

VOLUME 76 SEPTEMBER 28, 1972 NUMBER 20

JPCA X

---

THE JOURNAL OF  
PHYSICAL  
CHEMISTRY

---

PUBLISHED BIWEEKLY BY THE AMERICAN CHEMICAL SOCIETY

## Thirteen Ways to keep Informed

### KINETIC SYSTEMS

Mathematical Description of Chemical Kinetics in Solution

By Christos Capellos, *Feltman Research Laboratory, Picatinny Arsenal, Dover* and Benon H. J. Bielski, *Brookhaven National Laboratory*

This book presents step-by-step developments of important mathematical equations used in solving chemical kinetic systems. Forty different systems are discussed, including zero- to  $n^{\text{th}}$ -order reactions, reversible and consecutive irreversible reactions, catalytic reactions, parallel reactions, and electron transfer reactions in polar solvents. Equations describing the effect of Coulomb interactions and ionic strength on reaction velocities are also covered. The authors provide supplementary exercises and a list of selected differentials and integrals, as well as a short guide to the Operator Method of solving equations.

1972 138 pages \$11.95

### THE THEORY OF MAGNETIC RESONANCE

By Charles P. Poole, Jr. and Horacio A. Farach, *both of the University of South Carolina*

*The Theory of Magnetic Resonance* presents a uniform theoretical treatment of magnetic resonance and its various subfields. Utilizing a consistent matrix formulation, the authors develop general quantum-mechanical concepts, then derive principles relating to electron spin resonance, nuclear magnetic resonance, quadrupole spectroscopy, and the Mossbauer effect. Covering both generalized and specific phenomena, this book is an excellent preparation for advanced studies in magnetic resonance.

1972 452 pages \$19.95

### ADVANCES IN RADIATION CHEMISTRY

Volume 3

Edited by Milton Burton and John L. Magee, *both of the University of Notre Dame*

This series reflects the latest developments in areas fundamental to radiation chemistry.

**CONTENTS, VOLUME 3:** Short-Lived Transients—*Peter K. Ludwig*; Some Topics in Radiation Chemical Synthesis of Organic Compounds—*I. V. Vereshchinskii*; Radiation Chemical Mechanisms in Radiation Biology—*G. E. Adams*; X-ray Damage to DNA and Loss of Biological Function: Effect of Sensitizing Agents—*Peter T. Emerson*; Author Index; Subject Index.

1972 297 pages \$19.95

### CARBON-13 NMR SPECTRA

A Collection of Assigned, Coded, and Indexed Spectra

By Leroy F. Johnson and William C. Jankowski, *both of NMR Applications Laboratory, Varian, Palo Alto*

This unique reference contains 500 proton noise decoupled Carbon-13 NMR spectra of a variety of organic molecules. The spectra are supplemented with special diagrams, shift assignments and instrument parameters, and are reproduced in 200 ppm displays, allowing convenient laboratory comparison with spectra of unknown substances. An extensive structural coding system allows spectral correlation of a proposed structure with closely related compounds of known structure.

1972 680 pages (approx.) In Press

*Two volumes in the Wiley-Interscience Series on Atomic and Molecular Collision Processes, edited by C. F. Barnett*

### EXCITATION IN HEAVY PARTICLE COLLISIONS

By E. W. Thomas, *Georgia Institute of Technology*

This book tabulates and critically reviews an immense volume of published data on excitation induced by heavy particle collisions. Studies encompassing 147 different interactions involving helium, heavy monoatomic gases, and various molecular targets are considered in detail. To reconcile diverse experimental results, the author has adopted a three-step approach consisting of the formulation of experimental criteria, the collection and enumeration of data, and the examination of techniques against criteria with identification of deficiencies.

1972 436 pages \$22.50

### DISSOCIATION IN HEAVY PARTICLE COLLISIONS

By Gordon W. McClure and James M. Peek, *Sandia Laboratories, Albuquerque*

A companion to the above volume, this book covers the literature of dissociation processes in heavy particle collisions. After a general introduction, the authors present an extended discussion of experimental methods which includes a tabular guide to research papers, recommended experimental criteria, and a summary of significant qualitative findings. The last chapter is devoted to theoretical approximations applied to dissociative collisions.

1972 198 pages \$13.95

## SURFACE AND COLLOID SCIENCE

### Volume 5

Edited by Egon Matijevic, *Clarkson College*

This series presents research and critical reviews, written by specialists, on applications and advances in an increasingly important field.

**CONTENTS, VOLUME 5:** Rheological Properties of Monomolecular Films—*M. Joly*; The Physical Chemistry of Detergency—*Anthony M. Schwartz*; Friction, Lubrication, and Wear—*D. Tabor*; Author Index, Subject Index.

1972 331 pages \$22.50

## PROGRESS IN POLAROGRAPHY

### Volume 3

Edited by P. Zuman and L. Meites, *both of Clarkson College*, and I. M. Kolthoff, *University of Minnesota*

**CONTENTS:** Double Layer and Related Effects in Classic Polarography—*S. G. Mairanovskii*; Application of Polarography and Related Electrochemical Methods to the Study of Labile Complexes in Solution—*R. Tamamushi and G. P. Sato*; Effects of Acidity in the Elucidation of Organic Electrode Processes—*P. Zuman*; Intermetallic Compounds in Amalgams—*M. Kozlovsky and A. Zebrev*; Free Radicals in Organic Polarography—*B. Kastening*; Author Index; Subject Index.

1972 464 pages (approx.) In Press

## TOPICS IN PHOSPHOROUS CHEMISTRY

### Volume 7

Edited by Edward J. Griffith, *Monsanto Corporation*, and Martin Grayson, *American Cyanamid Company*

**CONTENTS:** Addition of Reactions of Tertiary Phosphorous Compounds with Electrophilic Olefins and Acetylenes—*M. A. Shaw and R. S. Ward*; Oligophosphonates—*J. D. Curry and D. A. Nicholson*; Nonenzymic Hydrolysis at Phosphate Tetrahedra—*R. K. Osterheld*; Cyclophosphates—*S. Y. Kalliney*; Compilation of Physical Data of Phosphazo Trihalides—*M. Berman*; Peroxophosphates—*I. I. Creaser and J. O. Edwards*; Author Index; Subject Index.

1972 528 pages (approx.) In Press

## LOW ENERGY ELECTRON SPECTROMETRY

By Kenneth D. Sevier

This book presents an extensive review of a rapidly expanding field. It covers both the instrumentation and methods used in electron spectrometry, and the related topics in atomic physics including Auger and Coster-Kronig effects, autoionization, internal conversion of nuclear transitions, atomic recoil following alpha-decay, and energy losses due to scattering in solids. The energy region of interest ranges over seven decades, from approximately 5 meV to 50 KeV.

1972 432 pages \$35.00

Available at your bookstore, or from Wiley-Interscience, Dept. 092

**wiley**

**WILEY-INTERSCIENCE** a division of

JOHN WILEY & SONS, INC. 605 Third Avenue, New York, N.Y. 10016. In Canada: 22 Worcester Road, Rexdale, Ontario

## UNIMOLECULAR REACTIONS

By P. J. Robinson, *University of Manchester*, and K. A. Holbrook, *University of Hull*

An extensive treatment of unimolecular reactions, this book provides derivations and comparisons of several important theories and their applications. Particular attention is given to the RRKM (Marcus-Rice) theory, and procedures for evaluating the necessary vibrational and rotational energy level densities are described and assessed. The book also furnishes up-to-date kinetic data for unimolecular equations, and discusses chemical activation, kinetic isotope effects, and collisional energy transfer in unimolecular reaction systems.

1972 371 pages \$19.95

## SEMI-EMPIRICAL SELF-CONSISTENT-FIELD MOLECULAR ORBITAL THEORY OF MOLECULES

By J. N. Murrell and A. J. Harget, *both of University of Sussex*

Starting from the limitations of Hückel techniques, this book develops the more exact, computer-adaptable methods of the self-consistent-field molecular orbital theory. The initial chapters introduce the Pariser-Parr-Pople-electron theory and the zero-overlap SCF methods for all valence electrons, covering molecular properties in both ground and excited states. This information is then applied to aspects of chemical structure, reactivity, and magnetic resonance spectroscopy. The book includes an extensive list of current references as well as appendices providing variation and perturbation methods, and a derivation of the Hartree-Fock equations.

1972 180 pages \$13.95

## THE INTERNATIONAL JOURNAL OF QUANTUM CHEMISTRY

Editor-in-Chief: Per-Olov Lowdin, *University of Uppsala, Sweden and University of Florida*

Assistant Editors: Jean-Louis Calais, *University of Uppsala*, Yngve Ohrn, *University of Florida*

Edited by internationally prominent scientists, this distinguished journal presents the most advanced information available on all important aspects of quantum chemistry. Subscribers receive six issues a year, plus the annual Sanibel Island Symposia on atomic, molecular and solid-state physics. There is no better way of keeping up with current developments in the field.

**PARTIAL CONTENTS, SEPT. 1972:** Unrestricted Hartree-Fock Calculations of Spin Densities with Orthogonalized Atomic Orbitals—*D. Nanda and P. T. Narasimhan*; Eigenspace Manipulation in SCF Theory—*C. Arnau, R. Carbo and S. Huzinaga*; Quasi-Relativistic Approximations in the SCF-MO-LCAO Method—*B. Bersuker et. al.*; The Electronic States of Icosahedral Molecules—*L. L. Boyle*; Vibrational Matrix Elements of the Quadrupole Moment Functions of H<sub>2</sub>, N<sub>2</sub>, and CO—*D. G. Trular*; An Alternative Formalism for the Method of Intermediate Hamiltonians—*R. A. Sack*.

Subscription price \$120.00 per volume (six issues plus symposia). Foreign postage \$5.00 per volume.

**WILEY-INTERSCIENCE**

# THE JOURNAL OF PHYSICAL CHEMISTRY

---

**BRYCE CRAWFORD, Jr.**, *Editor*  
STEPHEN PRAGER, *Associate Editor*  
ROBERT W. CARR, Jr., FREDERIC A. VAN-CATLEDGE, *Assistant Editors*

**EDITORIAL BOARD:** A. O. ALLEN (1970-1974), J. R. BOLTON (1971-1975),  
F. S. DAINTON (1972-1976), M. FIXMAN (1970-1974),  
H. S. FRANK (1970-1974), R. R. HENTZ (1972-1976), J. R. HUIZENGA (1969-1973),  
W. J. KAUZMANN (1969-1973), R. L. KAY (1972-1976), W. R. KRIGBAUM (1969-1973),  
R. A. MARCUS (1968-1972), W. J. MOORE (1969-1973), J. A. POPLE (1971-1975),  
B. S. RABINOVITCH (1971-1975), H. REISS (1970-1974), S. A. RICE (1969-1975),  
F. S. ROWLAND (1968-1972), R. L. SCOTT (1968-1972),  
R. SEIFERT (1968-1972), W. A. ZISMAN (1972-1976)

---

CHARLES R. BERTSCH, *Manager, Editorial Production*

---

**AMERICAN CHEMICAL SOCIETY**, 1155 Sixteenth St., N.W., Washington, D. C. 20036

#### **Books and Journals Division**

JOHN K CRUM, *Director*  
JOSEPH H. KUNEY, *Head, Business Operations Department*  
RUTH REYNARD, *Assistant to the Director*

©Copyright, 1972, by the American Chemical Society. Published biweekly by the American Chemical Society at 20th and Northampton Sts., Easton, Pa. 18042. Second-class postage paid at Washington, D. C., and at additional mailing offices.

All manuscripts should be sent to *The Journal of Physical Chemistry*, Department of Chemistry, University of Minnesota, Minneapolis, Minn. 55455.

*Additions and Corrections* are published once yearly in the final issue. See Volume 75, Number 26 for the proper form.

*Extensive or unusual alterations in an article after it has been set in type are made at the author's expense*, and it is understood that by requesting such alterations the author agrees to defray the cost thereof.

The American Chemical Society and the Editor of *The Journal of Physical Chemistry* assume no responsibility for the statements and opinions advanced by contributors.

Correspondence regarding accepted copy, proofs, and reprints should be directed to Editorial Production Office, American Chemical Society, 20th and Northampton Sts., Easton, Pa. 18042. Manager: CHARLES R. BERTSCH. Assistant Editor: EDWARD A. BORGER. Editorial Assistant: JOSEPH E. YURVATI.

Advertising Office: Centcom, Ltd. (formerly Century Communications Corporation), 142 East Avenue, Norwalk, Conn. 06851.

#### **Business and Subscription Information**

Remittances and orders for subscriptions and for single copies,

notices of changes of address and new professional connections, and claims for missing numbers should be sent to the Subscription Service Department, American Chemical Society, 1155 Sixteenth St., N.W., Washington, D. C. 20036. Allow 4 weeks for changes of address. Please include an old address label with the notification.

Claims for missing numbers will not be allowed (1) if received more than sixty days from date of issue, (2) if loss was due to failure of notice of change of address to be received before the date specified in the preceding paragraph, or (3) if the reason for the claim is "missing from files."

Subscription rates (1972): members of the American Chemical Society, \$20.00 for 1 year; to nonmembers, \$60.00 for 1 year. Those interested in becoming members should write to the Admissions Department, American Chemical Society, 1155 Sixteenth St., N.W., Washington, D. C. 20036. Postage to Canada and countries in the Pan-American Union, \$5.00; all other countries, \$6.00. Single copies for current year: \$3.00. Rates for back issues from Volume 56 to date are available from the Special Issues Sales Department, 1155 Sixteenth St., N.W., Washington, D. C. 20036.

This publication and the other ACS periodical publications are now available on microfilm. For information write to: MICROFILM, Special Issues Sales Department, 1155 Sixteenth St., N.W., Washington, D. C. 20036.

Notice to Authors last printed in the issue of June 22, 1972

# THE JOURNAL OF PHYSICAL CHEMISTRY

Volume 76, Number 20 September 28, 1972

JPCA<sub>x</sub> 76(20) 2801-2940 (1972)

Photochemical Production of Hot Hydrogen and Deuterium Atoms. Reactions with Hydrogen Halides and Halogens Richard A. Fass,* John W. Hoover, and Linda M. Simpson	2801
Exchange Reaction of Methane- <i>d</i> <sub>4</sub> with Hydrogen Chloride R. D. Kern* and G. G. Nika	2809
Gas-Phase Thermolysis Kinetics of Small Ring Nitriles Stanley F. Sarnier, David M. Gale,* Henry K. Hall, Jr., and Adah B. Richmond	2817
A Study of Ionization Processes by the Angular Distribution Technique. The AgCl System L. C. Wagner and R. T. Grimley*	2819
Shock Tube Cis-Trans Isomerization Studies. II Peter M. Jeffers	2829
Gas-Phase Homogeneous Catalysis in Shock Waves. III. The Oxidation of Carbon Monoxide by Oxygen in the Presence of Nickel Carbonyl Shimpei Matsuda	2833
Ultrasonic Attenuation in Basic Purine Solutions Maureen Brennan and Kenneth Kustin*	2838
A Manometric Study of the Oxygen-Peroxide-Superoxide Reaction in Nitrate Melts James M. Schlegel* and Douglas Priore	2841
Synergistic Catalysis of Ammonium Nitrate Decomposition. Visible Spectra of Ammine, Chloro, and Nitrate Complexes of Copper, Nickel, and Cobalt in Fused Ammonium Nitrate A. G. Keenan* and I. J. Ferrer	2844
Electron Spin Resonance Evidence for Dissociative Electron Capture in $\gamma$ -Irradiated Phosphate Esters Carolyn M. L. Kerr, Kathleen Webster, and Ffrancon Williams*	2848
Interaction of Arsine with Evaporated Metal Films I. M. Al-Daher and J. M. Saleh*	2851
Electron Spin Resonance Spectra of Di- and Trimethylaminium Radicals Richard W. Fessenden* and P. Neta	2857
Electron Paramagnetic Resonance Study of Copper(II)-Ammonia Complexes in Y-Type Zeolites E. F. Vansant and J. H. Lunsford*	2860
A Solvent Effect on Metal Hyperfine Constants in Alkali Metal Radical Anion Ion Pairs T. R. Tuttle, Jr.,* J. C. Danner, and Philip Graceffa	2866
Nitrogen and Boron Spin-Lattice Relaxation in Borazole George M. Whitesides,* Steven L. Regen, John B. Lisle, and Robert Mays	2871
Steric Interactions in <i>tert</i> -Butylethylenes Observed through Proton <sup>13</sup> C Satellite Spectra P. P. Nicholas,* C. J. Carman, A. R. Tarpley, Jr., and J. H. Goldstein	2877
Structure and Orientation of Phenols Chemisorbed on $\gamma$ -Alumina D. R. Taylor* and K. H. Ludlum	2882
Preparation and Structure of Bromobis(2-(2-aminoethyl)pyridine)copper(II) Bromide Phirtu Singh, Vicki C. Copeland, William E. Hatfield, and Derek J. Hodgson*	2887
Dielectric Properties and Relaxation in Ethylene Carbonate and Propylene Carbonate Richard Payne* and Ignatius E. Theodorou	2892
Second Virial Coefficients for the Polar Species in Steam R. J	2901
Strong Crystalline Field Perturbation Calculations for d <sup>3</sup> ,d <sup>7</sup> Pentacoordinate Complexes. I. The Trigonal Bipyramid J. A. Varga and C. A. L	
Calculated Free Energies of Adsorption of Halide and Hydroxide Ions by Mercury, Silver, and Gold Elec Donald D.	

Association of Alkali Perchlorates in Anhydrous Methanol at 25° . . . . .	Allesandro D'Aprano	2920
Ionic Association of Potassium Perchlorate in Sulfolane-Water Mixtures from Conductance Measurements at 25° . . . . .	A. D'Aprano,* I. D. Donato, and R. Palombo	2923
Effect of High Pressure on the Formation of Aqueous $\text{EuSO}_4^+$ at 25° . . . . .	Clarence F. Hale and F. H. Spedding*	2925

#### COMMUNICATIONS TO THE EDITOR

Quasi-Equilibrium Analysis of the Reaction of Atomic and Molecular Fluorine with Tungsten . . . . .	Philip C. Abbott and Robert E. Stickney*	2930
Reply to "Quasi-Equilibrium Analysis of the Reaction of Atomic and Molecular Fluorine with Tungsten" . . . . .	Daniel E. Rosner* and Paul C. Nordine	2930
Optical Absorption of Solvated Electrons in Alcohols and Their Mixtures with Alkanes . . . . .	Robert R. Hentz* and Geraldine Kenney-Wallace	2931
Calculation of $\Delta H_d^\circ(g) - \Delta H_d^\circ(l)$ for Dissociating Dimers <i>via</i> the "Dissociation-Vaporization" Rule. The $\Delta H_d^\circ(l)$ of Trimethylaluminum . . . . .	Martin B. Smith	2933
Resolution of Components of the Optical Rotation Tensor of Collagen . . . . .	I. V. Yannas,* N.-H. Sung, and C. Huang	2935
Hydrogen Displacement in <i>n</i> -Butane by Fast $T_2$ Collisions . . . . .	Michael Menzinger,* Rodney L. LeRoy, and Andrew J. Yench	2937
Comments on "Hydrogen Displacement in <i>n</i> -Butane by Fast $T_2$ Collisions" . . . . .	S. Wexler	2939

#### AUTHOR INDEX

Abbott, P. C., 2930	Gale, D. M., 2817	Kern, R. D., 2809	Nordine, P. C., 2930	Sung, N.-H., 2935
Al-Daher, I. M., 2851	Goldstein, J. H., 2877	Kerr, C. M. L., 2848	Palombo, R., 2923	Tarpley, A. R., Jr., 2877
Becker, C. A. L., 2907	Graceffa, P., 2866	Kubin, R. F., 2901	Payne, R., 2892	Taylor, D. R., 2882
Bodé, D. D., Jr., 2915	Grimley, R. T., 2819	Kustin, K., 2838	Priore, D., 2841	Theodorou, I. E., 2892
Brennan, M., 2838	Hale, C. F., 2925	LeRoy, R. L., 2937	Regen, S. L., 2871	Tuttle, T. R., Jr., 2866
Carman, C. J., 2877	Hall, H. K., Jr., 2817	Lisle, J. B., 2871	Richmond, A. B., 2817	Vansant, E. F., 2860
Copeland, V. C., 2887	Hatfield, W. E., 2887	Ludlum, K. H., 2882	Rosner, D. E., 2930	Varga, J. A., 2907
Danner, J. C., 2866	Hentz, R. R., 2931	Lunsford, J. H., 2860	Saleh, J. M., 2851	Wagner, L. C., 2819
D'Aprano, A., 2920, 2923	Hodgson, D. J., 2887	Matsuda, S., 2833	Sarner, S. F., 2817	Webster, K., 2848
Donato, I. D., 2923	Hoover, J. W., 2801	Mays, R., 2871	Schlegel, J. M., 2841	Wexler, S., 2939
Fass, R. A., 2801	Huang, C., 2935	Menzinger, M., 2937	Simpson, L. M., 2801	Whitesides, G. M., 2871
Ferrer, I. J., 2844	Jeffers, P. M., 2829	Neta, P., 2857	Singh, P., 2887	Williams, F., 2848
Fessenden, R. W., 2857	Keenan, A. G., 2844	Nicholas, P. P., 2877	Smith, M. B., 2933	Yannas, I. V., 2935
	Kennedy-Wallace, G., 2931	Nika, G. G., 2809	Spedding, F. H., 2925	Yench, A. J., 2937
			Stickney, R. E., 2930	

In papers with more than one author the name of the author to whom inquiries about the paper should be addressed is marked with an asterisk in the by-line.

## Photochemical Production of Hot Hydrogen and Deuterium Atoms.

Reactions with Hydrogen Halides and Halogens<sup>1a</sup>by Richard A. Fass,\* John W. Hoover,<sup>1b</sup> and Linda M. Simpson<sup>1c</sup>*Department of Chemistry, Pomona College, Claremont, California 91711 (Received February 18, 1972)**Publication costs assisted by the Research Corporation*

The reactions of photolytically produced hot hydrogen and deuterium atoms with hydrogen halides and halogens have been studied in both moderated and unmoderated gas-phase systems. The ratios of the rates of the reactions  $H + HX \rightarrow H_2 + X$  (2) and  $H + X_2 \rightarrow HX + X$  (3) have been determined when HX is HBr, DBr, and HCl, and the results have been compared with similar data available in the literature for HCl, DCl, and HI. In the absence of inert gas moderators the ratios  $k_3^*/k_2^*$  for the reactions of hot atoms are  $5.6 \pm 0.25$  for HBr,  $6.7 \pm 0.13$  for DBr, and  $8 \pm 4$  for HCl. The data for D atoms from the photolysis of DBr in the presence of D<sub>2</sub> moderator ( $[D_2]/[DBr] > 70$ ) give  $k_3/k_2 = (12 \pm 2.8) \exp(0.9 \pm 0.16)/RT$ .

## Introduction

The photodissociation of hydrogen halides leads to the production of "hot" hydrogen atoms, *i.e.*, hydrogen atoms with excess translation energies with respect to the threshold energies of some possible reactions. These hot hydrogen atoms may react while they are hot (H\*) or may be moderated by collision with other molecules or the walls of the reaction vessel, after which they react like thermal hydrogen atoms. The reactions of hot hydrogen atoms with molecular hydrogen (or the isotopic variations of these reactions),<sup>2-5</sup> with hydrocarbons,<sup>1,6-11</sup> and with hydrogen halides and halogens<sup>12-17</sup> have been the subject of considerable study. The reactions with hydrogen halides and halogens are of interest not only for the intrinsic information they yield about the reactivity of hot hydrogen atoms, but also for their implications in one of the more convenient methods of gas-phase ultraviolet actinometry. This paper presents additional data on the reactions of hot and thermal D atoms with DBr and Br<sub>2</sub>, and on the reaction of hot H atoms with HCl and Cl<sub>2</sub>. The effects of inert moderators are discussed and the relative Arrhenius parameters for the reaction of D atoms with DBr and Br<sub>2</sub> are calculated.

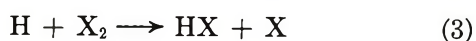
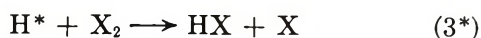
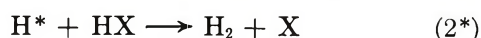
For the system consisting of HX (X = Br, I, and Cl), X<sub>2</sub>, and inert moderator (M), the mechanism of photodecomposition of the hydrogen halide is as follows.

- (1) (a) This research has been supported in part by a Frederick Gardner Cottrell grant from Research Corporation. (b) NSF Undergraduate Research Participant (NSF-URP), Summer, 1971. (c) Supported by a fellowship from the California Foundation for Biochemical Research, Summer, 1970.
- (2) R. M. Martin and J. E. Willard, *J. Chem. Phys.*, **40**, 3007 (1964).
- (3) A. Kuppermann and J. M. White, *ibid.*, **44**, 4352 (1966).
- (4) D. Seewald and R. Wolfgang, *ibid.*, **46**, 1207 (1967).
- (5) J. M. White, *Chem. Phys. Lett.*, **4**, 441 (1969).
- (6) J. C. Biondi, Y. Rousseau, and G. J. Mains, *J. Chem. Phys.*, **49**, 2642 (1968).
- (7) R. Gann and J. Dubrin, *ibid.*, **50**, 535 (1969).
- (8) C. C. Chou, T. Smail, and F. S. Rowland, *J. Amer. Chem. Soc.*, **91**, 3104 (1969).
- (9) R. T. K. Baker, M. Silber, and R. Wolfgang, *J. Chem. Phys.*, **52**, 1120 (1970).
- (10) R. G. Gann, W. M. Ollison, and J. Dubrin, *J. Amer. Chem. Soc.*, **92**, 450 (1970).
- (11) J. E. Nicholas, F. Bayrakceken, and R. D. Fink, *J. Phys. Chem.*, **75**, 841 (1971).
- (12) H. A. Schwarz, R. R. Williams, Jr., and W. H. Hamill, *J. Amer. Chem. Soc.*, **74**, 6007 (1952).
- (13) J. L. Holmes and P. Rodgers, *Trans. Faraday Soc.*, **64**, 2348 (1968).
- (14) R. D. Penzhorn and B. deB. Darwent, *J. Phys. Chem.*, **72**, 1639 (1968).

Table I: Quantum Yields of Br<sub>2</sub> from Photolysis of Unmoderated HBr-Br<sub>2</sub> Mixtures

HBr-Br <sub>2</sub> or DBr-Br <sub>2</sub>	λ, Å	T, °C	P <sub>HBr</sub> or P <sub>DBr</sub> , Torr <sup>a</sup>	([Br <sub>2</sub> ]/ [HBr]) <sub>avg</sub> or ([Br <sub>2</sub> ]/ [DBr]) <sub>avg</sub>	1/φ <sub>Br<sub>2</sub></sub>	HBr-Br <sub>2</sub> or DBr-Br <sub>2</sub>	λ, Å	T, °C	P <sub>HBr</sub> or P <sub>DBr</sub> , Torr <sup>a</sup>	([Br <sub>2</sub> ]/ [HBr]) <sub>avg</sub> or ([Br <sub>2</sub> ]/ [DBr]) <sub>avg</sub>	1/φ <sub>Br<sub>2</sub></sub>
HBr-Br <sub>2</sub> (2.0- 2.3 eV)	2139	25	9.04	0.0401	1.13	HBr-Br <sub>2</sub> (ref 15, 2.9 eV)	1850	25	15.8	0.105	1.48
				0.0549	1.12					0.139	1.71
				0.0684	1.28					0.193	1.93
				0.0846	1.14					0.223	2.23
				0.0995	1.35					0.267	2.36
				0.1115	1.67					0.339	2.64
				0.1235	1.71					0.100	1.52
				0.1395	1.64					0.121	1.56
				0.1647	1.80					0.210	2.01
				0.1924	2.15					0.244	2.42
HBr-Br <sub>2</sub> (2.0- 2.3 eV)	2139	25	16.06	0.0457	1.17	DBr-Br <sub>2</sub> (1.9- 2.2 eV)	2139	25	11.05	0.075	1.29
				0.0565	1.16					0.102	1.57
				0.0667	1.15					0.209	2.71
				0.0748	1.43					0.358	3.37
				0.0832	1.56					0.415	3.56
				0.0970	1.56					0.576	5.30
				0.1150	1.61					0.850	6.50
				0.1319	2.14					0.104	1.64
				0.1483	1.96					0.226	1.78
				0.0459	1.32					0.323	3.26
HBr-Br <sub>2</sub> (2.0- 2.3 eV)	2139	25	16.23	0.0652	1.28	DBr-Br <sub>2</sub> (1.9- 2.2 eV)	2139	120	10.93	0.381	3.35
				0.0735	1.57					0.550	5.00
				0.0824	1.34					0.829	6.85
				0.0961	1.69					0.113	1.79
				0.1130	1.68					0.240	2.50
				0.1297	2.13					0.382	3.43
				0.1452	2.11					0.551	4.63
				0.1631	2.14					0.118	1.91
				0.2211	2.11					0.233	2.67
				0.2530	2.08					0.366	3.47
0.3331	3.09	0.546	4.67								
		0.468	4.08								
		0.546	4.37								

<sup>a</sup> Pressures reported here are initial pressures, *i.e.*, HBr or DBr pressures initially added to each cell. As the photolysis proceeds, [HBr] or [DBr] of course decrease as Br<sub>2</sub> is produced.



When DX is photolyzed instead of HX the mechanism is the same, except D atoms are involved instead of H atoms. In the subsequent discussions of the mechanism it is implied that the reactions and equations apply to D atoms as well as H atoms, with the appropriate substitution of D for H in the formulas.

In pure HX, the H atoms must form H<sub>2</sub> by reaction

2\* and/or 2, leading to a quantum yield of 2.0 for HX consumption and 1.0 for X<sub>2</sub> formation. In the limit where [X<sub>2</sub>]/[HX] ≫ 1, inhibition from reactions 3\* and 3 results in a quantum yield of 0.0 for both HX decomposition and X<sub>2</sub> formation. Measurement of quantum yields as a function of [X<sub>2</sub>]/[HX] leads to values of k<sub>3</sub>\*/k<sub>2</sub>\*, as discussed below. When the photolysis is done in the presence of an excess of inert moderator, it is only k<sub>3</sub>/k<sub>2</sub>, the thermal rate constant ratio, that is observed.

In the absence of added inert moderator k<sub>3</sub>\*/k<sub>2</sub>\*, a ratio corresponding to an average H atom energy derived from a non-Boltzmann distribution, is the

(15) R. A. Fass, *J. Phys. Chem.*, **74**, 984 (1970).

(16) R. J. Letelier, H. L. Sandoval, and R. D. Penzhorn, *ibid.*, **75**, 835 (1971).

(17) G. O. Wood and J. M. White, *J. Chem. Phys.*, **52**, 2613 (1970).

measured quantity. All that is known about the energy distribution in these systems is that the maximum energy of H relative to HX and X<sub>2</sub> (ignoring the effects of thermal motion of the HX and X<sub>2</sub>) is equal to the difference between the energy of the exciting photon and the HX bond energy, calculated from the center of mass of HX.<sup>18</sup> Because of the large mass of X compared to H or D, practically all of the photon energy in excess of the bond energy ends up as kinetic energy of the H or D atom, assuming no electronic excitation of the halogen atom.<sup>19</sup> Calculated values of the initial energy for each wavelength and halide used are given with the data in Tables I and II. This is sometimes a gross approximation because of the effects of thermal motion; Kuppermann, *et al.*,<sup>20</sup> and Gann and Dubrin<sup>21</sup> have shown how to determine the initial (*i.e.*, before any collisions) energy distribution of the H atoms taking this motion into account. Since we find no wavelength effect (*i.e.*, no energy effect) for  $k_3^*/k_2^*$  in unmoderated systems (see below) it is sufficient in this work to separate our discussion into that applying to "thermal" atoms and to "hot" atoms without specifying the details of the hot atom energy and distribution.

There is now a substantial body of data on the relative rates of reactions of hydrogen atoms in HX-X<sub>2</sub>

systems and several patterns have begun to emerge. The original data of Schwarz, *et al.*,<sup>12</sup> on the reactions of hot H atoms in the HBr-Br<sub>2</sub> and HI-I<sub>2</sub> systems have been shown to be in error,<sup>12,14,15</sup> and corrected values of  $k_3^*/k_2^*$  for these systems have been given. The ratios of thermal rate constants and the relative Arrhenius parameters for these reactions have also been measured in some of these systems.<sup>14-16</sup> Data on the hot and thermal reactions of D atoms in DCl-Cl<sub>2</sub> systems have been provided by Wood and White,<sup>17</sup> and the present paper provides similar data for D atoms in the DBr-Br<sub>2</sub> system and for the reactions of hot H atoms in the HCl-Cl<sub>2</sub> systems. These data are compared in the last section of this paper and the implications of this comparison are discussed.

### Experimental Section

Matheson HBr was used as received (99.8% minimum purity) except for degassing and distillation under vacuum. It was stored in a Pyrex flask on a vacuum line and showed no appreciable decomposition over a period of several months. DBr was purchased from International Chemical and Nuclear Corp. (isotopic purity 99 atom %) and was similarly stored in a Pyrex flask. HCl (electronic grade) and Cl<sub>2</sub> (high-purity grade) were purchased in lecture bottles from Air Products and Chemicals, Inc., and were used in the same way as the HBr. Br<sub>2</sub> was Matheson Coleman and Bell ACS Reagent grade, and was stored in an evacuated Pyrex tube. All of these chemicals were stored behind Teflon stopcocks. Matheson D<sub>2</sub> (CP grade, 99.5 atom %) was used as received.

The light sources used in this work were a Phillips No. 93106 zinc vapor arc and a Hanovia low-pressure mercury arc. The zinc arc emits only three strong lines in the absorption region of HBr and DBr, 2026, 2062, and 2139 Å. Actinometry performed with and without a *cis*-2-butene filter to cut out the lines below 2100 Å (approximately 200 Torr *cis*-2-butene in a 1-cm quartz cell) indicated that roughly half of the output of the lamp is below 2100 Å, half at 2139 Å. In most of the work described below, this distribution was not a problem and the *cis*-2-butene filter was not used for the photolyses. A typical intensity available from the zinc lamp is  $5 \times 10^{14}$  photons/sec. It was necessary, however, to make small corrections for the changing rate of photon absorption due to the changing concentration of HBr or DBr in the cells during a photolysis, and for this purpose it was necessary to know the wavelength distribution approximately. The low-pressure mercury arc had a Suprasil window

**Table II:** Quantum Yields of Br<sub>2</sub> from the 2139-Å Photolysis of DBr-Br<sub>2</sub> Mixtures Moderated with 700 Torr D<sub>2</sub>

T, °C	P <sub>DBr</sub> , Torr	([Br <sub>2</sub> ]/ [DBr]) <sub>avg</sub>	1/φ <sub>Br<sub>2</sub></sub>
25	9.90	0.065	4.17
		0.102	6.38
		0.138	7.25
		0.194	12.5
		0.250	16.3
25	8.04	0.065	5.00
		0.109	7.46
		0.178	9.40
		0.227	13.8
		0.298	19.8
25	8.00	0.105	5.62
		0.128	6.50
		0.405	25.7
60	8.27	0.120	5.62
		0.149	7.30
		0.295	15.6
		0.350	15.6
120	8.00	0.014	1.24
		0.072	3.03
		0.147	5.38
		0.338	13.3
155	8.21	0.014	1.42
		0.094	3.75
		0.205	8.20
		0.328	13.1
		0.468	15.4
200	8.33	0.085	2.39
		0.186	5.43
		0.314	10.3
		0.468	15.4

(18) R. A. Fass, Ph.D. Thesis, University of Wisconsin, 1969.

(19) R. M. Martin and J. E. Willard, *J. Chem. Phys.*, **40**, 2999 (1964).

(20) A. Kuppermann, J. Stevenson, and P. O'Keefe, *Discuss. Faraday Soc.*, **44**, 46 (1967).

(21) R. G. Gann and J. Dubrin, *J. Amer. Chem. Soc.*, **92**, 450 (1970).

and therefore emitted both the 1850- and the 2537-Å lines. Only the 1850-Å line is absorbed significantly by HBr, DBr, or HCl so filters were not necessary for these photolyses.

In several of the experiments it was useful to have a very intense, but not necessarily monochromatic, ultraviolet source so that HBr or DBr could be decomposed rapidly in order to change the ratio of Br<sub>2</sub> to HBr or DBr in the cell. A Hanovia Model 673A-36, high-pressure mercury lamp was used for this purpose; it provided enough uv radiation to decompose HBr more than 100 times faster than the zinc source used for quantum yield measurements.

All cells were filled on a mercury-free vacuum line; contamination from stopcock grease was avoided by using Teflon stopcocks and Viton-A O-ring seals on all standard taper connections. Pressures were metered on a Wallace and Tiernan FA-141 low-pressure gauge (0–37 Torr) or an FA-145 gauge (0–800 Torr). The accuracy of the FA-141 gauge is given by the manufacturer as approximately 0.1 Torr, and that of the FA-145 gauge as approximately 1 Torr. These were verified by comparing the pressure reading on the gauge with the corresponding concentration of HBr in a photolysis cell as measured with a Cary Model 14 spectrophotometer at 2100 Å. The molar extinction coefficient of HBr used in this calculation is  $154.5 \pm 0.8 M^{-1} \text{ cm}^{-1}$ , as measured by Huebert and Martin.<sup>22</sup>

The photolysis cells were Suprasil, 22-mm cylindrical cells with 100 mm path length. They were fitted with graded seals and greaseless stopcocks. When DBr was used, the vacuum line and cells were always treated with DBr prior to filling the cells in order to assure the isotopic purity of the DBr in the photolysis cell. DBr (approximately 20 Torr) was metered into the line, allowed to remain for about 0.5 hr, and then pumped out. This procedure was used because of the tendency of DBr to exchange rapidly with the walls of a Pyrex system.<sup>2</sup>

When unmoderated HBr–Br<sub>2</sub> or DBr–Br<sub>2</sub> systems were being examined, the H<sub>2</sub> or D<sub>2</sub> produced during photolysis was periodically pumped out of the cells to prevent it from building up to a point where it might have a significant moderating effect on the hot atoms.

Extinction coefficients for HBr and DBr used in this work were those given by Huebert and Martin<sup>22</sup> and those of Gordus and Caughey.<sup>18, 23</sup> Interpolation of these data gave values at 2139 Å of 115.6 and 82.5  $M^{-1} \text{ cm}^{-1}$  for HBr and DBr, respectively. A value of 170  $M^{-1} \text{ cm}^{-1}$  at 4160 Å was used for the extinction coefficient of Br<sub>2</sub> at 4160 Å.<sup>24</sup> Quantum yields were determined by measuring the rate of formation of Br<sub>2</sub> spectrophotometrically at 4160 Å in the HBr and DBr systems, and the rate of formation of Cl<sub>2</sub> as measured at 3300 Å in the HCl systems. Actinometry was based on the fact that the quantum yield of decomposition

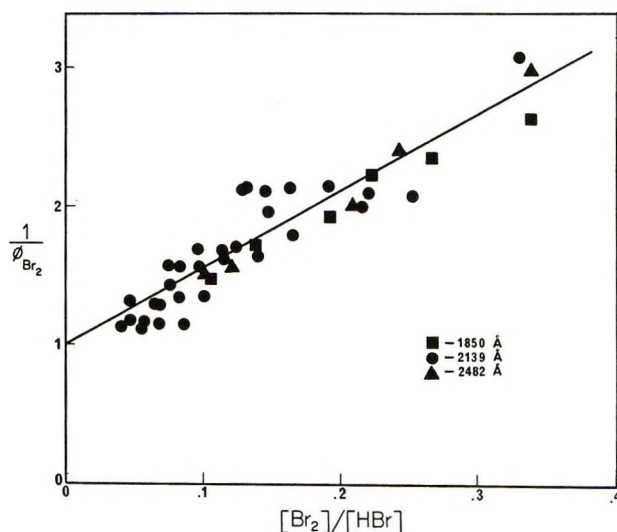


Figure 1. Reciprocal Br<sub>2</sub> quantum yields vs. [Br<sub>2</sub>]/[HBr] for unmoderated systems ( $k_3^*/k_2^* = 5.6 \pm 0.25$ ).

of HX (X = Br or Cl) is 2.0 in the absence of X<sub>2</sub>, and the quantum yield of formation of X<sub>2</sub> is therefore 1.0. The small amount of X<sub>2</sub> formed in a typical actinometric measurement usually had a very small effect on the quantum yield of decomposition of HX, but this inhibitory effect was corrected for when necessary. Accurate extinction coefficients for Cl<sub>2</sub> were not available, so in the HCl–Cl<sub>2</sub> systems the relative concentrations were calculated solely from the readings on the Wallace and Tiernan pressure gauges when the gases were metered into the photolysis cells. In the HBr and DBr systems the concentrations were also checked spectrophotometrically.

Most of the experiments with DBr were done at initial DBr or HBr pressures between 8 and 16 Torr. Experiments with the HBr–Br<sub>2</sub> system (see Figure 1 and discussion below) verified that the rate constants were, as expected, independent of pressure in this range. As each sample was photolyzed, giving successively higher [Br<sub>2</sub>]/[HBr] or [Br<sub>2</sub>]/[DBr] ratios, the total HBr or DBr pressure decreased accordingly. At the pressures used in these experiments the optical densities of HBr and DBr in the photolysis cells at 2139 Å were such that there was incomplete absorption of the radiation from the zinc lamp, and it was necessary to correct for this incomplete absorption in the calculations as the HBr or DBr concentration changed. The HCl pressure used in the HCl–Cl<sub>2</sub> systems was 200 Torr, and there was virtually complete absorption of all of the 1850-Å radiation from the mercury lamp. Under

(22) B. J. Huebert and R. M. Martin, *J. Phys. Chem.*, **72**, 3046 (1968).

(23) A. A. Gordus and D. A. Caughey, Abstracts, 150th National Meeting of the American Chemical Society, Atlantic City, N. J., Sept, 1965.

(24) A. A. Passchier, J. D. Christian, and N. W. Gregory, *J. Phys. Chem.*, **71**, 937 (1967).

these conditions, the quantum yield of  $\text{Cl}_2$  formation in a particular  $\text{HCl}-\text{Cl}_2$  mixture could be calculated as the ratio of the rate of optical density change at  $3300 \text{ \AA}$  in the mixture to the same rate in 200 Torr of pure  $\text{HCl}$ . This procedure obviated the need to obtain accurate extinction coefficients for  $\text{HCl}$  and  $\text{Cl}_2$ .

The photolysis train consisted of the zinc or mercury lamp, a biconvex  $f/1.0$  fused silica lens, and a thermostatically-controlled aluminum block housing for the photolysis cell. The temperature for  $25^\circ$  studies was controlled by passing water from a Haake Series F temperature-regulated circulator through coils in the aluminum block. For the higher temperature studies a different block was used, heated electrically and controlled by a Fenwal thermostatic switch. The temperature control in this housing was  $\pm 1^\circ$  as measured with a thermocouple inserted into the center of the block.

## Results

The mechanism described by reactions 1 through 5 leads, through the usual steady-state considerations, to the expression

$$\frac{1}{\phi_{X_2}} = \frac{k_3'[\text{X}_2]}{k_2'[\text{HX}]} + 1 \quad (\text{I})$$

In this equation,  $k_3'$  and  $k_2'$  are the rate constants characteristic of the particular hydrogen atom energy distribution in each experiment. Thus, in experiments with an excess of inert moderator  $k_3'/k_2' = k_3/k_2$ , the ratio of thermal rate constants. In "unmoderated" systems (containing  $\text{HX}$  or  $\text{DX}$ , and  $\text{X}_2$ , but no inert moderator)  $k_3'/k_2'$  represents an average ratio for all of the H or D atoms in the system. As discussed below there is evidence which indicates that in unmoderated systems of  $\text{HBr}$  and  $\text{Br}_2$  all of the hydrogen atoms react before reaching thermal energies, so that  $k_3'/k_2' = k_3^*/k_2^*$ , the ratio for some unspecified distribution of hot atoms. It has been assumed here that the same is true for the  $\text{DBr}-\text{Br}_2$  system.

In their discussion of the reactions of D atoms with  $\text{DCl}$  and  $\text{Cl}_2$ , Wood and White<sup>17</sup> found it necessary to consider the effect of moderation of the hot D atoms by  $\text{DCl}$  and  $\text{Cl}_2$ . If this effect is significant, then there is, of course, no such thing as an unmoderated system. They found that their data for systems in which no inert moderator was added were described by the equation

$$1/\phi = 1 + (k_4^{\text{DCl}}/k_2^*) + \left\{ (k_3^*/k_2^*) + (k_4^{\text{Cl}_2}/k_2^*) \right\} \left\{ [\text{Cl}_2]/[\text{DCl}] \right\} \quad (\text{II})$$

where the rate constants refer to the reactions as given in this paper, with  $\text{DCl}$  and  $\text{Cl}_2$  substituted for  $\text{HX}$  and  $\text{X}_2$ , respectively. The rate constants  $k_4^{\text{DCl}}$  and  $k_4^{\text{Cl}_2}$  refer to the moderation of hot D atoms by  $\text{DCl}$  and  $\text{Cl}_2$ , respectively. Wood and White<sup>17</sup> find that  $k_4^{\text{DCl}}/k_2 = 0.65$  and  $k_4^{\text{Cl}_2}/k_2^* = 1$  for D atoms of approximately

2 eV initial energy. If a similar mechanism were operative in the  $\text{DBr}-\text{Br}_2$  system we would expect that (a) plots of  $1/\phi$  vs.  $[\text{HBr}]/[\text{Br}_2]$  would have intercepts differing from unity by an amount equal to the ratio  $k_4^{\text{HBr}}/k_2^*$  and (b) the slopes of these plots would vary with initial H atom energy since one would expect that  $k_4^{\text{Br}_2}$  would increase and  $k_2^*$  would decrease as the initial H atom energy is decreased. None of the plots from the earlier work<sup>15</sup> on the  $\text{HBr}-\text{Br}_2$  system or the present work on the  $\text{DBr}-\text{Br}_2$  system deviated significantly from linearity or gave intercepts significantly different from unity, and variation of the initial energy of H atoms from approximately 1 to 3 eV (by photolyzing at three different wavelengths) resulted in no significant change in the slopes (see results below). It is therefore concluded that within the limits of detection in these studies, eq I is an adequate description of the reaction mechanism for the  $\text{HBr}-\text{Br}_2$  and  $\text{DBr}-\text{Br}_2$  systems, i.e.,  $k_4^{\text{HBr}}/k_2^* \ll 1$ ,  $k_4^{\text{DBr}}/k_2^* \ll 1$ , and  $k_4^{\text{Br}_2}/k_2^* \ll k_3^*/k_2^*$ .

Data for the  $\text{HBr}-\text{Br}_2$  system are shown in Figure 1, where earlier data<sup>15</sup> on the photolysis of unmoderated systems of  $\text{HBr}$  and  $\text{Br}_2$  photolyzed at 1850 and at 2482  $\text{\AA}$  are combined with recent measurements for the same mixtures photolyzed at 2139  $\text{\AA}$ . The 2139- $\text{\AA}$  data include measurements at several initial  $\text{HBr}$  pressures from 9 to 15 Torr. The slope of this plot is  $0.97 \pm 0.05$  when all points are used. Since this is, within experimental error, in agreement with I, the line drawn in Figure 1 is the least-squares line forced through an intercept of 1.0. The linear correlation coefficient is 0.93, and the lines calculated individually for each initial  $\text{HBr}$  pressure and wavelength are in agreement with each other within their uncertainty ranges. All uncertainties reported in this paper are standard deviations unless otherwise specified. The data for Figure 1 are also summarized in Table I, and the slope of the line forced through an intercept of 1.0 is  $k_3^*/k_2^* = 5.6 \pm 0.25$ . The value reported previously,<sup>15</sup> based on fewer points, was  $5.3 \pm 0.4$ .<sup>24a</sup>

Quantum yields were measured for unmoderated  $\text{DBr}-\text{Br}_2$  systems photolyzed at 2139  $\text{\AA}$ , with the results shown in Figure 2 and given in Table I. Included on this plot are several measurements made at 120 and 200 $^\circ$  as well as 25 $^\circ$ . The intercept calculated from these points is  $0.9 \pm 0.10$ . The slopes of the lines drawn through an intercept of unity in Figure 2, in accordance with eq I, are  $6.78 \pm 0.19$  at 25 $^\circ$  and  $6.65 \pm 0.09$  at 120 $^\circ$ , verifying that in these unmoderated systems we are seeing only hot, and therefore temperature-independent reactions. The correspond-

(24a) NOTE ADDED IN PROOF. J. M. White and H. Y. Su generously provided a prepublication copy of a paper in which they report a small wavelength effect for  $k_3^*/k_2^*$  in  $\text{HBr}-\text{Br}_2$  systems. They find  $k_3^*/k_2^* = 4.11 \pm 0.16$  for 1850- $\text{\AA}$  photolysis, and  $k_3^*/k_2^* = 5.48 \pm 0.22$  for 2290- $\text{\AA}$  photolysis. Although these data disagree somewhat with those in ref 15 and this paper, the disagreement does not affect any of the qualitative conclusions of this paper.

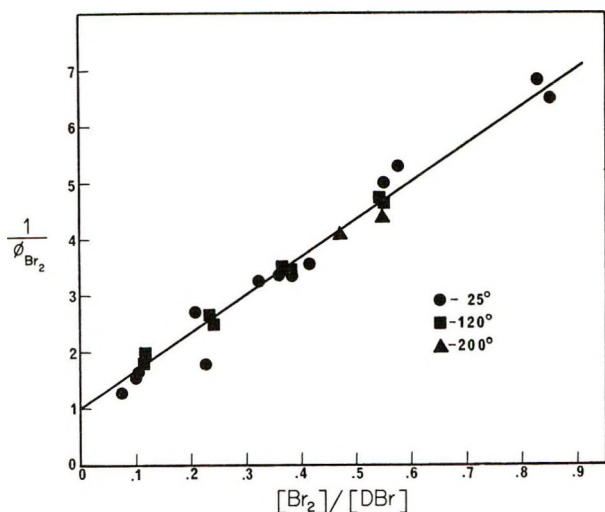


Figure 2. Reciprocal  $\text{Br}_2$  quantum yields vs.  $[\text{Br}_2]/[\text{DBr}]$  for unmoderated systems photolyzed with zinc resonance lamp. Initial D atom energy  $\approx 2$  eV ( $k_3^*/k_2^* = 6.7 \pm 0.13$ ).

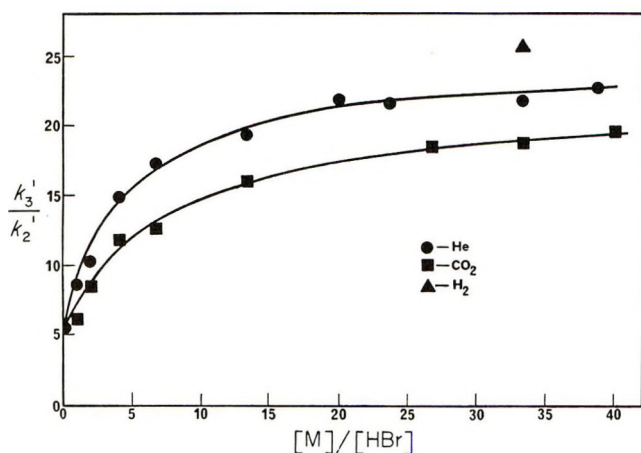


Figure 3. Effect of inert moderators on  $k_3'/k_2'$  for HBr. Photolysis with zinc resonance lamp at  $25^\circ$ ; initial HBr pressures = 15 Torr.

ing slopes for *thermalized* D atoms are (see below)  $58 \pm 1.7$  at  $25^\circ$  and  $35 \pm 1.5$  at  $120^\circ$ . The linear correlation coefficient of the data in Figure 2, using all points, is 0.99 and the slope of the line shown in the figure is  $k_3^*/k_2^* = 6.7 \pm 0.13$ .

Earlier work with the HBr- $\text{Br}_2$  system photolyzed at  $1850 \text{ \AA}$ <sup>15</sup> indicated that a ratio of at least 40/1 of  $[\text{He}]/[\text{HBr}]$  is necessary to thermalize essentially all of the  $\text{H}^*$  atoms before they react with HBr or  $\text{Br}_2$ . Furthermore, these studies<sup>15</sup> showed that the same ratio of  $\text{CO}_2$  to HBr was clearly insufficient to thermalize all of the 3-eV  $\text{H}^*$  atoms despite the appearance of an apparent plateau in plots of  $k_3'/k_2'$  vs. moderator concentration. Despite this, several reports have appeared of studies of reactions of "thermal" hydrogen atoms from photolysis of HI,<sup>14</sup> HBr,<sup>16</sup> or  $\text{H}_2\text{S}$ .<sup>25,26</sup> In order to provide a check on the possibility that the relatively inefficient moderation by  $\text{CO}_2$  was unique to

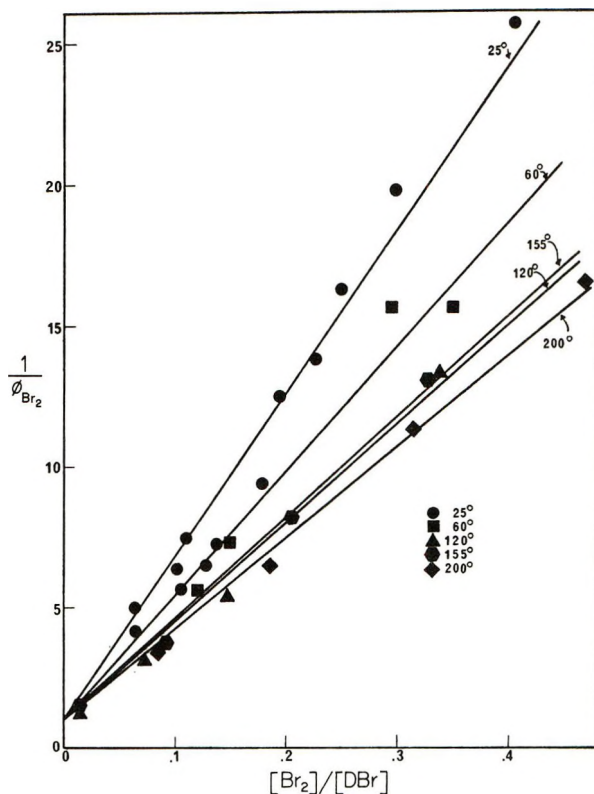


Figure 4. Reciprocal  $\text{Br}_2$  quantum yields vs.  $[\text{Br}_2]/[\text{DBr}]$  for systems moderated with 700 Torr of  $\text{D}_2$  and photolyzed with zinc resonance lamp.

the experiments with 3-eV hydrogen atoms, similar studies were undertaken with 2-eV hydrogen atoms produced from the  $2139\text{-\AA}$  photolysis of HBr. The results are shown in Figure 3. It is clear that in this case also,  $\text{CO}_2$  is less efficient than He, and that a ratio of 40/1 of  $[\text{CO}_2]/[\text{HBr}]$  is insufficient to completely thermalize all of the hot hydrogen atoms. Compared to the earlier data,<sup>15</sup> the moderating efficiencies of both  $\text{CO}_2$  and He seem to have increased slightly, probably due to the lower initial H atom energy in the present work. Complete thermalization would have given a value of  $k_3'/k_2'$  of approximately 25, the value for thermalized H atoms calculated from the Arrhenius equation reported previously.<sup>15</sup> In the present studies on reactions of D atoms with DBr and  $\text{Br}_2$ , a ratio of  $> 70/1$  of  $\text{D}_2$  to DBr was used to thermalize the D atoms. Since  $\text{D}_2$  can remove energy from D atoms by the exchange reaction  $\text{D}^* + \text{D}_2 = \text{D}_2^* + \text{D}$  as well as by elastic collisions, it was assumed that this concentration of  $\text{D}_2$  was sufficient to thermalize all of the 2-eV D atoms.

Data on the quantum yields of  $\text{Br}_2$  formation in thermalized systems photolyzed at five temperatures from 25 to  $200^\circ$  are given in Figure 4 and included in

(25) G. R. Woolley and R. J. Cvetanovic, *J. Chem. Phys.*, **50**, 4697 (1969).

(26) R. D. Penzhorn and B. deB. Darwent, *ibid.*, **55**, 1508 (1971).

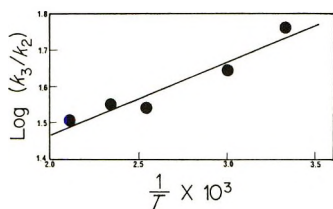


Figure 5. Temperature dependence of  $k_3/k_2$  for DBr-Br<sub>2</sub> system:  $A_3/A_2 = 12 \pm 2.8$  and  $E_2 - E_3 = 0.9 \pm 0.16$  kcal mol<sup>-1</sup>.

Table II. The least-squares slopes of the straight lines (drawn through an intercept of 1.0) are  $k_3'/k_2' = 58 \pm 1.7$ ,  $44 \pm 2.2$ ,  $35 \pm 1.5$ ,  $36 \pm 1.5$ , and  $32 \pm 0.6$  at 25, 60, 120, 155, and 200°, respectively. An Arrhenius plot of these data is shown in Figure 5, and it yields values of  $E_2 - E_3 = 0.9 \pm 0.16$  kcal mol<sup>-1</sup>, and  $A_3/A_2 = 12 \pm 2.8$ .

In order to provide some data on reaction of hot H atoms with HCl and Cl<sub>2</sub> for comparison with data on the other hydrogen halide-halogen systems now available in the literature, several quantum yield measurements were made of Cl<sub>2</sub> formation in unmoderated HCl-Cl<sub>2</sub> systems photolyzed at 1850 Å. The energetics of this system indicate that the initial energy of the hydrogen atom is approximately 2 eV. Because of the extremely long photolysis times required for these measurements it was not practical to obtain a very precise value of  $k_3^*/k_2^*$ . The best estimate, based on four quantum yield measurements, is  $k_3^*/k_2^*$  (for HCl-Cl<sub>2</sub>) =  $8 \pm 4$ .

## Discussion

*Energy Distribution of H Atoms in Unmoderated Systems.* The data presented in this paper, taken together with earlier data on the HBr-Br<sub>2</sub> system, provide strong evidence that thermalization of H\* atoms by HBr, Br<sub>2</sub>, or the walls of the reaction vessel is undetectable relative to reactive collisions of the hot hydrogen atoms with HBr and Br<sub>2</sub>, *i.e.*,  $k_4^{\text{HBr}}/k_2^* \ll 1$  and  $k_4^{\text{Br}_2}/k_2^* \ll k_3^*/k_2^*$ . In summary, the evidence is that (a) plots of  $1/\phi$  vs.  $[\text{Br}_2]/[\text{HBr}]$  are linear and, within experimental error, have intercepts of 1.0; (b) the slopes of these plots were identical, within experimental error, for H atoms produced by HBr photolysis at 1850, 2139, and 2480 Å; and (c) the quantum yields in the unmoderated systems give no detectable temperature dependence. It is clear, then, that all hydrogen atoms react while hot in this system, contrary to the conclusions of Wood and White<sup>17</sup> for the DCl-Cl<sub>2</sub> system. A possible explanation for this discrepancy is that absolute reactive cross sections for H atoms with DCl and Cl<sub>2</sub> are considerably lower than those for H atoms with HBr and Br<sub>2</sub>, a fact which is expected from the higher activation energies of the former compared to the latter. In the DCl-Cl<sub>2</sub> system, therefore, ther-

malization processes compete more favorably for hot H atoms than they do in the HBr-Br<sub>2</sub> system.

The fact that  $k_3^*/k_2^*$  is independent of H atom energy from about 1 to 3 eV suggests that the reaction cross sections for reactions 2 and 3 are relatively constant over this energy range. These studies provide no means of measuring absolute reaction cross sections.

*Effect of Inert Moderator on Br<sub>2</sub> Quantum Yields.* The results shown in Figure 3 indicate clearly that He and H<sub>2</sub> are both much more efficient than CO<sub>2</sub> for moderating hot H atoms with initial energies from 1 to 2 eV. This casts some doubt on the quantitative results obtained for the rate constants of some of the reactions of these thermal hydrogen atoms produced by photochemical means.<sup>14,16,25,26</sup> In agreement with Wood and White for the DCl-Cl<sub>2</sub> system,<sup>17</sup> we find that very small amounts of moderator have a very marked effect on the quantum yields and thus on the relative reaction rates. An apparent "plateau" is soon reached, however, beyond which the approach to complete thermalization is very slow but not insignificant. This apparent plateau is what led several workers to assume that complete thermalization has been achieved. The results of Figure 3, in which the efficiency of moderation by He is seen clearly, suggest that this conclusion is in error.

There is some disagreement in the literature about the mechanism of moderation of hot hydrogen atoms by inert gases. Penzhorn and Darwent<sup>14</sup> concluded that moderation of 2.0- and 0.8-eV hot H atoms by CO<sub>2</sub> proceeded *via* elastic "hard-sphere" collisions. Wood and White<sup>17</sup> disagree, citing their results as evidence for a substantial amount of inelasticity in the collisions of D with CO<sub>2</sub>. They suggest that the relative moderating efficiencies of three moderators, DCl, CO<sub>2</sub>, and Xe, are very sensitive to the number of internal energy levels which are available in the moderator. The moderation data given in Figure 3 are not sufficiently accurate to draw any quantitative conclusions about relative moderating efficiencies, but they do suggest that H<sub>2</sub> and He are much more efficient than CO<sub>2</sub> for moderating hot H atoms. Only elastic collisions are possible with He, and the low mass of this atom would tend to make it relatively efficient as an H atom moderator. CO<sub>2</sub> has many accessible internal energy levels, so it could be an efficient moderator if collisions are inelastic, whereas the high mass of CO<sub>2</sub> compared to H would make CO<sub>2</sub> an inefficient moderator *via* elastic collisions. It is therefore not too surprising that He turns out to be a more efficient moderator than CO<sub>2</sub>. Conclusions regarding the elasticity of collisions are made much more difficult, however, by the fact that even if all moderating collisions were elastic it is known that a hard-sphere potential can be a very poor approximation. For example, Estrup<sup>27</sup> has shown that in reactions of hot recoil tritium atoms with methane in helium-moderated

systems, the tritium-helium potential is considerably "softer" than a hard-sphere potential and considerable errors will be encountered if a more realistic potential is not used. It is clear that more accurate data on the relative moderating efficiencies for H and D atoms in these HX-X<sub>2</sub> and DX-X<sub>2</sub> systems are needed, and such studies are now underway in this laboratory. Without such data it is premature to speculate about the reasons for the behavior of the moderator curves in Figure 3.

*Comparison of D + DBr and Br<sub>2</sub> Data with other Data.* The data of Table III present all of the available information on the relative rate constants for H + HX and H + X<sub>2</sub>, both hot and thermal. Uncertainties have been included in this table only for data from this work and ref 15 because it is difficult to obtain estimates which have the same significance from each of the references used. It should be noted that in many cases differences which appear on Table III may not be significant because of experimental error.

**Table III:** Rate Parameters for Reactions of Hydrogen Atoms

$$\text{H}^a + \text{HX} \xrightarrow{(2)} \text{H}_2 + \text{X}$$

$$\text{H} + \text{X}_2 \xrightarrow{(3)} \text{HX} + \text{X}$$

HX <sup>a</sup>	$E_2 - E_3$ , kcal mol <sup>-1</sup>	$A_3/A_2$	$k_3^*/k_2^*$
DCl	1.9 <sup>c</sup>	12.9 <sup>c</sup>	6.5 <sup>d</sup>
HCl	1.5 <sup>e</sup>	6.9 <sup>e</sup>	8 <sup>f</sup>
DBr	0.9 ± 0.16 <sup>f</sup>	12 ± 2.8 <sup>f</sup>	6.7 ± 0.13 <sup>f</sup>
HBr	0.8 ± 0.3 <sup>g</sup>	6.8 ± 2 <sup>g</sup>	5.6 ± 0.25 <sup>f,g</sup>
HI	0.6 <sup>h</sup>	5.0 <sup>h</sup>	4.2 <sup>h</sup>

<sup>a</sup> The same equations apply to DX-X<sub>2</sub> systems with H replaced by D. <sup>b</sup> This is the ratio of reaction probabilities for hot H or D atoms. See text. <sup>c</sup> A calculated value based on the HCl data in ref 28 (see ref 17). <sup>d</sup> Reference 17. <sup>e</sup> Reference 28. <sup>f</sup> This work. <sup>g</sup> Reference 15. <sup>h</sup> Reference 14.

There are clear trends from X = I to Br to Cl, both for the H atom systems and the D atom systems, and

few of the features are very surprising. It has been suggested<sup>14-16</sup> that there might be a direct correspondence between the ratios of Arrhenius preexponential factors and the ratios of rate constants for corresponding hot reactions. This would be predicted from the very simple collision theory interpretation of the Arrhenius equation which attributes the preexponential factor to a collision frequency and a steric factor. The data of Table III indicate that this correlation is at best only an approximation, and it may, in fact, be that the ratio of preexponential factors is always slightly higher than the ratio of hot reaction probabilities. In the deuterated systems the difference between thermal and hot ratios appear to be beyond the limits of experimental error. The significance of this fact is not yet clear.

It should be noted that this comparison between thermal and hot atom rate constants is based on the assumption that for the thermal studies in HI-I<sub>2</sub>, HBr-Br<sub>2</sub>, and DBr-Br<sub>2</sub> systems the hot atoms have been completely thermalized by the added inert moderator. As discussed above, there is some doubt about this<sup>29</sup> and it is certainly not known to what extent a small deviation of the steady-state hydrogen atom energy distribution from a Boltzmann distribution will affect the relative rate constants. It is conceivable, because of the relatively low thresholds for these reactions, that the effect might be considerable. Since the ratios of preexponential factors appear to be slightly larger than the corresponding ratios of hot reaction probabilities, the former should be considered lower limits to the values for completely thermal atoms. Likewise, the activation energy differences might also be considered lower limits.

(27) P. J. Estrup, *J. Chem. Phys.*, **41**, 164 (1964).

(28) F. S. Klein and M. Wolfsberg, *ibid.*, **34**, 1494 (1961).

(29) One reviewer reports that extensive calculations have shown that the moderator to reactant ratios used here result in energy distributions which are significantly different from the Boltzmann distribution. This is due to the effect of "activating" collisions in which H (or D) atoms gain energy from the thermal moderator molecules.

## Exchange Reaction of Methane- $d_4$ with Hydrogen Chloride<sup>1</sup>

by R. D. Kern\* and G. G. Nika

Department of Chemistry, Louisiana State University in New Orleans, New Orleans, Louisiana 70122  
(Received June 5, 1972)

Publication costs assisted by the National Science Foundation

A shock tube coupled to a time-of-flight mass spectrometer was used to study the exchange reaction,  $CD_4 + HCl \rightleftharpoons CD_3H + DCl$ , over a density range  $1.7\text{--}4.1 \times 10^{-6}$  mol  $cm^{-3}$  in the temperature region 1600–2500°K. In the lower temperature range (1600–1900°K) DCl exhibits a quadratic time-dependent growth rate while at higher temperatures (2200–2500°K) increase of DCl is a linear function of time. The only chlorine-containing product is deuterium chloride. Rate constants extracted from the quadratic and linear regions yielded activation energies of 51 and 30 kcal  $mol^{-1}$ , respectively. An atomic mechanism for the exchange predicts both time dependencies and the transition between them. Pyrolysis of methane occurred along with the exchange but the growth rate of the products ethane, acetylene, and diacetylene was shown not to be catalyzed by the presence of HCl. Acetylene was the major product of the pyrolysis. Exchange was observed in both major and minor products. The ratio  $CH_3:CH_4$  was less than one when pyrolysis products were not detected and greater than one when they were present. This finding suggests the presence of methyl radical in the reaction mixture. The results are discussed in terms of an atomic mechanism.

### Introduction

Exchange reactions of diatomic and simple polyatomic molecules have been studied by two shock tube techniques: one, the single pulse method (SPST) which utilizes static samplings, and the other, a complementary facility composed of two shock tubes equipped to monitor infrared emission and time-of-flight (TOF) mass spectrometry, both tubes employing dynamic sampling of reacting gases. The reactions of  $HCl^{2a}$  and  $HCN^{2b}$  exchanging with  $D_2$  have been studied by the complementary techniques. Reaction of  $H_2 + D_2$  and the self-exchange of HD were followed by TOF<sup>2c,d</sup> and single-pulse<sup>3</sup> techniques and agreement between the two methods has been demonstrated.<sup>2c,d</sup>

These exchange reactions are characterized by low activation energies when comparison is made to molecular or atomic mechanisms, inert gas dependencies, a variety of orders for reactants, and, as revealed by the dynamic sampling experiments, a nonlinear time dependence for product formation.

In exchange reactions involving diatomic molecules, the only species detected are diatomic exchange products. However, the products from  $HCN + D_2$  include  $C_2N_2$  in small amounts.<sup>2b</sup> It has not been established whether the mechanism for production of  $C_2N_2$  involves radicals, but it is known that the formation involves more than a single reaction step.<sup>4</sup> Notwithstanding the presence of cyanogen, the rate of exchange is well described by the quadratic growth of DCN. Whether or not a more complicated system with respect to abundance of pyrolysis products follows a pattern exhibited by simpler exchange systems is the subject of this investigation.

Professor Bauer and his coworkers studied the  $CH_4 + D_2$  reaction in the temperature range 1440–1755°K

(SPST) under conditions of negligible  $O_2$  impurities.<sup>5</sup> Samples extracted from the reflected zone were analyzed with a mass spectrometer for  $CH_4$ ,  $D_2$ ,  $CH_3D$ , and HD. Evidence for methane pyrolysis was not found. The reaction is reported to proceed through a four-center complex in accordance with the vibrational excitation mechanism proposed by Bauer.<sup>3a</sup>

Burcat and Lifshitz (BL)<sup>6</sup> studied the exchange system  $CH_4 + CD_4$  in the temperature region 1340–1745°K (SPST). They report a zero-order dependence with respect to inert gas although Bauer found an order of 0.6 for the inert diluent. BL interpreted their results in terms of a methyl radical chain mechanism resulting from the pyrolytic initiation step  $CH_4 \rightarrow CH_3 + H$ , followed by the exchange reaction  $CH_3 + CD_4 \rightarrow CH_3D + CD_3$ .

Several questions are apparent from a comparison of these two methane exchange reactions. Both studies are in the same temperature range, yet Bauer argues against the importance of pyrolysis in the exchange

(1) (a) Support of this work by the National Science Foundation under Grant No. GP-23137 and also funds for equipment from NSF Departmental Science Development Program GU-2632 are gratefully acknowledged. (b) Paper presented in part at the Southwest Regional Meeting of the American Chemical Society, San Antonio, Tex., Dec 1971.

(2) (a) R. D. Kern and G. G. Nika, *J. Phys. Chem.*, **75**, 171 (1971); (b) J. M. Bruppacher and R. D. Kern, *ibid.*, **76**, 285 (1972); (c) R. D. Kern and G. G. Nika, *ibid.*, **75**, 1615 (1971); (d) R. D. Kern and G. G. Nika, *ibid.*, **75**, 2541 (1971).

(3)  $H_2 + D_2$ : (a) S. H. Bauer and E. Ossa, *J. Chem. Phys.*, **45**, 434 (1966); (b) A. Burcat and A. Lifshitz, *ibid.*, **47**, 3079 (1967); HD + HD: (c) D. Lewis and S. H. Bauer, *J. Amer. Chem. Soc.*, **90**, 5390 (1968).

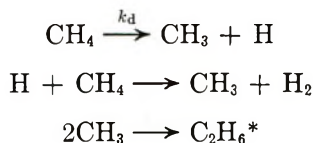
(4) J. M. Bruppacher and R. D. Kern, work in progress.

(5) W. S. Watt, P. Borrell, D. Lewis, and S. H. Bauer, *J. Chem. Phys.*, **45**, 444 (1966).

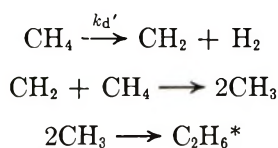
(6) A. Burcat and A. Lifshitz, *ibid.*, **52**, 3613 (1970).

sequence while BL rely entirely on methane decomposition to furnish a supply of methyl radicals in order to explain their results. The neglect of pyrolytic pathways in the Bauer study might be reconciled by the proposal that hydrogen, a major product of the pyrolysis, may have an inhibitory effect on the decomposition. The following two shock tube investigations reported no such effect.

Skinner and Ruehrwein<sup>7</sup> studied the thermal decomposition of methane (SPST). Their data did not support an inhibitory function for H<sub>2</sub> and led to a proposed mechanism



where  $k_d = 10^{14.71}e^{-101,000/RT} \text{ sec}^{-1}$ . A later study (SPST) by Heath and coworkers<sup>8</sup> substantiated a non-inhibition role for H<sub>2</sub>. However, these workers interpreted their data in terms of a pyrolysis sequence that involved methylene radical



where  $k_d' = 10^{14.12}e^{-93,000/RT} \text{ sec}^{-1}$ . According to these investigators, an activation energy of 93 kcal mol<sup>-1</sup> is indicative of decomposition to CH<sub>2</sub> but does not rule out an initiation step yielding CH<sub>3</sub>. An overall reaction rate expression is derived which accounts for homogeneous shock tube results and flow reactor studies where H<sub>2</sub> was observed to inhibit the pyrolysis (see ref 8).

A clear decision as to whether the initiation step yields methyl or methylene radical cannot be found in the literature. A review of shock tube studies<sup>9</sup> and a recent summary of paraffin pyrolysis<sup>10</sup> concluded that the question of initiation remains unanswered. This problem is not limited to thermal decomposition. Ausloos and Lias<sup>11</sup> in their review of methane photochemistry point out the perplexing nature in choosing an initiating step. They also discuss several theoretical studies which have not yielded a definite judgment.

The present investigation has a twofold purpose: (1) to study the time dependence of the exchange products, and (2) to probe the methane pyrolysis with the CD<sub>4</sub> + HCl reaction. The dynamic aspect of a shock tube-TOF mass spectrometer permits testing of the time dependence for product formation. Earlier papers from this laboratory have demonstrated that a nonlinear time-dependent growth for exchange products is a manifestation of a complex mechanism. Growth of DCl as a nonlinear function of time would provide a measure of support to an atomic mechanism

for HCl exchanging with CD<sub>4</sub>. Proposal of an atomic process for the exchange would be strengthened by the observation of mixed acetylene, C<sub>2</sub>HD, along with the pyrolysis products. Furthermore, the TOF-shock tube facility permits almost continuous observation of the cracking ratio of methane, CH<sub>3</sub>:CH<sub>4</sub>. By comparison with static tests and experiments exhibiting negligible pyrolysis, an increase in this ratio during observable decomposition would suggest the presence of methyl radical in the reaction sequence.

### Experimental Section

Three equimolar mixtures of CD<sub>4</sub> and HCl were blended with inert gases. The mole percentages for each reactant gas in the mixtures were 3, 2, and 1.5%, respectively. Similar mixtures of CH<sub>4</sub> with and without an equal amount of HCl were also prepared. CD<sub>4</sub> was obtained from Merck Sharp and Dohme and HCl (99%) and CH<sub>4</sub> (99%) from Matheson. The diluent for all nine mixtures was Ne-1% Ar research grade gases from Matheson. It was used without further purification.

Hydrogen chloride was purified prior to use by two liquid nitrogen bulb-to-bulb distillations. The middle fraction was accepted at each stage. Methane and the fully deuterated compound were purified as follows. A liquid nitrogen trap was filled with Matheson Coleman and Bell activated Linde Type 4A(4-8 mesh) molecular sieve. A thermocouple gauge was used for a 12-hr test to ensure that the baked trap exhibited an immeasurable amount of outgassing at room temperature. After cooling the trap with liquid nitrogen, the hydrocarbon was introduced at an initial room temperature pressure of 100 Torr. With the exception of about 2 Torr, all of the gas was collected on the trap. Removal of the liquid nitrogen for periods of 1-5 min permitted withdrawal of successive fractions for analysis by the TOF analog units. Fractions containing O<sub>2</sub> impurity levels less than 21 ppm were subsequently used for mixture preparation.

Mass spectrometric analysis of each gas indicated an impurity level for oxygen and chlorine (in HCl) indistinguishable from background. Mixtures were allowed to stand at least 24 hr prior to use. A reference mixture of 21 ppm O<sub>2</sub> dilute in Ne-1% Ar was used to establish the impurity levels of the test mixtures. Background levels of O<sub>2</sub> were determined to be 17 ppm. All test mixtures exhibited signals indicating O<sub>2</sub> contents below background. Oxygen was the only detected impurity.

(7) G. B. Skinner and R. A. Ruehrwein, *J. Phys. Chem.*, **63**, 1736 (1959).

(8) V. Kevorkian, C. E. Heath, and M. Boudart, *ibid.*, **64**, 964 (1960).

(9) S. H. Bauer, *Annu. Rev. Phys. Chem.*, **16**, 282 (1965).

(10) D. A. Leathard and J. H. Purnell, *ibid.*, **21**, 221 (1970).

(11) P. J. Ausloos and S. G. Lias, *ibid.*, **22**, 94 (1971).

Most of the experiments were carried out at an initial pressure of 5 Torr, the exception being runs with the 2% mixtures which were also shocked at 10 Torr. The test gas for each run was allowed to reside in the shock tube no longer than 20 sec prior to diaphragm rupture. During this time static analysis of the test gas for  $O_2$  content was performed with the TOF. In all experiments the impurity level was  $\leq 21$  ppm of  $O_2$ . Incident shock wave velocities and physical properties were treated as described previously.<sup>2a</sup> Polaroid Type 410 film was used to record the mass spectra for each run. Four oscilloscopes were used to display the mass spectra generated at 20- $\mu$ sec intervals.

## Results

At the outset of this study, mixtures of  $CH_4 + HCl$  were shocked to establish the contribution of  $^{37}Cl$  to the mass spectral position  $m/e$  37 and to measure the ratio  $m/e$  (15:16). Contribution of  $^{37}Cl$  to the DCl peak height in reacting mixtures was determined in the following manner. Peak heights from the  $H^{37}Cl$  cracking pattern were normalized by the peak height from  $m/e$  40 (1% argon). Thus  $R_{37}$  (= peak height  $m/e$  37 divided by the peak height  $m/e$  40) was calculated at each 20- $\mu$ sec interval. The method of least squares was employed to fit the data to the following equation

$$R_{37} = (R_{37})_0 + mt \quad (1)$$

where  $m$  is the slope and  $t$  the independent variable in  $\mu$ seconds. Experiments on four  $CH_4$ -HCl mixtures covering the temperature range 1600–2500°K disclosed constant values for  $R_{37}$  independent of temperature. This constancy implies the absence of chlorine compounds other than HCl and DCl and also the limited decomposition of these halides in the presence of methane for the experimental conditions reported herein. Table I lists the parameters used in correcting the signal obtained for DCl in reacting mixtures.

Table I: Calibration Data

Mixture (diluent, Ne-1% Ar)	$P_1$ , Torr	$(R_{37})_0$	$m \times 10^6$ , $\mu\text{sec}^{-1}$
3% $CH_4 + 3\%$ HCl	5	0.115	7.22
2% $CH_4 + 2\%$ HCl	5	0.103	-2.56
2% $CH_4 + 2\%$ HCl	10	0.155	6.51
1.5% $CH_4 + 1.5\%$ HCl	5	0.061	5.28

The need for determining the ratio  $m/e$  15:16 stems from the use of neon as diluent. The mass spectral position of  $^{20}Ne$  is superimposed on  $CD_4$ . A decrease in peak height at  $m/e$  20 during reaction of  $CD_4 + HCl$  would not be directly related to the concentration of  $CD_4$ . The ratio  $m/e$  18:20 is important since the species  $CD_3$  originates from the cracking pattern of  $CD_4$  and possibly from a pyrolysis-initiating step.

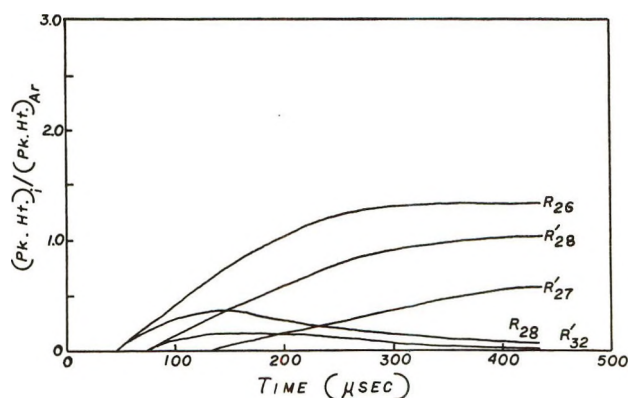


Figure 1. Reaction profiles of  $C_2H_4$  ( $R_{28}$ ) and  $C_2H_2$  ( $R_{26}$ ) from pyrolysis of  $CH_4$  with and without HCl:  $C_2D_4$  ( $R'_{32}$ ),  $C_2D_2$  ( $R'_{28}$ ), and  $C_2HD$  ( $R'_{27}$ ) from  $CD_4 + HCl$ ;  $T_0 = 2200^\circ K$ ;  $P_1 = 5$  Torr; 3% mixtures.

Results of shocking  $CH_4$ -HCl mixtures yielded a ratio of  $m/e$  15:16  $< 1$  under conditions where the pyrolysis of methane is negligible that was in agreement with the ratio obtained in static tests at room temperature. Ratios greater than one occurred when the pyrolysis products, ethane, ethylene, and acetylene, were observed. Similar results were obtained when methane diluted with inert gas was pyrolyzed.

Within the detectability limits of the equipment, these three products occur simultaneously. However, the reaction  $2CH_3 \rightarrow C_2H_6$  is 88 kcal  $\text{mol}^{-1}$  exothermic resulting in rapid dissociation of ethane. As a consequence, peak heights of  $m/e$  30 are too small for collection of meaningful data for ethane production. At temperatures above 2000°K, peak heights of  $m/e$  28 reach a maximum and then decrease while peak heights of  $m/e$  26 continue to grow. Above 2200°K, acetylene peak heights attain a constant level as does  $m/e$  50, diacetylene. This latter species is first observed at temperatures above 2000°K.

After normalizing the various peak heights to argon,  $R_{26}$  and  $R_{28}$  were plotted vs. pyrolysis reaction time to compare growth rates with and without the presence of HCl. Catalytic effects due to hydrogen chloride were not observed as demonstrated in Figure 1. Also shown in this figure are the reaction profiles for the deuterated products from  $CD_4$  pyrolysis. Of particular importance is the presence of the mixed acetylene,  $C_2HD$ . The species  $C_4D_2$  and  $C_4HD$  were also observed during the exchange experiments. Evidence was not found in this study for the sequence  $C_2H_2 \rightarrow C_4H_3 \rightarrow C_4H_2$ . The species  $C_4H_3$  is proposed to be a precursor to  $C_4H_2$  when acetylene is singularly pyrolyzed.<sup>12</sup> The absence of  $C_4H_3$  was reported previously in an investigation of ethylene decomposition.<sup>13</sup> At temperatures

(12) I. D. Gay, G. B. Kistiakowsky, J. V. Michael, and H. Niki, *J. Chem. Phys.*, **43**, 1720 (1965).

(13) I. D. Gay, R. D. Kern, G. B. Kistiakowsky, and H. Niki, *ibid.*, **45**, 2371 (1966).

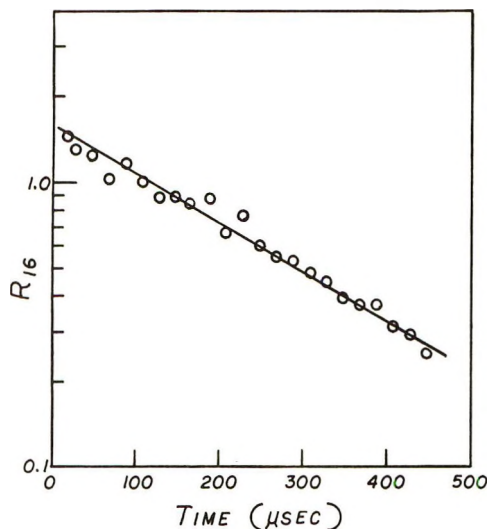


Figure 2. First-order plot of  $\text{CH}_4$  decomposition in an equimolar 3%  $\text{CH}_4 + \text{HCl}$  mixture:  $P_1 = 5$  Torr;  $T_s = 2302^\circ\text{K}$ ;  $k_d = 3.82 \times 10^{-3} \mu\text{sec}^{-1}$ ;  $R_{16} = (\text{peak height})_{16}/(\text{peak height})_{40}$ .

above  $2000^\circ\text{K}$ , the major product  $\text{C}_2\text{H}_2$  in turn formed  $\text{C}_4\text{H}_2$  without the radical  $\text{C}_4\text{H}_3$ . A further observation is that no chlorine containing product other than  $\text{DCl}$  is present in the  $\text{CH}_4\text{-HCl}$  and  $\text{CD}_4\text{-HCl}$  experiments.

First-order plots were constructed using the logarithm of the ratio of  $m/e$  16:40 vs. reaction time for the  $\text{CH}_4 + \text{HCl}$  mixtures. A typical experiment is depicted in Figure 2. The amount of conversion with respect to methane disappearance varied from 35% at  $1886^\circ\text{K}$  to 97% at  $2733^\circ\text{K}$ . Arrhenius plots constructed for each of the three mixtures revealed that the values for  $\log A$  and  $E^*$  agree within one standard deviation. A mixture of 3%  $\text{CH}_4$  and diluent was pyrolyzed over the same temperature range. The individual experiments displayed first-order decay of methane. The Arrhenius parameters agreed within one standard deviation with those obtained from the 3%  $\text{CH}_4\text{-3% HCl}$  mixture. A combined plot of the 3% data is presented in Figure 3. The activation energy is  $41.24 \pm 1.76 \text{ kcal mol}^{-1}$  and the value of  $\log A$  is  $7.56 \pm 0.18$ . The units of  $A$  are  $\text{seconds}^{-1}$ .

A less than ideal situation exists in the  $\text{CD}_4\text{-HCl}$  reaction; specifically, exchange and  $\text{CD}_4$  pyrolysis take place concurrently. The rate of exchange was determined by measuring the  $\text{DCl}$  mass peak height as a function of reaction time. Values of  $R_{37}$  from reacting mixtures are composed of  $\text{DCl}$  and the  $\text{HCl } m/e$  38 cracking pattern. Correction for the latter was accomplished by using the data in Table I and eq 1. The mole fraction of  $\text{DCl}$  ( $f_{37}$ ) was calculated by dividing the corrected value of  $R_{37}$  by the sum of  $R_{36}$  and  $R_{37}$ . At temperatures greater than  $2200^\circ\text{K}$ , reaction profiles of  $f_{37}$  indicate an equilibrium condition. Experimental values of  $(f_{37}/f_{36})_{\text{eq}}$  agreed with those calculated from statistical thermodynamic formulas for the reaction  $\text{CD}_4 + \text{HCl} \rightleftharpoons \text{CD}_3\text{H} + \text{DCl}$ .

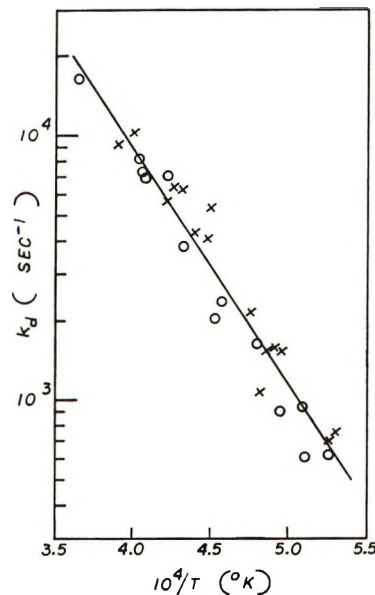


Figure 3. Arrhenius plot of apparent first-order rate constants:  $\times$ , 3%  $\text{CH}_4$ ;  $\circ$ , equimolar 3%  $\text{CH}_4 + \text{HCl}$ .

For equimolar amounts of  $\text{CD}_4$  and  $\text{HCl}$ ,  $f_{37}$  profiles are given by the general expression which includes the back reaction

$$1 - 1.52f_{37} = \exp(-kt^z) \quad (2)$$

where  $z$  is the time dependence parameter and

$$k = k_1(\text{CD}_4)_0^x(\text{HCl})_0^{x'}(M)^\nu$$

Expanding the exponential of eq 2 leads to an expression for growth of  $\text{DCl}$  mole fraction at low conversions

$$f_{37} = \frac{k}{1.52} t^z = k_{\text{obsd}} t^z$$

Mole fraction was then plotted as a function of reaction time raised to various powers. Values of  $z = 1, 3/2,$  and  $2$  were tested, yielding estimates for the observed rate constant,  $k_{\text{obsd}}$ . The initial appraisal of  $k_{\text{obsd}}$  along with its corresponding value of  $z$  was used as input to a computer solution of eq 2. The computer then iterated over a range of rate constants selecting the value which generated a profile possessing a minimum deviation when compared to experimental points.

An assessment of  $z$  was made by constructing  $\log(-\log)$  plots of eq 2. An average value of  $1.5$  was obtained from these plots. In order to represent the overall temperature coefficient of the exchange, the rate constants for all experiments were calculated on a time power basis of  $3/2$ . Figure 4 is a display of  $\log k$  vs.  $1/T(^\circ\text{K})$  for the four reacting mixtures. The four least-squares lines have an average slope of  $54 \text{ kcal mol}^{-1}$  as indicated by the solid line.

Closer inspection of the  $\log(-\log)$  plots in the intermediate temperature range ( $1900\text{-}2200^\circ\text{K}$ ) revealed the possibility of two time dependencies occurring in

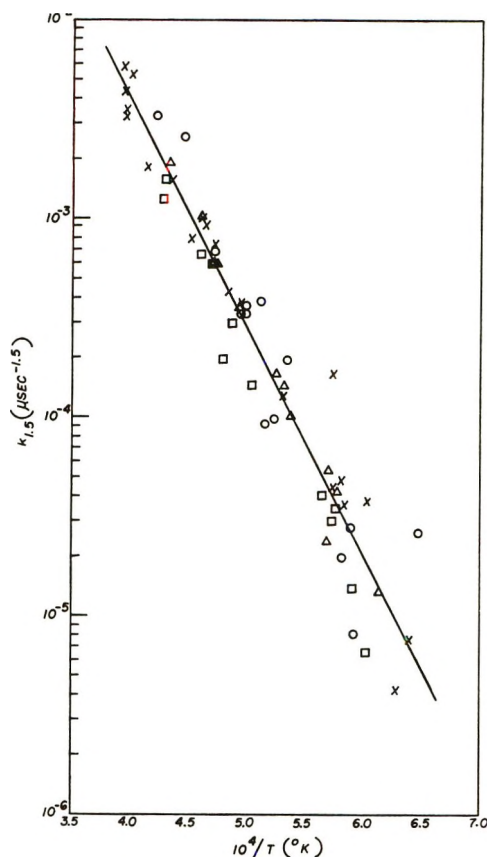


Figure 4. Plot of observed rate constants fitted to a  $3/2$  time dependence: average slope = 54 kcal mol $^{-1}$ . Equimolar mixtures:  $\times$ , 3%,  $P_1 = 5$  Torr;  $\circ$ , 2%,  $P_1 = 5$  Torr;  $\Delta$ , 2%,  $P_1 = 10$  Torr;  $\square$ , 1.5%,  $P_1 = 5$  Torr.

the same experiment. An example is depicted in Figure 5, where at early reaction times a quadratic time dependence is observed. At longer times a linear time dependence best describes the growth of  $f_{37}$ .

All experimental data were therefore fit with the three time dependencies mentioned above. Figure 6 demonstrates profile fits to a low-temperature run in the range 1600–1900°K where an assumed  $t^2$  dependence is the best fit to the data. A linear time-dependent profile adequately describes data from a run in the high-temperature range 2200–2500°K as shown in Figure 7. A profile fit with a 1.5 exponent is depicted in Figure 8.

It is possible to extract from this data quadratic and linear time-dependent rate constants at the temperature extremes of this study. Thus  $k_Q$  (1600–1900°K) and  $k_L$  (2200–2500°K) replace  $k$  in eq 2. Figures 9 and 10 are plots of  $k_Q$  and  $k_L$  vs.  $1/T$ , respectively. The quadratic rate constant data lead to an activation energy of 51 kcal mol $^{-1}$  while the high-temperature linear time-dependent results indicate an activation energy of 30 kcal mol $^{-1}$ .

A possible complication exists in the calculation of  $k_L$  and  $z$  for the higher temperature runs. Extensive pyrolytic conversion of methane to acetylene is an

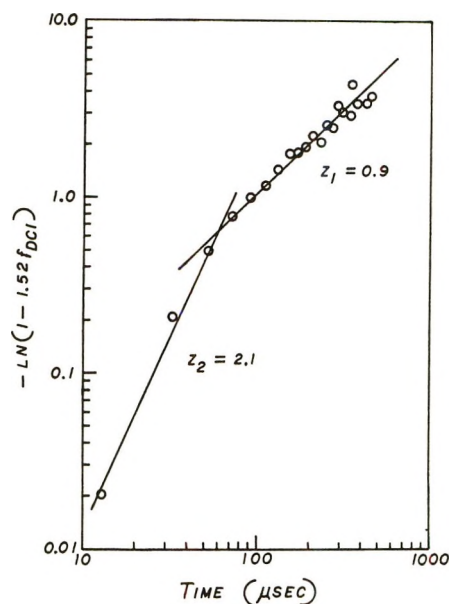


Figure 5. Plot of  $\log(-\ln[1 - 1.52f_{37}])$  vs.  $\log t$  from TOF data for a run at 2100°K. Values of slope are represented by  $z_1, z_2$ .

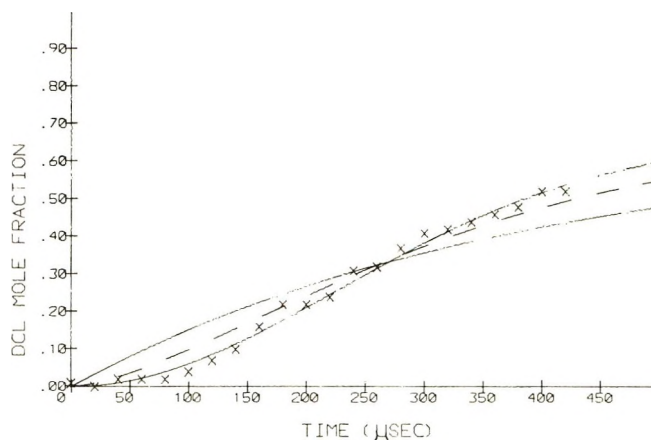


Figure 6. Computer plots of reaction profiles using different time parameters with equimolar 3% CD $_4$  + HCl,  $P_1 = 5$  Torr,  $T_0 = 1745$ °K:  $\times$ , experimental points; — (uppermost),  $t^2$ ; ---,  $t^{1.5}$ ; — (lower),  $t^2$ ; point of reference, 50  $\mu$ sec.

endothermic process which would lower the reflected shock zone temperature and consequently decrease the rate of the reaction. Taking the most extreme endothermic reaction,  $\text{CH}_4 \rightarrow 1/2\text{C}_2\text{H}_2 + 3/2\text{H}_2$ , the temperature decrease would be no more than 45° at one-third methane decomposition. The high-temperature profiles ( $>2000$ °K) were recalculated using those points which were recorded before one-third methane disappearance. It was determined that when methane was one-third decomposed, the exchange was 75% complete with respect to the mole fraction of DCl at equilibrium. Analyzing 75% of the profile yielded the result that the values for  $k_L$  and  $z$  were practically unchanged. The quadratic region ( $<1900$ °K) was unaffected.

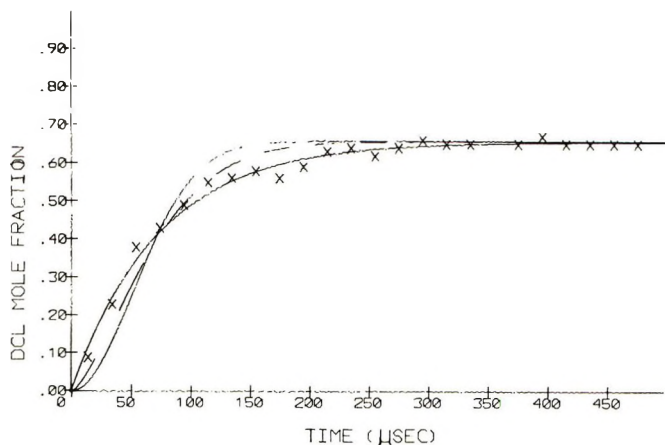


Figure 7. Mixture, initial conditions, and symbols same as Figure 6,  $T_3 = 2297^\circ\text{K}$ .

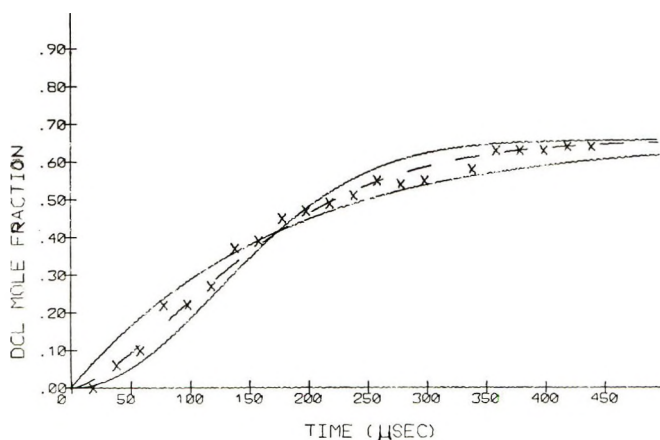


Figure 8. Mixture, initial conditions, and symbols same as Figure 6,  $T_3 = 2068^\circ\text{K}$ .

Plots of the ratio of  $m/e$  19:40 vs. reaction time were complicated by the disappearance of  $\text{CD}_3\text{H}$  due to further exchange to  $\text{CD}_2\text{H}_2$  and pyrolysis. In the early parts of the  $\text{CD}_3\text{H}$  profile when these effects were not as pronounced, the shape of the profile was similar to the DCl profile at comparable temperatures.

### Discussion

Three significant points may be summarized from the results: (1) deuterium chloride, the only chlorine containing product, is formed with a varying time dependence from quadratic at the lower temperatures to linear at the higher temperatures; (2) the presence of HCl does not appreciably affect the decomposition of methane; and (3) atomic exchange was observed in both major and minor products. These results are most readily accounted for by an atomic mechanism.

The basic premise is that DCl is produced by reactions of radicals and atoms with the major components of the mixture. While it is not the intention here to offer a mechanistic scheme for methane pyrolysis, sev-

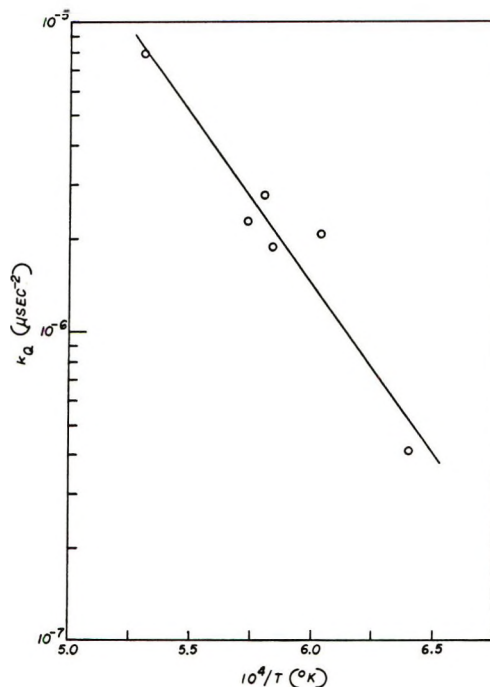
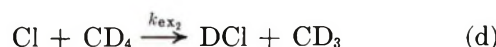
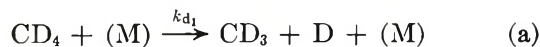


Figure 9. Arrhenius plot of observed rate constants from an equimolar 3% mixture exhibiting quadratic time dependence:  $E_Q^* = 51.00 \pm 7.37 \text{ kcal mol}^{-1}$ .

eral of the more probable steps will be discussed. The rate constants are listed in Table II.<sup>14-19</sup>



Deuterium atoms are not likely to play an important role in the exchange sequence. Reaction b competes for deuterium atoms quite favorably with the following reactions.



(14) (a) R. Hartig, J. Troe, and H. G. Wagner, *Symp. Combust.*, 13th, 1970, 147 (1971); (b) A. M. Dean and G. B. Kistiakowsky, *J. Chem. Phys.*, 54, 1718 (1971).

(15) R. R. Baldwin, D. E. Hopkins, A. C. Norris, and R. W. Walker, *Combust. Flame*, 15, 33 (1970).

(16) H. O. Prichard, J. B. Pyke, and A. F. Trotman-Dickenson, *J. Amer. Chem. Soc.*, 77, 2629 (1955).

(17) G. Chiltz, R. Eckling, P. Goldfinger, G. Huybrechts, H. S. Johnston, L. Meyers, and G. Verbeke, *J. Chem. Phys.*, 38, 1053 (1963).

(18) Rate constant expression based on  $\text{D} + \text{HCl} \rightarrow \text{HD} + \text{Cl}$ , (a) H. Steiner and E. K. Rideal, *Proc. Roy. Soc., Ser. A*, 173, 503 (1939); relative rates of abstraction/exchange, (b) G. O. Wood, *J. Chem. Phys.*, 56, 1723 (1972); and corrections in preexponential and activation energy terms due to isotopic effects, (c) A. A. Westenberg and N. deHaas, *ibid.*, 47, 1393 (1967).

(19) M. C. Lin and M. H. Back, *Can. J. Chem.*, 44, 2357 (1966).

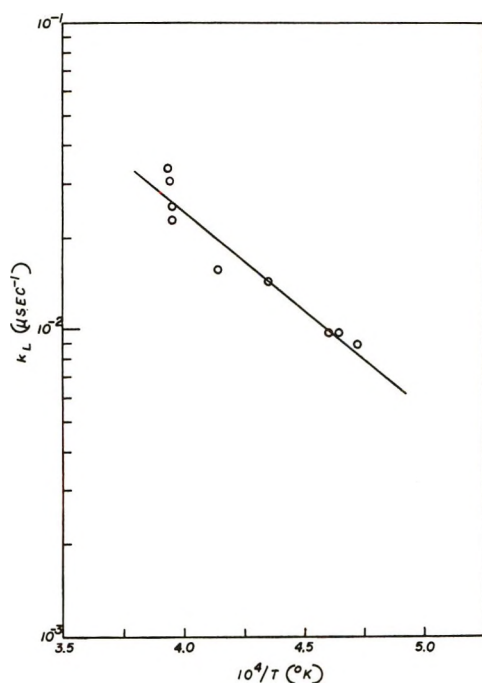


Figure 10. Arrhenius plot of observed rate constants from an equimolar 3% mixture exhibiting linear time dependence:  $E_L^* = 29.85 \pm 2.08$  kcal mol $^{-1}$ .

Table II: Rate Constants for Reactions a-g

Reaction	Rate constant <sup>a</sup>	Ref
a	$10^{14.7} \exp(-101,000/RT)$	7
	$10^{17.6} \exp(-88,000/RT)$	14a
	$10^{18.2} \exp(-103,000/RT)$	14b
b	$10^{14.1} \exp(-11,900/RT)$	15
c	$10^{12.1} \exp(-4,510/RT)$	16
d	$10^{13.7} \exp(-5,760/RT)$	17
e	$10^{13.0} \exp(-2,350/RT)$	18
f	$10^{10.1} \exp(-130/RT)$	18
g	$10^{13.1} \exp(-400/RT)$	19

<sup>a</sup> Units are cc mol $^{-1}$  sec $^{-1}$  except for ref 7 which is sec $^{-1}$ .

Reaction e has recently been shown to be faster than f although this finding<sup>18b</sup> differs with previous work.<sup>20</sup> The decomposition of methane exceeds that of hydrogen chloride as demonstrated by the results of pyrolyzing the CH $_4$ -HCl mixture. The disappearance of methane and the subsequent formation of the pyrolysis products produces additional radicals and atoms which may enter into the reaction mechanism.

It is instructive to analyze the time dependence of DCl formation using reaction d as a possible pathway. The rate of DCl growth at early times is given by the expression

$$d(\text{DCl})/dt = k_{\text{ex}_2}(\text{Cl})(\text{CD}_4) \quad (3)$$

Assuming that the production of chlorine atoms is mainly from reaction c rather than the dissociation of hydrogen chloride, it follows that the rate of c will de-

pend upon the concentration of methyl radicals which are generated *via* reactions a and b. If it is further assumed that under the reaction conditions of this investigation the growth of methyl radical is linear with respect to reaction time, there arise two conditions that lead to different time dependencies for DCl formation. It will be helpful to refer to Figure 10 of ref 2b which will be called the *profile* in the discussion that follows.

If the time required to produce a steady-state concentration is long compared to the observation time for the exchange, the formation of methyl radical will correspond to position a in the *profile*. It follows that if chlorine atoms are generated mostly from reaction c, the concentration of Cl will be at position a on the chlorine atom reaction *profile*, a non-steady-state condition. Therefore, the concentration of chlorine atoms will be given by the expression

$$(\text{Cl}) = k_d(\text{N})^z t \quad (4)$$

where  $k_d$  is a collection of rate constants that describe the overall decomposition of methane which is the rate-determining process for the formation of chlorine atoms. The order dependence for the formation is represented by  $(\text{N})^z$ . Substitution of (4) into (3) and integrating yields eq 5.

$$(\text{DCl}) = 1/2 k_d k_{\text{ex}_2} (\text{CD}_4) (\text{N})^z t^2 \quad (5)$$

The predicted activation energy  $E_Q^*$  is composed of the overall dissociation of methane and subsequent exchange of Cl with CD $_4$ . Thus,  $E_Q^*$  can be related to the observed rate constants which have a temperature coefficient of about 51 kcal mol $^{-1}$ .

$$E_Q^* = E_d^* + E_{\text{ex}_2}^* = 51 \text{ kcal mol}^{-1} \quad (6)$$

However, if production of Cl atoms is rapid compared to observed times for exchange, position b of the *profile*, then the formation of DCl is linear. The steady-state expression for chlorine atoms using reactions c and d is given by eq 7.

$$\begin{aligned} d(\text{Cl})/dt &= k_{\text{ex}_1}(\text{CD}_3)(\text{HCl}) - k_{\text{ex}_2}(\text{Cl})(\text{CD}_4) \\ (\text{Cl})_{\text{ss}} &= \frac{k_{\text{ex}_1}(\text{CD}_3)(\text{HCl})}{k_{\text{ex}_2}(\text{CD}_4)} \end{aligned} \quad (7)$$

Assuming that methyl radicals disappear *via* reaction g, the steady-state expression using reactions a, b,



and g is given by eq 8. The steady-state concentration of D atoms is taken to be  $k_{d1}/k_1$  from reactions a and b.

$$\begin{aligned} d(\text{CD}_3)/dt &= k_{d1}(\text{CD}_4) + \\ & k_1(\text{D})(\text{CD}_4) - 2k_3(\text{CD}_3)^2 = 0 \end{aligned}$$

(20) A. E. deVries and F. S. Klein, *J. Chem. Phys.*, **41**, 3428 (1964).

$$(\text{CD}_3)_{ss} = \left(\frac{k_{d1}}{k_3}\right)^{1/2} (\text{CD}_4)^{1/2} \quad (8)$$

Substituting (8) into (7) and setting  $(\text{CD}_4) \simeq (\text{HCl})$  under the condition of low conversions yields eq 9.

$$(\text{Cl})_{ss} = \left(\frac{k_{ex1}}{k_{ex2}}\right) \left(\frac{k_d}{k_3}\right)^{1/2} (\text{CD}_4)^{1/2} \quad (9)$$

Integrating eq (3) with the substitution for chlorine atoms results in a linear formation of the product DCl.

$$(\text{DCl}) = k_{ex1} \left(\frac{k_d}{k_3}\right)^{1/2} (\text{CD}_4)^{1/2} t \quad (10)$$

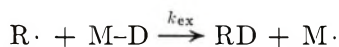
The activation energy expected for eq 10 can be related to the observed linear rate constants.

$$E_L^* = E_{ex1}^* + 1/2(E_d^* - E_3^*) = 30 \text{ kcal mol}^{-1} \quad (11)$$

Taking the activation energy for reaction g to be zero and  $E_{ex1}^* \simeq E_{ex2}^*$ , simultaneous solution of eq 6 and 11 gives  $E_d^* = 42 \text{ kcal mol}^{-1}$  and  $E_{ex}^* = 9 \text{ kcal mol}^{-1}$ .

The intermediate region of the profile corresponds to the 1900–2200°K range where the growth of DCl depends in a more complicated fashion upon the concentration of chlorine atoms.

Knowledge of the reaction profile for an exchange product can lead to conclusions about the radical or atom that attacks a reactant molecule even though the identity of the radical or atom may be unknown. Reactions c and d may be generalized by the following equation



where  $\text{R}\cdot$  is the radical or atom attacking the reactant molecule  $\text{M-D}$  which contains a hydrogen or deuterium atom,  $\text{RD}$  is the exchange product, and  $\text{M}\cdot$  is a radical. The rate of formation of the product  $\text{RD}$  is given by

$$d(\text{RD})/dt = k_{ex}(\text{R}\cdot)(\text{M-D})$$

If the reaction profile for  $\text{RD}$  resembles Figure 7, a linear production, then the concentration of  $\text{R}\cdot$  is that of a steady-state condition. If the profile is more like Figures 6 or 8, the attacking species  $\text{R}\cdot$  has not attained a steady-state concentration. Although the variance of the time power constant  $z$  from quadratic to linear is not by itself an absolute diagnostic of a radical mechanism, it is highly suggestive. In the work presented here, a specific identification of the attacking radicals or atoms can not be made, but statements concerning the steady-state levels of the species responsible for the formation of the exchange products can be offered.

The evidence for the existence of radicals in this system is indirect. It is improbable to imagine the production of ethane from methane occurring without radical intermediates. The increased ratio of  $\text{CH}_3:\text{CH}_4$  observed during appreciable decomposition indi-

cates the presence of methyl radicals but does not rule out the existence and importance of  $\text{CH}_2$  in the reaction scheme. The extensive scrambling of the pyrolytic products also supports the proposal of radicals and atoms playing an active role.

Assuming that the results presented here are free of impurity effects, an explanation would appear to be in order for the experimental activation energy of 42 kcal mol<sup>-1</sup> determined for the decomposition of methane. There are reports in the literature of apparent rate constants for hydrocarbon pyrolysis that yield "low" values for the activation energy. Two recent shock tube studies dealing with pyrolysis of higher hydrocarbons relate to this point. Bradley and Frend reported that the pyrolysis of ethane occurs with a complex temperature dependence in agreement with previous work.<sup>21</sup> The activation energy decreased from a value of 87 kcal mol<sup>-1</sup> at 1250°K to almost zero around 1600°K. In an azomethane pyrolysis paper, one of the products, *n*-butane, is reported to exhibit a varying activation energy for decomposition.<sup>22</sup> An abnormally low value for  $E^*$  was determined at the upper end of the temperature range 1160–1550°K. Although a satisfactory explanation has not been offered for this unexpected behavior as yet, low activation energies for decomposition are a well-established fact in shock tube work.<sup>23</sup>

Most of the studies of methane pyrolysis were accomplished at low conversions in order to arrive at a value for the rate constant of reaction a,  $k_{d1}$ . The experiments pertaining to decomposition presented herein involve a substantial conversion to products within the 500 μsec of observation time. A larger variety and concentration of radicals are present under such conditions and thereby provide several alternate routes by which methane may disappear. It is not certain whether methane is in the fall-off region given the temperature and pressure regime of this study. For this reason, the quantity  $M$  is written in parentheses in reaction a (and also in reaction g) and may be used in the derivation of the steady-state expressions. However, BL reported an absence of total density order dependence in their rate expression which implies that methane is decomposing in the first-order region.<sup>6</sup> Other workers working in approximately the same region as BL have considered the decomposition to be second order.<sup>14b, 24</sup>

At 2100°K, the value of  $k_{d1}$ , using the equation contained in ref 7, is  $1.6 \times 10^4 \text{ sec}^{-1}$  compared to a value of

(21) J. N. Bradley and M. A. Frend, *J. Phys. Chem.*, **75**, 1492 (1971).

(22) T. P. J. Izod, G. B. Kistiakowsky, and S. Matsuda, *J. Chem. Phys.*, **56**, 1337 (1972).

(23) R. L. Belford and R. A. Strehlow, *Annu. Rev. Phys. Chem.*, **20**, 260 (1967).

(24) G. B. Skinner, A. Lifshitz, K. Scheller, and A. Burcat, *J. Chem. Phys.*, **56**, 3853 (1972).

$1.6 \times 10^3 \text{ sec}^{-1}$  calculated from the apparent rate constant for the overall decomposition of methane reported herein.

The relationships between the two polyatomic-diatomic exchange systems,  $\text{CH}_4 + \text{D}_2$  and  $\text{CD}_4 + \text{HCl}$ , and the polyatomic-polyatomic exchange system  $\text{CD}_4 + \text{CH}_4$  are worth noting. The reported activation energies for exchange covering the 1600–1750°K range are 52( $\text{CH}_4 + \text{D}_2$ ), 51( $\text{CD}_4 + \text{HCl}$ ), and 70( $\text{CD}_4 + \text{CH}_4$ ) kcal mol<sup>-1</sup>. Although the mixed methane exchange has a somewhat higher activation energy, all temperature coefficients are much lower than the almost equal bond dissociation energies of reactants; namely, 104( $\text{CH}_3\text{-H}$ ), 102( $\text{H-Cl}$ ), and 104( $\text{D-D}$ ) kcal mol<sup>-1</sup>. These similarities and the postulation of atomic mechanisms for two of these exchange studies indicate that the molecular complexity of the exchanging partners is not the determining factor with respect to the mechanistic pathway in contrast to the earlier suggestion of BL.<sup>6</sup> An investigation of the

$\text{CD}_4 + \text{CH}_4$  and  $\text{CH}_4 + \text{D}_2$  exchange systems is currently underway in this laboratory with particular attention focussed on purification procedures, impurity levels, and determination of product time dependence.

In summary it can be stated that there are other diagnostic features that are more definite than an interpretation of the activation energy. In the  $\text{CD}_4\text{-HCl}$  system, the changing time dependence from quadratic to linear for product formation, the changing  $\text{CH}_3:\text{CH}_4$  ratio during extensive decomposition, and the presence of pyrolytic products whose formation most certainly involves radicals are facts which support an atomic mechanism for the exchange.

*Acknowledgments.* The authors gratefully recognize the assistance of Mr. D. Olivier and Mr. T. Dupuy in the collection of data. Mr. Dupuy and Mrs. M. E. Bopp are thanked for their role in the tedious task of data reduction. The authors also thank the referees for several helpful suggestions.

## Gas-Phase Thermolysis Kinetics of Small Ring Nitriles

by Stanley F. Sarnier, David M. Gale,\* Henry K. Hall, Jr., and Adah B. Richmond

Central Research Department, Experimental Station, E. I. du Pont de Nemours and Company, Wilmington, Delaware 19898 (Received April 13, 1972)

Publication costs assisted by E. I. du Pont de Nemours and Company

Gas-phase thermolysis kinetic data have been obtained for five cyano-substituted, four-membered ring compounds. The products formed were entirely analogous to those found in reactions with unsubstituted substrates. It is proposed that the decomposition reactions of cyclobutanecarbonitrile ( $k = 10^{15.5}e^{-56,700/RT} \text{ sec}^{-1}$ ), *trans*-1,2-cyclobutanedicarbonitrile ( $k = 10^{12.4}e^{-41,200/RT} \text{ sec}^{-1}$ ), and 3-methylenecyclobutanecarbonitrile ( $k = 10^{12.7}e^{-49,100/RT} \text{ sec}^{-1}$ ) occur *via* a two-step mechanism with a biradical intermediate, while the rearrangement reactions of bicyclobutanecarbonitrile ( $k = 10^{13.9}e^{-40,100/RT} \text{ sec}^{-1}$ ) and 1-cyclobutenecarbonitrile ( $k = 10^{13.4}e^{-33,600/RT} \text{ sec}^{-1}$ ) proceed through a concerted transition complex. It has been shown that the presence of the cyano group reduces the activation energy of the decomposition reactions (by stabilization of the biradical by about 6–10 kcal/group), but has no effect on the rearrangement reactions.

### Introduction

The mechanisms involved in the pyrolysis of four-membered ring compounds have been the subject of much discussion.<sup>1,2</sup> In this work, we have studied the kinetics of thermal decomposition or rearrangement of several four-membered ring compounds containing the cyano group. The effect of the presence of this group on the kinetic parameters gives strong indications as to the mechanisms involved in the thermal reactions of these substrates, by comparison with previously obtained data for similar substrates which do not contain the cyano group.

### Results

Equipment and techniques similar to those used to obtain the kinetic data in this study have been described previously.<sup>3</sup> The degradation of cyclobutanecarbonitrile to acrylonitrile and ethylene was measured over

(1) (a) H. M. Frey, "Gas-Phase Pyrolysis of Some Small Ring Hydrocarbons," *Advan. Phys. Org. Chem.*, **4**, 147 (1966); (b) S. W. Benson, "Thermochemical Kinetics," Wiley, New York, N. Y., 1968.

(2) R. B. Woodward and R. Hoffmann, "The Conservation of Orbital Symmetry," Academic Press, New York, N. Y., 1970.

(3) H. Kwart, S. F. Sarnier, and J. H. Olson, *J. Phys. Chem.*, **73**, 4056 (1969).

the range 460–510° in one series of tests, and over the range 453–519° in another series. The activation energies obtained were identical, but the two sets of data were barely within experimental error in the value of the preexponential term and in the absolute values of the reaction rates. A third set of measurements was also made, but using approximation methods. These results gave values intermediate between the above sets of data, thus confirming the values obtained, although there were indications that the activation energy may be lower than obtained above. An average value for the rate equation (see Tables I and II)<sup>4</sup> was

$$k = 2.03 \times 10^{15} e^{-56,700/RT} \text{ sec}^{-1}$$

Both *cis*- and *trans*-cyclobutane-1,2-dicarbonitrile were found to decompose to give acrylonitrile as the only product. The *trans* isomer was studied over the range 320–410° using two different reactor coils, with no *cis* isomer forming in the products. The resulting rate equation (Table III)<sup>4</sup> was

$$k = 2.51 \times 10^{12} e^{-41,200/RT} \text{ sec}^{-1}$$

The formation of the *trans* isomer complicates the reaction of *cis*-cyclobutanedicarbonitrile. Precise data were therefore not attainable, but approximation methods gave the indication that the same rate equation governing the decomposition of the *trans* isomer also fits the data for *cis*-cyclobutanedicarbonitrile.

The decomposition of 3-methylene-1-cyclobutanedicarbonitrile proceeds to give acrylonitrile and allene as products. In the temperature range 450–500° (Table IV)<sup>4</sup> the rate equation obtained was

$$k = 5.27 \times 10^{12} e^{-49,100/RT} \text{ sec}^{-1}$$

The thermal rearrangement of bicyclobutanedicarbonitrile to 2-cyanobutadiene was studied over the temperature range 270–320°. The rate equation obtained (Table V)<sup>4</sup> was

$$k = 8.43 \times 10^{13} e^{-40,100/RT} \text{ sec}^{-1}$$

The thermal rearrangement of cyclobutenedicarbonitrile to 2-methylene-3-butenitrile was studied over the range 190–225°, with the resulting rate equation (Table VI)<sup>4</sup>

$$k = 2.39 \times 10^{13} e^{-33,600/RT} \text{ sec}^{-1}$$

### Discussion of Kinetic Results

The pyrolysis of cyclobutane appears to proceed through the biradical mechanism. This has been previously concluded by Frey<sup>1a</sup> who noted that the observed entropy could be calculated using a model based on this mechanism, and by Benson<sup>1b,5</sup> who noted that the observed isotope effect could be explained on this basis. The high observed values of the preexponential term ( $10^{15}$ ), the activation energy (*ca.* 60 kcal/mol), and the activation entropy (+9 eu) tend to corroborate this conclusion. In addition, the isomerization of *cis*-

and *trans*-1,2-dimethylcyclobutane is considerably slower than their decomposition reactions, indicating that the actual mechanism is most likely a two-step process in which the biradical is an intermediate, and in which the energy for isomerization from the biradical is higher than that for decomposition.<sup>1a</sup> In the measurements in this work of the kinetics of the *cis*-cyclobutanedicarbonitrile reaction, it was noted that isomerization took place more readily than decomposition, indicating that the relative sizes of these energy barriers need not be uniform.

The decomposition of cyclobutanedicarbonitrile is faster than that of cyclobutane with the difference in rate due entirely to a difference in activation energies. This difference can be explained in terms of the stabilization effect of the cyano group on the biradical. In the decomposition of *trans*-cyclobutanedicarbonitrile, the biradical is doubly stabilized since conjugation with both cyano groups is feasible at the point of ring opening, resulting in appreciable lowering of the activation energy. The situation is similar to that occurring

(4) Table I–VI listing data will appear following these pages in the microfilm edition of this volume of the journal. Single copies may be obtained from the Business Operations Office, Books and Journals Division, American Chemical Society, 1155 Sixteenth St., N.W., Washington, D. C. 20036, by referring to code number JPC-72-2817. Remit check or money order for \$3.00 for photocopy or \$2.00 for microfiche.

- (5) S. W. Benson and P. S. Nangia, *J. Chem. Phys.*, **38**, 18 (1963).
- (6) (a) G. S. Hammond and C. D. DeBoer, *J. Amer. Chem. Soc.*, **86**, 899 (1964); (b) R. J. Ellis and H. M. Frey, *Trans. Faraday Soc.*, **59**, 2076 (1963).
- (7) R. W. Carr, Jr., and W. D. Walters, *J. Phys. Chem.*, **67**, 1370 (1963).
- (8) F. Kern and W. D. Walters, *Proc. Nat. Acad. Sci. U. S.*, **39**, 937 (1952).
- (9) F. Kern and W. D. Walters, *J. Amer. Chem. Soc.*, **75**, 6196 (1953).
- (10) G. T. Geneaux and W. D. Walters, *ibid.*, **73**, 4497 (1951).
- (11) M. N. Das and W. D. Walters, *Z. Phys. Chem. (Frankfurt am Main)*, **15**, 22 (1958).
- (12) R. E. Wellman and W. D. Walters, *J. Amer. Chem. Soc.*, **79**, 1542 (1957).
- (13) S. M. E. Kellner and W. D. Walters, *J. Phys. Chem.*, **65**, 466 (1961).
- (14) M. Zupan and W. D. Walters, *ibid.*, **67**, 1845 (1963).
- (15) H. R. Gerberich and W. D. Walters, *J. Amer. Chem. Soc.*, **83**, 3935 (1961).
- (16) H. R. Gerberich and W. D. Walters, *ibid.*, **83**, 4884 (1961).
- (17) D. J. Trecker and J. P. Henry, *ibid.*, **86**, 902 (1964).
- (18) J. P. Chesick, *J. Phys. Chem.*, **65**, 2170 (1961).
- (19) R. L. Brandauer, B. Short, and S. M. E. Kellner, *ibid.*, **65**, 2269 (1961).
- (20) R. Srinivasan, A. A. Levi, and I. Haller, *ibid.*, **69**, 1775 (1965).
- (21) H. M. Frey and I. D. R. Stevens, *Trans. Faraday Soc.*, **61**, 90 (1965).
- (22) J. P. Chesick, *J. Phys. Chem.*, **68**, 2033 (1964).
- (23) W. Cooper and W. D. Walters, *J. Amer. Chem. Soc.*, **80**, 4220 (1958).
- (24) W. P. Hauser and W. D. Walters, *J. Phys. Chem.*, **67**, 1328 (1963).
- (25) H. M. Frey, *Trans. Faraday Soc.*, **58**, 957 (1962).
- (26) H. M. Frey, *ibid.*, **60**, 83 (1964).
- (27) H. M. Frey and R. F. Skinner, *ibid.*, **61**, 1918 (1965).
- (28) H. M. Frey, *ibid.*, **59**, 1619 (1963).

in *trans*-1,2-divinylcyclobutane, where the biradical is stabilized to the extent of the allylic resonance energy of 13 kcal.<sup>6</sup> The stabilization energy provided by the cyano group can be deduced to about 6–10 kcal. A single cyano group evidences only 6-kcal stabilization in cyclobutanecarbonitrile decomposition. Two cyano groups acting in concert resulted in a lowering of the activation energy for thermal decomposition of 10–11 kcal/cyano group in the *trans*-1,2-cyclobutanedicarbonitrile reaction, and a cyano group possibly aided by the external methylene group resulted in a stabilization energy of 13–14 kcal.

The evidence obtained in this work indicates that the rearrangements of the unsaturated four-membered rings (cyclobutenes and bicyclobutanes) occur *via* a concerted mechanism.<sup>2</sup> In contrast to the situation in the mechanism involving a biradical intermediate, a cyano group should offer no additional stabilization energy in the concerted reaction path. The activation parameters obtained for the rearrangements of cyclobutenecarbonitrile and bicyclobutanecarbonitrile in this work are virtually identical with those obtained for the respective noncyano compounds in previously reported experiments.<sup>6–28</sup>

## A Study of Ionization Processes by the Angular Distribution Technique.

### The AgCl System<sup>1</sup>

by L. C. Wagner and R. T. Grimley\*

Department of Chemistry, Purdue University, Lafayette, Indiana 47907 (Received June 16, 1972)

Publication costs assisted by the U. S. Atomic Energy Commission

The angular distributions of species effusing through an orifice have been used to investigate the fragmentation processes which occur in the ion source of a mass spectrometer. The silver chloride vapor system has been studied in the temperature range 933–973°K. The monomer, dimer, trimer, tetramer, and pentamer have been observed, and the fragmentation processes associated with the electron bombardment of each of these species have been identified by use of this newly developed method in combination with standard methods. A metastable ion corresponding to the reaction  $\text{Ag}_3\text{Cl}_3^+ \rightarrow \text{Ag}_3\text{Cl}_2^+ + \text{Cl}$  was found in addition to 13 other ions. A seeming discrepancy in the heat of vaporization data for  $\text{Ag}_3\text{Cl}_3$  has been attributed to temperature-dependent fragmentation reactions.

### Introduction

One of the major problems encountered in the application of mass spectrometry to the study of high-temperature inorganic vapor systems is the identification of the various neutral species. The stoichiometry of the solid or liquid phase often provides little or no insight into the nature of the inorganic vapor species. The mass spectrum itself is frequently of little value since ionization of molecules often results not only in the formation of "parent" ions of the same mass but also in a group of ionized fragments of differing masses. Over the past decade a variety of techniques have been devised by high-temperature mass spectroscopists which aid in the identification of the neutral species. The techniques and information commonly used include (1) appearance potentials, (2) ionization efficiency curves, and (3) thermodynamic properties. It is most often the case that no one technique is suitable for use

in assigning each ion of a mass spectrum to the molecule or molecules from which the ion is formed. In addition, combinations of existing techniques are frequently inadequate. In this paper a new mass spectrometric technique which utilizes the angular distribution properties of the effusing vapor species is applied in conjunction with existing techniques to a study of the complex silver chloride vapor system.

The earliest measurements of the vapor pressure of silver chloride were reported by von Wartenberg and Bosse<sup>2</sup> and by Maier,<sup>3</sup> both of whom used static techniques. More recently a mass spectrometric study of the vaporization of silver chloride from a platinum foil

(1) This work was supported by the U. S. Atomic Energy Commission.

(2) H. von Wartenberg and D. Bosse, *Z. Elektrochem.*, **28**, 384 (1922).

(3) C. G. Maier, *U. S. Bur. Mines, Tech. Papers*, **360** (1925).

was reported by Rosenstock, Walton, and Brice<sup>4</sup> who obtained the mass spectrum and determined the heat of trimerization. The mass spectrum of silver chloride was also reported by Gusarov and Gorokhov.<sup>5</sup> A more detailed mass spectrometric investigation was recently published by Visnapuu and Jensen<sup>6</sup> who obtained second-law heat of vaporization data for the monomer and trimer. These authors also claimed to show the existence of the  $\text{Ag}_3\text{Cl}_2$  molecule in the vapor phase.

### Experimental Section

Details of the mass-spectrometric technique as applied to high-temperature vaporization phenomena have previously been discussed.<sup>7</sup> The data were obtained with a 60° single-focusing, 30.5-cm radius-of-curvature mass spectrometer. The mass spectrometer was unaltered from previous studies except for the following minor changes. Intensity data were collected using a 640 Keithley vibrating capacitor electrometer in series with a 399 Keithley isolating amplifier. The output from the amplifier was simultaneously fed to a strip chart recorder and a Hewlett-Packard Model 2212A voltage to frequency converter whose output was measured with a Hewlett-Packard 5202L scaler-timer. The V-to-F converter and scaler-timer functioned as an integrator with a variable time base. Integration times ranged from 10 sec for intense, low-noise peaks to 60 sec for low intensity, high-noise peaks.

Two molecular beam sources were used: (1) a standard static Knudsen cell system, and (2) a rotary Knudsen cell system. Each unit used a multiturn, bifilarly wound, platinum-10% rhodium resistance furnace. The temperature measurements of the Knudsen cells were made by means of chromel-alumel thermocouples which were peened into the bottom of the cells. All thermocouples used had previously been calibrated against a Pt/Pt-10% Rh secondary reference thermocouple which had in turn been calibrated against a National Bureau of Standards calibrated thermocouple (test No. G36304). While the static unit allows flux measurements only at the normal to the orifice exit, the rotary Knudsen cell assembly permits sampling of the molecular flux not only at the orifice normal but at various off-axis angles up to 75°. The details of construction and operation of the rotary effusion unit have been described by Muenow and Grimley.<sup>8</sup>

One of the major initial problems of this study was the extremely reactive nature of silver chloride. At 660° the  $\text{AgCl}$  reacted violently when in direct contact with an Inconel cell. Silver chloride also reacted vigorously with the copper in sterling silver as illustrated by the fact that when  $\text{AgCl}$  was heated in a sterling silver cell with only a partial  $\text{Al}_2\text{O}_3$  liner, mixed halides containing both copper and silver were formed. A partial mass spectrum includes  $\text{Ag}_4\text{Cl}_3^+$ ,  $\text{Ag}_3\text{CuCl}_4^+$ ,  $\text{Ag}_3\text{CuCl}_3^+$ ,  $\text{Ag}_2\text{Cu}_2\text{Cl}_4^+$ ,  $\text{AgCu}_3\text{Cl}_4^+$ ,  $\text{Ag}_3\text{Cl}_3^+$ ,  $\text{Ag}_3\text{Cl}_2^+$ ,  $\text{Ag}_2\text{CuCl}_3^+$ ,  $\text{Ag}_3\text{Cu}^+$ ,  $\text{Ag}_2\text{CuCl}_2^+$ ,  $\text{AgCu}_2\text{Cl}_3^+$ ,  $\text{AgCu}_2\text{Cl}_2^+$ ,  $\text{Cu}_3\text{Cl}_3^+$ ,

$\text{Ag}_2\text{Cl}^+$ , and  $\text{AgCuCl}^+$ . Due to this reactivity, alumina cell liners were used for all other experiments. It was also observed that the  $\text{AgCl}$  vapor phase reacted with the tantalum radiation shields as evidenced by the presence of  $\text{TaCl}_3^+$  and  $\text{TaCl}_4^+$  in the mass spectrum. As a consequence, pure silver foil shields were used in place of the normal tantalum shields for all work reported here. Use of these precautions eliminated all ionic species from the mass spectrum other than those directly attributable to the  $\text{AgCl}$ . All samples consisted of Mallinckrodt analytical reagent grade silver chloride.

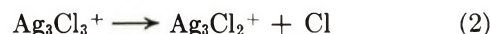
### Results

A total of eight ions has been reported by previous workers,<sup>4-6</sup> and they are as follows:  $\text{Ag}^+$ ,  $\text{AgCl}^+$ ,  $\text{Ag}_2^+$ ,  $\text{Ag}_2\text{Cl}^+$ ,  $\text{Ag}_3^+$ ,  $\text{Ag}_3\text{Cl}^+$ ,  $\text{Ag}_3\text{Cl}_2^+$ , and  $\text{Ag}_3\text{Cl}_3^+$ . In addition to these ions, the present study revealed five additional ionic species:  $\text{Ag}_2\text{Cl}_2^+$ ,  $\text{Ag}_4\text{Cl}_3^+$ ,  $\text{Ag}_4\text{Cl}_4^+$ ,  $\text{Ag}_5\text{Cl}_4^+$ , and  $\text{Cl}^+$ . Each of the ions in the mass spectrum was identified by the mass numbers and the isotopic abundances. Except for  $\text{Ag}_5\text{Cl}_4^+$ , which was of extremely low intensity, the predicted mass spectrum of each ion was in good agreement with the observed spectrum. Magnetic field measurements could not be made with sufficient accuracy to positively confirm the mass number of the  $\text{Ag}_5\text{Cl}_4^+$  species. However, the observed abundances are closer to  $\text{Ag}_5\text{Cl}_4^+$  than to the other possible species with a somewhat similar mass spectrum, namely,  $\text{Ag}_5\text{Cl}_5^+$  and  $\text{Ag}_5\text{Cl}_3^+$ .

A previously unreported metastable peak was also found which overlaps the  $\text{Ag}_3\text{Cl}^+$  spectrum. The reaction which results in the metastable peak was determined by use of the relationship<sup>9</sup>

$$m^* = (m_2)^2/m_1 \quad (1)$$

where  $m^*$  is the apparent mass of the metastable,  $m_1$  is the mass of the reacting ion, and  $m_2$  is mass of the product ion, and the metastable reaction was found to be



The reaction is characterized by the type of behavior normally associated with metastable reactions.<sup>10</sup> Since

(4) H. M. Rosenstock, J. R. Walton, and L. V. Brice, Jr., *U. S. Atomic Energy Comm. Report*, ORNL-2772 (1959).

(5) A. V. Gusarov and L. N. Gorokhov, *Vestn. Mosk. Univ., Khim., Ser. II*, 17(5), 14 (1962).

(6) A. Visnapuu and J. W. Jensen, *J. Less-Common Metals*, 20, 141 (1970).

(7) R. T. Grimley in "The Characterization of High-Temperature Vapors," J. L. Margrave, Ed., Wiley, New York, N. Y., 1967, Chapter 8.

(8) D. W. Muenow and R. T. Grimley, *Rev. Sci. Instrum.*, 42, 455 (1971).

(9) J. A. Hipple, R. E. Fox, and E. V. Condon, *Phys. Rev.*, 69, 347 (1946).

(10) F. H. Field and J. L. Franklin, "Electron Impact Phenomena and the Properties of Gaseous Ions," Academic Press, New York, N. Y., 1957.

the metastable has a distinct isotopic abundance spectrum, a predicted pattern based on the naturally occurring isotopic abundances was calculated. It was assumed that a  $^{35}\text{Cl}$  or  $^{37}\text{Cl}$  atom was lost with equal probability. Each isotope of  $\text{Ag}_3\text{Cl}_3^+$  was assumed to undergo the transition, and the resulting predicted intensities were then summed into mass bands with widths of approximately 0.3 mass units. A comparison of the predicted and observed metastable intensities is shown in Table I. In view of the approximations used in the calculation and the low intensities of the metastable peaks, the agreement is seen to be quite good.

**Table I:** Comparison of the Predicted and Observed Metastable Intensities

Mass number	Predicted abundance	Experimental abundance
359	0.130	0.122
361	0.301	0.284
363	0.332	0.346
365	0.186	0.179
367	0.050	0.070

Appearance potentials for all species except  $\text{Ag}_2^+$  were determined by the linear extrapolation method, and values are given in Table II. The spectroscopic ionization potential of mercury<sup>11</sup> (10.43 eV) was used as a reference for the energy scale. The ionization efficiency curve of  $\text{Ag}_2^+$  is nonlinear as shown in Figure 1. Nonlinearity of this type may occur when an ionic species is formed from more than one neutral species. Two breaks in the ionization efficiency curve for  $^{35}\text{Cl}^+$  are observed and are seen in Figures 2 and 3.

**Table II:** Appearance Potentials, Relative Intensities, and Heats of Vaporization for the Species of the  $\text{AgCl}$  Mass Spectrum

Ionic species	Appearance potential, eV	Rel intensities <sup>a</sup>	Heat of vaporization, <sup>b</sup> kcal mol <sup>-1</sup>
$\text{Cl}^+$	$13.0 \pm 0.8$	2.3	$46.1 \pm 1.3$
$\text{Ag}^+$	$12.7 \pm 0.5$	11.0	$46.0 \pm 0.7$
$\text{AgCl}^+$	$11.3 \pm 0.5$	100.0	$46.3 \pm 0.4$
$\text{Ag}_2^+$		2.0	$39.2 \pm 1.3$
$\text{Ag}_2\text{Cl}^+$	$13.7 \pm 0.5$	13.9	$38.8 \pm 1.0$
$\text{Ag}_2\text{Cl}_2^+$	$10.3 \pm 0.5$	0.4	$46.7 \pm 1.5$
$\text{Ag}_3^+$	$18.4 \pm 0.5$	1.2	$36.7 \pm 1.0$
$\text{Ag}_3\text{Cl}^+$	$14.9 \pm 0.5$	1.5	$37.6 \pm 1.0$
$\text{Ag}_3\text{Cl}_2^+$	$11.1 \pm 0.5$	41.5	$38.0 \pm 1.0$
$\text{Ag}_3\text{Cl}_3^+$	$10.0 \pm 0.5$	12.5	$32.4 \pm 0.6$
$\text{Ag}_4\text{Cl}_3^+$	$10.9 \pm 0.5$	1.9	$40.6 \pm 1.1$
$\text{Ag}_4\text{Cl}_4^+$	$9.6 \pm 1.0$	<0.1	c
$\text{Ag}_5\text{Cl}_4^+$	$10.0 \pm 1.5$	<0.1	c

<sup>a</sup> Determined at 25 eV and 700°. <sup>b</sup> Determined at 25 eV. <sup>c</sup> Too low intensity to measure.

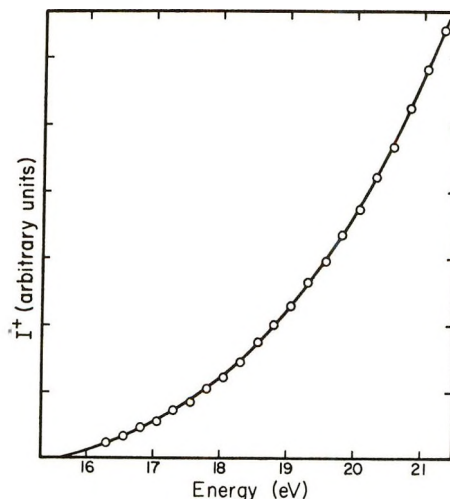


Figure 1. Ionization efficiency curve for the  $\text{Ag}_2^+$  ion.

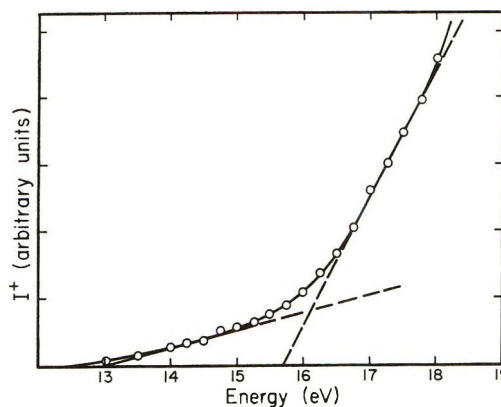


Figure 2. Low-energy portion of the ionization efficiency curve for  $\text{Cl}^+$ .

The intensity of each of the ions was determined as a function of temperature over the range 660–700°. The equilibrium vapor pressure  $P$  of a neutral vapor species in a Knudsen cell at temperature  $T$  is related to the intensity  $I^+$  of the ionic species which results from electron bombardment of the neutral vapor species by the relation  $P = kI^+T$  where  $k$  is a constant.<sup>12</sup> If an ionic species results from ionization of only one neutral vapor species, then the heat of vaporization of the vapor species is obtained from the  $\log I^+T$  vs.  $1/T$  plot for the ion. For ease of expression and identification we will use the term “heat of vaporization of an ion.” It should be clearly understood that use of this terminology in no way implies that we are measuring a thermodynamic heat of vaporization of an ion. The thermodynamic property which is measured is the heat of vaporization of the neutral precursor which forms the ion. Heats of vaporization are given in Table II for all species except  $\text{Ag}_4\text{Cl}_4^+$  and  $\text{Ag}_5\text{Cl}_4^+$  whose intensities were too low to give good second-law results. All data

(11) C. E. Moore, *Nat. Bur. Stand. (U. S.), Circ.*, **467** (1949).

(12) R. E. Honig, *J. Chem. Phys.*, **22**, 126 (1954).

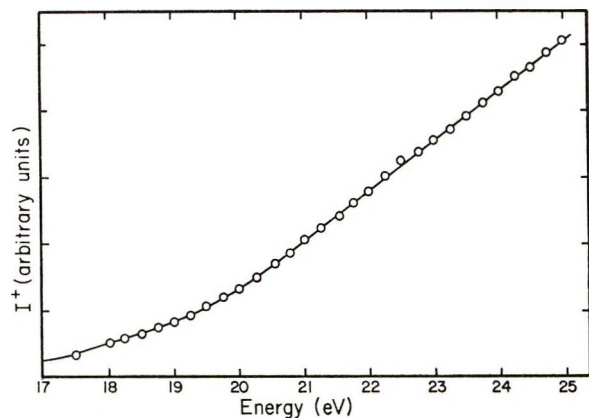


Figure 3. Higher energy portion of the ionization efficiency curve for  $\text{Cl}^+$ .

were taken at an electron bombardment energy of 25 eV. Since a pressure calibration was not obtained for each run, intercomparison of intensity data among the runs for a species was not possible. The data from each run were treated by the least-squares method. The tabulated heats are averages of the least-squares data for between three and five runs per ionic species. Similarly, the uncertainties are the standard deviations from these averages.

The theoretical treatment by Clausing<sup>13-15</sup> of molecular flow through cylindrical orifices predicts that the angular number distribution is a function of the orifice geometry. Recent work by Grimley, Muenow, and LaRue<sup>16</sup> has demonstrated that the angular distributions of related polymeric vapor species such as  $\text{KCl}$  and  $\text{K}_2\text{Cl}_2$  do not obey the Clausing theory and that the angular distributions of the two species differ from one another. These differences become more pronounced as the length to radius ratio ( $L/R$ ) of the orifice increases. The main purpose of this study was to determine the potential usefulness of the angular distribution technique as a tool for the investigation of ionization processes of complex vapor systems.

The information required to characterize each angular distribution curve includes the cell angle  $\theta$ , the molecular beam intensity  $I(\theta)$  as a function of angle, and the temperature of the Knudsen cell. The beam intensities are normalized to the beam intensity at  $0^\circ$  by taking the ratio of the intensity at each angle  $\theta$  to the intensity at  $0^\circ$ . The relative intensities  $I(\theta)/I(0)$  are then plotted as a function of the angle  $\theta$ .

The normalized angular distribution data for 12 ionic species observed in the  $\text{AgCl}$  mass spectrum are shown in Table III and are illustrated in Figure 4. An electron bombardment energy of 25 eV was employed for all species, and the Knudsen cell temperature was  $660^\circ$  for all species except  $\text{Cl}^+$  and  $\text{Ag}_4\text{Cl}_3^+$ . All data reported here were obtained from an orifice with a geometry of  $L/R = 4$ . Additional angular distribution curves were obtained at several electron bombardment

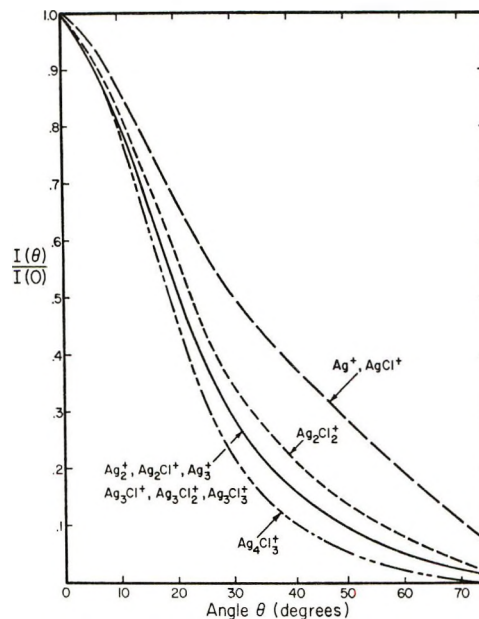


Figure 4. Angular distribution curves of species in the  $\text{AgCl}$  mass spectrum. Data points used to obtain these curves are contained in Table III.

energies, and these will be considered in the analysis of the fragmentation process.

## Discussion

Since most high-temperature vapor systems consist at equilibrium of a mixture of gases, the procedures used must be capable of treating simultaneously the ions resulting from electron bombardment of such a mixture. If the ionization potential of an atom or molecule has previously been determined, then measurement of appearance potentials can be useful. Let us consider the  $\text{Ag}^+$  ion as an example. If  $\text{Ag}^+$  is formed by ionization of elemental silver vapor, then the appearance potential will equal the spectroscopic ionization potential. If, on the other hand,  $\text{Ag}^+$  is formed by dissociative ionization of  $\text{AgCl}$ , then the appearance potential for  $\text{Ag}^+$  will exceed the ionization potential of elemental silver by the dissociation energy of  $\text{AgCl}$  plus any kinetic energy contributions. The appearance potential for  $\text{Ag}^+$  of 12.7 eV is greatly in excess of the reported spectroscopic value of the first ionization potential for silver of 7.54 eV<sup>17</sup> and one may reasonably conclude that  $\text{Ag}^+$  is a fragment ion. In a study of the silver vapor system Schissel<sup>18</sup> found the appearance potential of  $\text{Ag}_2^+$  to be less than the ionization potential of  $\text{Ag}^+$ . Consequently, the appear-

(13) P. Clausing, *Physica*, **9**, 65 (1929).

(14) P. Clausing, *Z. Phys.*, **66**, 471 (1930).

(15) P. Clausing, *Ann. Phys. (Leipzig)*, **12**, 961 (1932).

(16) R. T. Grimley, D. W. Muenow, and J. L. LaRue, *J. Chem. Phys.*, **56**, 490 (1972).

(17) C. E. Moore, *Nat. Bur. Stand. (U. S.), Circ.*, **467** (1958).

(18) P. Schissel, *J. Chem. Phys.*, **26**, 1276 (1957).

**Table III:** Normalized Angular Distribution Data of Ionic Species Observed in the AgCl Mass Spectrum<sup>a</sup>

$\theta$ , deg	Cl <sup>+</sup> <sup>b</sup>	Ag <sup>+</sup>	AgCl <sup>+</sup>	Ag <sub>2</sub> <sup>+</sup>	Ag <sub>2</sub> Cl <sup>+</sup>	Ag <sub>2</sub> Cl <sub>2</sub> <sup>+</sup>	Ag <sub>3</sub> <sup>+</sup>	Ag <sub>3</sub> Cl <sup>+</sup>	Ag <sub>3</sub> Cl <sub>2</sub> <sup>+</sup>	Ag <sub>3</sub> Cl <sub>3</sub> <sup>+</sup>	Ag <sub>4</sub> Cl <sub>3</sub> <sup>+</sup>	Ag <sub>4</sub> Cl <sub>4</sub> <sup>+</sup> <sup>b</sup>
0.00	1.000	1.000	1.000	1.000	1.000	1.000	1.000	1.000	1.000	1.000	1.000	1.000
4.68	0.957	0.964	0.957	0.956	0.946	0.946	0.951	0.955	0.939	0.940	0.931	0.936
9.42	0.869	0.879	0.876	0.830	0.826	0.841	0.843	0.821	0.816	0.818	0.796	0.799
14.22	0.776	0.792	0.787	0.703	0.691	0.707	0.709	0.703	0.683	0.686	0.641	0.653
18.93	0.696	0.691	0.691	0.560	0.557	0.577	0.551	0.562	0.545	0.554	0.496	0.508
23.78	0.599	0.598	0.601	0.427	0.426	0.468	0.438	0.425	0.416	0.423	0.361	0.351
28.65	0.517	0.503	0.517	0.308	0.315	0.365	0.313	0.316	0.307	0.309	0.242	0.258
33.55	0.423	0.443	0.455	0.242	0.241	0.292	0.240	0.238	0.234	0.237	0.167	0.184
38.48	0.389	0.391	0.400	0.188	0.189	0.243	0.183	0.183	0.182	0.184	0.124	0.119
43.38	0.336	0.343	0.349	0.145	0.147	0.195	0.141	0.145	0.143	0.145	0.091	0.100
48.28	0.293	0.297	0.303	0.111	0.114	0.160	0.114	0.113	0.111	0.109	0.065	0.060
53.24	0.253	0.250	0.257	0.086	0.089	0.123	0.087	0.087	0.085	0.085	0.047	0.039
58.19	0.202	0.211	0.213	0.064	0.067	0.095	0.063	0.063	0.064	0.063	0.035	0.029
63.25	0.164	0.171	0.166	0.047	0.049	0.072	0.042	0.045	0.046	0.045	0.023	0.022
68.31	0.134	0.128	0.128	0.033	0.033	0.050	0.030	0.031	0.030	0.030	0.015	0.011
73.37	0.114	0.091	0.088	0.019	0.020	0.030	0.018	0.016	0.017	0.018	0.008	0.009

<sup>a</sup> Data were taken at 25 eV with a cell temperature of 660° except as noted and an  $L/R = 4$  cell geometry. <sup>b</sup> Data taken at 700° cell temperature.

ance potential for Ag<sub>2</sub><sup>+</sup> of approximately 15.8 eV found in this work is greatly in excess of the appearance potential of the parent Ag<sub>2</sub><sup>+</sup> ion. Furthermore, it has been indicated that curvature in the ionization efficiency curve of Ag<sub>2</sub><sup>+</sup> suggested that at least two neutral molecules were responsible for this ion. Even when an ionization potential is unknown, the observations made with regard to the energetics of formation of Ag<sup>+</sup> may be usefully applied to other more complex species. If a parent ion is formed, its appearance potential will be lower than that of any of the fragment ions which may be formed by dissociative ionization of the same neutral precursor. The appearance potentials for Ag<sub>3</sub>Cl<sub>4</sub><sup>+</sup> (9.6 eV), Ag<sub>3</sub>Cl<sub>3</sub><sup>+</sup> (10.0 eV), and Ag<sub>2</sub>Cl<sub>2</sub><sup>+</sup> (10.3 eV) are low in comparison with the other species. Furthermore, the stoichiometries of the ions are such that simple ionization of the appropriate neutral polymer could easily give rise to the observed ions. It is likely, therefore, that these are parent ions. Where two elements combine to form a series of binary compounds, it is generally found that the appearance potentials of the parent ions are within a few eV of each other. When ions are observed whose appearance potentials are several (on the order of three or more) eV greater than the appearance potentials of the proposed parent ions and which may be formed by dissociative ionization of the proposed neutral precursors, it is assumed that these are likely candidates for fragment ions. The appearance potentials for Ag<sub>2</sub>Cl<sup>+</sup> (13.7 eV), Ag<sub>3</sub><sup>+</sup> (18.4 eV), and Ag<sub>3</sub>Cl<sup>+</sup> (14.9 eV) are sufficiently high relative to the appearance potentials of the proposed parent ions that these ions most likely result from fragmentation. We can say at this juncture that the Ag<sup>+</sup>, Ag<sub>2</sub><sup>+</sup>, Ag<sub>2</sub>Cl<sup>+</sup>, Ag<sub>3</sub><sup>+</sup>, and Ag<sub>3</sub>Cl<sup>+</sup> ions result from ionization accompanied by fragmentation. This information, however, is insufficient for

one to identify the neutral vapor species which produces a given ion.

Another technique which has been used to identify the neutral vapor species employs heat of vaporization data. If several ionic species are produced from one neutral species, the  $\log I^+T$  plot for each of these ions should yield the same heat of vaporization. Two complicating factors arise with this interpretation. First, the possibility exists that an ionic species may be formed from more than one neutral vapor species. Because the heat of vaporization would be of intermediate value, the ion could erroneously be attributed to a separate vapor species. When a molecule is ionized it may decompose or fragment by a series of parallel or consecutive reactions and form additional ionic species. The use of heat of vaporization data assumes that the rate constants for these ionic decomposition reactions are independent of the thermodynamic temperature of the neutral species. Any change with temperature of ion intensity is therefore associated with a change in the partial pressure of the vapor. Any temperature dependence of these rate constants could result in variation in the heats of vaporization for ions which have a common precursor. Should the temperature effect be pronounced, erroneous conclusions regarding the identity of the neutral vapor species are again possible. In the vast majority of previous high-temperature studies, it has been assumed that ionic decomposition reactions were temperature independent.

For the AgCl system the heat of vaporization data cluster around four values; 46, 41, 38, and 32 kcal mol<sup>-1</sup>. Using the standard arguments one would conclude that ionization of four neutral vapor species is responsible for the observed ions. There are, however, several disquieting aspects about such a con-

clusion. The species  $\text{Ag}_2\text{Cl}_2^+$ ,  $\text{AgCl}^+$ , and  $\text{Ag}^+$  all have approximately the same heat of vaporization. The appearance potential of  $\text{Ag}_2\text{Cl}_2^+$  is low, and a low intensity of the parent peak is not unusual in the case of halide compounds. The appearance potential of  $\text{AgCl}^+$  is of intermediate value and could easily be attributed to a fragment. The  $\text{Ag}_2\text{Cl}_2^+$  ion is assumed to be a parent ion, but the question of whether  $\text{AgCl}^+$  is a parent ion from  $\text{AgCl}$  or a fragment from  $\text{Ag}_2\text{Cl}_2$  remains open. The  $\text{Ag}_2^+$ ,  $\text{Ag}_2\text{Cl}^+$ ,  $\text{Ag}_3^+$ ,  $\text{Ag}_3\text{Cl}^+$ , and  $\text{Ag}_3\text{Cl}_2^+$  ions have approximately the same heats of vaporization and apparently come from the same molecule. Visnapuu and Jensen<sup>6</sup> claim that the difference in the heats of vaporization between  $\text{Ag}_3\text{Cl}_3^+$  and  $\text{Ag}_3\text{Cl}_2^+$  indicate that the  $\text{Ag}_3\text{Cl}_2$  molecule exists in addition to  $\text{Ag}_3\text{Cl}_3$ , and that fragmentation of  $\text{Ag}_3\text{Cl}_2^+$  results in formation of the other ions such as  $\text{Ag}_3\text{Cl}^+$ ,  $\text{Ag}_3^+$ ,  $\text{Ag}_2\text{Cl}^+$ , and  $\text{Ag}_2^+$ . As is readily seen the use of the conventional methods in the interpretation of the  $\text{AgCl}$  mass spectrum leaves many questions unresolved.

In the specific case of the  $\text{AgCl}$  system, the angular distribution technique enables one to answer many of these questions. For brevity we shall hereafter refer to this as the AD technique. The application of AD measurements to the analysis of fragmentation patterns depends on each molecular species having a different angular distribution pattern. Thus each ion formed from the same molecule will exhibit an identical AD curve. If an ion is produced from more than one neutral species, the AD curve will be a weighted superposition of the curves of the individual neutral species. The probability is remote that the ionization potentials and the ionization efficiency curves of the involved species are identical. As a result one would expect the AD curve for an ion formed from more than one neutral species to change with the energy of the ionizing electrons. In those instances where an ion is formed from only one neutral species, the form of the AD curve should be independent of the energy of the ionizing electrons.

The AD curves for the ions observed in the mass spectrum of the  $\text{AgCl}$  system are shown in Figure 4. All data were taken at 25 eV. Four distinct curves may be seen, and these are associated with four different molecules.

The AD curves of the  $\text{Ag}_4\text{Cl}_3^+$  and  $\text{Ag}_4\text{Cl}_4^+$  ions are identical and are highly focused. The AD measurements for  $\text{Ag}_4\text{Cl}_3^+$  were made at 18 and 25 eV and produced identical curves. Because of the low intensity of  $\text{Ag}_4\text{Cl}_4^+$ , AD measurements were made only at 25 eV. The low appearance potential for  $\text{Ag}_4\text{Cl}_4^+$  (9.6 eV) and the distinct heat of vaporization for  $\text{Ag}_4\text{Cl}_3^+$  of  $40.6 \text{ kcal mol}^{-1}$  provide further evidence for the existence of  $\text{Ag}_4\text{Cl}_4$ . We conclude that  $\text{Ag}_4\text{Cl}_4$  and  $\text{Ag}_4\text{Cl}_3^+$  are produced by ionization of one species,  $\text{Ag}_4\text{Cl}_4$ .

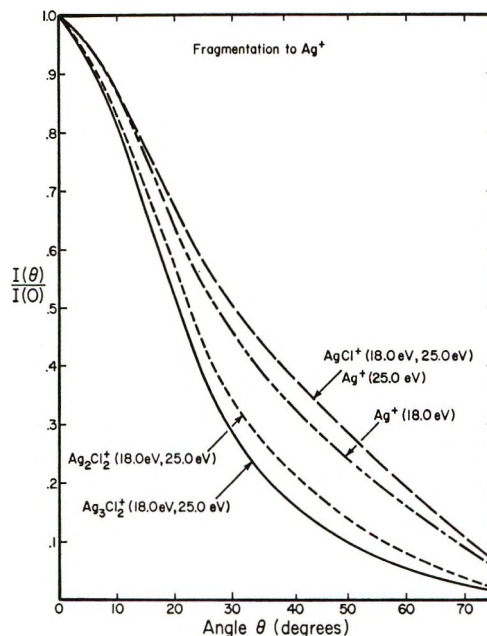


Figure 5. The effect of the energy of the ionizing electrons on the angular distribution curves of  $\text{Ag}^+$ .

The existence of  $\text{Ag}_5\text{Cl}_5$  is suggested by the observation of the  $\text{Ag}_5\text{Cl}_4^+$  ion. Measurement of the angular distribution of  $\text{Ag}_5\text{Cl}_4^+$  was attempted. However, data scatter was great even with the integration technique because of the extremely low intensity of the peak. Even though the AD curve for  $\text{Ag}_5\text{Cl}_4^+$  is poorly resolved, it appears to be more focused than any of the other AD curves. Furthermore, the appearance potential of 10 eV is similar in magnitude to those of  $\text{Ag}_3\text{Cl}_2^+$  and  $\text{Ag}_4\text{Cl}_3^+$  (See Table II). The presence of  $\text{Ag}_5\text{Cl}_5$  is suggested but at very low partial pressures at the temperatures of this study.

The three remaining molecular species  $\text{AgCl}$ ,  $\text{Ag}_2\text{Cl}_2$ , and  $\text{Ag}_3\text{Cl}_3$  also undergo fragmentation processes. The simplest of these is  $\text{AgCl}$ . The  $\text{Ag}^+$  and  $\text{AgCl}^+$  ions have a distribution curve which is more diffuse than any of the other ions at 25 eV. In addition, the  $\text{Ag}^+$  and  $\text{AgCl}^+$  heats of vaporization are identical within measurement error. For  $\text{AgCl}^+$ , AD curves were obtained at 18 and 25 eV and proved to be independent of the energy of the ionizing electrons. Since the higher molecular weight species which might contribute to the  $\text{AgCl}^+$  peak all possess more highly focused distribution curves, any fragment contribution to this peak would appear as a shifting of the AD curves toward the more focused configuration. This effect is in fact observed for  $\text{Ag}^+$  as shown in Figure 5. Measurements at 18 eV reveal a substantial increase in the focusing of the AD curve. The most likely sources of the  $\text{Ag}^+$  fragment are  $\text{Ag}_3\text{Cl}_3$  and  $\text{Ag}_2\text{Cl}_2$ . Both species have more highly focused distribution curves than  $\text{AgCl}$ . The heat of vaporization for  $\text{Ag}_3\text{Cl}_3$  is  $37.1 \pm 1.5 \text{ kcal mol}^{-1}$  and for  $\text{Ag}_2\text{Cl}_2$  is  $46.7 \text{ kcal mol}^{-1}$ .

If  $\text{Ag}^+$  is formed from  $\text{Ag}_2\text{Cl}_2$ , the value of the heat of vaporization at 18 eV would be essentially unchanged since the heat of vaporization for  $\text{AgCl}$  is  $46.3 \text{ kcal mol}^{-1}$ . Since the heat of vaporization for  $\text{Ag}_3\text{Cl}_3$  is  $37.1 \text{ kcal mol}^{-1}$ , a fragment contribution to  $\text{Ag}^+$  from  $\text{Ag}_3\text{Cl}_3$  would cause a decrease in the heat of vaporization of  $\text{Ag}^+$  when measured at 18 eV. Obviously the energy of the electrons which are used to form the ions cannot change the heat of vaporization of the neutral species. The measured value for the heat of vaporization of  $\text{Ag}^+$  at 18 eV is  $46.3 \pm 0.7 \text{ kcal mol}^{-1}$ . Because of the sensitivity limitations of both the thermodynamic and AD techniques, some trimer contribution to  $\text{Ag}^+$  is possible. However the major contributors to  $\text{Ag}^+$  are  $\text{AgCl}$  and  $\text{Ag}_2\text{Cl}_2$ .

The  $\text{Ag}_2\text{Cl}_2^+$  AD curve is considerably more focused than the monomer curve but is more diffuse than the curves for any of the higher molecular weight species. Furthermore, the  $\text{Ag}_2\text{Cl}_2^+$  distribution is also independent of the ionizing energy as shown in Figure 5. There can be no monomer fragment contribution to the  $\text{Ag}_2\text{Cl}_2^+$  ion and consequently to the AD curve. The  $\text{Ag}_2\text{Cl}_2^+$  AD curve cannot be formed wholly from  $\text{Ag}_3\text{Cl}_3$  or  $\text{Ag}_4\text{Cl}_4$  since both species have a more highly focused distribution than does  $\text{Ag}_2\text{Cl}_2^+$ . The low appearance potential of 10.3 eV provides further evidence that  $\text{Ag}_2\text{Cl}_2^+$  is formed from  $\text{Ag}_2\text{Cl}_2$ . It was previously mentioned that, because the heats of vaporization of  $\text{Ag}_2\text{Cl}_2^+$ ,  $\text{AgCl}^+$ , and  $\text{Ag}^+$  were equivalent, one could not identify the sources of  $\text{AgCl}^+$  and  $\text{Ag}^+$  from thermodynamic data. This example provides a graphic illustration of the value of the AD method.

The AD curves of  $\text{Ag}_3\text{Cl}_3^+$ ,  $\text{Ag}_3\text{Cl}_2^+$ ,  $\text{Ag}_3\text{Cl}^+$ ,  $\text{Ag}_3^+$ ,  $\text{Ag}_2\text{Cl}^+$ , and  $\text{Ag}_2^+$  at 25 eV are identical. The AD curves of  $\text{Ag}_3\text{Cl}_3^+$ ,  $\text{Ag}_3\text{Cl}_2^+$ ,  $\text{Ag}_3\text{Cl}^+$ , and  $\text{Ag}_3^+$  were also measured at 18 eV and were found to be in agreement with the 25-eV curves. Using the type of argument previously employed for the dimer, one would conclude that these ions are formed from the  $\text{Ag}_3\text{Cl}_3$  molecule. The appearance potential of  $\text{Ag}_3\text{Cl}_3^+$  is low (10.0 eV) and is a reasonable value for a parent ion. The magnitude of the spread in appearance potentials of the parent  $\text{Ag}_3\text{Cl}_3^+$  and the fragment  $\text{Ag}_3\text{Cl}_2^+$  is in the range observed for ions of this type. The appearance potentials of  $\text{Ag}_3\text{Cl}^+$  and  $\text{Ag}_3^+$  clearly classify these ions as fragments. However, a gross discrepancy between the heats of vaporization of  $\text{Ag}_3\text{Cl}_3^+$  and the other ions exists. The possible reasons for this seeming inconsistency will be considered shortly.

While the remaining silver containing ions,  $\text{Ag}_2\text{Cl}^+$  and  $\text{Ag}_2^+$ , have trimer type distributions at 25 eV, at lower ionizing energies the curves become more diffuse in shape. The dependence of the AD curves on the energy of the ionizing electrons is shown in Figures 6 and 7. Because the energy shift tends to make the curve more diffuse, the second or nontrimer contribution must be made by a species whose angular distribution

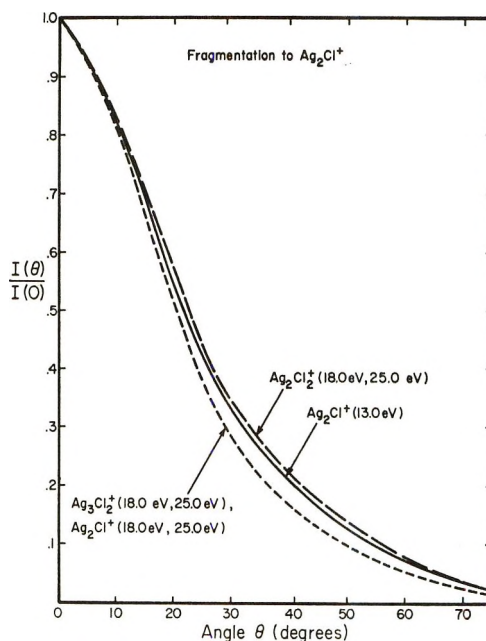


Figure 6. The effect of the energy of the ionizing electrons on the angular distribution curves of  $\text{Ag}_2\text{Cl}^+$ .

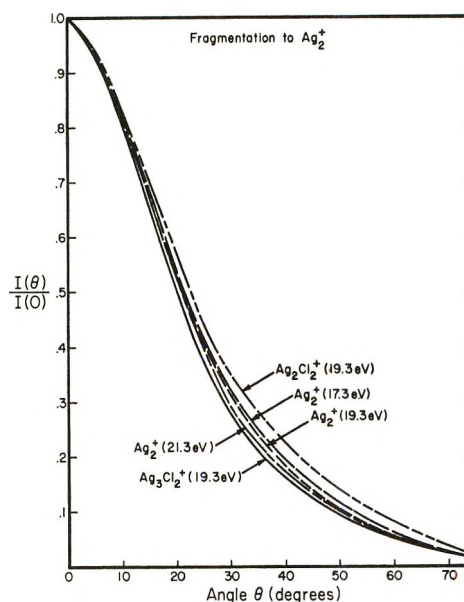


Figure 7. The effect of the energy of the ionizing electrons on the angular distribution curves of  $\text{Ag}_2^+$ .

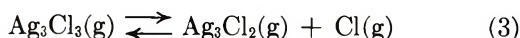
is more diffuse than the trimer. An additional and perhaps trivial requirement is that the vapor species must be capable of producing the ion. Only  $\text{Ag}_2\text{Cl}_2$  fulfills these requirements. Figure 6 shows that at 18 and 25 eV, the contribution of dimer to the  $\text{Ag}_2\text{Cl}^+$  ion intensity is not detectable. However, as the voltage is lowered to a point just above the onset of ionization, the relative dimer contribution increases and may be observed. Because of the curvature of the ionization efficiency curve, the appearance potential of 13.7 eV obtained by the linear extrapolation method is above

the energy at which these measurements were made, namely, 13 eV. A similar phenomena is observed for  $\text{Ag}_2^+$  (Figure 7) except that even close to the onset energy for  $\text{Ag}_2^+$ , a substantial trimer contribution to  $\text{Ag}_2^+$  is still found.

Based upon the behavior of organic systems one has generally assumed that fragmentation of complex inorganic systems would be minimized and analysis simplified if low ionizing energies were employed. This system provides a warning that this assumption may not be valid.

The discrepancy between the thermodynamic and AD data for the ions formed from  $\text{Ag}_3\text{Cl}_3$  has previously been mentioned. Since the standard deviation of second-law heat of vaporization measurements is of the order of  $\pm 1$  kcal mol<sup>-1</sup>, differences less than this cannot be considered to be significant. Except for  $\text{Ag}_3\text{Cl}_3^+$  the data for the trimer-related ions fall in the 38 kcal mol<sup>-1</sup> range. The slightly higher values for  $\text{Ag}_2\text{Cl}^+$  and  $\text{Ag}_2^+$  could possibly be attributed to the dimer fragmentation contributions to these ions. On the surface, at least, several explanations for the low heat of vaporization value for  $\text{Ag}_3\text{Cl}_3^+$  may be suggested. (1) Two separate vapor species  $\text{Ag}_3\text{Cl}_3$  and  $\text{Ag}_3\text{Cl}_2$  exist each with its own distinct heat of vaporization. (2) Two forms of  $\text{Ag}_3\text{Cl}_3$  with differing structures and heats of vaporization are present. (3) The rate constants for the various fragmentation processes are temperature dependent.

Visnapuu and Jensen<sup>6</sup> concluded that two separate and distinct species,  $\text{Ag}_3\text{Cl}_3$  and  $\text{Ag}_3\text{Cl}_2$ , exist in the vapor phase. The primary evidence cited in support of this conclusion was the differences in the heats of vaporization between  $\text{Ag}_3\text{Cl}_3^+$  and  $\text{Ag}_3\text{Cl}_2^+$  and the low appearance potentials of these species. There are a number of reasons why we feel that this explanation is incorrect. The angular distribution curves of  $\text{Ag}_3\text{Cl}_3^+$  and  $\text{Ag}_3\text{Cl}_2^+$  are identical and are independent of the energy of the ionizing electrons. An interrelationship between  $\text{Ag}_3\text{Cl}_3^+$  and  $\text{Ag}_3\text{Cl}_2^+$  has been demonstrated by means of the metastable transition (eq 2). Thus the heat of vaporization of  $\text{Ag}_3\text{Cl}_2^+$  cannot be solely representative of  $\text{Ag}_3\text{Cl}_2$ , and the thermodynamic argument cannot be invoked. In addition, if  $\text{Ag}_3\text{Cl}_2$  exists as a molecule in the gas phase, then the equilibrium



must exist in the Knudsen cell. In order for the stoichiometries of the liquid and gaseous phases to remain constant at a given temperature, the flux of  $\text{Ag}_3\text{Cl}_2$  molecules leaving the cell must be equal to the flux of Cl atoms. For the type of ion source used in this work the ion intensity  $I^+$  is related to the flux  $\nu$  by means of the equation  $I^+ = K\nu\sigma/\bar{c}$  where  $\sigma$  is the ionization cross section,  $\bar{c}$  is the average speed of the molecules, and  $K$  is a constant related to the machine geometry. If

$\text{Ag}_3\text{Cl}_2$  exists then the main ionic species associated with  $\text{Ag}_3\text{Cl}_2$  are  $\text{Ag}_3\text{Cl}_2^+$  and  $\text{Ag}_2\text{Cl}^+$ . Accordingly, the ion intensity for  $\text{Ag}_3\text{Cl}_2$  was taken to be the sum of  $I^+_{\text{Ag}_3\text{Cl}_2^+}$  and  $I^+_{\text{Ag}_2\text{Cl}^+}$ . Using the total ion intensity for  $\text{Ag}_3\text{Cl}_2$  one may predict the ion intensity for  $\text{Cl}^+$ . Dependent on whether the Otvos and Stevenson<sup>19</sup> or Mann<sup>20</sup> cross sections were used, the observed ion intensity was found to be low by factors of approximately 30 or 80 from the predicted intensity. These factors are greatly in excess of cross-section uncertainties or approximations, and we are forced to conclude that  $\text{Ag}_3\text{Cl}_2$  does not exist in the vapor phase.

The decomposition involving the formation of  $\text{Cl}_2$  has not been considered since no  $\text{Cl}_2^+$  was observed in the mass spectrum. The source of the  $\text{Cl}^+$  peak does, however, deserve further comment. In obtaining the ionization efficiency curve for  $\text{Cl}^+$  a substantial background of  $\text{Cl}^+$  was observed. Several potential sources of background  $\text{Cl}^+$  ion exist. The  $\text{Ag}_2\text{Cl}_x$  species thermally decompose on hot surfaces exterior of the Knudsen cell with the formation of a metallic silver film and atomic chlorine. Also hydrogen halides are commonly observed when a halogen is introduced into a mass spectrometer.<sup>21</sup> Thus fragmentation of HCl may also be expected to produce some  $\text{Cl}^+$  background.<sup>22</sup> The ionization efficiency curve for  $\text{Cl}^+$  with background removed is shown in Figures 2 and 3. The lower portion of the curve is seen in Figure 2 scaled up ten times relative to the upper portion of the curve shown in Figure 3. It is clear that the major intensity contribution to  $\text{Cl}^+$  results from the ionization process whose onset occurs at approximately 19 eV. An additional break in the curve is observed in Figure 2 at approximately 15.5 eV. The angular distribution curve for  $\text{Cl}^+$  was measured at 25 eV, and the data are shown in Table III. At 25 eV the AD curve of  $\text{Cl}^+$  coincides with the AD curve of  $\text{AgCl}^+$ . We conclude, therefore, that the major portion of the  $\text{Cl}^+$  ion intensity results from dissociative ionization of  $\text{AgCl}$ .

Microscopic examination of the cell orifice and the  $\text{AgCl}$  remaining in the cell after a run revealed the presence of a few small crystals of silver. While the major process which occurs is vaporization, a small amount of  $\text{AgCl}$  is simultaneously decomposing to elemental silver and chlorine. The appearance potential of  $13.0 \pm 0.8$  eV agrees with spectroscopic ionization potential for atomic chlorine of 13.01 eV.<sup>11</sup> The first section of the ionization efficiency curve is assigned to ionization of Cl.

(19) J. W. Otvos and D. P. Stevenson, *J. Amer. Chem. Soc.*, **78**, 546 (1956).

(20) J. B. Mann in "Recent Developments in Mass Spectroscopy," K. Ogata and T. Hayakawa, Ed., Baltimore University Press, Baltimore, Md., 1970, p 814.

(21) J. T. Herron and V. H. Dibeler, *J. Chem. Phys.*, **32**, 1884 (1960).

(22) R. Thorburn, *Proc. Phys. Soc. (London)*, **73**, 122 (1959).

The onset of the second segment of the ionization efficiency curve at approximately 15.5 eV could energetically result from fragmentation of  $\text{Cl}_2^{22,23}$  to  $\text{Cl}^+$ . If  $\text{Cl}_2$  were responsible for this segment of the curve, then one would also expect to observe a parent  $\text{Cl}_2^+$  peak, but none was found at any temperature. The possibility of HCl absorbed by the AgCl sample contributing to the  $\text{Cl}^+$  peak was considered. A large  $\text{HCl}^+$  peak was observed, but none was found to come from the cell. In addition, the onset of the second segment was well below the value of 17.6 eV reported by Thorburn<sup>22</sup> for the fragmentation of HCl to  $\text{Cl}^+$ . The only remaining chlorine containing species are the  $\text{Ag}_z\text{Cl}_z$  polymers. Because  $\text{Ag}_3\text{Cl}_3$  is present in the greatest amount, the best guess as to the cause of the second segment of the ionization efficiency curve seems to be fragmentation of  $\text{Ag}_3\text{Cl}_3$  to  $\text{Cl}^+$ . Unfortunately, the intensity levels of  $\text{Cl}^+$  were so low along the second segment of the ionization efficiency curve as to preclude the use of AD measurements to confirm the trimer as a source of  $\text{Cl}^+$ .

The possibility of linear and cyclic forms of  $\text{Li}_2\text{F}_2$  have been proposed by Abramowitz,<sup>24</sup> *et al.*, and by Snelson<sup>25</sup> who used the matrix isolation technique to determine the heats of vaporization for the isomeric vapor species. One needs to consider the possibility of two forms of  $\text{Ag}_3\text{Cl}_3$ . Two cyclic structures are easily conceived, one consisting of a three-membered ring of silver atoms with the chlorine atoms located in radial positions. This structure will be termed form A. The other possible cyclic structure, form B, consists of a six-membered ring of alternate silver and chlorine atoms. It is reasonable to expect that some differences in appearance potentials and fragmentation patterns of the two proposed trimer species might occur. However, the ionization efficiency curve of the  $\text{Ag}_3\text{Cl}_3^+$  parent ion exhibited no breaks or abnormal curvature of the type frequently found when more than one neutral precursor contributes to an ionic species.

On the basis of the heat of vaporization data it is possible to conceive of a situation where  $\text{Ag}_3\text{Cl}_3$  form A ionizes to  $\text{Ag}_3\text{Cl}_3^+(\text{A})$ ,  $\text{Ag}_3\text{Cl}_2^+$ , and other fragments. The  $\text{Ag}_3\text{Cl}_3^+(\text{A})$  ion is assumed to undergo the metastable decomposition to  $\text{Ag}_3\text{Cl}_2^+$ . Form B  $\text{Ag}_3\text{Cl}_3$  ionizes only to  $\text{Ag}_3\text{Cl}_3^+(\text{B})$ . Based upon these assumptions, the heats of vaporization of  $\text{Ag}_3\text{Cl}_2^+$ ,  $\text{Ag}_3\text{Cl}^+$ , etc. would be representative of the heat of vaporization of  $\text{Ag}_3\text{Cl}_3^+(\text{A})$ . The resulting heat of vaporization observed for  $\text{Ag}_3\text{Cl}_3^+$  would then be a weighted value of the contributions from forms A and B. Under these circumstances the plot of  $\log P_{\text{Ag}_3\text{Cl}_3^+}$  vs.  $1/T$  should be nonlinear. However, since a forced linear fit is generally used, an intermediate value of the heat of vaporization would be observed. Assuming this, model  $\text{Ag}_3\text{Cl}_3^+(\text{A})$  would have a heat of vaporization of approximately 38 kcal mol<sup>-1</sup> and form B would have a heat of vaporization of less than 32 kcal mol<sup>-1</sup>. Since the ionization

efficiency curves for the two forms would be expected to be somewhat different, the heat of vaporization should show some change as a function of the ionizing electron energy. Measurements made over the same temperature range at 18 and 25 eV give values of 32.9 and 32.4 kcal mol<sup>-1</sup>, respectively. Furthermore, unless the AD curves of both these species were identical, a change in the ionizing energy would cause some shifting of the AD curve. We are unable to demonstrate any of the possible effects which might result from the presence of two isomers. Lacking any spectroscopic evidence to the contrary, we conclude that only one form of  $\text{Ag}_3\text{Cl}_3$  is present in the vapor; and based on the fragmentation patterns, the three-membered silver ring form is the most likely structure.

In previous high-temperature studies of inorganic systems there has been no obvious evidence of temperature-dependent ionization processes. However, this phenomenon has been clearly demonstrated by the studies of Osberghaus, *et al.*,<sup>26-28</sup> in the study of a number of organic molecules. The total ion intensity which is defined as the sum of the intensities of all the ions produced from a given molecule was found to be independent of temperature for a series of  $\text{C}_2$ - $\text{C}_7$  hydrocarbons over a range of several hundred degrees. Cassuto<sup>29</sup> has confirmed this behavior in the case of methane, propane, and *n*-pentane. Qualitative agreement between experiment and the quasi-equilibrium theory has been reported by Ehrhardt and Osberghaus.<sup>28</sup> Of immediate importance insofar as the present work is concerned is the experimental behavior of the hydrocarbon systems. The parent ion shows a decrease in intensity with increasing temperature. The intensities of the fragment ions may either increase, decrease, or exhibit a maximum with temperature. The lowest molecular weight fragments all showed an increase of intensity with temperature. In most cases, the parent ion showed the largest dependence of intensity on temperature. It is interesting to examine the AgCl system in view of these observations. Since the total cross section and, therefore, the total ion of intensity is independent of temperature, any change in the flux for a given neutral species should be observable as a change in the total ion intensity. Thus a plot of  $\log I^+_{\text{total}}T$  vs.  $1/T$  should give the correct value of the second-law heat of vaporization. A least-squares fit

(23) D. C. Frost and C. A. McDowell, *Can. J. Chem.*, **38**, 407 (1960).

(24) S. Abramowitz, N. Acquista, and I. W. Levin, *J. Res. Nat. Bur. Stand.*, **72A**, 487 (1968).

(25) A. Snelson, *J. Phys. Chem.*, **73**, 1919 (1969).

(26) O. Osberghaus and R. Taubert, *Z. Phys. Chem. (Frankfurt am Main)* **4**, 264 (1955).

(27) H. Ehrhardt and O. Osberghaus, *Z. Naturforsch. A*, **13**, 16 (1958).

(28) H. Ehrhardt and O. Osberghaus, *ibid.*, **15**, 575 (1960).

(29) A. Cassuto, *Advan. Mass Spectrom.*, **2**, 296 (1963).

**Table IV:** Ions Formed by the Electron Bombardment of the AgCl Vapor System

Neutral	Ion												
	Cl <sup>+</sup>	Ag <sup>+</sup>	AgCl <sup>+</sup>	Ag <sub>2</sub> <sup>+</sup>	Ag <sub>2</sub> Cl <sup>+</sup>	Ag <sub>2</sub> Cl <sub>2</sub> <sup>+</sup>	Ag <sub>3</sub> <sup>+</sup>	Ag <sub>3</sub> Cl <sup>+</sup>	Ag <sub>3</sub> Cl <sub>2</sub> <sup>+</sup>	Ag <sub>3</sub> Cl <sub>3</sub> <sup>+</sup>	Ag <sub>4</sub> Cl <sub>3</sub> <sup>+</sup>	Ag <sub>4</sub> Cl <sub>4</sub> <sup>+</sup>	Ag <sub>5</sub> Cl <sub>4</sub> <sup>+</sup>
AgCl	X	X	X										
Ag <sub>2</sub> Cl <sub>2</sub>		X		X	X	X							
Ag <sub>3</sub> Cl <sub>3</sub>				X	X		X	X	X	X			
Ag <sub>4</sub> Cl <sub>4</sub>											X	X	
Ag <sub>5</sub> Cl <sub>5</sub>													X

of the  $I^+_{\text{total}}T$  data for Ag<sub>3</sub>Cl<sub>3</sub> yielded the trimer heat of vaporization of 37.1 kcal mol<sup>-1</sup>.

The measurements by Osberghaus, *et al.*,<sup>26</sup> indicate that the temperature variation of the cross sections for the individual ions is generally small compared to the temperature dependence of the vapor pressure for most inorganic compounds. One would expect that the superposition of the cross-section effects on the vapor pressure curve would cause some nonlinearity in the log  $I^+T$  vs.  $1/T$  plot for a given species. However, since the heat of vaporization is obtained from an assumed linear plot, the net effect would be to cause a decrease in the heat of vaporization when, as in the case of the parent ion, the cross section decreases with increased temperature. The heats of vaporization of Ag<sub>3</sub>Cl<sup>+</sup>, Ag<sub>3</sub>Cl<sub>2</sub><sup>+</sup>, and Ag<sub>3</sub><sup>+</sup> do not differ appreciably from the 37.1 ± 1.5 kcal mol<sup>-1</sup> value, and thus a small cross-section effect is likely. The Ag<sub>2</sub>Cl<sup>+</sup> and Ag<sub>2</sub><sup>+</sup> ions show an increase in the heat of vaporization. Since these ions are the smallest fragments, a slight positive temperature effect is in agreement with the results for the hydrocarbons. The contribution from Ag<sub>2</sub>Cl<sub>2</sub> is also a likely cause of the slightly higher heat of vaporization values found for these ions.

It is seen that the conclusions arrived at on the basis of AD data are consistent with the assumptions and observations of temperature-dependent cross sections. The ions which occur as a result of electron bombardment of the AgCl vapor system are compiled in Table IV.

The agreement of our data with that of Visnapuu and Jensen is quite poor. The heats of vaporization and the appearance potentials reported by these workers differ markedly from our results. The heats of vapor-

ization measured in this work are 3–6 kcal mol<sup>-1</sup> higher than those reported by Visnapuu and Jensen. Examination of the Visnapuu and Jensen data reveals differences of 8 to 9 kcal mol<sup>-1</sup> between the maximum and minimum values for the heat of vaporization of a given species. This spread is inordinately large and difficult to explain. Direct comparisons of the data are not possible in any event since Visnapuu and Jensen failed to indicate the energy of the ionizing electrons used in their work.

This and our earlier investigations have demonstrated that, where polymers are involved, angular distribution measurements are an effective aid in the study of ion source fragmentation processes. The possible danger in the use of thermodynamic data to interpret fragmentation patterns has been clearly demonstrated in the case of Ag<sub>3</sub>Cl<sub>3</sub>. It appears that, in order to obtain the most accurate thermodynamic data by mass spectrometric methods, total ion intensities should be used. This means that it is essential for one to be able to identify the neutral precursor of each ion. Possible exceptions to this requirement include (1) those instances where the cross sections are essentially temperature independent as evidenced by identical heats of vaporization for all ions associated with a given neutral precursor and (2) those instances where the ion intensity contributions from all but one ion are insignificant. Another important and frequently ignored observation is that the heats of vaporization of an ion may change with the energy of the ionizing electrons. Thus when an ion is formed from more than one neutral precursor, heat of vaporization data taken at low-electron energies may differ substantially from data for the same ion taken in the 50–70 eV range.

Shock Tube Cis-Trans Isomerization Studies. II<sup>1</sup>

by Peter M. Jeffers

*Department of Chemistry, State University College, Cortland, New York 13045 (Received April 12, 1972)*

Rates of isomerization of *cis*- and *trans*-1,2-dichloroethylene and *cis*- and *trans*-perfluoro-2-butene were measured relative to *cis*-2-butene isomerization. A  $\frac{3}{4}$ -in. single-pulse shock tube served as the reactor. Rate constants derived for the isomerizations agree well with available results of low-temperature studies. Rate constants found for the temperature range 1050–1350°K are  $\log k_{c \rightarrow t}(C_4F_8) = 13.21 - 54,700/4.58T$ ,  $\log k_{t \rightarrow c}(C_4F_8) = 12.98 - 55,000/4.58T$ ,  $\log k_{c \rightarrow t}(C_2H_2Cl_2) = 12.35 - 53,400/4.58T$ ,  $\log k_{t \rightarrow c}(C_2H_2Cl_2) = 12.26 - 52,700/4.58T$ . Combination of shock tube and low-temperature conventional results yields values of  $\log k_{c \rightarrow t}(C_2H_2Cl_2) = 13.2 - 57,400/4.58T$  and  $\log k_{c \rightarrow t}(C_4F_8) = 13.2 - 54,900/4.58T$ .

Part I of this series reported results on *cis*-*trans* isomerization of *cis*-2-butene and *cis*- and *trans*-1,2-difluoroethylene. It was evident from that work that the shock tube relative rate technique employed was excellently suited for finding the limiting high-pressure rate constants for homogeneous gas-phase isomerization reactions. A recent summary<sup>2</sup> of thermal isomerizations lists only nine studies spread over a 35-year period, and in most of these investigations some difficulties were experienced due to heterogeneous or free-radical catalysis. Neither of these problems arises with the shock tube method. In addition, the shock tube results for a given reaction usually cover a considerably higher temperature range than is found with conventional methods due to the inherent very short residence times. For these reasons, this series of studies continues.

This paper includes results on *cis*- and *trans*-1,2-dichloroethylene which can be compared with the study reported in Part I of difluoroethylene and on *cis*- and *trans*-perfluoro-2-butene which is of interest to compare with both 2-butene and difluoroethylene. There have been conventional studies of *trans*-C<sub>4</sub>F<sub>8</sub><sup>3</sup> and *cis*-C<sub>2</sub>H<sub>2</sub>Cl<sub>2</sub><sup>4</sup> both at a 300° lower temperature range, while study of the reactions in each direction as was done here allows a check for consistency with the known equilibrium constants for these systems.

**Experimental Section**

The 19-mm i.d. Pyrex shock tube has already been described.<sup>1</sup> The only alteration was a new end block still housing a BaTiO<sub>3</sub> pressure-sensing crystal, but with a 1-mm hole leading to a rubber septum through which samples were withdrawn directly into a Precision Sampling Co. gas tight syringe. Direct use of the syringe, a completely grease-free system, gave much better results with dichloroethylene experiments than were obtained in preliminary work where gas samples were withdrawn into sample bulbs and subsequently compressed in a mercury transfer system before being injected into the gas chromatograph. Apparently,

some of the C<sub>2</sub>H<sub>2</sub>Cl<sub>2</sub> absorbed on grease of the shock tube valve, the sampling bulb stopcock or joint, or the stopcocks or joint of the transfer apparatus.

**Materials.** Phillips research grade *cis*-2-butene was used as supplied and contained 0.08% of the *trans* isomer. A *cis*-*trans* mixture of Matheson perfluoro-2-butene was separated using a 6 mm × 15 m column of 20% Kel-F-oil No. 3 (Hewlett-Packard) on 80–100 mesh Chromosorb-P. The column was kept at 0°. About 0.5 ml of the liquid C<sub>4</sub>F<sub>8</sub> mixture (bp 0°) was injected at a time, and two repeat chromatographic separations of the crude products yielded *trans*-C<sub>4</sub>F<sub>8</sub> containing 0.3% of the *cis* isomer and *cis*-C<sub>4</sub>F<sub>8</sub> with 0.8% *trans* impurity. No other impurities were noted. Eastman practical grade 1,2-dichloroethylene (*cis*-*trans* mixture) was separated with a 25 mm × 1.83 m 10% silicon gum rubber column at room temperature. Two chromatographic separations gave 99.97% pure *trans*- and 99.3% pure *cis*-C<sub>2</sub>H<sub>2</sub>Cl<sub>2</sub>, with the other isomer as the only impurity. Linde high-purity Ar was used for sample preparation, and high-purity He served as the driver gas.

**Analysis.** All analyses were performed with a Hewlett-Packard Model 5750 gas chromatograph using the flame ionization detector. Samples containing perfluoro-2-butene and 2-butene were passed through a 6 mm × 1.83 m AgNO<sub>3</sub>-saturated polypropylene glycol column at room temperature, then through a 6 mm × 3.05 m column of Porapak T at 150°. Areas were determined by triangulation, and calibrations indicated the *trans*-C<sub>4</sub>F<sub>8</sub> area had to be multiplied by a factor of 1.03. Mixtures containing dichloroethylene and 2-butene could be separated

(1) Part I: P. M. Jeffers and W. Schaub, *J. Amer. Chem. Soc.*, **91**, 7706 (1969).

(2) S. W. Benson, "Thermochemical Kinetics," Wiley, New York, N. Y., 1968, p 74.

(3) E. W. Schlag and E. W. Kaiser, Jr., *J. Amer. Chem. Soc.*, **87**, 1171 (1965).

(4) L. D. Hawton and G. P. Semeluk, *Can. J. Chem.*, **44**, 2142 (1966).

using only the  $\text{AgNO}_3$  column. The  $\text{trans-C}_2\text{H}_2\text{Cl}_2$  areas were increased by a factor of 1.02. Shocked gas samples were withdrawn from the shock tube into a 2-ml syringe at about 200–400 Torr and were injected directly into the chromatograph. Usually, only a single analysis was performed per shock, although at times a second sample was also processed.

**Shock Experiments.** Mixtures of the reactants were prepared by pressure in a 5000-ml Pyrex bulb. Argon was used to dilute initial concentrations to the 0.02–2% range. Initial test section pressures of the unshocked gas ranged from 150 to 300 Torr. The 0.75-mil Mylar diaphragms ruptured at about 85 psig. These shocks yielded reflected shock temperatures of 1050–1350°K, with density ratio for shocked to unshocked gas of 4.2–5.2. Reflected shock dwell times at the end of the tube were 160–250  $\mu\text{sec}$ .

**Calculations.** Rate constants for the *cis*–*trans* isomerizations were calculated using the integrated rate expression for a reversible first-order process. Equilibrium constants (*cis*  $\rightarrow$  *trans*) used were  $K(\text{C}_4\text{H}_8) = 2.25$ ,<sup>5</sup>  $K(\text{C}_4\text{F}_8) = 1.8$ ,<sup>3</sup> and  $K(\text{C}_2\text{H}_2\text{Cl}_2) = 0.85$ .<sup>4</sup>

## Results

**Perfluoro-2-butene Isomerization.** Three sets of shocks were run with both *cis*-perfluoro-2-butene and *cis*-2-butene initial concentrations of 2, 0.2, and 0.02%. The same initial concentrations were used for three sets of shocks using *trans*- $\text{C}_4\text{F}_8$  with *cis*- $\text{C}_4\text{H}_8$ . Rate constants were evaluated from the measured per cent conversions and the residence times and were plotted as  $\log k(\text{C}_4\text{F}_8)$  vs.  $\log k(\text{C}_4\text{H}_8)$ . It has been shown<sup>1</sup> that the slope of such a relative rate plot gives the ratio of the activation energies for the two systems. With activation energy determined, evaluation of a preexponential factor is a simple matter. The isomerization rates were all measured with *cis*-2-butene as the standard for comparison, and a value of 62.0 kcal/mol was

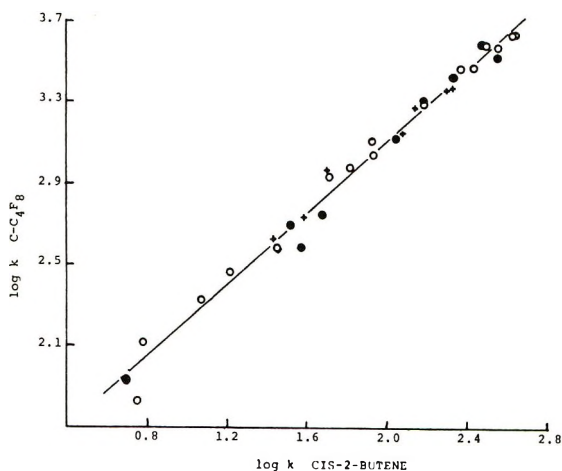


Figure 1. Plot of  $\log k(c \rightarrow t)$  for  $\text{C}_4\text{F}_8$  vs.  $\log k(c \rightarrow t)$  for  $\text{C}_4\text{H}_8$ :  $\circ$ , 2% of each reactant;  $+$ , 0.2% of each reactant;  $\bullet$ , 0.02% of each reactant.

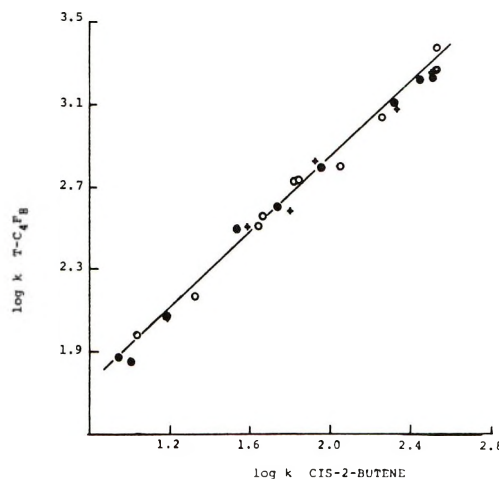


Figure 2. Plot of  $\log k(t \rightarrow c)$  for  $\text{C}_4\text{F}_8$  vs.  $\log k(c \rightarrow t)$  for  $\text{C}_4\text{H}_8$ :  $\bullet$ , 2% of each reactant;  $\circ$ , 0.2% of each reactant;  $+$ , 0.02% of each reactant.

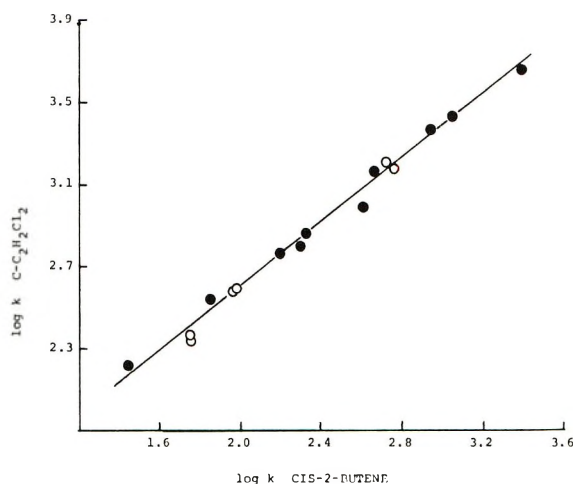


Figure 3. Plot of  $\log k(c \rightarrow t)$  for  $\text{C}_2\text{H}_2\text{Cl}_2$  vs.  $\log k(c \rightarrow t)$  for  $\text{C}_4\text{H}_8$ :  $\circ$ , 0.2% of each reactant;  $\bullet$ , 0.04% of each reactant.

chosen as  $E_a$  for *cis*-2-butene. Results for *cis*- $\text{C}_4\text{F}_8$  are shown in Figure 1. The least-squares slope is  $0.888 \pm 0.03$  which implies an activation energy of  $55.0 \pm 1.9$  kcal/mol. The preexponential factor is then found to be  $10^{13.22 \pm 0.2}$ . The temperature range can be determined from the experimental rate constants for 2-butene and the known Arrhenius parameters, and is 1060–1250°K. *trans*- $\text{C}_4\text{F}_8$  was studied from 1080 to 1240°K, with results as shown in Figure 2. The slope of  $0.893 \pm 0.015$  gives an activation energy of  $55.3 \pm 1.0$  kcal/mol and a preexponential factor of  $10^{13.01 \pm 1.15}$ .

**Dichloroethylene Isomerization.** Three sets of shocks were made with *cis*-1,2-dichloroethylene and *cis*-2-butene mixtures with initial concentrations of each reactant of 2, 0.2, and 0.04%. The slope of the relative rate plot, Figure 3, is  $0.860 \pm 0.03$  which gives  $E_a =$

(5) R. E. Duff and S. H. Bauer, *J. Chem. Phys.*, **36**, 1754 (1962).

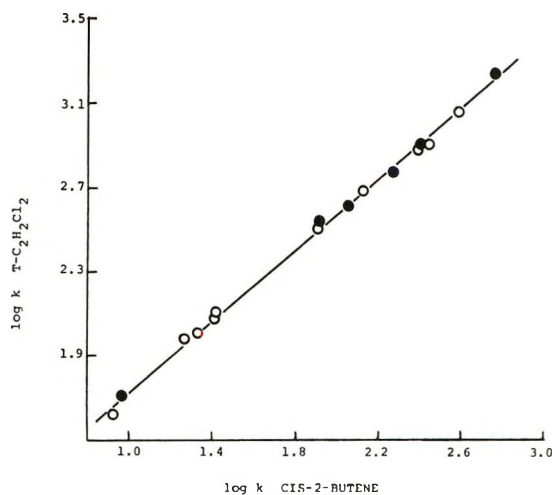


Figure 4. Plot of  $\log k(t \rightarrow c)$  for  $C_2H_2Cl_2$  vs.  $\log k(c \rightarrow t)$  for  $C_4H_8$ :  $\circ$ , 2%  $C_2H_2Cl_2$ -1%  $C_4H_8$ ;  $\bullet$ , 0.2%  $C_2H_2Cl_2$ -0.1%  $C_4H_8$ .

$53.4 \pm 2.0$  kcal/mol and  $\log A = 12.36 \pm 0.3$ . The temperature range is 1120–1350°K. Two series of shocks with *trans*- $C_2H_2Cl_2$  and *cis*- $C_4H_8$  had initial concentrations of 2–1% and 0.2–0.1%, respectively. Figure 4, which shows the results, has slope of 0.85  $\pm$  0.01 and implies a rate constant of  $10^{12.26 \pm 0.1} \exp(-52,700 \pm 600/RT)$  sec<sup>-1</sup> over the temperature range 1080–1275°K.

With the previously stated initial pressures in the shock tube, the shock compression yielded total reaction pressures of 3500–4000 Torr, so that the isomerizations should have all been in the unimolecular high-pressure regions.

The per cent conversion in the isomerizations ranged from 2 to 5% as a lower limit up to as much as 40%. The lower bound was set by the detector sensitivity and by the difficulty of quantitatively measuring conversions just slightly larger than the background impurity level. The upper conversion limit was selected sufficiently below the temperature range where side products appeared to give reasonable assurance that the isomerization was not free-radical catalyzed. All shock experiments where the conversion was acceptable are represented on the relative rate plots.

## Discussion

The comparison standard for the  $C_2H_2Cl_2$  and  $C_4F_8$  isomerizations was *cis*-2-butene, for which a rate constant of  $k_1 = 10^{13.4} \exp(-62,000/RT)$  was chosen. This value is a "rounded off" version of the previously determined<sup>1</sup>  $k_1 = 10^{13.38} \exp(-61,600/RT)$ , and is within the experimental uncertainty. Both the  $A$  factor and the activation energy agree exactly with the values calculated by Benson.<sup>2</sup>

The value found by Schlag and Kaiser<sup>3</sup> for perfluoro-2-butene isomerization is  $k_t = 10^{13.52 \pm 0.11} \exp(-56,400 \pm 160/RT)$  and agrees with the previously stated results within the sum of experimental uncertainties. Using

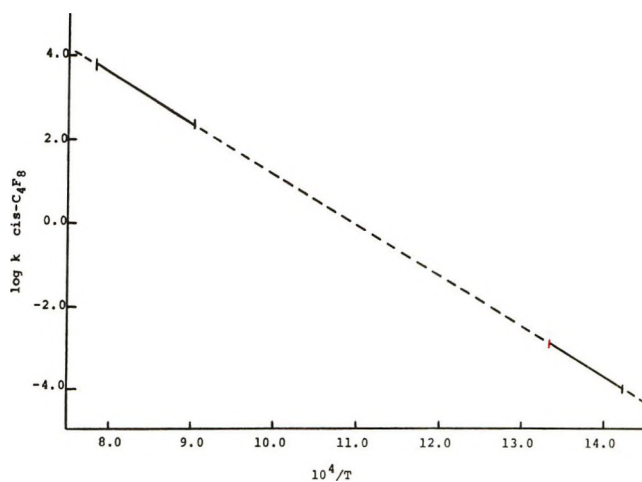


Figure 5. Arrhenius plot for *cis*-perfluoro-2-butene showing low  $T$  results<sup>3</sup> ( $k = 10^{13.42-55,100/4.58T}$ ), high  $T$  results of this study ( $k = 10^{13.21-54,700/4.58T}$ ), and the best line connecting the two sets ( $k = 10^{13.21-54,900/4.58T}$ ).

their values of  $\Delta H(t \rightarrow c) = 816.8$  kcal/mol and  $\Delta S = -0.486$  eu, one finds  $k(c \rightarrow t) = k(t \rightarrow c)/K = 10^{13.42} e^{-55,100/RT}$ . Schlag and Kaiser's results cover the temperature range 703–750°K while the present study was at 1060–1250°K. Plotting both sets of data on a  $\log k$  vs.  $1/T$  graph (Figure 5) and connecting them yields a value of  $k(\text{cis} \rightarrow \text{trans}) = 10^{13.21} \exp(-54,900/RT)$ , in excellent agreement with each individually determined value and especially with the shock tube result. Benson's calculated value for  $\log A$  is 13.1 which is also in excellent agreement.

The ratio of  $k_1/k_{-1}$  for perfluoro-2-butene found here is  $10^{0.23+(300/4.58T)} = 1.9$  at 1200°K, in agreement with  $K_{1200} = 1.8$  deduced from Schlag and Kaiser's<sup>3</sup> thermodynamic parameters. The difference of 300 cal/mol in forward and reverse activation energies agrees reasonably with Schlag and Kaiser's value of  $\Delta H^\circ = 816.8$  cal/mol. The activation energy for *cis*-2-butene now seems rather well established at 62 kcal/mol, so that the decrease in  $E_a$  in going to the perfluoro molecule is about 7 kcal. For comparison, Part I<sup>1</sup> of this series reported  $E_a$  for *cis*-difluoroethylene as 62.8 kcal/mol.

The present study indicated  $k(c \rightarrow t)$  for dichloroethylene to be  $10^{12.36} \exp(-53,400/RT)$ , compared to  $10^{12.76} \exp(-56,000/RT)$  found by Hawton and Semeluk.<sup>4</sup> The agreement in activation energies is probably within experimental error. However, if the shock tube results (1120–1350°K) are combined with the conventional data (807–845°K) on a  $\log k$  vs.  $1/T$  plot, (Figure 6), a value of  $k(c \rightarrow t) = 10^{13.2} \exp(-57,400/RT)$  is obtained. For this reaction Benson<sup>2</sup> calculates  $\log k = 13.2 - 57,000/4.58T$  which is nearly exact agreement. The differences between the relative rate value for *cis*- $C_2H_2Cl_2$  and the value determined from combination of high- and low-temperature data appear surprisingly large in view of the low relative

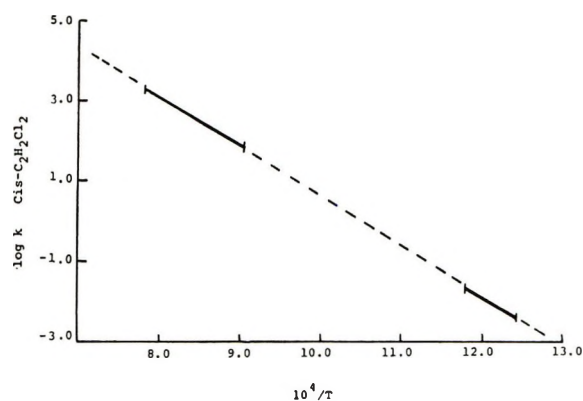


Figure 6. Arrhenius plot for *cis*-1,2-dichloroethylene showing low  $T$  results<sup>4</sup> ( $k = 10^{12.76 - 66,000/4.58T}$ ), high  $T$  results of this study ( $k = 10^{12.36 - 53,400/4.68T}$ ), and the best line connecting the two sets ( $k = 10^{13.2 - 57,400/4.57T}$ ).

rate experimental scatter. However, the value of the log of  $k(\text{relative})/k(\text{combined data})$  is 0.06 at 1120°K and 0.19 at 1350°K, and variations of this amount are not beyond the observed scatter. The experimental section mentions difficulties in preliminary studies of the dichloroethylenes which required development of very careful sample handling procedures. Since the  $\text{C}_2\text{H}_2\text{Cl}_2$  analysis did cause more trouble than usual, some small systematic error could have entered the results.

Hawton and Semeluk's suggested rate constant was obtained by extrapolating to surface/volume ratio = 0, indicating that they experienced some heterogeneous contributions to their reaction. In view of these difficulties, the rate constant obtained by combining the low- and high-temperature studies is undoubtedly the best choice of the three.

The relative rate results for  $\text{C}_2\text{H}_2\text{Cl}_2$  give  $k_1/k_{-1} = 10^{0.09 - (700/4.58T)} = 0.91$  at 1200°K, which is in reasonable agreement with a value of  $K_{1200^\circ} = 0.75$  derived from Pitzer and Hollenberg's<sup>6</sup> thermodynamic data. The difference of 700 cal/mol in forward and reverse activation energies is within experimental limits of  $\Delta H(c \rightarrow t) = 442$  cal/mol.<sup>6</sup>

Only minor differences are found in the preexponential factors of 2-butene, perfluoro-2-butene, difluoroethylene, and dichloroethylene, so that direct comparison of the activation energies might be expected to be meaningful. Table I contains some relevant physical quantities.

Table I

	$E_a$ , kcal/mol	$\Delta H_{298}(\text{hydro-}$ $\text{genation})^a$ , kcal/mol	$r_{\text{C}=\text{C}}^b$ , Å
$\text{C}_2\text{H}_2\text{D}_2^c$	65	-32.7	1.337
$\text{C}_2\text{H}_2\text{F}_2^d$	62	-28.4	1.331
$\text{C}_4\text{H}_8^d$	62	-27.1	1.346
$\text{C}_2\text{H}_2\text{Cl}_2$	57	-32.5	1.354
$\text{C}_4\text{F}_8$	55	-26.2	1.346

<sup>a</sup> Heats of hydrogenation were calculated from known heats of formation or from heats of formation estimated from Benson's tables of group contributions.<sup>2</sup> <sup>b</sup> S. H. Bauer, private communication. <sup>c</sup> B. S. Rabinovitch and F. S. Looney, *J. Chem. Phys.*, **23**, 2439 (1955); **23**, 315 (1955). <sup>d</sup> Reference 1.

The entries in Table I are listed in decreasing order of activation energy, and the same trend is observed in heat of hydrogenation, with the exception of dichloroethylene. Lin and Laidler<sup>7</sup> suggest the correlation  $E_a \approx 2\Delta H(\text{hydrogenation})$  for *cis*-*trans* isomerization, but there are significant deviations from that simple relation. The correlation between activation energies and double bond lengths is not as good as the heat of hydrogenation relation. Both Benson<sup>8</sup> and Lin and Laidler<sup>7</sup> recognize the close and direct relation between double bond strength ( $\Delta H$  for  $\text{RHC}=\text{CHR}' \rightleftharpoons \text{RH}\cdot\text{C}-\text{C}\cdot\text{HR}'$ ) and activation energy for isomerization. However, few data are available on double bond strengths, and estimations<sup>8</sup> require knowledge of specific C-H bond strengths and resonance stabilization energies which are not always available.

In view of the activation energy changes in going from  $\text{C}_2\text{H}_2\text{D}_2$  to  $\text{C}_2\text{H}_2\text{F}_2$  to  $\text{C}_2\text{H}_2\text{Cl}_2$  and from  $\text{C}_4\text{H}_8$  to  $\text{C}_4\text{F}_8$ , investigation of  $\text{C}_4\text{Cl}_8$  could prove quite interesting.

*Acknowledgments.* The author would like to thank the State University of New York Research Foundation for financial support of this project. The following undergraduate students contributed to the development of this work: Thomas McCarrick, David Tyminski, Ronald Yost, Water Schaub, and Robert Utter.

(6) K. S. Pitzer and J. L. Hollenberg, *J. Amer. Chem. Soc.*, **76**, 1493 (1954).

(7) M. C. Lin and K. J. Laidler, *Can. J. Chem.*, **46**, 973 (1968).

(8) S. W. Benson, D. M. Golden, and K. Egger, *J. Amer. Chem. Soc.*, **87**, 468 (1965).

# Gas-Phase Homogeneous Catalysis in Shock Waves. III. The Oxidation of Carbon Monoxide by Oxygen in the Presence of Nickel Carbonyl

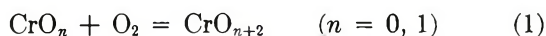
by Shimpei Matsuda<sup>1</sup>

Department of Chemistry, Harvard University, Cambridge, Massachusetts 02138 (Received March 3, 1972)

The oxidation of carbon monoxide by oxygen in the presence of small amounts of nickel tetracarbonyl was investigated in incident and reflected shock waves. A reaction mixture, typically containing 300 ppm of Ni(CO)<sub>4</sub>, 4% CO, and 2% O<sub>2</sub> in Ar, was shock heated to temperatures between 1100 and 2400°K at a total concentration of  $6 \times 10^{17}$  molecules/cc in incident shock waves. The CO<sub>2</sub> formation was followed by the infrared emission at 4.27  $\mu$  over 2-msec particle time. The CO<sub>2</sub> concentration was found to increase linearly with time, the rate of CO oxidation being much greater than in the absence of Ni(CO)<sub>4</sub>. A time-of-flight mass spectrometer coupled to a shock tube was used to investigate the formation of transient species containing Ni during the reaction behind reflected shock waves. Mass peaks due to Ni and NiO were identified, the peak height of the latter species being less than 10% of the former. A cyclic process involving Ni, NiO, and NiCO is proposed to account for the homogeneous catalytic oxidation of CO in the presence of Ni(CO)<sub>4</sub>.

## Introduction

The acceleration of combustion reactions by the addition of small amounts of metallic compounds has been a subject of several studies. Thus induction periods of the flash-initiated C<sub>2</sub>H<sub>2</sub>-O<sub>2</sub> reaction were shortened by the addition of Ni(CO)<sub>4</sub>, Fe(CO)<sub>5</sub>, and Cr(CO)<sub>6</sub>.<sup>2a</sup> The C<sub>2</sub>H<sub>2</sub>-O<sub>2</sub> reaction in shock waves (which is a strictly homogeneous system) is greatly enhanced in the presence of only 10 ppm of Cr(CO)<sub>6</sub>.<sup>2b</sup> The strong catalytic effects of Cr(CO)<sub>6</sub> and Fe(CO)<sub>5</sub> on the oxidation of carbon monoxide in shock waves have been thoroughly studied by Kistiakowsky and co-workers.<sup>3,4</sup> In the case of the Cr(CO)<sub>6</sub>-CO-O<sub>2</sub> reaction the formation of Cr, CrO, CrO<sub>2</sub>, and CrO<sub>3</sub> in steady-state concentrations was confirmed by means of a time-of-flight mass spectrometer coupled to a shock tube and a catalytic chain process



has been proposed.<sup>3</sup> A similar mechanism was proposed for the Fe(CO)<sub>5</sub>-CO-O<sub>2</sub> reaction.<sup>4</sup>

The spontaneous ignition of Ni(CO)<sub>4</sub> as well as the combustion of *n*-butane induced by Ni(CO)<sub>4</sub> have been studied by several workers.<sup>5-8</sup> The mechanism, however, is not well understood, mainly because of the heterogeneous nature of the reaction.

Nickel oxide as well as Fe<sub>2</sub>O<sub>3</sub> and Cr<sub>2</sub>O<sub>3</sub> are good catalysts for the CO oxidation in the gas-solid heterogeneous reaction systems.<sup>9,10</sup> The purpose of this paper is to present details of the homogeneous catalytic effect of Ni, added in the form of Ni(CO)<sub>4</sub>, on the CO-O<sub>2</sub> reaction. Shock waves have proved to be the ideal media for this type of study.

## Experimental Section

**Apparatus.** A 3-in. i.d. shock tube equipped with two InSb infrared detectors (IRST apparatus) has been described in detail previously.<sup>11,12</sup> One infrared detector monitored the emission at 4.20  $\mu$  from CO<sub>2</sub> and the other the emission at 5.03  $\mu$  from CO. The emission intensity at 4.20  $\mu$  was calibrated to absolute CO<sub>2</sub> concentration by shock heating known CO<sub>2</sub>-Ar mixtures over a temperature range used in this study. Shocks were generated in 5 or 10 Torr of reactant mixtures using He or He-N<sub>2</sub> as a driver gas.

A 1-in. i.d. shock tube coupled to a time-of-flight mass spectrometer (TOFST apparatus) has also been described previously.<sup>13,14</sup> Consecutive mass spectra of a shocked gas flowing into the ion source of the time-

(1) Present address: Department of Chemistry, Cornell University, Ithaca, N. Y. 14850.

(2) (a) K. Erhard, *Z. Phys. Chem. (Frankfurt am Main)*, **36**, 126 (1963); (b) S. Matsuda and D. Gutman, *J. Phys. Chem.*, **75**, 2402 (1971).

(3) T. P. J. Izod, G. B. Kistiakowsky, and S. Matsuda, *J. Chem. Phys.*, **56**, 1083 (1972).

(4) S. Matsuda, *ibid.*, **57**, 807 (1972).

(5) E. J. Badin, P. C. Hunter, and R. N. Pease, *J. Amer. Chem. Soc.*, **70**, 2055 (1948).

(6) A. P. Garrat and H. W. Thompson, *J. Chem. Soc.*, 1822 (1934).

(7) C. E. H. Bawn, *Trans. Faraday Soc.*, **31**, 440 (1935).

(8) A. Egerton and S. Rudrakanchana, *Proc. Roy. Soc., Ser. A*, **225**, 427 (1954).

(9) M. Katz, *Advan. Catal.*, **8**, 177 (1953).

(10) J. K. Dixon and J. E. Longfield, "Catalysis," Vol. III, P. H. Emmett, Ed., Reinhold, New York, N. Y., 1960, p 281.

(11) A. M. Dean and G. B. Kistiakowsky, *J. Chem. Phys.*, **53**, 830 (1970).

(12) J. B. Homer and G. B. Kistiakowsky, *ibid.*, **46**, 4213 (1967).

(13) J. E. Dove and D. McL. Moulton, *Proc. Roy. Soc., Ser. A*, **283**, 216 (1965).

(14) I. D. Gay, G. B. Kistiakowsky, J. V. Michael, and H. Niki, *J. Chem. Phys.*, **43**, 1720 (1965).

of-flight mass spectrometer through a pin hole in the end wall of the shock tube were displayed on oscilloscopes every 20  $\mu\text{sec}$  over a total observation time of about 200  $\mu\text{sec}$  and recorded photographically. Mass spectra covered a range of  $m/e$  50 to 110. The ionizing electron energy was 22.5 eV in all experiments.

**Material.** Matheson research grade  $\text{CO}_2$ ,  $\text{O}_2$ , and Ar were used without further purification. Matheson research grade CO was passed through a packed column cooled at liquid nitrogen temperature before use. Matheson tank  $\text{Ni}(\text{CO})_4$  was vacuum distilled several times before use. In TOFST experiments Matheson research grade premixed  $\text{O}_2$ -Ne (8/92) gas was used without further purification.

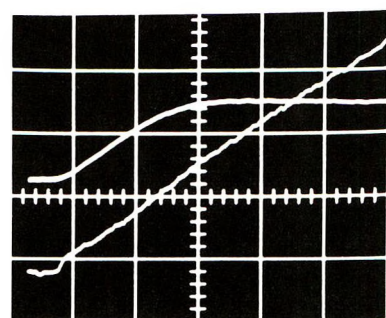
**Preparation of Gas Mixture.** Mixtures of  $\text{Ni}(\text{CO})_4$  and  $\text{O}_2$  ignite spontaneously after an induction period at room temperature.<sup>5-8</sup> Therefore, mixtures of  $\text{Ni}(\text{CO})_4$ -Ar and  $\text{CO}$ - $\text{O}_2$ -Ar were prepared and stored separately. All gas mixtures used in IRST experiments are listed in Table I. Mixture A was prepared from a mixture containing 3%  $\text{Ni}(\text{CO})_4$  in Ar. For each series of experiments with one of mixtures B-F a new sample of mixture A was prepared in order to avoid the change in  $\text{Ni}(\text{CO})_4$  concentration during storage, because the dissociation of  $\text{Ni}(\text{CO})_4$  might be appreciable even at room temperature.<sup>5-7, 15, 16</sup> All gas mixtures were used within 48 hr of preparation.

**Table I:** Composition of Reaction Mixtures

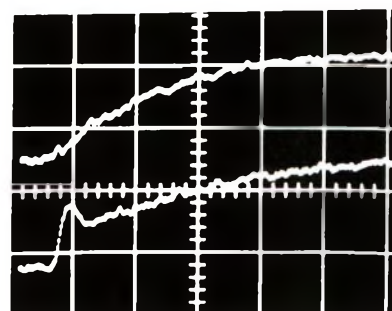
Mixture	$\text{Ni}(\text{CO})_4$ , ppm	$\text{CO}$ , %	$\text{O}_2$ , %	Ar, %
A	570			99.9
B		8.04	4.03	87.9
C		12.8	4.12	83.1
D		4.42	8.58	87.0
E		7.47	7.10	85.4
F		8.07	4.22	87.7

In IRST experiments the mixing of mixture A with one of mixtures B-F was carried out in the vacuum system ( $\approx 2$  l.) about 3 min before each shock experiment and the thus prepared  $\text{Ni}(\text{CO})_4$ - $\text{CO}$ - $\text{O}_2$ -Ar mixture was introduced into the shock tube approximately 1 min before shock firing. Usually a  $\text{CO}$ - $\text{O}_2$ -Ar mixture was introduced into the vacuum system first and then about an equal amount of the  $\text{Ni}(\text{CO})_4$ -Ar mixture. Since the duration for mixing is likely to be too short for complete mixing, the order of the introduction of two gases was reversed in some experiments. As will be shown later the rate of  $\text{CO}_2$  formation was not affected by this.

In TOFST experiments 0.2 Torr of  $\text{Ni}(\text{CO})_4$  vapor was mixed with 40 Torr of the  $\text{O}_2$ -Ne gas in the vacuum line about 5 min before each shock experiment. The  $\text{Ni}(\text{CO})_4$ - $\text{O}_2$ -Ne mixture was then introduced into the



(a)



(b)

Figure 1. Reaction profiles of the  $\text{Ni}(\text{CO})_4$ - $\text{CO}$ - $\text{O}_2$  reaction at high and low temperatures. (a) For reaction conditions see Table I. Upper trace, CO emission at 5.03  $\mu$ , 100 mV/division; lower trace,  $\text{CO}_2$  emission at 4.20  $\mu$ , 50 mV/division; one division corresponds to  $3.3 \times 10^{14}$   $\text{CO}_2$  molecules/cc. (b) mixture B + A,  $T_2 = 1268^\circ\text{K}$ ,  $(\text{Ni})_0 = 1.66 \times 10^{14}$ ,  $(\text{CO}) = 2.34 \times 10^{16}$  molecules/cc. Upper trace, CO emission, 20 mV/division; lower division,  $\text{CO}_2$  emission 20 mV/division; one division corresponds to  $2.6 \times 10^{14}$   $\text{CO}_2$  molecules/cc. Sweep time is 50  $\mu\text{sec}$ /division for all traces. Time increases from left to right. Arrival of shock waves is indicated by a sharp rise in the  $\text{CO}_2$  signals.

shock tube and the experiment completed within 1 min. It was found with the mass spectrometer that no  $\text{CO}_2$  was formed during the 5 min of mixing.

## Results

Figure 1 shows the typical reaction profiles in IRST experiments. The profile given in Figure 1a was observed in all experiments performed above  $1600^\circ\text{K}$ . The  $\text{CO}_2$  emission signal is seen to rise sharply upon shock arrival; after 40  $\mu\text{sec}$  particle time the  $\text{CO}_2$  concentration increases at a slower constant rate which is still much greater than in the absence of  $\text{Ni}(\text{CO})_4$ .<sup>11</sup> The initial sharp rise in the  $\text{CO}_2$  signal was unobservable above  $2200^\circ\text{K}$ . The amount of  $\text{CO}_2$  formed in this initial stage of the reaction was greater at lower temperatures. The linear growth region in the  $(\text{CO}_2)$  vs.

(15) A. Mittasch, *Z. Phys. Chem.*, 40, 1 (1902).

(16) J. P. Day, R. G. Pearson, and F. Basolo, *J. Amer. Chem. Soc.*, 90, 6933 (1968).

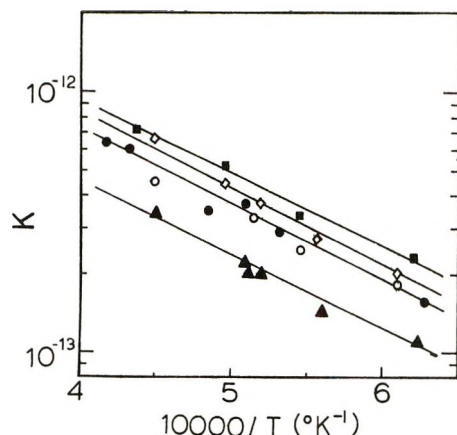


Figure 2. Plots of  $K (= d(\text{CO}_2)/dt/(\text{Ni})_0(\text{CO}))$  vs.  $10,000/T$  ( $K$  is in units of cc/molecules sec):  $\blacktriangle$ , mixture C + A;  $\bullet$ , mixture B + A;  $\circ$ , mixture F + A;  $\diamond$ , mixture E + A;  $\blacksquare$ , mixture D + A.

time plot was used to calculate the rates of  $\text{CO}_2$  formation. These rates of  $\text{CO}_2$  formation at high temperatures as well as experimental conditions are summarized in Table II and the rates of  $\text{CO}_2$  formation normalized by  $(\text{Ni})_0(\text{CO})$ , where  $(\text{Ni})_0$  is the initial concentration of  $\text{Ni}(\text{CO})_4$ , are plotted against  $T^{-1}$  in Figure 2.

Figure 1b shows a typical reaction profile at lower temperatures ( $<1400^\circ\text{K}$ ). It is seen that the  $\text{CO}_2$  emission signal rises very sharply upon shock heating, overshoots, and then after  $80 \mu\text{sec}$  (particle time) continues to rise slowly but not linearly with time. Similar observations were reported in the  $\text{Cr}(\text{CO})_6\text{-CO-O}_2$  and  $\text{Fe}(\text{CO})_5\text{-CO-O}_2$  reactions at lower temperatures.<sup>3,4</sup> It was observed that the overshoot in the  $\text{CO}_2$  emission signal was greater as the reaction temperature was lowered. The initially formed  $\text{CO}_2$ ,  $(\text{CO}_2)_i$ , is plotted against temperature in Figure 3 for a series of experiments with mixture B + A and F + A. It is seen that

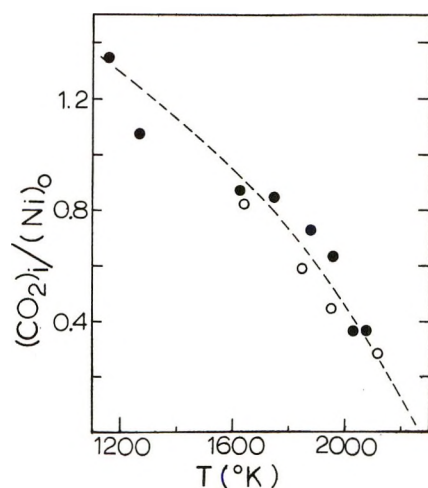


Figure 3. Plots of  $(\text{CO}_2)_i/(\text{Ni})_0$  vs. temperature for mixtures B + A and F + A.

Table II: Rate of  $\text{CO}_2$  Formation in the  $\text{Ni}(\text{CO})_4\text{-CO-O}_2$  Reaction

$T_1$ , $^\circ\text{K}$	$(\text{Ni})_0^a \times$ $10^{-14}$ , molecules/ cc	$(\text{CO}) \times$ $10^{-16}$ , molecules/ cc	$R^b \times$ $10^{-18}$ , molecules/ cc sec	$R/(\text{Ni})_0(\text{CO})$ $\times 10^{+13}$ , cc/molecules sec
Mixture B + A (1:1) <sup>c</sup>				
2390	1.59	2.37	2.41	6.40
2309	1.81	2.23	2.44	6.05
2070	2.00	2.32	1.59	3.43
1960	2.06	2.62	2.02	3.74
1882	1.69	2.27	1.12	2.92
1749	1.57	2.28	0.88	2.46
Mixture A + B (1:1)				
2404	1.62	2.16	2.96	6.17
2137	1.76	2.20	1.50	3.88
2014	1.67	2.16	1.32	3.53
Mixture C + A (1:1), Low Pressure				
2214	1.86	4.01	2.55	3.42
1963	1.92	4.55	1.88	2.15
1957	1.85	4.13	1.58	2.07
1922	1.67	3.89	1.32	2.03
1782	1.79	3.94	1.02	1.45
1601	1.80	4.12	0.83	1.11
Mixture C + A (1:1), High Pressure				
1928	3.20	7.21	3.84	1.67
1741	4.24	7.87	4.31	1.29
Mixture C + A (2:1)				
2044	1.18	5.47	1.73	2.18
1889	1.15	5.17	1.12	1.88
Mixture D + A (1:1)				
2293	1.91	1.35	1.86	7.22
2028	1.88	1.58	1.56	5.25
1831	1.93	1.50	0.95	3.26
1611	1.64	1.32	0.51	2.37
Mixture E + A (1:1)				
2231	1.62	2.27	2.54	6.90
2056	1.77	2.23	1.78	4.52
1926	1.87	2.58	1.80	3.73
1803	1.84	2.34	1.13	2.62
1642	1.54	2.18	3.22	1.94
Mixture F + A (1:1)				
2222	1.83	2.51	2.04	4.44
1945 <sup>d</sup>	1.58	2.46	1.27	3.26
1827	1.91	2.55	1.20	2.47
1637	1.63	2.42	0.72	1.82

<sup>a</sup> Initial concentration of  $\text{Ni}(\text{CO})_4$ . <sup>b</sup>  $R = d(\text{CO}_2)/dt =$  rate of  $\text{CO}_2$  formation. <sup>c</sup> Gas mixtures are listed in the order of the introduction to the vacuum system (see text). An approximate ratio of two mixtures is given in bracket. <sup>d</sup> Oscillogram from this experiment in Figure 1a.

the amount of  $\text{CO}_2$  formed at the initial stage of the reaction corresponds approximately to the initial concentration of  $\text{Ni}(\text{CO})_4$  at  $1400^\circ\text{K}$ .

As already noted the reactivity of  $\text{Ni}(\text{CO})_4$  toward  $\text{O}_2$  required fast mixing of  $\text{Ni}(\text{CO})_4\text{-Ar}$  with  $\text{CO-O}_2\text{-Ar}$  mixtures. Therefore, the effect of the sequence of gas introduction on the rate of  $\text{CO}_2$  formation was studied

using mixtures A and B. In the first series of experiments mixture B was introduced into the vacuum line first and then mixture A; in the second series the sequence was reversed. The results are given in Table II, which shows that the sequence of gas introduction has little effect on the measured rate of CO<sub>2</sub> formation, so that the homogeneity of the reactant gases was adequate despite the short mixing time. However, it should be noted that the scatter in the present data was considerably larger than that in the Cr(CO)<sub>6</sub>-CO-O<sub>2</sub> or Fe(CO)<sub>5</sub>-CO-O<sub>2</sub> experiments.<sup>3,4</sup>

The dependence of the rate of CO<sub>2</sub> formation on the total and on the Ni(CO)<sub>4</sub> concentration was investigated by shocking mixture C + A at 5 and 10 Torr initial pressures with the mixture ratio A/C = 1 and at 5 Torr with the mixture ratio A/C = 0.5, respectively. The results in Table II show that the rate of CO<sub>2</sub> formation depends approximately on the square of the total concentration and linearly on the Ni(CO)<sub>4</sub> concentration.

The dependence of the rate of CO<sub>2</sub> formation on the (CO)/(O<sub>2</sub>) ratio was investigated using mixtures A-E. The results are also given in Table II. Since the rate of CO<sub>2</sub> formation depends on the square of concentrations, the rate of CO<sub>2</sub> formation normalized by (Ni)<sub>0</sub>(CO) is plotted against  $T^{-1}$  in Figure 2. The rate of CO<sub>2</sub> formation is seen to have an apparent activation energy of about 13 kcal/mol for all mixtures and to depend only slightly on the O<sub>2</sub> concentration for mixtures with the (CO)/(O<sub>2</sub>) ratio less than 2. Empirically the rate of CO<sub>2</sub> formation is given by

$$\frac{d(\text{CO}_2)}{dt} = 1.1 \times 10^{-11} (\pm 20\%) \times \exp\left(-\frac{13 \pm 2 \text{ kcal/mol}}{RT}\right) (\text{Ni})_0^{1.0} (\text{CO})^{0.8} (\text{O}_2)^{0.2} \quad (\text{I})$$

(molecules/cc sec)

when the (CO)/(O<sub>2</sub>) ratio is less than 2. The order of dependence on (O<sub>2</sub>) (or (CO)) in eq I was obtained in the plot of  $\log [(d(\text{CO}_2)/dt)/(\text{Ni})_0(\text{CO})]$  vs.  $\log [(CO)/(O_2)]$ . Equation I is presented here for comparison with the Cr(CO)<sub>6</sub>-CO-O<sub>2</sub> and Fe(CO)<sub>5</sub>-CO-O<sub>2</sub> reaction systems<sup>3,4</sup> and to show the overall rate constant of the reaction. The correct functional dependence of the rate of CO<sub>2</sub> formation on the O<sub>2</sub> and CO concentration will be discussed later. It was found that the rate of CO<sub>2</sub> formation depends more on the O<sub>2</sub> concentration when the (CO)/(O<sub>2</sub>) ratio exceeds 2.

It was feared that in the mixture containing 3% Ni(CO)<sub>4</sub> in Ar from which mixture's A were prepared the Ni(CO)<sub>4</sub> concentration changed by decomposition during the course of the experiments. Therefore the last series of experiments was undertaken with mixtures A and F which had nearly the same composition as mixtures A and B. The results, given in Figure 2,

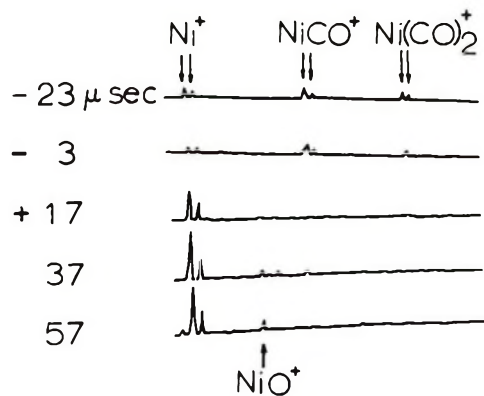


Figure 4. Tracing of consecutive mass spectra from a TOFST experiment:  $T_s = 2060^\circ\text{K}$ ;  $C_s = 1.1 \times 10^{18}$  molecules/cc. Time with respect to the shock reflection is given at the left of each mass spectra.

show that there is little difference in the rates of CO<sub>2</sub> formation between mixture B + A and F + A.

**TOFST Experiments.** About 10 shocks were performed with a mixture containing 0.5% Ni(CO)<sub>4</sub> and 8% O<sub>2</sub> in Ne between 1600 and 2400°K, so that this mixture contained 2% CO from the decomposition of Ni(CO)<sub>4</sub> upon shock heating. Figure 4 shows a tracing of consecutive mass spectra from a typical TOFST experiment at high temperatures (>2000°K). It is seen that the decomposition of Ni(CO)<sub>4</sub> is very rapid, the half-life of Ni(CO)<sub>4</sub> being much less than 20 μsec at 2060°K and at a total concentration of  $1.1 \times 10^{18}$  molecules/cc. After shock heating mass peaks due to Ni<sup>+</sup> ( $m/e$  58 and 60) and NiO<sup>+</sup> ( $m/e$  74) were observed. The peak height of NiO<sup>+</sup> was only 10% of Ni<sup>+</sup>. Although very small NiCO<sup>+</sup> peaks were observed frequently in mass spectra, the existence of NiCO in appreciable amounts could not be conclusively shown.

Below 1900°K Ni<sup>+</sup> and NiO<sup>+</sup> were not observed in mass spectra taken 40 μsec after shock heating (Ni<sup>+</sup> was observed in a mass spectrum taken within 20 μsec), although the disappearance of Ni(CO)<sub>n</sub><sup>+</sup> ( $n = 1,2$ ) peaks clearly showed that more than 90% of Ni(CO)<sub>4</sub> decomposed within 40 μsec. This indicated that Ni atoms formed from the decomposition of Ni(CO)<sub>4</sub> were removed from the gas phase by a condensation process, the Ni vapor being highly supersaturated below 1900°K.<sup>17</sup> The same phenomenon, a rapid condensation of Cr and Fe vapor from supersaturated gases, has been reported in the Cr(CO)<sub>6</sub>-CO-O<sub>2</sub><sup>3</sup> and Fe(CO)<sub>5</sub>-CO-O<sub>2</sub><sup>4</sup> studies.

## Discussion

The vaporization of a solid NiO has been studied by Grimley, *et al.*,<sup>18</sup> the vapor phase species containing

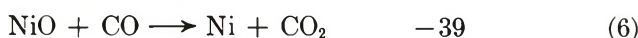
(17) R. C. Weast, Ed., "Handbook of Chemistry and Physics," 51st ed, Chemical Rubber Publishing Co., Cleveland, Ohio, 1970.

(18) R. T. Grimley, R. P. Burns, and M. G. Ingram, *J. Chem. Phys.*, **35**, 551 (1961).

Ni detected by a mass spectrometer as Ni and NiO. No additional species were formed even under conditions of increased oxygen partial pressure. Using their raw data for the equilibrium constant of the reaction



it can be calculated that  $(\text{NiO})_{\text{eq}}/(\text{Ni})_{\text{eq}} \approx 0.5$  at 1709°K and at an oxygen partial pressure of  $1 \times 10^{-3}$  atm. In the present study with the TOFST apparatus it was found that  $(\text{NiO})/(\text{Ni}) < 0.1$  at 2060°K, which is much less than the equilibrium value extrapolated to the same temperature using the data in ref 18. Therefore, it may be concluded that the observed  $(\text{NiO})/(\text{Ni})$  ratio represents a steady-state value during the Ni-CO-O<sub>2</sub> reaction instead of an equilibrium value. First consider a mechanism which is similar to the one proposed for the catalytic oxidation of CO in the presence of Cr(CO)<sub>6</sub>.<sup>3</sup>



For the calculation of the heat of reaction the dissociation energy of NiO was taken from ref 18 and the heat of formation of other species from ref 19. It should be noted that the reaction



has been specifically excluded from the present scheme because the rate of CO<sub>2</sub> production in reaction 7 is less than 5% of the observed rate of CO<sub>2</sub> formation even at the highest temperatures employed in this study.<sup>11</sup> Using a steady-state assumption for Ni and NiO concentrations and a mass balance equation, *i.e.*,  $(\text{Ni})_{\text{ss}} + (\text{NiO})_{\text{ss}} = (\text{Ni})_0$ , we obtain

$$\frac{d(\text{CO})_2}{dt} = (\text{Ni})_0 \left/ \left( \frac{1}{k_5(\text{O}_2)} + \frac{1}{k_6(\text{CO})} \right) \right. \quad (\text{II})$$

$$(\text{NiO})_{\text{ss}}/(\text{Ni})_{\text{ss}} = k_5(\text{O}_2)/k_6(\text{CO}) \quad (\text{III})$$

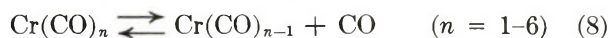
Since it was found that  $(\text{NiO})_{\text{ss}}/(\text{Ni})_{\text{ss}} \ll 1$ , *i.e.*,  $k_6(\text{CO}) \gg k_5(\text{O}_2)$ , eq II reduces to

$$d(\text{CO}_2)/dt \approx k_5(\text{Ni})_0(\text{O}_2) \quad (\text{IV})$$

which is not consistent with the experimental finding that the rate of CO<sub>2</sub> formation is strongly dependent on the CO concentration (see eq I).

The study of the Cr(CO)<sub>6</sub> decomposition (0.4% Cr(CO)<sub>6</sub> in Ne) using the TOFST apparatus showed that the CrCO<sup>+</sup> and Cr(CO)<sub>2</sub><sup>+</sup> peaks disappeared completely within 40 μsec of the shock reflection above 1500°K.<sup>3</sup> At lower temperatures (<1200°K) the CrCO<sup>+</sup> and Cr(CO)<sub>2</sub><sup>+</sup> peak height decreased rapidly to some low levels after 20 μsec but then decreased very

slowly, being observable even at 150 μsec.<sup>20</sup> This suggests that the reaction



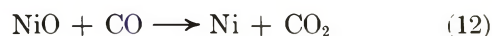
is measurably reversible at these low temperatures.

The average metal-carbon monoxide bond energy in Cr(CO)<sub>6</sub>, Fe(CO)<sub>5</sub>, and Ni(CO)<sub>4</sub> is estimated to be 27.1, 27.7, and 35.2 kcal/mol, respectively.<sup>21</sup> Thus, since the metal-carbon monoxide bond is considerably stronger in Ni(CO)<sub>4</sub>, it may be suggested that the reverse reaction in



remains significant to higher temperatures than in the Cr(CO)<sub>6</sub> and Fe(CO)<sub>5</sub> cases, although NiCO stays in such low concentrations that is not reliably observable by the present TOFST apparatus.

The following mechanism is proposed



The concentration of Ni(CO)<sub>2</sub> being very low, it is not included in the mechanism. Using a steady-state assumption for Ni, NiO, and NiCO (steady-state concentrations are attained within 50 μsec, see also Figure 1a) the rate of CO<sub>2</sub> formation is obtained as

$$\frac{d(\text{CO})_2}{dt} = \frac{2k_{10}(\text{Ni})_0(\text{CO})}{\frac{k_{-10}}{k_{11}(\text{O}_2)} + 1} \quad (\text{V})$$

where the relation  $(\text{Ni})_0 \approx (\text{Ni})_{\text{ss}}$  is used. In the IRST experiments it was found that the rate of CO<sub>2</sub> formation depends almost linearly on the CO concentration, which follows if  $k_{11}(\text{O}_2)$  is larger than  $k_{-10}$  in eq V. The observation that the dependence of the rate on the O<sub>2</sub> concentration becomes stronger as the latter decreases (mixture C and A, see Figure 2) also follows if  $k_{11}(\text{O}_2)$  is not very much greater than  $k_{-10}$ . The greater rate of CO<sub>2</sub> formation at the very initial stage of the reaction (see Figure 1a) could be due to the NiCO concentration being greater in the initial stage of the reaction, since then NiCO is formed in a stepwise dissociation of Ni(CO)<sub>4</sub>



The fast initial rate of CO<sub>2</sub> formation indicates that reaction 11'



competes with reaction 13. Since the rate constant of

(19) D. R. Stoll, Ed., "JANAF Thermochemical Table," Dow Chemical Co., Midland, Mich., 1965.

(20) S. Matsuda, unpublished results.

(21) F. A. Cotton, A. K. Fisher, and G. Wilkinson, *J. Amer. Chem. Soc.*, **81**, 800 (1959).

reaction 13 must be at least of the order of  $1 \times 10^5$   $\text{sec}^{-1}$ ,  $k_{11}$  (or  $k_{11'}$ ) has to be of the order of  $1 \times 10^{-11}$   $\text{cc/molecules sec}$  at about  $2000^\circ\text{K}$ .

In the IRST experiments the Ni vapor pressure exceeds the equilibrium pressure by a factor of 10 around  $1600^\circ\text{K}$ . Therefore, a rapid condensation of Ni vapor could be expected below  $1600^\circ\text{K}$ , this explaining that the linear growth of the  $\text{CO}_2$  formation was not observed below  $1600^\circ\text{K}$ . The overshoot in the  $\text{CO}_2$  emission signal observed below  $1400^\circ\text{K}$  (see Figure 1b) indicates that  $\text{CO}_2$  molecules formed in reaction 11 are vibrationally excited.<sup>4</sup> Taking 35 kcal/mol for the Ni-CO bond energy<sup>21</sup> reaction 11 is found indeed to be exothermic by 60 kcal/mol which is sufficient to produce  $\text{CO}_2$  molecules in vibrationally excited states.

Finally the effect of nonidealities of shock waves due to a boundary layer growth should be mentioned briefly, since the initial pressures employed in this study were fairly low (5 and 10 Torr). The importance of corrections due to nonideal flow was emphasized by Belford and Strehlow<sup>22</sup> who presented simplified

formulas for these corrections using a theory developed by Mirel.<sup>23</sup> Under the present conditions these non-idealities (increase in density, temperature, etc.) change the observed rate of  $\text{CO}_2$  formation consistently by about 15%. Therefore, the effects of a boundary layer growth do not change the conclusion of this study but numerically the rate constants should be reduced by about 15%.

*Acknowledgment.* The author wishes to thank Professor G. B. Kistiakowsky for the use of his laboratory which made this work possible and also for helpful discussions in the course of the work. The author also thanks Dr. T. P. J. Izod, Mr. R. Santro, and Mrs. M. Matsuda for their assistance in the experiments. In addition the author thank the National Science Foundation for a grant which made this work possible.

(22) R. L. Belford and R. A. Strehlow, *Annu. Rev. Phys. Chem.*, **20**, 247 (1969).

(23) H. Mirel, *Phys. Fluids*, **6**, 1201 (1963); **9**, 1907 (1966); *AIAA J.*, **2**, 84 (1964).

## Ultrasonic Attenuation in Basic Purine Solutions<sup>1</sup>

by Maureen Brennan and Kenneth Kustin\*

*Department of Chemistry, Brandeis University, Waltham, Massachusetts 02154 (Received June 16, 1972)*

*Publication costs assisted by the National Institute of General Medical Sciences*

The kinetics of the reaction  $\text{PH} + \text{OH}^- \rightleftharpoons \text{P}^- + \text{H}_2\text{O}$  (1), where PH and  $\text{P}^-$  represent purine and purinate ion, respectively, have been determined by an ultrasonic attenuation technique. The effect of a dimerization process (formation of  $(\text{PH})_2$ ) on the equilibrium purine concentration has been included in the kinetic analysis. Measurements were performed at  $25^\circ$ , pH 9.88, and in an ionic strength range 0.6–1.0  $M$ . The measured rate constants are  $k_f = (1.13 \pm 0.05) \times 10^{10} M^{-1} \text{sec}^{-1}$  and  $k_r = (4.0 \pm 2.0) \times 10^6 \text{sec}^{-1}$ .

Studies on the kinetics of protolytic reactions in basic media have been reported for some substituted purines.<sup>2</sup> However, for purine itself, the kinetics have been studied only in an acidic medium.<sup>3</sup> There is strong evidence that purine is highly associated in aqueous solutions.<sup>4–9</sup> The equilibrium of the postulated molecular stacking process has been studied using osmotic pressure techniques.<sup>4</sup> In addition, the effect of polymerization on the rate of proton transfer in an acidic medium has been considered.<sup>3</sup> Thus far, however, the kinetics of stacking have not been directly examined. We are reporting on an ultrasonic absorption study of basic aqueous purine to gain insight into the kinetics of processes in these solutions.

The sound absorption technique is applicable to the measurement of relaxation processes in the range  $2 \times$

(1) The authors gratefully acknowledge support from Public Health Service Research Grant No. GM-08893-10 from the National Institute of General Medical Sciences.

(2) H. G. Busse and G. Maass, *Z. Phys. Chem. (Frankfurt am Main)*, **66**, 92 (1969).

(3) T. H. Marshall and E. Grunwald, *J. Amer. Chem. Soc.*, **91**, 4541 (1969).

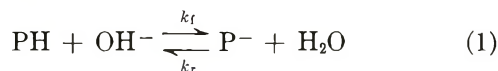
(4) P. O. P. T'so, I. S. Melvin, and A. C. Olsen, *ibid.*, **85**, 1289 (1963).

(5) S. I. Chan, M. P. Schweizer, P. O. P. T'so, and G. K. Helmkamp, *ibid.*, **86**, 4182 (1964).

(6) S. J. Gill, M. Downing, and G. F. Sheats, *Biochemistry*, **6**, 272 (1967).

(7) E. L. Farquhar, M. Downing, and S. J. Gill, *ibid.*, **7**, 1224 (1968).

$10^{-8}$  to  $8 \times 10^{-10}$  sec.<sup>10-12</sup> Therefore, one might expect that if stacking is observable, it would appear coupled with one or more protolytic processes, some or all of which might be outside the range of the technique. Consequently, preliminary ultrasonic measurements were made in three different pH ranges corresponding to predominance of different protolytic species in order to ascertain what reactions might be observable experimentally. A measurable sound absorption effect was obtained only in the basic pH region (pH  $\sim$ 10), where the principal protolytic reaction is



where PH refers to undissociated purine and  $\text{P}^-$  refers to the purinate ion. The kinetics of (1) has been determined; the stacking equilibrium has been included in the analysis of the experimental data, its kinetic parameters being beyond the range of the apparatus.

### Materials and Methods

Purine obtained from Aldrich Chemical Co. was used without further purification. The pH of the purine solutions was adjusted to  $9.88 \pm 0.02$  by adding the required amount of a 10 N NaOH solution (Fisher certified reagent). The pH of a solution was determined using a Corning Model 12 pH meter in conjunction with a standard combination electrode.

Ultrasonic absorption measurements were made with an apparatus which employs the pulse technique. This equipment has been fully described in earlier publications.<sup>11,12</sup> The ultrasonic attenuation coefficient per wavelength,  $\alpha\lambda$ , was measured as a function of frequency for a series of purine solutions of varying concentration. All experiments were performed at a temperature of  $25 \pm 0.5^\circ$ .

In order to determine rate constants from sound absorption data, a knowledge of the concentrations of the species in solution is necessary. A value of the pK for acid dissociation of neutral purine is available,<sup>7</sup> from which an equilibrium constant for reaction 1 can be calculated. However, due to the variation in ionic strength in the ultrasonic experiments ( $\sim$ 0.6 to 1.0 M), it would be unreasonable to expect that this equilibrium constant would yield accurate values for purine and purinate ion concentrations without first applying suitable activity coefficient corrections. Furthermore, these are mixed electrolyte solutions since both NaOH and sodium purinate are present. It is difficult either to measure or to calculate activity coefficients for such solutions at high ionic strengths. Therefore, the following procedure was adopted to determine working values for the concentrations required in the kinetic evaluation.

A series of solutions having varying initial purine concentrations was titrated with a standard NaOH solution. It was possible to determine  $[\text{Na}^+]$  for pH

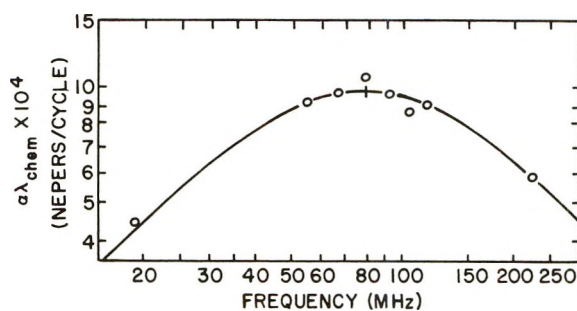


Figure 1. Plot of  $\alpha\lambda_{\text{chem}}$  vs.  $f$ . The initial purine concentration for this experiment was 0.40 M. The sound absorption of the solution less that of water is given by  $\alpha\lambda_{\text{chem}}$ ;  $\alpha\lambda_{\text{H}_2\text{O}} = 3.24 \times 10^{-11} \times f$  neper at  $25^\circ$  for  $\alpha/f^2 = 21.7 \times 10^{17}$  neper sec<sup>2</sup>/cm. The vertical dash denotes  $f_{\text{max}}$ . The theoretical curve was fitted to the data by means of a template. This procedure introduces a maximum  $\pm 5\%$  error in determining  $f_{\text{max}}$  and, therefore, in determining  $1/\tau$ ; this error is propagated through the calculation of rate constants, and is the chief source of error in the forward rate constant.

9.88 from the titration curves. Using appropriate charge and material balance equations and taking advantage of the fact that  $[\text{OH}^-]$  was too low to contribute additively to any other concentration, it was possible to calculate  $[\text{P}^-]$  and  $[\text{PH}]$  (*vide infra*). A plot of initial  $[\text{PH}]$  vs.  $[\text{P}^-]$  provided a calibration curve for determination of concentration parameters appropriate to each ultrasonic experiment.

A solution prepared from Fisher reagent grade NaOH pellets and standardized by titration of primary standard potassium hydrogen phthalate (Fisher ACS, certified standard) was used as the titrant. A Beckman Model 39142 electrode was used to measure pH in the small volume of purine solution titrated (4 to 6 ml). Titrations were carried out in a thermostated vessel in order to maintain the temperature at  $25 \pm 0.5^\circ$ .

### Results and Discussion

Relaxation times are obtained from the sound absorption data by plotting  $\alpha\lambda_{\text{chem}}$  vs. frequency for each acoustic experiment. A typical plot is shown in Figure 1. The data can be fitted quite well to the theoretical function corresponding to a single relaxation time. Therefore, the relaxation time  $\tau$  is defined by

$$1/\tau = 2\pi f_{\text{max}} \quad (2)$$

where  $f_{\text{max}}$  is the frequency of maximum sound absorption. The data for all the ultrasonic experiments are collected in Table I.

To determine the rate constants, a relaxation equa-

(8) G. K. Helmkamp and N. S. Kondo, *Biochim. Biophys. Acta*, **145**, 27 (1967).

(9) G. K. Helmkamp and N. S. Kondo, *ibid.*, **157**, 242 (1968).

(10) M. Eigen and L. DeMaeyer in "Technique of Organic Chemistry," Vol. VIII, 2nd ed, A. Weissberger, Ed., Interscience, New York, N. Y., 1963, Part II, p 895.

(11) R. S. Brundage, Ph.D. Thesis, Brandeis University, 1969.

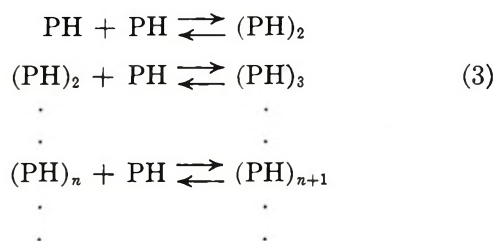
(12) R. S. Brundage and K. Kustin, *J. Phys. Chem.*, **74**, 672 (1970).

**Table I:** Frequencies of Maximum Absorption for Aqueous Purine Solutions at pH 9.88

$C^0_{\text{PH}}$ , $M^a$	$[\text{PH}]$ , $M$	$f_{\text{max}}$ , MHz	$1/\tau \times 10^{-8}$ , $\text{sec}^{-1}$
0.70	0.087	158	996
0.64	0.077	140	879
0.48	0.056	100	628
0.44	0.050	90	565
0.40	0.043	79	496

<sup>a</sup>  $C^0_{\text{PH}}$  refers to the initial purine concentration.

tion is derived which relates observed relaxation times to equilibrium concentrations of appropriate species in solution. (The corresponding rate law is also formulated in terms of concentrations, not activities.) Concentrations were determined as described below because they cannot be calculated from a thermodynamic equilibrium constant, the activity coefficients being unknown but certainly not unity. The relaxation equation must account for all processes that could conceivably contribute to the experimentally observed relaxation process. For the aqueous purine system at pH 9.88 the pertinent processes are reaction 1 and molecular stacking. Stacking may be described by the following scheme.



where  $(\text{PH})_n$  refers to a polymer composed of  $n$  purine molecules or monomers.

Existing evidence indicates that stacking occurs to an infinite degree and that the equilibrium constants for separate steps in (3) are equal. The available value for this constant,  $K_D$ , is  $2.1 \text{ m}^{-1}$  at  $25^\circ$ .<sup>4</sup> In the literature,  $K_D$  is given as a thermodynamic equilibrium constant; it has been derived from osmotic pressure data assuming that all species participating in (3) have unit activity coefficients. In this study of purine kinetics all polymers beyond the dimer are neglected since they are present in very low concentrations relative to the monomer. (In the most concentrated solution, trimers represent less than 1.0% of the net stoichiometric purine concentration.)

The appropriate relaxation equation based on (1), and assuming the first reaction of (3) to be equilibrated at all times is<sup>13</sup>

$$1/\tau = k_f\{[\text{PH}] + [\text{OH}^-]/[1 + 4K_D]\} + k_r \quad (4)$$

The term in (4) involving  $[\text{OH}^-]$  is three to four orders of magnitude smaller than that involving  $[\text{PH}]$  for the

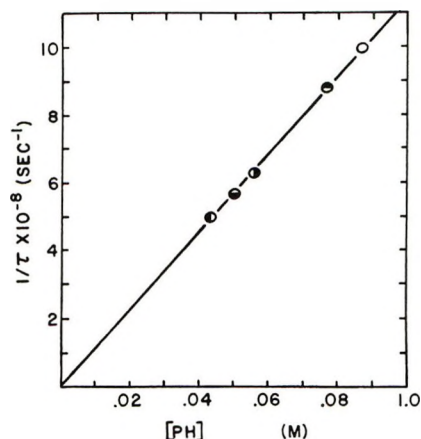


Figure 2. Concentration dependence of the relaxation time given by eq 5. The initial purine concentrations are the following:  $\circ$ , 0.70  $M$ ;  $\bullet$ , 0.64  $M$ ;  $\ominus$ , 0.48  $M$ ;  $\omin�$ , 0.44  $M$ ;  $\bullet$ , 0.40  $M$ . The slope of the line is  $k_f$  and the intercept is  $k_r$ . The slope and intercept have been determined by a standard least-squares analysis; the solid line is the best straight line as determined by this procedure.

given experimental conditions. Therefore, it can be neglected and the final relaxation equation is

$$1/\tau \cong k_f[\text{PH}] + k_r \quad (5)$$

A plot of  $1/\tau$  vs.  $[\text{PH}]$  should yield a straight line having slope  $k_f$  and intercept  $k_r$ . This plot is given in Figure 2.

The values of  $[\text{PH}]$  were obtained from the titration experiments described above using the following charge and material balance conditions.

$$[\text{Na}^+] \cong [\text{P}^-] + [\text{OH}^-] \cong [\text{P}^-] \quad (6)$$

$$C^0_{\text{PH}} = [\text{P}^-] + [\text{PH}] + 2[(\text{PH})_2] \quad (7)$$

Using (6), (7), and the equilibrium expression for stacking,  $[\text{PH}]$  is given by

$$2K_D[\text{PH}]^2 + [\text{PH}] + [\text{Na}^+] - C^0_{\text{PH}} = 0 \quad (8)$$

The values of  $[\text{PH}]$  obtained from (8) are also listed in Table I.

It is important to note that (1) is an ion-dipole reaction. Therefore, it is not expected that its rate constants would vary appreciably with ionic strength.<sup>14</sup> These rate constants are functions of the dielectric constant of the medium. However, in these experiments the dielectric constant varies only slightly and is effectively constant throughout. The resulting rate constants are, therefore, those for reaction 1 occurring in a medium having a constant dielectric strength.

(13) D. Pörschke and F. Eggers, *Eur. J. Biochem.*, **26**, 490 (1972). This sound absorption study on the stacking kinetics of  $N^6,N^9$ -dimethyladenine, a related system, indicates that our assumption of rapid purine monomer-dimer equilibration with respect to reaction 1 is a justifiable approximation.

(14) I. Amdur and G. G. Hammes, "Chemical Kinetics," McGraw-Hill, New York, N. Y., 1966, pp 115, 116.

The rate constants for (1) found by analysis of (5) are  $k_t = (1.13 \pm 0.05) \times 10^{10} M^{-1} \text{ sec}^{-1}$ ,  $k_r = (4.0 \pm 2.0) \times 10^6 \text{ sec}^{-1}$ , and  $K = k_t/k_r = (3.0 \pm 1.7) \times 10^3 M^{-1}$ .

The equilibrium constant found in this work is in reasonable agreement with the literature value of  $2.58 \times 10^3 M^{-1}$ .<sup>3</sup> (High accuracy is not expected here; there is a large uncertainty in  $k_r$  compared with  $k_t$  since  $k_r$  is given by the difference of two relatively large numbers in (5).) The presence of purine stacks does not appear to influence the rate constant for  $\text{OH}^-$  attack, an observation also made for  $\text{H}^+$  attack on purine in acidic media.<sup>3</sup>

The reaction with  $\text{OH}^-$  is presumably deprotonation of the only proton on purine, namely, H(9) on the imidazole portion of the molecule. To see whether the rate constant for this reaction represents diffusion control, we first calculate the expected theoretical value for diffusion control.<sup>15</sup>

$$k = 4\pi N_A a (D_{\text{OH}^-} + D_{\text{PH}}) \Phi / 10^3 M^{-1} \text{ sec}^{-1} \quad (9)$$

where  $N_A$  is Avogadro's number,  $a$  is the distance of closest approach,  $D$  is the diffusion coefficient, and  $\Phi$  is a function which depends on the interaction potential between the reaction partners. Let  $\Phi = e^0 = 1$  for an ion-dipole reaction and let  $a$  be  $7 \text{ \AA}$  for  $\text{PH} + \text{OH}^-$  due to the large effective radius for  $\text{OH}^-$ . The dominant diffusion coefficient will be that of  $\text{OH}^-$ , which we have calculated to be  $5.26 \times 10^{-5} \text{ cm}^2 \text{ sec}^{-1}$  at  $25^\circ$ .<sup>16</sup> Letting  $D_{\text{PH}}$  range from zero to  $1 \times 10^{-5}$  yields  $2.79 \times$

$10^{10} \leq k \leq 3.33 \times 10^{10} M^{-1} \text{ sec}^{-1}$ . Since not all solid angles of approach between purine and  $\text{OH}^-$  will lead to reaction, steric hindrance should reduce the observed rate constant to a value below the theoretical limit. In fact, if the measured rate constant is taken as an indication of diffusion control, the steric factor corresponds to about  $1/3$  favorably oriented encounters.

Closely related systems have similar rate constants; for example, those for reactions of  $\text{OH}^-$  with phenol, uracil, and adenine are 1.4, 0.98, and  $1.0 \times 10^{10} M^{-1} \text{ sec}^{-1}$ , respectively.<sup>2,15</sup> Reactions with  $\text{OH}^-$  that are appreciably less than diffusion controlled have been observed when the proton to be removed is directly H bonded to two atoms; the associated rate constants are often in the range  $10^7$  to  $10^8 M^{-1} \text{ sec}^{-1}$ . The rate constants for purine and adenine are essentially the same, and are less than that of phenol. The steric factor for phenol is approximately  $1/2$ , which should also hold for the purine bases. It is possible that the proton attached to N(9) is H bonded at N(3) (perhaps through one or more intervening water molecules). The binding energy of this additional bond adds to the activation energy, thus lowering the rate constant. The effect, if present, is certainly small, indicating that any internal H bonding in the purine bases is relatively weak.

(15) M. Eigen, W. Kruse, G. Maass, and L. DeMaeyer, *Progr. React. Kinet.*, **2**, 287 (1964).

(16) R. A. Robinson and R. H. Stokes, "Electrolyte Solutions," Butterworths, London, 1959, p 465.

## A Manometric Study of the Oxygen-Peroxide-Superoxide

### Reaction in Nitrate Melts

by James M. Schlegel\* and Douglas Priore

*Department of Chemistry, Rutgers University, Newark, New Jersey 07102 (Received April 10, 1972)*

The thermodynamics and kinetics of the reaction  $2\text{O}_2^- \rightleftharpoons \text{O}_2^{2-} + \text{O}_2$  have been studied in molten alkali metal nitrates by measuring oxygen absorption into a nitrate melt containing peroxide ion. An equilibrium constant of  $2 \times 10^{-5}$  was obtained for this reaction at  $260^\circ$ . This reaction was also found to be exothermic, having an enthalpy change of approximately  $-9.90 \text{ kcal/mol}$ . The rate of disproportionation and comproportionation were found to be  $1.0$  and  $5 \times 10^4 \text{ l./mol sec}$ , respectively.

Recent investigations by Zambonin and Jordan<sup>1</sup> have revealed that when oxide ion,  $\text{O}^{2-}$ , is added to fused alkali metal nitrates, it is oxidized by  $\text{NO}_3^-$  to give a mixture of peroxide ion,  $\text{O}_2^{2-}$ , and superoxide,  $\text{O}_2^-$ . This result is quite surprising in view of the

Lux-Flood acid-base theory that has been used to describe the many reactions which take place in nitrate melts.<sup>2-4</sup> Zambonin and Jordan also report that, al-

(1) P. G. Zambonin and J. Jordan, *J. Amer. Chem. Soc.*, **91**, 2225 (1969).

though the peroxide ion is the predominant oxygen anion that is produced, the peroxide ion is converted almost exclusively into superoxide ion in an atmosphere of oxygen,  $O_2^{2-} + O_2 = 2O_2^-$ . Based on voltametric studies at Levich's rotated platinum electrode, they calculated the equilibrium constant for the reverse of the above reaction to be  $3.5 \times 10^{-6}$  at  $229^\circ$  in a eutectic mixture of  $NaNO_3$  and  $KNO_3$ .

This equilibrium constant has a value which is the same order of magnitude as the Henry's law constant which they cite for oxygen. Therefore, we felt that the equilibrium constant for this reaction could be determined using a manometric method. We equilibrated  $O_2$  over  $NaNO_3$ - $KNO_3$  melts containing peroxide ion and obtained results which support Zamboni and Jordan's findings.

We have studied the temperature dependence of the equilibrium constant for this reaction and have also made some rate measurements. The thermodynamics and the kinetics of this reaction are discussed in the present paper.

### Experimental Section

**Chemicals.** Baker reagent grade  $NaNO_3$  and  $KNO_3$  were dried at  $120^\circ$  before being used.  $KO_2$  from Alfa Inorganics assayed at 98%  $KO_2$  and Mallinckrodt analytical reagent grade  $Na_2O_2$  containing approximately 5%  $NaO_2$  were kept dry in a desiccator. The amount of  $NaO_2$  impurity in  $Na_2O_2$  was determined using a method described by Seyb and Kleinberg.<sup>5</sup>

**Procedure.**  $NaNO_3$ - $KNO_3$  solvent (40 g) was placed in a platinum container. The container was placed in a reaction vessel which was attached to a vacuum system and heated by a large molten salt constant temperature bath. The reaction vessel consisted of a 30-mm glass tube with a 30-mm side arm containing a 29/42 standard taper female joint. A glass rod having a cup at one end was attached to a 29/42 male joint and extended through the center of the joint. Prior to a run, the cup was filled with a weighed quantity of  $Na_2O_2$  or  $KO_2$  in a dry atmosphere, and this male joint was put into the side arm of the reaction vessel. By rotating the joint, the solid reactants can be added to the nitrate solvent while maintaining a vacuum.

The apparent volume of our system was determined by introducing known amounts of gas and measuring resultant pressures. Only an apparent volume could be calculated since an appreciable volume of our system is contained in the bath at a temperature of  $250$ - $300^\circ$  while the rest of the system is at room temperature. After each run an apparent volume was determined.

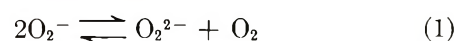
The pure fused nitrate solvent was kept *in vacuo* for at least a day to ensure complete removal of water and to check for small leaks. A known quantity of oxygen gas was added to the system, and a pressure reading was recorded. Then a weighed quantity of peroxide

was added from the cup. The manometer reading would begin to increase as oxygen was absorbed, and the reaction was allowed to equilibrate overnight. If very little superoxide is present initially, the change in pressure readings is considerable, *ca.* 85% of the original pressure.

### Results and Discussion

Within a specially designed vacuum system, 0.3-2 mmol of dry oxygen was equilibrated over a  $NaNO_3$ - $KNO_3$  melt which contained known quantities of  $Na_2O_2$  and  $KO_2$ . Equilibrium was established within 12 to 24 hr. We found that equilibrium was attained sooner if the oxygen was allowed to be in contact with the melt for a day before adding the peroxide. Therefore, most of the runs were performed using this order of addition.

To calculate an equilibrium constant for the reaction



the equilibrium expression is written in a form which incorporates a Henry's law constant for oxygen in nitrate melts

$$K/k = P_{O_2} \frac{[O_2^{2-}]}{[O_2^-]^2} \quad (2)$$

where  $P_{O_2}$  represents the pressure of oxygen after equilibrium is attained and  $k$  is the Henry's law constant for oxygen. This expression can be written in a form which allows us to calculate an equilibrium constant directly from our experimental data

$$K/k = \frac{P_f(a - \Delta P/S)(40)}{(b + 2\Delta P/S)^2} \quad (3)$$

$P_f$  is the final pressure in mm,  $\Delta P$  is the final pressure minus the initial pressure,  $a$  is the initial millimoles of  $O_2^{2-}$ ,  $b$  is the initial millimoles of  $O_2^-$ , and  $S$  is the pressure in mm that 1 mmol of gas exerts in our vacuum system.  $S$  is a function of the temperature of the melt, room temperature, and the barometric pressure and therefore varies slightly from day to day. Its value was determined at the end of each run and in most cases did not vary by more than 3%. The number 40 represents the grams of solvent that was used. In the above expression  $k$  has units of molal per millimeters.

The equilibrium constant for reaction 1 is determined by the value chosen for the Henry's law constant for  $O_2$ . Studies by Copeland and Seibles<sup>6</sup> indicate the solubility of argon and nitrogen in sodium nitrate melt to be approximately  $1 \times 10^{-3}$  mol/kg atm between

(2) F. R. Duke in "Fused Salts," B. R. Sundheim, Ed., McGraw-Hill, New York, N. Y., 1964, pp 409-417.

(3) B. J. Brough, D. A. Habboush, and D. H. Kerridge, *J. Inorg. Nucl. Chem.*, **30**, 2870 (1968).

(4) J. M. Schlegel and J. J. Robinson, submitted for publication.

(5) E. Seyb and J. Kleinberg, *Anal. Chem.*, **23**, 115 (1951).

(6) J. Copeland and L. Seibles, *J. Phys. Chem.*, **72**, 603 (1968).

Table I: Data Relevant to Equilibrium Studies

Temp, °C	$P_f$	$P$	$a^a$	$b^a$	$S$	$K/k$
257	5.2	18	1.95	0.145	56	547
255	5.0	17	1.93	0.143	56	578
258	20	33.5	1.90	0.142	54	534
277	16	41	1.98	0.140	55	297
278	3.5	17	1.88	0.133	56	403
279	3.5	18.5	1.89	0.134	58	367
273	3.0	18	1.93	0.137	57	329
269	18	38	1.89	0.134	56	392
280	49.5	53	3.59	1.723	58	420
257	75	26	0.99	0.775	56	543
272	76	20.5	0.83	1.210	56	394
265	49	19.5	1.03	1.020	56	453

<sup>a</sup> Corrected values assuming  $\text{KO}_2$  was 98% pure and  $\text{Na}_2\text{O}_2$  contained 5%  $\text{Na}_2\text{O}$ .

370 and 450°. Their manometric method requires relatively high pressures exceeding 300 atm. More recently, Field and Green<sup>7</sup> have measured the solubility of nitrogen and argon near 1 atm of pressure using a method involving an elution process. The two methods give values which differ by an order of magnitude and the heat of solution is of opposite sign. Both papers give a temperature dependence of Henry's law constant for the gases studied. We chose to use Field and Green's results because their data were obtained at pressures close to our studies and extrapolation of Henry's law constant,  $k$ , to 500° using Field and Green's temperature dependence equation gives a value which compares very well with the value reported by Zamboni and Jordan. This latter observation adds credence to our assumption that  $k$  for  $\text{N}_2$  is very close to  $k$  for  $\text{O}_2$  in nitrate melts. Field and Green's relationship,  $\log k = -599.15/T - 5.71$  becomes  $\log k = -599.15/T - 5.89$  when  $k$  is expressed in units of moles per kilogram millimeter. We used the latter expression to calculate Henry's law constant for oxygen and finally the equilibrium constant using eq 2.

Assuming that reaction 1 is the only reaction occurring in the nitrate melt within the temperature range 255–282°, a plot of  $\log K/k$  vs.  $1/T$  would yield a straight line having a slope of  $-\Delta H/2.3R + 599.15$ , where  $\Delta H$  is the enthalpy change in calories per mole for reaction 1 (Figure 1). There is considerable scatter in the points at higher temperatures; however, the points that are farthest from the line represent runs in which the equilibration time was longer than the other runs.

We attribute this scatter to a possible decomposition of the nitrate melt which is known to occur especially at temperatures approaching 300°. Extrapolating the best straight line in Figure 1 to a temperature of 229°, the equilibrium constant for reaction 1 is  $9.3 \times 10^{-5}$ . This value is within an order of magnitude of

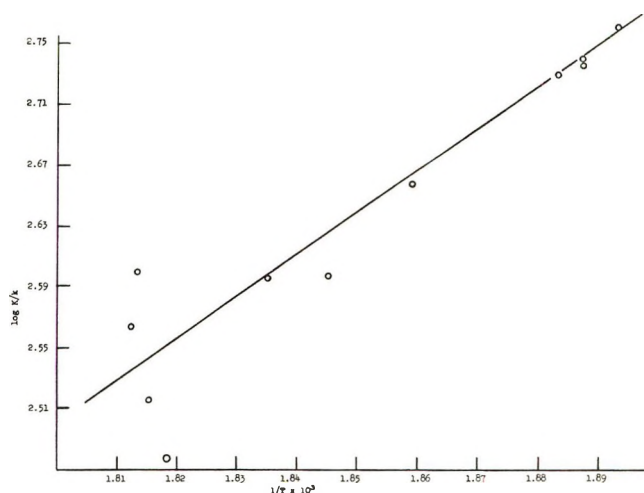


Figure 1. Dependence of  $\log K/k$  on the reciprocal of the absolute temperature.

the value reported by Zamboni and Jordan and represents good agreement considering the two completely independent methods used to obtain this equilibrium constant.

*Thermodynamics.* It is interesting that reaction 1 is exothermic. The slope of the line in Figure 1 yields a value of  $-9.90$  kcal/mol for the enthalpy change of this reaction. We calculated the enthalpy change for  $2\text{MO}_2 \rightleftharpoons \text{M}_2\text{O}_2 + \text{O}_2$  (the standard state being pure compounds) using standard enthalpies of formation and heat capacity data.<sup>9</sup> Both the sodium salt and potassium salt gave endothermic values of  $+2.40$  and  $+15.1$  kcal/mol, respectively, at 260°.

The difference between an average of these values,  $+8.5$  kcal/mol, and our value,  $-9.90$  kcal/mol, may be due to the difference in solvation energies of  $\text{O}_2^{2-}$  and  $\text{O}_2^-$  in alkali metal nitrate melts, the energy released upon solvation  $\text{O}_2^{2-}$  being more than twice the energy released upon solvating  $\text{O}_2^-$ . Considering that solvation energies in aqueous systems are proportional to the charge squared of the ion divided by its radius, the above result is reasonable.

We attempted to obtain a more quantitative measure of solvation effects by studying reaction 1 in a nitrate melt which contains only  $\text{Na}^+$ . Equilibrating oxygen over pure  $\text{NaNO}_3$  which contained  $\text{Na}_2\text{O}_2$  gave very high values for  $K/k$  and the data were not reproducible. These results may be due to side reactions as a result of the decomposition of the nitrate melt. The melting point of  $\text{NaNO}_3$  is considerably higher than the temperatures of our other equilibration studies.

*Kinetics.* Most of our equilibrations were performed without stirring. Recently, however, our laboratory

(7) P. E. Field and W. J. Green, *J. Phys. Chem.*, **75**, 821 (1971).

(8) R. N. Kust and J. D. Burke, *Inorg. Nucl. Chem. Lett.*, **6**, 335 (1970).

(9) JANAF Thermochemical Tables (1965).

devised a method which allows us to efficiently stir the contents of our reaction vessel while maintaining a good vacuum and good temperature control.<sup>10</sup> The new method of stirring reduced equilibration times from 20 to 3 hr. This observation led us to calculate the rate at which a nonreacting gas is absorbed into a quiescent liquid using the expression<sup>11</sup>

$$\text{rate} = 2(A^* - A^\circ)(D_A/\pi t)^{1/2}$$

where  $D_A$  is the diffusion coefficient for the gas,  $A^*$  is the concentration which corresponds to the solubility of the gas at the partial pressure prevailing above the surface of the liquid, and  $A^\circ$  is the initial concentration of the gas in the liquid. We calculated what this rate would be after 1 hr at the prevailing pressure of our system, 20 mm, using the diffusion coefficient reported by Zambonin, *et al.*,<sup>12</sup> and using Henry's law constant previously cited. We obtained a value of  $4.42 \times 10^{-14}$  mol/cm<sup>2</sup> sec. The initial rate at which O<sub>2</sub> is absorbed into our melt containing O<sub>2</sub><sup>2-</sup> with no stirring is  $7.34 \times 10^{-10}$  mol/cm<sup>2</sup> sec. This value is based on the surface area of our reaction vessel, 20.26 cm<sup>2</sup>, and the rate,

after 1 hr, at which the mercury in our manometer rose, 3 mm/hr. The ratio of the experimental rate to the rate we calculated for no chemical reaction is referred to as an enhancement factor. The enhancement factor for our reaction, 6000, is large enough such that the approximate relationship,  $R = [O_2](D_{O_2}k_1[O_2^{2-}])^{1/2}$ , is valid.<sup>11</sup>  $R$  is the experimental rate and  $k_1$  is the rate constant for the reaction  $O_2 + O_2^{2-} = 2O_2^-$ .

The above relationship yields a rate constant,  $k_1$ , for the electron transfer reaction of  $5 \times 10^7$  cm<sup>3</sup>/mol sec or  $5 \times 10^4$  l./mol sec. Using the equilibrium constant at 260°,  $2 \times 10^{-5}$ , a value of 1.0 l./mol sec is obtained for the rate of disproportionation of O<sub>2</sub><sup>-</sup> in alkali metal nitrates.

*Acknowledgment.* This investigation was supported in part by Undergraduate Research Participation Grant No. GY-8891 from the National Science Foundation.

(10) D. Uhr and J. Schlegel, *J. Chem. Educ.*, **49**, 243 (1972).

(11) P. V. Danckwerts, "Gas-Liquid Reactions," McGraw-Hill, New York, N. Y., pp 30-69.

(12) P. Zambonin, V. Cardetta, and G. Signorile, *J. Electroanal. Chem.*, **28**, 237 (1970).

## Synergistic Catalysis of Ammonium Nitrate Decomposition. Visible Spectra of Ammine, Chloro, and Nitrate Complexes of Copper, Nickel, and Cobalt in Fused Ammonium Nitrate

by A. G. Keenan\* and I. J. Ferrer

Department of Chemistry, University of Miami, Coral Gables, Florida 33124 (Received February 22, 1972)

Publication costs assisted by the Office of Naval Research, Power Program

Spectrophotometric studies in the visible region have confirmed details of the mechanism, previously proposed on the basis of kinetic evidence alone, for the chloride-transition metal ion synergistically catalyzed thermal decomposition of ammonium nitrate. Thus ammine, nitrate, and chloro complexes of copper(II) and nickel(II) and chloro complexes of cobalt(II) have been detected in the decomposing melt. The ammine complexes of copper and nickel have not previously been observed in any molten nitrates.

### Introduction

A recent publication<sup>1</sup> described a pronounced synergistic catalysis of fused ammonium nitrate decomposition which occurred when the individual catalytic species, namely, chloride ion and transition metal cations, were combined. Mechanisms based on kinetic evidence were proposed for the synergesis. Chromium

was thought to operate through oxo complexes but other transition metal ions such as copper, silver, nickel, and cobalt were considered to involve ammine complexes initially, which changed to chloro complexes

(1) A. G. Keenan, K. Notz, and N. B. Franco, *J. Amer. Chem. Soc.*, **91**, 3168 (1969).

as the melt became more acidic during the course of decomposition.

In the present work, direct spectrophotometric evidence in the visible region is presented for the existence of ammine and chloro, and also nitrate, complexes of copper, nickel, and cobalt in fused ammonium nitrate. The general features of the previously proposed mechanism are thus confirmed.

### Experimental Section

Spectra were taken on a Beckman Model DU spectrophotometer with a cell housing modified for use with fused salts similar to one already described in the literature.<sup>2</sup> Spectra for copper and nickel salts were taken at 175° and for cobalt at 185°. Quartz cells with path lengths ranging from 0.5 to 0.005 cm were used (Pyro-cell Manufacturing Co.). Ternary nitrate eutectic (TNE) consisting of 34, 19, and 47 mol % of lithium, sodium, and potassium nitrates, respectively, was used as a solvent for reference spectra. The transition metal ions were added as nitrates. Commercially available reagent grade chemicals dried in an appropriate manner were used in general, except for Co(NH<sub>3</sub>)<sub>6</sub>(NO<sub>3</sub>)<sub>3</sub> which was synthesized according to a published procedure.<sup>3</sup>

In general, the concentrations of chloride and transition metal ion were the same as used in the kinetic catalytic studies,<sup>1</sup> *i.e.*, 0.1 wt % metal and a chloride to metal ion mole ratio of 36. Where necessary, these concentrations were varied somewhat so that, by choice of available path lengths for the optical cells, the absorbances could be brought into a reasonably sensitive range of the spectrophotometer. In some cases even larger excesses of chloride ion were added to ensure formation of the highest chloro complexes. In some cases Na<sub>2</sub>CO<sub>3</sub> was added to ammonium nitrate melts since it released NH<sub>3</sub> and enhanced formation of ammine complexes.

Charges of a size large enough to allow accurate weighing of the components (usually 10 g) were made up in separate test tubes immersed in a fused salt thermostat,<sup>1</sup> thoroughly stirred after melting, and suitable portions then poured into the cells contained in the heated compartment of the spectrophotometer.

### Results and Discussion

1. *Copper Complexes.* Table I shows a sequence of spectral measurements and visual color changes observed during the cupric and chloride ion synergistically catalyzed decomposition of ammonium nitrate. About 100 mg of Na<sub>2</sub>CO<sub>3</sub> was added to the standard charge to stabilize it initially. This disappeared rapidly as the melt became acid during the course of its decomposition.<sup>1</sup> A strong smell of NH<sub>3</sub> was noted initially.

The spectrum of Cu(II) in TNE showed a single peak at 840 nm with a molal absorptivity of 124 in the region

Table I: Ammonium Nitrate-Cu<sup>2+</sup>-Cl<sup>-</sup> System

Time, hr	$\lambda_1$ , nm	$\lambda_2$ , nm	Color
0		680	Blue
1.5		760	Blue-green
3		780	Green
4		780	Yellow-green
5	370		Greenish-yellow

from 500 to 1000 nm. Cu(II) in fused NH<sub>4</sub>NO<sub>3</sub> showed the peak shifted to 790 nm with a molal absorptivity of 98. Figure 1 shows the peak shifting further to successively lower wavelengths as the concentration of free NH<sub>3</sub> is increased by adding increasing amounts of Na<sub>2</sub>CO<sub>3</sub>.

Figure 2 shows the spectrum of Cu(II) in fused NH<sub>4</sub>NO<sub>3</sub> with added chloride ions. Without chloride ions, the shoulder peak at 370 nm is missing. The steeply rising absorption below 360 nm is part of the known strong absorption peak of nitrate ion whose maximum lies at 300 nm.<sup>4</sup> Identical spectra were observed in this region for TNE with and without chloride ions, respectively.

Using results from the literature and considering the reference spectra taken in the present work, the data of Table I can be interpreted unequivocally as follows. Initially at time zero with excess Na<sub>2</sub>CO<sub>3</sub> and therefore free NH<sub>3</sub> present, the copper is octahedrally complexed with ammine groups and gives the characteristic blue band at 680 nm. As the reaction slowly commences, the melt grows acid,<sup>1</sup> the ammine ligands are replaced by nitrate, and the absorption shifts to the region of 780 nm. In the last recorded stage of the reaction, where the acidity is highest and the chloride ion concentration has increased due to decomposition of NH<sub>4</sub>NO<sub>3</sub>, the copper is present as chloro complexes with absorption at 370 nm.

To substantiate this assignment, the complexes will be discussed in the above order. The spectra of copper(II) ammine complexes do not appear to have been studied previously in fused nitrates but the absorption regions of complexes do not appear generally to vary drastically with solvent as will appear later. Hare<sup>5</sup> states that Dq for Cu(II) complexes having NH<sub>3</sub> ligands in octahedral symmetry is expected to be about 1500 cm<sup>-1</sup>. This would give an absorption at 667 nm.

(2) B. R. Sundheim and J. Greenberg, *Rev. Sci. Instrum.*, **27**, 703 (1956).

(3) J. Bjerrum and J. P. McReynolds, "Inorganic Synthesis," Vol. II, W. C. Fernelius, Ed., McGraw-Hill, New York, N. Y., 1957, p 218.

(4) G. P. Smith, "Molten Salt Chemistry," M. Blander, Ed., Interscience, New York, N. Y., 1964.

(5) C. R. Hare, "Spectroscopy and Structure of Metal Chelate Compounds," K. Nakamoto and P. J. McCarthy, S. J., Ed., Wiley, New York, N. Y., 1968.

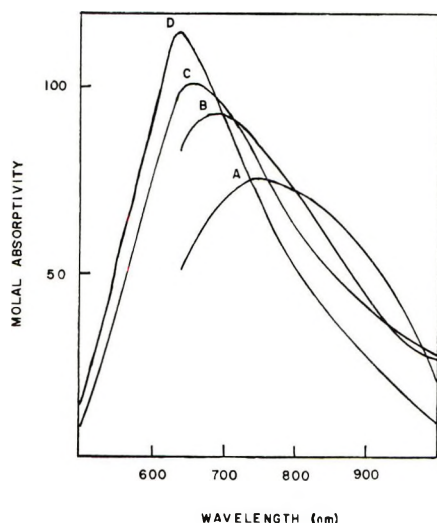


Figure 1. Spectra of 0.02 *m* Cu(NO<sub>3</sub>)<sub>2</sub> in 10 g of fused NH<sub>4</sub>NO<sub>3</sub> at 175° with Na<sub>2</sub>CO<sub>3</sub> added as follows: curve A, 0.01 g; curve B, 0.03 g; curve C, 0.10 g; and curve D, 0.20 g.

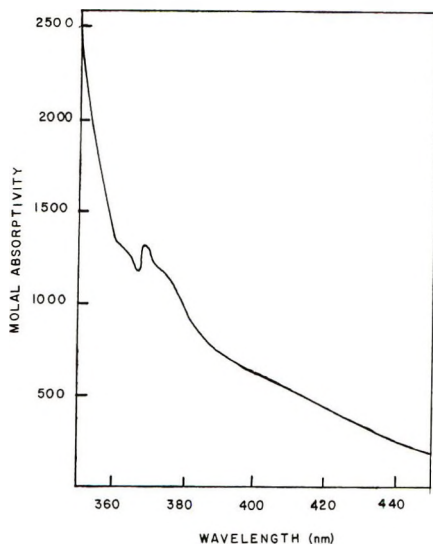


Figure 2. Spectrum of 0.02 *m* Cu(NO<sub>3</sub>)<sub>2</sub> in fused NH<sub>4</sub>NO<sub>3</sub> at 175° with 50-fold excess of NaCl.

Other authors,<sup>6,7</sup> studying aqueous solutions of ammonium salts, concluded that complexes of the formula [Cu(NH<sub>3</sub>)<sub>*n*</sub>(H<sub>2</sub>O)<sub>6-*n*</sub>]<sup>2+</sup>, where *n* varies from 0 to 5, were present. As *n* increased to 4, the spectrum in the visible region consisted of bands that moved from 800 to 590 nm and then shifted to 647 nm again for *n* = 5.

The visible spectrum of Cu(II) in LiNO<sub>3</sub>-KNO<sub>3</sub> eutectic has already been studied<sup>8</sup> and a single band observed at 850 nm. This agrees almost exactly with the value we have observed in TNE and must correspond to a nitrate complex. Cu(II) is a d<sup>9</sup> transition metal which forms distorted octahedral and tetrahedral complexes. The position of the d-d transition band with different ligands has been studied extensively.<sup>9,10</sup> It was concluded that in a tetrahedral environment the band appeared at about 1666 nm, while in an octa-

hedral environment it was at about 833 nm. In still another work,<sup>11</sup> the complex ion [Cu(NO<sub>3</sub>)<sub>4</sub>]<sup>2-</sup> containing six-coordinated copper with two nitrates acting as bidentate ligands was found to have an absorption at 785 nm.

Based on the above information, therefore, it seems quite clear that in Figure 1, predominantly ammine complexes with an absorption around 630 nm (curve D) are gradually exchanged into mixed nitrate-ammine complexes with absorption around 750 nm (curve A) as the amount of Na<sub>2</sub>CO<sub>3</sub> is decreased. The nitrate complexes contain Cu(II) in an octahedral environment surrounded by four nitrate groups, two of which act as bidentate ligands. The same exchange process is occurring in the first four entries of Table I.

The spectrum of Cu(II) in a LiCl-KCl eutectic melt at 364° shows bands at 260 and 370 nm.<sup>12-14</sup> Aqueous solutions of Cu(II) with high chloride concentrations show peaks at 270 and 380 nm.<sup>15,16</sup> Only the higher wavelength peak would be visible in nitrate melts and indeed it appears as a shoulder at the correct wavelength (370 nm) superimposed on the strong nitrate absorption edge in the present data (Figure 2). The form of this complex is generally considered to be a highly distorted tetrahedron.

2. *Nickel Complexes.* Table II shows a sequence of spectral measurements and visual color changes observed during the nickel and chloride ion synergistically catalyzed decomposition of ammonium nitrate. As in the case of copper, about 100 mg of Na<sub>2</sub>CO<sub>3</sub> was added initially.

Based on reference spectra and literature data to be discussed below, the Ni(II) data in Table II can be interpreted in the same manner as the Cu(II) data of Table I. Initially in the bluish solutions, ammine complexes predominate. The 6-, 8-, and 9-hr entries represent predominantly nitrate complexes while the 14- and 15-hr entries are essentially chloro complexes.

Thus when Ni(II) was added to NH<sub>4</sub>NO<sub>3</sub> containing Na<sub>2</sub>CO<sub>3</sub> or to TNE containing NH<sub>4</sub>NO<sub>3</sub> and Na<sub>2</sub>CO<sub>3</sub> the resulting bluish solutions showed a sharp peak from

(6) D. M. Grant and R. Kollrack, *J. Inorg. Nucl. Chem.*, **23**, 25 (1961).

(7) J. Bjerrum, C. J. Ballhausen, and C. K. Jørgensen, *Acta Chem. Scand.*, **8**, 1275 (1954).

(8) D. M. Gruen, *J. Inorg. Nucl. Chem.*, **4**, 74 (1957).

(9) R. Pappalardo, *J. Mol. Spectrosc.*, **6**, 554 (1961).

(10) R. Pappalardo and R. E. Dietz, *Phys. Rev.*, **123**, 1188 (1961).

(11) D. K. Straub, R. S. Drago, and J. T. Donoghue, *Inorg. Chem.*, **1**, 848 (1962).

(12) G. W. Harrington, Ph.D. Thesis, New York University, 1958.

(13) G. W. Harrington and B. R. Sundheim, *Ann. N. Y. Acad. Sci.*, **79**, 950 (1960).

(14) D. M. Gruen and R. L. McBeth, *Pure Appl. Chem.*, **6**, 23 (1963).

(15) S. Lindenbaum and G. E. Boyd, *J. Phys. Chem.*, **67**, 1238 (1963).

(16) C. A. Angell and D. M. Gruen, *J. Amer. Chem. Soc.*, **88**, 5192 (1966).

**Table II:** Ammonium Nitrate-Ni<sup>2+</sup>-Cl<sup>-</sup> System

Time, hr	$\lambda_1$ , nm	$\lambda_2$ , nm	Color
0	385	640	Light blue
1	390	650	Blue green
2.5	410	670	Blue green
4	420	680	Light green
6	425	700	Yellow green
8	425	725	Greenish yellow
9	425	780	Yellow
14	450	780-925	Amber
15	460	725-800	Light brown

372 to 390 nm with a molal absorptivity of about 50 and a broader peak from 640 to 670 nm with a molal absorptivity of about 25.

The spectrum of Ni(II) ammine complexes does not appear to have been studied previously in fused salts. In aqueous solution, ammine complexes have been reported<sup>17</sup> showing absorptions ranging from 570 to 700 nm depending on the free ammonia concentration. In other work,<sup>18,19</sup> Ni(II) complexes with six NH<sub>3</sub> ligands in octahedral symmetry were found to show absorptions at 930, 571, and 355 nm. An absorption at 930 nm would not have been observable in the present work.

It was found that when the Na<sub>2</sub>CO<sub>3</sub> concentration was reduced to zero, an identical spectrum was obtained for Ni(II) in both NH<sub>4</sub>NO<sub>3</sub> and in TNE. This consisted of a narrow peak at 423 nm with a molal absorptivity of about 50 and a broader peak at 765 nm with a molal absorptivity of about 20. This spectrum is identical with the one obtained for Ni(II) in LiNO<sub>3</sub>-KNO<sub>3</sub> eutectic<sup>20</sup> and attributed to an octahedral field.<sup>4,21,22</sup> Nitromethane solutions of [Ni(NO<sub>3</sub>)<sub>4</sub>]<sup>2-</sup> have been found to give peaks at 415, 700-785, and 1250 nm.<sup>11</sup> The field was considered to be octahedral with two of the nitrate groups acting as bidentates. Other models have been discussed for the octahedral nitrate complex of Ni(II).<sup>23</sup>

Successive additions of chloride ion to Ni(II) in TNE produced drastic changes in the spectrum. The major peak at 423 nm shifted to slightly higher wavelengths but in addition a characteristic sequence of three smaller peaks appeared in the region between 550 and 1000 nm. The locations of these three peaks depended on the chloride concentration. For example, Figure 3 shows the spectrum of  $1.26 \times 10^{-2}$  m Ni(II) ion in TNE containing Cl<sup>-</sup> at a concentration of 2.7 m.

Similar concentrations of Cl<sup>-</sup> added to fused NH<sub>4</sub>NO<sub>3</sub> containing the same concentration of Ni<sup>2+</sup> gave spectra essentially identical with Figure 3. The rate of decomposition, however, was so high that accurate spectral readings could not be taken.

Spectra of Ni(II) in LiNO<sub>3</sub>-KNO<sub>3</sub> eutectic with varying chloride concentrations have been reported<sup>8,20</sup> with absorptions at 495, 590, 630, and 705 nm. At

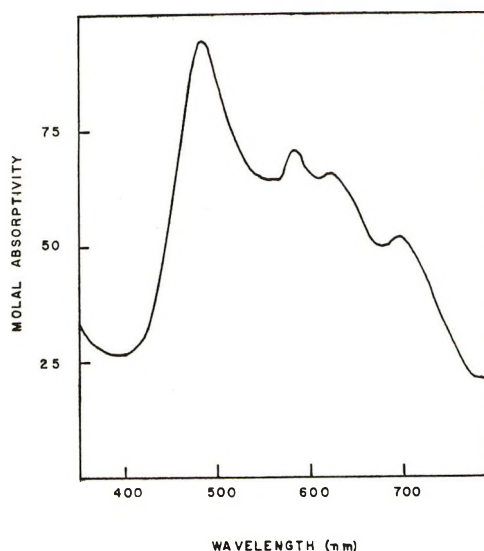


Figure 3. Spectrum of 0.01 m Ni(NO<sub>3</sub>)<sub>2</sub> in fused TNE at 175° with 100-fold excess of NaCl.

230° this spectrum was interpreted as being due to a distorted tetrahedral [NiCl<sub>4</sub>]<sup>2-</sup> complex. These results agree almost exactly with the present results in TNE. Many other studies of Ni(II) chloro complexes in fused salts have been reported<sup>4,23</sup> and it is known that octahedral chloro complexes also exist and absorb at lower wavelengths. The last entries in Table II for decomposing NH<sub>4</sub>NO<sub>3</sub> may therefore represent equilibria between octahedral and tetrahedral chloro complexes or the higher wavelength absorptions may be due to solvent effects on the distorted tetrahedral complexes.

3. *Cobalt Complexes.* Only a blue chloro complex of Co(II) with overlapping absorption peaks at 625, 665, and 690 nm was detected during the Co(II) and chloride ion synergistically catalyzed decomposition of NH<sub>4</sub>NO<sub>3</sub>. The molal absorptivities were 375, 560, and 490, respectively. Co(II) in TNE with excess chloride gave an almost identical spectrum. This spectrum has already been well characterized in the literature<sup>8,12-14,24,25</sup> and attributed to the species (CoCl<sub>4</sub>)<sup>2-</sup>.

(17) J. Bjerrum, "Metal Ammine Formation in Aqueous Solution," P. Haase and Son, Copenhagen, 1941, pp 190-198.

(18) C. K. Jørgensen, *Acta Chem. Scand.*, 9, 1362 (1955).

(19) A. D. Liehr and C. J. Ballhausen, *Ann. Phys. (Leipzig)*, 2, 134 (1959).

(20) D. M. Gruen and R. L. McBeth, *J. Phys. Chem.*, 63, 393 (1959).

(21) S. J. Strickler and M. Kash, "Molecular Orbitals in Chemistry, Physics, and Biology," P. Löwdin and B. Pullman, Ed., Academic Press, New York, N. Y., 1964.

(22) D. M. Gruen, *Quart. Revs., Chem. Soc.*, 19, 349 (1965).

(23) D. M. Gruen, "Fused Salts," B. R. Sundheim, Ed., McGraw-Hill, New York, N. Y., 1964.

(24) I. V. Tananaev and B. F. Dzhurinskii, *Dokl. Akad. Nauk SSSR*, 134, 1374 (1960).

(25) D. M. Gruen, S. Fried, P. Graf, and R. L. McBeth, *Proc. U. N. Int. Conf. Peaceful Uses At. Energy*, 2nd, 12, 112 (1958).

Co(II) in both TNE and in  $\text{NH}_4\text{NO}_3$ , without chloride, gave the known nitrate complex with a single absorption at 560 nm and molal absorptivity of 160. This complex has been variously interpreted as having octahedral<sup>20,22,24</sup> or tetrahedral<sup>11,26</sup> symmetry. This complex was not, however, observed in the synergistically catalyzed decomposing melt at any stage.

No evidence for Co(II) ammine complexes was obtained when  $\text{Na}_2\text{CO}_3$  was added to a melt of  $\text{NH}_4\text{NO}_3$  containing the metal. The nitrate peak at 260 nm remained unchanged. No references to ammine complexes of Co(II) in fused salts have been found in the literature. In aqueous solution absorptions for these species occur at 350 and 500 nm.<sup>27</sup> If Co(II) ammine complexes do occur in fused nitrate melts and have absorptions near the aqueous values, the lower wavelength would be obscured by nitrate absorption and the higher wavelength by the nitrate complex. The present results, therefore, indicate at most that Co(II) ammine complexes in fused nitrates have low stability.

When the synthesized Co(III) ammine complex of formula  $\text{Co}(\text{NH}_3)_6(\text{NO}_3)_3$  was dissolved in either TNE or  $\text{NH}_4\text{NO}_3$  a single peak at 490 nm with a molal absorptivity of about 100 was observed. This has already been reported in the literature<sup>28,29</sup> and assigned to the species  $[\text{Co}(\text{NH}_3)_6]^{3+}$ . When  $\text{Co}(\text{NH}_3)_6(\text{NO}_3)_3$  and chloride ion were added to fused  $\text{NH}_4\text{NO}_3$  to pro-

duce a synergistically catalyzed melt, the 490-nm peak gradually disappeared over the first hour and the Co(II) chloro complex peak described earlier appeared. Co(III) is known to be unstable in acid media and the decomposing  $\text{NH}_4\text{NO}_3$  melt becomes acid as the reaction proceeds.

### Conclusions

The present spectrometric results provide substantial direct support for the occurrence and transformations of the types of transition metal complexes which were called for in the mechanisms previously postulated<sup>1</sup> on the basis of kinetic evidence alone for the synergistically catalyzed thermal decomposition of ammonium nitrate. Explicit discussion of the role of the complexes in the proposed mechanism of the synergistic decomposition is given in the reference cited.

*Acknowledgment.* This work was supported by the Office of Naval Research, Material Sciences Division, Power Program.

(26) F. A. Cotton and T. G. Dunne, *J. Amer. Chem. Soc.*, **84**, 2013 (1962).

(27) C. J. Ballhausen and C. K. Jørgensen, *Acta Chem. Scand.*, **9**, 397 (1955).

(28) A. Tomita and Y. Tamai, *J. Phys. Chem.*, **75**, 649 (1971).

(29) H. Kuroya and R. Tsuchida, *Bull. Chem. Soc. Jap.*, **15**, 429 (1940).

## Electron Spin Resonance Evidence for Dissociative Electron Capture in $\gamma$ -Irradiated Phosphate Esters<sup>1</sup>

by Carolyn M. L. Kerr, Kathleen Webster, and Ffrancon Williams\*

*Department of Chemistry, University of Tennessee, Knoxville, Tennessee 37916 (Received February 23, 1972)*

Alkyl radicals are formed during  $\gamma$  irradiation of alkyl phosphates at 77°K. Inclusion of an electron scavenger virtually eliminates this reaction, and a comparable yield of radicals derived from the scavenger is obtained. This proves that alkyl radicals are formed only by dissociative electron capture in the pure esters. Possible biological implications are discussed.

### Introduction

The mechanism of interaction of ionizing radiation with phosphate esters is of interest as these compounds are closely related to many important constituents of biological materials. The effect of  $\gamma$  irradiation on alkyl phosphates has been investigated by product analysis,<sup>2</sup> and more recently by esr examination of the radical intermediates at low temperatures.<sup>3,4</sup> Although

various reaction steps have been postulated on the basis of the information obtained, definitive proof of these is

(1) This work was supported by the U. S. Atomic Energy Commission under Contract No. AT-(40-1)-2968, and this is AEC Document No. ORO-2968-72.

(2) R. W. Wilkinson and F. Williams, *J. Chem. Soc.*, 4098 (1961).

(3) S. Sugimoto, K. Kuwata, S. Ohnishi, and I. Nitta, *Rep. Jap. Assoc., Rad. Res. Polymers*, **7**, 199 (1965-1966).

lacking. Here we present the results of an esr study which demonstrates conclusively that the alkyl radicals observed in  $\gamma$ -irradiated alkyl phosphates are formed by dissociative electron capture. This finding confirms a previous suggestion along these lines.<sup>4</sup>

### Experimental Section

Trimethyl phosphate, triethyl phosphate, dimethyl methyl phosphonate, and dimethyl acid pyrophosphate were supplied by Aldrich Chemical Co. and used without purification. Samples of each compound were prepared both with and without a quantity of a known electron scavenger,<sup>5</sup> ethyl bromide being used as the scavenger for the methyl esters and methyl bromide for the ethyl ester. The alkyl halide concentration was nominally 1 mol % or greater. It was found necessary to use low ethyl bromide concentrations (1–2 mol %) to avoid formation of the  $\cdot\text{C}_2\text{H}_4\text{Br}$  radical since its spectrum tended to obscure that of the ethyl radical. All samples formed glasses when quenched to 77°K. The doped and undoped samples of each compound were irradiated at this temperature to the same total dose (0.1 to 0.2 Mrad), and their esr spectra recorded immediately using identical spectrometer conditions. The esr spectrometer and accessories have been described elsewhere.<sup>6</sup>

### Results and Discussion

In all the methyl esters that were examined, the quartet esr spectrum of the methyl radical ( $A_{\text{iso}}^{\text{CH}_3} = 23 \text{ G}$ ) was superimposed on a broad triplet which can be assigned to a  $>\text{P}(=\text{O})\text{OCH}_2\cdot$  radical.<sup>7</sup> On the other hand, the somewhat anisotropic 12-line spectrum obtained in the sample doped with ethyl bromide appeared to be mainly due to the ethyl radical ( $A_{\text{iso}}^{\text{CH}_2} = 27 \text{ G}$ ,  $A^{\text{CH}_2} = 21 \text{ G}$ ), indicating that a large fraction of the electrons had been captured by the ethyl bromide. Representative spectra obtained for trimethyl phosphate are shown in Figures 1A and B, with stick diagrams indicating the spectral analyses.<sup>8</sup> Although the spectra of the two radicals are quite different, the positions of the four lines in the methyl radical spectrum lie close to those of lines 3, 5, 8, and 10 of the ethyl radical spectrum, thus rendering a relatively small amount of methyl radical difficult to detect in the presence of ethyl. However, the methyl radicals disappeared at 77°K so that any contribution to the spectrum in the doped sample could be determined by recording the spectrum again after the decay was observed to be complete in the spectrum of the pure sample (Figure 1C). The corresponding spectrum of the doped sample is shown in Figure 1D. Comparison of Figures 1B and D shows that the intensities of lines 3 and 10 relative to the adjacent outer lines (which are due only to the ethyl radical) are diminished in Figure 1D. The difference, however, represents only a small contribution to the initial spectrum by methyl radicals,

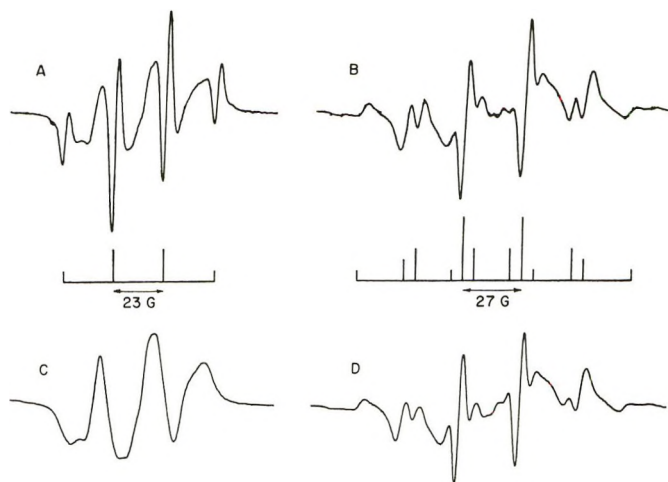


Figure 1. ESR spectra of  $\gamma$ -irradiated trimethyl phosphate with and without ethyl bromide. The radiation dose was 0.2 Mrad. All spectra were recorded at 77°K under the same spectrometer conditions. The spectra refer to samples as follows: A, pure trimethyl phosphate immediately after  $\gamma$  irradiation; B, trimethyl phosphate containing 1–2 mol % ethyl bromide immediately after  $\gamma$  irradiation; C, same sample as A, 6 days after irradiation; and D, same sample as B, 6 days after irradiation.

and scavenging is probably better than 90% complete. Results similar to the above were obtained for the phosphonate and acid pyrophosphate. In the case of the triethyl phosphate, ethyl radicals were observed in the pure material and methyl in the doped sample. As the ethyl radical signal was almost unchanged after 6 days whereas the methyl had decayed out leaving no trace of ethyl, scavenging by methyl bromide was judged to be complete.

Since complete scavenging was observed for triethyl phosphate containing  $\sim 8$  mol % of methyl bromide, it is reasonable to assume that the incomplete scavenging occurring in the methyl esters was due to the much lower (1–2 mol %) scavenger concentration used

(4) A. Begum, S. Subramanian, and M. C. R. Symons, *J. Chem. Soc. A*, 1334 (1970).

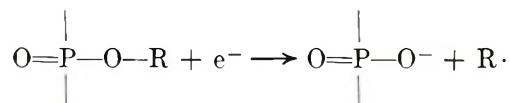
(5) (a) J. M. Warman, K.-D. Asmus, and R. H. Schuler, *Advan. Chem. Ser.*, No. 88, 25, (1968); (b) E. D. Sprague and F. Williams, *J. Chem. Phys.*, 54, 5425 (1971).

(6) J. Lin, K. Tsuji, and F. Williams, *J. Amer. Chem. Soc.*, 90, 2766 (1968).

(7) Since the yield of the  $(\text{CH}_2\text{O})_2\text{P}(=\text{O})\text{OCH}_2\cdot$  radical from trimethyl phosphate is considerably smaller in the sample doped with ethyl bromide than in the undoped sample (Figure 1), it is very probable that this radical originates largely from the decay of methyl radicals by hydrogen atom abstraction from the trimethyl phosphate. For other examples of hydrogen atom abstraction by methyl radicals at 77°K, see (a) E. D. Sprague and F. Williams, *J. Amer. Chem. Soc.*, 93, 787 (1971); (b) R. J. Le Roy, E. D. Sprague, and F. Williams, *J. Phys. Chem.*, 76, 546 (1972); (c) J.-T. Wang and F. Williams, *J. Amer. Chem. Soc.*, 94, 2930 (1972); (d) A. Campion and F. Williams, *ibid.*, in press.

(8) In the powder spectrum of the ethyl radical (Figure 1D), the signal heights of the sharp lines (2, 5, 8, and 11) are enhanced relative to the heights of the other lines as compared to the intensity ratios indicated in the stick diagram. This is due to a line width difference which arises from anisotropic hyperfine broadening. For a detailed explanation, see E. L. Cochran, F. J. Adrian, and V. A. Bowers, *J. Chem. Phys.*, 34, 1161 (1961).

in this case. The fact that the parent alkyl radical is largely but not completely replaced by radicals derived from the scavenger when the latter is present in low concentration is evidence for competition between the highly efficient ethyl bromide<sup>6a</sup> and the methyl esters for the electrons. The observation of comparable yields of parent alkyl and scavenger alkyl radicals in the doped and undoped samples further indicates that the parent alkyl radicals originate from dissociative electron capture by the phosphate esters. The reaction can be written as follows, where R = CH<sub>3</sub> or C<sub>2</sub>H<sub>5</sub>



Although it is clear to us that the results reported here provide definitive evidence for the formation of parent alkyl radicals from the phosphate esters by dissociative electron capture, this interpretation has been questioned by one of the reviewers of this paper. Therefore some elaboration seems to be necessary. If we assume that the parent alkyl radicals are not formed by dissociative electron capture, then the presence of an electron scavenger should not affect their

initial formation and these radicals must be removed by a rapid (*i.e.*, unobservable) secondary reaction with the scavenger. This would require that methyl radicals (which decay only slowly in the absence of scavenger<sup>7</sup>) react with ethyl bromide and that ethyl radicals react with methyl bromide. The only reasonable course of these reactions would involve radical displacement, and since one is the reverse of the other, it is difficult to understand why both should proceed efficiently. Therefore, this alternative explanation to dissociative electron capture may be dismissed.

The present findings may have some bearing on the mechanism of radiation damage in biological molecules containing phosphate ester linkages. For example, dissociative electron capture processes similar to those observed here could bring about main chain scission in polynucleotides. A significant feature of this process is that the products are very unlikely to recombine. This is in contrast to the case of homolytic fission where two free radicals are formed adjacent to one another and a repair mechanism is feasible. Another aspect of this study which deserves comment is the possibility that the incorporation of suitable electron scavengers might be useful in protecting biological material from inactivation by radiation.

## Interaction of Arsine with Evaporated Metal Films

by I. M. Al-Daher and J. M. Saleh\*

Department of Chemistry, College of Science, University of Baghdad, Baghdad, Republic of Iraq (Received December 9, 1971)

Publication costs assisted by the University of Baghdad

The interaction of  $\text{AsH}_3$  with evaporated films of Fe, Ni, Pd, W, Ag, and Pb has been studied in the temperature range from  $-80$  to  $\sim 200^\circ$ . The extent of adsorption was expressed by  $X$ , representing the ratio of the volume of  $\text{AsH}_3$  adsorbed to the volume of krypton corresponding to a monolayer. Rapid dissociative chemisorption, which was accompanied by  $\text{H}_2$  evolution, occurred on the first three metals at  $-80^\circ$ . The total  $\text{AsH}_3$  uptake was very much the same ( $X \simeq 1.7$ ) for these three metals at this temperature irrespective of the different amounts of hydrogen which remained in the adsorbed phases. On W film, both dissociative and weak molecular adsorption took place at  $-80^\circ$  while physical adsorption was the main feature of the  $\text{AsH}_3$  uptake on Ag and Pb films at this temperature. The structure of the adsorbed phase at  $-80^\circ$  corresponded mainly to  $\text{AsH}$  on Fe,  $\text{AsH}_2$  on Ni, and to a mixture of  $\text{AsH}_2$  and  $\text{AsH}_3$  on Pd and W films. The uptake of  $\text{AsH}_3$  on oxidized films of Fe, Ni, Pd, and W at  $-80^\circ$  was more extensive than on the corresponding clean films. The adsorption on oxide sites gave rise probably to the formation of  $\text{H}_3\text{AsO}_m$  on the surface in which the hydrogen atoms were strongly bound to As atoms so that  $\text{H}_2$  evolution was not possible at such low temperature. The tarnishing of clean and oxidized films by  $\text{AsH}_3$  at temperatures  $\geq 30^\circ$  occurred with constant energies of activation and the parameter  $X$  was regarded as a measure of the extent of arsenidation. The rate of arsenidation, at constant temperature and  $\text{AsH}_3$  pressure, became slower as  $X$  increased due to the decrease of the frequency factor ( $A$ ) in the rate expression; the concentration of the reacting sites decreased with increasing thickness of the arsenide layer ( $X$ ). The relationship between  $\log A$  and  $X$  was quite linear in each case from which the rate of  $\text{AsH}_3$  adsorption was determined. Oxidized Ni and W films were less active, while oxidized Fe and Pd were more active, than the corresponding clean metals for reaction with  $\text{AsH}_3$ . When Ni film was coated with a thick film of Pb, the resulting "two-metal" film of Pb-Ni became less active than either Ni or Pb film in reacting with arsine; this was ascribed to the formation of a stable solid solution or alloy by such binary system. When Pd film was covered with Pb film, the activity toward  $\text{AsH}_3$  became surprisingly higher than that of either Pd or Pb or any other film. The resulting solid solution or alloy was assumed to be so unstable as to enhance the outward diffusion of the metal atoms to interact with the gas phase.

### Introduction

Arsine is known as a poison for a number of catalytic reactions on metals,<sup>1,2</sup> but its role in this respect is not quite understood because of the lack of fundamental data on the adsorption of this gas on metal surfaces. Moreover, the thermal decomposition of arsine on certain surfaces was thought to be inhibited by the evolved hydrogen but catalyzed by the arsenic which was separated throughout the decomposition;<sup>3</sup> so far the evidence in support of these results is very little.

Arsine reacts with metals at elevated temperatures to form arsenides which in many cases do not correspond to the usual oxidation states of metals or arsenic.<sup>4</sup> From these standpoints it would be interesting to investigate the adsorption of arsine on clean metal films and to follow the formation of metal arsenides under controlled vacuum conditions.

### Experimental Section

The apparatus, the materials used, and the procedure for the preparation of the evaporated metal films (Fe, Ni, W, Pd, Pb, and Ag) have already been described.<sup>5-10</sup> The films were always sintered at  $60^\circ$  for 20 min before surface area determination by krypton adsorption at  $-195^\circ$  and the subsequent interaction with  $\text{AsH}_3$ . The procedure for outgassing the apparatus and the metal

filaments has also been described in previous papers.<sup>5-10</sup> In a typical experiment, after the apparatus had been thoroughly outgassed, the rate of degassing, with the reaction vessel maintained at  $450^\circ$ , was  $<10^{-3}$  N m<sup>-2</sup> hr<sup>-1</sup>. During the deposition of the film the reaction vessel was maintained open to the pumps and the pressure was always  $<10^{-4}$  N m<sup>-2</sup>.

Arsine was prepared from dilute sulfuric acid, sodium arsenate, and zinc powder at room temperature. The gas was passed through a trap which was kept at  $-80^\circ$ , and finally freed from permanent gases by condensing at  $-195^\circ$  and pumping. New supplies of

- (1) R. D. Clay and E. E. Petersen, *J. Catal.*, **16**, 30 (1970).
- (2) E. B. Maxted, *Advan. Catal.*, **3**, 129 (1951).
- (3) G. G. Devyatikh, *Poluch. Anal. Veshchestv Osoboi Chist., Mater. Veses. Konf.*, **1963**, 5 (1966).
- (4) J. L. Gay Lussac and L. J. Thenard, *Ann. Chim. Phys.*, **73**, 229 (1810).
- (5) J. M. Saleh, C. Kemball, and M. W. Roberts, *Trans. Faraday Soc.*, **57**, 259 (1961).
- (6) A. M. Al-Haidery and J. M. Saleh, *ibid.*, **66**, 3113 (1970).
- (7) J. M. Saleh, *ibid.*, **67**, 1830 (1971).
- (8) Y. M. Dadiza and J. M. Saleh, *J. Chem. Soc., Faraday Trans. 1*, **68**, 269 (1972).
- (9) J. M. Saleh, *Trans. Faraday Soc.*, **66**, 242 (1970).
- (10) J. M. Saleh, B. R. Wells, and M. W. Roberts, *ibid.*, **62**, 2301 (1964).

the gas were prepared frequently and its vapor pressure at  $-195^\circ$ , as measured by a McLeod gauge, was  $10^{-3}$  N m $^{-2}$  and this value was quite reproducible for different samples of the gas. The gas was condensed at  $-195^\circ$  and pumped for few minutes before use. The doses were admitted to the reaction system through a trap which was cooled to  $-80^\circ$ . A series of careful blank experiments showed that arsine was quite stable in the temperature range  $-80$  to  $250^\circ$  in absence of evaporated metal films. Mixtures of AsH $_3$  plus H $_2$  were analyzed by condensing the former gas in a cold glass finger immersed in liquid nitrogen; the condensation occurred within 1 min when the total pressure was  $\leq 9$  N m $^{-2}$ .

After preparing and sintering the film, the general procedure was to determine the volume of krypton required to form a monolayer on the film at  $-195^\circ$ . Then, the krypton was removed by pumping at room temperature for 30 min and subsequently the AsH $_3$  was admitted to the film at  $-80^\circ$ . After the initial fast chemisorption, the interaction was investigated using pressures in the range 6–8 N m $^{-2}$ . The reaction was followed until the rate of change of gas composition had become small and the film was then warmed in successive stages to about  $200^\circ$ , the products being analyzed continuously. The area of the film was redetermined at the end of each run.

## Results

The extent of AsH $_3$  uptake was expressed as  $X = V_{\text{AsH}_3}/V_{\text{Kr}}$ , where  $V_{\text{AsH}_3}$  was the volume of AsH $_3$  adsorbed and  $V_{\text{Kr}}$  was the mono layer of krypton which was determined using the point B method.<sup>5</sup>

*Adsorption at  $-80^\circ$ .* There was an initial rapid uptake of AsH $_3$  (at  $-80^\circ$  and  $P_{\text{AsH}_3} = 6$  N m $^{-2}$ ) on films of Fe, Ni, Pd, and W until  $X$  was  $\sim 1.5$  on the first three metals and  $X = 0.6$  on W. Thereafter, adsorption became slow and proceeded at a measurable rate. Hydrogen evolution began at low coverages of the surface by AsH $_3$  ( $X \simeq 0.2$ ) and the extent increased as  $X$  increased. The structure of the surface phase was represented as AsH $_n$ , where  $n$  was calculated at various values of  $X$  from the relationship

$$n = (3V_{\text{AsH}_3} - 2\bar{V}_{\text{H}_2})/V_{\text{AsH}_3} \quad (1)$$

where  $V_{\text{AsH}_3}$  and  $\bar{V}_{\text{H}_2}$  were the volumes of the adsorbed AsH $_3$  and the desorbed H $_2$  at the same value of  $X$ , respectively. Figure 1 shows the plot of  $n$  against  $X$  on the previous four metals at  $-80^\circ$ . The lowest value of  $n$  at the latter temperature was  $\sim 1.0$  on Fe,  $\sim 2.0$  on Ni, and just below 3.0 on Pd and W films. The maximum value of  $X$  at  $-80^\circ$  on the first three metals was  $\sim 1.7$ , but on W it was not possible to attain, at this temperature, values of  $X > 0.76$ . Furthermore, some  $\sim 15\%$  of AsH $_3$  adsorption on W film at  $-80^\circ$  was molecular and reversible.

Adsorption of AsH $_3$  on both Ag and Pb films at

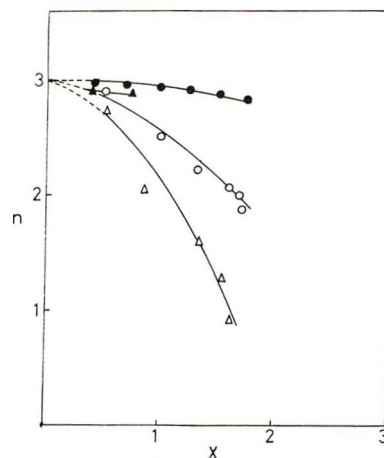


Figure 1. Composition of the surface phase  $n$ , representing AsH $_n$ , plotted against  $X$  on Fe ( $\Delta$ ), Ni ( $\circ$ ), Pd ( $\bullet$ ), and W ( $\blacktriangle$ ) films at  $-80^\circ$ .

$-80^\circ$  was entirely molecular and reversible; the adsorbate was completely desorbed on warming the film to  $30^\circ$  and a similar amount could be re-adsorbed on cooling back to  $-80^\circ$ . It was also possible to remove the adsorbed AsH $_3$  merely by evacuation of the reaction vessel down to  $10^{-2}$  N m $^{-2}$ . Table I gives the relationship of the initial surface area ( $V_{\text{Kr}}$ ) to the total AsH $_3$  uptake ( $V_{\text{AsH}_3}$ ) at  $-80^\circ$  and the subsequent H $_2$  evolution ( $\bar{V}_{\text{H}_2}$ ) at this temperature for typical experiments on various metals. The final values of  $X$  and  $n$  at  $-80^\circ$  as well as the volume of AsH $_3$  which was desorbed on warming each film to  $30^\circ$  ( $\bar{V}_{\text{AsH}_3}$ ) are also indicated in the table.

Table I: Adsorption of AsH $_3$  on Films of Fe, Ni, Pd, W, Ag, and Pb at  $-80^\circ$  and a Gas Pressure of  $\sim 6.0$  N m $^{-2}$ <sup>a</sup>

Film	$V_{\text{Kr}}$	$V_{\text{AsH}_3}$	$X$	$\bar{V}_{\text{H}_2}$	$n$	$\bar{V}_{\text{AsH}_3}$
Fe	94.3	157.68	1.67	160.75	0.96	
Ni	86.1	146.37	1.70	74.0	1.92	
Pd	76.3	129.71	1.70	19.00	2.70	
W	91.2	79.7	0.86	5.00	2.86	12
Ag	3.78	3.78	1.0		3.0	3.5
Pb	3.78	3.63	0.96		3.0	3.5

<sup>a</sup> Volumes are expressed in  $\mu\text{l}$  (stp).

*Effect of Oxidation on the Subsequent AsH $_3$  Uptake at  $-80^\circ$ .* In a series of experiments, the film was first saturated at  $30^\circ$  and a gas pressure of  $\sim 6$  N m $^{-2}$  with oxygen. The total volume of oxygen adsorbed was denoted  $V_{\text{O}_2}$  and the extent of oxidation was represented by  $Y = V_{\text{O}_2}/V_{\text{Kr}}$ . Oxygen adsorption, at  $30^\circ$  under a pressure of 6 N m $^{-2}$ , on clean films of Fe, Ni, Pd, and W caused a substantial sintering to occur. This is shown in Table II by comparing the original surface area  $V_{\text{Kr}}$  of a film with its area  $\bar{V}_{\text{Kr}}$  after saturation, at  $30^\circ$  and  $P_{\text{O}_2} = 6$  N m $^{-2}$ , with oxy-

gen ( $V_{O_2}$ ); a better representation of the extent of sintering is indicated in the values of  $S = \bar{V}_{Kr}/V_{Kr}$  (Table II). The heavy oxidation ( $Y = 8.5$ ) of Fe film was parallel with the ease of sintering of this metal ( $S = 0.15$ ). Although oxidation of W film ( $Y = 0.84$ ) was less extensive under the same conditions than that of Ni film ( $Y = 3.45$ ), yet nearly the same extent of sintering resulted ( $S = 0.34-0.37$ ).

**Table II:** Adsorption of  $AsH_3$  on Oxidized Films of Fe, Ni, Pd, and W at  $-80^\circ$  and  $P_{AsH_3} = 6.0 \text{ N m}^{-2}$ <sup>a</sup>

Film	$V_{Kr}$	$V_{O_2}$	$Y$	$\bar{V}_{Kr}$	$S$	$V_{AsH_3}$	$X$
Fe	36.0	307.7	8.5	5.33	0.15	29.36	5.51
Ni	42.6	147.3	3.45	14.76	0.34	41.03	2.78
Pd	39.5	46.1	1.56	16.4	0.41	88.07	5.37
W	70.6	59.3	0.84	26.6	0.37	18.6	0.70

<sup>a</sup>  $Y = V_{O_2}/V_{Kr}$  and  $S = \bar{V}_{Kr}/V_{Kr}$ .

Fast irreversible adsorption of  $AsH_3$  took place at  $-80^\circ$  on films of Fe, Ni, Pd, and W which had been saturated with oxygen as described above. The maximum values of  $X$ , as calculated in terms of  $\bar{V}_{Kr}$ , on oxidized Fe, Ni, and Pd films (Table II) were appreciably higher than the values obtained with the corresponding clean metals (Table I). The extent of  $AsH_3$  uptake on oxidized W film at  $-80^\circ$  was ( $X = 0.7$ ) small as compared with the amounts adsorbed on the other three oxidized films at the same temperature. The volume of  $H_2$ , which was desorbed subsequent to  $AsH_3$  adsorption at  $-80^\circ$ , was so small that values of  $n$  remained always close to  $\sim 3.0$ . No gas ( $H_2$  or  $H_2O$ ) was desorbed on pumping the film at  $-80^\circ$  down to  $10^{-3} \text{ N m}^{-2}$  or on heating the film to  $200^\circ$ .

*Tarnishing by  $AsH_3$ .* Extensive arsenidation of Fe, Ni, and Pd films occurred by  $AsH_3$  at temperatures  $\geq 25^\circ$  at a rate which increased with temperature. The reaction became appreciably fast at temperatures  $> 160^\circ$ ; and at any temperature the total gas pressure increased with time on Fe and Ni films as shown in Figure 2. The amount of  $H_2$  evolved at a given time, on either Fe or Ni film, was always  $3/2$  times as much as  $AsH_3$  adsorbed. The relationship between the extent of  $AsH_3$  adsorption and the subsequent  $H_2$  evolution in the same period of time is indicated for three typical experiments in Table III.

The total pressure ( $P_{AsH_3} + P_{H_2}$ ) on W film at a constant temperature in the range  $25-200^\circ$  remained virtually constant (Table III) because of the desorption of one  $H_2$  molecule for each  $AsH_3$  molecule adsorbed. The rate of the reaction at the same temperature and  $P_{AsH_3}$  decreased considerably over a limited increase in  $X$  (from 1.5 to 2.5); the rate at  $200^\circ$  and  $P_{AsH_3} = 6 \text{ N m}^{-2}$  became  $\sim 2.0 \mu\text{l hr}^{-1} \text{ cm}^{-2}$  when  $X$  approached 2.5.

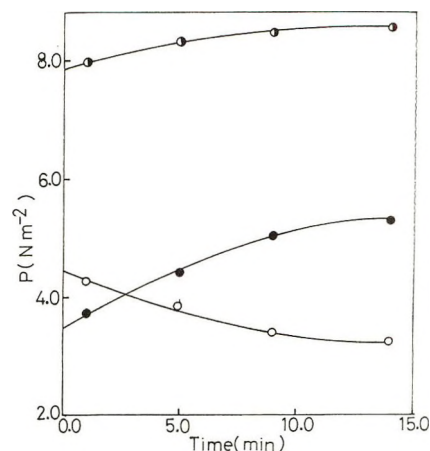


**Figure 2.** Interaction of  $AsH_3$  with Fe film at  $80^\circ$ : (●), total pressure; (○), pressure of  $AsH_3$ ; (●), pressure of  $H_2$ .

**Table III:** Extent of Increase in the Total ( $\Delta P$ ) and Hydrogen Pressures ( $\Delta P_{H_2}$ ) while  $AsH_3$  Pressure Decreased ( $-\Delta P_{AsH_3}$ ) in the Same Period and Temperature<sup>a</sup>

Film	$\Delta P$	$\Delta P_{H_2}$	$-\Delta P_{AsH_3}$	Period, min	Temp, $^\circ\text{C}$
Fe	1.235	2.820	1.600	9	58
	0.546	1.534	1.000	6	80
Ni	2.067	5.980	3.900	16	60
	1.482	3.562	2.080	7	80
W		1.82	1.82	14	28
		0.75	0.75	14	100
		1.482	1.482	12	150

<sup>a</sup>  $P$  is expressed in  $\text{N m}^{-2}$ .

On Pb film at any temperature above  $80^\circ$  there was a continuous decrease in the total gas pressure with time because  $H_2$  evolution was much slower than  $AsH_3$  adsorption. The main feature of  $AsH_3$  interaction with Ag films between  $30$  and  $200^\circ$  was similar to that with Pb although both the rates of  $AsH_3$  uptake and of subsequent  $H_2$  evolution, under similar conditions, were faster on Ag than on Pb.

Oxidized Pd and Fe were in general more active, while oxidized Ni and W were much less active, toward  $AsH_3$  than the corresponding clean films. A steady  $H_2$  evolution as a consequence of  $AsH_3$  adsorption with oxidized films began only beyond certain values of  $X$ . The minimum value of  $X$  at which a steady  $H_2$  evolution was detected depended both on the extent of the preoxidation ( $Y$ ) and the temperature of the film as indicated in Table IV. Beyond such values of  $X$  at the specified temperatures, the behavior of the oxidized film approached that of the corresponding clean film with respect to the relation of  $\bar{V}_{H_2}$  to that of  $V_{AsH_3}$  for the same period of time.

*Kinetics of Metal Tarnishing by  $AsH_3$ .* The rate of the reaction depended directly on  $AsH_3$  pressure. This was done by measuring the rate of  $AsH_3$  uptake

**Table IV:** Relationship between the Extent of Preoxidation ( $Y$ ) and the Subsequent Value of  $X$  at which a Steady Evolution of  $H_2$  Began

Film	$Y$	$X$	— $H_2$ evolution at— Temp, °C
Fe	8.5	10	$\geq 100$
Ni	3.45	6	$\geq 120$
Pd	1.56	4	$\geq 60$
W	0.84	2.7	$\geq 200$

( $r_1$ ) at an initial pressure  $P_1$ , the pressure was then rapidly changed to a different constant pressure  $P_2$  at which the new rate ( $r_2$ ) of adsorption was estimated. Both rates were assumed to depend on  $P^n$ , consequently the exponent  $n$  was evaluated from the relation<sup>6</sup>

$$r_1/r_2 = (P_1/P_2)^n \quad (2)$$

The values of  $n$  thus obtained ranged from 0.85 to 1.0, from which we assumed a pressure dependence of  $n = 1$  since the experimental procedure used (eq 2) always tends to give results which are slightly smaller than the true value.

From the rates of  $AsH_3$  adsorption at two different temperatures and the same value of  $X$ , activation energies ( $E$ ) of the tarnishing reaction were obtained. The reaction proceeded on each metal with a constant energy of activation ( $E$ ) which was independent of  $X$  as indicated in Table V. The rate ( $r$ ) of the reaction at constant temperature and  $P_{AsH_3}$  decreased steadily as  $X$  increased and this was reflected in the values of the frequency factor ( $A$ ) in the rate expression

$$r = Ae^{-E/RT} \quad (3)$$

where  $A$  contains a  $(P_{AsH_3})^{1.0}$  term. The rates of adsorption at different values of  $X$  were first determined under the same  $AsH_3$  pressure of  $\sim 6 \text{ N m}^{-2}$ . Using the appropriate value of  $E$  for each film, the corre-

**Table V:** Activation Energies ( $E$ ) of Metal Tarnishing by  $AsH_3$ 

Film	$X$	Temp range, °C	$E$ , kJ mol <sup>-1</sup>
Fe	1.6–2.4	–45–100	35.5
Ni	1.56–3.64	–80–100	35.5
Pd	1.86–2.0	–45–50	50.3
W	0.76–1.67	–80–150	58.1
Ag	1.0–9.7	–80–200	42.5
Pb	3.66–6.66	80–200	44.0
Oxidized Fe	5.5–8.05	–80–180	25.5
Oxidized Ni	2.7–3.9	–80–150	23.3
Oxidized Pd	5.37–6.15	–80–50	21.5
Oxidized W	0.7–1.2	60–200	46.7
Pb–Pd	1.58–7.73	–80–100	56.5
Pb–Ni	4.14–7.25	–80–50	13.0

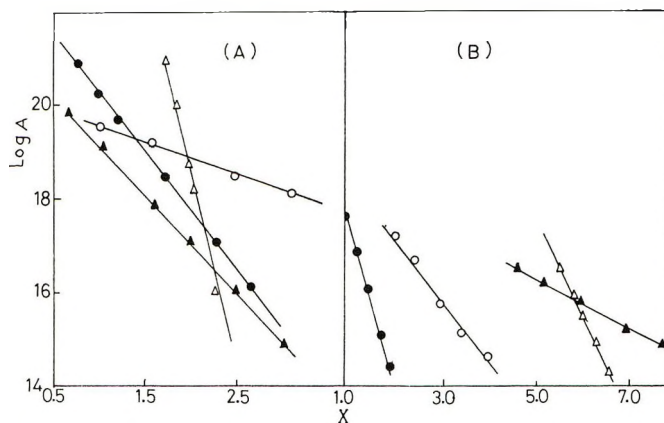


Figure 3.  $\log A$  plotted against  $X$ : (A) clean Ni ( $\circ$ ), Pd ( $\Delta$ ), W ( $\bullet$ ), and Fe ( $\blacktriangle$ ) films; (B) oxidized films of Fe ( $\blacktriangle$ ), Pd ( $\Delta$ ), W ( $\bullet$ ), and Ni ( $\circ$ ). The points represented various temperatures in the range 30–120°. The units of  $A$  are molecules  $\text{cm}^{-2} \text{sec}^{-1}$ .

sponding values of  $A$  were estimated. Figure 3 shows the relationship of  $\log A$  against  $X$  for various systems and the plots are shown to be quite linear over a wide range of  $X$ .

**Two-Metal Films.** In a series of experiments, a metal film of Pd (or Ni) was first deposited on the glass walls of the reaction vessel which was kept at  $-195^\circ$ . The film was then sintered (at  $60^\circ$  for 20 min) and its area was measured from krypton adsorption. The film was then pumped to remove the krypton until a vacuum of  $10^{-4} \text{ N m}^{-2}$  was established in the system. The film was then cooled to  $-195^\circ$  and a thick film of Pb was deposited on top of the former film. The resulting two-metal film of Pb–Pd (or Pb–Ni) was resintered and its area ( $\bar{V}_{Kr}$ ) was subsequently determined prior to interaction with  $AsH_3$ .

**Pb–Pd.** The area of a Pd film decreased on subsequent deposition of a thick Pb film. In a typical experiment, the area of a Pd film weighing 70 mg was  $V_{Kr} = 50.9 \mu\text{l}$  and this decreased to  $\bar{V}_{Kr} = 17.5 \mu\text{l}$  when a thick Pb film (weight = 250 mg) was deposited on top of the former; the reduction in area was by a factor of  $\sim 3.0$ . Such a relationship between  $V_{Kr}$  and  $\bar{V}_{Kr}$  was quite reproducible as confirmed by a number of similar experiments.

Rapid adsorption of  $AsH_3$  to the extent  $X = 1.77$  took place on the resulting Pb–Pd film at  $-80^\circ$  without  $H_2$  evolution. Further, but extensive  $AsH_3$  uptake was observed at temperatures  $\geq 30^\circ$  with a constant energy of activation of  $56.5 \text{ kJ mol}^{-1}$ . Values of  $A$  were obtained at various values of  $X$  and temperatures as described before and the results were plotted as  $\log A$  vs.  $X$  in Figure 4.

**Pb–Ni.** The area of a nickel film, on top of which a thick Pb film was deposited (Pb–Ni), was less than the area of the underlying Ni film; there was a reduction in the area of Ni film due to the deposition of Pb film. In an experiment, the area of a nickel film (weighing

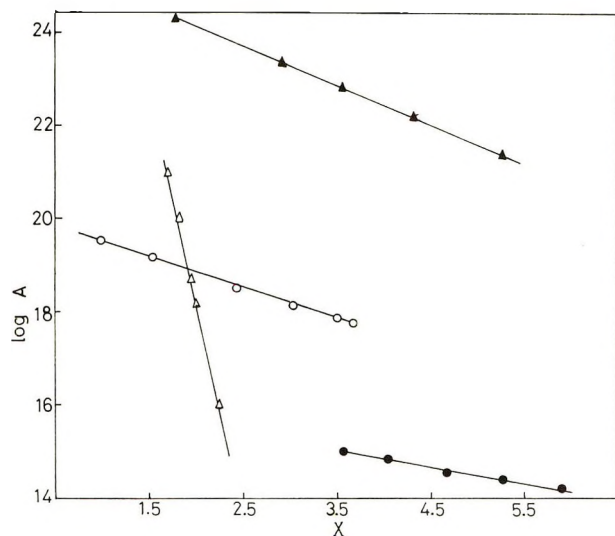


Figure 4.  $\log A$  plotted against  $X$  for two-metal films of Pb-Ni (●) and Pb-Pd (▲). The points for clean Ni (○) and Pd (△) points are also given for comparison.

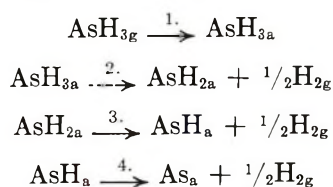
30 mg) was  $29.6 \mu\text{l}$  and this decreased to ( $\bar{V}_{kr}$ )  $26.6 \mu\text{l}$  on deposition of a thick Pb film (240 mg) on top of the former metal.

Fast adsorption of  $\text{AsH}_3$  occurred on a Pb-Ni film to the extent  $X = 4.14$  at  $-80^\circ$  and gas pressure of  $6 \text{ N m}^{-2}$ . Above this temperature there was only a very slow  $\text{AsH}_3$  uptake despite the low energy of activation of  $\sim 13 \text{ kJ mol}^{-1}$ . The values of  $\log A$  were plotted against  $X$  for this system as shown in Figure 4.

### Discussion

At  $-80^\circ$ . The results (Table I) indicate that films of Fe, Ni, Pd, and W chemisorbed  $\text{AsH}_3$  dissociatively at  $-80^\circ$  as extensive  $\text{H}_2$  evolution was observed at this temperature. The fact that chemisorption on each of Fe, Ni, and Pd films occurred at  $-80^\circ$  to the same extent of  $X = 1.7$  may suggest that the interaction of  $\text{AsH}_3$  with these metals at this temperature was confined exclusively to the surface. On the other hand values of  $X > 1.7$  were obtained on oxidized surfaces (see Table II) at  $-80^\circ$ ; these probably correspond to incorporation of As in the solid phase. The surface structures on clean films corresponded to  $1.7 \text{ AsH}_n$ , where  $n$  equals  $\sim 1.0$  on Fe,  $\sim 2.0$  on Ni, and just below 3.0 on Pd.

The results of adsorption at  $-80^\circ$  suggest that  $\text{AsH}_3$  molecules breakdown on metal surfaces by a number of steps involving the following.



where g and a refer to the gaseous and the adsorbed states, respectively. The surface phase at  $-80^\circ$  may

be composed mainly of  $\text{AsH}_a$  on Fe and  $\text{AsH}_{2a}$  on Ni. The minimum values of  $n$ , which were slightly  $< 1.0$  on Fe and slightly  $< 2.0$  on Ni films (Table I), indicate that, beside the main reactions on these metals, reaction 4 on Fe and reaction 3 on Ni were also taking place, though to a small extent, resulting in the formation of few  $\text{As}_a$  and  $\text{AsH}_a$  on these films, respectively. The complete breakdown of  $\text{AsH}_3$  molecules into adsorbed As and H is less likely to take place on these metals at  $-80^\circ$  because of the following facts.

(1) No  $\text{H}_2$  desorption was ever observed on rapid warming the films from  $-80$  to  $30^\circ$  or higher temperatures.

(2) The total surface sites are insufficient to accommodate the products (As and H) if complete dissociation takes place. The size of an arsenide ion ( $0.16 \text{ nm}^2$ ) is twice as large as of either Fe or Ni site ( $\sim 0.07 \text{ nm}^2$ ) and, on the assumption of complete breakdown, each AsH on Fe will occupy three surface sites while four sites are needed for each  $\text{AsH}_2$  on Ni film. Such a number of surface sites would not be available if the adsorption at  $-80^\circ$  to the extent  $X = 1.7$  was confined entirely to the surface even if it is assumed that each krypton atom (cross-sectional area =  $0.19 \text{ nm}^2$ ) covers three surface sites; to accommodate all the adsorbate to the surface there would be a need for surface areas which are greater than those available by factors of 1.7 for Fe and 2.3 for Ni. This argument still applies even if As adatoms were only partially ionic.

(3) The maximum value of  $X$  before incorporation occurred (at  $-80^\circ$ ) on Fe and Ni films was  $\sim 1.7$  corresponding, according to the previous scheme of gradual breakdown of  $\text{AsH}_3$ , approximately to one AsH (or  $\text{AsH}_2$ ) on two sites; the surface sites would be just sufficient to hold the adsorbed species at  $-80^\circ$  without necessary incorporation. In this way, the same extent of  $\text{AsH}_3$  adsorption ( $X = 1.7$ ) at this temperature, despite the different values of  $n$  in the adsorbed  $\text{AsH}_n$ , can thus be accounted for. This conclusion is again based on the assumption of taking the krypton atom to be equivalent to three surface sites.

(4) The results of Table III probably refer to the formation of  $\text{AsH}_a$  on W film at temperatures  $> 30^\circ$ , and this in turn may be an evidence in support of gradual breakdown mechanism which is depicted in the above scheme.

From the foregoing discussion, it would be reasonable to suggest the following types of surface states on Fe and Ni films at  $-80^\circ$ .



where the Ni site denoted 2 is assumed to be blocked by  $\text{AsH}_{2a}$  and the angle H-As-H remains almost similar to that in  $\text{AsH}_3$  ( $\sim 92^\circ$ ).

On Pd and W films both reactions 1 and 2 may take place at  $-80^\circ$  with the result that the value of  $n$  lies between 2 and 3. The desorption of molecular  $\text{AsH}_3$  on warming the films (particularly W film) from  $-80$  to  $30^\circ$  is evidence for the existence of  $\text{AsH}_{3a}$  on the surface. These molecules may be coordinated to the surface through As atom in a similar manner to the coordination of sulfur atoms in dimethyl sulfide with Pd.<sup>11</sup>  $\text{AsH}_3$  is known<sup>1,2</sup> as a poison toward a variety of catalytic reactions on transition metals due probably to the tendency of As atoms for coordination with metals. The comparatively low value of  $X$  on W film at  $-80^\circ$  may be ascribed to the high energy of activation for further  $\text{AsH}_3$  adsorption on the metal at this temperature.

*Oxidized Films at  $-80^\circ$ .* The final values of  $X$  at  $-80^\circ$  on oxidized films of Fe, Ni, and Pd, which were calculated in terms of  $\bar{V}_{Kr}$ , were substantially higher (Table II) than the corresponding values on clean films (Table I). Such high values of  $X$  on oxidized films provide evidence for incorporation of  $\text{AsH}_3$  even at  $-80^\circ$ . Both the metal and the oxide sites were likely involved in chemisorption of  $\text{AsH}_3$ . On oxide sites such "compounds" as  $\text{H}_3\text{AsO}_m$  may be formed, where  $m$  refers to the number of oxygen atoms taking part in the adsorption of  $\text{AsH}_3$  molecule. The hydrogen atoms of the adsorbed  $\text{AsH}_3$  may be strongly attached to the surface phase so that no  $\text{H}_2$  evolution takes place at temperatures below  $200^\circ$ .

*Kinetics of Tarnishing by  $\text{AsH}_3$ .* The tarnishing of clean and oxidized metal films at  $\geq 30^\circ$  by  $\text{AsH}_3$  took place with constant energies of activation (Table V). The rate of tarnishing, at constant temperature and  $\text{AsH}_3$  pressure, decreased as  $X$  increased due to the decrease of the frequency factor ( $A$ ) in eq 3 which was given before. Since the pressure dependence ( $n$ ) is  $\sim 1.0$ , it would be reasonable to express  $A$  as<sup>8,12</sup>

$$A = C_g C_s kT/h \exp(\Delta S^\ddagger/R) \quad (4)$$

where  $\Delta S^\ddagger$  is the entropy of activation,  $C_g$  is the concentration of the gas molecules per  $\text{cm}^3$ , and  $C_s$  is the concentration of bare sites per  $\text{cm}^2$  of the surface. For an ideal gas  $P = C_g kT$  so that

$$A = C_s (P/h) \exp(\Delta S^\ddagger/R) \quad (5)$$

If  $\Delta S^\ddagger$  remains constant, which is likely because of the constancy of  $E$  for each system,<sup>8,13</sup> then the decrease in  $A$  at constant  $P$  would be attributed to the  $C_s$  term. Since  $C_s = n_s f(X)$ , where  $n_s$  is the total number of reacting sites per  $\text{cm}^2$  of the surface and  $f(X)$  is the fraction of the sites which is available for reaction with  $\text{AsH}_3$ , it would be possible to write

$$A = n_s (P/h) f(X) \exp(\Delta S^\ddagger/R) \quad (6)$$

The linear relationship between  $\log A$  and  $X$  in Figure 3 suggests that

$$A = A_0 \exp(-\alpha X) \quad (7)$$

where  $A_0$  is the value of  $A$  at  $X = 0$  and  $\alpha$  is a constant independent of temperature. Since the terms  $n_s$ ,  $P$ , and  $\Delta S^\ddagger$  are constants, then by comparing eq 6 with 7 it would be concluded that

$$f(X) = \exp(-\alpha X) \quad (8)$$

and

$$A_0 = n_s (P/h) \exp(\Delta S^\ddagger/R) \quad (9)$$

The reactivity toward  $\text{AsH}_3$  of the different metals having the same value of  $E$  can be deduced by comparing (i) the values of  $A$  (or  $\log A$ ) at the same value of  $X$  and (ii) the extent of the decrease in  $A$  with increasing  $X$ , that is, by comparing the slopes of the  $\log A$  vs.  $X$  plots of Figure 3. Since  $E$  is the same for both Ni and Fe films (Table V), it would be, therefore, reasonable to assign higher reactivity toward  $\text{AsH}_3$  to the former metal because of the greater  $A$  values on one hand, and due to the less decrease of  $A$  values with increasing  $X$  on the other hand. Also the values of  $E$  for both W and Pd films were almost the same (Table V) and for the same previous reasons W may be considered more reactive than Pd particularly at  $X > 2.0$ . Pd seems, from Figure 3, to be more active than W at some values of  $X$ , but such activity, nevertheless, is compensated by the sharp drop of  $A$  to very low values over a small decrease in  $X$  (Figure 3).

*Reactivity of the Oxidized Films.* The effect of surface oxide on subsequent  $\text{AsH}_3$  uptake, as indicated in Figure 3, seems to differ as in the following ways.

(1) A decrease in activity toward  $\text{AsH}_3$  was observed due to the oxidation of Ni and W films; the values of  $A$  at the same value of  $X$  were in general lower on oxidized Ni and W films than on the corresponding clean films, and also, the inclination of the plot ( $\log A$  against  $X$ ) of Figure 3 for oxidized films was sharper than for clean surfaces. On oxidized W in particular, the reaction of  $\text{AsH}_3$  proceeded to a much less extent as compared with either clean W or with the other oxidized films. This comparison ignored the slightly lower values of  $E$  on oxidized than on clean films (Table V).

(2) The reactivity of Fe, and to a less extent of Pd, increased considerably toward  $\text{AsH}_3$  on preoxidation; this is substantiated by the comparatively higher values of  $A$ , even at  $X > 5.0$ , and the smaller decrease of these values with increasing  $X$  on oxidized than on clean Fe and Pd films.

The presence of an oxide layer on a metal probably

(11) M. H. Dilke, D. D. Eley, and E. B. Maxted, *Nature (London)*, **161**, 804 (1948).

(12) S. Glasstone, K. J. Laidler, and H. Eyring, "The Theory of Rate Processes," McGraw-Hill, New York, N. Y., 1941.

(13) C. Kemball, *Proc. Roy. Soc., Ser. A*, **217**, 376 (1953).

alters the potential energy barrier to the outward diffusion of the metal atoms; on oxidized Fe and Pd the barrier is likely to be lowered and thus increasing the concentration of the reacting sites on the surface. If we assume that 0.4 nm of oxide is equivalent to one oxide layer ( $X = 1$ ), then the thickness of the oxide phase in any case did not exceed 3.0 nm. Up to an oxide thickness of  $\sim 4.0$  nm, the presence of the superimposed electric field was assumed<sup>14</sup> to have a marked influence on the observed kinetics of the tarnishing reaction on metals.

*Behavior of the "Two-Metal" Film.* A solid solution or an alloy, with a superlattice structure, may be formed<sup>15, 18</sup> on a slow cooling or annealing at low temperatures of two metals together. The tendency to form such structures increases with increasing difference in the atomic diameter.<sup>15-18</sup> In the present work, each of the binary systems (Pd-Pd and Pd-Ni) was exposed to the following heat effects: (i) the heat of condensation of Pb on Pd (or Ni), (ii) the effect of sintering of the two-metal film, and (iii) the gradual heating of the film during the experiment with  $\text{AsH}_3$ . These factors may enhance the mobility of the metal atoms and consequently facilitate the diffusion of Pd (or Ni) atoms into Pb lattice resulting in the formation of a solid solution or an alloy. Since the difference in the atomic diameter between Pb ( $r = 0.175$  nm) and Ni ( $r = 0.124$  nm) is greater than

the difference between Pb and Pd ( $r = 0.134$  nm), we would expect a more stable solid solution or alloy to be formed by the system Pb-Ni than from Pb-Pd. The surface potential of the chemisorbed gas ( $\text{AsH}_3$ ) may lower the potential energy barrier to the outward movement of Pd (or Ni) atoms through the Pb lattice.<sup>19</sup> Such an outward diffusion of metal atoms is likely to be greater in the less stable system, that is, Pb-Pd. This may account for the increased reactivity of the latter system toward  $\text{AsH}_3$ . The introduction of a metal into another metal disturbs the ease with which the electron and the defect can migrate through the solid. The lattice spacing in an alloy almost invariably lies between the values of the two component metals. There are also important changes in magnetic properties associated with the filling of the d band. These and other factors probably operate together to form the characteristic properties of a solid solution or an alloy.

(14) M. W. Roberts, *Quart. Rev., Chem. Soc.*, **16**, 71 (1962).

(15) W. Hume-Rothery and H. M. Powell, *Z. Kristallogr.*, **91**, 23 (1935).

(16) H. Lipson, *Progr. Metal Phys.*, **2**, 1 (1950).

(17) G. C. Bond, "Catalysis by Metals," Academic Press, New York, N. Y., 1962, pp 24-28 and 484-487.

(18) Y. M. Dadiza and J. M. Saleh, *J. Chem. Soc., Faraday Trans. 1*, **68**, 1513 (1972).

(19) N. Cabrera and N. F. Mott, *Rep. Progr. Phys.*, **12**, 163 (1948)

## Electron Spin Resonance Spectra of Di- and Trimethylaminiium Radicals<sup>1</sup>

by Richard W. Fessenden\* and P. Neta

Radiation Research Laboratories, Center for Special Studies and Department of Chemistry, Mellon Institute of Science, Carnegie-Mellon University, Pittsburgh, Pennsylvania 15213 (Received April 4, 1972)

Publication costs assisted by the Carnegie-Mellon University and the U. S. Atomic Energy Commission

The esr spectra obtained during radiolysis of acid solutions of di- and trimethylamine are shown to be due to the radicals  $(\text{CH}_3)_2\text{NH}\cdot^+$  and  $(\text{CH}_3)_3\text{N}\cdot^+$  formed by OH attack on the respective ammonium ions. The parameters which give the minimum rms error between observed and calculated positions are the following: for  $(\text{CH}_3)_2\text{NH}\cdot^+$ ,  $a^N = 19.23$  G,  $a_{\text{NH}}^H = 21.96$  G,  $a_{\text{CH}_3}^H = 33.61$  G, and  $g = 2.00354$  and for  $(\text{CH}_3)_3\text{N}\cdot^+$ ,  $a^N = 20.55$  G,  $a_{\text{CH}_3}^H = 28.56$  G, and  $g = 2.00357$ . The radical  $(\text{CH}_3)_2\text{NH}\cdot^+$  and its conjugate base  $(\text{CH}_3)_2\text{N}\cdot$  were also produced by the reaction of  $e_{\text{aq}}^-$  with  $(\text{CH}_3)_2\text{NCl}$ . The pK for the dissociation of  $(\text{CH}_3)_2\text{NH}\cdot^+$  is estimated to be 6.5-7.5.

A previous paper<sup>2</sup> reported esr spectra obtained during the steady-state radiolysis of acid solutions of di- and trimethylamine. However, problems were encountered in attempting to assign the observed spectra to radicals resulting directly from reaction of H and OH with the solutes. As a result the observed spectra

were attributed to radicals arising in secondary processes. The assignments given did not seem wholly satisfactory on a chemical basis and the need for fur-

(1) Supported in part by the U. S. Atomic Energy Commission.

(2) P. Neta and R. W. Fessenden, *J. Phys. Chem.*, **75**, 738 (1971).

ther study was suggested. The results of that study are reported here.

The approach to be used in this reinvestigation was suggested by a recent photolysis study by Danen and Rickard.<sup>3</sup> They report esr spectra of dialkylammonium radicals as formed by photolysis of dialkyl *N*-chloroamines and provide an unambiguous assignment of the spectrum of  $(\text{CH}_3)_2\text{NH}\cdot^+$ . Their parameters ( $a^{\text{N}} = 19.28$  G,  $a_{\text{NH}}^{\text{H}} = 22.73$  G,  $a_{\text{CH}_3}^{\text{H}} = 34.27$  G and  $g = 2.0036$ ) are essentially the same as found by us for the radical in irradiated solutions of dimethylammonium ion<sup>2</sup> suggesting rather strongly that the same radical is responsible for the two spectra. Our previous assignment,<sup>2</sup> now known to be incorrect, was to an aminium radical with only four equivalent protons. This misassignment is clearly the result of having insufficient signal-to-noise ratio to detect the unit-intensity lines at both the extremes of the spectrum and in the second-order structures.<sup>4</sup> The results reported here further substantiate this suggestion and show that a similar problem was encountered with trimethylammonium ion.

The improved signal-to-noise ratio, which made possible the detection of those lines missed previously, was largely the result of a recent improvement in magnetic field homogeneity through a new cavity design.<sup>5</sup> Experiments were carried out as described previously<sup>2</sup> with  $\sim 0.5$  M solutions of amine in  $\text{HClO}_4$  at pH 1. Experiments with dimethylammonium ion were also carried out at pH values of 3 and 6 in the presence of  $\text{N}_2\text{O}$ . Essentially the same spectrum was found at pH 3 as at pH 1 while no lines were found at pH 6. In addition to the studies of di- and trimethylammonium ions reported below monomethylammonium ion was also reinvestigated but (as found before) no radicals could be detected at pH 1.

The spectrum found with dimethylammonium ion consists of six septets with line positions and second-order structure appropriate to the radical  $(\text{CH}_3)_2\text{NH}\cdot^+$ . The six isolated unit-intensity lines at each end of the spectrum and many of the second-order groups were recorded and parameters fit by the computer program EXCALIES.<sup>6</sup> The spectral parameters obtained in the present work for  $(\text{CH}_3)_2\text{NH}\cdot^+$  are given in Table I along with those of Danen and Rickard.<sup>3</sup> The two sets of parameters are in satisfactory agreement although the values of  $a_{\text{NH}}^{\text{H}}$  and  $a_{\text{CH}_3}^{\text{H}}$  differ in each case by about 0.7 G. We attribute this difference to the effect of the solvent ( $\text{H}_2\text{O}$  vs. 90%  $\text{H}_2\text{SO}_4$ ). In the case of trimethylammonium ion the spectrum consists of three decets for nine equivalent protons as appropriate to the radical  $(\text{CH}_3)_3\text{N}\cdot^+$ . Again it was possible to detect the six unit-intensity lines at each end of the spectrum as well as those in the second-order groups. The parameters obtained from the computer calculation are given in Table I together with those of Tench<sup>7</sup> for  $(\text{CH}_3)_3\text{N}\cdot^+$  in the solid. The hyperfine constants in the solid are each 2 G lower than those reported here

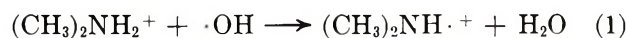
**Table I:** ESR Parameters of Di- and Trimethylammonium Radicals

	$(\text{CH}_3)_2\text{NH}\cdot^+$		$(\text{CH}_3)_3\text{N}\cdot^+$	
	Present work <sup>a,b</sup>	Danen and Rickard <sup>c</sup>	Present work <sup>a,d</sup>	Tench <sup>e</sup> (solid phase)
<i>g</i> factor	2.00354	2.0036	2.00357	
$a^{\text{N}}$	19.23	19.28	20.55	18.0
$a_{\text{NH}}^{\text{H}}$	(- )21.96	22.73		
$a_{\text{CH}_3}^{\text{H}}$	33.61	34.27	28.56	26.7

<sup>a</sup> The irradiated solutions contained 0.3–0.5 M of the amine at pH 1 or 3 and were saturated with  $\text{N}_2\text{O}$ . The hyperfine constants are given in Gauss and are accurate to  $\pm 0.03$  G. The *g* factors are measured relative to the peak from the silica cell and are accurate to  $\pm 0.00003$ . <sup>b</sup> Parameters were calculated using 53 lines. The rms error between observed and calculated spectra was 0.02 G. The maximum change in line position upon changing  $a_{\text{NH}}^{\text{H}}$  from - to + is less than the rms error so the sign cannot be determined. <sup>c</sup> Reference 3. <sup>d</sup> Parameters were calculated using 65 lines. The rms error was 0.02 G. <sup>e</sup> Reference 7.

for aqueous solution.

The formation of aminium radicals can be written as



and regarded as either an oxidation by electron transfer or H abstraction from the NH position. The fact that the spectrum observed at pH 3 in the presence of  $\text{N}_2\text{O}$  ( $G(\text{OH}) = 5.6$ ) was more intense than that at pH 1 ( $G(\text{OH}) = 2.8$ ,  $G(\text{H}) = 3.6$ ) shows that OH is the main contributor to the radical formation under these experimental conditions. The rate for this reaction can be estimated from the fact that 3 mM *tert*-butyl alcohol caused  $\sim 50\%$  drop in the signal of  $(\text{CH}_3)_2\text{NH}\cdot^+$  with 0.5 M  $(\text{CH}_3)_2\text{NH}_2^+$ . The rate constant for reaction 1 so obtained is  $\sim 10^6$  M<sup>-1</sup> sec<sup>-1</sup>. Because the overall rate constant for reaction of OH with these amines is  $\sim 10^7$  M<sup>-1</sup> sec<sup>-1</sup> in acid solution<sup>8</sup> a major fraction of the OH must react by another path. This path has been shown by both the product analysis<sup>9</sup> and esr spectra<sup>2</sup> to be the abstraction of hydrogen from methyl groups to form carbon-centered radicals. In acid solutions the esr spectra of these carbon-centered radicals are not evident, apparently as a result of line broadening by exchange of the ammonium protons.

(3) W. C. Danen and R. C. Rickard, *J. Amer. Chem. Soc.*, **94**, 3254 (1972).

(4) Even with this misassignment the parameters obtained by us<sup>2</sup> are accurate because the positions of the observed lines in the second-order groups are the same with either four or six equivalent protons.

(5) D. Behar and R. W. Fessenden, *J. Phys. Chem.*, **76**, 1710 (1972).

(6) R. W. Fessenden, *J. Magn. Resonance*, **1**, 277 (1969).

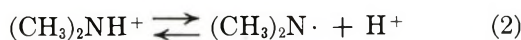
(7) A. J. Tench, *J. Chem. Phys.*, **38**, 593 (1963).

(8) N. Getoff and F. Schwörer, *Int. J. Radiat. Phys. Chem.*, **3**, 429 (1971).

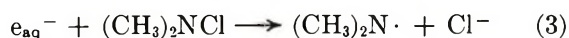
(9) See the review by W. M. Garrison in "Current Topics in Radiation Research," M. Ebert and A. Howard, Ed., North-Holland Publishing Co., Amsterdam, 1968, p 43.

The large total signal intensity of the aminium radicals<sup>10</sup> together with only partial conversion of OH imply that the disappearance rate constants for these species are relatively low.

Although strong signals of  $(\text{CH}_3)_2\text{NH}\cdot^+$  were found at pH 3 in experiments with  $(\text{CH}_3)_2\text{NH}_2^+$  no signals were found at pH 6. This result was interpreted as the effect of the dissociation



and consequent line broadening. To investigate this dissociation further a source of radicals applicable over a wider range of pH was necessary. Following preliminary experiments with a sample of *N*-chlorodiisopropylamine<sup>11</sup> it was found that the reaction



is a source of  $(\text{CH}_3)_2\text{N}\cdot$  (or of its conjugate acid  $(\text{CH}_3)_2\text{NH}\cdot^+$ ). Experiments with  $(\text{CH}_3)_2\text{NCl}$ <sup>12</sup> at pH 4.0 and 4.3 showed essentially the same signal intensity from  $(\text{CH}_3)_2\text{NH}\cdot^+$  while at pH 5.2 the lines were much weaker. No lines at all were detected at pH 7.2 and 8.0 but at pH 8.7 lines attributable to  $(\text{CH}_3)_2\text{N}\cdot$  were found. Somewhat higher intensities of this latter species were found at pH 9–11. The parameters found for  $(\text{CH}_3)_2\text{N}\cdot$  are shown in Table II together with those reported by Danen and Kensler.<sup>13</sup> It should be noted that this radical was not found in a previous study<sup>2</sup> with dimethylamine solutions although its formation was expected.

The absence of lines in the region  $5.2 < \text{pH} < 8.7$  is taken to mean that proton exchange (net result reaction 2) causes line broadening and that the *pK* of  $(\text{CH}_3)_2\text{NH}\cdot^+$  is 6.5–7.5. The exchange cannot involve  $\text{H}^+$  or  $\text{OH}^-$  directly because of the near neutral conditions. Several solutes such as the  $\sim\text{mM}$  phosphate buffer and

Table II: ESR Parameters of  $(\text{CH}_3)_2\text{N}\cdot$

	Present work <sup>a</sup>	Danen, <i>et al.</i> <sup>b</sup>
<i>g</i> factor	2.00440	2.0044
<i>a</i> <sup>N</sup>	15.65	14.78
<i>a</i> <sub>CH<sub>3</sub>H</sub>	28.48	27.36

<sup>a</sup> The irradiated solution contained  $\sim 10^{-3}$  M  $(\text{CH}_3)_2\text{NCl}$  at pH 10.0 and was deoxygenated by bubbling with pure nitrogen. The hyperfine constants are given in Gauss and are accurate to  $\pm 0.03$  G. The *g* factor is measured relative to the peak from the silica cell and is accurate to  $\pm 0.00003$ . Second-order corrections have been made. The unit-intensity lines both at the ends of the spectrum and in the second-order patterns were too weak to be observed. <sup>b</sup> References 3 and 13. The radical was prepared by photolysis of the corresponding tetrazene in cyclopropane solution at  $-90^\circ$ .

the  $(\text{CH}_3)_2\text{NCl}$  are, however, present at sufficient concentration to mediate the exchange. A more quantitative study of the *pK* and of the exchange is precluded by the weakness of the spectra of the two forms of the radical when produced in this way.

*Acknowledgment.* We are indebted to Dr. W. C. Danen for communicating his results prior to publication and for supplying a sample of *N*-chlorodiisopropylamine.

(10) The unit-intensity lines represent  $1/381$  and  $1/1536$  of the total ESR intensity for  $(\text{CH}_3)_2\text{NH}\cdot^+$  and  $(\text{CH}_3)_2\text{N}\cdot^+$ , respectively.

(11) Kindly supplied by Dr. W. C. Danen.

(12) Prepared as described by W. S. Metcalf [*J. Chem. Soc.*, 148 (1942)] by mixing phosphate-buffered solutions of  $(\text{CH}_3)_2\text{NH}_2^+$  and HOCl. The reaction mixture was then diluted to a nominal 1 mM of  $(\text{CH}_3)_2\text{NCl}$  and used immediately after adjustment of the pH.

(13) W. C. Danen and T. T. Kensler, *J. Amer. Chem. Soc.*, **92**, 5235 (1970).

# Electron Paramagnetic Resonance Study of Copper(II)-Ammonia Complexes in Y-Type Zeolites

by E. F. Vansant<sup>1</sup> and J. H. Lunsford\*

Department of Chemistry, Texas A & M University, College Station, Texas 77843 (Received February 28, 1972)

Publication costs assisted by the National Science Foundation

The epr spectra of some cupric ammonia, monomethylamine, and monoethylamine complexes in various ion-exchanged Y zeolites were studied. Particular attention was given to the influence of the adsorption and desorption temperature on the symmetry and composition of the copper(II)-amine complexes. Ammonia adsorption in Cu(II)Y zeolites at different temperatures resulted in the formation of a complex having a square planar symmetry with four ammonia molecules per  $\text{Cu}^{2+}$  ion. Desorption of the amines produced spectral changes corresponding to the transition from a square planar to a distorted tetrahedral symmetry with one amine per  $\text{Cu}^{2+}$  ion. Complete removal of the amine from the complex resulted in the formation of nonlinear pairs of  $\text{Cu}^{2+}$  ions in the sodalite cages.

## Introduction

Complexes of the copper(II) cations in zeolite crystals have been the subject of a number of electron paramagnetic resonance (epr) studies.<sup>2-6</sup> Small concentrations of  $\text{Cu}^{2+}$  yield a characteristic hyperfine spectrum, which may be correlated to a crystallographic coordination in the lattice framework. The hyperfine structure is sensitive to the symmetry and bonding character of the  $\text{Cu}^{2+}$  ions to their ligands. Nicula, *et al.*,<sup>2a</sup> Richardson,<sup>2b</sup> and Naccache and Ben Taarit<sup>3</sup> reported that the dehydration process of the copper-containing zeolites results in a transition from a distorted octahedral to a square planar symmetry for the  $\text{Cu}^{2+}$  ions. Moreover, Richardson<sup>2b</sup> observed that the relative energy of the  $d_{x^2-y^2}$  levels increased with increasing polarizing power,  $e/r$ , of the neighboring cations. The spectrum also indicated a fully ionic bond between the copper(II) ions and the surrounding lattice oxygens. For ammoniated and hydrated Cu(II)NaY zeolites, Naccache, *et al.*,<sup>3</sup> and Nicula, *et al.*,<sup>2a</sup> pointed out that the  $\text{Cu}^{2+}$ -ligand bond had considerable covalent character, and they suggested a hexacoordinated copper(II) complex in the large cavities.

The purpose of this epr study was to examine the copper-ammonia complexes that were formed in Y zeolites under various adsorption and desorption conditions. Complexes with monomethylamine and monoethylamine were also investigated to determine the influence of the size of the ligand.

## Experimental Section

The copper(II) zeolites were prepared by treating Linde type Y zeolites (NaY Lot No. 13544-76) with aqueous 1 to 5 mixtures of  $\text{Cu}^{2+}$  and  $\text{Na}^+$ ,  $\text{Ba}^{2+}$ ,  $\text{Ca}^{2+}$ , or  $\text{Mg}^{2+}$  salts. After the exchange, the zeolite samples were washed several times with distilled water to re-

move the excess salts and dried at  $100^\circ$ . After an oxygen pretreatment the zeolite samples were then evacuated stepwise from room temperature to  $500^\circ$  under a vacuum of  $10^{-5}$  Torr. The analyses of the Cu(II)NaY, Cu(II)MgY, Cu(II)CaY, and Cu(II)BaY zeolites indicated 3.5, 10.1, 5.1, and 3  $\text{Cu}^{2+}$  ions per unit cell, respectively.

The adsorption and desorption of ammonia on the copper(II)Y zeolites were carried out at different temperatures in a vacuum system. The  $^{14}\text{NH}_3$ ,  $^{15}\text{NH}_3$  enriched to 95%  $\text{N-15}$ ,  $\text{CH}_3\text{NH}_2$ , and  $\text{C}_2\text{H}_5\text{NH}_2$  were obtained from commercial sources and were used without further purification.

The epr measurements were made with a Varian spectrometer (Model V4502). The instrument was operated either at about 9.3 GHz (X band) or at 35 GHz (Q band). The  $g$  values were determined by using a 2,2-diphenyl-1-picrylhydrazyl ( $g = 2.0036$ ) standard. The sample tubes were usually filled with zeolite powder to a height greater than that of the TE<sub>102</sub> mode microwave cavity. All of the epr measurements were made at room temperature and at  $-196^\circ$ .

## Results and Discussion

*A. Paramagnetic Properties of the Copper(II) Ions in Various Ion-Exchanged Y Zeolites.* The relative simplicity of the epr spectra of copper(II) ions and their complexes makes them ideal species to study in

(1) On leave from the Laboratorium voor Oppervlaktescheikunde, Heverlee, Belgium.

(2) (a) A. Nicula, D. Stamires, and J. Turkevich, *J. Chem. Phys.*, **42**, 3684 (1965); (b) J. T. Richardson, *J. Catal.*, **9**, 178 (1967).

(3) C. Naccache and Y. Ben Taarit, *Chem. Phys. Lett.*, **11**, 11 (1971).

(4) D. Mikheikin, V. A. Shvets, and V. B. Kazanskii, *Kinet. Katal.*, **29**, 1395 (1968).

(5) C. C. Chao and J. H. Lunsford, *J. Chem. Phys.*, in press.

(6) H. B. Slot and J. L. Verbeek, *J. Catal.*, **12**, 216 (1968).

**Table I:** Magnetic Parameters<sup>a, b</sup> of Copper(II) Ions in Y Zeolites

Sample	Temp, °C	$g_{  }^{(1)c}$	$g_{  }^{(2)}$	$A_{  }^{(1)}$	$A_{  }^{(2)}$	$g_{\perp}$	$A_{\perp}$
Cu(II)NaY	RT <sup>d</sup>	$\pm 0.005$ 2.32	$\pm 0.005$ 2.27	$\pm 2$ 150	$\pm 2$ 130	$\pm 0.005$ 2.063	$\pm 2$ 20
	-196	2.32	2.26	154	130	2.062	20
Cu(II)BaY	RT	2.33	2.248	150	131	2.061	20
	-196	2.32	2.248	153	132	2.062	20
Cu(II)CaY	RT	2.33		135		2.058	
	-196	2.34		135		2.056	20
Cu(II)MgY	RT	2.34		136		2.051	
	-196	2.34		136		2.052	20

<sup>a</sup>  $A_{||}$  and  $A_{\perp}$  are in Gauss. <sup>b</sup>  $g_{\perp}$  computed from  $1/g_{\perp} = 1/g_m - 0.342(1/g_m - 1/g_c)$ , where  $g_m$  is the  $g$  value at the high-field minimum and  $g_c$  is the  $g$  value taken where the spectrum crosses the baseline.<sup>8</sup> <sup>c</sup> Superscripts refer to a particular spectrum. <sup>d</sup> RT denotes room temperature.

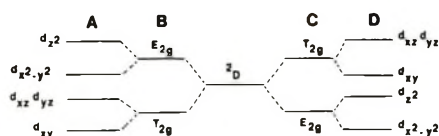


Figure 1. The scheme of the splitting of the energy levels for a  $3d^9$  hole: A, tetrahedral symmetry with tetragonal elongation; B, tetrahedral symmetry; C, octahedral symmetry; D, octahedral symmetry with tetragonal elongation or square planar symmetry.

zeolites. The free  $\text{Cu}^{2+}$  ion has an electron configuration  $1s^2 2s^2 2p^6 3s^2 3p^6 3d^9$  giving rise to a  $^2D$  spectroscopic ground state, which splits in a crystal field. The scheme of the splitting of the energy levels of  $d^9$  ions for different types of symmetry is shown in Figure 1. The epr spectra of the copper(II) ions in zeolite crystals may be generally described by the axially symmetrical spin Hamiltonian

$$\mathcal{H} = \beta[g_{||}H_zS_z + g_{\perp}(H_xS_x + H_yS_y)] + A_{||}I_zS_z + A_{\perp}(I_xS_x + I_yS_y) \quad (1)$$

where  $z$  is the symmetry axis;  $H$  is the external magnetic field;  $S$  is the effective electron spin;  $g_{||}$  and  $g_{\perp}$  are the spectroscopic splitting factors, parallel or perpendicular to the symmetry axis;  $I$  is the nuclear spin;  $A_{||}$  and  $A_{\perp}$  are the hyperfine constants; and  $\beta$  is the Bohr magneton. The principal values of the  $g$  and hyperfine tensors may be readily extracted from the polycrystalline spectra.<sup>2a</sup>

The epr spectra of dehydrated Cu(II)Y zeolites varied in appearance with the copper(II) concentration and the nature of the major compensating cations, but apart from the line width, no difference in paramagnetic parameters was found in the spectra recorded at room temperature or at  $-196^\circ$ . At room temperature the epr lines were rather broad. Kivelson, *et al.*,<sup>7</sup> attributed the broad epr lines to rapid spin-lattice relaxation which results from modulated spin-orbit interactions. This relaxation rate is reduced at low temperatures.

The different paramagnetic parameters for the copper(II) ions in various ion-exchanged Y zeolites are summarized in Table I.<sup>8</sup>

These parameters have been previously interpreted as evidence for the copper(II) ions existing in square planar or octahedral symmetry with tetragonal elongation.<sup>2</sup> It is apparent from the work of Bleaney, *et al.*,<sup>9a</sup> that one should also consider trigonal symmetry with tetragonal distortions as a possible coordination which would produce the observed magnetic parameters. The analyses of the Cu(II)NaY and Cu(II)BaY zeolites show two different  $g_{||}$  values. Such spectra reflect the presence of  $\text{Cu}^{2+}$  ions in two different sites. Indeed, in an X-ray study of a dehydrated Cu(II)NaY zeolite, Gallezot, *et al.*,<sup>9b</sup> pointed out that the cation sites  $S_7$  and especially  $S_7'$  in the small cavities were occupied by  $\text{Cu}^{2+}$  ions. Moreover, CO adsorption on the dehydrated Cu(II)NaY sample indicated that no  $\text{Cu}^{2+}$  ions are present in the large cavities. The paramagnetic parameters of Cu(II)CaY and Cu(II)MgY zeolites are fairly close to those obtained by Richardson<sup>2b</sup> and confirmed the influence of the major compensating cations on the splitting of the  $\text{Cu}^{2+}$  levels. In addition, these Cu(II)CaY and Cu(II)MgY samples produced spectra with epr lines attributed to a spin exchange phenomena. An epr study by Chao and Lunsford<sup>5</sup> has shown that coupled  $\text{Cu}^{2+}$  ions are present in the sodalite cages of these samples.

*B. Copper(II)-Ammonia Complexes.* Several investigators<sup>10-12</sup> have studied the ammonia-zeolite

(7) D. Kivelson and R. Neiman, *J. Chem. Phys.*, **35**, 149 (1961).

(8) J. W. Searl, R. C. Smith, and S. J. Wyard, *Proc. Phys. Soc., London, Sect. A*, **78**, 1174 (1961).

(9) (a) B. Bleaney, K. D. Bowers, and R. S. Trenam, *Proc. Roy. Soc., Ser. A*, **228**, 157 (1955); (b) P. Gallezot, Y. Ben Taarit, and B. Imelik, *C. R. Acad. Sci.*, **272**, 261 (1971).

(10) R. M. Barrer and R. M. Gibbons, *Trans. Faraday Soc.*, **59**, 2569 (1963).

(11) P. A. Jacobs and J. B. Uytterhoeven, *J. Catal.*, submitted for publication.

equilibria. Barrer, *et al.*,<sup>10</sup> examined the adsorption of ammonia in various ion-exchanged X-type zeolites over a range of adsorption temperatures. They reported that the ammonia can enter both the sodalite cages and the supercages; however, the principal amount of the adsorbed ammonia must be situated in the large cavities. The amount varied from 4 to 1 NH<sub>3</sub> molecule per cation.

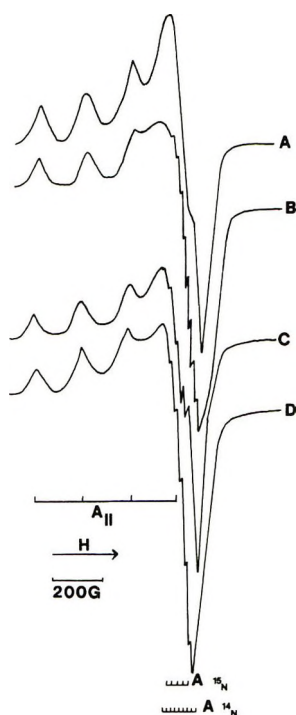


Figure 2. Effect of the ammonia adsorption temperature on the epr spectra (recorded at  $-196^\circ$ ): A, Cu(II)Ca- $^{14}\text{NH}_3$  complex formed at room temperature; B, Cu(II)Ca- $^{14}\text{NH}_3$  complex formed at  $100^\circ$ ; C, Cu(II)Ca- $^{15}\text{NH}_3$  complex formed at room temperature; D, Cu(II)Ca- $^{15}\text{NH}_3$  complex formed at  $100^\circ$ .

The epr lines of ammoniated zeolite samples are very broad at room temperature but sharpen at  $-196^\circ$ . The spectra of Cu(II)Ca-NH<sub>3</sub> complexes are shown in Figure 2. The magnetic parameters at  $-196^\circ$  for the copper(II)-ammonia complexes in different ion-exchanged Y zeolites, formed at room temperature or at  $100^\circ$ , are  $g_{\parallel} = 2.235 \pm 0.005$ ,  $g_{\perp} = 2.035 \pm 0.005$ , and  $A_{\parallel} = 175 \pm 2$  G. Comparing the  $g$  values of the dehydrated and ammoniated zeolite samples we may conclude that the symmetry of the Cu(II)-NH<sub>3</sub> complexes is also either square planar, octahedral with tetragonal elongation, or trigonal with tetragonal distortions.

The change in parameters during the adsorption of ammonia indicates that these ligands are coordinated with the copper(II) ions. The decrease of the  $g$  factors in the complexation process may result from two factors: (1) the increase in the splitting between the ground and excited orbital levels of the Cu<sup>2+</sup> ions or (2) the decrease of spin density in the Cu<sup>2+</sup> ions as a result of a

delocalization of the unpaired electron by the NH<sub>3</sub> ligands.

The adsorption temperature of NH<sub>3</sub>, as shown in Figure 2, has no influence on the magnetic parameters; however, a small decrease of the Cu<sup>2+</sup> epr signals occurs, which may be due to a reduction of Cu<sup>2+</sup> into Cu<sup>1+</sup>. For the Cu(II)- $^{14}\text{NH}_3$  complexes the high-magnetic field band was better resolved after adsorption at  $100^\circ$ . Nine hyperfine lines of nitrogen with a hyperfine splitting constant of  $14 \pm 2$  G were observed. In order to determine the composition of the copper(II)-ammonia complexes similar experiments were carried out with  $^{15}\text{NH}_3$ . For the adsorption of  $^{15}\text{NH}_3$  at room temperature and at  $100^\circ$  (Figure 2) no difference in epr parameters was observed; however, again the resolution in the high-field region was better at  $100^\circ$ . For both adsorption temperatures five hyperfine lines of  $^{15}\text{N}$  in the high-field region were detected.

The number of the hyperfine lines can be interpreted to mean that the unpaired electron is interacting with four equivalent nitrogen nuclei. One would expect  $2NI + 1$  or 9 and 5 hyperfine lines for  $^{14}\text{NH}_3$  and  $^{15}\text{NH}_3$ , respectively. Very similar spectra have been observed by Adato, *et al.*,<sup>13</sup> for planar bis(acetylacetonedi-oximate)copper(II), a nitrogen chelate complex. The nitrogen hyperfine structure indicates that in the large cavities the Cu<sup>2+</sup> ions are surrounded by four identical ammonia molecules in a square planar symmetry. This complex formation requires a migration of Cu<sup>2+</sup> ions from the sodalite cages into the large cavities where they take positions which are favorable for the fourfold coordination. The independency of the  $g$  values and hyperfine splitting constants with the coexchanged cations indicates that the ammonia molecules tend to stabilize the environment of the copper(II) ions and remove them from perturbations by the neighboring cations. From these observations one may conclude that upon adsorption of NH<sub>3</sub> a redistribution of the exchangeable cations occurs which confirms the theory that a zeolite is a dynamic system.

Because the NH<sub>3</sub> molecules are predominantly  $\sigma$  bonding ligands, a strong delocalization of the unpaired electron may be expected. For the copper(II) complexes in which the unpaired electron occupies the B<sub>1g</sub> orbital, the density of the unpaired electron at the central atom can be computed from<sup>7</sup>

$$\alpha^2 = \left( \frac{A_{\parallel}}{P} \right) + (g_{\parallel} - 2) + \frac{3}{7}(g_{\perp} - 2) + 0.04 \quad (2)$$

where  $1 - \alpha^2$  measures the covalency associated with the bonding of the Cu<sup>2+</sup> ions to the ligands and  $P = 0.036 \text{ cm}^{-1}$ .<sup>7</sup> Values of  $\alpha^2 = 1$  or  $\alpha^2 = 0.5$  refer to a completely ionic and covalent bond, respectively. All

(12) J. E. Benson, K. Ushiba, and M. Boudart, *J. Catal.*, **9**, 91 (1967).

(13) I. Adato, A. H. I. Ben Bassat, and S. Sarel, *J. Phys. Chem.*, **75**, 3828 (1971).

$\alpha^2$  values are about  $0.75 \pm 0.02$  for the different ammoniated copper(II)Y zeolites. This indicates a partial delocalization of the unpaired electron to the ligand. The degree of delocalization is approximately the same for all of the ion-exchanged copper(II) zeolites; hence, it does not depend on the nature of the neighboring cations.

To calculate the density  $\rho_N$  of the unpaired electron on the coordinating nitrogen atoms, the following equation may be used<sup>14</sup>

$$\rho_N = 1/4(\sqrt{1 - \alpha^2} + \sqrt{\alpha^2 S})^2 \quad (3)$$

where  $S$  is the overlapping integral, which is equal to 0.093 for the Cu-N bond.<sup>7</sup> Calculations with this formula show that  $\rho_N$  was  $0.086 \pm 0.003$ . This means that the spin density at the nitrogen nuclei arises as a result of the delocalization of the unpaired electron into the  $sp^3$  orbital of the nitrogen.

Good agreement was found between the  $\rho_N$  values calculated from eq 3 and from the experimental nitrogen hyperfine splitting constant. The total wave function for an  $sp^3$  hybridization of the nitrogen in ammonia can be expressed as

$$\psi = C_1\psi_s + C_2\psi_{p_x} + C_3\psi_{p_y} + C_4\psi_{p_z} \quad (4)$$

where  $C_1 = C_2 = C_3 = C_4 = 1/2$ <sup>15</sup> with the normalization condition  $C_1^2 + C_2^2 + C_3^2 + C_4^2 = 1$ . Here  $\psi_s$ ,  $\psi_{p_x}$ ,  $\psi_{p_y}$ , and  $\psi_{p_z}$  are the wave functions associated with the  $s$ ,  $p_x$ ,  $p_y$ , and  $p_z$  orbitals. The nitrogen hyperfine interaction is isotropic due to the equal probability of finding the electron in the  $p_x$ ,  $p_y$ , or  $p_z$  orbitals. From the theoretical separation between <sup>14</sup>N-hyperfine lines<sup>16</sup> and the experimental <sup>14</sup>N-hyperfine constant, a  $\rho_N$  value of 0.089 was calculated.

In order to examine further the copper(II) complexes, adsorptions of monomethylamine (Me) and monoethylamine (Et) were carried out in Cu(II)NaY and Cu(II)CaY zeolite samples. Because of the size of the amines, copper(II) complexes are only possible in the large cavities. The magnetic parameters of these copper(II)-amine complexes at  $-196^\circ$  are shown in Table II. In the low-field region two different Cu<sup>2+</sup> centers were observed. In comparison with the  $g$  values of Table I we may assume that one Cu<sup>2+</sup> spectrum is due to a Cu<sup>2+</sup>-amine complex and the other to the original Cu<sup>2+</sup> ions. The  $g$  values of the copper(II)-amine complexes indicate an increasing influence of the major compensating cations with increasing size of the copper ligands. This indicates a larger perturbation of the copper environment from the neighboring cations through the intermediate lattice oxygens.<sup>2b</sup> Also the covalency of the Cu<sup>2+</sup>-ligand bond and the density of the unpaired electron on the nitrogen increase with increasing ligand size. Therefore, the orbital overlap between the orbitals of the central copper(II) ion and the  $sp^3$  orbital of the nitrogen becomes more important. The second  $g$  factor, attributed to the original Cu<sup>2+</sup>

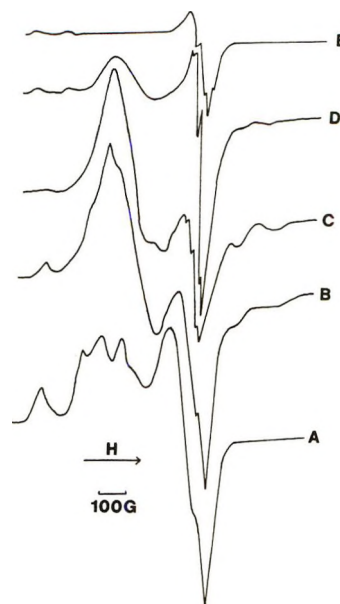


Figure 3. Effect of the desorption temperature on the Cu(II)Ca-<sup>14</sup>NH<sub>3</sub> spectra (recorded at  $-196^\circ$ ): A, room temperature; B,  $60^\circ$ ; C,  $100^\circ$ ; D,  $200^\circ$ ; E,  $300^\circ$ .

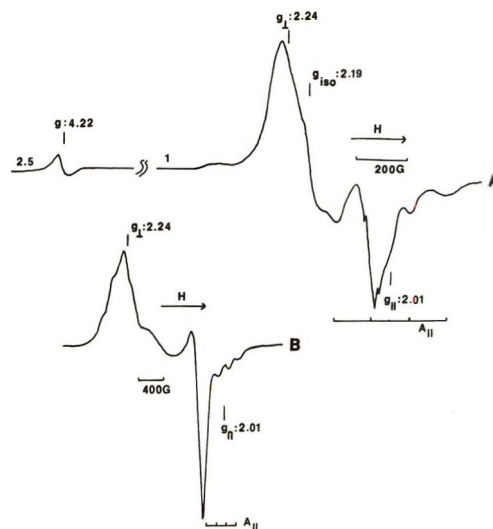


Figure 4. Epr spectra of a partially desorbed ( $100^\circ$ ) Cu(II)Ca-NH<sub>3</sub>Y zeolite: A, at X band; B, at Q band.

ions, indicates that part of the Cu<sup>2+</sup> ions do not react with the amines because of space requirement factors. These ions probably remain inside the sodalite cages.

*C. Effect of Desorption on the Copper(II)-Ammonia Complexes in Y Zeolites.* The different ammoniated zeolites were evacuated overnight at various temperatures. Figures 3 and 4 show the effects of the desorption temperature on the Cu(II)CaY-NH<sub>3</sub> complexes.

(14) A. N. Zhitomirskii and K. I. Zamaraer, *Zh. Fiz. Khim.*, **10**, 435 (1969).

(15) A. Liberles, "Introduction to Theoretical Organic Chemistry," Macmillan, New York, N. Y., 1968, pp 172, 173.

(16) H. Zeldes, G. T. Trammell, R. Livingston, and R. W. Holmberg, *J. Chem. Phys.*, **32**, 618 (1960).

**Table II:** Magnetic Parameters of the Copper(II)-Monomethylamine and Copper(II)-Monoethylamine Complexes

Complex	$g_{  }^{(1)}$	$g_{  }^{(2)}$	$A_{  }^{(1)}$	$A_{  }^{(2)}$	$g_{\perp}$	$a^2$	$\rho_N$
	$\pm 0.005$	$\pm 0.005$	$\pm 2$	$\pm 2$	$\pm 0.005$	$\pm 0.02$	$\pm 0.003$
Cu(II)Na-MeY	2.235	2.33	167	155	2.025	0.719	0.092
Cu(II)Ca-MeY	2.23		167		2.021	0.712	0.095
Cu(II)Na-EtY	2.229	2.328	170	154	2.024	0.72	0.094
Cu(II)Ca-EtY	2.22		170		2.015	0.70	0.096

**Table III:** Influence of the Desorption Temperature on the Magnetic Parameters of Cu(II)Ca-Amine Complexes

Complex	Desorption temp, °C	$g_{  }^{(1)}$	$A_{  }^{(1)}$	$g_{  }^{(2)}$	$A_{  }^{(2)}$	$g_{  }^{(3)}$	$A_{  }^{(3)}$	$g_{\perp}^{(1,2)}$	$A_{\perp}^{(1)}$	$g_{\perp}^{(3)}$
		$\pm 0.005$	$\pm 2$	$\pm 0.005$	$\pm 2$	$\pm 0.005$	$\pm 2$	$\pm 0.005$	$\pm 2$	$\pm 0.005$
Cu(II)Ca-NH <sub>3</sub>	RT <sup>a</sup>	2.23	170	2.276	140			2.035		
	60			2.275	140	2.012	141	2.035		2.24
	100			2.27	140	2.012	141	2.049	20	2.24
	200	2.33	135			2.012	141	2.051	20	2.24
	300	2.33	135					2.052	20	
Cu(II)Ca-Me	100			2.23	165	2.013	140	(2.023)		2.25

<sup>a</sup> See footnote d, Table I.

Three important phenomena can be observed with increasing desorption temperature: (1) reduction of Cu<sup>2+</sup> into Cu<sup>1+</sup>, (2) the change in symmetry of the Cu(II)-NH<sub>3</sub> complexes, and (3) the formation of coupled Cu<sup>2+</sup> pairs.

(1) *Reduction of Cu<sup>2+</sup>*. The intensity of the epr signals due to the different Cu<sup>2+</sup> centers decreased significantly with the desorption of NH<sub>3</sub>. An intensity study of the epr adsorption lines of Cu(II)-H<sub>2</sub>O and Cu(II)-NH<sub>3</sub> complexes as a function of the temperature, made by Krüerke, *et al.*,<sup>17</sup> indicates a reduction of Cu<sup>2+</sup> into Cu<sup>1+</sup> at about 150° when ammonia is present. The decrease of the epr signals with desorption could be the result of two phenomena: (1) the reduction of Cu<sup>2+</sup> into Cu<sup>+</sup> or (2) formation of a pure tetrahedral complex which would result in a very short relaxation time. With increasing desorption temperature the reduction of the Cu<sup>2+</sup> ions probably becomes more important.

(2) *Change in Symmetry of the Cu(II)-NH<sub>3</sub> Complexes*. The spectra of a Cu(II)Y zeolite following partial desorption of the ammonia (Figures 3 and 4) illustrate that three different Cu(II) centers can be distinguished: (a) original copper(II) ions, (b) a distorted octahedral Cu(II) complex, and (c) a distorted tetrahedral Cu(II)-NH<sub>3</sub> complex. The influence of the desorption temperature on the magnetic parameters is shown in Table III. The outgassing of ammoniated Cu(II)Y zeolites at room temperature created two copper(II) centers which are attributed to distorted octahedral Cu(II)-NH<sub>3</sub> complexes. Upon the partial desorption of NH<sub>3</sub> an evolution in symmetry of the Cu(II)-NH<sub>3</sub> complex from a square planar symmetry

to octahedral symmetry with tetragonal elongation must be assumed.

At an elevated desorption temperature an inverted anisotropy was observed ( $g_{\perp} > g_{||}$ ). The inversion of the anisotropy can be attributed to the formation of a tetragonally compressed octahedral or a tetragonally elongated tetrahedral Cu(II)-NH<sub>3</sub> complex. The Q band spectrum of a partially desorbed Cu(II)Ca-NH<sub>3</sub> sample, shown in Figure 4, confirms the change in symmetry. The same behavior was found in the Cu(II)-Me complex after a desorption at 100°. A similar inversion of the Cu(II) spectrum upon desorption of ammonia has been reported by Naccache and Ben Taarit,<sup>3</sup> however, they were unable to detect any hyperfine structure. Spectroscopic investigations of Klier, *et al.*,<sup>18,19</sup> indicated tetrahedrally coordinated Co(II)-NH<sub>3</sub> complexes in partially ammoniated A-type zeolites. A similar situation was found for partially hydrated Ni(II) and Co(II) A zeolites. Therefore, we assign the spectrum to a distorted tetrahedrally coordinated ammonia complex which is present in the large cavities. As shown in Figure 5, the complex is formed by three O<sub>4</sub> lattice oxygens and one ammonia molecule.

Upon further increases in the desorption temperature (200-300°) the importance of the original Cu<sup>2+</sup> center increases while the intensity of the tetrahedrally coordinated Cu(II)-NH<sub>3</sub> complex decreases. At a desorption temperature of 300° only the original copper(II) centers

(17) U. Krüerke and P. Jung, *Z. Phys. Chem. (Leipzig)*, **58**, 53 (1968).

(18) K. Klier and M. Ralek, *J. Phys. Chem. Solids*, **29**, 951 (1968).

(19) K. Klier, *Proc. Int. Conf. Molec. Sieve Zeolites, Worcester, 2nd*, 782 (1970).

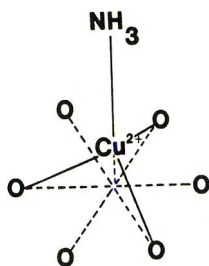


Figure 5. Symmetry model of the  $\text{Cu}^{2+}$ - $\text{NH}_3$  complexes after partial desorption.

were observed. Adsorption isotherms of  $\text{NH}_3$  on  $\text{Cu(II)NaY}$  and  $\text{NaY}$  zeolites confirmed the changes in composition of the copper(II)-ammonia complexes. Table IV gives the variation in  $\text{NH}_3$  content with the desorption temperature.

**Table IV:** Variation of the  $\text{NH}_3$  Content in the  $\text{Cu(II)NaY}$  Zeolite with the Desorption Temperature

Temp. °C	$\text{NH}_3$ molecules per $\text{Cu}^{2+}$ ion
RT <sup>a</sup>	$1.5 \pm 0.3$
100	$1.1 \pm 0.3$
200	$0.4 \pm 0.3$

<sup>a</sup> See footnote *d*, Table I.

Generally we may conclude that the desorption of  $\text{NH}_3$  changes the  $\text{Cu(II)-NH}_3$  complex from a square

planar to a distorted octahedral, and then to a distorted tetrahedral symmetry.

(3) *Formation of Coupled  $\text{Cu}^{2+}$  Pairs.* When ammonia was evacuated from the  $\text{Cu(II)Y}$  zeolites, a strong tendency of interaction between  $\text{Cu}^{2+}$  ions was observed. Figure 4b shows a complete spectrum of a partially desorbed  $\text{Cu(II)Ca-NH}_3$  Y zeolite. The magnetic parameters at  $-196^\circ$  for the spin exchange interaction are  $\Delta m = 1$ ,  $g_{\text{iso}} = 2.19$  and  $\Delta m = 2$ ,  $g = 4.22$ . The isotropic band at  $g_{\text{iso}} = 2.19$  partially overlaps the spectra of other copper(II) centers.

An extensive study of coupled  $\text{Cu}^{2+}$  ions was made by Chao and Lunsford<sup>5</sup> in  $\text{Cu(II)Y}$  zeolites, coexchanged with  $\text{Ca}^{2+}$  or  $\text{Mg}^{2+}$ , and in Y zeolites with a high  $\text{Cu}^{2+}$  content. These authors found that the symmetry of the linkage between a pair of  $\text{Cu}^{2+}$  ions depends on the  $\text{Cu}^{2+}$  concentration in the sodalite cages and the coexchanged cation. In the copper(II) zeolites following ammonia desorption the coupled  $\text{Cu}^{2+}$  ions form nonlinear pairs, which are probably linked together with an oxygen bridge in the sodalite cages. Chao and Lunsford<sup>5</sup> pointed out that the  $\text{Cu}^{2+}$  ions in nonlinear coupled pairs are localized in the  $S_7'$  sites. The absence of coupled  $\text{Cu}^{2+}$  ions at a desorption temperature of  $300^\circ$  must be due to the strong reduction of the  $\text{Cu}^{2+}$  ions.

*Acknowledgment.* The work was supported by the National Science Foundation under Grant No. GP-29898. We are grateful to Dr. Y. Huang for his CO and  $\text{NH}_3$  adsorption experiments and to Dr. C. C. Chao for valuable discussions.

# A Solvent Effect on Metal Hyperfine Constants in Alkali

## Metal Radical Anion Ion Pairs

by T. R. Tuttle, Jr.,\* J. C. Danner, and Philip Graceffa

Department of Chemistry, Brandeis University, Waltham, Massachusetts 02154 (Received May 5, 1971)

Alkali metal hyperfine coupling constants ( $a_M$ ) for metal naphthalenides are measured in a number of solvents and solvent mixtures. The variation of  $a_{Li}$  in mixtures of tetrahydrofuran and alkane are quantitatively interpreted in terms of an equilibrium between ion pairs which differ in their outer solvation layers. Accordingly, rough correlations between  $a_M$  and the solvent dielectric constant,  $D$ , are exemplified for Li and Na naphthalenides in a number of different solvents. A linear variation of  $a_M$  with  $D^{-3}$ , as is expected in case the solvent may be treated as a dielectric continuum, is shown to hold in some cases. A relationship between the hydrocarbon anion salts and the monomers observed in some alkali metal amine solutions is thereby inferred.

### Introduction

The effect of solvent on alkali metal hyperfine coupling constants in solutions of paramagnetic salts has been the subject of a number of investigations.<sup>1-13</sup> Studies on the effect of changing temperature have revealed a variety of behavior which indicates the complexity of the phenomenon. Alkali metal coupling constants may increase, decrease, or stay constant as temperature is increased. No clear picture has emerged as to what causes these changes, although an increase in coupling constant has been generally assumed to be associated with a change in structure of the ion pair such that the ions come closer together. The effect of lateral movement of the cation with respect to the anion has been investigated theoretically and has been shown to correlate with anion structure in the case of substituted naphthalenes.<sup>12</sup> However, the effect of changing solvent composition seems to be unpredictable. In some cases a change in solvent has a large effect on the metal hyperfine coupling constant, in other cases almost none.

In this paper we present determination of metal hyperfine coupling constants (hfc) in solutions of lithium, sodium, rubidium, and cesium naphthalenides in a number of solvents and solvent mixtures, and examine the results in terms of a model in which variations of hfc are attributed to changes in solvation of the cation in the ion pair.

### Experimental Section

Solvents were purified by predrying with Na wire or CaH<sub>2</sub>, followed by fractional distillation into a storage bulb with Na-K alloy and anthracene. Details are given elsewhere.<sup>14</sup> The alkanes, *i.e.*, pentane, heptane, and decane from Fisher Scientific Co., were stored over Na-K alloy. The mole fractions of the mixed solvents were determined by weighing the amounts of

each solvent. ESR spectra were obtained on a Strand Labs Model 602 B X-band spectrometer.

### Results

Lithium hfc were measured for solutions of lithium naphthalenide in mixed solvents of THF plus pentane, heptane, and decane. The results of these measurements are presented in Figure 1. Measurements for pure THF are given in Figure 2. The results for the different alkanes fall essentially all on the same curve. In each case at first, the metal coupling constant increases slowly and linearly with increasing mole fraction of alkane ( $X_A$ ) up to about  $X_A \approx 0.9$ . Beyond this point the coupling constant increases abruptly and more rapidly.

Sodium hfc were measured in solutions of sodium naphthalenide in THF-heptane mixtures. The results are presented in Figure 3. As for lithium, the hfc increases slowly and linearly up to a heptane mole frac-

- (1) N. M. Atherton and S. I. Weissman, *J. Amer. Chem. Soc.*, **83**, 1330 (1961).
- (2) H. Nishiguchi, Y. Nakai, K. Nakamura, I. Ishizu, Y. Deguchi, and H. Talaki, *Mol. Phys.*, **9**, 153 (1965); *J. Chem. Phys.*, **40**, 241 (1964).
- (3) A. H. Reddoch, *ibid.*, **43**, 225 (1965).
- (4) E. DeBoer, *Recl. Trav. Chim. Pays-Bas*, **84**, 609 (1965).
- (5) Iwaizumi and T. Isobe, *Bull. Chem. Soc. Jap.*, **37**, 1651 (1964).
- (6) P. B. Ayscough and P. F. Sargent, *J. Chem. Soc. B*, 900 (1966).
- (7) N. Hirota and R. Kreilick, *J. Amer. Chem. Soc.*, **88**, 614 (1966).
- (8) A. H. Crowley, N. Hirota, and R. Kreilick, *J. Chem. Phys.*, **46**, 4815 (1967); N. Hirota, *J. Phys. Chem.*, **71**, 127 (1967).
- (9) N. Hirota, *J. Amer. Chem. Soc.*, **90**, 3603 (1968).
- (10) P. Graceffa and T. R. Tuttle, Jr., *J. Chem. Phys.*, **50**, 1908 (1969).
- (11) N. Hirota, R. Carraway, and W. Schook, *J. Amer. Chem. Soc.*, **90**, 3611 (1968).
- (12) I. B. Goldberg and J. R. Bolton, *J. Phys. Chem.*, **74**, 1965 (1970).
- (13) C. L. Dodson and A. H. Reddoch, *J. Chem. Phys.*, **48**, 3226 (1968).
- (14) J. C. Danner, Thesis, Brandeis University, 1966.

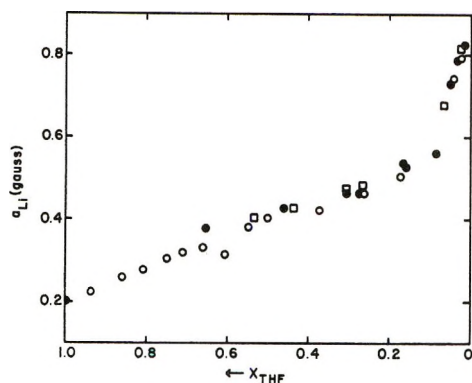


Figure 1. Lithium splittings in lithium naphthalenide as a function of solvent composition:  $\circ$ , pentane as second solvent component;  $\bullet$ , heptane;  $\square$ , decane.

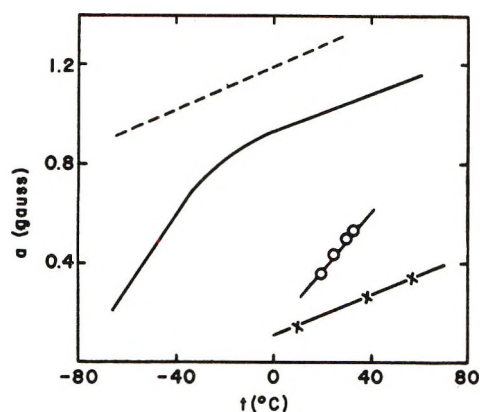


Figure 2. Metal splittings as a function of temperature for lithium and sodium naphthalenides: broken line, Na in THP (from ref 1); solid line, Na in THF (from ref 1 and 9);  $\circ$ , Na in DME;  $\times$ , Li in THF.

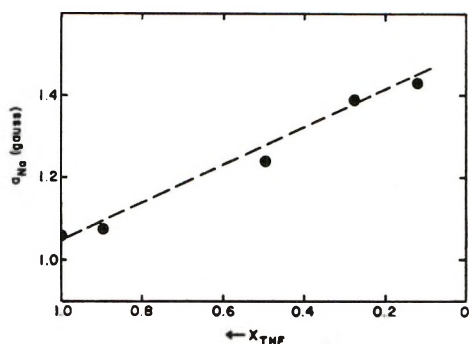


Figure 3. Sodium splittings in sodium naphthalenide in THF-heptane mixtures.

tion of about 0.9. Unfortunately, we were unable to prepare stable solutions of sodium naphthalenide in solvents with a mole fraction of heptane greater than 0.9. Our results for sodium naphthalenide dissolved in 1,2-dimethoxyethane (DME) are presented in Figure 2 along with the results of other investigations<sup>1,9</sup> in THF and tetrahydropyran (THP).

Rubidium-87 hfc were measured for rubidium naphthalenide dissolved in THF-heptane mixtures. The

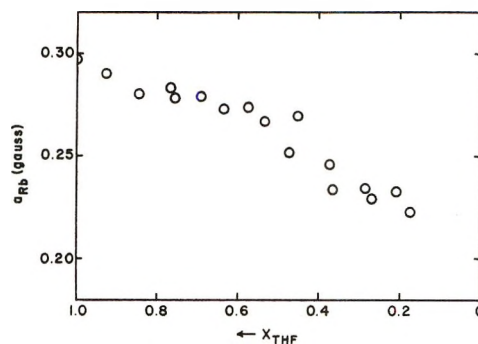


Figure 4. Rubidium-87 splittings in rubidium naphthalenide in THF-heptane mixtures.

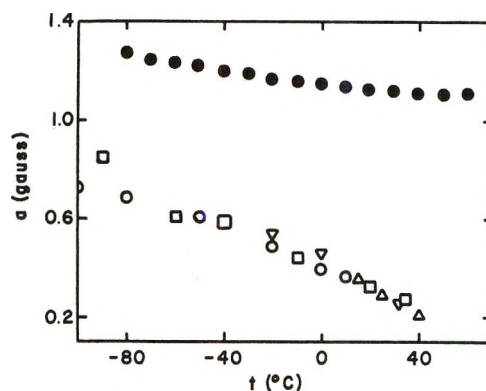


Figure 5. Metal splittings as a function of temperature for cesium and rubidium naphthalenides:  $\bullet$ , Cs-THF;  $\circ$ , Rb-THF;  $\square$ , Rb-DME;  $\Delta$ , Rb-paraldehyde;  $\nabla$ , Rb-THP.

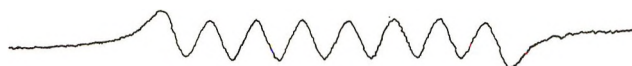


Figure 6. Spectrum of cesium naphthalenide in THF in the presence of excess naphthalene.

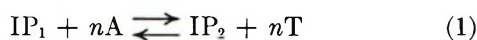
results are given in Figure 4. Results for rubidium naphthalenide dissolved in THF, 1,2-dimethoxyethane, paraldehyde, and THP are presented together in Figure 5. Our results are in agreement with those of Dodson and Reddoch<sup>13</sup> where there is overlap between the two studies.

Cesium hfc were measured for cesium naphthalenide in THF. These results are given in Figure 5. Because the cesium naphthalenide spectrum is so complicated we also measured the cesium hfc for a solution in which excess ( $\sim 5 M$ ) naphthalene was present. This solution yielded the simple eight-line spectrum shown in Figure 6 and gave essentially the same coupling constant as was extracted from the complex spectrum of solutions without added naphthalene. The coupling constants obtained in THF solution are close to those obtained previously for cesium naphthalenide dissolved in DME<sup>9,13</sup> and 2-methyltetrahydrofuran<sup>8,9</sup> (MTHF).

## Discussion

The naphthalenide ion pairs with alkali metal ions

may be divided roughly into two groups<sup>14</sup> according to whether the metal hfc depends strongly on environment or not. The sodium and lithium ion pairs clearly belong to the first-mentioned group since their metal hfc vary strongly as temperature or solvent is changed, while the rubidium and cesium ion pairs belong to the second group. The temperature dependence of hfc has been accounted for on the basis of an equilibrium between two different ion pairs, one of which called a "tight" ion pair dominates at high temperatures and one of which called a "loose" ion pair dominates at low temperatures.<sup>9</sup> A change in solvent can also change this equilibrium and hence the metal hfc. In order to test whether the equilibrium-involved expulsion of solvent molecules from the complex we measured the Li hfc in mixtures of THF and alkanes. The coupling constant showed no specific dependence on which alkane was used as diluent, but varied as a function of solvent composition in the nonlinear manner shown in Figure 1. It was tempting to separate the dependence of the coupling constant on  $X_T$  (mole fraction of THF) into two linear regions: (1) the gradual increase which persists down to  $X_T \approx 0.1$ , and (2) the steep increase which takes place for  $X_T < 0.1$ . However, since there was no obvious physical reason for performing this separation, we attempted and succeeded in fitting the data over the whole range of solvent composition to a single equilibrium expression. In order to account for this data consider the equilibrium<sup>15</sup>



in which the two ion pairs are related through exchange of  $n$  THF (T) molecules for an equal number of alkane molecules (A). If the metal hfc  $a_M$  is assumed to be a weighted average of the values for the two different ion pairs

$$a_M = f_1 a_1 + f_2 a_2 \quad (2)$$

in which the subscripts refer to the two ion pairs of eq 1 and  $f_1$  is the mole fraction of the total concentration of ion pair in form one. By combining the equilibrium constant for reaction 1

$$K = \frac{[\text{IP}_2][\text{T}]^n}{[\text{IP}_1][\text{A}]^n} = \frac{f_2 R^n}{f_1} \quad (3)$$

where  $R$  is the mole ratio of THF to alkane, with eq 2 we obtain

$$\frac{1}{a_M - a_1} = \frac{1}{a_2 - a_1} \left( 1 + \frac{R^n}{K} \right) \quad (4)$$

which is a useful expression for testing eq 1. According to eq 4 a proper choice of  $n$  should lead to a linear plot of  $1/(a_M - a_1)$  vs.  $R^n$ . Logically  $a_1$  may be chosen as the value of  $a_M$  in pure THF. Unfortunately, this quantity could not be obtained accurately because the lines overlapped seriously so  $a_1$  was left as an adjustable parameter. No linear fit could be obtained with  $n \geq$

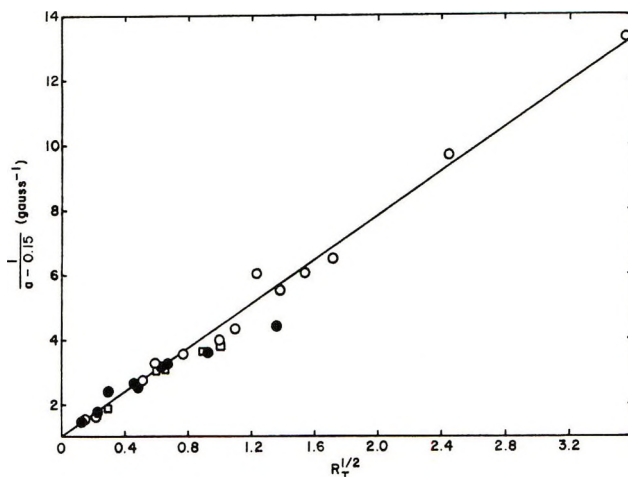
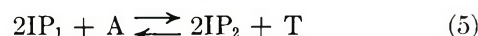


Figure 7. Fit of lithium data from Figure 1 to eq 4 with  $n = 1/2$  and  $a_1 = 0.15$  G.

1. However, the excellent fit shown in Figure 7 was obtained with  $n = 1/2$  and  $a_1 = 0.15$  G. This value of  $a_1$  was judged to be reasonable as we had estimated  $a_1 = 0.2 \pm 0.05$  G from direct measurement in the pure solvent. Also Dodson and Reddoch estimate  $a_1 \sim 0.18$  G.<sup>13</sup>

The value of  $n = 1/2$  leads to a problem of interpreting the chemical equilibrium which may be written



If taken literally this equation contains an inconsistency, for if two molecules of an ion pair either expel or accept one molecule of solvent these ion pairs cannot be identical as represented. A correct chemical representation of these solutions probably involves a complex set of coupled equilibria which are nevertheless well represented simply by eq 5. Equation 5 is interpreted to mean that relatively little exchange of solvating solvent between THF and alkane takes place over a very large change in solvent composition. What little exchange does take place affects the Li coupling constant markedly. The fit of eq 4 to the data gives  $a_2 = 1.15$  G and  $K = 0.27$ , or  $\Delta G^\circ = 0.75$  kcal/mol, a not unreasonable value for the change in solvation represented. For example, if the total solvation energy of an ion pair in THF is about 100 kcal/mol, the change in solvation free energy between THF and alkane can be represented roughly in terms of the Born equation as  $100(1/D_A - 1/D_T) \approx 100(1/2 - 1/7) = 36$  kcal/mol.  $D_A$  and  $D_T$  are the static dielectric constants of alkane and THF, respectively.<sup>16,17</sup> If there are about 20 molecules in-

(15) We also considered the equilibrium in which alkane molecules were excluded so that the mole ratio which appears in eq 4 is simply replaced by mole fraction of THF. This equation was explicitly tested for  $n = 1/2, 1$ , and  $2$  by plotting  $1/a - a_1$  vs.  $X_T$ . None of these plots came close to being linear. From the trends observed it was also clear that no value of  $n > 2$  or  $< 1/2$  would lead to a reasonable fit of the data.

(16) *Nat. Bur. Stand. (U. S.), Circ.*, **514**, 16 (1951).

involved in solvation then a change in half a molecule on the average should be accompanied by a change in free energy of about 1 kcal/mol as is in fact observed.

Insufficient data are available to tell precisely how changes in coupling constant are related to changes in solvation. However, it may be inferred that the change in solvation represented in eq 5 probably does not involve the primary layer of solvating solvent molecules because of the small free energy of reaction. The exchange of THF for alkane most probably involves the outer solvation sheath. If this is the case, representation of the solvent as a continuous dielectric medium may provide quantitative insight into variations of  $a_M$  which occur on changing temperature or solvent.

If such a model is applicable in explaining changes in  $a_M$ , a correlation between  $a_M$  and dielectric constant  $D$  is to be expected. For lithium naphthalenides<sup>6,9</sup> the correlation between  $a_{Li}$  and  $D$  is unmistakable. The value of  $a_{Li}$  increases either as temperature is increased or as nonpolar solvent is added to polar solvent. In both cases  $a_{Li}$  increases as  $D$  decreases. A similar correlation is apparent between  $a_{Na}$  and  $D$  for sodium naphthalenides<sup>1,8,9,13</sup> as shown in Figure 8. The value of  $a_{Na}$  increases regularly as  $D$  decreases for solutions in THF, MTHF, THP,<sup>1</sup> and ethyl ether.<sup>8</sup> However, a clear exception to this correlation occurs for solutions in DME. Another exception occurs for *p*-dioxane solutions.<sup>1</sup> Furthermore, the values of  $a_{Na}$  in ethyl ether solutions appear to be larger even at the same value of  $D$  than for the other solutions. Discussion of these exceptions to the correlation will be deferred for the moment.

Because of these rough correlations, the model of solvent as continuous dielectric medium is examined further. Solution of the quantum mechanical problem of a unit point positive charge immersed in a dielectric medium and interacting with an electron yields a set of hydrogenic orbitals for which the values of  $|\psi_{ns}(0)|^2$  depend on  $(1/D)^3$ . Accordingly, we expect that  $a_M$  which result from unpaired electron in the valence orbital of the metal should vary linearly<sup>18</sup> with  $(1/D)^3$ . In Figure 9,  $a_{Na}$  is plotted vs.  $(1/D)^3$  for sodium naphthalenide in THF, THP, MTHF, and methyl ether. The data for THP, MTHF, and THF at high temperature fall approximately on the straight line drawn in the figure. However, the data for ethyl ether and for THF at low temperature deviate from this line significantly. It is clear that all of the observed variations of  $a_{Na}$  may not be attributed to the effect of the solvent on the valence orbital of the metal. Nevertheless, some of the variations may, and these are identified by their adherence to the expectation of the continuum model, *i.e.*, linear plot of  $a_N$  vs.  $(1/D)^3$ .

This linear correlation may be written as

$$a_M = a_M^0 + SD^{-3} \quad (6)$$

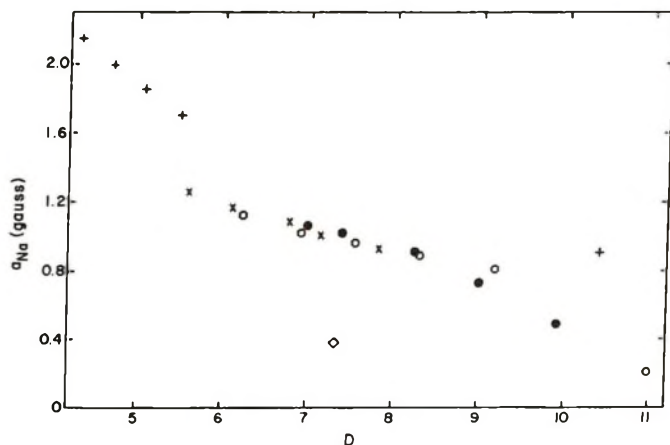


Figure 8. Correlation of sodium coupling constants with dielectric constant for solutions of sodium naphthalenide: ●, THF; ○, MTHF; ×, THP; +, ethyl ether; ◇, DME.

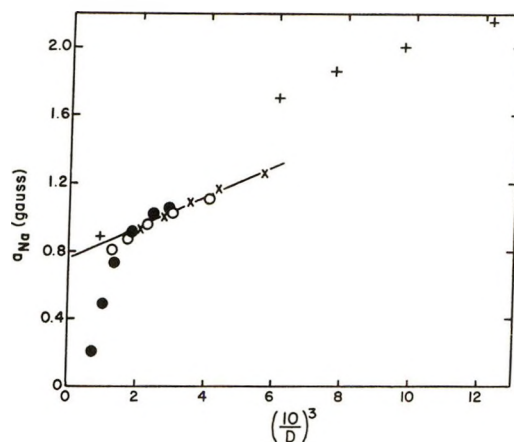


Figure 9. Variation of  $a_{Na}$  with  $D^{-3}$  for sodium naphthalenides: ●, THF; ○, MTHF; ×, THP; +, ethyl ether.

In terms of the model,  $S$  is interpreted as a measure of the amount of electron in the valence orbital of the metal, *i.e.*, the amount of electron transfer from anion to cation. The intercept  $a_M^0$  represents a contribution to  $a_M$  from a different mechanism. A natural candidate for this second mechanism is polarization of the core electrons<sup>4</sup> of the alkali metal ion by the unpaired electron of the nearby anion. The contribution to  $a_M$  from core polarization, *i.e.*,  $a_M^0$ , will be relatively insensitive to changes in temperature and/or solvent as long as the relative positions of anion and cation remain constant. The straight line in Figure 9 is defined by  $a_M^0 = 0.76$  G and  $S = 90$  G. The deviation of the low-temperature data for sodium naphthalenide

(17) C. Carvajal, J. K. Toelle, J. Smid, and M. Szwarc, *J. Amer. Chem. Soc.*, **87**, 5548 (1965); R. B. Slates and M. Szwarc, *J. Phys. Chem.*, **69**, 4124 (1965); P. Chang, R. V. Slates, and M. Szwarc, *ibid.*, **70**, 3180 (1966).

(18) Even though the mixed solvent experiments helped suggest representing the solvent as a continuous dielectric, the quantitative results of the model may not be applied in the case of mixed solvents because of preferential solvation.

in THF from the straight line presumably occurs because  $a_M^0$  becomes temperature dependent as a result of the relative positions of anion and cation changing. Alternatively, this deviation may be explained in terms of a temperature-dependent equilibrium between two species<sup>9</sup> each of which has characteristic values of  $a_{Na}^0$  and  $S$ . The other deviations from the correlation, *i.e.*, DME, *p*-dioxane, and ethyl ether, are also interpreted as reflecting a solvent, or temperature dependence of  $a_{Na}^0$  and/or  $S$ . For cesium naphthalenide the available data indicate that  $S \approx 0$  because  $a_{Cs}$  depends little on solvent or temperature (see Figure 5 and ref 8, 9, and 13) and that  $a_{Cs}^0 = -1.1 \pm 0.1$  G.<sup>19</sup> The data for rubidium naphthalenide indicate  $S \approx 0$ , as for cesium, because  $a_{Rb}$  is practically independent of solvent even though large changes in  $D$  are involved (see Figures 4 and 5), but that  $a_{Rb}^0$  depends on temperature, as does  $a_{Na}^0$  for sodium naphthalenide in THF.

Because more than one source of temperature and/or solvent dependence for  $a_M$  exists, it is important to be able to distinguish between the possibilities when a variable  $a_M$  is observed. One criterion is to see if the data conform to the requirements of eq 6. However, this may not be a very severe test when, as often is the case, both coupling constant and dielectric constant data<sup>20</sup> are available over a restricted range. Nevertheless, among the solutions of naphthalenide, biphenylide, and anthracenide<sup>1-3,6-11,13,14</sup> studied, a number yield  $a_M$ 's which satisfy eq 6. Others do not. For those solutions of sodium salts which do satisfy eq 6 values of  $S$  range from 60 to 100 G (see Table I).

**Table I:** Parameters of Eq 6 for Ion Pairs in Several Solvents<sup>a</sup>

Anion	Solvent	$a_{Na}^0$	$S$
A	Et <sub>2</sub> O	1.9	67
B	MTHF	-0.24	94
B	THP	-0.35	65
N	MTHF	0.76	90
N	THP	0.76	90

<sup>a</sup> A = anthracenide; B = biphenylide; N = naphthalenide.  $a_{Na}^0$  and  $S$  are in Gauss.

The value of  $S$  measures the total amount of electron transfer since it gives the contribution to  $a_{Na}$  from the electron transfer mechanism when  $D = 1$ . This range of values for  $S$  may be interpreted to mean that between 20 and 30% of the electron is transferred from the anion to cation. This appears to be an unreasonably large percentage of electron transfer in view of the fact that the hydrocarbon proton splittings are nearly independent of cation, upon which the amount of electron transfer depends. Thus, serious doubt arises about the source of the temperature dependence of  $a_M$  even when eq 6 is satisfied.

One possible explanation for these unreasonably large values for electron transfer is that the simple model which leads to eq 6 is inadequate. Clearly, the potential function from the continuum theory does not give a very good representation of the actual potential function near the ion, so that it is probably unrealistic to expect literal adherence of the data to the simple theory. On the other hand, the monomer species observed in solutions of alkali metals in amines<sup>21</sup> provide experimental tests of the model which can reveal inadequacies in an empirical manner. Plots of  $a_M$  vs.  $(1/D)^3$  for K, Rb, and Cs dissolved in ethylamine reveal linear relationships as shown in Figure 10. For convenience, values of  $a_M$  are in units of the respective atomic hyperfine coupling constants<sup>22</sup> which are 82.4 G for <sup>39</sup>K, 375 G for <sup>87</sup>Rb, and 821 G for <sup>133</sup>Cs. The values of  $a_M^0$  and  $S$  in these units are given in Table II. In spite of the linear variation of  $a_M$  with  $(1/D)^3$  in these three cases, deviation from the simple model is apparent. Most significantly the value of  $S$  for all three metals is 25 to 30 times too large; *i.e.*, extrapolation to  $D = 1$  gives values of  $a_M$  25 to 30 times the value for the gas-phase atom. In each case a value of  $a_M$  equal to that for the gas-phase atom is attained for  $D \approx 3$ . Clearly, a linear relationship between  $a_M$  and  $(1/D)^3$  cannot persist to very low values of  $D$ . Ap-

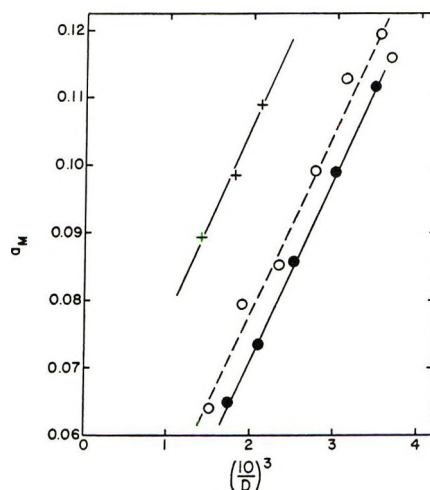


Figure 10. Variation of  $a_M$  with  $D^{-3}$  for metal solutions in ethylamine ( $a_M$  is in units of the atomic splitting):<sup>22</sup> ●, K; ○, Rb; +, Cs.

(19) The sign of the cesium coupling constant is obtained from nmr experiments. See T. Takeshita and N. Hirota, *Chem. Phys. Lett.*, **4**, 369 (1969); B. M. P. Hendriks, G. W. Canters, C. Corvaja, J. W. M. De Boer, and E. de Boer, *Mol. Phys.*, **20**, 193 (1971).

(20) Dielectric constant data were obtained from (a) ref 16, p 142; (b) C. Carvajal, K. J. Tölle, J. Smid, and M. Szwarc, *J. Amer. Chem. Soc.*, **87**, 5548 (1965); (c) D. Nicholls, C. Sutphen, and M. Szwarc, *J. Phys. Chem.*, **72**, 1021 (1968).

(21) K. Bar-Eli and T. R. Tuttle, Jr., *J. Chem. Phys.*, **40**, 2508 (1964); **44**, 114 (1966).

(22) N. F. Ramsey, "Nuclear Moments," Wiley, New York, N. Y., 1953, pp 12, 89.

**Table II:** Parameters for Eq 6 for Alkali Metals in Ethylamine<sup>a</sup>

Metal	$a_M^0$	$S$
K	0.015	0.27
Rb	0.025	0.26
Cs	0.048	0.29

<sup>a</sup>  $a_M^0$  and  $S$  are in units of atomic gas-phase hyperfine coupling constants.

preciable deviations from linearity may be expected for  $D < 3$ .

Returning to the ion pairs, we now estimate the amount of electron transfer by substituting  $D = 3$  instead of  $D = 1$ . This leads to values of the order of 1% for the total amount of electron transfer, a much

more reasonable value than the 30% previously estimated. Values of  $a_{Na}^0$  and  $S$  are listed in Table I for some systems which adhere to eq 6. Unfortunately, insufficient data are available at present to pick out trends in these quantities which may correlate with solvent structure, hydrocarbon structure, or metal. However, the efficacy of the analysis presented here may be tested by studying variations in  $a_M$  over wider ranges of  $D$  by varying both temperature and solvent. Obtaining results for a homologous series of solvents may be particularly useful in this respect because  $D$  may be changed a great deal without at the same time changing specific effects which relate to the molecular structure of the solvent.

*Acknowledgment.* This research was supported in part through a grant from the National Science Foundation (GP15517).

## Nitrogen and Boron Spin-Lattice Relaxation in Borazole<sup>1</sup>

by George M. Whitesides,\* Steven L. Regen,<sup>2</sup> John B. Lisle, and Robert Mays

Department of Chemistry, Massachusetts Institute of Technology, Cambridge, Massachusetts 02139  
(Received January 7, 1972)

Publication costs assisted by the National Institutes of Health

The observed line shapes of the <sup>1</sup>H nuclear magnetic resonance spectra of neat borazole and of borazole in toluene-*d*<sub>8</sub>, dimethyl-*d*<sub>6</sub> sulfoxide, chloroform-*d*, and cyclohexane-*d*<sub>12</sub> solutions are dominated by broadening due to the electric quadrupole-dependent nuclear spin-lattice relaxation of nitrogen and boron. Comparisons of observed spectra for borazole with those calculated for varying values of the nitrogen and boron spin-lattice relaxation rates establish that a parameter  $f = [\tau(eq)^2]_B / [\tau(eq)^2]_N$  characterizing the relative response of the boron and nitrogen nuclei to rotational diffusion (eq 3) is indistinguishable from unity ( $f = 1.0 \pm 0.1$ ) over a range of experimental conditions in these media. These observations are rationalized satisfactorily by eq 1 and provide empirical support for the usefulness of this equation in describing the influence of molecular motion on the rates of spin-lattice relaxation of quadrupolar nuclei. Spin-lattice relaxation of nitrogen is more rapid than that of boron in solutions containing the stable free radical di-*tert*-butylnitroxyl, presumably due to weak specific interactions between the borazole molecule and the nitroxyl radical. Combination of spin-lattice relaxation times inferred from the <sup>1</sup>H spectra of borazole with an estimate of its mean rotational correlation time in solution leads to approximate values for the quadrupole coupling constants:  $(e^2qQ/h) \cong 7.6 \pm 2.9$  MHz (<sup>10</sup>B);  $3.6 \pm 1.3$  MHz (<sup>11</sup>B);  $1.4 \pm 0.5$  MHz (<sup>14</sup>N).

### Introduction

The determination of spin-lattice relaxation times for quadrupolar nuclei is a technique of increasing importance in the study of molecular motions in solution.<sup>3-5</sup> Interpretation of these relaxation time measurements in terms of molecular motions rests on the assumption that relaxation is dominated by quadrupolar interactions and that contributions from dipole-dipole, anisotropic shielding, and spin-rotation interactions are unimportant. With this assumption,

equations having the form of eq 1 are used to relate re-

$$\frac{1}{T_{1X}} = \left(\frac{3}{40}\right) \left(\frac{2I + 3}{I^2(2I - 1)}\right) \left(\frac{e^2qQ}{\hbar}\right)^2 \left(1 + \frac{\eta^2}{3}\right) \tau_X \quad (1)$$

laxation times to molecular motion. Here  $T_{1X}$  is the

(1) Acknowledgment is made to the donors of the Petroleum Research Fund, administered by the American Chemical Society (Grant No. 4032), and to the National Institutes of Health (Grant No. GM-16020) for support of this research.

(2) A. D. Little Fellow, 1969-1970.

spin-lattice relaxation time of nucleus X,  $I$  is the nuclear spin of X,  $eQ$  is the electric quadrupole moment of the nucleus,  $eq = \partial E/\partial z = \partial^2 V/\partial z^2 = V_{zz}$  is the principal component of the electric field gradient tensor at the nucleus,  $\eta = [V_{xx} - V_{yy}]/V_{zz}$  is the asymmetry parameter describing the deviation of the electric field gradient tensor from axial symmetry, and  $\tau_X$ , at the simplest level of interpretation, is a mean correlation time characterizing the power spectrum of the electric field gradient fluctuations at the nucleus that are effective in inducing magnetic dipole transitions.<sup>6,7</sup>

The assumptions underlying this equation are undoubtedly tenable in the great majority of studies in solutions of normal viscosities, and the equation appears to have very generally applicable form. However, despite theoretical expansions of  $\tau_X$  in terms of other microscopic parameters, particularly the components of the rotational diffusion tensor,<sup>3</sup> the physical interpretation to be placed on this correlation time remains vague, depending significantly on the model chosen to generate the power spectrum of the electric field fluctuations resulting from molecular motion. In particular, the relative usefulness of inertial and diffusional models for molecular reorientation, and the interpretation of the "microscopic" viscosities commonly used in the diffusional treatments,<sup>4,8-10</sup> are not clear. Further, although there is some agreement that for most nonionic molecules the major contributions to the field gradient fluctuations responsible for spin-lattice relaxation arise from the reorientation of the molecule containing the quadrupolar nucleus being observed, rather than from motions of other molecules in solution,<sup>8</sup> the influence of relatively weak intermolecular interactions on the relaxation behavior of quadrupolar nuclei has not been thoroughly explored.

This paper describes measurements of the temperature, viscosity, and solvent dependence of the spin-lattice relaxation times of the nitrogen and boron atoms of borazole, obtained by examination of the <sup>1</sup>H nmr line shapes of this substance. These measurements were intended to search for deviations of the experimental relaxation times from the behavior expected from an equation having the form of eq 1 and to help to define, in an empirical sense, the sensitivity of quadrupole relaxation rates to the intermolecular and environmental effects that are presently impractical to include in theoretical discussion. Borazole was chosen for the subject of this study because the presence of two chemically distinct<sup>11</sup> quadrupolar nuclei in a single rigid molecule of high symmetry provides an opportunity to circumvent some of the uncertainties inherent in eq 1 by focusing attention on comparison of the magnitudes of nitrogen and boron spin-lattice relaxation rates rather than on the absolute magnitudes of these rates. Thus, on the basis of eq 1, the spin-lattice relaxation times of, e.g., <sup>11</sup>B and <sup>14</sup>N should be related by eq 2.<sup>12</sup> We assume at the outset that the term con-

$$\frac{T_{1,^{14}\text{N}}}{T_{1,^{11}\text{B}}} = \left(\frac{4}{15}\right) \left(\frac{\tau_{^{11}\text{B}}}{\tau_{^{14}\text{N}}}\right) \left(\frac{e^2qQ_{^{11}\text{B}}}{e^2qQ_{^{14}\text{N}}}\right)^2 \left(\frac{3 + \eta^2_{^{11}\text{B}}}{3 + \eta^2_{^{14}\text{N}}}\right) \quad (2)$$

taining the asymmetry parameters  $\eta$  in this equation can be neglected. The magnitudes of these terms are not known for borazoles; however, for most organic compounds  $\eta$  is sufficiently small that  $\eta^2$  is less than 0.1.<sup>12</sup> Thus, in all probability, the contributions from  $\tau_{^{11}\text{B}}$  and  $\tau_{^{14}\text{N}}$  could individually be safely neglected in eq 2; the error introduced by setting equal to unity the quotient that constitutes the last term in this equation is undoubtedly well within the final experimental uncertainty in this work ( $\sim \pm 10\%$  for the ratio  $T_{1,^{14}\text{N}}/T_{1,^{11}\text{B}}$ ; *vide infra*). Thus, since the nuclear quadrupole moments  $Q$  are known quantities,<sup>13,14</sup> eq 2 can be rewritten in more compact form (eq 3). It is not prac-

$$\frac{T_{1,^{14}\text{N}}}{T_{1,^{11}\text{B}}} = 1.64 \left(\frac{\tau_{^{11}\text{B}}}{\tau_{^{14}\text{N}}}\right) \left(\frac{eq_{^{11}\text{B}}}{eq_{^{14}\text{N}}}\right)^2 = 1.64f \quad (3a)$$

$$f = \frac{[\tau(eq)^2]_{\text{B}}}{[\tau(eq)^2]_{\text{N}}} \quad (3b)$$

tical to make a reliable *a priori* estimate of the ratio  $(eq_{\text{B}}/eq_{\text{N}})^2$ ; however, it is possible to estimate the ratio  $\tau_{\text{B}}/\tau_{\text{N}}$ . The nitrogen and boron nuclei occupy symmetry-equivalent positions in the borazole skeleton.

(3) Review: W. T. Huntress, Jr., *Advan. Magn. Resonance*, **4**, 2 (1970); *J. Chem. Phys.*, **48**, 3524 (1968); R. A. Dwek and R. E. Richards, *Discuss. Faraday Soc.*, **43**, 196 (1967); J. A. Pople, *ibid.*, 192 (1967).

(4) T. T. Bopp, *J. Chem. Phys.*, **47**, 3621 (1967); T. D. Alger and H. S. Gutowsky, *ibid.*, **48**, 4625 (1968); R. K. Harris and N. C. Pypers, *Mol. Phys.*, **20**, 467 (1971); and references in each.

(5) R. P. Hangland, L. Stryer, T. R. Stengle, and J. D. Balde-schiwiler, *Biochemistry*, **6**, 498 (1967); R. G. Bryant, *J. Amer. Chem. Soc.*, **89**, 2496 (1967); Ch. Brevard and J. M. Lehn, *ibid.*, **92**, 4987 (1970).

(6) A. Abragam, "The Principles of Nuclear Magnetism," Oxford University Press, London, 1961, Chapters VII and VIII; C. P. Slichter, "Principles of Magnetic Resonance," Harper and Row, New York, N. Y., 1963, Chapters 5 and 6.

(7) H. S. Gutowsky, R. L. Vold, and E. J. Wells, *J. Chem. Phys.*, **43**, 4107 (1965), and references therein.

(8) E. W. Randall and D. Shaw, *Spectrochim. Acta, Part A*, **23**, 1235 (1966); D. W. Aksnes, S. M. Hutchinson, and K. J. Packer, *Mol. Phys.*, **14**, 301 (1968); M. Arnold and K. J. Packer, *ibid.*, **10**, 141 (1966); C. Deverell, D. J. Frost, and R. E. Richards, *ibid.*, **9**, 564 (1965).

(9) W. A. Steele, *J. Chem. Phys.*, **38**, 2404 (1963); P. S. Hubbard, *ibid.*, **53**, 985 (1970); S. G. Brush, *Chem. Rev.*, **62**, 513 (1962); A. Bondi, *J. Amer. Chem. Soc.*, **88**, 2131 (1966).

(10) D. E. Woessner, *J. Chem. Phys.*, **40**, 2341 (1964); K. T. Gillen and J. H. Noggle, *ibid.*, **52**, 4905 (1970); W. B. Moniz and H. S. Gutowsky, *ibid.*, **38**, 1155 (1963); H. Shimizu, *ibid.*, **40**, 754 (1964).

(11) For a review of borazoles, see H. Steinberg and R. J. Brotherton, "Organoboron Chemistry," Vol. II, Wiley, New York, N.Y., 1966, pp. 174-434; O. T. Beachley, Jr., *J. Amer. Chem. Soc.*, **93**, 5066 (1971), and references therein.

(12) For examples, see C. T. O'Konski, "Determination of Organic Structures by Physical Methods," F. C. Nachod and W. D. Phillips, Ed., Academic Press, New York, N. Y., 1962, Chapter 11.

(13) The values of the nuclear quadrupole moments used in this paper are (in esu cm<sup>2</sup>)  $eQ(^{14}\text{N}) = 1.56 \times 10^{-26}$ ; <sup>14a</sup>  $eQ(^{10}\text{B}) = 8.04 \times 10^{-26}$ ; <sup>14b</sup>  $eQ(^{11}\text{B}) = 3.86 \times 10^{-25}$ ; <sup>14b</sup>

(14) (a) C. T. O'Konski and T. Ha, *J. Chem. Phys.*, **49**, 5354 (1968); see also C. C. Lin, *Phys. Rev.*, **119**, 1027 (1960); (b) H. Schaefer, R. Klemm, and F. Harris, *ibid.*, **176**, 49 (1968).

In consequence, in the absence of association between borazole and other components of the solution, the diffusional motion of boron and nitrogen nuclei with respect to the external magnetic field should be identical. Thus, the ratio  $\tau_B/\tau_N$ , at the simplest level of interpretation, would be expected to be unity.

The technique used to determine relaxation times in this work yields simultaneous measurements on nitrogen and boron, two nuclei having magnetic dipole transitions at different frequencies [ $\nu_0(^{14}\text{N}) = 4.33$  MHz,  $\nu_0(^{11}\text{B}) = 19.25$  MHz at 14 kG], and characterized by different chemical shift anisotropies and dipole-dipole interactions with other spins in the solution. Since comparison of the ratio of the relaxation times of these two nuclei should serve to reduce the importance of several possible types of experimental error, small contributions to relaxation rates from sources other than the fairly restricted set covered by eq 1 might be detectable in borazole that would be difficult to detect in other compounds. Thus, in particular, fluctuations in the magnitude of the parameter  $f$  (eq 3b) on changing solution composition, viscosity, or temperature should be attributable either to a failure of eq 1, or to the influence of specific intermolecular association between solvent and the boron or nitrogen nuclei, since eq 1 clearly implies that  $f$  should be invariant to the nature of the medium in the absence of intermolecular association effects.

The influence of quadrupole relaxation on the  $^1\text{H}$  nmr spectrum of borazole and its analogs has been discussed previously.<sup>15</sup>

## Results

The  $^1\text{H}$  nmr spectrum of a sample of neat borazole containing a small amount of benzene as an internal resolution standard at  $-8^\circ$  consists of a triplet arising from protons bonded to  $^{14}\text{N}$  [ $J(^1\text{H}, ^{14}\text{N}) = 54 \pm 2$  Hz] centered at  $\delta$  5.47, superimposed on a quartet due to protons on  $^{11}\text{B}$  [ $J(^1\text{H}, ^{11}\text{B}) = 135 \pm 3$  Hz,  $\delta$  4.43]; the expected septet due to protons on  $^{10}\text{B}$  ( $\sim 19\%$  natural abundance) is obscured by the more intense  $^{11}\text{B}$ -H resonances (Figure 1). Lowering the temperature of the sample to  $-72^\circ$  results in partial collapse of the NH and BH signals to broad superimposed singlets. Although complete collapse cannot be observed in samples composed mainly of borazole because these samples freeze at  $\sim -55^\circ$ , samples in dimethyl- $d_6$  sulfoxide (DMSO- $d_6$ , 68% v/v) show two relatively sharp peaks at  $-62^\circ$ . Samples of borazole in toluene- $d_8$  could be cooled to  $-80^\circ$  before freezing; spectra at these low temperatures resemble those observed for 68% borazole in DMSO- $d_6$ . The line widths characteristic of all of these spectra were never sufficiently narrow to permit observation of  $^1\text{H}$ -N-B- $^1\text{H}$ ,  $^1\text{H}$ -B- $^{14}\text{N}$ , or  $^1\text{H}$ -N- $^{11}\text{B}$  spin-spin coupling, although partial decoupling indicated that two bond heteronuclear couplings were not important: thus, the  $^1\text{H}$  nmr spectrum

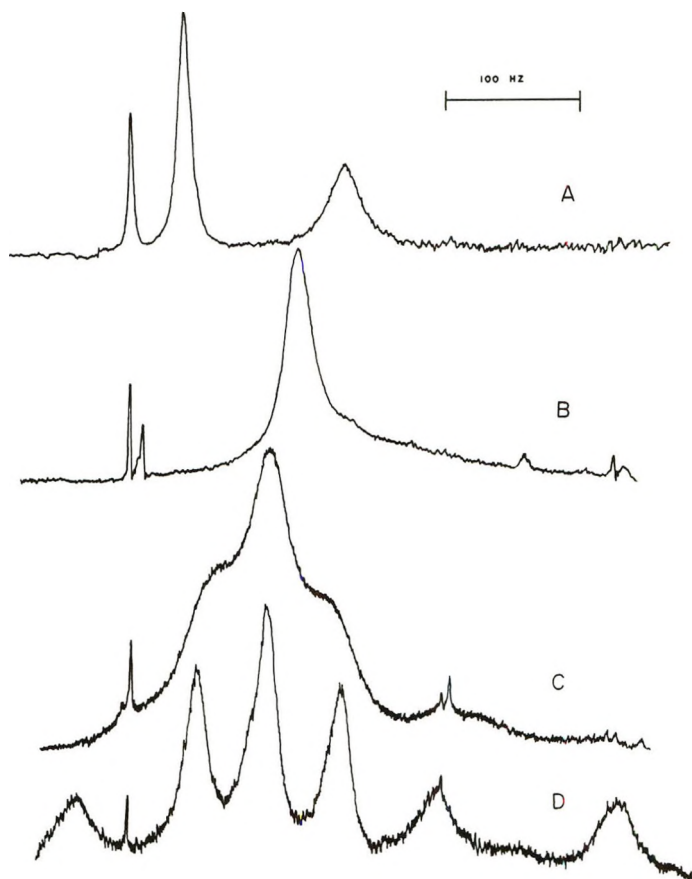


Figure 1.  $^1\text{H}$  nmr spectra at 60 MHz of (A) borazole in DMSO- $d_6$  (68% v/v) at  $-62^\circ$ , (B) borazole in toluene- $d_8$  (33% v/v) at  $-80^\circ$ , (C) borazole (neat) at  $-72^\circ$ , and (D) borazole (neat) at  $-8^\circ$ . The sharp line at low field in each spectrum is the benzene used as an internal line width standard.

of neat borazole at  $30^\circ$  showed that no significant change in the shape of the lines comprising the H- $^{14}\text{N}$  triplet accompanied collapse of the H- $^{11}\text{B}$  quartet on irradiation at the boron resonance frequency.

The difference in the appearance of the borazole spectra in neat samples and in toluene and DMSO solution are primarily a reflection of the differences in viscosities of these samples, rather than of sample temperatures.<sup>16</sup> The Gierer and Wirtz modification of the Stokes equation provides a fairly satisfactory empirical relation between the temperature and bulk viscosity of the sample, dimension of solvent and solute molecules, and the nmr rotational correlation times of the solute (eq 4).<sup>17</sup> This equation contains the assumptions that

(15) H. Watanabi, T. Totani, and M. Ohtsuru, *Mol. Phys.*, **14**, 367 (1968). A recent paper by E. K. Mellon, B. M. Coker, and P. B. Dillon, *Inorg. Chem.*, **11**, 852 (1972), describes an investigation of the nmr spectrum of borazole closely related to that described in this article.

(16) See G. M. Whitesides and H. L. Mitchell, *J. Amer. Chem. Soc.*, **91**, 2245 (1969), for a discussion of this point.

(17) A. Gierer and K. Wirtz, *Z. Naturforsch. A*, **8**, 532 (1953); D. Herbison-Evans and R. E. Richards, *Mol. Phys.*, **7**, 515 (1964). See R. A. Assink, J. DeZwaan, and J. Jonas, *J. Chem. Phys.*, **56**, 4975 (1972), for a recent experimental investigation of certain of the assumptions underlying this treatment.

one correlation time is sufficient to describe the rotational behavior of the solute and that the difference between the macroscopic and "microscopic" viscosities can be taken into account by the "microviscosity factor" of  $1/6$ .<sup>17</sup>

$$\tau_X = \frac{r_{\text{solute}}\tau_s}{6r_{\text{solvent}}} = \frac{(r_{\text{solute}})(V_{\text{solute}})\eta}{6kT(r_{\text{solvent}})} \quad (4)$$

Here  $r_{\text{solute}}$  and  $r_{\text{solvent}}$  are hard-sphere radii for solute and solvent molecules (cm),  $\tau_s$  is the Stokes correlation time (sec),  $V_{\text{solute}}$  is the hard-sphere "volume" of the solute, and  $\eta$  is the macroscopic solution viscosity (poise). On the basis of this equation,  $\tau_X$  should depend on both  $\eta$  and  $T$ ; however, in practice, the change in sample viscosity  $\eta$  on changing temperature is normally much larger proportionately than the change in the reciprocal temperature; hence, the spectra of Figure 1 illustrate primarily the influence of solution viscosity on the spin-lattice relaxation rates of  $^{11}\text{B}$  and  $^{14}\text{N}$  of borazole.

Relaxation rates for boron and nitrogen were extracted from the experimental spectra using a procedure outlined previously<sup>16</sup> by treating the relaxation processes responsible for the collapse of the  $^{14}\text{NH}$ ,  $^{11}\text{BH}$ , and  $^{10}\text{BH}$  multiplets separately as equivalent to chemical exchange between equally populated sites separated in frequency by  $m_I J_{X,H}$ , corresponding to the  $(2I + 1)$  substates of  $m_I$  of a nucleus having spin  $I$ . The appropriate transition rates between the  $m_I$  substates are given by eq 5-7.<sup>18</sup>

$$k_{m,m\pm 1} = k_{m+1,m} = \frac{(2m \pm 1)^2(I + m \pm 1)(I \mp m)}{2T_{1X}(2I - 1)(2I + 3)} \quad (5)$$

$$k_{m,m\pm 2} = k_{m\pm 2,m} = \frac{(I \mp m)(I \mp m - 1)(I \pm m + 1)(I \pm m + 2)}{2T_{1X}(2I - 1)(2I + 3)} \quad (6)$$

$$k_{m,m} = \sum_{m' \neq m} k_{m,m'} \quad (7)$$

With these equations, the calculation of the amplitude of the proton signal at frequency  $\omega$  for any values of  $T_{1,^{14}\text{N}}$ ,  $T_{1,^{11}\text{B}}$ , and  $T_{1,^{10}\text{B}}$  is reduced to the solution of eq 8.

$$I(\omega) \propto \text{Re}\left\{ \left(\frac{1}{3}\right)\mathbf{I} \cdot [i\omega_{^{14}\text{N}} + \mathbf{R}_{^{14}\text{N}} + (1/T_{1,^{14}\text{N}})\mathbf{K}_{^{14}\text{N}}]^{-1} \cdot \mathbf{I} + \left(\frac{1}{4}\right)0.81\mathbf{I} \cdot [i\omega_{^{11}\text{B}} + \mathbf{R}_{^{11}\text{B}} + (f/T_{1,^{11}\text{B}})\mathbf{K}_{^{11}\text{B}}]^{-1} \cdot \mathbf{I} + \left(\frac{1}{7}\right)0.19\mathbf{I} \cdot [i\omega_{^{10}\text{B}} + \mathbf{R}_{^{10}\text{B}} + (f/T_{1,^{10}\text{B}})\mathbf{K}_{^{10}\text{B}}]^{-1} \cdot \mathbf{I} \right\} \quad (8)$$

Here, e.g.,  $\omega_{^{14}\text{N}}$  is a diagonal matrix whose elements are the values  $(m_I J_{N,H} - \omega_{\text{N}} - \omega)$ ;  $\mathbf{R}_{^{14}\text{N}}$  is a diagonal matrix whose elements describe the widths of the  $\text{NH}$  lines in the absence of quadrupole relaxation; and the matrix  $(1/T_{1,^{14}\text{N}})\mathbf{K}_{^{14}\text{N}}$  contains the transition rate constants obtained from eq 5-7, describing the transfer of

magnetization between the various  $\text{NH}$  resonances under the influence of  $^{14}\text{N}$  relaxation.<sup>19</sup> The influence of unresolved  $^1\text{HNB}^1\text{H}$  couplings on the  $^1\text{H}$  line shapes was approximated by assuming a line width in the absence of relaxation that was uniformly 10 Hz broader than the observed width of the benzene internal resolution standard (typically 3 Hz in nonviscous solutions and 5 Hz in  $\text{DMSO}-d_6$  at  $-62^\circ$ ). The relative isotopic abundances of  $^{14}\text{N}$ ,  $^{11}\text{B}$ , and  $^{10}\text{B}$  (1.00:0.81:0.19) were taken into account by appropriate adjustment of intensities. The multiplicative factor  $f$  in eq 8 was used to adjust the fit of calculated to observed spectra independently for  $\text{NH}$  and  $\text{BH}$  resonances; it can be interpreted as the deviation of the ratio of relaxation times at  $^{11}\text{B}$  and  $^{14}\text{N}$  from the value calculated in eq 3 (eq 9).

$$\left(\frac{T_{1,^{14}\text{N}}}{T_{1,^{11}\text{B}}}\right)_{\text{obsd}} = f \left(\frac{T_{1,^{14}\text{N}}}{T_{1,^{11}\text{B}}}\right)_{\text{calcd}} = 1.64f \quad (9)$$

Calculated spectra were obtained from eq 8 using standard computer routines.<sup>19,20</sup> Representative spectra illustrating the dependence of the proton line shapes on the spin-lattice relaxation times are given in Figure 2; chemical shifts used in these calculations were obtained in neat borazole. Relaxation times characterizing the experimental spectra were obtained by visual fitting of spectra calculated by varying the boron and nitrogen relaxation times to these spectra; variations in chemical shifts and in the assumed proton  $T_2$  (as inferred from the benzene line width) with temperature were taken into account.

By varying viscosity and/or temperature, the  $^1\text{H}$  spectrum of borazole could be easily adjusted in a medium of interest to give spectra at any point between the limits in which  $\text{NH}$  and  $\text{BH}$  couplings were fully resolved or collapsed. For determinations of  $f$  (eq 8 and 9) it was found most convenient to compare calculated and experimental spectra in the region in which the  $\text{NH}$  and  $\text{BH}$  resonances were single, broad lines. Comparisons were carried out by varying  $T_{1,^{14}\text{N}}$  to give the best fit between calculated and experimental shapes for the  $\text{NH}$  line and then calculating several complete spectra for several values of  $f$  centered around  $f = 1.0$ . Three representative theoretical spectra are compared with the experimental spectrum of borazole in  $\text{DMSO}-d_6$  at  $-44^\circ$  in Figure 3. In this instance,  $f = 1.0$  ap-

(18) Numerical values for these rate constants are given in eq 4.43 (for  $I = 1$ ) and 4.44 (for  $I = 3/2$ ) of ref 7, and  $I = 3$  in J. Bacon, R. J. Gillespie, J. S. Hartman, and U. R. K. Rao, *Mol. Phys.*, **18**, 561 (1970). They will not be reproduced here. For discussions of the limitations of this computational procedure, see N. C. Pyper, *ibid.*, **21**, 977 (1971), and references therein.

(19) For reviews of techniques, see C. S. Johnson, Jr., *Advan. Magn. Resonance*, **1**, 33 (1965).

(20) Calculations were carried out using a version of the program NMRCTL (cf. J. K. Krieger, Ph.D. Thesis, Massachusetts Institute of Technology, Cambridge, Mass., 1971). Matrix inversions were carried out using procedures based on the routine ALLMAT (cf. G. Binsch, *J. Amer. Chem. Soc.*, **91**, 1304 (1969); R. E. Schirmer, J. H. Noggle, and D. F. Gaines, *ibid.*, **91**, 6240 (1969); R. G. Gordon and R. P. McGinnis, *J. Chem. Phys.*, **49**, 2455 (1968)).

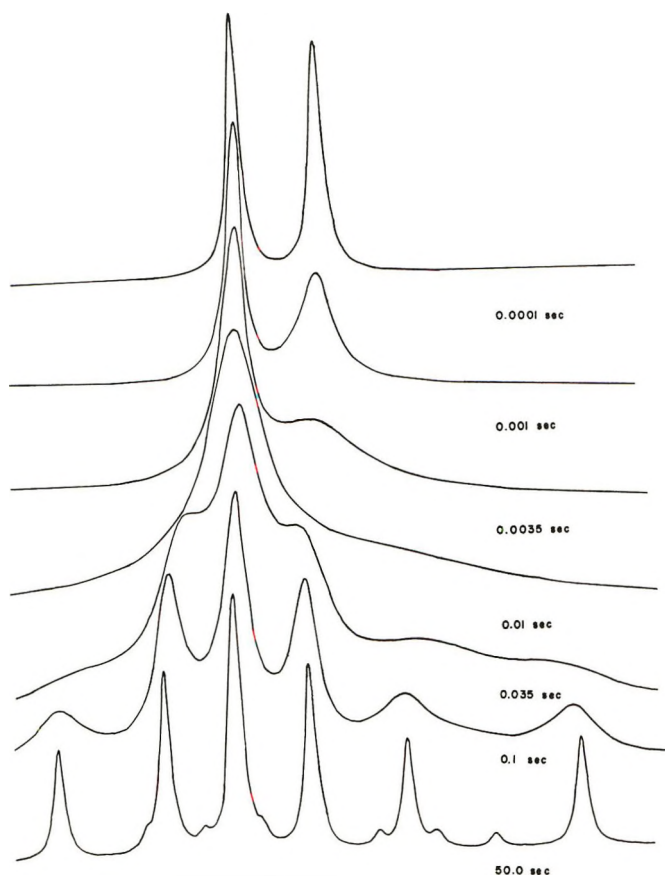


Figure 2. Calculated  $^1\text{H}$  nmr line shapes for borazole as a function of a uniform relaxation time  $T_1^0$ . The individual relaxation times are related to  $T_1^0$  by the following expressions:  $T_{1,^{14}\text{N}} = T_1^0/6.73$ ;  $T_{1,^{11}\text{B}} = T_1^0/11.06$ ;  $T_{1,^{10}\text{B}} = T_1^0/7.20$ .

pears to give better agreement between calculated and experimental line shapes than  $f = 1.1$  or  $f = 0.90$ . The results of similar experiments in several other media are summarized in Table I.

Table I: Values of  $f$  (Eq 8) for Borazole in Several Solvents

Solvent (concn, v/v)	$f$	Temp, °C
Neat	$1.0 \pm 0.1$	-37
DMSO- $d_6$ (68%)	$1.0 \pm 0.1$	-44
$\text{CDCl}_3$ (44%)	$1.0 \pm 0.1$	25
Toluene- $d_8$ (33%)	$1.0 \pm 0.1$	-11
Cyclohexane- $d_{12}$ (42%)	$1.0 \pm 0.1$	25
$\text{CCl}_4$ (60%) with added di- <i>tert</i> -butylnitroxyl <sup>a</sup>	$0.17 \pm 0.08$	25

<sup>a</sup> The concentration of nitroxyl radical was  $\sim 5\%$ .

The significant conclusion to be drawn from these data is that  $f = 1$  in a variety of "typical" solvents within the limits of the experimental technique ( $\sim \pm 10\%$ ). Thus, these data provide support for the contention that eq 1 does provide a useful functional relationship between the molecular motions charac-

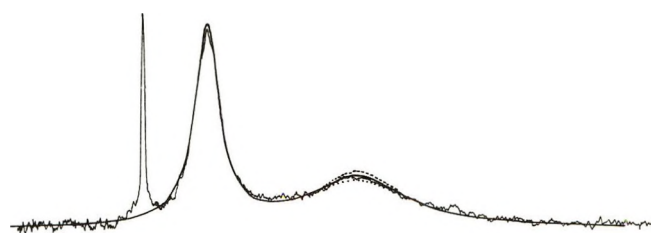


Figure 3. Comparison of the observed spectrum of borazole in DMSO- $d_6$  (68% v/v) at  $-44^\circ$  with spectra calculated assuming the following values of  $f$  (eq 7):  $f = 1.0$  (—);  $f = 1.1$  (---); and  $f = 0.9$  (····). The single resonance downfield from the  $\text{NH}$  line is benzene used as an internal line width standard.

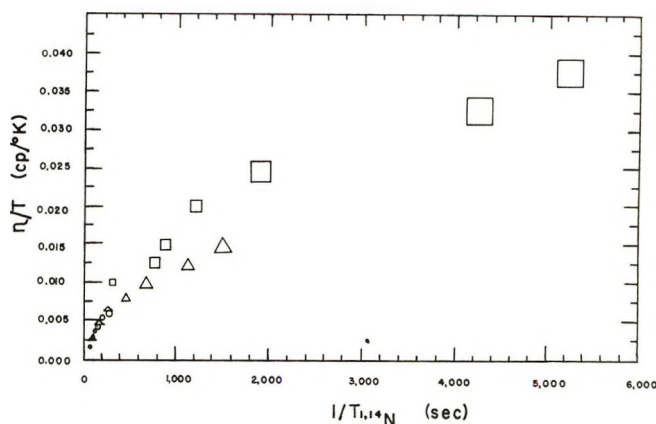
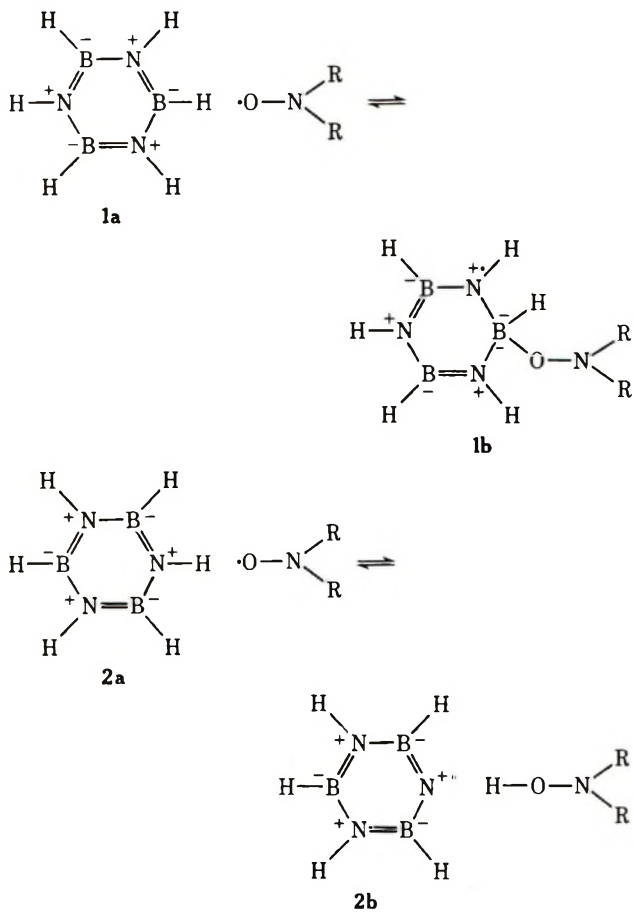


Figure 4. Plot of  $\eta/T$  as a function of  $1/T_{1,^{14}\text{N}}$  for borazole in DMSO- $d_6$  (68% v/v) ( $\square$ ); borazole in toluene- $d_8$  (33% v/v) ( $\triangle$ ); and borazole (neat) ( $\circ$ ). Relaxation times for  $^{11}\text{B}$  can be obtained from this plot using the relation  $1/T_{1,^{11}\text{B}} = 1.64(1/T_{1,^{14}\text{N}})$ .

terized by  $\tau_X$  and the spin-lattice relaxation time of a quadrupolar nucleus and that other factors not included in eq 1 that might in principal contribute to  $T_1$  apparently are not experimentally significant.

The one medium in which there is a significant deviation of  $f$  from unity is one composed of *ca.* 60% borazole in  $\text{CCl}_4$  containing the stable free radical di-*tert*-butylnitroxyl, in which the  $^{14}\text{N}$  is selectively relaxed.<sup>21</sup> Whether the selective relaxation of  $^{14}\text{N}$  is due to a  $\sigma$ -complex formation between a boron atom of borazole and nitroxyl radical (1) or hydrogen bonding between a proton bound to nitrogen and nitroxyl (2), both of which could selectively place the  $^{14}\text{N}$  nuclei in close proximity to an unpaired electron, or to some other more complex mechanism, is not clear. However, it is pertinent to considerations of the utility of eq 1 that only a drastic change in medium (*i.e.*, addition of a paramagnetic species to the solution containing borazole) is capable of inducing an observable deviation of  $f$  from its expected value.<sup>22,23</sup>

(21) Increasing the concentration of di-*tert*-butylnitroxyl broadens and collapses the  $\text{NH}$  resonances more rapidly than the  $\text{BH}$  resonances. Since the solvent viscosity is not appreciably changed by addition of nitroxyl, the deviation of  $f$  from unity thus appears to be due to a decrease in  $T_{1,\text{N}}$  rather than an increase in  $T_{1,\text{B}}$ .



The Gierer-Wirtz equation (eq 4) predicts a linear relation between  $1/T_{1,^{14}\text{N}}$  (and  $1/T_{1,^{11}\text{B}}$ ) and  $\eta/T$ . This relation is only approximately obeyed by the relaxation time data obtained in this study (Figure 4): a plot of the reciprocal relaxation times *vs.*  $\eta/T$  shows a significant curvature. This curvature has the sense that would be expected if reorientation of borazole around its  $C_3$  axis were faster than that around the  $C_2$  axes. However, the presently available data are not sufficient to distinguish between a failure of the approximations underlying the Gierer-Wirtz equation<sup>17</sup> and errors in the line shape analysis at the fast- or slow-exchange limits, due to neglect of spin-spin couplings, cross-relaxation effects, or other factors influencing line shapes.

Regardless, the observation that the relaxation data for borazole in toluene, DMSO, and borazole solutions fall approximately along a common curve provides support for the assertion that specific interactions between borazole and typical diamagnetic solvent molecules do not strongly influence the relaxation behavior of the former.

Keeping in mind the failure of the relaxation data obtained in this study to obey eq 4 in detail, these data can nonetheless be used in conjunction with eq 4 to obtain crude estimates of the quadrupole coupling constants of nitrogen and boron in borazole. To

evaluate the dimensional parameters contained in eq 4, borazole and toluene were assumed to be hard spheres:  $r_{\text{borazole}} = 2.96 \text{ \AA}$  and  $r_{\text{toluene}} = 3.09 \text{ \AA}$ .<sup>24-26</sup> Inserting these values and the experimentally determined viscosity of a 33% (v/v) solution of borazole in toluene (1.07 cP at  $-39^\circ$ ) into eq 4, the correlation time for reorientation  $\tau_X$  is estimated to be  $5.7 \times 10^{-12} \text{ sec}$ ;<sup>27</sup> this value, together with the experimental value for  $T_{1,^{14}\text{N}}$  in toluene at  $-39^\circ$  ( $= 5.5 \times 10^{-3} \text{ sec}$ ), yields values for the quadrupole coupling constants:  $(e^2qQ/h) \cong 3.6 \pm 1.3 \text{ MHz}$  ( $^{11}\text{B}$ );  $7.6 \pm 2.9 \text{ MHz}$  ( $^{10}\text{B}$ );  $1.4 \pm 0.5 \text{ MHz}$  ( $^{14}\text{N}$ ).<sup>28-31</sup>

### Experimental Section

**General.** Nmr spectra were taken on Varian HA-100 and A-60 spectrometers equipped with V-6040 variable-temperature controller. Calibration of the temperature control unit was accomplished by measuring peak separations in methanol or ethylene glycol samples. Viscosities of neat borazole as a function of temperature were taken from the literature;<sup>25</sup> viscosities of borazole in toluene (33% v/v) and borazole in DMSO (68% v/v) were measured using a Cannon-Manning semi-

(22) Di-*tert*-butylnitroxyl forms relatively stable complexes with a number of Lewis acids.<sup>23</sup> Nucleophilic attack on borazole seems to involve the boron centers.<sup>11</sup>

(23) B. M. Hoffman and T. B. Eames, *J. Amer. Chem. Soc.*, **91**, 5170 (1969); W. Beck and K. Schmidther, *Chem. Ber.*, **100**, 3363 (1967); L. A. Krinitskays and S. Dobryakov, *Bull. Acad. Sci. USSR*, **3**, 558 (1966); B. M. Hoffman and T. B. Eames, *J. Amer. Chem. Soc.*, **91**, 2169 (1969).

(24) The density of borazole at  $-39^\circ$  is  $0.904 \text{ g/cm}^3$ ;<sup>25</sup> the density of toluene at  $-39^\circ$  is  $0.921 \text{ g/cm}^3$ .<sup>26</sup> Hard sphere radii were calculated assuming a closest packing relation between the hard spheres and the molar volume  $= 0.74\nu_m = 4\pi r^3/3$ .

(25) L. B. Eddy, H. Smith, Jr., and R. R. Miller, *J. Amer. Chem. Soc.*, **77**, 2105 (1955).

(26) E. D. Washburn, Ed., "International Critical Tables," Vol. III, McGraw-Hill, New York, N. Y., 1928, p 29.

(27) For comparison, values of  $\tau_c$  of 1.3, 1.7, and  $2.4 \times 10^{-12} \text{ sec}$  have been determined for benzene-*d*<sub>6</sub> and benzene at  $\sim 30^\circ$ : D. E. Woessner and B. S. Snowden, *J. Chem. Phys.*, **52**, 1621 (1970); T. E. Bull and J. Jonas, *ibid.*, **52**, 4553 (1970); G. Bonera and A. Rigamonti, *ibid.*, **42**, 171 (1965); see also D. E. O'Reilly, *ibid.*, **53**, 850 (1970).

(28) The value of the coupling constant for  $^{11}\text{B}$  is of interest in a qualitative estimation of the  $\pi$ -bond order of the N-B bond of borazole. Ring and Koski<sup>29</sup> have suggested that the  $\pi$ -bond order of B-N multiple bond can be determined by the expression  $\pi_{\text{B-N}} = 1 - [e^2qQ/h]_{^{11}\text{B}}/5.39$ . Our estimate of the quadrupole coupling constant leads to  $\pi_{\text{B-N}} = 0.33 \pm 0.13$ , in rough agreement with previous estimates of this parameter ( $\sim 0.5$ ).<sup>30,31</sup> The estimate of this parameter by Mellon, *et al.*,<sup>15</sup> based on similar quadrupole coupling constants appears to be too high by a factor of 2.

(29) M. Ring and W. Koski, *J. Chem. Phys.*, **35**, 381 (1961). For other recent discussions pertinent to the electronic structure of borazole, see D. R. Armstrong and D. T. Clark, *Chem. Commun.*, 99 (1970); H. Bock and W. Fuss, *Agnew. Chem., Int. Ed. Engl.*, **10**, 182 (1971); G. J. Bullen and N. H. Clark, *J. Chem. Soc. A*, 992 (1970); S. D. Peyerimhoff and R. J. Buenker, *J. Chem. Phys.*, **49**, 312 (1968); K. E. Blick, J. W. Dawson, and K. Niedenzu, *Inorg. Chem.*, **9**, 1416 (1970); S. D. Peyerimhoff and R. J. Buenker, *Theor. Chim. Acta*, **19**, 1 (1970).

(30) R. W. Rector, G. W. Schaeffer, and J. R. Platt, *J. Chem. Phys.*, **17**, 460 (1949); H. Watanabe, K. Ito, and M. Kubo, *J. Amer. Chem. Soc.*, **82**, 3294 (1960).

(31) For a listing of representative  $^{14}\text{N}$  quadrupole coupling constants in heterocyclic compounds, see E. A. C. Lucken in "Physical Methods in Heterocyclic Chemistry," Vol. IV, A. R. Katritzky, Ed., Academic Press, New York, N. Y., 1971, Chapter 2.

micro viscometer modified for operation under a nitrogen atmosphere. The viscometer was calibrated against literature values for toluene<sup>32</sup> (temperature, viscosity in cP): 24°, 0.560; 6°, 0.720; -12°, 0.970. Measured values for the solutions of borazole in toluene were 24°, 0.410; 6°, 0.532; -12°, 0.759. Values for solutions of borazole in DMSO were 24°, 1.17; 6°, 1.61; -12°, 2.47.

*Borazole* was prepared using a literature procedure<sup>33</sup> and was purified by three successive bulb-to-bulb distillations immediately before use. Samples for spectroscopic examination were prepared on a vacuum

line in flame-dried glassware using standard procedures.<sup>34</sup>

*Acknowledgment.* We are indebted to Mr. Calvin Powell and Dr. Jeanne K. Krieger for extensive assistance with the computer programs used in this work.

(32) L. G. Belinskaya, *Uch. Zap., Mosk. Oblast. Pedagog. Inst.*, **33**, 221 (1955); *Chem. Abstr.*, **52**, 821i (1958).

(33) H. Watanabe and M. Kubo, *J. Amer. Chem. Soc.*, **82**, 2428 (1960).

(34) Borazole is inert to oxygen, but sensitive to moisture: A. Stock and E. Pohland, *Chem. Ber.*, **59**, 2215 (1926).

## Steric Interactions in *tert*-Butylethylenes Observed

### through Proton <sup>13</sup>C Satellite Spectra

by P. P. Nicholas,\* C. J. Carman,

*B. F. Goodrich Research Center, Brecksville, Ohio 44141*

A. R. Tarpley, Jr., and J. H. Goldstein

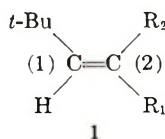
*Department of Chemistry, Emory University, Atlanta, Georgia 30322 (Received March 6, 1972)*

*Publication costs assisted by the B. F. Goodrich Research Center*

Steric interactions in a series of alkyl-substituted *tert*-butylethylenes have been studied through their proton <sup>13</sup>C satellite spectra. The parent compound, mono-*tert*-butylethylene, has an unusually low <sup>1</sup>J<sub>13C-H</sub> value for the ethylenic C-H bonded to *tert*-butyl (150.07 Hz). Further methyl or *tert*-butyl substitution, regardless of stereochemistry, causes little change in this value. Assuming that the inductive effect on <sup>1</sup>J<sub>13C-H</sub> for alkyl substituents is relatively small, the usual interpretation of <sup>1</sup>J<sub>13C-H</sub> leads to the conclusion that these low values reflect sterically induced changes in s character, but particularly interesting is the fact that most of this change occurs with the introduction of a single *tert*-butyl group on ethylene. *tert*-Butyl substituent effects have also been determined from the three ethylenic <sup>1</sup>J<sub>13C-H</sub> values in mono-*tert*-butylethylene. These accurately predict <sup>1</sup>J<sub>13C-H</sub> for *trans*-di-*tert*-butylethylene. The observed deviation from additivity of substituent effects for the *cis* isomer reflects the steric interaction of the *cis*-*tert*-butyl groups in this compound. <sup>13</sup>C chemical shifts and proton nmr parameters are also reported for this series.

### Introduction

There has been considerable interest in *cis*-di-*tert*-



a, R<sub>1</sub> = R<sub>2</sub> = H

b, R<sub>1</sub> = H; R<sub>2</sub> = *t*-Bu

c, R<sub>1</sub> = *t*-Bu; R<sub>2</sub> = H

d, R<sub>1</sub> = H; R<sub>2</sub> = CH<sub>3</sub>

e, R<sub>1</sub> = CH<sub>3</sub>; R<sub>2</sub> = H

f, R<sub>1</sub> = R<sub>2</sub> = CH<sub>3</sub>

butylethylene (**1b**) because of the apparently large steric effects of the *tert*-butyl substituents.<sup>1-5</sup> Examination of the Fisher-Hirschfelder model for this

compound indicates that an undistorted structure with normal bond angles and bond lengths would result in nearly rigid conformations of the *tert*-butyl groups. Strain in this molecule is reflected in the large differences in heats of combustion and hydrogenation be-

(1) W. Puterbaugh and M. S. Newman, *J. Amer. Chem. Soc.*, **81**, 1611 (1959).

(2) R. E. Turner, D. E. Nettleton, and M. Perelman, *ibid.*, **80**, 1430 (1958).

(3) F. H. A. Rummens, *Recl. Trav. Chem. Pays-Bas*, **84**, 5 (1965).

(4) R. C. Fahey, *J. Amer. Chem. Soc.*, **88**, 4681 (1966).

(5) R. W. Murray, R. D. Youssefyeh, and P. R. Story, *ibid.*, **89**, 2429 (1967).

tween it and its trans isomer **1c** (10.5 kcal/mol for combustion and 9.3 kcal/mol for hydrogenation).<sup>1,2</sup> Rummens<sup>3</sup> has reported on an infrared study of strain relief in alkyl-substituted ethylenes, including **1b**. His analysis was based upon frequency shifts for the =C-H stretch, the C=C stretch, and the in- and out-of-plane C=C-H deformations. He concluded that rehybridization of the sp<sup>2</sup> orbitals seemed to be most important for accommodating small distortions in bond angles, but that bond bending is likely the most important strain relief mechanism in molecules like **1b** which presumably require large bond angle distortions.

Strain caused by vicinal di-*tert*-butyl groups is also apparent in *o*-*tert*-butylbenzenes. For example, *o*-di-*tert*-butylbenzene itself is reported to have a strain energy of 22 kcal/mol.<sup>6</sup> This strain apparently causes significant geometric distortions. Although 1,2,4,5-tetra-*tert*-butylbenzene is coplanar, the interior bond angles between the *tert*-butyl substituents and the ring edge are increased from the usual 120 to 130° and the benzene ring bond angles are distorted.<sup>7</sup> In addition, the bonds connecting the *tert*-butyl groups are elongated somewhat compared to bonds in related but unstrained molecules.

There have been some reports on nmr studies of stereochemistry in *tert*-butyl-substituted molecules. Based upon proton nmr chemical shifts, it has been suggested that the *peri-tert*-butyl groups in *peri*-di-*tert*-butyl-naphthalene relieve strain by bending away from each other above and below the plane of the naphthalene ring.<sup>8</sup> Rummens<sup>9</sup> has recently reported on allylic proton coupling constants in disubstituted ethylenes where one substituent is *tert*-butyl. In this system, he finds that the relative magnitudes of the *cis* and *trans* allylic proton coupling constants are anomalous and attributes it to rehybridization of sp<sup>2</sup> bonds in the *cis* isomers caused by steric constraints. Cooper and Manatt<sup>10</sup> have published a detailed evaluation of the dependence of <sup>3</sup>J<sub>H-H</sub> on C=C-H bond angles in alkenes. Included in their report is the <sup>3</sup>J<sub>H-H</sub> value for **1b** (14.2 Hz), the largest value yet reported for a *cis*-dialkylethylene. They also proposed the interesting possibility of obtaining accurate estimates of bond angles from these coupling constants. Trends in <sup>3</sup>J<sub>H-H</sub> for *cis* hydrogen atoms with ring size in cycloolefins have also been reported.<sup>11-13</sup>

One would expect that ethylenic <sup>13</sup>C-H coupling constants would also be sensitive to strong steric interactions from double bond substituents. In fact, the low values of <sup>1</sup>J<sub>13C-H</sub> observed for the di-*tert*-butylethylenes<sup>10</sup> might suggest just that. For hydrocarbons, <sup>1</sup>J<sub>13C-H</sub> values generally provide an index of hybridization and stereochemistry of the C-H bond.<sup>14</sup> Unfortunately, very few <sup>1</sup>J<sub>13C-H</sub> values for *tert*-butylethylenes have been reported, but such data are essential if one is to understand the cause of the low <sup>1</sup>J<sub>13C-H</sub> values observed for the di-*tert*-butylethylenes.

Although these data are available from <sup>13</sup>C-H satellites of the proton spectra, no corrections have been made for isotope shifts and second-order effects for the few <sup>1</sup>J<sub>13C-H</sub> values reported.<sup>10</sup> An analysis of the <sup>13</sup>C-H satellite spectrum of mono-*tert*-butylethylene (**1a**) has never been reported. It is also reasonable to expect <sup>13</sup>C chemical shifts to be sensitive to strong steric effects, but no <sup>13</sup>C chemical shift data have been reported for the *tert*-butylethylenes.

This paper reports the results of a detailed study of <sup>1</sup>H, <sup>13</sup>C, and <sup>13</sup>C-H satellite spectra for a series of *tert*-butylethylenes and the stereochemical implications of these spectra.

### Experimental Section

All spectra were taken on a Bruker Scientific HFX-90 spectrometer operating at 90 MHz for protons and 22.63 MHz for carbon-13. All proton spectra were taken on the neat liquids with 1% TMS added for internal reference and for field-frequency lock. The carbon-13 spectra were taken on neat liquids in 10-mm sample tubes with a small capillary of hexafluorobenzene added for external <sup>19</sup>F lock. Most of the carbon-13 spectra were taken using broadband proton decoupling although some undecoupled spectra were taken in order to check <sup>13</sup>C chemical shift assignments and to determine if some long-range <sup>13</sup>C-H coupling information could be extracted from the spectra. When it was necessary to time average <sup>13</sup>C satellite or carbon-13 spectra, a Fabri-Tek 1074 signal averaging system was employed.

*trans*-Di-*tert*-butylethylene (**1c**) was a gift from Professor R. Murray, University of Missouri. This compound was further purified by preparative gas chromatography (gc) using a 20 ft × 0.25 in. 5% Bentone 34/5% DIDP on 60-80 M Chromosorb W column. *cis*-Di-*tert*-butylethylene was prepared by hydrogenation of di-*tert*-butylacetylene with 5% Pt on alumina using Newman's procedure.<sup>1</sup> This reduction was followed by gc and purified by preparative gc. The infrared spectra for both **1b** and **1c** were in accord with those previously reported.<sup>3</sup> Di-*tert*-butylacetylene was prepared according to the procedure described by Hennion and Banigan.<sup>15</sup> All other compounds in

(6) E. M. Arnett, J. C. Sanda, J. M. Bollinger, and M. Barber, *J. Amer. Chem. Soc.*, **89**, 5389 (1967).

(7) A. van Bruijnsvoort, C. Eilermann, H. van der Meer, and C. H. Stam, *Tetrahedron Lett.*, 2527 (1968).

(8) R. W. Franck and E. G. Leser, *J. Amer. Chem. Soc.*, **91**, 1577 (1969).

(9) F. H. A. Rummens and J. W. de Haan, *Org. Magn. Resonance*, **2**, 351 (1970).

(10) M. A. Cooper and S. L. Manatt, *ibid.*, **2**, 511 (1970).

(11) P. Laszlo and P. von R. Schleyer, *J. Amer. Chem. Soc.*, **85**, 2017 (1963).

(12) G. V. Smith and H. Kriloff, *ibid.*, **85**, 2016 (1963).

(13) O. L. Chapman, *ibid.*, **85**, 2014 (1963).

(14) J. N. Schoolery, *J. Chem. Phys.*, **31**, 1427 (1959).

(15) G. F. Hennion and T. F. Banigan, *J. Amer. Chem. Soc.*, **68**, 1202 (1946).

**Table I:** Proton Chemical Shifts<sup>a</sup> and <sup>13</sup>C Isotope Shifts<sup>b</sup> for *tert*-Butylethylenes

Compd	H (carbon 1)	<i>tert</i> -Butyl- methyl	H (R <sub>2</sub> )	H (R <sub>1</sub> )	Methyl (R <sub>2</sub> )	Methyl (R <sub>1</sub> )
<b>1a</b>	5.79 (+0.30) <sup>b</sup>	1.01	4.88 (+0.30) <sup>b</sup>	4.79 (+0.30) <sup>b</sup>		
<b>1b</b>	5.15 (+0.30)	1.15		5.15 (+0.30)		
<b>1c</b>	5.34 (+0.28)	0.99	5.34 (+0.28)			
<b>1d</b>	5.29 (+0.40)	1.12		5.23 (+0.34)	1.69	
<b>1e</b>	5.42 (+0.28)	0.97	5.30 (+0.39)			1.60
<b>1f</b>	5.16 (+0.21)	1.08			1.69	1.63

<sup>a</sup>The proton chemical shifts are given in parts per million downfield from internal TMS. <sup>b</sup>The isotope shifts observed are given in parentheses below the corresponding proton shifts and are reported in Hz at 90 MHz. For compound **1a** an isotope shift of 0.3 Hz was assumed in each instance.

this series were purchased from Aldrich Chemical Co. and were used without further purification.

### Spectral Analysis

The proton and <sup>13</sup>C-H satellite spectra for each compound in this series were analyzed to obtain values of the coupling constants and chemical shifts. LAOCN 4, a modification of the program LAOCN 3,<sup>16</sup> was used with a Digital Equipment Co. PDP-10 computer to obtain iterative fitted values. Resonance lines were calibrated in both the methyl and ethylenic regions in obtaining an iterative fit for compounds having methyl substituents. Multiple scans in both the forward and reverse frequency sweep directions were taken in order to minimize calibration errors. As has been pointed out before,<sup>2</sup> no measurable coupling was observed between the protons in the *tert*-butyl group and the ethylenic protons. Upfield and downfield <sup>13</sup>C satellite spectra were analyzed using LAOCN 4 to obtain the directly bonded <sup>13</sup>C-H coupling constants, isotope shifts, and H-H coupling constants. The satellite spectrum from the ethylenic hydrogen on the carbon bearing the *tert*-butyl group (carbon 1) overlaps with both the other ethylenic satellite spectra and the ABC vinyl spectrum. Only the downfield half of the geminal proton <sup>13</sup>C satellite spectrum could be analyzed, while only the upfield portions of the *cis* and *trans* proton <sup>13</sup>C satellite spectra could be analyzed. Assuming positive isotope shifts, as was the case for all other isotope shift determinations in this series (Table I), the <sup>1</sup>J<sub>13C-H</sub> (carbon 1) value obtained from the analysis of the downfield pattern for **1a** would understate the actual value by twice the magnitude of the isotope shift. Therefore, the <sup>1</sup>J<sub>13C-H</sub> values reported for **1a** were corrected for isotope effects by assuming approximately the same value found for the other members of this series (Table I). The chemical shifts and coupling constants obtained from our iterative analyses

accurately reproduced the <sup>1</sup>H and outer <sup>1</sup>H-<sup>13</sup>C satellite spectra observed for each compound. The rms errors between observed and calculated spectra for the ethylenic and methyl proton as well as the proton <sup>13</sup>C satellite spectra were less than 0.05 Hz in all cases.

We did not determine the absolute signs of the coupling constants in any instance. However, in agreement with Rummens,<sup>9</sup> we found that the spectra for *cis*- and *trans*-4,4-dimethyl-2-pentene (**1d** and **1e**) were sensitive to the relative signs of the vicinal and allylic H-H coupling constants. The signs shown in Table II for these two compounds are based on the assumption<sup>9</sup> of a positive value for the vicinal vinylic coupling. The proton <sup>13</sup>C satellite spectra were insensitive to differences in long-range <sup>1</sup>H-<sup>13</sup>C coupling constants. Although high-resolution <sup>13</sup>C spectra were obtained for this series of compounds, their complete analysis would be impractical at this time.

### Results

Shown in Table III are the carbon-13 chemical shifts for the substituted *tert*-butylethylenes **1a-f** expressed in parts per million upfield from external CS<sub>2</sub>. The absolute carbon-13 chemical shifts are estimated to be accurate to within 0.1 ppm. However, the relative shifts are more accurate. Table I gives the proton chemical shifts in parts per million relative to TMS. For compounds **1d** and **1e**, the assignments of the vinyl proton chemical shifts are reversed relative to the assignments given by Rummens.<sup>9</sup> Only the assignments shown in Table I lead to a fit of the observed spectra. Also listed in Table I are the <sup>13</sup>C isotope shifts which were determined for cases where it was possible to observe both the upfield and downfield <sup>13</sup>C satellite spectra. Table II gives the H-H coupling

(16) S. M. Castellano and A. A. Bothner-By, *J. Chem. Phys.*, **41**, 3863 (1964).

**Table II:**  $J_{H-H}$  and  ${}^1J_{{}^{13}C-H}$  Coupling Constants<sup>a</sup> for *tert*-Butylethylenes

Compd	$J_{H-H}$			${}^1J_{{}^{13}C-H}$		
	$J_{H,R_1}$	$J_{H,R_2}$	$J_{R_1,R_2}$	$J_{1,H}$	$J_{2,R_1}$	$J_{2,R_2}$
<b>1a</b>	10.69 (10.71) <sup>b</sup> (10.8) <sup>f</sup>	17.48 (17.46) <sup>b</sup> (17.5) <sup>f</sup>	1.42 (1.41) <sup>b</sup> (1.4) <sup>f</sup>	150.07 (150.3) <sup>c</sup>	157.21 (157.0) <sup>c</sup>	153.29 (152.6) <sup>c</sup>
<b>1b</b>	14.15 (14.2) <sup>b</sup>			148.33 (150.4) <sup>b</sup>	148.33 (150.4) <sup>b</sup>	
<b>1c</b>		15.92 (16.10) <sup>b</sup>		147.56 (149.4) <sup>d</sup>		147.56 (149.4) <sup>d</sup>
<b>1d</b>	11.93 (12.02) <sup>e</sup>	-1.91 (-1.82) <sup>e</sup>	7.32 (+7.41) <sup>e</sup>	149.95	152.24	
<b>1e</b>	-1.63 (-1.66) <sup>e</sup>	15.47 (15.50) <sup>e</sup>	6.37 (6.42) <sup>e</sup>	147.38		149.38
<b>1f</b>	1.4	1.4	0.3	148.01		

<sup>a</sup> All coupling constants are given in Hz. <sup>b</sup> Reference 10. <sup>c</sup> G. C. Graham, Ph.D. Dissertation, University of California, San Diego, Calif., 1967. <sup>d</sup> S. L. Manatt, private communication. <sup>e</sup> Reference 9. <sup>f</sup> S. Alexander, *J. Chem. Phys.*, **28**, 358 (1958).

**Table III:** Carbon-13 Chemical Shifts for *tert*-Butylethylenes<sup>a</sup>

Compd	Carbons					
	1	2	<i>tert</i> -Butyl- methine	<i>tert</i> -Butyl- methyl	Methyl (R <sub>2</sub> )	Methyl (R <sub>1</sub> )
<b>1a</b>	44.18	84.58	160.05	164.40		
<b>1b</b>	54.07	54.07	160.71	160.78		
<b>1c</b>	57.20	57.20	161.10	163.23		
<b>1d</b>	52.78	71.35	160.45	162.58	179.62	
<b>1e</b>	50.77	74.51	160.81	163.68		175.83
<b>1f</b>	58.22	63.91	161.42	162.31	174.89	165.64

<sup>a</sup> The chemical shift value given for each carbon is in parts per million upfield from external CS<sub>2</sub>.

constants and the directly bonded <sup>13</sup>C-H coupling constants along with literature comparisons where available. The H-H coupling constants are conservatively estimated to be accurate to within 0.1 Hz while the <sup>1</sup>J<sub><sup>13</sup>C-H</sub> values should be accurate to ±0.25 Hz.

## Discussion

The carbon-13 chemical shifts given in Table III for this series of *tert*-butylethylenes show that the largest variations occur among the ethylenic carbon atoms. However, the <sup>13</sup>C chemical shifts for these carbon atoms do not appear to establish any particular trend. The *tert*-butylmethine carbon shifts are almost constant throughout this series, indicating that this carbon atom is highly insulated from effects produced by the structural changes in this series. However, there is a definite trend in the *tert*-butylmethyl carbon chemical shifts. These decrease to lower field as the size of the *cis*-(R<sub>2</sub>) or *trans*-(R<sub>1</sub>) substituent increases. The largest effect results from the *cis* substituents where the *tert*-butylmethyl chemical shifts relative to CS<sub>2</sub> are in the order *cis*-*t*-Bu < *cis*-Me < *cis*-H. The trend is the same for the *trans* substituents. The overall order for all compounds in this series is **1b** < **1f** ≈ **1d** < **1c** < **1e** < **1a**. Coincidentally, the *tert*-butylmethyl

and methine carbon atoms for *cis*-*di-tert*-butylethylene (**1b**) have almost identical chemical shifts.

The coupling constants for this series of *tert*-butylethylenes show the most striking departures from normal values. Cooper and Manatt have previously called attention to the unusually large value for <sup>3</sup>J<sub>H-H</sub> (~14.2 Hz) in **1b**.<sup>10</sup> This appears to be the largest reported value for <sup>3</sup>J<sub>H-H</sub> in any alkylethylene. It has been interpreted as resulting from reduction of the C=C-H bond angle caused by steric repulsion of the *cis-tert*-butyl substituents.

Although only <sup>3</sup>J<sub>H-H</sub> for **1b** appears to be unusual among the H-H couplings (Table II), virtually every <sup>1</sup>J<sub><sup>13</sup>C-H</sub> value in Table II falls well below that expected for ethylenic hydrocarbons. Of the 12 <sup>1</sup>J<sub><sup>13</sup>C-H</sub> values listed, all are unusually low except that for J<sub>2,R<sub>1</sub></sub>, the unsubstituted carbon in mono-*tert*-butylethylene (**1a**).

The expression <sup>1</sup>J<sub><sup>13</sup>C-H</sub> = 500α<sup>2</sup>, where α<sup>2</sup> is the fractional s character in the bonding orbital, represents a simple interpretation of directly bonded <sup>13</sup>C-H coupling constants.<sup>14,17-19</sup> This relationship is reasonably

(17) N. Muller and D. E. Pritchard, *J. Chem. Phys.*, **31**, 768 (1959).

(18) N. Muller and D. E. Pritchard, *ibid.*, **31**, 1471 (1959).

(19) R. M. Lynden-Bell and N. Sheppard, *Proc. Roy. Soc., Ser. A*, **269**, 386 (1962).

valid in cases where inductive effects are minimal as is the case with hydrocarbons. There are examples in the literature to justify the assumption that alkyl substituents have only a minor inductive effect on  $^1J_{13C-H}$ . For example, the  $^1J_{13C-H}$  values for unhindered cycloalkenes are nearly identical with that for ethylene, even though they are di-*sec*-alkylethylenes.<sup>20-22</sup> Similarly, alkyl and even halomethyl substituents on methane cause little change in the original  $^1J_{13C-H}$  value for the  $sp^3$  bonds in methane.<sup>23</sup> The  $^1J_{13C-H}$  values in Table II are sufficiently lower than 156.4 Hz value for ethylene<sup>19</sup> as to indicate that appreciable perturbation of the ethylenic system has taken place. Assuming that the inductive effect on  $^1J_{13C-H}$  for alkyl substituents is relatively small, we can conclude that these low values reflect sterically induced changes in character.

The low values for  $^1J_{13C-H}$  in *cis*- and *trans*-di-*tert*-butylethylene have been noted,<sup>10</sup> but no explanation has yet been offered for the fact that their  $^1J_{13C-H}$  values are nearly equal. When considered alone, these data appear anomalous. One would normally expect the steric interaction of the two *tert*-butyl groups in **1b** to cause appreciable differences in  $^1J_{13C-H}$  for these two isomers, but as the present study reveals, most of the decrease in ethylenic  $^1J_{13C-H}$  results from the introduction of the first *tert*-butyl substituent. Subsequent methyl or *tert*-butyl substitution, regardless of stereochemistry, has little further effect on  $^1J_{13C-H}$  for the ethylenic C-H bonded to *tert*-butyl. So it must be concluded that a sizable steric interaction occurs between the *tert*-butyl and vinyl groups. Nevertheless, there are indications of measurable, though smaller, steric effects on  $^1J_{13C-H}$  caused by the interaction of the *cis*-*tert*-butyl groups in **1b**. Evidence for this is the fact that **1b** shows a deviation from additivity of *tert*-butyl substituent effects on  $^1J_{13C-H}$ .

From the three  $^1J_{13C-H}$  values for mono-*tert*-butylethylene (Table II), the following *tert*-butyl substituent effects on  $^1J_{13C-H}$  in ethylene can be easily determined: *gem*-*tert*-butyl = -6.33 Hz, *trans*-*tert*-butyl = +0.81 Hz, and *cis*-*tert*-butyl = -3.11 Hz. Whether or not these effects are additive in multiple substituted *tert*-butylethylenes will depend on the extent of interaction between the substituent groups. If we tentatively assume additivity of the above substituent effects, we predict  $^1J_{13C-H}$  values of 146.96 and 150.88 Hz for *trans*- and *cis*-di-*tert*-butylethylene, respectively. The predicted value for the *trans* isomer is very close to the observed value of 147.56 Hz, but the observed value for the *cis* isomer (148.33 Hz) is more than 2.5 Hz lower than predicted. This difference likely reflects the extra steric effect resulting from the interaction of the *cis*-*tert*-butyl groups. Additivity treatments for the methyl-substituted compounds **1d**, **e**, and **f** are not possible at this time since the substituent effects on  $^1J_{13C-H}$  in propylene are not known.

*Acknowledgment.* Our thanks to D. T. Miller, Emory University, for preparing the di-*tert*-butylacetylene used in this study. We are also grateful to Professor Robert Murray, University of Missouri, for his gift of *trans*-di-*tert*-butylethylene and Professor Robert Fahey, University of California, for his gift of di-*tert*-butylacetylene. Our thanks also to the B. F. Goodrich Co. for permission to publish this work and to the National Institutes of Health for partial support of that work carried out at Emory University.

(20) M. Karplus, *J. Amer. Chem. Soc.*, **85**, 2870 (1963).

(21) T. Schaefer and H. M. Hutton, *Can. J. Chem.*, **45**, 3153 (1967).

(22) S. M. Costellano and C. Sun, *J. Amer. Chem. Soc.*, **88**, 4741 (1966).

(23) J. W. Emsley, J. Feeney, and L. H. Sutcliffe, "High-Resolution Nuclear Magnetic Resonance Spectroscopy," Vol. 2, Pergamon Press, New York, N. Y., 1966, p 1016.

## Structure and Orientation of Phenols Chemisorbed on $\gamma$ -Alumina

by D. R. Taylor\* and K. H. Ludlum

Texaco Research Center, Beacon, New York 12508 (Received March 27, 1972)

Publication costs assisted by Texaco, Inc.

It has been found that phenol forms a strongly chemisorbed surface species on  $\gamma$ -alumina at 300° and that it resists evacuation up to 450°. The infrared spectrum of this surface species (in the region 4000–1200  $\text{cm}^{-1}$ ) differs markedly from that of liquid or physisorbed phenol and is characterized by loss of OH stretching and in-plane bending modes (3350 and 1360  $\text{cm}^{-1}$ , respectively), a ring stretching mode (1473  $\text{cm}^{-1}$ ), and a shift of the C–O stretching mode from 1259 to 1286  $\text{cm}^{-1}$ . Based on these data, a chemisorbed aluminum phenoxide surface species ( $>\text{Al}-\text{O}-\text{C}_6\text{H}_5$ ) is proposed and mechanisms for its formation are discussed. Related infrared studies for a series of methylated phenols suggest that the phenol molecule is oriented with the aromatic ring almost coplanar with the surface but tilted upward such that the para position is farther from the surface than the ortho position. This conclusion is based partly on the fact that a methyl group in the ortho position experiences a stronger interaction with the surface than a methyl group in the meta or para position.

### Introduction

Alumina reacts with a large number of chemical compounds to give chemisorbed species which can be studied by infrared techniques to yield information about the adsorbed species as well as the adsorption sites<sup>1,2</sup> themselves.

Phenol reacts with alcohols over dehydrated  $\gamma$ -alumina catalysts to yield ring-alkylated products;<sup>3</sup> recently, cyclohexadienone intermediates have been proposed<sup>4</sup> as key intermediates in this reaction. Since the alkylation of phenol is of interest, an attempt was made to detect this intermediate by infrared techniques. No evidence for a cyclohexadienone intermediate was found, but it was determined that phenol is strongly chemisorbed on  $\gamma$ -alumina and resists evacuation at 450°.

Although other chemisorbed hydroxy-containing compounds (mainly alcohols) have been studied by infrared techniques,<sup>5–8</sup> and phenol has been reported to be physisorbed on various catalysts,<sup>9–11</sup> no definitive infrared studies on chemisorbed phenol have been published. A study of the structure of chemisorbed phenol was therefore undertaken.

### Experimental Section

**Materials and Apparatus.** The  $\gamma$ -alumina used in these experiments has a surface area of 102  $\text{m}^2/\text{g}$  (determined by BET method using  $\text{N}_2$  adsorption). Examination by X-ray diffraction spectroscopy revealed the presence of some  $\chi$ -alumina.

About 100 mg of the catalyst was ground to a fine powder and pressed into a disk to be placed in the infrared cell of the spectrometer. The samples for chemisorbed phenol were heated under vacuum at 450° overnight prior to being exposed to phenol. Samples exposed to methylated phenols were heated at 550° under vacuum overnight, then cooled to 350° prior to exposure.

For deuterium studies the catalyst was outgassed under vacuum at 450° overnight, exposed to  $\text{D}_2\text{O}$  vapor at room temperature for 15 min, and evacuated (repeated three times), and the catalyst was heated to 450° for 2 hr and cooled to room temperature under vacuum. Repetition of this entire procedure and infrared examination of the catalyst showed that OH bands were barely observable and that the OD bands were quite large.

The  $\text{D}_2\text{O}$  used was from NMR Specialties Inc. reported to be 99.8%  $\text{D}_2\text{O}$  by the supplier. Before use it was put through several freeze–thaw cycles. Oxygen gas (99.0% minimum purity) was obtained from the Linde Co.

The phenol ((99+ % pure) used in these studies was obtained from James Hinton, 268 Ewing Court N.W., Fort Walton Beach, Fla. Before use it was put through several freeze–thaw cycles.

*o*-Cresol (puriss), *p*-cresol (puriss), 2,6-dimethylphenol (puriss), and 3,4-, 2,3-, and 3,5-dimethylphenol were obtained from Aldrich Chemical Co. and are claimed to be 97–100% pure (puriss grade is 99+ %

- (1) J. B. Peri and R. B. Hannan, *J. Phys. Chem.*, **64**, 1526 (1960).
- (2) J. B. Peri, *ibid.*, **69**, 231 (1965).
- (3) E. Briner, W. Plüss, and H. Paillard, *Helv. Chim. Acta*, **7**, 1046 (1924).
- (4) L. H. Klemm and D. R. Taylor, *J. Org. Chem.*, **35**, 3216 (1970), and references cited therein.
- (5) R. Greenler, *J. Chem. Phys.*, **37**, 2094 (1962).
- (6) D. Treibmann and A. Simon, *Naturwissenschaften*, **53**, 107 (1966).
- (7) R. Kagel, *J. Phys. Chem.*, **71**, 844 (1967).
- (8) R. Kagel, *J. Catal.*, **16**, 316 (1970).
- (9) V. N. Abramov, A. V. Kiselev, and V. I. Lygin, *Zh. Fiz. Khim.*, **38**, 1045 (1964).
- (10) G. A. Galkin, A. V. Kiselev, and V. I. Lygin, *Trans. Faraday Soc.*, **60**, 431 (1964).
- (11) (a) G. Karagounis and O. Peter, *Z. Elektrochem.*, **61**, 827 (1957); (b) *ibid.*, **63**, 1120 (1959).

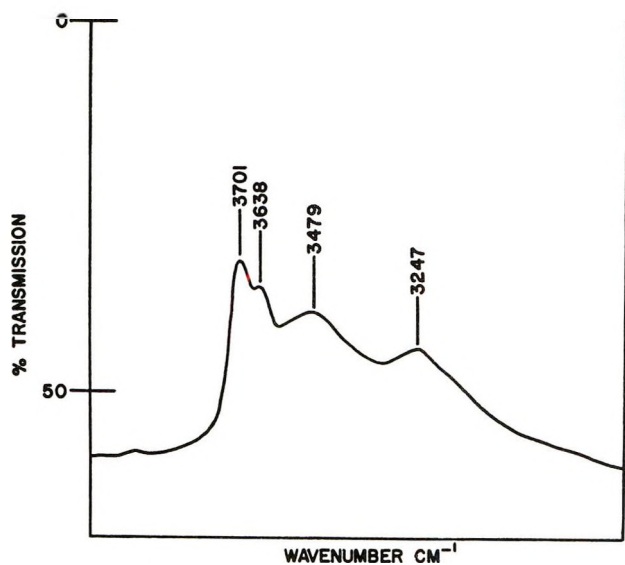


Figure 1. Spectrum of  $\gamma$ -alumina taken after heating *in vacuo* at 450° overnight (LiF prism).

pure). *m*-Cresol (99+ % pure) was obtained from K & K Rare Fine Chemicals. All chemicals were used without further purification.

The apparatus used in these experiments was a modified Perkin-Elmer Model 12B infrared spectrometer and has been described previously.<sup>12</sup> Associated with this instrument was a conventional Pyrex high-vacuum system for handling gases and volatile liquids. Both LiF and CaF<sub>2</sub> prisms were used in these studies for examination of various regions of the infrared spectrum.

## Results and Discussion

1. *Phenol Chemisorption.* After heating the catalyst to 450° under vacuum and cooling to room temperature, the  $\gamma$ -alumina showed infrared bands at 3701, 3638, 3479, and 3247 cm<sup>-1</sup> in the background spectrum which were attributed to OH stretching frequencies (see Figure 1). The catalyst was then exposed to phenol vapor (0.4 Torr) at 300° for 4 hr and evacuated at 150° for 1 hr, and spectra were obtained (see Figures 2 and 3). The phenyl C-H stretching vibrations<sup>13</sup> show up as bands at 3050 and 3020 cm<sup>-1</sup> in Figure 2. By comparing curve A with curves B and C in Figure 3, it is apparent that the phenol O-H stretching and in-plane bending vibrations (3350 and 1360 cm<sup>-1</sup>, respectively) as well as a phenyl ring vibration (1474 cm<sup>-1</sup>) disappear upon chemisorption.

Since the 1474-cm<sup>-1</sup> ring stretching vibration is thought to be coupled<sup>14</sup> with the 1360-cm<sup>-1</sup> O-H in-plane bending vibration, its disappearance is expected if the O-H in-plane bending vibration is also destroyed by chemisorption. The band at 1286 cm<sup>-1</sup> for chemisorbed phenol is believed to be due to a C-O stretching vibration and hence is shifted to a higher wave number than is normal for this vibration (Evans<sup>13</sup> reports a value of 1260 cm<sup>-1</sup> for this band). Although this shift indicates some strengthening of the C-O bond,

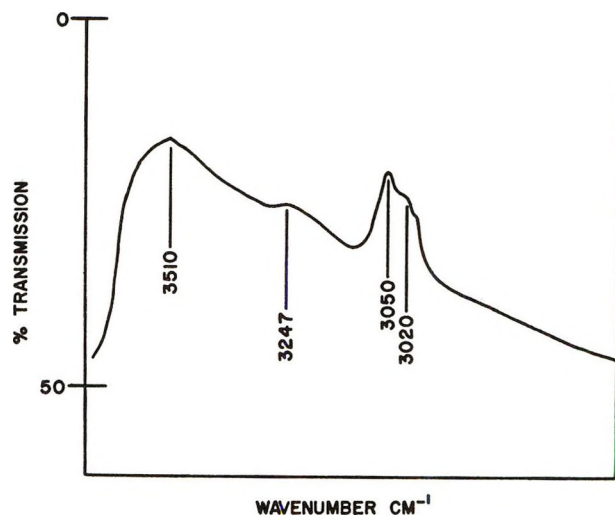


Figure 2. Spectrum of phenol chemisorbed on  $\gamma$ -alumina (at room temperature, LiF prism).

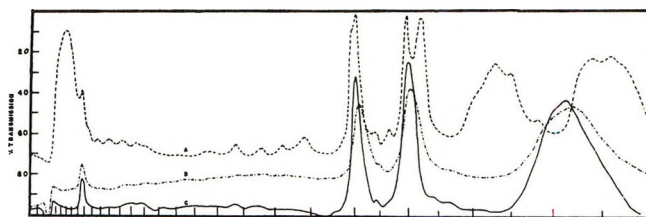


Figure 3. Comparison of spectrum of liquid phenol on alumina: (A) liquid phenol; (B) phenol on alumina at 450°; and (C) at 150° (CaF<sub>2</sub> prism).

and possibly even some partial double bond character (C=O), it does not even remotely approach a value of 1650 cm<sup>-1</sup> expected<sup>15</sup> of conjugated C=O vibration for a cyclohexadienone. The remaining very strong phenol bands at 1602 and 1490 cm<sup>-1</sup> are due to phenyl ring vibrations.<sup>13</sup> The two highest frequency OH bands of the  $\gamma$ -alumina are gone and, as shown in Figure 2, a broad band now extends from 3510 cm<sup>-1</sup> to lower frequencies. The 3247-cm<sup>-1</sup> band is still discernible, but the 3479-cm<sup>-1</sup> band, if present, is covered by the 3510-cm<sup>-1</sup> band. This broad OH band may indicate hydrogen bonding between chemisorbed phenol and surface hydroxide groups or between the surface hydroxide groups themselves.

A representation that is consistent with these observations is one in which the phenol molecule loses a proton to the surface and the resulting phenoxide ion is chemisorbed on an exposed surface aluminum ion (see below). The extent and character of bond for-

(12) R. P. Eischens and W. A. Pliskin, *Advan. Catal.*, **10**, 1 (1958).

(13) J. C. Evans, *Spectrochim. Acta*, **16**, 1382 (1960).

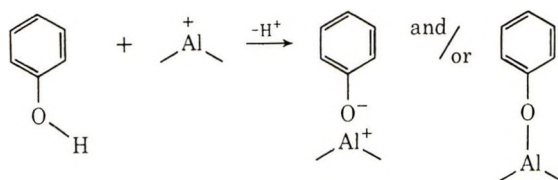
(14) R. Mecke and G. Rossmly, *Z. Elektrochim.*, **59**, 866 (1965).

(15) H. Hart, P. M. Collins, and A. J. Waring, *J. Amer. Chem. Soc.*, **88**, 1005 (1966).

**Table I:** Effect of Chemisorption on the Relative Intensity of CH<sub>3</sub> Symmetrical Bending Modes of Methylated Phenols

	<i>o</i> -Cresol	<i>m</i> -Cresol	<i>p</i> -Cresol	2,3-DMP	3,4-DMP	3,5-DMP	2,6-DMP
Position of CH <sub>3</sub> symmetrical bending mode (CCl <sub>4</sub> )	1383	1380	1384	1388	1377 1388	1380	1383
Position of CH <sub>3</sub> symmetrical bending mode (Al <sub>2</sub> O <sub>3</sub> )	1379	1384	1385	1361? 1382	1411?	1384	1383
Rel intensity (CCl <sub>4</sub> ) <sup>a,b</sup>	0.54	0.42	0.52	0.53	0.58 0.79	0.50	0.72
Rel intensity (Al <sub>2</sub> O <sub>3</sub> ) <sup>a</sup>	0.20	0.31	0.50	0.50 0.50	1.20	0.37	0.43
% decrease of rel intensity <sup>c</sup>	63	26	0.4	<i>d</i>	<i>d</i>	26	40

<sup>a</sup> Relative intensity = absorbance CH<sub>3</sub> symmetrical bending mode/absorbance aromatic C-H stretching mode. <sup>b</sup> Solution spectra were obtained on a Beckman IR-12 using 6 wt % phenol in CCl<sub>4</sub>. <sup>c</sup> Per cent decrease of relative intensity = [relative intensity (CCl<sub>4</sub>) - relative intensity (Al<sub>2</sub>O<sub>3</sub>)/relative intensity (CCl<sub>4</sub>)] × 100. <sup>d</sup> The presence of ortho methyl groups apparently leads to a doubling (or coalescence) of bands due to changes of state in a manner similar to that observed by Richards and Thompson, *Proc. Roy. Soc., Ser. A*, **195**, 1 (1948), for CH<sub>2</sub> deformation frequencies of hydrocarbons. Since there might be unknown intensity components associated with the phenomenon, no attempt was made to calculate a per cent decrease in relative intensity for 2,3- and 3,4-dimethylphenol.



mation between the phenoxide oxygen and the aluminum surface ion cannot be determined from our data. A known ionic compound such as aluminum phenoxide, Al(OC<sub>6</sub>H<sub>5</sub>)<sub>3</sub>, would provide an excellent model for spectral comparisons but attempts to purchase or prepare pure samples of aluminum phenoxide were unsuccessful, and unfortunately, no infrared spectral data on aluminum phenoxide have been published. However, the infrared spectrum of a related compound,<sup>16</sup> thallos phenoxide, is practically identical with spectra reported here (especially with regard to loss of OH stretching and in-plane bending vibrations and the 1473-cm<sup>-1</sup> ring stretching mode) and suggests considerable ionic character for the surface species.

2. *Methylated Phenol Chemisorption.* Examination of curve A, Figure 3, reveals a number of low-intensity, out-of-plane combination bands<sup>13</sup> at 1705, 1772, 1843, 1930, and 2050 cm<sup>-1</sup>. Comparison of curve A with curves B and C shows that these bands have practically disappeared for the chemisorbed phenol molecule even though the intensities of the remaining bands are comparable. Karagounis and coworkers<sup>11a,17</sup> have interpreted a decrease in the intensity of out-of-plane C-H vibrations of chemisorbed aromatic molecules to mean that these molecules are adsorbed with the plane of the aromatic ring parallel to the adsorbent surface. Applying a similar interpretation to the above observations leads to the conclusion that the chemisorbed phenol molecule also has its benzene ring more or less coplanar with the surface such that interaction with the surface results in a lack of bands in the region 1700–2050 cm<sup>-1</sup>. It was felt that an independent check for

this hypothesis could be obtained by studying the changes of intensity for the methyl symmetrical bending vibrations (1375–1390 cm<sup>-1</sup>) for a series of methylated phenols.

For these studies, the catalyst was heated to 550° under vacuum and then lowered to 350° at which time the catalyst was exposed to vapors of the methyl phenol. Exposure was continued overnight at 350°, the system was evacuated, and a spectrum obtained (at 350°) as in Figure 3 over the region 1200–4000 cm<sup>-1</sup>.

For methylated phenols, methyl groups exhibit a characteristic symmetrical bending mode in a narrow frequency range between 1375 and 1390 cm<sup>-1</sup>. By comparing the absorbance of the C-H aromatic stretching mode with the absorbance of the symmetrical CH<sub>3</sub> bending mode, a relative intensity value (relative intensity = the absorbance of CH<sub>3</sub> symmetrical bending mode divided by the absorbance of aromatic C-H stretching mode) can be obtained. This was done for a series of monomethylphenols and dimethylphenols, both in solution (CCl<sub>4</sub>) and chemisorbed on  $\gamma$ -alumina; the results are presented in Table I.

Using the absorbance of the aromatic C-H stretching mode as an internal standard of comparison has precedent in the work of Kiselev, *et al.*,<sup>10</sup> who employed a similar method in studying the effect of surface OH groups on C-H out-of-plane bending vibrations. One assumption is that if the extinction coefficient of the aromatic C-H stretching mode is altered by chemisorption,<sup>17</sup> then the extent or degree of that alteration must be approximately the same for each of the phenols in Table I. The assumption seems intuitively correct because the compounds are practically identical and it would be expected that the mode of their attachment to the surface (and hence effects on the extinction co-

(16) C. J. Pouchert, "The Aldrich Library of Infrared Spectra," Spectrum No. 15,389-3, Aldrich Chemical Co., Milwaukee, Wis.

(17) G. Karagounis and O. Peter, *Z. Elektrochem.*, **61**, 1094 (1957).

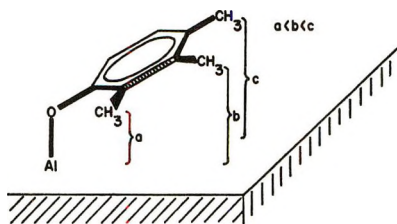


Figure 4.

efficient for the aromatic C-H stretching bands) would also be similar.

Examination of the relative intensity values for the  $\text{CH}_3$  symmetrical bending modes in Table I reveals (in all cases) a decrease in passing from solution to the chemisorbed state and is expected if the methyl groups interact in some manner with the surface.<sup>18</sup> Even more important, however, is the observation that a correlation exists between the value for the percentage decrease in intensity and the position of the methyl group with respect to the oxygen; *i.e.*, compare the series *o*-, *m*-, *p*-cresol and compare 2,6- with 3,5-dimethylphenol.

Attempts to quantitatively interpret the data in Table I were considered premature because relative intensity values for the chemisorbed state, obtained from the symmetrical  $\text{CH}_3$  bending bands with a prism instrument, suffer somewhat from poor resolution (and concomitant loss of accuracy). However, the qualitative picture that emerges and is most consistent with a trend of smaller values for the percentage decrease in intensity with increasing distance between methyl groups and oxygen is one in which the benzene ring is more or less coplanar but tilted upward such that a methyl group in the para position is more removed from the surface than one in the ortho or meta position (see Figure 4). In this configuration, a decreasing interaction of the methyl groups with the surface in going from ortho to meta to para is expected and supported by observation. A strictly parallel and coplanar orientation between the benzene ring and the surface ( $\text{Al-O-C}$  bond angle of  $90^\circ$ ) should result in essentially no difference in the effect of the surface on the  $\text{CH}_3$  symmetrical bending intensities as a function of position, but on the basis of data presented here, this possibility seems unlikely. Although the  $\text{Al-O-C}$  bond angle for compounds like aluminum phenoxide has not been reported, it seems likely that it would fall close to the range  $118$ – $121^\circ$  ( $\angle\text{COH}$  for phenol and  $\angle\text{COC}$  for anisole, respectively).

As with phenol itself, the C-O stretching bands for chemisorbed methyl phenols are found in a relatively narrow region between  $1263$  and  $1294\text{ cm}^{-1}$  which represents a shift ( $\Delta\nu$   $25$ – $40\text{ cm}^{-1}$ ) to higher frequencies upon chemisorption; O-H stretching and in-plane bending modes are, of course, absent. Although a previous study<sup>19</sup> of isomeric cresols assigns bands in the

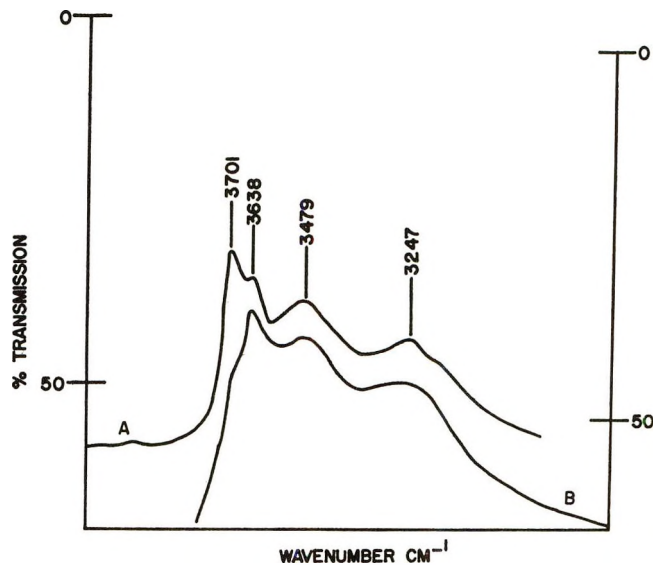


Figure 5. Spectrum of  $\gamma$ -alumina taken after phenol burnoff: (A) Figure 1 replotted; (B) after phenol burnoff.

$1260$ – $1290\text{-cm}^{-1}$  region to  $\text{Al-CH}_3$  symmetrical deformation vibrations, phenol (no methyl groups possible) exhibits a band at  $1286\text{ cm}^{-1}$  which supports the idea that bands in this region should be assigned to chemisorbed C-O stretching vibrations.

**3. Mechanism of Phenol Chemisorption.** As mentioned previously, the two highest frequency hydroxide bands for alumina,  $3701$  and  $3638\text{ cm}^{-1}$ , disappear when phenol is chemisorbed on the surface while the two low-frequency bands at  $3479$  and  $3247\text{ cm}^{-1}$  are relatively unaffected (see Figures 1 and 2). This observation was confirmed using a deuterated surface; of the four OD bands ( $2750$ ,  $2701$ ,  $2596$ , and  $2440\text{ cm}^{-1}$ ) only the first two disappear when phenol is chemisorbed.

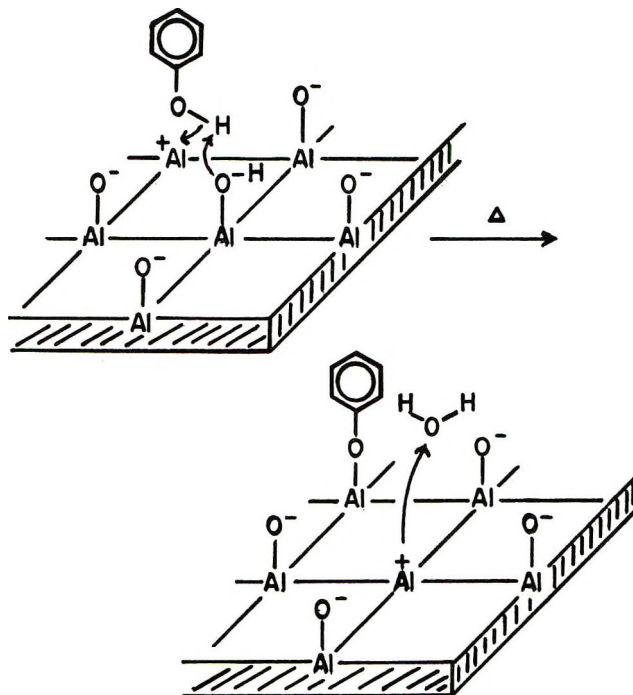
If the chemisorbed phenol is burned off (flowing  $\text{O}_2$  for 3 hr at  $450^\circ$ ) and a new background spectrum obtained (Figure 5), we see that the  $3701\text{-cm}^{-1}$  band is still gone, or at best has shifted to a very weak shoulder on the  $3638\text{-cm}^{-1}$  band which is itself restored. The  $3479$ - and  $3247\text{-cm}^{-1}$  infrared bands remain unchanged. Exposure of this sample to phenol a second time gives a spectrum identical with Figure 2 (even though the  $3701\text{-cm}^{-1}$  band was not originally present in this case). Finally, burnoff (as before) gives a spectrum identical with that obtained in Figure 5, *i.e.*,  $3701\text{-cm}^{-1}$  band gone,  $3638\text{-cm}^{-1}$  band restored,  $3479$ - and  $3247\text{-cm}^{-1}$  bands unaffected. Only by heating the catalyst (after phenol burnoff) to  $450^\circ$  in the presence of water vapor could the  $3701\text{-cm}^{-1}$  band be restored; exposure to water vapor at room temperature was not sufficient to restore it.

(18) L. H. Little, "Infrared Spectra of Adsorbed Species," Academic Press, New York, N. Y., 1966, pp 382–405.

(19) L. A. Ignat'eva, A. Sideridu, and T. Slovokhotova, *Kinet. Katal.*, **5**, 1069 (1964).

All of these observations can be interpreted in terms of Peri's description<sup>20</sup> of the surface of  $\gamma$ -alumina catalysts. In his paper, it is suggested that different kinds of isolated hydroxyl groups exist on the surface depending on the arrangement of next nearest neighbors (*i.e.*, adjacent hydroxyls, oxide ions, or exposed aluminum ions). It is also proposed that the highest frequency OH band has four oxide nearest neighbors, and furthermore, *that this is the most basic hydroxyl group on the surface* (conversely, the lowest frequency OH band is associated with the most *acidic* surface hydroxyl). The following mechanism (Scheme I) is suggested to

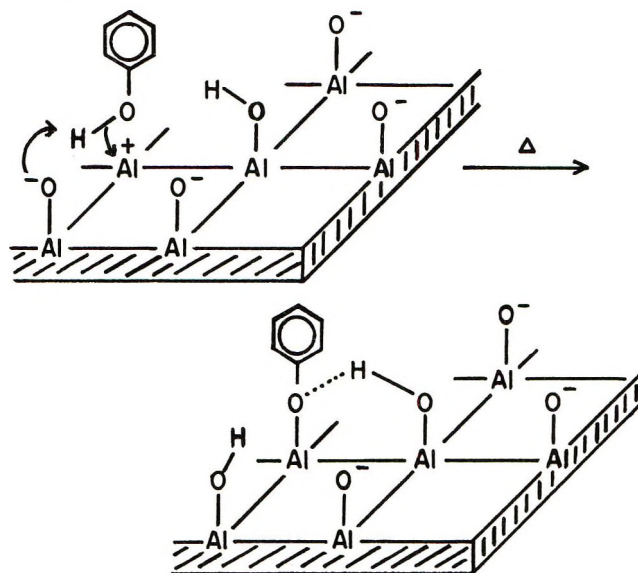
**Scheme I:** Loss of 3701-cm<sup>-1</sup> Band via Dehydration



account for the disappearance of the 3701-cm<sup>-1</sup> band and the fact that it can not be restored by phenol burnoff. Here, the phenol molecule loses a proton to the high-frequency (most basic) hydroxyl and is chemisorbed on a nearby exposed aluminum ion. The water molecule that results by combination of the phenol proton and the surface hydroxyl is then desorbed and the corresponding high-frequency OH band is lost. Thus, the 3701-cm<sup>-1</sup> OH group is removed not by burnoff, but by a classical acid-base-type reaction.

The mechanism in Scheme II can account for the disappearance of the 3638-cm<sup>-1</sup> OH band upon phenol chemisorption and its subsequent restoration with phenol burnoff. According to Peri's interpretation, the next most basic surface hydroxyl would have three oxide nearest neighbors and one adjacent exposed aluminum ion. The difference here is that this surface

**Scheme II:** Loss of 3638-cm<sup>-1</sup> Band via Hydrogen Bonding



hydroxyl does not have the necessary basicity to abstract a phenol proton, and a nearby oxide ion performs this operation. However, once the phenoxide ion has settled over the exposed aluminum ion, hydrogen bonding (between the phenoxide oxygen and/or the phenyl ring  $\pi$  cloud) and the surface hydroxyl will shift the frequency of this band to a lower value and it will, in effect, disappear. The mechanism proposed here is similar to that proposed by Kagel<sup>7</sup> for the adsorption of ROH compounds on  $\gamma$ -Al<sub>2</sub>O<sub>3</sub> and supports the present contention. In contrast to the previous case (where the OH band can not be restored by phenol burnoff because that hydroxyl group has actually been removed from the surface as water), phenol burnoff here will destroy the hydrogen bonding and the 3638-cm<sup>-1</sup> OH band should reappear, in agreement with observation.

The reason for two of the four OH groups not becoming involved in the reaction with phenol remains obscure.

### Summary

Phenols are strongly chemisorbed on  $\gamma$ -alumina to form phenoxide surface species whose orientation with respect to the surface is more or less coplanar but tilted upward such that the para position is more removed from the surface than the ortho. The two highest frequency OH groups interact with the chemisorbed phenol; the highest frequency OH group is removed from the surface as water, the next highest frequency OH group forms a hydrogen bond with an adjacent chemisorbed phenoxide.

(20) J. B. Peri, *J. Phys. Chem.*, **69**, 220 (1965).

## Preparation and Structure of

## Bromobis(2-(2-aminoethyl)pyridine)copper(II) Bromide

by Phirtu Singh, Vicki C. Copeland, William E. Hatfield, and Derek J. Hodgson\*

Department of Chemistry, University of North Carolina, Chapel Hill, North Carolina 27514 (Received March 13, 1972)

Publication costs assisted by the Materials Research Center of the University of North Carolina

Bromobis(2-(2-aminoethyl)pyridine)copper(II) bromide,  $[\text{Cu}(\text{C}_7\text{N}_2\text{H}_{10})_2\text{Br}]\text{Br}$ , has been prepared by the reaction of copper(II) bromide with excess 2-(2-aminoethyl)pyridine (AEP) in 95% ethanol, and its crystal and molecular structure has been determined from three-dimensional X-ray data collected by counter methods. The material crystallizes in the monoclinic space group  $C2/c$  with four formula units in a cell of dimensions  $a = 8.883(6) \text{ \AA}$ ,  $b = 11.853(13) \text{ \AA}$ ,  $c = 16.940(14) \text{ \AA}$  and  $\beta = 67.57(3)^\circ$ . The observed and calculated densities are  $1.87(2)$  and  $1.885 \text{ g cm}^{-3}$ , respectively. The structure has been refined by least-squares methods to a final value of the  $R$  factor (on  $F$ ) of 0.044 for 1620 independent data. The complex consists of five-coordinate  $[\text{Cu}(\text{AEP})_2\text{Br}]^+$  cations which are well separated from discrete  $\text{Br}^-$  anions. The copper atoms and both bromine atoms lie on a twofold rotation axis in the cell, and the geometry at the copper atoms is intermediate between tetragonal pyramidal and trigonal bipyramidal. The pyridine nitrogen atoms are trans, the N-Cu-N angle being  $178.0(2)^\circ$ , while the N(amine)-Cu-N(amine) and Br-Cu-N(amine) angles are  $149.4(3)^\circ$  and  $105.3(1)^\circ$ , respectively. The Cu-Br bond length of  $2.702(2) \text{ \AA}$  is very long, but does not appear to result from intramolecular contacts. The monomeric nature of the complex, which is in contrast to the structure of  $\text{Cu}(\text{AEP})_2\text{Br}_2$ , is consistent with its magnetic properties.

## Introduction

The preparations of complexes of the types  $\text{Cu}(\text{AEP})_2\text{X}_2$  and  $\text{Cu}(\text{AEP})\text{X}_2$ , where AEP is 2-(2-aminoethyl)pyridine, have been reported by Uhlig and Maaser,<sup>1</sup> and these workers suggested that the complexes  $\text{Cu}(\text{AEP})\text{X}_2$  are dimeric with five-coordinate geometry at the copper atoms while those of formulation  $\text{Cu}(\text{AEP})_2\text{X}_2$  are monomeric and six coordinate. Our recent report of the structure<sup>2</sup> of  $\text{Cu}(\text{AEP})\text{Br}_2$ , however, shows that this complex is polymeric, containing both Cu-Br-Cu chains and dimer-type Cu-Br-Cu-Br linkages, and that the copper atoms are six coordinate.

The magnetic properties of the complex of formulation  $\text{Cu}(\text{AEP})_2\text{Br}_2$  are consistent with a monomeric structure, since the Curie-Weiss law is obeyed to  $2.9^\circ\text{K}$ ,<sup>3</sup> but weak dimeric or polymeric interactions cannot be ruled out on the basis of magnetic susceptibility data alone. The great water solubility of this complex, however, did not seem to us to be consistent with any polymeric model, but suggested that the complex might be ionic. Such an ionic species could not be ruled out in view of the known, five-coordinate geometry of the complex  $\text{Cu}(\text{bipy})_2\text{I}_2$  (where bipy = 2,2'-bipyridine), in which there are  $[\text{Cu}(\text{bipy})_2\text{I}]^+$  cations and discrete  $\text{I}^-$  anions.<sup>4</sup>

In order to further our studies of the relationship between structural and magnetic properties,<sup>2,3,5-10</sup> and especially to make a comparison between the complexes  $\text{Cu}(\text{AEP})_2\text{X}_2$  and  $\text{Cu}(\text{AEP})\text{X}_2$ , we have under-

taken a precise three-dimensional structural investigation of the complex  $\text{Cu}(\text{AEP})_2\text{Br}_2$ .

## Experimental Section

The preparations of complexes of formulation  $\text{Cu}(\text{AEP})_2\text{X}_2 \cdot \text{H}_2\text{O}$ , where AEP is 2-(2-aminoethyl)pyridine and X is chlorine or bromine, have been reported by Uhlig and Maaser.<sup>1</sup> These authors report that the complex  $\text{Cu}(\text{AEP})_2\text{Br}_2 \cdot \text{H}_2\text{O}$ , for example, is formed by the reaction of  $\text{CuBr}_2$  with excess AEP in aqueous solution, and assumed that the complex is probably a tetragonally distorted octahedron with trans bromine atoms, analogous to the known structure<sup>11</sup> of *trans*-dinitrotetraamminecopper(II).

(1) E. Uhlig and M. Maaser, *Z. Anorg. Allg. Chem.*, **322**, 25 (1963).

(2) V. C. Copeland, P. Singh, W. E. Hatfield, and D. J. Hodgson, *Inorg. Chem.*, **11**, 1826 (1972).

(3) D. Y. Jeter, W. E. Hatfield, and D. J. Hodgson, *J. Phys. Chem.*, **76**, 2707 (1972).

(4) G. A. Barclay, B. F. Hoskins, and C. H. L. Kennard, *J. Chem. Soc.*, 5691 (1963).

(5) D. L. Lewis, W. E. Hatfield, and D. J. Hodgson, *Inorg. Chem.*, in press.

(6) J. A. Barnes, D. J. Hodgson, and W. E. Hatfield, *ibid.*, **11**, 144 (1972).

(7) D. J. Hodgson, P. K. Hale, and W. E. Hatfield, *ibid.*, **10**, 1061 (1971).

(8) D. Y. Jeter, D. J. Hodgson, and W. E. Hatfield, *Inorg. Chim. Acta*, **5**, 257 (1971).

(9) D. Y. Jeter, D. J. Hodgson, and W. E. Hatfield, *Inorg. Chem.*, **11**, 185 (1972).

(10) J. A. Barnes, W. E. Hatfield, and D. J. Hodgson, *Chem. Commun.*, 1593 (1970).

We find that the reaction of  $\text{CuBr}_2$  with excess AEP in 95% ethanol gives a deep blue solution from which blue crystals of formulation  $\text{Cu}(\text{AEP})_2\text{Br}_2$  (anhydrous) precipitate. The complex melts at  $140^\circ$ , while  $\text{Cu}(\text{AEP})_2\text{Br}_2 \cdot \text{H}_2\text{O}$  melts<sup>1</sup> at  $130^\circ$ . *Anal.* Calcd for  $\text{CuBr}_2\text{C}_{14}\text{N}_4\text{H}_{20}$ : C, 35.95; N, 11.98; H, 4.31; Br, 34.17. Found:<sup>12</sup> C, 35.84; N, 12.04; H, 4.50; Br, 33.99.

Examination of the crystals by precession and Weissenberg photography indicated that the crystals belong to the monoclinic system, and the observed systematic absences of  $hkl$  for  $h + k$  odd and  $h0l$  for  $l$  odd suggest that the space group is either  $C2/c$  or  $Cc$ ; examination of the statistical distribution of the normalized structure factors obtained from a Wilson plot suggested that the centrosymmetric space group ( $C2/c$ ) is appropriate, and this was confirmed by the successful refinement of the structure. The cell constants, obtained by the least-squares procedure of Busing and Levy,<sup>13</sup> are  $a = 8.883(6) \text{ \AA}$ ,  $b = 11.853(13) \text{ \AA}$ ,  $c = 16.940(14) \text{ \AA}$  and  $\beta = 67.57(3)^\circ$ . A density of  $1.885 \text{ g cm}^{-3}$  calculated for four formula units in the cell is in acceptable agreement with the value of  $1.87(2) \text{ g cm}^{-3}$  obtained experimentally by flotation in dibromomethane-dichloromethane solution. Hence, the copper atom is constrained to lie either on a twofold axis or on an inversion center.

Diffraction data were obtained from a hexagonal plate crystal with hexagonal faces (110) and ( $\bar{1}\bar{1}0$ ) and rectangular faces (001), (00 $\bar{1}$ ), ( $\bar{1}\bar{1}0$ ), ( $\bar{1}10$ ), ( $\bar{1}\bar{1}1$ ), and ( $\bar{1}11$ ). The separations between opposite faces were the following: (001) and (00 $\bar{1}$ ), 0.074 cm; ( $\bar{1}\bar{1}0$ ) and ( $\bar{1}10$ ), 0.033 cm; ( $\bar{1}\bar{1}1$ ) and ( $\bar{1}11$ ), 0.074 cm; (110) and ( $\bar{1}\bar{1}0$ ), 0.027 cm. The crystal was mounted normal to the (103) planes, and data were collected using Mo  $K\alpha$  radiation and a Nb filter on a Picker four-circle automatic diffractometer in the manner previously described,<sup>7</sup> at a scan rate of  $1^\circ/\text{min}$  and with scans from  $-0.7^\circ$  from the calculated  $K\alpha_1$  peak to  $+0.7^\circ$  from the calculated  $K\alpha_2$  peak position. Data were collected out to a value of  $2\theta = 55^\circ$ , a total of 2061 independent intensities being recorded. Most of the data with  $2\theta > 52^\circ$  were extremely weak, and there were very few intensities above background at values of  $2\theta > 55^\circ$ .

The data were processed by the method of Corfield, Doedens, and Ibers,<sup>14</sup> the standard deviations of the intensities being estimated from the usual expression

$$\sigma(I) = [C + 0.25(t_s/t_b)^2(B_H + B_L) + p^2I^2]^{1/2}$$

with  $p$  chosen as 0.05.<sup>15</sup> An absorption correction was applied to the data; the linear absorption coefficient  $\mu$  for these atoms and Mo  $K\alpha$  radiation is  $65.2 \text{ cm}^{-1}$ , and for the crystal used the transmission coefficients were found to lie in the range 0.138–0.311.<sup>16</sup> Of the 2061 independent intensities measured, 1539 exceeded three times their estimated standard deviations and 1620 exceeded twice their estimated standard deviations.

## Solution and Refinement

The locations of the copper atom and two independent bromine atoms were found in a three-dimensional Patterson function. The presence of two independent bromine atoms instead of the expected single bromine atom is due to the bromine's lying on special positions in the cell; both bromine atoms and the copper atom were found to lie on the twofold axis. Four cycles of least-squares refinement of these positions were run. All least-squares refinements in this analysis were carried out on  $F$ , the function minimized being  $\sum w(|F_o| - |F_c|)^2$  and the weights  $w$  being taken as  $4F_o^2/\sigma^2(F_o^2)$ . In all calculations of  $F_c$  the atomic scattering factors for Cu and Br were taken from Cromer and Waber,<sup>17</sup> that for H was taken from Stewart, Davidson, and Simpson,<sup>18</sup> and those for C and N were taken from the tabulation of Ibers.<sup>19</sup> The effects of anomalous dispersion were included in calculations of  $F_c$ ,<sup>20</sup> the values of  $\Delta f'$  and  $\Delta f''$  being taken from the tabulation of Cromer.<sup>21</sup> Only the 1539 independent intensities which were greater than three times their estimated standard deviations were used in the initial refinement of the structure.

Initially, the three atoms were assigned variable isotropic thermal parameters. After four cycles of least-squares refinement, using the data before they had been corrected for absorption effects, the usual agreement factors  $R_1 = \sum ||F_o| - |F_c|/\sum |F_o|$  and  $R_2 = (\sum w(|F_o| - |F_c|)^2/\sum w(F_o^2))^{1/2}$  were 0.249 and 0.283, respectively. A difference Fourier synthesis revealed the carbon and nitrogen atoms of the AEP ligand, and two cycles of least-squares with variable isotropic thermal parameters assigned to all atoms gave values of 0.122 and 0.159 for  $R_1$  and  $R_2$ . The positions of the hydrogen atoms were located in a difference Fourier synthesis. After the absorption correction had been applied (*vide supra*), two cycles of least-squares refinement using the 1620 intensities which were greater than twice their

(11) M. A. Porai-Koshits and M. Bukovska, *Kristallografiya*, **6**, 381 (1961).

(12) Analyses were performed by Galbraith Laboratories, Inc., Knoxville, Tenn.

(13) W. R. Busing and H. A. Levy, *Acta Crystallogr.*, **22**, 457 (1967).

(14) P. W. R. Corfield, R. J. Doedens, and J. A. Ibers, *Inorg. Chem.*, **6**, 197 (1967).

(15) W. R. Busing and H. A. Levy, *J. Chem. Phys.*, **26**, 563 (1957).

(16) The programs for the IBM 360/75 used in this analysis were local modifications of Hamilton's GONO absorption correction program, Ibers' NUCLS least-squares program, Busing, Martin, and Levy's ORFFE function and error program, Zalkin's FORDP Fourier program, Doedens' RSCAN program, and various local programs.

(17) D. T. Cromer and J. T. Waber, *Acta Crystallogr.*, **18**, 104 (1965).

(18) R. F. Stewart, E. R. Davidson, and W. T. Simpson, *J. Chem. Phys.*, **42**, 3175 (1965).

(19) J. A. Ibers, "International Tables for X-Ray Crystallography," Vol. III, Kynoch Press, Birmingham, England, Table 3.3.1A.

(20) J. A. Ibers and W. C. Hamilton, *Acta Crystallogr.*, **17**, 781 (1964).

(21) D. T. Cromer, *ibid.*, **18**, 17 (1965).



**Table II:** Thermal Parameters for  $[\text{Cu}(\text{C}_7\text{N}_2\text{H}_{10})_2\text{Br}]\text{Br}$ 

Atom	$\beta_{11}^a$ or $B(\text{\AA}^2)$	$\beta_{22}$	$\beta_{33}$	$\beta_{12}$	$\beta_{13}$	$\beta_{23}$
Cu	0.0081 (1)	0.00586 (6)	0.00220 (3)	0	-0.00076 (4)	0
Br(1)	0.0153 (1)	0.00486 (4)	0.00311 (3)	0	-0.00276 (4)	0
Br(2)	0.0114 (1)	0.00944 (7)	0.00405 (3)	0	-0.00261 (5)	0
N(1)	0.0101 (5)	0.0047 (2)	0.0024 (1)	0.0007 (3)	-0.0010 (2)	-0.0001 (1)
N(2)	0.0101 (6)	0.0081 (3)	0.0031 (2)	0.0018 (3)	-0.0014 (2)	-0.0002 (2)
C(1)	0.0097 (6)	0.0043 (3)	0.0026 (2)	0.0001 (3)	-0.0010 (3)	-0.0002 (2)
C(2)	0.0114 (7)	0.0061 (3)	0.0022 (2)	0.0002 (4)	0.0000 (3)	-0.0002 (2)
C(3)	0.0149 (8)	0.0073 (4)	0.0021 (2)	-0.0004 (4)	-0.0017 (3)	0.0002 (2)
C(4)	0.0130 (8)	0.0060 (3)	0.0038 (2)	0.0010 (4)	-0.0032 (3)	-0.0002 (2)
C(5)	0.0087 (6)	0.0057 (3)	0.0029 (2)	0.0016 (4)	-0.0012 (3)	-0.0005 (2)
C(6)	0.0126 (7)	0.0053 (3)	0.0028 (2)	0.0027 (4)	-0.0003 (3)	0.0000 (2)
C(7)	0.0079 (6)	0.0072 (4)	0.0031 (2)	0.0017 (4)	-0.0005 (3)	0.0008 (2)
H(2)	3.3 (12)					
H(3)	4.0 (12)					
H(4)	2.6 (10)					
H(5)	2.3 (10)					
H(61)	4.1 (13)					
H(62)	5.1 (13)					
H(71)	4.3 (13)					
H(72)	4.3 (11)					
H(N1)	9 (3)					
H(N2)	10 (2)					

<sup>a</sup> The form of the anisotropic thermal ellipsoid is  $\exp[-(\beta_{11}h^2 + \beta_{22}k^2 + \beta_{33}l^2 + 2\beta_{12}hk + 2\beta_{13}hl + 2\beta_{23}kl)]$ .

**Table III:** Internuclear Distances and Angles in  $[\text{Cu}(\text{C}_7\text{N}_2\text{H}_{10})_2\text{Br}]\text{Br}^a$ 

Distance, $\text{\AA}$		Angle, deg	
Cu-Br(1)	2.702 (2)	N(1)-Cu-N(1)'	178.0 (2)
Cu-Br(2)	4.034 (4)	N(2)-Cu-N(2)'	149.4 (3)
Cu-N(1)	2.065 (3)	N(1)-Cu-N(2)	92.8 (2)
Cu-N(2)	2.027 (4)	N(1)-Cu-N(2)'	87.7 (2)
N(1)-C(1)	1.342 (5)	Br(1)-Cu-N(1)	89.01 (9)
N(1)-C(5)	1.342 (5)	Br(1)-Cu-N(2)	105.3 (1)
N(2)-C(7)	1.475 (6)	C(1)-N(1)-C(5)	117.6 (4)
C(1)-C(2)	1.388 (6)	N(1)-C(1)-C(2)	120.9 (4)
C(2)-C(3)	1.355 (7)	N(1)-C(1)-C(6)	118.1 (4)
C(3)-C(4)	1.387 (7)	C(2)-C(1)-C(6)	121.0 (4)
C(4)-C(5)	1.359 (7)	C(1)-C(2)-C(3)	121.1 (4)
C(1)-C(6)	1.493 (6)	C(2)-C(3)-C(4)	117.8 (4)
C(6)-C(7)	1.495 (7)	C(3)-C(4)-C(5)	119.0 (5)
C(2)-H(2)	0.77 (6)	N(1)-C(5)-C(4)	123.7 (4)
C(3)-H(3)	0.89 (5)	C(1)-C(6)-C(7)	112.4 (4)
C(4)-H(4)	0.77 (5)	C(6)-C(7)-N(2)	112.1 (4)
C(5)-H(5)	0.70 (5)		
C(6)-H(61)	1.08 (6)		
C(6)-H(62)	1.03 (6)		
C(7)-H(71)	1.02 (7)		
C(7)-H(72)	1.01 (5)		
N(2)-H(N1)	0.86 (10)		
N(2)-H(N2)	1.14 (9)		

<sup>a</sup> Atoms designated with a prime are related to the reference atom by the twofold rotation.

per(II),<sup>26</sup> but is shorter than the value of 2.16(1)  $\text{\AA}$  found in 2-methylpyridinecopper(II) chloroacetate.<sup>27</sup> Similarly, the Cu-N(2) bond length of 2.027(4)  $\text{\AA}$  is

consistent with the copper(II)-amine bond lengths of 1.971(2) and 1.984(2)  $\text{\AA}$  in carbonatodiamminecopper(II),<sup>28</sup> 2.012(9) and 2.017(9)  $\text{\AA}$  in selenatotetraamminecopper(II),<sup>29</sup> 2.031(6) and 2.032  $\text{\AA}$  in sulfatotetraamminecopper(II),<sup>29</sup> and in many other related systems,<sup>30-35</sup> all of which fall in the range 1.97-2.07  $\text{\AA}$ .

The bonded Cu-Br(1) distance is longer than any terminal Cu-Br bond that could be found in the literature. In dibromobis(2,3-dimethylpyridine)copper(II),<sup>36</sup>  $\text{Cu}(\text{AEP})\text{Br}_2$ ,<sup>2</sup> and dibromobis(2-methylpyridine)copper(II),<sup>23</sup> the terminal Cu-Br bond lengths fall in the range 2.388-2.413  $\text{\AA}$ , which might, therefore, be considered "normal" for systems of this type. In  $\text{CuBr}_5^{3-}$ , the Cu-Br distances are<sup>37</sup> 2.450(2) and 2.519(2)  $\text{\AA}$ , and this latter is the longest terminal Cu-Br bond length found in the literature; the sum of the

(26) J. D. Dunitz, *Acta Crystallogr.*, **10**, 307 (1957).

(27) G. Davey and F. S. Stephens, *J. Chem. Soc. A*, 2803 (1970).

(28) M. H. Meyer, P. Singh, W. E. Hatfield, and D. J. Hodgson, *Acta Cryst., Sect. B*, **28**, 1607 (1972).

(29) B. Morosin, *Acta Crystallogr., Sect. B*, **25**, 19 (1969).

(30) M. B. Cingi, C. Guastini, A. Musatti, and M. Nardelli, *ibid.*, **26**, 1836 (1970).

(31) I. Agrell, *Acta Chem. Scand.*, **20**, 1281 (1966).

(32) T. Distler and P. A. Vaughan, *Inorg. Chem.*, **6**, 126 (1967).

(33) Y. Iitaka, K. Shimizu, and T. Kwan, *Acta Cryst.*, **20**, 803 (1966).

(34) B. W. Brown and E. C. Lingafelter, *ibid.*, **17**, 254 (1964).

(35) Y. Komiyama and E. C. Lingafelter, *ibid.*, **17**, 1145 (1964).

(36) W. Stahlin and H. R. Oswald, *Acta Crystallogr., Sect. B*, **27**, 1368 (1971).

(37) S. A. Goldfield and K. N. Raymond, *Inorg. Chem.*, **10**, 2604 (1971).

covalent radii<sup>38</sup> of Cu(II) (1.35) and Br (1.14) leads to a single bond value of 2.49 Å, in good agreement with these values. The bond length of 2.702(2) Å found here is significantly greater than all of these examples, and is very similar to the value of 2.70 Å found for the Cu-I bond<sup>4</sup> in [Cu(bipy)<sub>2</sub>I]<sup>+</sup>; the sum of the covalent radii<sup>38</sup> of Cu(II) and I is 2.68 Å.

In an attempt to discover the cause of this anomalous Cu-Br bond length, we made a series of calculations in which the Br(1) atom was bonded more closely to the Cu atom but the other atoms maintained their observed positions. When the Cu-Br bond length was set to 2.41 Å there were Br···N and Br···C contacts of 3.146 and 3.235 Å, respectively, and with a Cu-Br bond length of 2.52 Å these contacts were 3.230 and 3.290 Å, respectively; in the observed molecule, the closest separations are 3.372 and 3.388 Å. While these Br···N contacts are less than the sum of the atomic van der Waals radii reported by Pauling,<sup>38</sup> none of them can be regarded as severe since in dibromobis(2-methylpyridine)copper(II) there are four Br···N separations in the range 3.118(7)–3.148(7) Å,<sup>23</sup> in Cu(AEP)Br<sub>2</sub> there is a Br···N distance of 3.195 Å,<sup>2</sup> and in dibromobis(2,3-dimethylpyridine) there are Br···N contacts of 3.101(9) and 3.105(9) Å.<sup>36</sup> In none of these cases cited is the apparent contraction of the Br···N separations due to hydrogen bonding, since the nitrogen atoms involved are pyridine nitrogen atoms and have no hydrogen atom attached. Hence, the lengthening of the Cu-Br bond cannot be attributed to intramolecular contacts. There is no evidence of any hydrogen bonding involving this bromine; the closest Br(1)···N(2) separation is 3.702(3) Å, with a corresponding Br(1)···H separation of 3.11 Å and an associated Br(1)···H-N(2) angle of 112°. These values preclude any hydrogen bond formation,<sup>39</sup> since the Br···N separation is considerably larger than the sum of the van der Waals radii and the Br···H distance in hydrogen bonded systems has been reported to be approximately 2.43 Å.<sup>40,41</sup>

The geometry of the substituted pyridine ring is normal. The C-N(1) bond lengths of 1.342(5) and 1.342(5) in the AEP ligand are in excellent agreement with the mean value of 1.342(11) Å in dibromobis(2-methylpyridine)copper(II)<sup>23</sup> and the values of 1.33(1) and 1.342(9) Å in the AEP ligand in Cu(AEP)Br<sub>2</sub>,<sup>2</sup> and also with the mean value of 1.352 Å reported for heterocyclic compounds by Sutton.<sup>42</sup> While there are wide variations in the C-C bond lengths in the ring, it is evident that the C(1)-C(2) bond, which is adjacent to the exocyclic portion of the ligand, is slightly longer (1.388(6) Å) than the average length of 1.367(13) Å for the other ring C-C bonds. The exocyclic C-C bond lengths of 1.493(6) and 1.495(7) Å, however, are

relatively short. This shortening of the exocyclic C-C bond and lengthening of the adjacent ring C-C bond have been observed in analogous systems,<sup>2,23-25</sup> and can be ascribed to a drift of electron density from the ring toward the exocyclic moiety.<sup>23</sup> The bond angles in the ring are normal, falling in the range of 117.6(4)–123.7(4)°. The pyridine ring is planar, with no atom deviating from the least-squares plane by more than 0.018 Å.

The geometry at the copper(II) atoms is quite different from that proposed by Uhlig and Maaser,<sup>1</sup> and we have made some calculations of the intramolecular contacts which would result if the AEP ligands maintained their observed geometry and position but the non-bonded Br(2) ion were within bonding distance of the metal. In these models as in the previous calculations involving Br(1) (*vide supra*) the bromine atom was constrained to lie on the twofold axis. With a normal bonded Cu-Br separation of 2.41 Å, there would be Br···N(2) contacts as short as 2.709 Å, and when the Cu-Br distance is increased to 2.52 Å there are still Br···N(2) interactions of 2.786 Å; this contact is increased to only 2.919 Å when the Cu-Br(2) bond length is set equal to the very long Cu-Br(1) value of 2.702 Å. All of these Br···N contacts would cause severe strain in the molecule and are significantly shorter than any Br···N contacts which could be found in the literature. While these calculated contacts do explain why the Br(2) ion cannot bond to the [Cu(AEP)<sub>2</sub>Br]<sup>+</sup> moiety if the cation maintains its present geometry, there is no obvious reason why the AEP ligands could not move upward (in the direction of Br(1)) to reduce this strain. It would be of great interest to compare this structure with those of the corresponding iodo and chloro complexes to see whether any further light can be shed on this problem.

*Acknowledgments.* This research was supported by the Materials Research Center of the University of North Carolina under Contract No. DAHC-15-67-C-0223 with the Advanced Research Projects Agency, and by the National Science Foundation under Grant No. GP-10300. We are grateful for this continuing support.

(38) L. Pauling, "The Nature of the Chemical Bond," 3rd ed, Cornell University Press, Ithaca, N. Y., 1960.

(39) W. C. Hamilton and J. A. Ibers, "Hydrogen Bonding in Solids," W. A. Benjamin, New York, N. Y., 1968.

(40) H. A. Levy and S. W. Petersen, *J. Amer. Chem. Soc.*, **75**, 1536 (1953).

(41) H. S. Gutowsky, G. B. Kistiakowsky, G. E. Pake, and E. M. Purcell, *J. Chem. Phys.*, **17**, 972 (1949).

(42) L. E. Sutton, "Tables of Interatomic Distances and Configurations in Molecules and Ions," The Chemical Society, London, 1958.

# Dielectric Properties and Relaxation in Ethylene Carbonate and Propylene Carbonate

by Richard Payne\* and Ignatius E. Theodorou

*Air Force Cambridge Research Laboratories, L. G. Hanscom Field, Bedford, Massachusetts 01730  
(Received May 22, 1972)*

*Publication costs assisted by the Air Force Cambridge Research Laboratories*

The dielectric properties of ethylene carbonate and propylene carbonate have been studied by a pulse reflection technique and ac measurements in the frequency range 1–9000 MHz. Equilibrium dielectric constants for the pure liquids and mixtures with other liquid dielectrics are consistent with the absence of specific intermolecular forces. The dipole relaxation process is described by the Debye equations with relaxation times in the picosecond region at room temperature and the nanosecond region for supercooled propylene carbonate at  $-78^\circ$ . The apparent limiting high-frequency dielectric constant in both liquids is approximately 10 suggesting the existence of a second dispersion region at frequencies above 9000 MHz. The relaxation times and the viscosity of propylene carbonate are described by an empirical rate equation of the form previously applied by Davidson and Cole to their measurements for 1-propanol, propylene glycol, and glycerol.

## Introduction

Several studies of the dielectric properties of the cyclic carbonates have been reported in the literature.<sup>1–3</sup> They show that these compounds have unusually high dielectric constants which in general can be attributed to large permanent dipole moments rather than to specific intermolecular association of the type responsible for the high dielectric constant of, for example, water or the N monoalkyl amides.<sup>4</sup> However, the evidence is not entirely unambiguous. For example, the Trouton's constants for both ethylene carbonate and propylene carbonate are significantly higher than the usual value for nonassociated liquids. Also the occurrence of doublets in the carbonyl stretching band of the ir spectrum has been reported in the case of ethylene carbonate and some closely related compounds, but not however in propylene carbonate.<sup>5</sup> Similar effects in the ir spectra of halogenated esters of acetic acid have been attributed to molecular association<sup>6</sup> or rotational isomerism.<sup>7</sup> Since the latter could hardly explain the phenomenon in the case of ethylene carbonate the spectroscopic data seem to point to the possibility of association.

In order to explore this problem further, we have investigated the dipole relaxation process in these compounds by extending the dielectric measurements into the microwave frequency range. Accurate measurements of the static dielectric constant at 1 MHz for ethylene carbonate, propylene carbonate, and mixtures of the latter with methanol, 4-butyrolactone, and diethyl carbonate are also reported.

## Experimental Section

*A. Purification and Manipulation of Solvents.* Propylene carbonate (Matheson Coleman and Bell) was

purified by distillation under reduced pressure on a Podbielniak Semi-Cal (Series 3650) adiabatic fractional distillation column using a reflux ratio of 10. The pressure and temperature at the head of the column were maintained at 0.1–0.3 Torr and  $55$ – $60^\circ$ , respectively. The kettle temperature was kept below  $110^\circ$  to avoid decomposition. The middle fraction was collected and analyzed by gas chromatography using a 2-ft copper column packed with cross-linked polystyrene beads (Porapak Q) in a Model 500 F & M chromatograph with thermal conductivity detector. The distillate contained less than 10 ppm of water and no other detectable low-boiling impurities. Specific conductance was in the range  $10^{-7}$ – $10^{-8}$  (ohm cm)<sup>-1</sup>. Ethylene carbonate (Matheson Coleman and Bell) was dried with 4A molecular sieves then distilled twice under reduced pressure on a 40-cm heated glass column packed with glass helices. Chromatographic analysis of the middle fraction indicated less than 10 ppm of water and one other unidentified low-boiling impurity of low concentration. The melting point was  $36.6^\circ$  and the specific conductance  $10^{-7}$ – $10^{-8}$  (ohm cm)<sup>-1</sup>.

Diethyl carbonate, methanol, and 4-butyrolactone were likewise purified by distillation after drying with molecular sieves. All solvents were routinely analyzed for water and other impurities. All manipulation of

- (1) R. P. Seward and E. C. Vieira, *J. Phys. Chem.*, **62**, 127 (1958).
- (2) R. Kempa and W. H. Lee, *J. Chem. Soc.*, 1936 (1958).
- (3) L. Simeral and R. L. Amey, *J. Phys. Chem.*, **74**, 1443 (1970).
- (4) C. P. Smyth, "Dielectric Behavior and Structure," McGraw-Hill, New York, N. Y., 1955.
- (5) J. L. Hales, J. I. Jones, and W. Kynaston, *J. Chem. Soc.*, 618 (1957).
- (6) E. T. McBee and D. L. Christman, *J. Amer. Chem. Soc.*, **77**, 755 (1955).
- (7) M. Josien and M. R. Callas, *C. R. Acad. Sci.*, **240**, 1641 (1955).

nonaqueous solvents was performed in a drybox (Vacuum Atmospheres Model HE-553-2).

Ordinary distilled water was redistilled from alkaline permanganate and again distilled under reduced pressure on a 1-m insulated Pyrex column packed with Raschig rings. The specific conductance of the product was in the range  $2-5 \times 10^{-7}$  (ohm cm)<sup>-1</sup>.

*B. Measurement of Static Dielectric Constant.* The static dielectric constant was measured at a fixed frequency of 1 MHz using a cell similar to that described by Connor, Clarke, and Smyth.<sup>8</sup> Concentric brass electrodes were threaded onto a Teflon base which also formed part of a water circulation jacket. Banana plugs screwed into the electrodes at the base of the cell enabled the cell to be plugged directly into General Radio Type 938 binding posts.

The cell capacitance was measured by a substitution method using a General Radio Type 1606A bridge and Type 1722N precision variable capacitor. The overall sensitivity of the arrangement was 0.05 pf or 0.01% for the water-filled cell. The accuracy of the 1722N capacitor was improved from the nominal value of  $\pm 0.3$  pf to better than  $\pm 0.1$  pf by calibration against a General Radio Type 1615A transformer ratio-arm bridge at 1 kHz.

The cell constants were determined from measurements made with air, water, and methanol in the cell using standard dielectric constant values at 25° of 78.30 for water<sup>9</sup> and 32.63 for methanol.<sup>10</sup> The capacitance of the air-filled cell measured on a Hewlett-Packard Type 250A RX bridge at 1 MHz was 8.26 pf. The capacitance of the cell filled with a liquid of dielectric constant  $\epsilon$  is given by

$$C = C_0\epsilon + C' \quad (1)$$

where  $C_0$  is the geometric capacitance of the air-filled space and  $C'$  is the invariant capacitance associated with the Teflon-spaced portion of the electrode area and the terminals. The values of  $C_0$  and  $C'$  were established as 5.890 and 2.37 pf, respectively. A small change in  $C_0$  was observed over a long period of time.

In arriving at the cell constants (and in subsequent measurements) due consideration was given to the effects of solvent conductance and residual inductance of both the precision condenser and the cell. The 1606A bridge measures the equivalent series RC combination. It was necessary therefore to transform the cell impedance to the equivalent parallel combination in cases where the effect of solvent conductance was measurable. However, the difference between the series capacitance and equivalent parallel capacitance was usually negligible and amounted to less than 1% in the worst case (*i.e.*, in the case of water). The correction for inductance from all sources was usually less than 0.1%.

The temperature of the cell was controlled to  $\pm 0.03^\circ$  by circulating water through the jacket from a thermo-

stat bath. The water temperature was measured in the jacket using NBS calibrated ASTM thermometers with a precision of 0.02°. Partial immersion errors were shown to be negligible under the experimental conditions. The variation with temperature of  $C_0$ , the air capacitance of the cell, was calculated from consideration of the thermal expansion of the electrodes. This was considered a more accurate procedure than measuring the cell constant at different temperatures using a standard calibration liquid such as water. This was however also done routinely as a check on the procedure using the accurate water data of Malmberg and Maryott.<sup>9</sup> The total calculated variation of  $C_0$  between 0 and 70° was 0.13% which was confirmed within experimental error by the measurements.

*C. Measurement of Dielectric Constant and Loss at 1-250 MHz.* Measurements at frequencies up to 250 MHz were made with a coaxial displacement cell similar to the cell described by Lovell and Cole,<sup>11</sup> using a Hewlett-Packard Type 250A bridge. Improved electrical characteristics were obtained by constructing the cell from General Radio Type 900 precision rod and tubing using a Type 900 BT precision coaxial connector with a slightly modified bead to form the base of the cell.

For a perfectly fitting plunger the complex dielectric constant of the liquid ( $\epsilon^*$ ) is related to the measured changes in the parallel capacitance ( $\Delta C$ ) and conductance ( $\Delta G$ ) for a given displacement ( $l$ ) according to

$$C_0 l (\epsilon^* - \epsilon_t) = \Delta C - j \frac{\Delta G}{\omega} \quad (2)$$

where  $C_0$  is the geometric capacitance per unit length of the cell,  $\epsilon_t$  is the dielectric constant of the plunger material, and  $\omega$  is the angular frequency of the ac signal. By equating real and imaginary parts in eq 2, the dielectric constant ( $\epsilon'$ ) and loss ( $\epsilon''$ ) are shown to be

$$\epsilon' = \epsilon_t + \Delta C / C_0 l \quad (3)$$

$$\epsilon'' = \Delta G / \omega C_0 l \quad (4)$$

From a prior knowledge of  $\epsilon_t$  and the dimensions of the cell the method in principle allows absolute measurement of the complex dielectric constant by measuring the changes of capacitance and conductance with displacement of the plunger. In practice, however, the cell is imperfect since the plunger does not fit tightly. Also the fringing capacitance at the end of the inner electrode varies at small plunger settings due to collec-

(8) W. P. Connor, R. P. Clarke, and C. P. Smyth, *J. Amer. Chem. Soc.*, **64**, 1379 (1942).

(9) C. G. Malmberg and A. A. Maryott, *J. Res. Nat. Bur. Stand.*, **56**, 1 (1956).

(10) R. Parsons, "Handbook of Electrochemical Constants," Butterworths, London, 1959.

(11) S. E. Lovell and R. H. Cole, *Rev. Sci. Instrum.*, **30**, 361 (1959)

tion of liquid above the electrode. This effect causes curvature of the capacitance *vs.* displacement plot at small (<0.05 cm) displacements. This problem was solved by extending the inner electrode with a Teflon cap 0.5 cm long. The cell capacitance was then found to be linearly dependent on the plunger displacement at least down to 0.005 cm above the cell floor. The problem of the imperfectly fitting plunger was considered by Lovell and Cole, who treated that part of the cell occupied by the plunger as two series connected capacitors, *i.e.*, the capacitance of the plunger ( $C_1$ ) and the capacitance of the annular gap ( $C_2$ ). The change in the cell impedance with plunger displacement is then given by

$$\Delta C^* = \epsilon^* C_0 l - \left(1 + \frac{C_1}{C_2}\right) \frac{\epsilon^* \epsilon_t C_0 l}{\epsilon^* + \epsilon_t C_1 / C_2} \quad (5)$$

where  $\Delta C^*$  is defined by

$$\Delta C^* = \Delta C - j \frac{\Delta G}{\omega} \quad (6)$$

An approximation for  $\epsilon^*$  from eq 5 valid when  $|\epsilon^*| > 3$  and  $C_1/C_2 < 0.1$  is

$$\epsilon^* = \epsilon_t (1 + C_1/C_2) + \frac{\Delta C^*}{C_0 l} - \frac{C_1}{C_2} \left[ \frac{\epsilon_t^2 C_0 l}{\Delta C^* + \epsilon_t C_0 l} \right] \quad (7)$$

from which by equating real and imaginary parts

$$\epsilon' = \epsilon_t (1 + C_1/C_2) +$$

$$\frac{\Delta C}{C_0 l} - \frac{C_1}{C_2} \left[ \frac{\epsilon_t + \Delta C/C_0 l}{(1 + \Delta C/\epsilon_t C_0 l)^2 + (\Delta G/\epsilon_t C_0 l \omega)^2} \right] \quad (8)$$

$$\epsilon'' = \frac{\Delta G}{\omega C_0 l} - \frac{C_1}{C_2} \left[ \frac{\Delta G/C_0 l \omega}{(1 + \Delta C/\epsilon_t C_0 l)^2 + (\Delta G/\epsilon_t C_0 l \omega)^2} \right] \quad (9)$$

The value of  $C_1/C_2$  for our cell was 0.08 obtained from measurements on the air-filled cell using the exact formula of eq 5. The specified value of  $C_0$  (0.6667 pf  $\pm$  0.07%) for the GR Type 900 coaxial stock was assumed. The value of  $\epsilon_t$  was taken as 2.08. As a check of the correctness of the cell constants, calibration measurements were made at 1 MHz with air, methanol, and dimethyl sulfoxide which gave dielectric constants in satisfactory agreement with established values. The conditions for the approximation involved in eq 7–9 were met for all the liquids studied. The last terms in eq 8 and 9 were negligibly small under all experimental conditions encountered.

The problem of the impedance transforming properties of the internal transmission line connecting the bridge to the bridge terminal at high frequencies was solved by isolating the cell from the bridge by a  $\lambda/2$  section. For measurements on nonconducting liquids below 20 MHz the cell could be mounted directly on the bridge using a GR Type 900-QNP adaptor. The effect of the series inductance of the internal line (0.019  $\mu$ H) at 20 MHz calculated from the lead correction

equations given by Lovell and Cole proved to be negligible. For higher frequencies  $\lambda/2$  sections were constructed from General Radio Type 874 50-ohm line using a Type 874 LK10L adjustable line for the final adjustment of the length. For a loss-free line the measured impedance is equal to the impedance of the cell.<sup>12</sup> The effect of resistive losses in the line on the measured impedance was checked by measurements with standard transmissions. The correction to the measured values of the cell capacitance and conductance was always less than 1%.

The temperature of the cell was controlled by circulating water through a copper coil wrapped around the cell surrounded by fiber glass insulation. For measurements at low temperatures the cell was surrounded by a reservoir filled with a mixture of Dry Ice in methanol.

*D. Dielectric Constant and Loss at 250–9000 MHz.* Impedance measurements at frequencies over 250 MHz were made by means of a General Radio Type 900 LB precision-slotted line. Up to 1000 MHz it was found possible to use the coaxial cell described in the previous section after replacing the inner electrode with a shorter electrode of only 1 mm total length. With this arrangement the cell could be treated as a lumped impedance up to 1000 MHz. The cell was connected to the slotted line in a vertical orientation using a 90° ell section (GR 900L) and its impedance obtained as a function of plunger displacement from measurements of the voltage standing wave ratio (VSWR) and the location of the voltage nodes on the line. The equivalent parallel RC components of the impedance were obtained directly from the measurements by solution of the transmission line equations.

At frequencies above 1000 MHz the dielectric constant and loss were obtained by measuring the input impedance of a short-circuited section of coaxial line filled with the dielectric using the method of Roberts and Von Hippel.<sup>13</sup> Details of the cell and experimental procedure are given elsewhere.<sup>14</sup>

*E. Pulse Reflection Measurements.* The response of a dielectric-filled section of transmission line to a fast rise-time square pulse was investigated using the method of time-domain reflectometry (TDR). The TDR method can, under favorable conditions, give quantitative information on the dielectric constant and loss.<sup>15,16</sup> We have used the technique in this work to supplement the more accurate bridge and slotted line measurements.

The instrumentation used is essentially that described

(12) H. H. Skilling, "Electric Transmission Lines," McGraw-Hill, New York, N. Y., 1951.

(13) S. Roberts and A. Von Hippel, *J. Appl. Phys.*, **17**, 610 (1946).

(14) R. Payne and I. E. Theodorou, *Rev. Sci. Instrum.*, **42**, 218 (1971).

(15) H. Fellner-Feldegg, *J. Phys. Chem.*, **73**, 616 (1969).

(16) H. Fellner-Feldegg and E. F. Barnett, *ibid.*, **74**, 1962 (1970).

previously.<sup>17</sup> A transmission line of approximately 250-cm electrical length was constructed from 40-cm lengths of General Radio Type 874 50-ohm air line. The cell consisted of a General Radio Type 900 LZ30 reference air line terminated with a Type 900 WNC short circuit to give a dielectric-filled length of 30 cm. Hewlett-Packard pulse generators Type 215A (1 nsec rise time) and 213B (150 psec rise time) supplied the square pulses. The pulse and reflections were observed on the line at the generator end by means of a Tektronix VPI coaxial tee and P6034 or P6035 passive probe connected to a Tektronix Type 661 sampling oscilloscope with Type 4S2 sampling unit. The signal was usually recorded directly on a Moseley 135M XY recorder. The overall rise time of this system is approximately 100 psec.

## Results

*A. Low-Frequency Measurements.* Equilibrium dielectric constants were measured at 1 MHz for ethylene carbonate from 40 to 70° and for propylene carbonate from 0 to 65°. The results given in Table I were cor-

**Table I:** Static Dielectric Constant ( $\epsilon_0$ ) Measured at 1 MHz and Kirkwood Correlation Factor ( $g$ ) for Ethylene Carbonate and Propylene Carbonate<sup>a</sup>

Liquid	$T, ^\circ\text{C}$	$\epsilon_0$	$g$
Ethylene carbonate	25	5.4	
	40	89.78	1.20 (1.10)
	50	85.81	1.20 (1.09)
	60	82.01	1.19 (1.08)
	70	78.51	1.18 (1.06)
	Propylene carbonate	-78	89
0		71.03	0.99 (0.89)
10		68.64	
15		67.41	
20		66.14	
25		64.92	1.01 (0.89)
30		63.70	
35		62.58	
40		61.42	1.02 (0.89)
45		60.27	
50		59.17	
55		58.05	
60	56.89	1.02 (0.88)	

<sup>a</sup> Estimated accuracy of dielectric constant 0.1%. Correlation factor calculated from eq 17.

rected for scale errors and inductance in the standard capacitor and cell inductance, and for the temperature dependence of the cell constant. The dielectric constant of propylene carbonate was also measured at -78° with the coaxial displacement cell using a General Radio Type 1615A bridge at 10 kHz. The uncertainty of the 1-MHz measurements is estimated at 0.1%. The results are compared with previous measurements in Figures 1 and 2. The agreement is generally good.

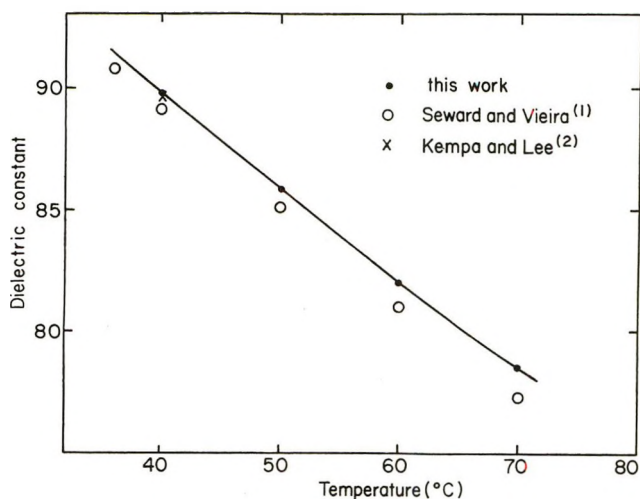


Figure 1. Static dielectric constant as a function of temperature for ethylene carbonate.

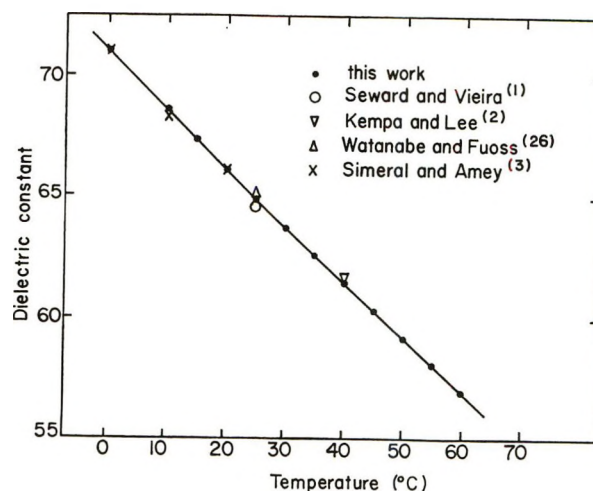


Figure 2. Static dielectric constant as a function of temperature for propylene carbonate.

However, the ethylene carbonate data of Seward and Vieira<sup>1</sup> are systematically lower than our results by up to 3%. A sample of propylene carbonate rigorously purified by the method of Jasinski and Kirkland,<sup>18</sup> and supplied by them, gave results indistinguishable from those found with our material.

Dielectric constants were measured at 1 MHz for mixtures of propylene carbonate with water, diethyl carbonate, and 4-butyrolactone. The results are summarized in Figure 3 in the form of plots of the excess dielectric constant  $\Delta\epsilon$  defined by

$$\Delta\epsilon = \epsilon_m - (x_1\epsilon_1 + x_2\epsilon_2) \quad (10)$$

where  $\epsilon_m$  is the measured value for the mixture,  $\epsilon_1$  and  $\epsilon_2$  are the values for the pure components, and  $x_1$  and  $x_2$  are their respective mole fractions in the mixture.

(17) R. Payne, *J. Electroanal. Chem.*, **19**, 1 (1968).

(18) R. J. Jasinski and S. Kirkland, *Anal. Chem.*, **39**, 1663 (1967).

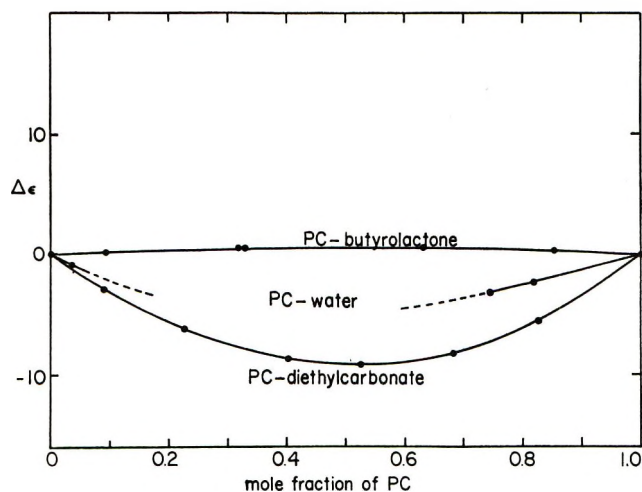


Figure 3. Excess dielectric constant as defined by eq 10 for mixtures of propylene carbonate with 4-butyrolactone, water, and diethyl carbonate at 25°.

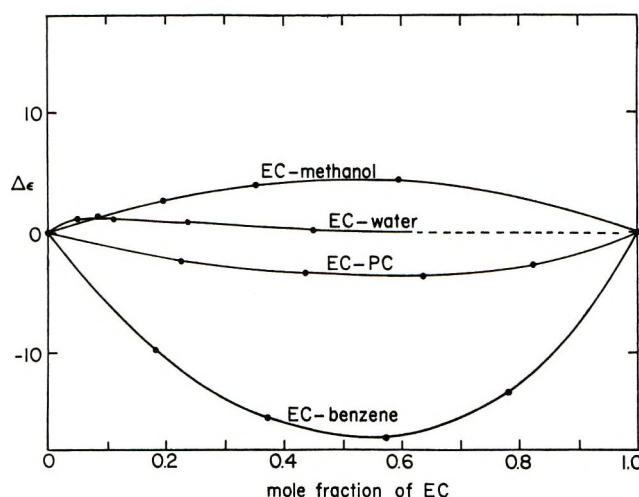


Figure 4. Excess dielectric constant as defined by eq 10 for mixtures of ethylene carbonate with methanol, water, propylene carbonate, and benzene at 25° (data of Seward and Vieira<sup>1</sup>).

Similar results for ethylene carbonate mixtures calculated from the data of Seward and Vieira<sup>1</sup> are shown in Figure 4. In both cases mixtures of the cyclic carbonate with strongly polar liquids (and with each other) produce small deviations from ideal behavior whereas large negative deviations occur in mixtures with low-dielectric constant liquids. A miscibility gap occurs in the propylene carbonate-water system between approximately 30 and 90 mol % of water at 25°.

**B. Pulse Reflection Measurements.** The pulse reflection technique gives two experimental parameters related to the dielectric constant of the liquid: the propagation time and the reflection coefficient. For a system which remains in equilibrium (no dispersion) the propagation time is proportional to the square root of the dielectric constant which can therefore be determined.

The reflection coefficient is the ratio of the height of the reflected pulse ( $E_r$ ) at the impedance discontinuity to that of the incident pulse ( $E_i$ ) and is given by transmission line theory

$$\rho = \frac{E_r}{E_i} = \frac{Z - Z_0}{Z + Z_0} \quad (11)$$

where  $Z$  is the input impedance of the dielectric-filled line and  $Z_0$  the characteristic impedance of the transmission line. For a loss-free dielectric the impedance at the surface of the liquid is a pure resistance given by

$$Z = Z_0/\sqrt{\epsilon} \quad (12)$$

Since  $Z$  is always less than  $Z_0$ , the reflection coefficient is negative and the reflected pulse for the loss-free dielectric is an inverted square pulse. Combination of eq 11 and 12 gives

$$\epsilon = \left( \frac{1 - \rho}{1 + \rho} \right)^2 \quad (13)$$

Hence the dielectric constant is also obtained from the measured reflection coefficient. For the general case of a dielectric with loss the reflection coefficient varies with time. If the relaxation is slow compared to the response of the system the infinite frequency dielectric constant is obtained from the height of the reflected pulse at  $t = 0$ . Similarly the static dielectric constant follows from the height of the pulse when  $t \gg \tau_0$  (the relaxation time). Determination of the relaxation time from the time dependence of the reflection coefficient is difficult even for the simple case of a Debye liquid and requires a full analysis of the spectrum of the input and reflected wave forms.<sup>19</sup> A simplified analysis of this type was given recently by Fellner-Feldegg and Barnett using the Laplace transform method.<sup>16</sup>

A typical pulse reflection measurement for propylene carbonate at room temperature is shown in Figure 5. The delay time of the transmission line in this case is approximately 10.5 nsec giving a time separation of the incident pulse and the first reflection of 21 nsec. The various features of Figure 5 are identified as follows. The first pulse is the incident signal sampled as it passes the probe. The second (inverted pulse) is the reflection from the dielectric discontinuity at the liquid surface: it is inverted because the reflection coefficient of the discontinuity "seen" by the line is negative (see eq 11). The next pulse, also inverted, is the reflection of the transmitted portion of the signal from the short circuit at the floor of the cell. Subsequent pulses are due to repeated internal reflection with partial transmission occurring at the dielectric-air interface and total reflection at the short circuit. The amplitude of the  $n$ th reflected pulse is easily shown to be

$$E_r^n = E_i(1 - \rho^2)(-\rho)^{n-2}(-1)^{n-1} \quad (14)$$

(19) T. A. Whittingham, *J. Phys. Chem.*, **74**, 1824 (1970).

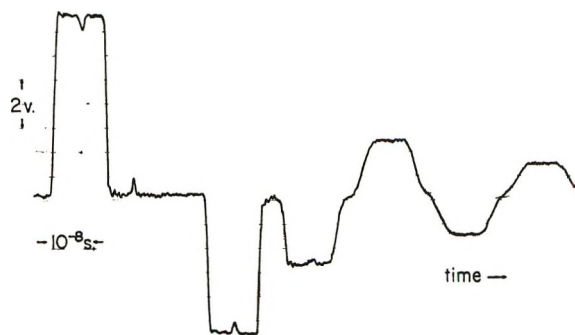


Figure 5. Pulse reflections from a 30-cm section of 50-ohm coaxial transmission line terminated by a short circuit and filled with propylene carbonate at  $21^\circ$ .

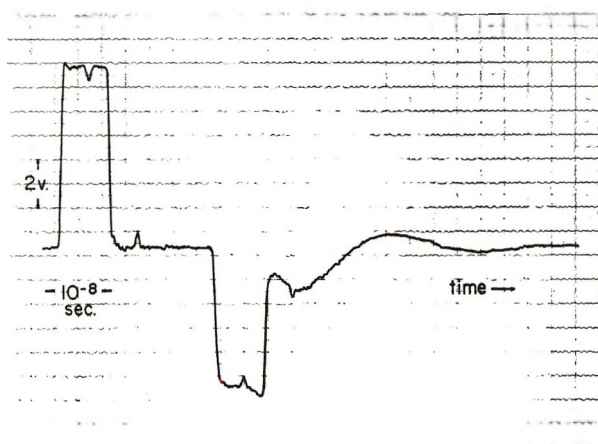


Figure 6. Pulse reflections from a 30-cm section of 50-ohm coaxial transmission line terminated by a short circuit and filled with propylene carbonate at  $-78^\circ$ .

for  $n \geq 2$  where  $\rho$  is the forward reflection coefficient (*i.e.*, air to dielectric).

A qualitative examination of Figure 5 shows that the dipole relaxation process in propylene carbonate at room temperature is extremely rapid. The measurements for ethylene carbonate at  $40^\circ$  are similar and closely resemble the behavior of water (relaxation time at  $25^\circ$ ,  $8.3 \times 10^{-12}$  sec).<sup>4</sup> However, some high-frequency absorption is indicated in Figure 5 by the rounding of later reflections. At  $-40^\circ$  the high-frequency attenuation is marked and at  $-78^\circ$  the pulse is completely attenuated after two passes through the cell (Figure 6).

The ac measurements described below show that the relaxation time at  $-78^\circ$  is  $1.3 \times 10^{-9}$  sec. Some time dependence of the dielectric constant (and hence the reflection coefficient) therefore should be apparent at times  $< 5$  nsec. The rounding of the first reflection in Figure 6 confirms that this is the case. Closer examination of the rise of this pulse using a 150-psec rise-time pulse showed that the pulse rises "instantaneously" to a height of  $\sim E_i/2$  corresponding to  $\rho = -0.5$  and  $\epsilon = 9$

according to eq 13. The subsequent rise is approximately exponential and is substantially complete after 5 nsec. This behavior is consistent with the ac measurements. The equilibrium reflection coefficients are also consistent with the static dielectric constant values. The time separation of the first and second reflections in Figure 5 is 16.2 nsec giving a value for  $\epsilon$  of 66 in excellent agreement with the bridge value.

At room temperature ethylene carbonate is a solid. The reflection coefficient and propagation time indicate a dielectric constant of 2.5 to 3.

*C. High-Frequency Measurements.* Dielectric constant and loss measurements were made in the frequency range 10–250 MHz for ethylene carbonate at a single temperature ( $40^\circ$ ), and for propylene carbonate at six temperatures ranging from  $-78$  to  $70^\circ$  using the Hewlett-Packard 250A bridge and the coaxial displacement cell. Dispersion was observed in this frequency range for both liquids. The dielectric constant and loss were determined from plots of the measured parallel capacitance and conductance, respectively, against plunger displacement using eq 8 and 9, neglecting the last term in each case.

The relaxation times given in Table II were obtained

Table II: Dielectric Relaxation Times for Ethylene Carbonate and Propylene Carbonate Calculated from Eq 16

Liquid	$T$ , $^\circ\text{C}$	$10^{11}\tau_0$ , sec	$\epsilon_\infty$
Ethylene carbonate	40	3.1	2.62
Propylene carbonate	$-78$	13.0	2.63
	2	5.6	2.63
	25	4.3	2.63
	44.6	3.2	2.63
	68.9	2.6	2.63

directly from the conductance by assuming a Debye relaxation function for which the loss conductance is given by<sup>4</sup>

$$G = \omega C_0 \left[ \frac{(\epsilon_0 - \epsilon_\infty)\omega\tau_0}{1 + \omega^2\tau_0^2} \right] \quad (15)$$

which reduces to

$$G = (\epsilon_0 - \epsilon_\infty)C_0\omega^2\tau_0 \quad (16)$$

when  $\omega\tau_0 \ll 1$ . Since the decrease in the dielectric constant was usually only a few per cent up to 250 MHz the approximation in eq 16 is valid and the conductance should be proportional to the square of the frequency. This was generally confirmed by the experimental results which are therefore consistent with either a simple Debye relaxation function or a more complicated function which reduces to the Debye form at low frequencies. The relaxation times were calculated from

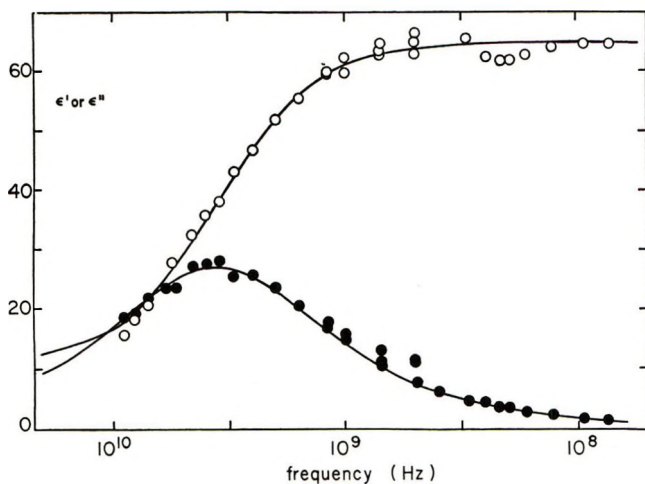


Figure 7. Dielectric constant and loss for propylene carbonate at 25°. Lines were calculated from the Debye equations with  $\epsilon_0 = 64.9$ ,  $\epsilon_\infty = 10.8$ , and  $\tau_0 = 4.6 \times 10^{-11}$  sec.

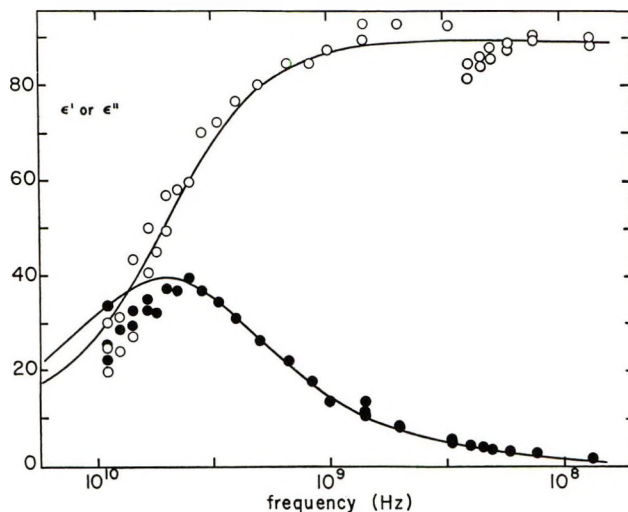


Figure 9. Dielectric constant and loss for ethylene carbonate at 40°. Lines calculated from the Debye equations with  $\epsilon_0 = 89.8$ ,  $\epsilon_\infty = 11.0$ , and  $\tau_0 = 3.1 \times 10^{-11}$  sec.

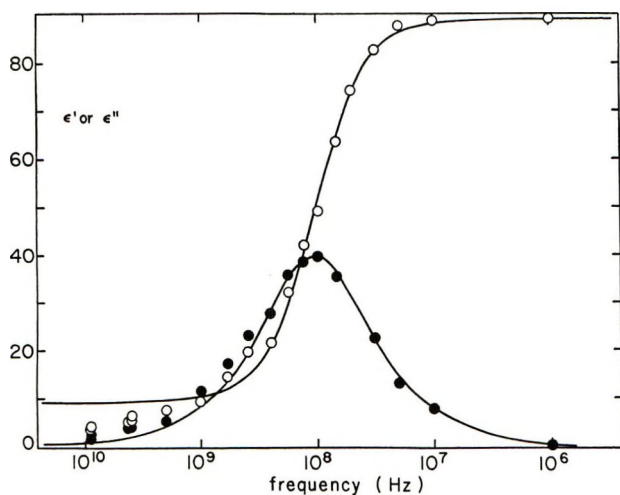


Figure 8. Dielectric constant and loss for propylene carbonate at  $-78^\circ$ . Solid lines were calculated from the Debye equations with  $\epsilon_0 = 88.9$ ,  $\epsilon_\infty = 9.4$ , and  $\tau_0 = 1.3 \times 10^{-9}$  sec.

the plots of conductance against square of the frequency assuming an arbitrary value for  $\epsilon_\infty$  equal to  $1.3n^2$  in eq 16 where  $n$  is the optical refractive index.

Substantially complete dispersion curves were obtained for ethylene carbonate at 40° and propylene carbonate at 25 and  $-78^\circ$  by extending the frequency range to 9000 MHz using the slotted-line technique. The results shown in Figures 7–9 were compared with Debye curves calculated from the relaxation times in Table II with  $\epsilon_\infty$  again set equal to  $1.3n^2$ . In each case the experimental loss factors were found to be systematically low, close to the critical frequency. The results, however, could be fitted satisfactorily to Debye curves calculated from an assumed value of  $\epsilon_\infty$  close to 10 as shown in the semicircular arc plots of Figure 10. This implies the existence of a second dispersion region at higher frequencies of the type reported by Davidson and Cole<sup>20</sup> for 1-propanol at  $-140^\circ$  and previously

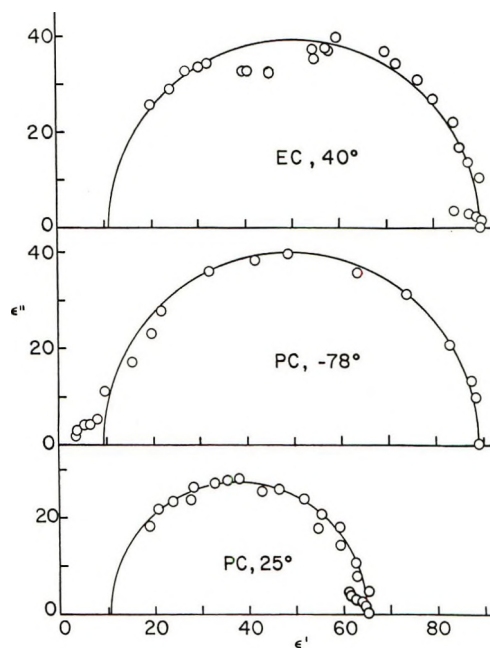


Figure 10. Cole-Cole semicircular arc plots for propylene carbonate at 25 and  $-78^\circ$  and ethylene carbonate at 40°. Solid lines drawn for Debye parameters given in Figures 7–9.

observed in the dispersion curves for aliphatic alcohols.<sup>21,22</sup> This is confirmed by the low-temperature propylene carbonate measurements which show the second dispersion region (Figure 10). None of the results could be fitted to the Cole and Cole circular arc function,<sup>23</sup> or the Davidson and Cole skewed arc func-

(20) D. W. Davidson and R. H. Cole, *J. Chem. Phys.*, **19**, 1484 (1951).

(21) P. and Girard P. Abadie, *Trans. Faraday Soc.*, **42A**, 40 (1946).

(22) J. A. Saxton, *Proc. Roy. Soc., Ser. A*, **213**, 473 (1952).

(23) K. S. Cole and R. H. Cole, *J. Chem. Phys.*, **9**, 341 (1941).

tion<sup>20</sup> for any value of the empirical argument. The Debye curves in Figures 7–9 and the Cole and Cole plots in Figure 10 were calculated from the parameters indicated. The relaxation times are in good agreement with the bridge values in Table II which, however, were obtained with lower assumed values of  $\epsilon_\infty$ .

## Discussion

A. *Static Dielectric Constants.* The possibility of molecular association through short-range specific forces was investigated by calculating the Kirkwood correlation factor  $g$ .<sup>24</sup> Kirkwood's extension of the Onsager<sup>25</sup> equation can be written

$$\epsilon - \epsilon_\infty = \frac{4\pi N_0 \mu_0^2}{9kTV} \frac{\epsilon_0(\epsilon_\infty + 2)^2}{(2\epsilon_0 + \epsilon_\infty)} g \quad (17)$$

where  $\mu_0$  is the permanent dipole moment,  $N_0$  is Avogadro's number,  $V$  is the molar volume, and  $k$  is Boltzmann's constant. Correlation factors were calculated from eq 17 assuming dipole moment values of 4.87 for ethylene carbonate and 4.94 for propylene carbonate.<sup>2</sup> Molar volumes were calculated from density data given by Watanabe and Fuoss<sup>26</sup> (ethylene carbonate) and Simeral and Amey<sup>3</sup> (propylene carbonate).  $\epsilon_\infty$  was calculated from published values of the optical refractive index<sup>2</sup> assuming as before a 30% increase in the total induced polarizability between optical and microwave frequencies. The resultant  $g$  values given in Table I are close to unity for propylene carbonate as reported by Simeral and Amey<sup>3</sup> in the lower temperature range. The ethylene carbonate values are somewhat higher although still close to unity. Seward and Vieira<sup>1</sup> obtained a value of 1.6 for ethylene carbonate at 40° and hence concluded that some association was present. They evidently used the approximation  $\epsilon_\infty = n^2$  in eq 17 which accounts for the discrepancy with our result. In view of the sensitivity of the calculation to the assumed value of  $\epsilon_\infty$  and the uncertainty of this value no firm conclusion can be drawn. The  $g$  values shown in parentheses in Table I were calculated from a form of eq 17 used by Davidson and Cole<sup>20</sup> in which  $\epsilon_\infty$  is equated to  $n^2$  on the right-hand side and the experimentally measured value for the *low-frequency* dispersion on the left-hand side. In our experiments this value is close to 10. The justification for this procedure is unclear but in any case it has little effect on the results. The sensitivity to  $\epsilon_\infty$  arises from the quadratic dependence on the right-hand side of eq 17. Calculations of this kind therefore lead to the conclusion that propylene carbonate and probably also ethylene carbonate obey Onsager's equation within the limits of uncertainty of the calculation.

Some qualitative inferences concerning the possibility of association can be drawn from the excess dielectric constant function for various mixtures shown in Figures 3 and 4. Ethylene carbonate–water mixtures show surprisingly little deviation from ideal behavior whereas

strong negative deviations might be expected due to breakup of the water structure. Similar behavior of the dimethyl sulfoxide–water system has been attributed to strong interaction of the two components which is supposed to compensate for the disruption of the water structure.<sup>27</sup> Large negative deviations from ideality for ethylene carbonate–benzene and propylene carbonate–diethyl carbonate mixtures could be interpreted as evidence of structure in the high dielectric constant components by analogy with the similar effect of dioxane on water, for example.<sup>27,28</sup> An alternative interpretation which seems more plausible in view of the earlier discussion is that the low-dielectric constant component promotes association of the dipoles of the high-dielectric constant component to form dimers or larger aggregates of low moment. Mixtures with other high-dielectric constant liquids, *i.e.*, propylene carbonate–butyrolactone and propylene carbonate–ethylene carbonate show only small deviations from ideality, which seems consistent with the general conclusion that there is little or no specific association. However, it is worth noting that both ethylene carbonate and propylene carbonate have Trouton's constants of approximately 23 which is significantly higher than the "normal" value of 21 for a nonassociated liquid. There is also some evidence of association in chloroethylene carbonate and chloromethylene carbonate (chloropropylene carbonate) for which the correlation factors calculated from the data of Kempa and Lee<sup>2</sup> are 1.38 and 1.85, respectively. Possible modes of association in these compounds are suggested by the extensive polymerization of the carbonic acid esters of trimethylene glycol and higher glycols of the OH–(CH<sub>2</sub>)<sub>*n*</sub>–OH type described by Carothers and Van Natta.<sup>29</sup> However, these authors also stress that extensive studies of ethylene carbonate have revealed no evidence of polymerization in the five-membered ring compounds.

B. *Dielectric Relaxation.* As noted earlier, the principal relaxation process in both ethylene carbonate and propylene carbonate obeys the Debye equations. In propylene carbonate the Debye behavior is also found in the supercooled state at –78°. The relaxation times summarized in Table II are comparable with values for normal polar liquids of high dielectric constant, *e.g.*, dimethylformamide ( $\tau_0 = 1.3 \times 10^{-11}$  sec at 37.3°)<sup>30</sup> and 4-butyrolactone ( $\tau_0 = 2.1 \times 10^{-11}$  sec at 0°).<sup>31</sup>

(24) J. G. Kirkwood, *J. Chem. Phys.*, **7**, 911 (1939).

(25) L. Onsager, *J. Amer. Chem. Soc.*, **58**, 1486 (1936).

(26) M. Watanabe and R. Fuoss, *ibid.*, **78**, 527 (1956).

(27) J. J. Lindberg and J. Kenttamaa, *Suom. Kemistilehti B*, **33**, 104 (1960).

(28) F. E. Critchfield, J. A. Gibson, and J. L. Hall, *J. Amer. Chem. Soc.*, **75**, 1991 (1953).

(29) W. H. Carothers and F. J. Van Natta, *ibid.*, **52**, 314 (1930).

(30) S. J. Bass, W. I. Nathan, R. M. Meighan, and R. H. Cole, *J. Phys. Chem.*, **68**, 509 (1964).

(31) R. Payne and I. E. Theodorou, unpublished data.

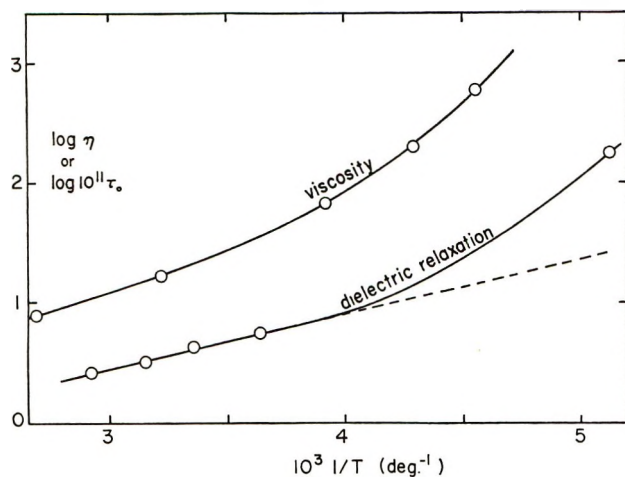


Figure 11. Arrhenius plots for dielectric relaxation and viscosity in propylene carbonate. Viscosity data taken from "Propylene Carbonate Technical Bulletin," Jefferson Chemical Co., Houston, Tex., 1962.

Liquids which are known to be associated, *e.g.*, *N*-methylformamide and ethanol, on the other hand generally have relaxation times an order of magnitude larger. However, the two examples cited also have correlation factors in the range 2–5 indicating far more extensive association than is likely to be present in the cyclic carbonates. The relaxation time for supercooled propylene carbonate at  $-78^\circ$  ( $1.3 \times 10^{-9}$  sec) is five orders of magnitude shorter than the value of  $1.89 \times 10^{-4}$  sec reported by Davidson and Cole<sup>20</sup> for propylene glycol at  $-75^\circ$  where a distribution of relaxation times was also found. The dispersion measurements therefore seem consistent with the inference drawn from the static dielectric constant measurements that significant intermolecular association is absent.

The temperature dependence of the relaxation time for propylene carbonate in the temperature range  $0$ – $70^\circ$  can be satisfactorily represented by the Arrhenius rate equation

$$\tau_0 = A \exp[-\Delta H^*/RT] \quad (18)$$

with a heat of activation ( $\Delta H^*$ ) of 2.1 kcal/mol and preexponential factor ( $A$ ) of  $1.23 \times 10^{-12}$  sec. However,  $\Delta H^*$  apparently increases at lower temperatures as shown by the deviation of the  $-78^\circ$  point from the straight line plot of  $\log \tau_0$  against  $1/T$  in Figure 11. The Arrhenius plot for the viscosity is markedly curved over the whole temperature range from  $-54$  to  $99^\circ$  (Figure 11). The apparent activation energy increases from a value of  $\sim 3$  kcal/mol at  $40^\circ$  to  $\sim 7$  kcal/mol at  $-40^\circ$ . This is substantially higher than the activation energy for the relaxation process as usually found.<sup>4</sup> Both the relaxation time and the viscosity can be fitted to an empirical expression of the form

$$\tau_0 = A \exp[B/(T - T_\infty)] \quad (19)$$

over the whole temperature range with  $B = 139^\circ\text{K}$  and  $T_\infty = 140^\circ\text{K}$  for the relaxation process and  $B = 187^\circ\text{K}$  and  $T_\infty = 150^\circ\text{K}$  for the viscosity. Equation 19 was previously applied by Davidson and Cole<sup>20</sup> to their low-temperature data for 1-propanol, propylene glycol, and glycerol where the constants  $B$  and  $T_\infty$  proved to be the same for viscous flow as for the dielectric relaxation process. In propylene carbonate, however, they appear to be significantly different. The significance of  $T_\infty$  according to eq 19 is that the relaxation time and the viscosity become infinite when  $T = T_\infty$ . This seems physically reasonable since supercooled propylene carbonate becomes highly viscous at temperatures below  $-50^\circ$  and forms a glassy solid below  $-100^\circ$ .

The correlation between the dielectric relaxation process and the viscosity can be further explored through Debye's hydrodynamic model of the dipole reorientation according to which the microscopic relaxation time is given by<sup>4</sup>

$$\tau_0 = 4\pi\eta a^3/kT \quad (20)$$

where  $\eta$  is the viscosity,  $a$  is the molecular radius, and  $k$  is the Boltzmann constant. Equation 20 is based on Stokes' calculation for motion of a spherical particle in a viscous medium and is therefore subject to the well-known uncertainties which arise when the particle is nonspherical and of molecular dimensions. A further difficulty is the unknown relationship between the microscopic relaxation time  $\tau_0$  and the measured relaxation time which depends on whether the local field acting on the dipole is taken as the Lorentz field or the Onsager field. On the reasonable assumption that the latter is more appropriate the value of  $\tau_0$  in eq 20 can be approximated by the measured relaxation time which together with the ordinary macroscopic viscosity leads to molecular radii of 1.7 Å for ethylene carbonate and 1.8 Å for propylene carbonate. The diameter of the ethylene carbonate ring along the direction of the dipole estimated from molecular models is  $\sim 6$  Å. The radii given by eq 20 are therefore smaller than expected although surprisingly close in view of the assumptions involved. The assumption of a Lorentzian field would reduce the value of  $\tau_0$  in eq 20 by a factor  $(\epsilon_\infty + 2)/(\epsilon_0 + 2)$  which would yield substantially lower values of the molecular radius.

In the absence of more detailed measurements at frequencies higher than 9 GHz, little discussion of the high-frequency dispersion is possible. The low-temperature measurements for propylene carbonate seem to indicate a central frequency approximately 30 times greater than that of the principal dispersion. Roughly 10% of the total dispersion is accounted for by the high-frequency dispersion.

## Second Virial Coefficients for the Polar Species in Steam

by R. F. Kubin<sup>1</sup>

Ames Research Center, National Aeronautics and Space Administration, Moffett Field, California 94035  
(Received March 15, 1972)

Publication costs assisted by Ames Research Center, National Aeronautics and Space Administration

Recent experimental *PVT* data on the second virial coefficients of steam over the temperature range 100–1000° have been fitted using both a Stockmayer and a modified Stockmayer potential that includes the dipole–quadrupole term. When the experimental value of the  $Q_{zz}$  component of the quadrupole moment tensor is used in the simplified potential function, the contribution from the dipole–quadrupole term to the second virial coefficient is found to be unimportant. The Stockmayer potential with parameters  $\mu = 1.86$  D,  $\sigma = 2.60$  Å, and  $\epsilon/k = 280^\circ\text{K}$  is found to fit the experimental values to 5% or better. The calculations were extended to OH–OH and OH–H<sub>2</sub>O interactions. For the latter case the formalism for computing the interaction virial coefficient to include the dipole–quadrupole terms is given. The second virial coefficients and their first and second temperature derivatives are given in tabular form from 100° to 2000°.

Recent work<sup>2</sup> using various curve fitting techniques for virial coefficients of steam provides little means for extending these results outside the range of experimental values. In the past, the virial equation of state has been used to provide more accurate thermodynamic calculations (*e.g.*, references 3 and 4a) over fairly wide temperature and pressure ranges. However, use of the virial equation of state implies some means of estimating the virial coefficients, usually only the second being used because of a lack of knowledge of even the two body forces involved in the multipole potential function expansion.

In estimating second virial coefficients for polar molecules, in particular, the Stockmayer potential<sup>4b</sup> and the Kihara core potential<sup>5</sup> have been applied with essentially equal success,<sup>6–8</sup> though Suh and Storvick<sup>6a</sup> have shown that the Kihara core potential provides a slightly better fit except for strongly polar molecules (including water). However, in the latter calculations cognizance was not taken of the reported<sup>7b</sup> importance of the dipole–quadrupole term in the potential. The Stockmayer potential as modified by Rowlinson<sup>7b</sup> to include this dipole–quadrupole term was found by him to provide good agreement with experimentally measured values of the second virial coefficient over the range 100–400° and is somewhat simpler to handle than the Kihara core potential. Using Rowlinson's method as outlined in Hirschfelder, Curtiss, and Byrd,<sup>9</sup> we have recalculated the second virial coefficient for the H<sub>2</sub>O–H<sub>2</sub>O interaction to high temperatures in light of newly available *PVT* data<sup>10,11</sup> and quadrupole moment data.<sup>12</sup> Since there are now available the highly accurate theoretical calculations (*e.g.*, the recent work of Moskowitz and coworkers<sup>13,14</sup>) having excellent agreement with the experimental work of Verhoeven and Dymanus,<sup>12</sup> evaluation of the dipole–quadrupole interaction effects is now possible.

Previous comparisons of experimental and calculated virial data for water have been made using the data of Keyes, *et al.*<sup>15</sup> Comparison of these data to those of Kell, McLaurin, and Whalley<sup>11</sup> shows a divergence of the values of  $B(T)$ , the second virial coefficient, at lower temperatures. This divergence has been explained as due to absorbed water in the Keyes experiments. Therefore, in this paper we have taken the

(1) Address correspondence to Propulsion Development Department, Naval Weapons Center, China Lake, Calif. 93555.

(2) (a) J. M. H. Levelt Sengers, M. Klein, and J. S. Gallagher, "Pressure-Volume-Temperature Relationships of Gases Virial Coefficients," AEDC-TR-71-39 (March 1971); (b) R. L. Halm and L. I. Stiel, *AIChE J.*, **17**, 259 (1971); (c) R. G. Kung and R. S. Kapner, *ibid.*, **17**, 562 (1971).

(3) (a) J. Hilsenrath and M. Klein, "Tables of Thermodynamic Properties of Air in Chemical Equilibrium Including Second Virial Corrections from 1500°K to 15,000°K," AEDC-TDR-63-161 (1963); (b) "Tables of Thermodynamic Properties of Nitrogen in Chemical Equilibrium Including Second Virial Corrections from 1500°K to 15,000°K," AEDC-TDR-63-162 (1963).

(4) (a) O. Sinanoglu, M. S. Vardya, E. M. Mortensen, and W. C. Johnson, Jr., *Phys. Fluids*, **5**, 665 (1962); (b) W. H. Stockmayer, *J. Chem. Phys.*, **9**, 398 (1941).

(5) (a) T. Kihara, *Rev. Mod. Phys.*, **25**, 831 (1953); (b) *Advan. Chem. Phys.*, **5**, 147 (1963).

(6) (a) K. W. Suh and T. S. Storvick, *J. Phys. Chem.*, **71**, 1450 (1967); (b) T. S. Storvick and T. H. Spurling, *ibid.*, **72**, 1821 (1968).

(7) (a) J. S. Rowlinson, *Trans. Faraday Soc.*, **45**, 974 (1949); (b) *ibid.*, **47**, 120 (1951).

(8) R. A. Svehla, *NASA Spec. Publ.*, 3011 (1964).

(9) J. O. Hirschfelder, C. F. Curtiss, and R. B. Bird, "Molecular Theory of Gases and Liquids," Wiley, New York, N. Y., 1954.

(10) S. Sugawara, T. Sato, and T. Minamiyama, *Bull. Jap. Soc. Mech. Engr.*, **7**, 136 (1964).

(11) G. S. Kell, G. E. McLaurin, and E. Whalley, *J. Chem. Phys.*, **48**, 3805 (1968).

(12) J. Verhoeven and A. Dymanus, *ibid.*, **52**, 3222 (1970).

(13) D. Neumann and J. W. Moskowitz, *ibid.*, **49**, 2056 (1968).

(14) D. Hankins, J. W. Moskowitz, and T. H. Stillinger, *ibid.*, **53**, 4544 (1970).

(15) (a) F. G. Keyes, L. B. Smith, and H. T. Gerry, *Proc. Amer. Acad. Arts Sci.*, **70**, 319 (1936); (b) S. C. Collins and F. G. Keyes, *ibid.*, **72**, 283 (1938).

work of Kell, *et al.*, as being more accurate and have determined the potential function parameters to fit these data. The data of Kell, *et al.*, cover the temperature range 150–450°; data for the temperature range 500–1000° are from Sugawara, Sato, and Minamiyama.<sup>10</sup>

These calculations have been extended to include OH–OH and OH–H<sub>2</sub>O pairwise interactions. For the latter interaction the formalism was extended to the case of unequal dipole and quadrupole moments in the potential function for the interacting species. Our initial objective was estimation of the thermodynamic properties for the high-temperature and low-pressure H<sub>2</sub>O system.

### Modified Stockmayer Potential

If we choose a central axis for each interacting species, for water this is the figure or dipole axis, and choose a model such that we have cylindrical symmetry, the quadrupole moment, which is really a tensor, can be expressed by a single moment. Then making the usual assumption of ideal point dipoles and quadrupoles, the Stockmayer potential with added dipole–quadrupole terms can be written for two unlike interacting species as

$$\Phi = 4\epsilon \left[ \left( \frac{\sigma}{r} \right)^{12} - \left( \frac{\sigma}{r} \right)^6 \right] \frac{\mu_1 \mu_2}{r^3} g(\theta_1, \theta_2, \phi_2 - \phi_1) + \frac{3\mu_1 Q_2}{2r^4} h_{12}(\theta_1, \theta_2, \phi_2 - \phi_1) - \frac{3\mu_2 Q_1}{2r^4} h_{21}(\theta_1, \theta_2, \phi_2 - \phi_1) \quad (1)$$

Here  $\mu_i$  is the dipole moment of species  $i$ ,  $Q_i$  the cylindrically symmetric quadrupole moment, and  $g$  and  $h_{ij}$  are the geometric orientation relations given by

$$g(\theta_1, \theta_2, \phi_2 - \phi_1) = 2 \cos \theta_1 \cos \theta_2 - \sin \theta_1 \sin \theta_2 \cos(\phi_2 - \phi_1) \quad (2)$$

and

$$h_{ij} = \frac{1}{2} [\cos \theta_i (3 \cos \theta_j - 1) - 2 \sin \theta_i \sin \theta_j \cos \theta_j \cos(\phi_2 - \phi_1)] \quad (3)$$

It is noted that because of the induced symmetry  $g$  and  $h$  are functions of only two of the Euler angles in each species and are independent of the third Euler angle. Figure 1 shows the coordinate system; the origins of the axes are at the centers of mass of each interacting species.

If in eq 1,  $\mu_1 = \mu_2$  and  $Q_1 = Q_2$  the resulting potential form is the same as given in ref 9 (except that the sign of the dipole–quadrupole term should be positive and not negative as it is given).

### Second Virial Coefficient

1. *H<sub>2</sub>O–H<sub>2</sub>O and OH–OH.* The second virial coefficient,  $B(T)$ , for the angle dependent potential (eq 1) is given by the expression

$$B(T^*) = -\frac{N_0}{4} \int_0^\infty \int_0^{2\pi} \int_0^\pi \int_0^\pi (e^{-\Phi/kT} - 1) r^2 \times \sin \theta_1 \sin \theta_2 d\theta_1 d\theta_2 d\phi dr \quad (4)$$

where  $d\phi = d(\phi_2 - \phi_1)$ . Equation 4 is evaluated by expansion of all but the repulsive term of the potential function of the exponential, followed by repeated application of the binomial theorem to obtain a product of series sums, then term by term integration, first over angles (which removes the divergence of the  $r^{-3}$  term), and finally integration over  $r$ . Using the common definition of parameters,  $T^* = kT/\epsilon$ ,  $l = \mu^2/(\sqrt{8}\epsilon\sigma^3)$ , and  $u = 3\mu Q/(\sqrt{32}\epsilon\sigma^4)$ , the second virial coefficient is

$$B(T^*) = b_0 \left( \frac{4}{T^*} \right)^{1/4} \left[ \Gamma \left( \frac{3}{4} \right) - \frac{1}{4} \sum_{m=1}^\infty \sum_{n=0}^m \sum_{l=0}^{\leq n/2} \times \frac{2^{(m-1/3)}}{m!} x \binom{m}{n} \binom{n}{2l} l^{n-2l} u^{2l} H_{nl} \Gamma \times \left( \frac{6m - 3n + 2l - 3}{12} \right) T^{*-(6m+3n-2l)/12} \right] \quad (5)$$

where  $\Gamma(x)$  is the  $\gamma$  function of  $\arg x$ , the notation  $\binom{j}{i}$  is a binomial coefficient, and  $b_0 = 2\pi N_0 \sigma^3/3$ . The  $H_{nl}$  are expansion coefficients as given in the Appendix. This expression for  $B(T^*)$  is an infinite series and could involve a large number of terms. In practice it was found that convergence of the series expression 5 was reasonably rapid for  $T^*$  in the range 1.2–10 such that for  $m$  (and hence  $n$ ) an upper limit of 25 in this range provided precision greater than that to which the data are known. For  $T^*$  less than 1.2 progressively more terms must be added, *e.g.*, for  $T^* = 0.8$ , 50 terms were required to achieve convergence to four places. As a further remark on eq 5, it is noted that if in the triple sum the terms for  $l = 0$  are separated out they give the dipole–dipole correction (the result of the Stockmayer potential) and the remaining terms give the dipole–quadrupole correction.<sup>16</sup> In making the calculation the dipole–dipole and the dipole–quadrupole terms

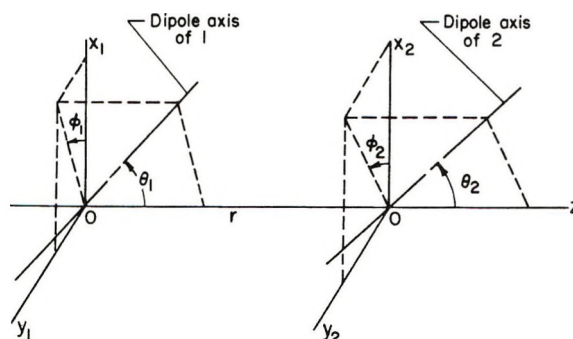


Figure 1. The coordinate system:  $\theta_i$  and  $\phi_i$  are usual spherical coordinates of the dipole axis of molecule  $i$ .

(16) There are several misprints in the dipole–quadrupole eq 3.10–20 of ref 9.

were evaluated separately in order to see the effect of the latter. It was found that the series expression for the contribution from the dipole-quadrupole term  $\Delta B(T^*)$  converges somewhat more rapidly than for the dipole-dipole term. Also since  $\Delta B(T^*)$  is only a small correction term, adequate precision even at the lower temperatures is obtained with the upper limit of  $m$  equal to 20 for this correction term.

2. *OH-H<sub>2</sub>O*. The treatment of the cross interaction OH-H<sub>2</sub>O again involves essentially the same procedure described above. When (1) is used in (4), the resulting expression one obtains for  $B(T^*)$  is

$$B(T^*) = b_0 \left( \frac{4}{T^*} \right)^{1/2} \left[ \Gamma \left( \frac{3}{4} \right) - \frac{1}{4} \sum_{m=1}^{\infty} \sum_{n=0}^m \sum_{l=0}^{\leq n/2} \sum_{q=0}^{2l} \times \right. \\ \left. \frac{(-1)^{q_2} 2^{m-l/3}}{(m-n)!(n-2l)!(2l-q)!} \times \right. \\ \left. t_{12}^{n-2l} u_{12}^{2l-q} u_{21}^q \Gamma \left( \frac{6m-3n+2l-3}{12} \right) \times \right. \\ \left. H_{nlq} T^{*-(6m+3n-2l)/12} \right] \quad (6)$$

where  $t_{12} = \mu_1 \mu_2 / (\sqrt{8\epsilon\sigma^3})$  and  $u_{ij} = 3\mu_i Q_j / (\sqrt{32\epsilon\sigma^4})$ . The expansion coefficients  $H_{nlq}$  are given by the expression

$$H_{nlq} = \frac{1}{8\pi} \int_0^{2\pi} \int_0^\pi \int_0^\pi q^{n-2l} h_{12}^{2l-q} h_{21}^q \times \\ \sin \theta_1 \sin \theta_2 d\theta_1 d\theta_2 d\phi \quad (7)$$

which can be expressed in analytic form similar to the  $H_{nl}$  (see Appendix). As can be seen, the numerical computation is increased, though it is noted that a great many of the  $H_{nlq}$  are zero. Here again the dipole-quadrupole correction can be separated and since this correction was found to be quite small, the upper limit on  $m$  was arbitrarily set to 10, providing a precision of three to four places in passing from low to high temperatures.

### Potential Function Parameters

The magnitude of the quadrupole moment depends on the choice of origin and the quadrupole definition, there being several of the latter in the literature. (See Buckingham<sup>17</sup> for a discussion of quadrupole moments.) We use the following definition of the quadrupole moment tensor

$$Q_{\alpha\beta} = \sum e_i (3\bar{r}_{i\alpha} \bar{r}_{i\beta} - r_i^2 \delta_{\alpha\beta}) \quad (8)$$

or its integral representation for a charge distribution. Here  $e_i$  is the magnitude of the  $i$ th charge and  $\bar{r}_i$  is its radius vector from the origin. This definition is the same as used by Hirschfelder, *et al.*,<sup>9</sup> but differs by a factor of 2 from that of Buckingham<sup>17</sup> and from that used in several theoretical papers<sup>13,14,18,19</sup> on water which contained calculated values of the quadrupole

moment tensor. In this work the factor  $1/2$  is included in the definition of  $h_{ij}$ , eq 3.

Initial results of this study, before the work of Verhoeven and Dymanus appeared, were based on a simple rotating water molecule<sup>7b,9</sup> and we mention it here because for this model we found  $Q_{zz} = -0.183 \times 10^{-26}$  esu cm<sup>2</sup> in fair agreement with the experimental value<sup>12</sup> of  $Q_{zz}$  of  $-0.266 \times 10^{-26}$  esu cm<sup>2</sup> (using our definition). We note here that while the potential function 1 assumes a cylindrically symmetric quadrupole, *i.e.*, one averaged over rotations about the  $z$  axis, such averaging has no effect on the value of  $Q_{zz}$ . Therefore we can compare values of the  $Q_{zz}$  component of the quadrupole moment tensor for cylindrically symmetric and unsymmetric models.

For the H<sub>2</sub>O-H<sub>2</sub>O interaction the dipole moment and the quadrupole moment are available from experiment. Thus (5) is a two-parameter equation (in  $\sigma$  and  $\epsilon$ ) to fit to the available experimental data. These were determined from a best fit to the data.

For the purpose of estimating its multipole moments, the OH radical is assumed to be represented by the two point charges separated by a distance  $l$ , equal to the spectroscopic bond distance as given by Herzberg<sup>20</sup> ( $0.9706 \times 10^{-8}$  cm). The dipole moment was taken from the work of Powell and Lide<sup>21</sup> whose careful measurement determined  $\mu$  to be  $1.66 \pm 0.01$  D. The quadrupole moment can now be estimated. Our estimate is quite large,  $Q_{zz} = 2.84 \times 10^{-26}$  esu/cm<sup>2</sup>. Since there are no experimental data the parameters  $b_o$  and  $\epsilon/k$  were determined by the methods of Woolley.<sup>22</sup> His rule applied to the OH-OH interaction takes the form

$$(\epsilon/k)_{O-O}(b_o^2)_{O-O} + 2(\epsilon/k)_{O-H}(b_o^2)_{O-H} + \\ (\epsilon/k)_{H-H}(b_o^2)_{H-H} = (\epsilon/k)_{OH-OH}(b_o^2)_{OH-OH} \quad (9)$$

The usual combinatorial rules were used to evaluate  $b_o$  and  $\epsilon/k$  for the OH-H<sub>2</sub>O interaction. That is,  $\sigma_{ij}$  was estimated using the arithmetic mean and  $\epsilon_{ij}$  was estimated using the geometric mean of the values for the single species interactions.

The potential function parameters are summarized in Table I.

### Results and Discussion

1. *Polar Forces*. The recent experimental<sup>12</sup> and theoretical<sup>13,14,18,19</sup> work already mentioned has ended speculation about various point charge models for water, at least from the standpoint of using them to

(17) A. D. Buckingham, *Chem. Soc., Quart. Rev.*, 183 (1959).

(18) S. Aung, R. M. Pitzer, and S. I. Chan, *J. Chem. Phys.*, **49**, 2071 (1968).

(19) C. W. Kern and R. L. Matcha, *ibid.*, **49**, 2081 (1968).

(20) G. Herzberg, "Molecular Structure and Molecular Spectra," Vol. I, Van Nostrand, New York, N. Y., 1950.

(21) F. X. Powell and D. R. Lide, Jr., *J. Chem. Phys.*, **42**, 4201 (1965).

(22) H. W. Woolley, "The Calculation of Thermodynamic Properties of Gases at High Temperature," AFSWC-TDR-62-21 (1962).

**Table I:** Parameters Used in the Potential Function

A. Values of Dipole and Quadrupole Moments			
	H <sub>2</sub> O	OH	
$\mu$ , D	1.86	1.66	
$Q$ , $10^{-26}$ esu cm <sup>2</sup>	-0.266	2.84	
B. Interaction Parameters			
	H <sub>2</sub> O-H <sub>2</sub> O	OH-OH	OH-H <sub>2</sub> O
$\sigma$ , Å	2.60	3.24	2.96
$\epsilon/k$ , °K	280	83.7	153

predict the quadrupole moment. Using the experimental value of  $Q_{zz}$  we find the contribution of the dipole-quadrupole term to be 1% or less over the entire temperature range, 100–1000°. The simplified rotating water model of our early calculations gives a similar result.

Rowlinson<sup>7b</sup> used a computed value of  $Q_{zz} = 1.81 \times 10^{-26}$  esu/cm<sup>2</sup> and found that the dipole-quadrupole term for H<sub>2</sub>O-H<sub>2</sub>O made an approximately 15% correction to his results. On this basis, he felt the derived parameters would be better even though the dipole-quadrupole correction did not improve his fit of the then known experimental  $B(T)$  values. The  $Q_{zz}$  component for water has been shown to be about an order of magnitude less than his estimate and does not affect the value of  $B(T)$ .

We also note that in eq 5 the terms involving the quadrupole moment appear as even powers only; thus  $B(T)$  is independent of the sign of the quadrupole moment. We point out that the early point charge models were all in error as to the correct sign of  $Q_{zz}$  and some cases an order of magnitude too large, which would overestimate the contribution of the dipole-quadrupole term. Additionally, this theory considers only approximate models that must be cylindrically symmetric; thus molecular geometry is omitted. Including this aspect, *i.e.*, all the components of the quadrupole moment tensor in eq 1 (and now we must consider the three Euler angles) results in a burdensome calculation. However, it is expected that the results of this improved calculation will not change the conclusions drawn in this paper.

For the OH-OH interaction a quadrupole moment has been determined for a very crude model and its value is probably just as unreliable as similar estimates were for water. This is true even though we have experimental data for the dipole moment. Nor are there reliable data on  $\sigma$  and  $\epsilon$ . The large quadrupole moment estimated here does make a noticeable contribution to the virial coefficient of approximately 20% at low temperatures, falling to less than 5% at 1000°. However, its use in estimating the virial coefficient is unjustified on other grounds too. An error of about

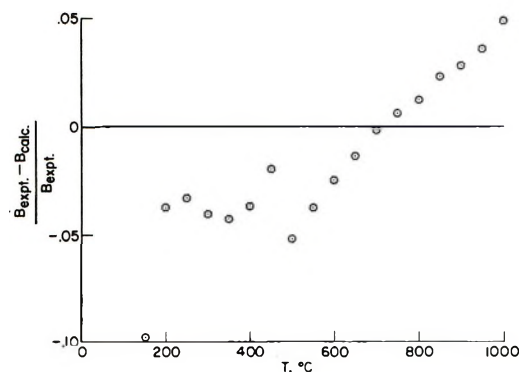


Figure 2. Comparison of experimental and calculated second virial coefficients.  $B_{\text{expt}}$  is the experimental value of  $B(T)$  and  $B_{\text{calc}}$  is the value calculated in this paper.

5% in the dipole moment introduces an uncertainty in the second virial coefficient approximately equal to that of the above estimated dipole-quadrupole term.

Again using the crude quadrupole moment of OH in the OH-H<sub>2</sub>O interaction estimate, the dipole-quadrupole term contribution was found to be on the order of 2% or less of  $B(T)$  over the entire temperature range. The correction to  $B(T)$  from the dipole-quadrupole terms in this case would be expected to be smaller than for OH-OH since the quadrupole for water is small and has been shown to make essentially no contribution to  $B(T)$  for H<sub>2</sub>O-H<sub>2</sub>O. Also there is a large change in  $\epsilon/k$  for OH-H<sub>2</sub>O over OH-OH contributing to the reduction of the contribution from the dipole-quadrupole terms to  $B(T^*)$ .

We find that the dipole-dipole term is the dominant one at the low temperatures contributing over 95% of the value of  $B(T)$  at 100° for the H<sub>2</sub>O-H<sub>2</sub>O interaction. Even at 1000°, its contribution to  $B(T)$  is about 40% greater than the contribution from the Lennard-Jones terms. In Figure 2 we have compared the experimental and calculated values of  $B(T)$ . This graph is particularly interesting in the lower region where the deviation is approximately constant at 4%. This observation strengthens the neglect of the dipole-quadrupole term in the very region where it would be expected to make its greatest contribution. The difficulty at the lowest temperature may be experimental since this is the most difficult experimental range. Both Keyes, *et al.*,<sup>15</sup> and Kell, *et al.*,<sup>11</sup> claim a precision greater than the difference in their results. At 150° Kell reports  $B(T) = 338$  cm<sup>3</sup>/mol and Keyes 284 cm<sup>3</sup>/mol and this theory gives a result in between, 305 cm<sup>3</sup>/mol.

In summary of the dipole-quadrupole term we find that in general for the steam system considered here if  $Q_{zz}$  is  $\sim 2 \times 10^{-26}$  esu cm<sup>2</sup> this term contributes on the order of 15% of the virial coefficient for the interaction of like species at low temperatures ( $\sim 100^\circ$ ) and this contribution will diminish to essentially nothing at high enough temperatures. We would expect the latter result since the dipole-quadrupole term corresponds

Table II: Second Virial Coefficients and Their Temperature Derivatives for H<sub>2</sub>O–H<sub>2</sub>O, OH–OH, and OH–H<sub>2</sub>O Interactions<sup>a</sup>

$T$ , °C	$-B(T)$ exptl <sup>b</sup>	H <sub>2</sub> O–H <sub>2</sub> O $-B(T)$	$T \frac{dB}{dT}$	$-T^2 \frac{d^2B}{dT^2}$	OH–OH $B(T)$	$T \frac{dB}{dT}$	$-T^2 \frac{d^2B}{dT^2}$	OH–H <sub>2</sub> O $B(T)$	$T \frac{dB}{dT}$	$-T^2 \frac{d^2B}{dT^2}$
100		510	$2.26 \times 10^3$	$1.52 \times 10^4$	-50.6	160	553	-128	372	$1.57 \times 10^3$
150	338	305	$1.16 \times 10^3$	$6.81 \times 10^3$	-33.2	118	392	-89.7	253	986
200	213.2	205	692	$3.65 \times 10^3$	-21.6	92.0	295	-65.5	185	679
250	153.1	148	461	$2.22 \times 10^3$	-13.3	74.0	231	-49.1	143	500
300	116.8	112	331	$1.48 \times 10^3$	-7.12	61.1	188	-37.4	115	386
350	91.95	88.0	250	$1.05 \times 10^3$	-2.43	51.4	156	-28.6	94.7	309
400	73.54	70.8	197	$7.85 \times 10^2$	1.25	44.0	132	-21.9	79.8	254
450	59.15	58.0	160	$6.10 \times 10^2$	4.18	38.1	114	-16.6	68.4	213
500	50.79	48.2	134	$4.90 \times 10^2$	6.57	33.4	99.5	-12.4	59.4	183
550	42.07	40.5	113	$4.03 \times 10^2$	8.53	29.5	87.8	-8.87	52.3	158
600	35.17	34.3	97.8	$3.38 \times 10^2$	10.2	26.2	78.2	-5.97	46.4	139
650	29.60	29.2	85.5	$2.89 \times 10^2$	11.7	23.5	70.1	-3.52	41.6	124
700	25.04	25.0	75.6	$2.50 \times 10^2$	12.7	21.2	63.3	-1.44	37.5	111
750	21.26	21.4	67.4	$2.19 \times 10^2$	13.7	19.1	57.5	0.352	34.0	99.8
800	18.07	18.3	60.6	$1.94 \times 10^2$	14.6	17.4	52.6	1.90	31.0	90.6
850	15.35	15.7	55.0	$1.73 \times 10^2$	15.4	15.8	48.2	3.25	28.4	82.7
900	13.03	13.4	50.1	$1.56 \times 10^2$	16.0	14.5	44.4	4.44	26.1	76.0
950	10.99	11.4	45.9	$1.41 \times 10^2$	16.6	13.3	41.1	5.49	24.1	70.0
1000	9.21	9.65	42.2	$1.29 \times 10^2$	17.1	12.2	38.1	6.42	22.4	64.9
1100		6.69	36.2	$1.09 \times 10^2$	18.0	10.4	33.1	8.00	19.4	56.2
1200		4.31	31.5	93.4	18.6	8.87	29.0	9.28	17.0	49.3
1300		2.37	27.7	81.3	19.2	7.62	25.6	10.3	15.0	43.7
1400		0.763	24.6	71.7	19.6	6.56	22.8	11.2	13.3	39.0
1500		+0.590	22.1	63.8	20.0	5.66	20.4	11.9	11.9	35.1
1600		1.74	19.9	57.2	20.3	4.89	18.4	12.5	10.6	31.8
1700		2.73	18.0	51.8	20.5	4.21	16.6	13.1	9.60	29.0
1800		3.58	16.5	47.1	20.7	3.62	15.1	13.5	8.68	26.5
1900		4.32	15.1	43.1	20.9	3.10	13.7	13.9	7.87	24.4
2000		4.97	13.9	39.6	21.0	2.64	12.5	14.2	7.15	22.5

<sup>a</sup> Units are cm<sup>3</sup>/mol. <sup>b</sup> The data through 450° are from ref 11 and from 500 to 1000° from ref 10.

to long-range forces and the high-temperature region is the domain of short-range forces. For the H<sub>2</sub>O–H<sub>2</sub>O interaction, the measured  $Q_{22}$  component is so small that the contribution from this term can be neglected.

2. *Derived Potential Parameters.* Comparison of the calculated values of  $B(T)$  with Sugawara, *et al.*,<sup>10</sup> in the temperature range above 500° shows a deviation ranging from -5 to +5%. With the present limited theory this variation could be reduced only at the expense of the low-temperature fit, tending toward the values of Keyes. However, we said we feel the work of Kell, *et al.*, to be the more accurate. Actually in the higher temperature region exchange forces are becoming important and their effect is inadequately taken into account through  $\epsilon/k$  and  $\sigma$ . Also in this region the Lennard-Jones part of the potential is becoming increasingly important and this potential in general has too narrow a potential well, *i.e.*, the radial dependence is not correct. Thus the regular, almost linear, difference between experiment and calculation may be the result of use of the Stockmayer potential.

Rowlinson fitted his modified Stockmayer potential to the then available limited range of experimental values for the H<sub>2</sub>O–H<sub>2</sub>O interaction. He determined

$\sigma = 2.725 \text{ \AA}$  and  $\epsilon/k = 356^\circ\text{K}$  for this potential and  $\sigma = 2.65 \text{ \AA}$  and  $\epsilon/k = 380^\circ\text{K}$  for the Stockmayer potential. We find that the Stockmayer potential fits a large (900°) temperature range with  $\sigma = 2.60 \text{ \AA}$  and  $\epsilon/k = 280^\circ\text{K}$ . The lowering of  $\epsilon/k$  over that of Rowlinson is fairly large and even larger compared to the value of 506°K recommended by Monchick and Mason.<sup>23</sup> Our value does fall within the estimated range for  $\epsilon/k$  given by these authors. Rowlinson's remarks<sup>7a</sup> concerning the interpretation of  $\epsilon/k$  are pertinent to the low-temperature region. He has shown that when the total interaction energy becomes large compared to  $\epsilon$ , *i.e.*, for this case when the dipole-dipole energy becomes large compared to the contribution from the nonpolar forces (measured by  $\epsilon$ ) the accuracy of the determination of  $\epsilon$  suffers. However, in this study the high-temperature data provide more information on  $\epsilon$ . At the highest experimental temperature (1000°) the nonpolar forces are contributing 40% to  $B(T)$ . Therefore, the accuracy of  $\epsilon$  is improved over prior results. We note that the actual well depth is orientation dependent and the value determined here corresponds to an integrated average.

(23) L. Monchick and E. A. Mason, *J. Chem. Phys.*, **35**, 1676 (1961).

**Table III:** Values of the Joule-Thomson Coefficient<sup>a</sup>

$T, ^\circ\text{C}$	Exptl	This work <sup>b</sup>	Ref 11 <sup>b,c</sup>	Ref 15 <sup>b,c</sup>
150	3.81	4.23	[5.10] <sup>f</sup>	3.44
200	2.52 <sup>d</sup>	2.56	2.60	2.20
260	1.68	1.64		
300	1.25	1.23	1.28	1.20
350	0.97 <sup>e</sup>	0.92	1.02	

<sup>a</sup> Units are  $^\circ\text{C}/\text{bar}$ . <sup>b</sup>  $C_p$  data taken from the steam tables, ref 25. <sup>c</sup>  $\text{dB}/\text{dT}$  determined graphically. <sup>d</sup> This value is for  $T = 196^\circ$ . <sup>e</sup> This value is for  $T = 347^\circ$ . <sup>f</sup> See text.

The inclusion of higher multipole terms to the Lennard-Jones 12-6 potential has proven to be practical even for the highly polar water molecule. Only one such term is required to give essential agreement with experiment in this lower temperature region where the multipole expansion is still valid.

3.  $B(T)$  Tables. Table II gives the estimated second virial coefficients and their first and second temperature derivatives for  $\text{H}_2\text{O}-\text{H}_2\text{O}$ ,  $\text{OH}-\text{OH}$ , and  $\text{OH}-\text{H}_2\text{O}$  interactions up to  $2000^\circ$ . This table is based on the Stockmayer potential only. We have included the temperature derivatives in order that thermodynamic quantities may be calculated directly. The first derivative provides a further test of the potential function. At relatively low pressures the Joule-Thomson coefficient can be expressed as

$$\mu_{\text{JT}} = -\frac{1}{C_p} \left[ B - T \frac{\text{dB}}{\text{dT}} \right] \quad (10)$$

where  $B$  is the second virial coefficient  $B(T)$  and  $C_p$  is the constant pressure heat capacity. In Table III we have compared the experimental data for  $\mu_{\text{JT}}$  with values calculated in this work and from the experimental virial coefficient data of ref 11 and 15. In the latter cases we had to estimate  $\text{dB}/\text{dT}$  graphically and the comparison suffers from errors in that method. The error is quite noticeable in the value of  $\mu_{\text{JT}}$  at  $150^\circ$  estimated from the work of Kell, *et al.*,<sup>11</sup> since this point is the end point of the graph. Thus still unresolved are which low-temperature  $B(T)$  data are the better, *i.e.*, Kell, *et al.*,<sup>11</sup> or Keyes, *et al.*<sup>15</sup>

The experimental  $\mu_{\text{JT}}$  values used in Table III are from the work of Juza as given by Potter<sup>24</sup> and the work of Davis and Kleinschmidt as given in the steam tables.<sup>25</sup> The  $C_p$  data used were also taken from the steam tables.<sup>25</sup>

*Acknowledgment.* The author wishes to thank Mrs. D. Lyon and especially Mrs. E. Williams for their assistance in the computer programming for this work.

## Appendix

The expansion coefficients  $H_{nl}$  are given by the expression

$$H_{nl} = \frac{1}{8\pi} \int_0^{2\pi} \int_0^\pi \int_0^\pi g^{n-2l} h^{2l} \times \sin \theta_1 \sin \theta_2 \, d\theta_1 \, d\theta_2 \, d\phi \quad (\text{A-1})$$

where as in the text  $d\phi = d(\phi_2 - \phi_1)$ . The usual method of evaluation is using the binomial theorem followed by integration. If the terms for  $l = 0$  are evaluated separately, a simple expression is obtained ( $n$  must be even or the integral in (A-1) is zero for this case).

$$H_{no} = G_k = \frac{(k+1)}{(2k+1)\Gamma[k+(3/2)]} \times \sum_{q=0}^k \frac{2^{2q-1}\Gamma[g+(1/2)]}{\Gamma(g+1)} \quad (\text{A-2})$$

where  $k = n/2$  for  $n$  even. The coefficients in (A-2) are just those for the dipole-dipole interaction alone. The complete expression for the  $H_{nl}$ <sup>26</sup> is

$$H_{nl} = \frac{1}{4} \sum_{p=0}^{n-2l} \sum_{q=0}^{2l} \sum_{r=0}^{2l} \sum_{s=0}^{2l-r} (-1)^{p+q+r} \left(\frac{1}{2}\right)^{k-2p} 3^s \times \frac{(n-2l)!(2l)!(n-2l-p+r)!}{p!q!r!s!(n-2l-p)!(2l-q)!(2l-r-s)!} \times \frac{\Gamma\left(\frac{p+q+s+1}{2}\right)\Gamma\left(\frac{2l+p-q+s+1}{2}\right)}{\Gamma\left(\frac{n-2l+q+r+s+3}{2}\right)\Gamma\left(\frac{k-q+r+s}{2}\right)} \quad (\text{A-3})$$

where  $x!$  is the factorial function of  $x$ .

Similar considerations apply to the evaluation of (7) in the text except that the result is quite involved and requires a large amount of computation. The final result is

$$H_{nlq} = \frac{1}{4} \sum_{r=0}^{n-2l} \sum_{s=0}^{2l-q} \sum_{t=0}^{2l-q-s} \sum_{u=0}^q \sum_{v=0}^{q-u} (-1)^{t+v} \times (2)^{n-4t-2r} (3)^{2l-s-t-u-v} x \binom{n-2l}{r} \times \binom{r+s+u}{(r+s+u)/2} \binom{2l-q}{s} \times \binom{2l-q-s}{t} \binom{q}{u} \binom{q-u}{v} \times \left[ \frac{\Gamma\left(\frac{r+s+u+1}{2}\right)^2 \Gamma\left(\frac{n+q-r-s-u-2v+1}{2}\right)}{\Gamma\left(\frac{n+2l-q-r-s-2t-u+1}{2}\right)} \right] \frac{\Gamma\left(\frac{n+q-2v+2}{2}\right)\Gamma\left(\frac{n+2l-q-2t+2}{2}\right)}{\Gamma\left(\frac{n+q-2v+2}{2}\right)\Gamma\left(\frac{n+2l-q-2t+2}{2}\right)} \quad (\text{A-4})$$

(24) J. H. Potter, *J. Eng. Ind.*, **92**, 257 (1970).

(25) J. H. Keenan, F. G. Keyes, P. G. Hill, and J. G. Moore, "Steam Tables," International ed, Wiley, New York, N. Y., 1969.

(26) The first few of these coefficients as given in Table 3. 10-6 of ref 9 are all in error, being exactly four times too large.

Strong Crystalline Field Perturbation Calculations for  $d^3, d^7$ 

## Pentacoordinate Complexes. I. The Trigonal Bipyramid

by J. A. Varga and C. A. L. Becker\*

*Department of Chemistry, The University of Texas, Austin, Texas 78712 (Received January 24, 1972)**Publication costs assisted by The Petroleum Research Fund*

Crystal field theory within the context of the strong-field approximation is used to treat the  $d^3, d^7$  system in a trigonal bipyramidal environment. The strong-field basis functions are taken as Slater determinants, and the  $D_{3h}$  crystalline field symmetry eigenfunctions specified as individual members of this basis set or linear combinations thereof. Although spin is only implicitly included, the two distinct types of doublet wave functions for three particles of half-integral spin are successfully identified. The crystalline field and Coulombic perturbation energy matrices are calculated in the limit of zero spin-orbit coupling. All such matrices are shown to be consistent with results available from the weak-field limit. Numerical values are substituted into the parametric form of the perturbation matrices. The resulting energies of the strong crystalline field states are presented in the form of an energy level diagram in order to discuss the expected spectroscopic behavior of a  $d^7$  trigonal bipyramidal system.

## Introduction

Crystal-field calculations of varying degrees of complexity have been carried out for most  $d^n$  configurations. Although both the weak- and strong-field approximations are well represented, the majority of the existent calculations pertain to systems of octahedral geometry or derivable therefrom.<sup>1,2</sup> Noncubic calculations (*i.e.*, not based on cubically disposed eigenfunctions) have focused on  $d^n$  systems in a trigonal bipyramidal environment. Simple crystal-field calculations are available for the atomic  $d$  orbitals (and the  $d^9$  system *via* the hole formalism)<sup>3,4</sup> as well as the  $d^2, d^8$  system.<sup>4</sup> Becker, Meek, and Dunn have extended the treatment of the  $d^1, d^9$  and  $d^2, d^8$  configurations to include spin-orbit coupling as well as both weak and strong crystalline field effects.<sup>5</sup> For the remaining  $d^n$  configurations, available calculations have been based on the weak crystalline field formalism. Norgett, Thornley, and Venanzi<sup>6</sup> have calculated the splitting of the free ion terms for  $d^{6-8}$  systems subjected to a weak crystalline field from which they constructed energy level diagrams for discussing spectroscopic data. Wood<sup>7</sup> has published energy level diagrams for the  $d^2, d^8$  and  $d^3, d^7$  systems and has discussed the magnetic properties of the  $d^{1-4}$  and  $d^{6-9}$  configurations including spin-orbit coupling effects.

Trigonal bipyramidal coordination has been well established for the  $d^8$  ions, Ni(II), Pd(II), Pt(II), and Co(I).<sup>8,9</sup> Recently, however, trigonal bipyramidal complexes of the  $d^7$  ion Co(II) have been prepared with ligands capable of producing a strong crystalline field and are receiving serious consideration.<sup>10-12</sup> The present calculation formulates the  $d^3, d^7$  system within the context of the strong crystalline field approxima-

tion. In the limit of vanishingly small spin-orbit interaction, the appropriate Hamiltonian consists of a crystalline field potential and the electron-electron repulsion operator

$$\mathcal{H} = V_{CF}(r, \theta, \phi) + \sum_{i < j}^3 \frac{e^2}{r_{ij}} \quad (1)$$

An electron within a trigonal bipyramidal crystalline field, as shown in Figure 1, is subject to a potential which, in the ionic model system of calculation,<sup>13</sup> has the explicit form

- (1) A. D. Liehr, *J. Phys. Chem.*, **64**, 43 (1960); **67**, 1314 (1963).
- (2) J. Perumareddi, *ibid.*, **71**, 3144 (1967), and references therein.
- (3) P. Day, *Proc. Chem. Soc., London*, 18 (1964).
- (4) M. Ciampolini, *Inorg. Chem.*, **5**, 35 (1966).
- (5) (a) C. A. L. Becker, D. W. Meek, and T. M. Dunn, *J. Phys. Chem.*, **72**, 3588 (1968); (b) *ibid.*, **74**, 1568 (1970).
- (6) (a) M. J. Norgett, J. H. M. Thornley, and L. M. Venanzi, *J. Chem. Soc. A*, 540 (1967); (b) see also the refined extension of this work, M. J. Norgett and L. M. Venanzi, *Inorg. Chim. Acta*, **2**, 107 (1968).
- (7) (a) J. S. Wood, *Inorg. Chem.*, **7**, 852 (1968); (b) *ibid.*, **8**, 491 (1969); (c) *J. Chem. Soc. A*, 1582 (1969).
- (8) R. L. Dutta, D. W. Meek, and D. H. Busch, *Inorg. Chem.*, **9**, 1215 (1970); **9**, 2098 (1970); and references contained therein.
- (9) F. A. Cotton, T. G. Dunne, and J. S. Wood, *ibid.*, **4**, 318 (1965).
- (10) D. W. Meek, data reported in part at the 162nd National Meeting of the American Chemical Society, Washington, D. C., Sept 1971, Abstract No. 96 (inorganic division); *Inorg. Chem.*, submitted for publication.
- (11) L. Sacconi, data reported in part at the 162nd National Meeting of the American Chemical Society, Washington, D. C., Sept 1971, Abstract No. 95 (inorganic division).
- (12) C. A. L. Becker, data reported in part at the 162nd National Meeting of the American Chemical Society, Washington, D. C., Sept 1971, Abstract No. 106 (inorganic division).
- (13) T. M. Dunn, D. S. McClure, and R. G. Pearson, "Some Aspects of Crystal Field Theory," Harper and Row, New York, N. Y., 1965, Chapter 1.

$$V_{CF}(r,\theta,\phi) = e^2 \left[ \frac{3Z_E}{a} + \frac{2Z_A}{b} + \frac{(9x^2 + 9y^2 - 6r^2)Z_E}{4a^3} + \frac{(3z^2 - r^2)Z_A}{b^3} + \frac{(15x^3 - 45xy^2)Z_E}{8a^4} + \frac{(315[x^4 + 2x^2y^2 + y^4] - 360r^2[x^2 + y^2] + 72r^4)Z_E}{65a^5} + \frac{(35z^4 - 30z^2r^2 + 3r^4)Z_A}{4b^5} \right] \quad (2)$$

For the case of a regular trigonal bipyramid ( $Z_E \equiv Z_A$  and  $a \equiv b$ ), this potential becomes<sup>5a</sup>

$$V_{CF}(r,\theta,\phi) = \frac{Ze^2}{a} \left[ 5 + \frac{9x^2 + 9y^2 + 12z^2 - 10r^2}{4a^2} + \frac{15x^3 - 45xy^2}{8a^5} + \frac{315(x^4 + 2x^2y^2 + y^4) + 560z^4 + 120r^2(r^2 - 3x^2 - 3y^2 - 4z^2)}{64a^4} \right] \quad (3)$$

In order to maintain agreement with previous  $D_{3h}$  calculations, as, for example, according to Wood,<sup>7a</sup> the crystalline field parameters are taken as

$$D_s = \frac{Ze^2}{14a^3} \langle r^2 \rangle \quad (4a)$$

and

$$D_t = \frac{25Ze^2}{168a^5} \langle r^4 \rangle \quad (4b)$$

in which case, the non-vanishing one-electron matrix elements become

$$\begin{aligned} \langle 2, \pm 2 | V_{CF}(r,\theta,\phi) | \pm 2, 2 \rangle &= \epsilon_0 - 2D_s + Dt \\ \langle 2, \pm 1 | V_{CF}(r,\theta,\phi) | \pm 1, 2 \rangle &= \epsilon_0 + D_s - 4Dt \\ \langle 2, 0 | V_{CF}(r,\theta,\phi) | 0, 2 \rangle &= \epsilon_0 + 2D_s + 6Dt \end{aligned} \quad (5)$$

Spectroscopic data for trigonal bipyramidal complexes of Cu(II)<sup>14</sup> and Ni(II)<sup>6,15</sup> suggest that  $D_t > D_s$ . Therefore, the ordering of the one-electron crystalline field energy levels is clearly  $e''(\phi_{\pm 1}) < e'(\phi_{\pm 2}) \ll a_1'(\phi_0)$ .

The crystalline field treatment of the  $d^3, d^7$  system involves the determination of multi-electron strong crystalline field basis functions, construction of the symmetry eigenfunctions, and, finally, calculation of the perturbation energy matrices in parametric form. From these matrices energy level diagrams are then obtainable upon substitution of actual numerical values for the various parameters.

### Basis Functions

The strong-field basis functions are of the one-electron product type, *i.e.*, Slater determinants constructed from one-electron energy levels. Three electrons may occupy the trigonal bipyramidal one-electron energy levels in the nine different configurations:  $[(e'')^3]$ ,  $[(e'')^2(e')]$ ,  $[(e'')(e')^2]$ ,  $[(e')^3]$ ,  $[(e'')^2(a_1')]$ ,  $[(e'')(e')-(a_1')]$ ,  $[(e')^2(a_1')]$ ,  $[(e'')(a_1')^2]$ , and  $[(e')(a_1')^2]$ . The basis functions are obtained by assembling the one-electron energy levels corresponding to each of the configurations into a Slater determinant:  $|\phi_i(1)\phi_j(2)-\phi_k(3)|$ , where electron 1 occupies energy level  $i$ ; electron 2, energy level  $j$ ; and electron 3, energy level  $k$ . Spin is implicitly included to distinguish between quartets,

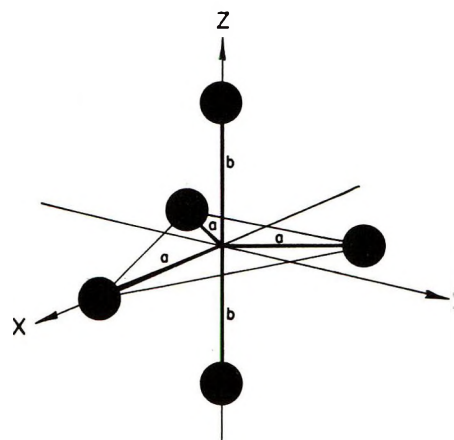


Figure 1. Trigonal bipyramidal coordination sphere.

$|\phi_i^+(1)\phi_j^+(2)\phi_k^+(3)|$ , and doublets,  $|\phi_i^+(1)\phi_j^+(2)\phi_k^-(3)|$  (including the allowed permutations of two like and one unlike spin among  $\phi_i$ ,  $\phi_j$ , and  $\phi_k$ ).

By standard group theoretical methods,<sup>16,17</sup> it is possible to deduce the symmetries of the states belonging to each of the nine configurations. The multiplicities of the states are tentatively assigned by distributing the total (spin and orbital) multiplicity of a given configuration among the several states arising therefrom. For cases in which more than one assignment is possible, correlation with the weak-field limit removes the ambiguity, since the strong- and weak-field states must be isomorphic. By such methods the  $d^3$  strong field states under trigonal bipyramidal geometry ( $D_{3h}$  symmetry) were determined to possess the symmetries and multiplicities listed in Table I. The weak-field states are shown also for comparison.

The construction of the symmetry eigenfunctions depends ultimately on the transformation properties of the three-electron basis functions. Application of the appropriate  $D^2(\alpha,\beta,\gamma)$  matrices<sup>5b</sup> to the orbital

(14) G. C. Allen and N. S. Hush, *Inorg. Chem.*, **6**, 4 (1967).

(15) G. S. Benner, W. E. Hatfield, and D. W. Meek, *ibid.*, **3**, 1544 (1964).

(16) F. A. Cotton, "Chemical Applications of Group Theory," Interscience, New York, N. Y., 1963, Chapters 5 and 8.

(17) M. Tinkham, "Group Theory and Quantum Mechanics," McGraw-Hill, New York, N. Y., 1964, Chapter 3.

**Table I:** Correlation of the  $d^3$  Weak- and Strong-Field States in a Trigonal Bipyramidal ( $D_{3h}$ ) Environment

$d^3$	Total multiplicity <sup>a,b</sup>	Symmetry states										
		${}^2A_1'$	${}^2A_2'$	${}^2E'$	${}^2A_1''$	${}^2A_2''$	${}^2E''$	${}^4A_2'$	${}^4E'$	${}^4A_1''$	${}^4A_2''$	${}^4E''$
Strong-Field Configuration												
$[(e'')^3] \equiv [(e'')]^c$	4						1					
$[(e'')^2(e')]$	24	1	1	3				1				
$[(e'')(e')^2]$	24				1	1	3					1
$[(e'')^2(a_1')]$	12	1	1	1				1				
$[(e'')(e')(a_1')]$	32				2	2	2			1	1	1
$[(e'')(a_1')^2]$	4						1					
$[(e')^3] \equiv [(e')]^c$	4			1								
$[(e')^2(a_1')]$	12	1	1	1				1				
$[(e')(a_1')^2]$	4			1								
$\Sigma$	120	3	3	7	3	3	7	2	1	1	1	2
Weak-Field Terms												
${}^3P$	6		1				1					
${}^3D + {}^3D$	20	2		2			2					
${}^3F$	14		1	1	1	1	1					
${}^3G$	18	1		2	1	1	1					
${}^3H$	22		1	2	1	1	2					
${}^4P$	12							1				1
${}^4F$	28							1	1	1	1	1
$\Sigma$	120	3	3	7	3	3	7	2	1	1	1	2

<sup>a</sup> Total multiplicity = (spin degeneracy)  $\times$  (orbital degeneracy). <sup>b</sup> Strong-field total multiplicity

$$\prod_{q=a_1', e', e''} q[C_r] = \prod_{q=a_1', e', e''} q \left[ \frac{(r-1)(r-2)\dots(r-n+1)}{n!} \right]$$

where  $r$  is the number of spin orbitals available to the  $n$  electrons in the  $q$ th energy level. For  $q = a_1'$ ,  $r = 2$ ; for  $q = e', e''$ ,  $r = 4$ . <sup>c</sup> Since an  $e$  level is exactly half-filled with two electrons, the three electron configuration must be treated *via* the hole formalism, *i.e.*,  $[(e)^3] \equiv [(e)]$ .

portion of the basis functions (the spin being unaffected) generates the rotation characters of each member of the basis set. Linear combinations of the basis functions are then taken, where necessary, to reproduce the symmetries required for the various  $d^3$  strong-field states.

The identification of the  $d^3$  symmetry eigenfunctions as individual members of the basis set, or linear combinations thereof, proceeds quite straightforwardly for those configurations from which only doublets can arise:  $[(e'')^3]$ ,  $[(e')^3]$ ,  $[(e'')(a_1')^2]$ , and  $[(e')(a_1')^2]$ . For the remaining configurations  $[(e'')^2(a_1')]$ ,  $[(e')^2(a_1')]$ ,  $[(e'')(e')(a_1')]$ ,  $[(e'')^2(e')]$ , and  $[(e'')(e')^2]$ , however, a caveat is in order. To accommodate the orbital degeneracy of these configurations more than one type of doublet is necessary. Use of the Löwdin projection operator according to standard procedures<sup>18-20</sup> readily generates the two orthonormal doublet wave functions

$$\begin{aligned} & 1/\sqrt{6}[2|\phi_a^\beta \phi_b^\alpha \phi_c^\alpha\rangle - |\phi_a^\alpha \phi_b^\beta \phi_c^\alpha\rangle - |\phi_a^\alpha \phi_b^\alpha \phi_c^\beta\rangle] \\ & 1/\sqrt{6}[2|\phi_a^\alpha \phi_b^\beta \phi_c^\beta\rangle - |\phi_a^\beta \phi_b^\alpha \phi_c^\beta\rangle - |\phi_a^\beta \phi_b^\beta \phi_c^\alpha\rangle] \quad (6) \end{aligned}$$

and

$$\begin{aligned} & 1/\sqrt{2}[|\phi_a^\alpha \phi_b^\beta \phi_c^\alpha\rangle = |\phi_a^\alpha \phi_b^\alpha \phi_c^\beta\rangle] \\ & 1/\sqrt{2}[|\phi_a^\beta \phi_b^\alpha \phi_c^\beta\rangle - |\phi_a^\beta \phi_b^\beta \phi_c^\alpha\rangle] \quad (7) \end{aligned}$$

Hereafter, those doublets with  $1/\sqrt{6}$  normalization factor will be termed type I; those with  $1/\sqrt{2}$ , type II.

The symmetry eigenfunctions obtained for the  $d^3$  case are listed in Table II. It should be noted, however, that for those wave functions arising from the  $[(e'')(e')(a_1')]$  configuration symmetry arguments indicate that the choice of the particular three-electron basis function to appear with coefficient  $2/\sqrt{6}$  in the type I doublet is perfectly arbitrary provided the remaining members of the basis are completely distributed between the type I and type II doublets. The  ${}^2A_1''$ ,  ${}^2A_2''$ , and  ${}^2E''$  eigenfunctions from  $[(e'')(e')(a_1')]$  listed in Table II are those which give all integral coefficients in the diagonal Coulombic matrix elements. Alternate choices, which give fractional coefficients, could also be used since the effective Coulombic perturbation (*i.e.*, net perturbation due to combined diagonal and off-diagonal terms) is identical in all cases.

(18) P. O. Löwdin, *Phys. Rev.*, **97**, 1509 (1955).

(19) A. Carrington and A. D. McLachlan, "Introduction to Magnetic Resonance," Harper and Row, New York, N. Y., 1967, Appendix C.

(20) M. J. S. Dewar, "The MO Theory of Organic Chemistry," McGraw-Hill, New York, N. Y., 1969, pp 254-268.

**Table II:**  $D_{3h}$  Strong-Field Wave Functions for the  $d^3$  Configuration

$(e'')^3 \equiv (e'')$	${}^2E''$	$ \phi_1^+\phi_1^-\phi_{-1}^+ ,  \phi_1^+\phi_{-1}^-\phi_{-1}^+ $	$\Psi_8$
$(e'')(a_1')^2$	${}^2E''$	$ \phi_1^+\phi_0^-\phi_0^+ ,  \phi_0^+\phi_0^-\phi_{-1}^+ $	$\Psi_9$
$(e')(a_1')^2$	${}^2E'$	$ \phi_2^+\phi_0^-\phi_0^+ ,  \phi_0^+\phi_0^-\phi_{-2}^+ $	$\Psi_{10}$
$(e')^3 \equiv (e')$	${}^2E'$	$ \phi_2^+\phi_2^-\phi_{-2}^+ ,  \phi_2^+\phi_{-2}^-\phi_{-2}^+ $	$\Psi_{11}$
$(e'')^2(a_1')$	${}^4A_2'$	$ \phi_1^+\phi_0^+\phi_{-1}^+ $	$\Psi_{12}$
	${}^2E'$	$ \phi_1^+\phi_1^-\phi_0^+ ,  \phi_0^+\phi_{-1}^-\phi_{-1}^+ $	$\Psi_{13}$
	${}^2A_2'$	$1/\sqrt{6}[2 \phi_1^+\phi_0^-\phi_{-1}^+  -  \phi_1^+\phi_0^+\phi_{-1}^-  -  \phi_1^-\phi_0^+\phi_{-1}^+ ]$	$\Psi_{14}$
	${}^2A_1'$	$1/\sqrt{2}[ \phi_1^+\phi_0^+\phi_{-1}^-  -  \phi_1^-\phi_0^+\phi_{-1}^+ ]$	$\Psi_{15}$
	${}^4A_2'$	$ \phi_2^+\phi_0^+\phi_{-2}^+ $	$\Psi_{16}$
	${}^2E'$	$ \phi_2^+\phi_2^-\phi_0^+ ,  \phi_0^+\phi_{-2}^-\phi_{-2}^+ $	$\Psi_{17}$
	${}^2A_2'$	$1/\sqrt{6}[2 \phi_2^+\phi_0^-\phi_{-2}^+  -  \phi_2^+\phi_0^+\phi_{-2}^-  -  \phi_2^-\phi_0^+\phi_{-2}^+ ]$	$\Psi_{18}$
	${}^2A_1'$	$1/\sqrt{2}[ \phi_2^+\phi_0^+\phi_{-2}^-  -  \phi_2^-\phi_0^+\phi_{-2}^+ ]$	$\Psi_{19}$
$(e'')^2(e')$	${}^4E'$	$ \phi_2^+\phi_1^+\phi_{-1}^+ ,  \phi_1^+\phi_{-1}^+\phi_{-2}^+ $	$\Psi_4$
	${}^2E'$	$ \phi_2^+\phi_1^-\phi_{-1}^+ ,  \phi_{-1}^+\phi_{-1}^-\phi_{-2}^+ $	$\Psi_{18}$
	${}^2E'$	$\left\{ \begin{array}{l} 1/\sqrt{2}[ \phi_2^+\phi_1^+\phi_{-1}^-  -  \phi_2^+\phi_1^-\phi_{-1}^+ ] \\ 1/\sqrt{2}[ \phi_1^+\phi_{-1}^-\phi_{-2}^+  -  \phi_1^-\phi_{-1}^+\phi_{-2}^+ ] \end{array} \right\}$	$\Psi_{20}$
	${}^2E'$	$\left\{ \begin{array}{l} 1/\sqrt{6}[2 \phi_2^+\phi_1^+\phi_{-1}^+  -  \phi_2^+\phi_1^-\phi_{-1}^+  -  \phi_2^+\phi_1^+\phi_{-1}^- ] \\ 1/\sqrt{6}[2 \phi_2^+\phi_1^+\phi_{-1}^+  -  \phi_1^+\phi_{-1}^-\phi_{-2}^+  -  \phi_1^-\phi_{-1}^+\phi_{-2}^+ ] \end{array} \right\}$	$\Psi_{21}$
	${}^2A_2'$	$1/\sqrt{2}[ \phi_1^+\phi_1^-\phi_{-2}^+  +  \phi_2^+\phi_{-1}^-\phi_{-1}^+ ]$	$\Psi_{22}$
	${}^2A_1'$	$1/\sqrt{2}[ \phi_1^+\phi_1^-\phi_{-2}^+  -  \phi_2^+\phi_{-1}^-\phi_{-1}^+ ]$	$\Psi_6$
$(e'')(e')^2$	${}^4E''$	$ \phi_2^+\phi_1^+\phi_{-2}^+ ,  \phi_2^+\phi_{-1}^+\phi_{-2}^+ $	$\Psi_6$
	${}^2E''$	$ \phi_2^+\phi_2^-\phi_1^+ ,  \phi_1^+\phi_{-2}^-\phi_{-2}^+ $	$\Psi_{23}$
	${}^2E''$	$\left\{ \begin{array}{l} 1/\sqrt{2}[ \phi_2^+\phi_1^+\phi_{-2}^-  -  \phi_2^-\phi_1^+\phi_{-2}^+ ] \\ 1/\sqrt{2}[ \phi_2^+\phi_{-1}^+\phi_{-2}^-  -  \phi_2^-\phi_{-1}^+\phi_{-2}^+ ] \end{array} \right\}$	$\Psi_{24}$
	${}^2E''$	$\left\{ \begin{array}{l} 1/\sqrt{6}[2 \phi_2^+\phi_1^-\phi_{-2}^+  -  \phi_2^+\phi_1^+\phi_{-2}^-  -  \phi_2^-\phi_1^+\phi_{-2}^+ ] \\ 1/\sqrt{6}[2 \phi_2^+\phi_1^-\phi_{-2}^+  -  \phi_2^+\phi_{-1}^+\phi_{-2}^-  -  \phi_2^-\phi_{-1}^+\phi_{-2}^+ ] \end{array} \right\}$	$\Psi_{25}$
	${}^2A_1''$	$1/\sqrt{2}[ \phi_2^+\phi_2^-\phi_{-1}^+  -  \phi_1^+\phi_{-2}^-\phi_{-2}^+ ]$	$\Psi_{26}$
	${}^2A_2''$	$1/\sqrt{2}[ \phi_2^+\phi_2^-\phi_{-1}^+  +  \phi_1^+\phi_{-2}^-\phi_{-2}^+ ]$	$\Psi_{27}$
$(e'')(e')(a_1')$	${}^4A_2''$	$1/\sqrt{2}[ \phi_2^+\phi_1^+\phi_0^+  +  \phi_0^+\phi_{-1}^+\phi_{-2}^+ ]$	$\Psi_5$
	${}^4A_1''$	$1/\sqrt{2}[ \phi_2^+\phi_1^+\phi_0^+  -  \phi_0^+\phi_{-1}^+\phi_{-2}^+ ]$	$\Psi_3$
	${}^4E''$	$ \phi_2^+\phi_0^+\phi_{-1}^+ ,  \phi_1^+\phi_0^+\phi_{-2}^+ $	$\Psi_7$
	${}^2E''$	$\left\{ \begin{array}{l} 1/\sqrt{2}[ \phi_2^+\phi_0^-\phi_{-1}^+  -  \phi_2^+\phi_0^+\phi_{-1}^- ] \\ 1/\sqrt{2}[ \phi_1^+\phi_0^-\phi_{-2}^+  -  \phi_1^-\phi_0^+\phi_{-2}^+ ] \end{array} \right\}$	$\Psi_{28}$
	${}^2E''$	$\left\{ \begin{array}{l} 1/\sqrt{6}[2 \phi_2^-\phi_0^+\phi_{-1}^+  -  \phi_2^+\phi_0^-\phi_{-1}^+  -  \phi_2^+\phi_0^+\phi_{-1}^- ] \\ 1/\sqrt{6}[2 \phi_1^+\phi_0^+\phi_{-2}^-  -  \phi_1^+\phi_0^-\phi_{-2}^+  -  \phi_1^-\phi_0^+\phi_{-2}^+ ] \end{array} \right\}$	$\Psi_{29}$
	${}^2A_1''$	$1/2[ \phi_2^+\phi_1^-\phi_0^+  -  \phi_0^+\phi_{-1}^-\phi_{-2}^+  -  \phi_2^+\phi_1^+\phi_0^-  +  \phi_0^-\phi_{-1}^+\phi_{-2}^+ ]$	$\Psi_{30}$
	${}^2A_2''$	$1/2[ \phi_2^+\phi_1^-\phi_0^+  +  \phi_0^+\phi_{-1}^-\phi_{-2}^+  -  \phi_2^+\phi_1^+\phi_0^-  -  \phi_0^-\phi_{-1}^+\phi_{-2}^+ ]$	$\Psi_{31}$
	${}^2A_1''$	$1/2\sqrt{3}[2 \phi_2^-\phi_1^+\phi_0^+  - 2 \phi_0^+\phi_{-1}^+\phi_{-2}^-  -  \phi_2^+\phi_1^-\phi_0^+  +  \phi_0^+\phi_{-1}^-\phi_{-2}^+  -  \phi_2^+\phi_1^+\phi_0^-  +  \phi_0^-\phi_{-1}^+\phi_{-2}^+ ]$	$\Psi_{32}$
	${}^2A_2''$	$1/2\sqrt{3}[2 \phi_2^-\phi_1^+\phi_0^+  + 2 \phi_0^+\phi_{-1}^+\phi_{-2}^-  -  \phi_2^+\phi_1^-\phi_0^+  -  \phi_0^+\phi_{-1}^-\phi_{-2}^+  -  \phi_2^+\phi_1^+\phi_0^-  -  \phi_0^-\phi_{-1}^+\phi_{-2}^+ ]$	$\Psi_{33}$

### Perturbation Energy Matrices

The one-electron crystal-field symmetry eigenfunctions (*i.e.*,  $a_1'$ ,  $e'$ ,  $e''$ ) completely diagonalize the parametric form of the perturbation matrix: in the instance of  $D_{3h}$  symmetry, the perturbation matrix of the one-electron orbital functions (*i.e.*,  $\phi_0$ ,  $\phi_{\pm 1}$ ,  $\phi_{\pm 2}$ ) is even strictly diagonal. Thus no off-diagonal crystal-field matrix elements can exist in the perturbation matrices for  $d^3, d^7$  in strong  $D_{3h}$  crystalline field. The diagonal matrix element for a given state depends only upon the strong-field configuration which gives rise to that state, and is simply the algebraic sum of the energies of the one-electron levels composing that strong-field configuration. The crystal-field energies of the various  $d^3$  trigonal bipyramidal strong-field configurations are listed in Table III.

**Table III:**  $D_{3h}$  Crystalline Field Energies for the  $d^3$  Strong-Field Configurations

Configuration	Crystal-field energy
$[(e'')^3]$	$3\epsilon_0 + 3Ds - 12Dt$
$[(e'')^2(e')]$	$3\epsilon_0 - 7Dt$
$[(e'')(e')^2]$	$3\epsilon_0 - 3Ds - 2Dt$
$[(e')^3]$	$3\epsilon_0 - 6Ds + 3Dt$
$[(e'')^2(a_1')]$	$3\epsilon_0 + 4Ds - 2Dt$
$[(e'')(e')(a_1')]$	$3\epsilon_0 + Ds + 3Dt$
$[(e')^2(a_1')]$	$3\epsilon_0 - 2Ds + 8Dt$
$[(e'')(a_1')^2]$	$3\epsilon_0 + 5Ds + 8Dt$
$[(e')(a_1')^2]$	$3\epsilon_0 + 2Ds + 13Dt$

Nonzero Coulombic matrix elements can occur, of course, only between eigenfunctions of the same sym-





${}^2E'$	$\psi_{10}[(e')^2(a_1')]^2$	$3e_0 + 2Ds + 13Dt + 3A - 8B + 4C - E$	$4B + C$	$\sqrt{6}B$	$\sqrt{2}(B + C)$	0	0
	$\psi_{11}[(e')^2]$	$4B + C$	$3e_0 - 6Ds + 3Dt + 3A + 12B + 4C - E$	0	$\sqrt{2}(3B + C)$	$3\sqrt{6}B$	0
	$\psi_{12}[(e'')^2(a_1')]$	$\sqrt{6}B$	0	$3e_0 + 4Ds - 2Dt + 3A + 4B + 3C - E$	$5\sqrt{3}B$	3B	0
	$\psi_{19}[(e'')^2(e')]$	$\sqrt{2}(B + C)$	$\sqrt{2}(3B + C)$	$5\sqrt{3}B$	$3e_0 - 7Dt + 3A + 5C - E$	$3\sqrt{3}B$	0
	$\psi_{20}[(e'')^2(e')]$	0	$3\sqrt{6}B$	3B	$3\sqrt{3}B$	$3e_0 - 7Dt + 3A - 6B + 3C - E$	0
	$\psi_{15}[(e')^2(a_1')]$	0	0	0	0	0	$3e_0 - 2Ds + 8Dt + 3A - 8B + 3C - E$
	$\psi_{16}[(e'')^2(e')]$	0	0	0	0	0	$6\sqrt{6}B$
							$3e_0 - 7Dt + 3A - 9B + 3C - E$
							= 0

and Shortley's text.<sup>23</sup> The  ${}^2P$  and  ${}^2H$  terms have the same Coulomb energy. The fact that two  ${}^2D$  terms arise in the  $d^3$  case necessitates invoking second-order effects to sort out their exact Coulomb energies, since consideration of first-order effects alone gives only their mean value. According to the diagonal sum rule<sup>24,25</sup>

$$a^2D \begin{vmatrix} 3A + 7B + 7C - E & 3\sqrt{21}B \\ 3\sqrt{21}B & 3A + 3B + 3C - E \end{vmatrix} = 0$$

$$E = 5A + 5B + 5C \pm \sqrt{193B^2 + 8BC + 4C^2}$$

(11)

$$E = 5A + 5B \pm \sqrt{193B}, \quad \text{if } C = 0$$

$$E = 5A + 7C, 5A + 3C, \quad \text{if } B = 0$$

To check the strong-field matrices against the weak-field limit, the parameters are simply assigned numerical values (either one at a time with the second parameter zeroed, or jointly) and the resulting perturbation energy matrices solved for the appropriate eigenvalues. The eigenvalues for the strong-field approximation must then agree identically with the (diagonal) weak-field limit. Verification of the parameter  $A$  is of course trivial since  $A$  occurs only along the diagonal in both approximations. All the matrices listed in Table IV were checked and found to be consistent with the weak-field limit.

To a first approximation, the undiagonalized form of the strong-field matrices can also be checked against the weak-field case. For each type of symmetry state the traces of the weak- and strong-field matrices are identical; this could not be otherwise because the weak- and strong-field perturbation matrices differ only by a similarity transformation.

### Energy Level Diagram

Complete perturbation energy matrices, such as those given in Table IV, are used to investigate the spectroscopic behavior of transition metal complexes. By way of illustration, numerical values for  $Ds$ ,  $Dt$ ,  $B$ , and  $C$  approximately suitable for  $\text{Co(II)}$  coordinated to five identical strong-field ligands were chosen and the matrices solved. Since  $\text{Co(II)}$  is very similar to  $\text{Ni(II)}$  in the spectrochemical series, crystal-field parametric values appropriate to strong-field trigonal bipyramidal  $\text{Ni(II)}$  complexes were deemed reasonable:  $Ds = 2580 \text{ cm}^{-1}$  and  $Dt = 2680 \text{ cm}^{-1}$ .<sup>5b,6</sup> The Racah parameters,  $B$  and  $C$ , were taken as 70% their free ion values,<sup>26</sup> 780 and  $3056 \text{ cm}^{-1}$ , respectively, to account for nephelauxetic effect due to five strong-field ligands. For application to specific strong-field  $d^3, d^7$  complexes,

(23) See ref 21, Chapter 7.

(24) See ref 21, Chapter 8.

(25) C. W. Ufford and G. H. Shortley, *Phys. Rev.*, **42**, 167 (1932).

(26) J. S. Griffith, "The Theory of Transition Metal Ions," Cambridge University Press, Cambridge, 1964, Appendix 6.

of course, the parameters  $Ds$ ,  $Dt$ ,  $B$ , and  $C$  would be assigned values which best fit the experimental electronic spectra.

When the strong-field energy levels are displayed as in Figure 2, qualitative features expected in the absorption spectrum become apparent. The ground state is well defined as  ${}^2E'[(e'')^4(e')^3]$ . Nine spin-allowed, symmetry-allowed transitions, listed in Table V, are possible below  $50,000\text{ cm}^{-1}$  ( $2000\text{ \AA}$ ).

**Table V:** Spin-Allowed, Symmetry-Allowed d-d Transitions for a Strong-Field  $d^7$  Trigonal Bipyramidal Complex<sup>a</sup>

$$\begin{array}{l}
 {}^2E'[(e'')^4(e')^3] \xrightarrow{(z)} {}^2E''[(e'')^3(e')^4] \\
 {}^2E'[(e'')^4(e')^3] \xrightarrow{(x,y)} {}^2E'[(e'')^4(e')^2(a_1)'] \\
 {}^2E'[(e'')^4(e')^3] \xrightarrow{(x,y)} {}^2A_1'[(e'')^4(e')^2(a_1)'] \\
 {}^2E'[(e'')^4(e')^3] \xrightarrow{(z)} {}^2E''[(e'')^3(e')^3(a_1)'] \\
 {}^2E'[(e'')^4(e')^3] \xrightarrow{(x,y)} {}^2A_2'[(e'')^4(e')^2(a_1)'] \\
 {}^2E'[(e'')^4(e')^3] \xrightarrow{(z)} {}^2E''[(e'')^3(e')^3(a_1)'] \\
 {}^2E'[(e'')^4(e')^3] \xrightarrow{(x,y)} {}^2A_2'[(e'')^2(e')^4(a_1)'] \\
 {}^2E'[(e'')^4(e')^3] \xrightarrow{(x,y)} {}^2E'[(e'')^2(e')^4(a_1)'] \\
 {}^2E'[(e'')^4(e')^3] \xrightarrow{(x,y)} {}^2A_1'[(e'')^2(e')^4(a_1)']
 \end{array}$$

<sup>a</sup> Calculated for the parametric values  $Ds = 2580\text{ cm}^{-1}$ ,  $Dt = 2680\text{ cm}^{-1}$ ,  $B = 780\text{ cm}^{-1}$ , and  $C = 3055\text{ cm}^{-1}$ ; with only those transitions expected below  $50,000\text{ cm}^{-1}$  ( $2000\text{ \AA}$ ) being included.

The  $d^7$  strong-field energy levels are shown in Figure 2 to both a first-order approximation (diagonal matrix elements only) and to a second-order calculation (diagonal and off-diagonal crystal-field and Coulombic terms). The ground state,  ${}^2E'[(e'')^4(e')^3]$ , is relatively insensitive to second-order effects, but most of

the excited states are strongly influenced by second-order interaction. For example, the lowest energy transition,  ${}^2E'[(e'')^4(e')^3] \rightarrow {}^2E''[(e'')^3(e')^4]$ , appears at significantly lower energy, whereas the transition,  ${}^2E'[(e'')^4(e')^3] \rightarrow {}^2E''[(e'')^3(e')^3(a_1)']$ , shifts to higher energy, under second-order considerations. The degeneracy of the  ${}^2E'[(e'')^4(e')^3] \rightarrow {}^2A_1'[(e'')^4(e')^2(a_1)']$ ,  ${}^2E'[(e'')^3(e')^3(a_1)']$ , and  ${}^2A_2'[(e'')^4(e')^2(a_1)']$  transitions is partially lifted, with the first two split away together toward lower energy and the third toward higher energy. The transitions  ${}^2E'[(e'')^4(e')^3] \rightarrow {}^2A_2'[(e'')^2(e')^4(a_1)']$ ,  ${}^2E'[(e'')^2(e')^4(a_1)']$ , however, become degenerate only in second order. Only the second lowest energy transition,  ${}^2E'[(e'')^4(e')^3] \rightarrow {}^2E'[(e'')^4(e')^2(a_1)']$ , remains unaffected in going from first to second order.

### Conclusion

The complete perturbation energy matrices for a  $d^3, d^7$  metal ion subject to a strong trigonal bipyramidal ( $D_{3h}$ ) crystalline field have been quantitatively evaluated in parametric form. A qualitatively correct energy level diagram has then been constructed to illustrate the use of these matrices in discussing the optical behavior of such a system.

*Acknowledgments.* Acknowledgment is made to the donors of The Petroleum Research Fund, administered by the American Chemical Society, for partial support of this research, in particular, for making available a Wang Model 320 Electronic Calculator and Model 320E Electronics Package to this laboratory. The authors wish also to gratefully acknowledge The Robert A. Welch Foundation for financial support of this research and for a graduate fellowship to J. A. Varga.

# Calculated Free Energies of Adsorption of Halide and Hydroxide Ions

## by Mercury, Silver, and Gold Electrodes<sup>1,2</sup>

by Donald D. Bodé, Jr.<sup>3</sup>

Lawrence Livermore Laboratory, University of California, Livermore, California 94550 (Received November 22, 1971)

Publication costs assisted by the Lawrence Radiation Laboratory

The free energies of specific adsorption ( $\Delta G^\circ$ ) for  $\text{Br}^-$ ,  $\text{Cl}^-$ ,  $\text{F}^-$ , and  $\text{OH}^-$  in aqueous solution on Hg, Ag, and Au electrodes are calculated. The model includes metal-ion interactions, ion-water interactions, water-metal interactions, and Born energy contributions. For the halide ions, the calculated  $\Delta G^\circ$  agree with previously reported experimental trends in adsorption although the magnitudes of  $\Delta G^\circ$  are too great. For  $\text{OH}^-$  adsorption, the calculated  $\Delta G^\circ$  do not agree with experimental data; reasons for the discrepancy are discussed. Adsorption for  $\text{Br}^-$  and  $\text{Cl}^-$  is accompanied by loss of primary waters of hydration and the ions situate in the inner Helmholtz plane. The  $\text{F}^-$  and  $\text{OH}^-$  ions are negligibly dehydrated and adsorb in the outer Helmholtz plane.

### Introduction

In this paper are calculations for the free energies of specific adsorption ( $\Delta G^\circ$ ) for halide and hydroxide ions in aqueous solutions on mercury, silver, and gold electrodes. The model used is that of Andersen and Bockris who first calculated the free energies of adsorption of simple, monovalent ions on mercury by assuming that adsorption is predominantly noncovalent.<sup>4</sup> Covalent bonding is believed to be unlikely since the order of increased bond strength of the metal-ion molecule does not correspond to the ordering of adsorbabilities.<sup>4-6</sup> Moreover, the water-metal and ion-water interactions are large compared to the differences in bond energies, so the degree of adsorption should be highly dependent on the amount of hydration. For the free energy of specific adsorption, they used the sum of the changes in entropy and enthalpy resulting from differences in ion-metal, ion-water, and water-metal interactions for the ion as it is removed from the bulk solution and brought near the electrode. The contributions for the enthalpy can be summarized as follows.

$\Delta H_1$  is the loss (*i.e.*,  $H$  becomes more positive) of interaction with the surroundings for the  $n$  water molecule which desorb from the surface. This includes losses from the hydrogen bonding with the second-layer water molecules and lateral interaction between these  $n$  molecules and their adsorbed neighbors and with the metal surface.

$\Delta H_2$  is the gain of interaction between those  $n$  water molecules and the bulk.

$\Delta H_3$  is the acquisition of image, dispersion, and repulsion energies.

$\Delta H_4$  is the difference in interaction with the  $n_1$  primary water molecules in the bulk solution and the  $n_1'$  at the electrode, *i.e.*,  $(n_1' - n_1)\Delta H_{\text{ion-w}}$ .

$\Delta H_5$  is the difference in energy as a result of the

change in hydrogen bonding for all the water molecules associated with the ion when going from the bulk to the surface; *i.e.*,  $(n_1' - n_1)\Delta H_{\text{H bond}}/2$ .

$\Delta H_6$  is the loss of interaction with water beyond nearest neighbors.

$\Delta H_7$  is the loss of interaction resulting from the reorientation of adsorbed neighboring water molecules around the adsorbed ion as a result of the ion-water interaction at the surface. In the Andersen-Bockris treatment this is taken as one-half of the water-metal interaction.

The changes in entropy are as follows.

$\Delta S_1$  is the gain resulting from the  $n$  water molecules on the electrode being desorbed into the solution.

$\Delta S_2$  is the loss as a result of the changes in the degrees of freedom for the ion upon adsorption.

$\Delta S_3$  is the gain due to the decrease in the number of primary waters of hydration bound to the ion after adsorption of the ion on the surface.

$\Delta S_4$  is the loss associated with the increase in hydrogen bonding for the nonprimary waters when the ion leaves the bulk and adsorbs.

In the Andersen-Bockris treatment, the equilibrium distance between the ion and the electrode,  $R_e$ , was determined by minimizing the image, dispersion, and repulsive energies ( $\Delta H_3$ ) with respect to distance. These

(1) This work was performed under the auspices of the U. S. Atomic Energy Commission.

(2) Presented in part at the 161st National Meeting of the American Chemical Society, Los Angeles, Calif., March, 1971.

(3) Address correspondence to Ph.D.-M.D. Program, School of Medicine, University of Miami, Miami, Fla. 33152.

(4) T. N. Andersen and J. O'M. Bockris, *Electrochim. Acta*, **9**, 347 (1964).

(5) T. N. Andersen, J. L. Anderson, and H. Eyring, *J. Phys. Chem.*, **73**, 3562 (1969).

(6) J. O'M. Bockris, M. A. V. Devanathan, and K. Muller, *Proc. Roy. Soc., Ser. A*, **274**, 55 (1963).

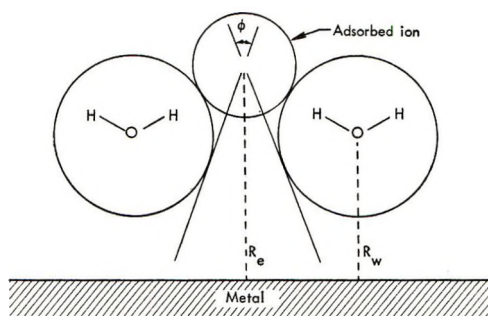


Figure 1. Electrode-solution interphase. The adsorbed anion is shown with two adsorbed primary waters of hydration; other surrounding water is not shown.

three ion-metal interactions have the greatest exponential dependence on distance of all the contributions.

The first of two modifications in this paper to the theory of Andersen and Bockris occurs in the determination of the equilibrium separation distance  $R_e$ . Instead of using only the ion-metal interactions to determine  $R_e$ , all contributions to  $\Delta G^\circ$  were included. This effect is most evident in the case of  $F^-$  adsorption. At the point where the ion-metal interactions are a minimum, the loss in hydration for this ion is about 25%. In other words, the angle  $\phi$  in Figure 1 must be large for that value of  $R_e$  if  $R_w$ , the separation distance of the water molecule from the electrode, is to remain near its equilibrium value. The result is a loss in energy of about 18 kcal/mol; that this is large can be seen by observing that for  $Cl^-$  the change in energy is only about 6 kcal/mol when ion-metal interactions are at a minimum. The large loss in energy for  $F^-$  is enough to make  $\Delta G^\circ$  positive and there is no adsorption at that distance. However, when the ion is further from the metal, fewer waters of hydration must be removed from the hydrated ion. Thus with a smaller  $\phi$ , the change in ion-water interaction upon adsorption of the ion is less significant. If the other contributions to  $\Delta G^\circ$  do not change significantly, the small loss in energy of hydration may result in a negative free energy of adsorption, and the ion will adsorb. Thus, the amount of hydration depends on the separation distance and  $\phi$ , which is a function of the water-metal separation, and the orientation of the water with respect to the ion.

The second modification of the theory of Andersen and Bockris involves the water-metal interaction. They assumed that the separation distance of the water molecule from the electrode was the same as its radius and that the molecules which reoriented in the presence of an adjacent, adsorbed ion lost one-half of their water-metal interaction ( $\Delta H_{w-m}$ ). In this paper the orientation of primary waters of hydration is constrained by both the metal surface and the ion. First, the water-metal orientation appears in  $\Delta H_{w-m}(R_w, \theta_w)$  where the  $R_w$  corresponds to the separation distance of the water and the electrode and the  $\theta_w$  refers to the angle that the dipole of the water molecule makes with the surface of

the electrode.<sup>7</sup> The zero angle is defined as the configuration in which the oxygen atom is closest to the metal and the hydrogens are at the greatest distance. Other angles result from a rotation about a normal to the plane of the water molecule so that each hydrogen comes closer to the metal in succession. Secondly, the ion-water orientation is such that the primary waters always have an O-H bond axis in the direction of the anion and remain the distance of a hydrogen bond from the ion. These constraints on  $R_w$ ,  $\theta_w$ , and the ion-water separation affect not only  $\Delta H_w$  but also describe the amount of hydration the ion experiences.

In obtaining  $\Delta G^\circ$  the ion-metal separation distance ( $R$ ) was varied incrementally from 1.0 to 4.0 Å, and for each value of  $R$ , the water molecules primary to the ion were moved about the ion by varying  $R_w$  and  $\theta_w$  to find a minimum  $\Delta G^\circ$  for that of distance  $R$ . The separation distance at which  $\Delta G^\circ$  is the least is expressed as  $R_e$ . Zero ionic coverage was assumed to allow the omission of ion-ion interactions and the solid metal electrodes were assumed to have smooth surfaces for this coverage.

The following section deals with problems encountered in determining values for certain of the contributions to the enthalpies.

### Theory

In calculating the free energy of adsorption of the halides on these electrodes there is a major problem in determining the repulsive energies. In evaluating the equation below, the constants  $A$  and  $n$  are unknown.<sup>4</sup>

$$U_{rep} = \frac{2\pi NA}{(n-2)(n-3)} \frac{1}{R^{n-3}} \quad (1)$$

$N$  is the number of adsorption sites per  $cm^3$ . These unknown constants depend on the metal, the ion, and their structure. This problem was first dealt with in the study of adsorption on mercury by using the values of  $A$  and  $n$  for rubidium compounds since  $Rb^+$  and  $Hg^+$  have nearly the same size.<sup>4</sup> This approximation led to quite reasonable results for  $\Delta G^\circ$ .

To derive  $A$  and  $n$  from the properties of the ions and metals themselves, one can use Born's theory of ionic crystals in which

$$n = 1 + \frac{9v_0 a_0}{\beta \alpha^2 z e^2} \quad (2)$$

where  $v_0$  is the cell volume,  $\alpha$  is the Madlung constant,  $a_0$  is the equilibrium separation of nearest charged species  $ze$ , and  $\beta$  is the compressibility.<sup>8</sup> Also

$$A = \alpha z^2 e^2 a_0^{n-1} / s_n n \quad (3)$$

where  $s_n$  is the sum of the nearest neighbors, each divided by the square root of their respective distance

(7) D. D. Bodé, *Advan. Chem. Phys.*, 21, 362 (1971).

(8) E. A. Moelwyn-Hughes, "Physical Chemistry," 2nd ed, Pergamon Press, London, 1961, p 556.

from a given atom and taken to the  $n$ th power. These equations allowed for too little repulsion when they were applied to adsorption on mercury if mercurous halides were used to obtain  $A$  and  $n$ . This would be expected when one examines the crystal structure of the mercurous halides. They are nonionic and tetragonal;<sup>9</sup> additionally, close packing is evident when one compares the Madelung constant for  $\text{Hg}_2\text{Cl}_2$  ( $\alpha = 2.62$ )<sup>10</sup> to that for simple cubic  $\text{RbCl}$  ( $\alpha = 1.75$ ). For the calculations in this paper I based  $A$  and  $n$  for mercury on the similarity in size of  $\text{Hg}^+$  and  $\text{Rb}^+$  as did Andersen and Bockris.<sup>4</sup>

Silver and gold halides are cubic,<sup>11</sup> and they are not purely ionic. However, reasonable values for  $A$  and  $n$  can be estimated by eq 2 and 3. Since only the values for  $\beta_{\text{AgCl}}$  and  $\beta_{\text{AgBr}}$  are known,<sup>12</sup> the other compressibilities must be approximated. That this is feasible from molar volumes<sup>13</sup> can be seen by comparing the known values of  $\beta_{\text{AgBr}}$  to the derived value  $\beta_{\text{AgBr}} = \beta_{\text{AgCl}}(V_{\text{AgBr}}/V_{\text{AgCl}})$ . There is a 2% difference. For the remaining ions that adsorb on the silver electrode,  $\beta_{\text{AgF}} = \beta_{\text{AgOH}} = \beta_{\text{AgCl}}(V_{\text{AgF}}/V_{\text{AgCl}})$ , where molar volumes were derived using known ionic distances.

For the gold electrode, none of the compressibilities are known; however, there is a proportionality between the silver and gold halides. The difference in the molar volume of  $\text{AuBr}$  derived directly from its ionic dimensions and that calculated by  $V_{\text{AuBr}} = V_{\text{AgBr}}(V_{\text{AuCl}}/V_{\text{AgCl}})$ , where  $V_{\text{AuCl}}$  was derived using known ionic distances, is 0.37%. Thus  $V_{\text{AuF}} = V_{\text{AuOH}} = V_{\text{AgF}}(V_{\text{AuCl}}/V_{\text{AgCl}})$ . For the compressibilities, one can then assume  $\beta_{\text{AuX}} = \beta_{\text{AgCl}}(V_{\text{AuX}}/V_{\text{AgCl}}) = \beta_{\text{AgCl}}(V_{\text{AgX}}V_{\text{AuCl}}/V_{\text{AgCl}}^2)$ , where X denotes the anion  $\text{F}^-$ ,  $\text{OH}^-$ ,  $\text{Cl}^-$ , and  $\text{Br}^-$ . To each of these estimated compressibilities, a 2% correction is made corresponding to the difference in experimental  $\beta_{\text{AgBr}}$  and the calculated value based on  $\beta_{\text{AgCl}}$ .

To calculate the dispersion energy ( $U_{\text{disp}}$ ) the polarizabilities of the metals are needed. These are approximated by taking  $\alpha_m = 3V_m/4\pi N_{\text{Av}}$ , where  $N_{\text{Av}}$  is Avagadro's number and  $V_m$  is the molar volume.<sup>14</sup> The calculated value of  $\alpha_m$  for Hg differs from the experimental value by 14%, so all calculated values of  $\alpha_m$  were adjusted by this amount. Also in obtaining  $U_{\text{disp}}$ , one needs diamagnetic susceptibilities; however,  $\chi_{\text{OH}^-}$  has not been reported. It was approximated from  $\text{NaOH}$  and  $\text{KOH}$  by taking

$$\chi^- = [(\chi_{\text{KOH}} - \chi_{\text{K}^+}) + (\chi_{\text{NaOH}} - \chi_{\text{Na}^+})]/2^{15,16}$$

The  $\chi_{\text{OH}^-}$  found in this manner differs from  $\chi_{\text{F}^-}$  for the fluoride ion, which is the same size and is isoelectronic with the hydroxyl ion, by 2%.

The ion-water interaction,  $\Delta H_{i-w}$ , for  $\text{OH}^-$  was calculated by the methods of Eley and Evans to be  $-21.5$  kcal/mol.<sup>17</sup>

The coverage for adsorbed water molecules has been

calculated and measured to be between 0.8 and 1.0.<sup>4, 18, 19</sup> Variations in the percentage of coverage changes the values of  $H_1$ ,  $H_2$ ,  $H_3$ , and  $S_1$  by approximately the same percentage and alters  $S_4$  by 8.2 eu/mol times the change in fractional coverage. For this work, as with Andersen and Bockris, the coverage is taken as 0.9.

## Results

The results from the estimation of some of the parameters used in these calculations as well as calculated values for the contributions to the free energy of specific adsorption are listed in Tables I-V.

**Table I:** Separation Distances and Free Energies of Adsorption

	$R_e$ , Å	$R_w$ , Å	$\Delta G^\circ$ , kcal/mol
Hg/Br	1.95	2.54	-11.9
Hg/Cl	1.77	2.54	-10.3
Hg/F	3.80	2.16	2.6
Hg/OH	3.79	2.15	2.6
Ag/Br	1.80	2.50	-17.3
Ag/Cl	1.71	2.54	-15.0
Ag/F	3.61	1.97	-2.4
Ag/OH	3.61	1.96	-3.4
Au/Br	2.01	2.57	-14.0
Au/Cl	1.91	2.53	-11.7
Au/F	3.67	2.03	-2.7
Au/OH	3.67	2.02	-3.7

For adsorption of the halides on silver, gold, and mercury the calculated  $\Delta G^\circ$  show the experimentally observed<sup>4, 20</sup> order  $\text{Br}^- > \text{Cl}^- > \text{F}^-$ . One finds experimentally that  $\text{OH}^-$  is adsorbed more than  $\text{Cl}^-$  on Au, less than  $\text{Cl}^-$  on Ag, and  $\text{OH}^-$  is not adsorbed at all on Hg. This repositioning of  $\text{OH}^-$  in order of adsorbability, depending on the electrode, is not evident in the calculations. The calculated  $\Delta G^\circ$  for  $\text{OH}^-$  is only

(9) R. W. G. Wyckoff, "Crystal Structure," Vol. I, 2nd ed. Wiley-Interscience, New York, N. Y., 1963, p 151.

(10) Q. C. Johnson and D. H. Templeton, *J. Chem. Phys.*, **34**, 2004 (1961). Madelung constant for  $\text{Hg}_2\text{Cl}_2$  was calculated by their computer code.

(11) See ref 9, p 10.

(12) E. D. Washburn, Ed., "International Critical Tables of Numerical Data, Physics, Chemistry and Technology," Vol. III, McGraw-Hill, New York, N. Y., 1928, p 50.

(13) P. A. Savintsev, *Izv. Tomsk. Politekh. Inst.*, **95**, 152 (1958).

(14) J. O'M. Bockris and D. A. J. Swinkles, *J. Electrochem. Soc.*, **111**, 737 (1964).

(15) F. E. Hoare and G. W. Bridley, *Proc. Phys. Soc.*, **49**, 619 (1937).

(16) "Handbook of Chemistry and Physics," 49th ed, Chemical Rubber Publishing Co., Cleveland, Ohio, 1968-1969, p E-112.

(17) D. D. Eley and M. G. Evans, *Trans. Faraday Soc.*, **34**, 1093 (1938).

(18) A. I. Sarakhov, *Proc. Acad. Sci. USSR, Phys. Chem. Sect.*, **112**, 55 (1957).

(19) J. R. MacDonald and C. A. Barlow, Jr., *Proc. Aust. Conf. Electrochem.*, **1st**, 1963 (1963).

(20) D. D. Bodé, T. N. Andersen, and H. Eyring, *J. Phys. Chem.*, **71**, 792 (1967).

**Table II:** Constants for the Anions and Metal Electrodes Used in Calculating  $\Delta G^\circ$ 

	Br <sup>-</sup>	Cl <sup>-</sup>	F <sup>-</sup>	OH <sup>-</sup>	Hg	Ag	Au
$r_i, \text{\AA}^a$	1.96	1.81	1.31	1.31			
$n_1^{b,c}$	1.0	1.6	3.9	4.0			
$\alpha, \text{cm}^3 \times 10^{24}{}^{b,d}$	4.24	2.98	0.81	1.80	5.05	3.51	3.48
$\chi, \text{cm}^3 \times 10^{22}{}^{b,e}$	-5.73	-4.02	-1.56	-1.61	-5.55	-3.23	-4.64
$\Delta H_{i-w}, \text{kcal/mol}^f$	-12.0	-13.6	-20.6	-21.5			
$W_a, \text{ergs} \times 10^{12}{}^{b,e,g}$					1.54	1.53	1.54
$N_s, \text{cm}^3 \times 10^{22}{}^h$					4.08	2.33	2.33

<sup>a</sup> Reference 8, p 24. <sup>b</sup> Reference 4. <sup>c</sup> Reference 28. <sup>d</sup> References 14 and 23 and J. A. A. Ketelaar, "Chemical Constitution," Elsevier, Amsterdam, 1958, p 91. <sup>e</sup> Reference 16. <sup>f</sup> Reference 17. <sup>g</sup> C. Kittel, "Introduction to Solid State Physics," 2nd ed, Wiley, New York, N. Y., 1956, p 250. <sup>h</sup> Reference 9, p 10, and ref 13.

**Table III:** Geometric Terms Obtained in Calculating  $\Delta G^\circ$ 

	$\phi,$ deg	$\theta_w,$ deg	$n$	$n_t$	$n_t'$	$n_1$
Hg/Br	75.8	47.7	1.4	14.1	9.8	0.6
Hg/Cl	78.3	51.5	1.2	12.8	8.7	1.0
Hg/F	22.1	0.3	0.5	9.3	8.2	3.8
Hg/OH	22.1	0.3	0.5	9.3	8.2	3.9
Ag/Br	77.7	49.6	1.0	14.1	7.5	0.6
Ag/Cl	79.4	52.6	0.8	12.8	6.6	0.9
Ag/F	22.1	0.3	0.5	9.3	8.2	3.8
Ag/OH	21.9	0.0	0.5	9.3	8.2	3.9
Au/Br	75.2	47.2	1.0	14.1	7.8	0.6
Au/Cl	75.6	48.7	0.8	12.8	7.0	1.0
Au/F	22.1	0.3	0.5	9.3	8.2	3.8
Au/OH	21.9	0.0	0.5	9.3	8.2	3.9

when it moves from the bulk solution and adsorbs on the electrode. Thus Cl<sup>-</sup> and Br<sup>-</sup> would be specifically adsorbed in the inner Helmholtz plane (iHp) while F<sup>-</sup> and OH<sup>-</sup> would be adsorbed in the outer Helmholtz plane (oHp). This conclusion is unusual since anions are normally considered to be adsorbed in the iHp and cations in the oHp.<sup>21</sup> The dependence of  $\Delta G^\circ$  on the separation distance for Cl<sup>-</sup> and F<sup>-</sup> with Hg and Ag are shown in Figure 2. Other results are not plotted since the small differences in values would not make their plots significantly unlike those in Figure 2.

### Discussion

The calculated  $\Delta G^\circ$  for Br<sup>-</sup>, Cl<sup>-</sup>, F<sup>-</sup>, and OH<sup>-</sup> on Hg are -11.9, -10.3, +2.6, and +2.6 kcal/mol, re-

**Table IV:** Calculated Contributions to  $\Delta H$  (kcal/mol)

	$U_{\text{image}}$	$U_{\text{disp}}$	$U_{\text{rep}}$	$\Delta H_{w-m}$ ( $R_e, \theta_e$ )	$A$	$n$	$\Delta H_1$	$\Delta H_2$	$\Delta H_3$	$\Delta H_4$	$\Delta H_5$	$\Delta H_6$	$\Delta H_7$
Hg/Br	-40.5	-29.4	19.9	-11.1	$8.8 \times 10^{-80}$	8.7	31.6	-14.7	-46.9	4.5	-9.8	15.2	2.7
Hg/Cl	-44.4	-24.8	21.9	-11.3	$3.8 \times 10^{-74}$	8.1	27.0	-12.6	-47.3	8.7	-9.6	15.4	4.2
Hg/F	-21.3	-0.5	0.1	-14.8	$1.6 \times 10^{-78}$	8.8	10.7	-5.3	-21.7	3.0	-2.3	18.0	4.4
Hg/OH	-21.3	-0.7	0.1	-14.8	$1.6 \times 10^{-78}$		10.7	-5.3	-22.0	3.2	-2.3	18.0	4.5
Ag/Br	-43.6	-12.2	8.0	-9.3	$1.8 \times 10^{-106}$	12.3	20.9	-10.5	-48.1	4.7	-14.9	15.3	2.7
Ag/Cl	-45.8	-10.0	7.7	-9.6	$2.8 \times 10^{-104}$	12.0	17.2	-8.4	-43.4	8.9	-14.0	15.5	4.3
Ag/F	-22.4	-0.3	0.0	-16.0	$1.8 \times 10^{-98}$	11.3	10.1	-5.3	-22.7	3.0	-2.3	18.8	0.0
Ag/OH	-22.4	-0.5	0.0	-16.0	$1.8 \times 10^{-98}$	11.3	10.1	-5.3	-22.9	3.1	-2.3	18.9	0.1
Au/Br	-39.3	-10.6	6.5	-9.0	$9.8 \times 10^{-112}$	13.1	20.3	-10.5	-43.4	4.5	-14.2	15.2	2.6
Au/Cl	-41.3	-8.6	6.3	-9.1	$5.3 \times 10^{-108}$	12.6	16.8	-8.4	-43.6	8.2	-13.1	15.4	4.4
Au/F	-22.0	-0.4	0.0	-15.5	$2.3 \times 10^{-103}$	12.0	10.8	-5.3	-22.4	3.0	-2.3	18.5	0.0
Au/OH	-22.0	-0.6	0.0	-15.5	$2.3 \times 10^{-103}$	12.0	10.8	-5.3	-22.6	3.1	-2.3	18.6	0.1

slightly more negative than that for F<sup>-</sup> and both are more positive than the  $\Delta G^\circ$  for Cl<sup>-</sup>.

The calculated minima for  $\Delta G^\circ$  with Cl<sup>-</sup> and Br<sup>-</sup> occurs very close for all these electrodes to the separation distances corresponding to the minima for the sums of the ion-metal interactions. However for F<sup>-</sup> and OH<sup>-</sup>, the minima for  $\Delta G^\circ$  occur when the separation distance for the water and the electrode is nearly equal to the minimum value for  $\Delta H_{w-m}(R_w, \theta_w)$ . At this distance there is little change in hydration of the ion

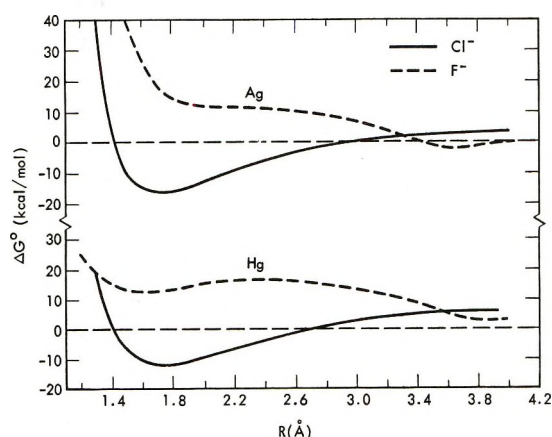
respectively (Table I). There are no experimental results with which these may be compared other than the value for I<sup>-</sup> adsorption on Hg, which is -8.5 kcal/mol.<sup>22</sup> Since I<sup>-</sup> is adsorbed more than the other halide ions, the calculated results must be too negative. Much of this error is due to the Kirkwood-Müller dispersion

(21) J. O'M. Bockris and A. K. N. Reddy, "Modern Electrochemistry," Vol. II, Plenum Press, New York, N. Y., 1970, Chapter 7.

(22) W. Anderson and R. Parsons, *Proc. Int. Congr. Surface Activ., 3rd*, 45 (1957).

**Table V:** Calculated Contributions to  $\Delta S$  (eu/mol)

	$\Delta S_1$	$\Delta S_2$	$\Delta S_3$	$\Delta S_4$
Hg/Br	14.7	-5.7	5.0	-32.0
Hg/Cl	12.5	-5.5	9.7	-28.8
Hg/F	4.7	-3.3	19.5	-7.3
Hg/OH	4.7	-3.3	19.9	-7.3
Ag/Br	10.2	-5.9	5.0	-50.6
Ag/Cl	8.7	-5.4	9.8	-45.6
Ag/F	4.7	-3.5	19.5	-7.2
Ag/OH	4.7	-0.4	19.9	-7.1
Au/Br	10.2	-5.1	5.0	-48.6
Au/Cl	8.7	-4.7	9.5	-42.8
Au/F	4.7	-3.3	19.5	-7.3
Au/OH	4.7	-0.3	19.9	-7.2

**Figure 2.** The free energy of adsorption for  $\text{Cl}^-$  and  $\text{F}^-$  as a function of the separation distance from the electrode for Hg and Ag.

formula, since it is only about 30% accurate and usually allows too much interaction.<sup>23,24</sup> Another error is present in the image energy because the lines of force passing from the ion through neighboring water molecules were assumed not to experience a change in dielectric. The effect of this approximation is to allow too much ion-metal interaction. This is offset by neglecting such secondary effects as metal-induced dipoles in the ion interacting with the metal. The repulsive energy is only approximate; the exact values of  $A$  and  $n$  in eq 1 are not known. On the other hand, an error in the value of  $A$  or  $n$  for an ion interacting with a given electrode will appear much to the same degree within the series of ions for that electrode and it should not alter the ordering of relative magnitudes for  $\Delta G^\circ$  for the ions adsorbing on that electrode. The ordering in magnitudes of the calculated  $\Delta G^\circ$  for a given electrode should correspond with experimentally observed trends in adsorption for those ions on that electrode.

The uncertainties in this type of calculation for the

water-metal and the ion-water interactions are discussed in detail by Andersen and Bockris. It is shown that the uncertainties in these interactions may affect the magnitudes of the free energies of adsorption, but they will not alter the relative order of adsorbabilities. Thus the calculated values are only approximations of the actual values for the free energies, but they are indications of the expected trends in adsorption.

The cause for the varying degree of adsorbability for  $\text{OH}^-$  is not clear. Several authors have argued that formation of compounds between the adsorbing ion and the electrode is unlikely since the order of bond strength for the compounds do not correspond to the order of adsorbability.<sup>4,5,25</sup> However, the contention that there is no compound formation on Au or Ag has not been proven.

Another explanation involves bridging, wherein adsorbed pairs of anions and cations induce greater adsorption of anions on the electrode.<sup>26,27</sup> The adsorption of ionic pairs would also decrease the dielectric constant in the double-layer region and make the potential of zero charge (pzc) more negative than for simple anionic adsorption. Since the relative adsorbabilities are based on the relative values of the pzc for the ions, bridging with  $\text{OH}^-$  would make the  $\text{OH}^-$  appear to be more adsorbed than one of the halide ions when it is actually not. However, for  $\text{OH}^-$  to give a pzc more negative than  $\text{Cl}^-$ , and thus appear to be more adsorbed than both  $\text{F}^-$  and  $\text{Cl}^-$ , the bridging would have to be markedly greater for  $\text{OH}^-$  than that of  $\text{F}^-$ .

A third alternative lies in the possibility for additional interaction of hydration that has not already been included in this theory. The small  $\text{OH}^-$  and  $\text{F}^-$  ions could interact with the water surrounding them and become more stable than the other halide ions.<sup>28-32</sup> Thus, during ionic adsorption there can be ordering of the surrounding water, and for want of a better description, an "ice-like" layer results.

*Acknowledgments.* I wish to thank T. N. Andersen and J. E. Harrar for their helpful suggestions on this work.

(23) A. Müller, *Proc. Roy. Soc., Sect. A*, **154**, 624 (1936).

(24) R. A. Pierotti and G. D. Halsey, Jr., *J. Phys. Chem.*, **63**, 680 (1959).

(25) T. N. Andersen, J. L. Anderson, D. D. Bodé, and H. Eyring, *J. Res. Inst. Catal., Hokkaido Univ.*, **16** (1), 449 (1968).

(26) A. N. Frumkin, *Trans. Faraday Soc.*, **55**, 156 (1959).

(27) D. D. Bodé, T. N. Andersen, and H. Eyring, *J. Electrochem. Soc.*, **114**, 72 (1967).

(28) T. Ackermann, *Discuss. Faraday Soc.*, **24**, 180 (1957).

(29) H. S. Frank and W. Wen, *ibid.*, **24**, 133 (1957).

(30) O. Y. Samoilov, *ibid.*, **24**, 141 (1957).

(31) R. E. Weston, Jr., *Spectrochim. Acta*, **18**, 1257 (1962).

(32) J. W. Schultz and D. F. Hoenig, *J. Phys. Chem.*, **65**, 2131 (1961).

## Association of Alkali Perchlorates in Anhydrous Methanol at 25°

by Alessandro D'Aprano

*Institute of Physical Chemistry, University of Palermo, Palermo, Italy (Received May 22, 1972)*

Equivalent conductance of alkali metal perchlorates in anhydrous methanol at 25° are reported. The  $K_A$  values have been determined by a new conductance equation including terms of order  $c^{3/2}$ , and contrary to a previous 1959 analysis, association has been found for all the perchlorates (including lithium and sodium). From a comparison of the association behavior of alkali perchlorates in different pure solvents in the range of dielectric constant between 80 and 30, the influence of cation solvation and the protic properties of solvent on the association process are considered.

### Introduction

A previous analysis of conductance data for lithium,<sup>1</sup> sodium,<sup>2</sup> potassium,<sup>2</sup> and cesium<sup>3</sup> perchlorate in anhydrous methanol by the Fuoss–Onsager conductance equation<sup>4,5</sup> indicated that lithium and sodium perchlorates are unassociated electrolytes. Recently, the association of alkali perchlorates has been found in water<sup>6</sup> by a new conductance equation, including terms of order  $c^{3/2}$ . Owing to the electrostatic nature of ion pair formation, these results are in disagreement; due to the lower dielectric constant, in fact, the association of alkali perchlorate in methanol ( $D = 32.66$ ) should be at least one order of magnitude greater than in water ( $D = 78.35$ ).

In order to investigate if the lack of association found for  $\text{LiClO}_4$  and the  $\text{NaClO}_4$  in pure methanol was due to the mathematical approximations of the Fuoss–Onsager previous treatment,<sup>4,5</sup> a new analysis of 1959 conductance data<sup>1,2</sup> has been made by the new equation.<sup>6</sup> The limiting conductance values obtained from this new analysis agree within 0.01  $\Lambda$  units with those derived by the 1959 treatment, while the more realistic values of  $K_A(\text{LiClO}_4) = 14$ ,  $K_A(\text{NaClO}_4) = 19$ ,  $K_A(\text{KClO}_4) = 34$ , and  $K_A(\text{CsClO}_4) = 54$  were obtained for the association constants.

To complete the series of alkali perchlorates, the conductance of rubidium perchlorate has been measured and the conductances of lithium, sodium, potassium, and cesium perchlorates were also redetermined in a concentration range below  $c_{\text{max}} < D^3 \times 10^{-7}$ , the critical concentration above which it is impossible to assign unique partners to ions to form pairs.<sup>7</sup>

The resulting association sequence  $K_A(\text{LiClO}_4) < K_A(\text{NaClO}_4) < K_A(\text{KClO}_4) < K_A(\text{RbClO}_4) < K_A(\text{CsClO}_4)$  found for the alkali perchlorates in methanol at 25° is in full agreement with that previously found<sup>6</sup> in pure water, where the alkali metal cations are assumed to be extensively solvated.

### Experimental Section

Methanol was refluxed over  $\text{AgNO}_3$  for 24 hr to remove traces of aldehydes or ketones, and then dis-

tilled in a closed system into a flask containing some magnesium turnings and traces of  $\text{I}_2$ . After a further 24-hr refluxing it was fractionally distilled. All outlets to the air were protected by drying tubes. The middle cut was used. Specific conductance was less than  $2 \times 10^{-8} \text{ ohm}^{-1} \text{ cm}^{-1}$  and the amount of water, tested by Karl Fisher reagent, was less than 0.01%. The anhydrous methanol was used immediately after distillation. A viscosity<sup>8</sup> of 0.5445 cP and dielectric constant<sup>9</sup> of 32.66 were used in the calculations.

Reagent grade perchlorates were recrystallized three times from conductivity water ( $\kappa_0 = 1-2 \times 10^{-6} \text{ ohm}^{-1} \text{ cm}^{-1}$ ) and dried by heating under vacuum for 4-6 weeks at 150°. The dried salts were kept in a desiccator containing  $\text{P}_2\text{O}_5$ .

Full details concerning electrical equipment and general technique have been outlined elsewhere.<sup>10</sup> The cell used was an erlenmeyer-type cell with an unplatinized electrodes and with a constant of  $1.6698 \text{ cm}^{-1}$  determined by the Lind–Zwolenick–Fuoss method<sup>11</sup> using aqueous solutions of potassium chloride.

Conductance runs were made by the concentration method. In order to test if the dried salts used were water free, two runs were made in dry methanol for each perchlorate after keeping the salts under vacuum (150°) for 4 and 6 weeks, respectively.

The experimental values of the equivalent conductance of alkali perchlorates in anhydrous methanol at 25° are given in Table I,<sup>12</sup> where  $\Lambda$  is the equivalent

- (1) F. Accascina and G. Craia, *Sci. Tec.*, **3**, 11 (1959).
- (2) F. Accascina and G. Craia, *ibid.*, **3**, 203 (1959).
- (3) F. Conti and G. Pistoia, *J. Phys. Chem.*, **72**, 2245 (1968).
- (4) R. M. Fuoss and L. Onsager, *ibid.*, **62**, 1339 (1958).
- (5) R. M. Fuoss, *J. Amer. Chem. Soc.*, **81**, 2659 (1959).
- (6) A. D'Aprano, *J. Phys. Chem.*, **75**, 3290 (1971).
- (7) R. M. Fuoss, *J. Amer. Chem. Soc.*, **57**, 2604 (1935).
- (8) G. Jones and H. J. Fonwalt, *ibid.*, **60**, 1683 (1938).
- (9) L. J. Gostin and P. S. Albright, *ibid.*, **68**, 1061 (1946).
- (10) F. Accascina, A. D'Aprano, and R. M. Fuoss, *ibid.*, **81**, 1058 (1959).
- (11) J. E. Lind, Jr., J. J. Zwolenick, and R. M. Fuoss, *ibid.*, **81**, 1557 (1959).

conductance ( $\text{ohm}^{-1} \text{cm}^{-2} \text{equiv}^{-1}$ ) an  $c$  the concentration ( $\text{equiv/l.}$ ).

All the conductance data including the previous 1959 data<sup>1-3</sup> were analyzed by a new conductance equation<sup>6</sup> in order to find the conductance parameters  $\Lambda_0$ ,  $K_A$ , and  $\bar{d}$ . All the calculations were made on a UNIVAC 1108 computer. Full details concerning the new equation and the search program have been reported in a previous paper.<sup>6</sup>

The results of the computer analysis are summarized in Table II where the various runs made in the present work are identified by the number given in Table I, while the 1959 data by the letters.

**Table II:** Derived Constants

Electrolyte	Run	$\Lambda_0$	$K_A$	$\bar{d}$	$\sigma$
LiClO <sub>4</sub>	1	110.58 ± 0.002	13.68 ± 0.01	7.9	0.004
	2	110.58 ± 0.000	13.66 ± 0.01	7.9	0.002
	a <sup>a</sup>	110.57 ± 0.003	13.71 ± 0.03	7.9	0.009
NaClO <sub>4</sub>	3	116.32 ± 0.002	18.96 ± 0.02	6.4	0.006
	4	116.32 ± 0.002	18.96 ± 0.02	6.4	0.004
	b <sup>b</sup>	116.29 ± 0.004	18.70 ± 0.04	6.4	0.01
KClO <sub>4</sub>	5	123.15 ± 0.001	34.22 ± 0.01	4.1	0.004
	6	123.16 ± 0.001	34.30 ± 0.01	4.1	0.005
	c <sup>b</sup>	123.16 ± 0.002	34.25 ± 0.02	4.1	0.005
RbClO <sub>4</sub>	7	127.01 ± 0.008	44.19 ± 0.09	3.4	0.03
	8	127.12 ± 0.007	44.96 ± 0.10	3.4	0.04
CsClO <sub>4</sub>	9	131.57 ± 0.02	53.80 ± 0.15	3.1	0.04
	10	131.55 ± 0.01	53.60 ± 0.16	3.1	0.05
	d <sup>c</sup>	131.58 ± 0.01	53.83 ± 0.10	3.1	0.03

<sup>a</sup> See ref 1. <sup>b</sup> See ref 2. <sup>c</sup> See ref 3.

## Discussion

From inspection of the results given in Table II, we note that all the perchlorates (including lithium and sodium) examined in the present work are associated in anhydrous methanol at 25°. The disagreement of this results from the 1959 analysis<sup>1,2</sup> can be easily explained considering the differences between the equations used. The linearized form of the Fuoss conductance equation<sup>5</sup>

$$\Lambda = \Lambda_0 - S\sqrt{c\gamma} + Ec\gamma \log c\gamma + Jc\gamma - K_A c\gamma f^2 \Lambda \quad (1)$$

or the simplified<sup>4</sup>

$$\Lambda = \Lambda_0 - S\sqrt{c} + Ec \log c + Jc \quad (2)$$

for an unassociated electrolyte, which have been used previously to analyze sodium, potassium, lithium, and cesium perchlorates conductance data, were obtained by retaining terms through those linear in concentration in the integration of the differential equation which describes the relaxation field. This approximation, made in order to simplify the form of the equation,

was found to be too drastic, especially for 1:1 ionophores in solvents with intermediate dielectric constants.

The anomalies accumulated in the literature for these systems using eq 1 and 2 have been examined recently by Justice.<sup>13</sup> In particular for the association constant, the  $K_A$  values derived from eq 1 must at least include all the effects due to terms higher than those linear in concentration which were not considered in the arbitrary truncated integration.

Recently the entire problem has been reexamined by Fuoss<sup>14</sup> and the arbitrary cutting of terms in concentration has been reduced by a new integration of the equations of continuity and motion, this time with retention of terms of order  $c^{3/2}$ . The resulting equation can be put in the form

$$\Lambda = \Lambda_0 - S\sqrt{c\gamma} + Ec\gamma \log c\gamma + Jc\gamma + J_2 c^{3/2} \gamma^{3/2} - K_A c\gamma f^2 \Lambda \quad (3)$$

The 1967 Fuoss-Hsia equation used in the present work is a recently revised version including some variation on the lower limit of integration of the function describing the relaxation terms, the use of a more complete Debye-Hückel expression for the activity coefficient of free ions, and several other changes previously<sup>6</sup> reported. As shown by the results obtained in the present research, the use of the new equation leads to much more reliable values of  $K_A$  for electrolytes in solvents with intermediate dielectric constants and demonstrates the influence of terms of the order  $c^{3/2}$  on the association of these systems when derived by numerical analysis of conductometric data.

Alkali perchlorates have been investigated so far by several authors in various solvent of high or intermediate dielectric constant, such as, water,<sup>6</sup> acetonitrile,<sup>15,16</sup> and sulfolane.<sup>17</sup> In order to have a complete set of specific information derived from each system, all these data have been reanalyzed by eq 3 used in the present research.

The results of the computer analysis for all the systems examined are summarized in Tables III, IV, and V where all the symbols have the usual meaning.

As may be noted in Tables II, III, IV, and V, for each solvent considered the association of alkali perchlorates increases as the cation crystallographic radii

(12) Table I will appear following these pages in the microfilm edition of this volume of the journal. Single copies may be obtained from the Business Operations Office, Books and Journals Division, American Chemical Society, 1155 Sixteenth St., N.W., Washington, D. C. 20036, by referring to code number JPC-72-2920. Remit check or money order for \$3.00 for photocopy or \$2.00 for microfiche.

(13) J. C. Justice, *Electrochim. Acta*, **16**, 701 (1971).

(14) K. L. Hsia and R. M. Fuoss, *Proc. Nat. Acad. Sci. U. S.*, **57**, 1550 (1967).

(15) R. L. Kay, B. J. Hales, and G. P. Gunningham, *J. Phys. Chem.*, **71**, 3925 (1967).

(16) F. Accascina and S. Schiavo, *Ric. Sci.*, **7**, 556 (1966).

(17) B. F. Prini and J. E. Prue, *Trans. Faraday Soc.*, **62**, 1257 (1966).

**Table III:** Derived Constants for the Alkali Perchlorates in Pure Water at 25°<sup>a</sup>

Salt	$\Lambda_0$	$K_A$	$\bar{d}$	$\sigma$
LiClO <sub>4</sub>	105.89 ± 0.4			0.04
NaClO <sub>4</sub>	117.32 ± 0.4	0.20 ± 0.14		0.04
KClO <sub>4</sub>	140.73 ± 0.1	0.98 ± 0.04	3.3	0.01
RbClO <sub>4</sub>	144.20 ± 0.1	1.35 ± 0.03	2.7	0.01
CsClO <sub>4</sub>	144.52 ± 0.3	1.69 ± 0.10	2.3	0.02

<sup>a</sup> See ref 6.**Table IV:** Derived Constants for the Alkali Perchlorates in Pure Acetonitrile at 25°<sup>a</sup>

Salt	$\Lambda_0$	$K_A$	$\bar{d}$	$\sigma$
LiClO <sub>4</sub> <sup>b</sup>	173.29 ± 0.04	19.55 ± 0.01	4.5	0.02
NaClO <sub>4</sub>	180.42 ± 0.13	20.77 ± 0.5	4.4	0.08
KClO <sub>4</sub>	187.66 ± 0.05	28.42 ± 0.14	3.4	0.02
RbClO <sub>4</sub>	189.59 ± 0.19	31.95 ± 0.4	3.2	0.06
CsClO <sub>4</sub>	191.16 ± 0.05	35.20 ± 0.15	3.0	0.02

<sup>a</sup> See ref 15. <sup>b</sup> See ref 16.**Table V:** Derived Constants for the Alkali Perchlorates in Pure Sulfolane at 30°<sup>a</sup>

Salt	$\Lambda_0$	$K_A$	$\bar{d}$	$\sigma$
LiClO <sub>4</sub>	11.057 ± 0.000	7.74 ± 0.2	4.7	0.05
NaClO <sub>4</sub>	10.334 ± 0.001	9.05 ± 0.04	4.2	0.08
KClO <sub>4</sub>	10.760 ± 0.001	9.86 ± 0.03	3.9	0.07
RbClO <sub>4</sub>	10.839 ± 0.001	10.16 ± 0.04	3.8	0.09
CsClO <sub>4</sub>	11.045 ± 0.002	11.25 ± 0.06	3.5	0.13

<sup>a</sup> See ref 17.

increase. This behavior has so far been explained by taking into account the effect of solvation of the cation on the ion pairing.<sup>18-23</sup> The behavior of association constants of the alkali perchlorates in the different solvent considered in the present analysis is shown in Figure 1 where  $\log K_A$  is plotted against  $1/DT$ . The most interesting fact evident in Figure 1 is that, while for CsClO<sub>4</sub> a linear relationship between  $\log K_A$  and

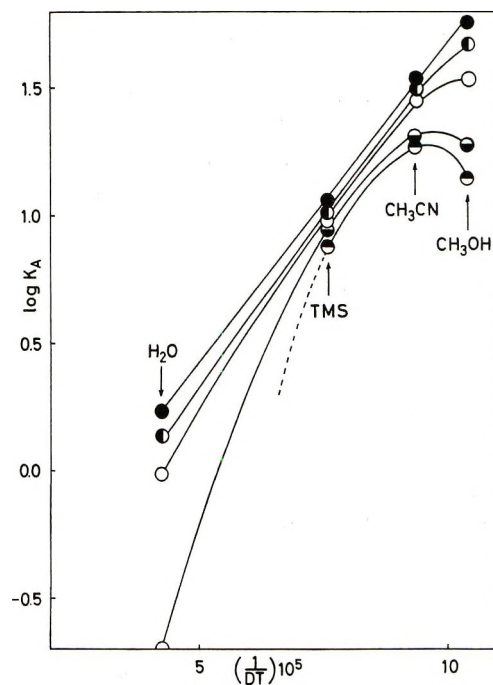


Figure 1.  $\log K_A$  vs.  $(1/DT) \times 10^5$  for the alkali perchlorates in different pure solvents: ●, CsClO<sub>4</sub>; ○, RbClO<sub>4</sub>; ○, KClO<sub>4</sub>; ○, NaClO<sub>4</sub>; ○, LiClO<sub>4</sub>.

$1/DT$  exists, the plots for the others alkali perchlorates become more concave down either if the atomic number of the cation decreases or if the hydrogen bonding capacity of the solvent increases. From these results, the association behavior of alkali perchlorates in different solvents appears to be governed on the one hand by the degree of solvation of the cations and on the other hand by the protic properties of solvent. The latter may be in relation with the postulated ability of perchlorate anion to form hydrogen bonds with protic solvents.<sup>23</sup>

- (18) A. D'Aprano and R. M. Fuoss, *J. Phys. Chem.*, **67**, 1704 (1963).
- (19) A. D'Aprano and R. M. Fuoss, *ibid.*, **67**, 1877 (1963).
- (20) A. K. Bodenseh and J. B. Ramsey, *ibid.*, **69**, 543 (1965).
- (21) W. R. Gilkerson and B. Ezell, *J. Amer. Chem. Soc.*, **87**, 3812 (1965).
- (22) W. R. Gilkerson and B. Ezell, *ibid.*, **88**, 3484 (1966).
- (23) F. Accascina, A. D'Aprano, and R. Triolo, *J. Phys. Chem.*, **71**, 3469 (1967).

# Ionic Association of Potassium Perchlorate in Sulfolane-Water Mixtures from Conductance Measurements at 25°

by A. D'Aprano,\* I. D. Donato,<sup>1a</sup> and R. Palombo<sup>1b</sup>

*Institute of Physical Chemistry, University of Palermo, Palermo, Italy (Received January 24, 1972)*

The ion pair association of potassium perchlorate in water-sulfolane mixtures has been computed by conductance measurements at 25°. Deviations from previous results in pure solvents are observed. An interpretation involving the water structure modification by sulfolane takes into account the observed behavior of ion pair association.

## Introduction

Over the past years a number of workers have made extensive investigations concerning the effects of the dielectric constant, the nature of ions, and the structure of the solvent on the ionic association. The main purpose of these studies has been to gain a further knowledge on the structure of the electrolyte species in solution. Among the different experimental techniques suitable for these investigations, conductance has been the most used, the conductometric method for determination of association constants being able to give exact experimental results within 0.01%. Owing to the limitation of the conductance theory<sup>2</sup> most of the published work has been made in solvents or solvent mixtures in the dielectric range below 30, where the association constant for the formation of electrostatic ion pair becomes detectable by the conductance equation.<sup>2b</sup> The lack of information about ionic association in solvents of higher dielectric constant has been recently eliminated by Fuoss with a new theoretical treatment of conductance theory.<sup>3</sup>

Recent studies on ionic association of alkali perchlorates in pure solvents,<sup>4,5</sup> covering the dielectric constant range between 80 and 30, have given experimental evidence of the large effects of solvent structure and ion solvation on the ion-pairing process.

In order to get a better understanding of the problem and to investigate the postulated<sup>6</sup> effect of water structure modification on the ionic association, the conductance of potassium perchlorate in water-sulfolane mixtures has been measured at 25°. The results are given and discussed in the present paper.

## Experimental Section

Reagent grade sulfolane (tetrahydrothiophene 1,1-dioxide) was distilled twice under reduced pressure (bp 130° (6.5 mm)). The middle fraction (60-70%) of each distillation was used.

Conductivity water ( $\kappa_0 = 1-2 \times 10^{-6}$  ohm<sup>-1</sup> cm<sup>-1</sup>) was purified as previously described.<sup>7</sup>

Water-sulfolane mixtures were made up by weight

and corrected to vacuum. For each solvent mixture used for conductance work, the physical properties were determined at 25°. Densities were measured in a Sprengel-type picnometer calibrated with distilled water. Viscosities were measured in a Ubbelohde viscometer. The flow time for water was 471.3 sec reproducible to 0.1 or 0.2 sec. Dielectric constants were measured on the General Radio 761 CSI capacitance bridge at 1 MHz using the stainless-steel cell previously described.<sup>8</sup> The physical properties of water-sulfolane mixtures are summarized in Table I,<sup>9</sup> where  $w$  is the weight per cent of water,  $D$  the dielectric constants,  $d$ (g/cm<sup>3</sup>) the densities,  $100\eta$  the viscosities in cP.

Reagent grade potassium perchlorate was recrystallized from conductivity water and dried by heating under vacuum at 150°. Conductance measurements were carried out by the concentration method using the bridge, bath, and electrical apparatus previously described.<sup>10</sup> All measurements were carried out at 25.00 ± 0.003°. Two erlenmeyer-type conductance

(1) (a) Postdoctoral Research Fellow CNR, Contract No. 69.00345/115/630, 1970. (b) Part of the results presented in this paper have been included in the thesis presented by R. Palombo to obtain the degree of "Docteur de Spécialité" in the University of Montpellier, France.

(2) (a) R. M. Fuoss and L. Onsager, *J. Phys. Chem.*, **61**, 668 (1957); (b) R. M. Fuoss, *J. Amer. Chem. Soc.*, **81**, 2659 (1959).

(3) R. M. Fuoss and K. L. Hsia, *Proc. Acad. Sci. U. S.*, **57**, 1550 (1967).

(4) A. D'Aprano, *J. Phys. Chem.*, **75**, 3290 (1971).

(5) A. D'Aprano, *ibid.*, **76**, 2920 (1972).

(6) A. D'Aprano and R. M. Fuoss, *J. Amer. Chem. Soc.*, **91**, 211 (1969).

(7) A. D'Aprano, *Ric. Sci.*, **34**(7), 433 (1964).

(8) J. Lind, Jr., and R. M. Fuoss, *J. Phys. Chem.*, **65**, 999 (1961).

(9) Tables I and II will appear following these pages in the microfilm edition of this volume of the journal. Single copies may be obtained from the Business Operations Office, Books and Journals Division, American Chemical Society, 1155 Sixteenth St., N.W., Washington, D. C. 20036, by referring to code number JPC-72-2923. Remit check or money order for \$3.00 for photocopy or \$2.00 for microfiche.

(10) F. Accascina, A. D'Aprano, and R. M. Fuoss, *J. Amer. Chem. Soc.*, **81**, 1058 (1959).

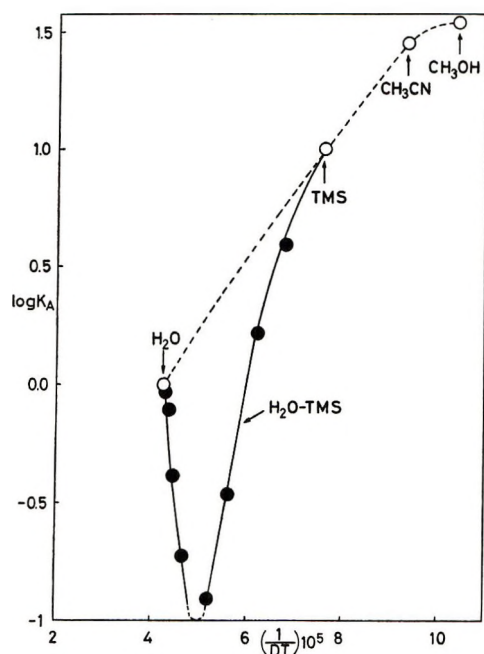


Figure 1.  $\log K_A$  vs.  $(1/DT) \times 10^6$  for  $KClO_4$  in (○) pure solvents and (●) water-sulfolane mixtures.

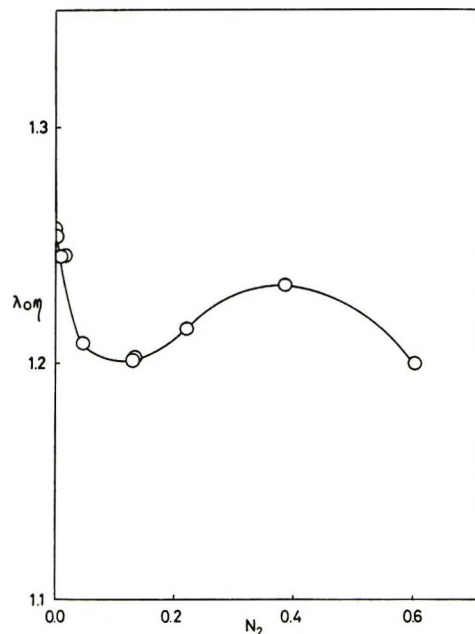


Figure 3. Walden product vs.  $N_2$  (mole fraction of sulfolane) for  $KClO_4$  in water-sulfolane mixtures at  $25^\circ$ .

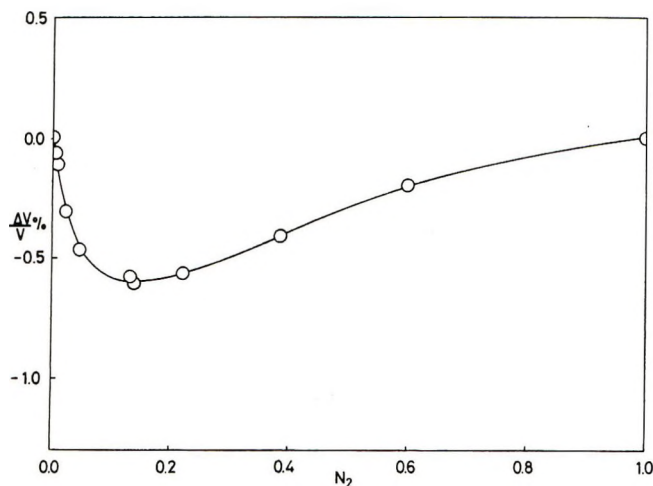


Figure 2.  $\Delta V/V 100$  vs. mole fraction of sulfolane ( $N_2$ ) in water-sulfolane mixtures at  $25^\circ$ .

cells were used. Cell constants  $1.6698 \pm 0.0002$  and  $7.0897 \pm 0.0005 \text{ cm}^{-1}$  were determined as previously described.<sup>11</sup>

The measured conductance of potassium perchlorate in sulfolane-water mixtures are summarized in Table II<sup>9</sup> where  $\Lambda$  is the equivalent conductance ( $\text{ohm}^{-1} \text{ cm}^2 \text{ equiv}^{-1}$ ) and  $c$  the concentration ( $\text{equiv}/\text{l}$ ). The values in pure water<sup>4</sup> and in pure sulfolane<sup>12</sup> are omitted since they were previously published.

### Discussion

The experimental data reported in Table II were analyzed by a new conductance equation<sup>4</sup>

$$\Lambda = \Lambda_0 - Sc^{1/2}\gamma^{1/2} + Ec\gamma \log c\gamma + Jc\gamma + J_2c^{3/2}\gamma^{3/2} - K_Ac\gamma f^2\Lambda \quad (1)$$

including terms of the order  $c^{3/2}$ . Equation 1, containing the four unknown  $\Lambda_0$ ,  $K_A$ ,  $J$ , and  $J_2$ , has been programmed for an electronic computer to find  $\Lambda_0$ ,  $K_A$ , and  $\bar{a}$  parameters. Full details concerning the new equation and the search program have been reported elsewhere.<sup>4</sup> We are indebted to Fuoss for making the Fortran computer program available to us.

The results of the computer analysis are summarized in the form of conductance parameters in Table III where the symbols have the usual meaning. All data are at  $25^\circ$  except in the case of pure sulfolane which has a melting point of  $28.45^\circ$ .<sup>13</sup> In this case the data are at  $30^\circ$ . From an inspection of Table II we note a minimum in the association of potassium perchlorate in water-sulfolane mixtures. This behavior is much more evident in Figure 1 where  $\log K_A$  for  $KClO_4$  in pure solvents<sup>5</sup> and in water-sulfolane mixtures is plotted against  $1/DT$ .

The minimum, already found by other workers<sup>6,14-16</sup> in several mixed solvents, demonstrates once more that the bulk dielectric constant is not the only factor involved in the association process, but other factors, strongly dependent on the nature and composition of solvent, must be considered. This means taking into

(11) J. E. Lind, Jr., J. Zwolenick, and R. M. Fuoss, *J. Amer. Chem. Soc.*, **81**, 1557 (1959).

(12) B. Fernández-Prini and J. E. Prue, *Trans. Faraday Soc.*, **62**, 1257 (1966).

(13) R. Garnsey and J. E. Prue, *ibid.*, **64**, 1206 (1968).

(14) Y. H. Inami, H. K. Bobenseh, and J. B. Ramsey, *J. Amer. Chem. Soc.*, **83**, 4745 (1961).

(15) F. Conti, P. Delogu, and G. Pistoia, *J. Phys. Chem.*, **72**, 1396 (1968).

(16) F. Conti and G. Pistoia, *ibid.*, **72**, 2245 (1968).

**Table III:** Derived Constants

$D$	$\Lambda_0$	$K_A$	$d$	$\sigma$
78.35	$140.73 \pm 0.1$	$0.98 \pm 0.04$	3.3	0.01
78.16	$138.78 \pm 0.03$	$0.99 \pm 0.01$	3.3	0.005
77.75	$135.19 \pm 0.04$	$0.93 \pm 0.02$	3.5	0.008
77.15	$130.19 \pm 0.09$	$0.79 \pm 0.09$	3.8	0.03
75.20	$118.14 \pm 0.1$	$(0.41 \pm 0.24)$		0.09
72.37	$98.25 \pm 0.05$	$(0.19 \pm 0.03)$		0.01
65.20	$63.63 \pm 0.06$	$(0.0 \pm 0.07)$		0.05
64.90	$63.05 \pm 0.08$	$(0.12 \pm 0.10)$		0.08
60.10	$46.46 \pm 0.03$	$(0.34 \pm 0.05)$		0.05
54.12	$31.168 \pm 0.008$	$1.64 \pm 0.04$	6.2	0.02
49.40	$21.287 \pm 0.004$	$3.95 \pm 0.01$	5.2	0.04
43.33 <sup>a</sup>	$10.760 \pm 0.001$	$9.86 \pm 0.03$	3.9	0.07

<sup>a</sup> Values at 30°, see ref 12.

account the influence on the association of the specific ion-solvent interactions connected to the solvent structure.

In order to investigate the dependence of ionic solvation on the solvent composition, the volumetric behavior of water-sulfolane mixtures was derived from the density values given in Table I. The results are shown in Figure 2 where the molar volume excess in per cent  $[(\Delta V/V)100]$  is plotted against the mole fraction of sulfolane ( $N_2$ ). As can be seen, a negative volume excess is found as sulfolane is added to pure water. Assuming that the increased packing density in the water-rich mixtures enhances the preferential solvation of ions by water, the observed decrease of association of potassium perchlorate can be rationalized considering the increased screening effect of the solvation shell on the ion-ion interaction.

A further comment should be made, finally, about the postulated increase of ionic solvation caused by the water structure modification. If such a process occurs, a decrease of ionic mobility must be observed in the water-rich region. The behavior of Walden product shown in Figure 3 seems to confirm, also from the hydrodynamic point of view, the above assumption.

## Effect of High Pressure on the Formation of Aqueous $\text{EuSO}_4^+$ at 25°

by Clarence F. Hale and F. H. Spedding\*

Ames Laboratory, U. S. Atomic Energy Commission and Department of Chemistry, Iowa State University, Ames, Iowa 50010 (Received March 30, 1972)

Publication costs assisted by Ames Laboratory, Iowa State University, Ames, Iowa

The formation of aqueous  $\text{EuSO}_4^+$  was studied at various pressures from atmospheric to 2040 atm at 25° using uv absorption spectrophotometry. Data were gathered at a constant ionic strength of 0.046  $m$  and as a function of ionic strength from 0.010 to 0.046  $m$ . The formation constants were found to be independent of wavelength from 240 to 250  $m\mu$ . The plots of  $\log \kappa$  and  $\log \kappa^\circ$  vs. pressure were found to exhibit distinct quadratic behavior. For the infinitely dilute solution,  $\Delta V^\circ$  of formation was calculated to be 25.6 and 12.0 ml/mol at atmospheric pressure and 2040 atm, respectively. The large  $\Delta V^\circ$  value at atmospheric pressure when compared to those from similar studies and from theories on ion-pair formation provides overwhelming evidence that  $\text{EuSO}_4^+$  is an inner-sphere complex in dilute aqueous solution.  $\bar{V}_{\text{EuSO}_4^+}^\circ$  was calculated to be  $-4.4$  ml/mol at 1 atm and 25°.

### Introduction

An earlier investigation from this laboratory employed differential uv absorption spectrophotometry<sup>1</sup> to study the association of aqueous  $\text{Eu}^{3+}$  and  $\text{SO}_4^{2-}$  ions as a function of dilute ionic strength, temperature, and wavelength. Analysis of the resulting  $\Delta H^\circ$  and  $\Delta S^\circ$  data provided strong evidence that  $\text{EuSO}_4^+$  in dilute aqueous solution at 25° exists primarily in the inner-sphere form; *i.e.*, the ions are in mutual contact with no solvent molecules separating them as in the case for

the outer-sphere type. Since the change in the partial molal volumes,  $\Delta V^\circ$ , for  $\text{EuSO}_4^+$  formation should also be sensitive to the type of complex formed,<sup>2</sup> it was decided to make a similar investigation of this system as a function of pressure.

Other studies made on the formation of aqueous com-

(1) C. F. Hale and F. H. Spedding, *J. Phys. Chem.*, **76**, 188 (1972).

(2) R. S. Bradley, "High Pressure Physics and Chemistry," Vol. 2, Academic Press, New York, N. Y., 1963, pp 131-162.

plex ions as a function of pressure have been rather scarce.<sup>1-7</sup> Discussions of those pertinent to the present investigation will be made later in this paper.

### Experimental Section

The methods employed in the volumetric preparation of the europium perchlorate, sodium perchlorate, and sodium sulfate stock solutions and sample and reference solutions were identical with those in the earlier temperature study.<sup>1</sup> The salt concentrations although not identical were very similar. Their concentrations were known to an accuracy of 0.2%. Between 15 and 17 sample solutions were prepared for use at each pressure and wavelength in the constant ionic strength studies. Eleven sample solutions were employed at each pressure and wavelength for those studies made at variable ionic strengths. As before, each sample had an identical companion reference solution except that it contained no sodium sulfate.

Since the ionic strength range studied was low, the changes in molar concentrations with pressure were safely calculated by assuming that the densities of the test solutions were those of pure water.

*Analysis of the Test Solutions.* A Cary Model 14 recording spectrophotometer equipped with a thermostatable cell compartment, supplied from an external water bath held at  $25.0 \pm 0.1^\circ$ , was employed to measure the experimental absorbancies.

The air-operated single-ended pump, 316-stainless steel tubing, valves, gauges, and high-pressure optical cell with sapphire windows were supplied by the American Instrument Co. and are all listed in their commercial catalog. However, some minor modifications were made. The pump was adapted to use distilled water as the pumping fluid. The path length of the optical cell was increased from 1.0 to 2.0 cm while its overall size was decreased, so that it would fit into the standard cell compartment of a Cary 14. The optical cell was also provided with a Hastelloy-C liner to inhibit corrosion and special O rings containing a high percentage of Teflon. The original O rings were found to discharge a substance whose absorbancy, relative to that of the test solutions, was too large to tolerate. These modifications to the optical cell reduced its pressure rating to 50,000 psi from 100,000 psi.

To compensate for the low-experimental absorbancies (less than 0.2) due to the short path length of 2.0 cm,<sup>8</sup> the normal slide wire was replaced with one which expanded the absorbancy scale by a factor of 10. All readings were taken manually at each wavelength and not from a recording of the spectra. The reference beam had to be masked due to excessive attenuation of the sample beam by the narrow aperture of the high-pressure optical cell.

To prevent mixing of the test solutions with the oil-contaminated distilled water used by the pump, a separator was positioned between the pump and optical cell.

It was composed of a movable Teflon plug with O ring contained in a stainless steel jacket having an inner lining of Hastelloy-C. The pressure was monitored by two Bourdon tube type gauges on the pump side of the separator and two on the optical cell side. These gauges provided an accuracy of  $\pm 7$  atm up to 680 atm and  $\pm 27$  atm from 680 to 2040 atm.

The optical cell was thoroughly flushed with distilled water before using and the reference baselines at 240, 245, and 250 m $\mu$  were checked and set, if necessary. The absorbancy of a single test solution was then measured at these three wavelengths at 11 pressures from 1 to 2040 atm. After the reading at 2040 atm the pressure was returned to 1 atm and the absorbancy rechecked. If any significant difference was found (*i.e.*, greater than 0.0005 absorbancy units) the run was repeated after locating and correcting the malfunction. In addition, at the conclusion of a days work, the optical cell was flushed with distilled water and the baselines rechecked.

Since only one high-pressure optical cell was used, all absorbancy readings were made *vs.* air. Therefore, unlike the previous study on this system<sup>1</sup> where the more accurate method of differential spectrophotometry was employed, the absorbancies of the reference solutions had to be subtracted manually from those of the sample solutions.

*Equations and Definition of Terms.* The molar thermodynamic equilibrium constant  $K^\circ$  for the association of europium(III) and sulfate ions as expressed by eq 1 is the product of its formation constant  $K$  and activity coefficient factor ( $Y_{\pm}$ ).



$$K = [\text{EuSO}_4^+]/([\text{Eu}^{3+}][\text{SO}_4^{2-}]) \quad (2a)$$

$$K^\circ = K\{Y_{\text{EuSO}_4^+}/((Y_{\text{Eu}^{3+}})(Y_{\text{SO}_4^{2-}}))\} \quad (2b)$$

For this investigation the unknown activity coefficient factor was assumed to have been invariant at each pressure for those studies made at constant ionic strength. For maximum clarity the hydration spheres of the ions have not been shown.

Equation 4 which assumed that Beer-Lambert's law and the law of mass action were applicable over the experimental conditions employed was used to evaluate  $K$  and  $(\epsilon_1 - \epsilon^\circ)$  from the experimental absorbancy data.

(3) S. D. Hamann, P. J. Pearce, and W. Strauss, *J. Phys. Chem.*, **68**, 375 (1964).

(4) F. H. Fisher and D. F. Davies, *ibid.*, **69**, 2595 (1965).

(5) F. H. Fisher and D. F. Davies, *ibid.*, **71**, 819 (1967).

(6) R. A. Horne, B. R. Myers, and G. R. Frysinger, *Inorg. Chem.*, **3**, 452 (1964).

(7) F. H. Fisher, *J. Phys. Chem.*, **66**, 1607 (1962).

(8) The analogous temperature study previously made on this system<sup>1</sup> employed optical cells having path lengths of 10 cm. Also, unlike the previous study which utilized differential spectrophotometry, the reference solutions which had very low absorbancies had to be measured separately.

It contains a term to correct for the presence of  $\text{NaSO}_4^-$  ion pairs. The derivation of this equation without the  $\text{NaSO}_4^-$  modification is well known and therefore will not be given here.<sup>9</sup> Light absorption by sodium sulfate was found to be insignificant at the concentrations and wavelengths employed. As in the previous temperature study on this system,<sup>1</sup> the formation of bisulfate ion was safely ignored. Due to the inability to obtain accurate  $K_2$  and  $(\epsilon_1 - \epsilon^\circ)$  values at pressures significantly above atmospheric, no corrections were made for the presence of the  $\text{Eu}(\text{SO}_4)_2^-$  complex.

$$[\text{NaSO}_4^-] = \frac{Q(N + 2S)[\text{SO}_4^{2-}]}{1 + Q[\text{SO}_4^{2-}]} \quad (3a)$$

$$Q = [\text{NaSO}_4^-]/([\text{Na}^+][\text{SO}_4^{2-}]) \quad (3b)$$

$$\bar{a} = (\epsilon_1 - \epsilon^\circ) - \frac{1}{K} \left\{ \frac{\bar{a}}{[\text{Eu}^{3+}]} \left( 1 + \frac{[\text{NaSO}_4^-]}{[\text{SO}_4^{2-}]} \right) \right\} \quad (4)$$

$$[\text{EuSO}_4^+] = (A_s - A_r)/(L(\epsilon_1 - \epsilon^\circ)) \quad (5)$$

$$[\text{SO}_4^{2-}] = S - [\text{EuSO}_4^+] - [\text{NaSO}_4^-] \quad (6)$$

$$[\text{Eu}^{3+}] = E - [\text{EuSO}_4^+] \quad (7)$$

$$K = \bar{a}/((\epsilon_1 - \epsilon^\circ) - \bar{a})[\text{SO}_4^{2-}] \quad (8)$$

$$I = 6\{E - [\text{EuSO}_4^+]\} + 3S + N - 2[\text{NaSO}_4^-] \quad (9)$$

where  $\bar{a} = (A_s - A_r)/SL$ ,  $\bar{a} = (A_s - A_r)/EL$ ,  $E$  = molar concentration  $\text{Eu}(\text{ClO}_4)_3$ ,  $S$  = molar concentration  $\text{Na}_2\text{SO}_4$ ,  $N$  = molar concentration  $\text{NaClO}_4$ ,  $L$  = path length in cm,  $A_s$  = absorbancy of sample solution,  $A_r$  = absorbancy of reference solution,  $\epsilon^\circ$  = molar extinction coefficient of  $\text{Eu}^{3+}$ ,  $\epsilon_1$  = molar extinction coefficient of  $\text{EuSO}_4^+$ ,  $[x]$  = molar concentration of  $x$  at equilibrium.

$$\left\{ \log K - \frac{\Delta Z^2 A I^{1/2}}{1 + I^{1/2}} \right\} = \log K^\circ - (\Delta Z^2 A D) I \quad (10)$$

where  $\Delta Z^2 = \sum Z^2(\text{products}) - \sum Z^2(\text{reactants})$ ,  $Z$  = charge on ion,  $A$  = Debye-Hueckel constant (pressure and temperature dependent),  $D$  = constant.

**Determination of the Formation Constants.** For the investigations at constant ionic strength  $K$  and  $(\epsilon_1 - \epsilon^\circ)$  were obtained from eq 4 in conjunction with eq 3a, 5, 6, and 7, in that order, by initially setting  $[\text{Eu}^{3+}] = E$  and  $[\text{SO}_4^{2-}] = S$ . An iterative process was then employed using refined values for  $[\text{SO}_4^{2-}]$ ,  $[\text{Eu}^{3+}]$ , and  $[\text{NaSO}_4^-]$ , until the change in  $K$  was less than 0.1%; this took four to five cycles.

For  $Q$ , the formation constant of  $\text{NaSO}_4^-$  as defined by eq 8, the value of 5.0 at infinite dilution as determined by Jenkins and Monk<sup>10</sup> at 25° was used. Its pressure dependence was estimated from the equation for ion-pair association proposed by Fuoss.<sup>11</sup> For these calculations Owen and Brinkley's<sup>12</sup> analysis of Kyropoulos<sup>13</sup> measurements on the dielectric constant of water at high pressures was employed.<sup>14</sup> Also the value of 4.8 calculated for  $\bar{a}$  at 1 atm and 25° was assumed to be

independent of pressure.  $Q$  was found to decrease from 5.0 at 1 atm to 4.3 at 2040 atm at 25°. The ionic strength dependence of  $Q$  was obtained from eq 10 after first setting  $D = 0.3$ , as recommended by Davies.<sup>16</sup> The adequacy of this value for  $D$  for such an extrapolation was discussed previously.<sup>1</sup>

For those studies made at various ionic strengths,  $K$  was calculated directly from eq 8 after assuming that the  $(\epsilon_1 - \epsilon^\circ)$  values obtained in the constant ionic strength investigation for any one wavelength and pressure remained constant over the entire ionic strength range studied; *i.e.*, 0.046–0.010  $m$ .

First an approximate ionic strength for a single sample solution was determined from eq 9 and 5 by ignoring the presence of  $\text{NaSO}_4^-$  ion pair. A value for  $Q$  was then calculated for this approximate ionic strength as described above, after which the initial  $[\text{NaSO}_4^-]$  concentration was obtained from eq 3a by first setting  $[\text{SO}_4^{2-}] = S$ . Then  $[\text{SO}_4^{2-}]$  was calculated from eq 5 and 6, which in turn was used in eq 8 and 9 to obtain  $K$  and a new ionic strength. After this process was repeated for all the sample solutions, the resulting  $K$  values were then extrapolated to infinite dilution by using eq 10 to obtain the initial molar thermodynamic formation constant  $K^\circ$ . This procedure was repeated, using progressively more accurate  $[\text{SO}_4^{2-}]$  concentrations, until the change in  $K^\circ$  was less than 0.1%; generally only three cycles were required.

Due to the pressure dependence of the molar concentration scale, these molar formation constants had to be corrected to the molal concentration scale before accurate  $\Delta V$  and  $\Delta V^\circ$  values could be determined. This was accomplished by multiplying the final  $K$  and  $K^\circ$  values by the density of pure water at that pressure. To distinguish the formation constants based on the molal scale from those on the molar scale, the molal formation constants have been written as  $\kappa$  and  $\kappa^\circ$ . The  $K^\circ$  to  $\kappa^\circ$  conversions were exact, but those for  $K$  to  $\kappa$  were not. However, due to the low-ionic strength of 0.046  $m$ , the resulting error in  $\kappa$  is negligible. Also, in the  $\Delta V$  calculations it is the change in density with pressure that is important and not its absolute value.

The method of least squares was employed for all the data fitting. The experimental points<sup>17</sup> were weighted

(9) C. B. Monk, "Electrolytic Dissociation," 1st ed, Academic Press, London, 1961, p 186.

(10) I. L. Jenkins and C. B. Monk, *J. Amer. Chem. Soc.*, **72**, 2695 (1950).

(11) R. A. Robinson and R. H. Stokes, "Electrolyte Solutions," Butterworths, London, 1959, p 551.

(12) B. B. Owen and S. R. Brinkley, Jr., *Phys. Rev.*, **64**, 32 (1943).

(13) S. Kyropoulos, *Z. Phys.*, **40**, 507 (1926).

(14) The more recent data of Owen, Miller, Milner, and Cogan<sup>15</sup> are probably more accurate but, unfortunately, only extend to 1000 atm.

(15) B. B. Owen, R. C. Miller, C. E. Milner, and H. L. Cogan, *J. Phys. Chem.*, **65**, 2065 (1961).

(16) C. W. Davies, "Ion Association," 1st ed, Butterworths, London, 1962, p 41.

in the manner described by Wolberg.<sup>18</sup> Any points falling outside the 95% confidence level were rejected.<sup>19</sup> If a point was rejected, that particular set of iterations was repeated from the beginning. All the calculations were executed by an IBM Model 360 digital computer.

## Results

Table I contains the final  $K$  and  $(\epsilon_1 - \epsilon^\circ)$  values obtained at 240, 245, and 250  $m\mu$  at a constant ionic strength of 0.046  $m$  over the pressure range of 1 to 2040 atm at 25°. The formation constants at each pressure were found to be independent of wavelength,<sup>20</sup> at least within the standard deviations which averaged about 2.5% up to 953 atm, 4% from 953 to 1770 atm, and 8% at 2040 atm.

**Table I:**  $K$  and  $(\epsilon_1 - \epsilon^\circ)$  for Aqueous  $\text{EuSO}_4^+$  Formation at  $I = 0.046 m$  and 25°

Pressure, atm	$\lambda, m\mu$					
	240		245		250	
	$K$	$(\epsilon_1 - \epsilon^\circ)$	$K$	$(\epsilon_1 - \epsilon^\circ)$	$K$	$(\epsilon_1 - \epsilon^\circ)$
1	557	81.26	571	73.66	564	62.02
136	504	79.01	517	71.24	506	59.95
272	453	76.88	444	70.21	443	58.71
408	398	75.24	397	67.95	405	56.20
545	358	73.28	353	66.36	353	54.94
680	317	71.75	324	63.87	320	53.04
953	261	67.54	268	59.48	255	49.96
1225	211	64.82	222	55.93	213	46.41
1497	182	61.12	186	53.02	186	43.18
1770	152	59.21	155	51.32	162	40.69
2040	139	54.71	142	47.73	127	40.59

The variable ionic strength studies were made from 0.011 to 0.046  $m$  at the same pressures and wavelengths as above. The resulting molar thermodynamic formation constants  $K^\circ$ , obtained after extrapolation to infinite dilution, are given in Table II. Again no trend with wavelength was noted within the standard deviations which averaged about 1.5 to 2.5% over the entire pressure range.

**Table II:**  $K^\circ$  for Aqueous  $\text{EuSO}_4^+$  Formation at 25°

Pressure, atm	$K^\circ \times 10^{-3}$		
	$\lambda, m\mu$		
	240	245	250
1	4.57	4.93	4.78
136	4.12	4.34	4.29
272	3.56	3.62	3.53
408	3.12	3.17	3.24
545	2.79	2.77	2.76
680	2.40	2.49	2.44
953	1.94	1.98	1.91
1225	1.53	1.66	1.58
1497	1.24	1.31	1.32
1770	1.05	1.07	1.11
2040	0.96	0.98	0.89

The final  $K$  and  $K^\circ$  values together with their standard deviations are reported in Table III. These molar formation constants were calculated by taking an average of the three given at each pressure in Table II. The uncertainties were determined in the same manner, although their individual values were not shown in Table II. Table III also contains the molal formation constants calculated from these final  $K$  and  $K^\circ$  values. At 1 atm the value of 560 for  $K$  is in excellent agreement with that of 570 obtained from the earlier temperature study made on this system, in which the presence of the  $\text{Eu}(\text{SO}_4)_2^-$  complex was taken into account.<sup>1</sup> This was to be expected since, in this previous work which used analogous salt concentrations, it was shown that at 25° only a 2% change in  $K$  would result if  $\text{Eu}(\text{SO}_4)_2^-$  were ignored.

**Table III:** Final Molar and Molal Formation Constants for Aqueous  $\text{EuSO}_4^+$  at 25°

Pressure, atm	Ionic strength			
	0.046 $m$		0 $m$	
	$K \times 10^{-2}$	$\kappa^\circ \times 10^{-2}$	$K^\circ \times 10^{-3}$	$\kappa^\circ \times 10^{-3}$
1	5.64 ± 0.15	5.62	4.76 ± 0.07	4.74
136	5.09 ± 0.12	5.10	4.25 ± 0.06	4.25
272	4.47 ± 0.11	4.50	3.57 ± 0.09	3.59
408	4.00 ± 0.11	4.05	3.18 ± 0.06	3.22
545	3.55 ± 0.10	3.61	2.77 ± 0.07	2.83
680	3.20 ± 0.08	3.28	2.44 ± 0.05	2.50
983	2.61 ± 0.07	2.70	1.94 ± 0.05	2.01
1225	2.15 ± 0.07	2.25	1.59 ± 0.05	1.66
1497	1.85 ± 0.08	1.95	1.29 ± 0.03	1.36
1770	1.56 ± 0.07	1.66	1.08 ± 0.02	1.14
2040	1.36 ± 0.12	1.46	0.94 ± 0.02	1.01

When  $\log \kappa$  and  $\log \kappa^\circ$  were plotted *vs.* pressure, a plot which exhibited distinct quadratic behavior was obtained. The following equations were found to best represent the data over the entire pressure range. The accompanying uncertainties are the standard deviations obtained from the least-squares fit of the data.

$$\log \kappa = 2.755 - 3.821 \times 10^{-4}P + 4.48 \times 10^{-8}P^2 \pm 0.0022$$

(17) The raw absorbancy data were far too numerous to be included in this paper. Therefore, all the  $A_s - A_t$  values for the test solutions at all the ionic strengths, wavelengths, and pressures employed will appear following these pages in the microfilm edition of this volume of the journal. Single copies may be obtained from the Business Operations Office, Books and Journals Division, American Chemical Society, 1155 Sixteenth St., N.W., Washington, D. C. 20036, by referring to code number JPC-72-2925. Remit check or money order for \$3.00 for photocopy or \$2.00 for microfiche.

(18) J. R. Wolberg, "Prediction Analysis," Van Nostrand, New York, N. Y., 1967.

(19) W. Chauvenet, "Spherical and Practical Astronomy," Vol. V, Lippincott, Philadelphia, Pa., 1868, p 558.

(20) The importance of  $K$  being constant as a function of wavelength was discussed fully in an earlier paper.<sup>1</sup>

$$\log \kappa^\circ = 3.682 - 4.540 \times 10^{-4}P + 5.89 \times 10^{-8}P^2 \quad \pm 0.0044$$

The desired  $\Delta V$  and  $\Delta V^\circ$  values were obtained from eq 11 and are reported in Table IV.

**Table IV:**  $\Delta V$  and  $\Delta V^\circ$  for Aqueous  $\text{EuSO}_4^+$  Formation at 25°

Pressure, atm	Ionic strength	
	0.046 <i>m</i> $\Delta V$ , ml/mol	$\rightarrow 0$ <i>m</i> $\Delta V^\circ$ , ml/mol
1	21.5	25.6
136	20.8	24.7
272	20.2	23.8
408	19.5	22.9
545	18.8	22.0
680	18.1	21.1
953	16.7	19.3
1225	15.3	17.4
1497	14.0	15.6
1770	12.6	13.8
2040	11.2	12.0

$$(RT \partial \ln \kappa^\circ / \partial P)_T = -\Delta V^\circ \quad (11)$$

## Discussion

The association of two ions to form an outer-sphere complex should be accomplished by only a slightly positive  $\Delta V^\circ$ , because the primary hydration sheaths and surrounding solvent molecules of both ions are but little affected. However, a large positive  $\Delta V^\circ$  would be expected for inner-sphere complex formation where mutual contact of the ions would lead to significant liberation of the solvent molecules due to the disruption of the hydration sheaths and the greater cancellation of charges.

Previous investigations concerning the effects of high pressure on the formation of complex ions have been rather scarce in the literature. Those which have a bearing on the present study are listed in Table V.

Hamann, Pearce, and Strauss<sup>3</sup> found  $\Delta V^\circ = 8.0$  ml/mol for the formation of aqueous lanthanum ferricyanide ion pairs at 25° and 1 atm. They compared this value and that of 7.3 ml/mol from Fisher's<sup>7</sup> study on  $\text{MgSO}_4$  with those calculated from the theories on ion association as proposed by Bjerrum<sup>21</sup> and Fuoss<sup>11</sup> and found good agreement. This led the authors to conclude that these two salts form true outer-sphere complexes in dilute aqueous solutions.

Since the  $\Delta Z^2$  for  $\text{EuSO}_4^+$  formation lies between that of  $\text{MgSO}_4$  and  $\text{LaFe}(\text{CN})_6$ , one would expect its  $\Delta V^\circ$  to be 5–9 ml/mol at 25° and 1 atm if  $\text{EuSO}_4^+$  were of the outer-sphere type. Instead, the much higher value of 25.6 ml/mol was obtained. This three- to five fold increase in  $\Delta V^\circ$  from that predicted by theory for outer-sphere ion pairs could only be reasonably explained by assuming that  $\text{EuSO}_4^+$  exists primarily<sup>22</sup> as an inner-sphere complex in dilute aqueous solution.

**Table V:**  $\Delta V^\circ$  of Formation for Some Aqueous Complex Ions at 25° and 1 atm

Complex	$\Delta V^\circ$	Ref
$\text{MgSO}_4$	7.3	18
$\text{MnSO}_4$	7.4	2
$\text{LaFe}(\text{CN})_6$	8.0	3
$\text{LaSO}_4^+$	21–26	5
$\text{EuSO}_4^+$	25.6	This study

The only previous high-pressure investigation made on an aqueous rare earth-sulfate complex was that on  $\text{La}_2(\text{SO}_4)_3$  by Fisher and Davies.<sup>5</sup> They studied the electrical conductance of  $\text{La}_2(\text{SO}_4)_3$  at various pressures up to 2000 atm at 25° and reported 21.2–26.2 ml/mol at atmospheric pressure and 6.8–11.8 ml/mol at 2000 atm for  $\Delta V^\circ$  of association. They employed three different equations in their calculations and found that each gave different  $\Delta V^\circ$  values. This and the fact that their values were also concentration dependent precluded their reporting a single  $\Delta V^\circ$  for each pressure. Nevertheless, their results over the entire pressure range agree very well with those from this investigation.<sup>23</sup> This is particularly noteworthy since they used completely different experimental and analytical methods as compared to those employed in this study.

(21) See ref 10, p 393.

(22) The  $K_1$  values calculated in this study actually represent the sum of the formation constants for the inner- and outer-sphere species. Merely making the spectroscopic studies at various wavelengths does not by itself enable one to separate  $K_1$  into its component parts.

(23) Due to the effective shielding of the 4f orbitals by the 5s and 5p orbitals aqueous rare earth(III) ions display many similar chemical properties. Therefore, since the partial molar volumes of aqueous lanthanum and europium salts are very similar,<sup>24</sup> e.g.,  $V^\circ_{\text{La}^{3+}} = -42.0$  and  $V^\circ_{\text{Eu}^{3+}} = -44.5$  ml/mol, it would be expected that their  $\Delta V^\circ$  values for monosulfate complex ion formation should also be similar.

(24) F. H. Spedding, M. J. Pikal, and B. O. Ayers, *J. Phys. Chem.*, **70**, 2550 (1966).

## COMMUNICATIONS TO THE EDITOR

### Quasi-Equilibrium Analysis of the Reaction of Atomic and Molecular Fluorine with Tungsten

Publication costs assisted by the Joint Services Electronics Program

Sir: Rosner and Allendorf<sup>1</sup> have recently reported experimental data on the fluorination rate of solid tungsten which revealed a sharp drop in reactivity above a filament temperature of 2000°K. Based on a comparison of these data with the quasi-equilibrium (QE) model of Batty and Stickney,<sup>2,3</sup> they concluded that<sup>1</sup> "the quasi-equilibrium model, combined with presently available thermochemical data, does not provide a self-consistent explanation of our observed Arrhenius behavior for the W(s)-F(g) reaction." However, one reason for reaching this conclusion was that, based on the quasi-equilibrium model and available thermochemical data for WF<sub>6</sub>(g) and F(g), Rosner and Allendorf found that the predicted transition in dominant reaction product from WF<sub>6</sub>(g) to F(g) occurred below 2000°K. We wish to point out here that while their analysis appears to be correct, the temperature at which the QE-predicted transition occurs is within 100°K of the value (~2000°K) corresponding to the experimental data. Hence, we suggest that the quasi-equilibrium model, when combined with available data, is not inconsistent with Rosner and Allendorf's data.

To provide a more detailed comparison of the QE predictions with the experimental data of Rosner and Allendorf, we have performed a complete analysis similar to that described in ref 3 for the O<sub>2</sub>-W reaction. The results are shown in Figure 1, which is a reproduction of Figure 4 of Rosner and Allendorf<sup>1</sup> except for

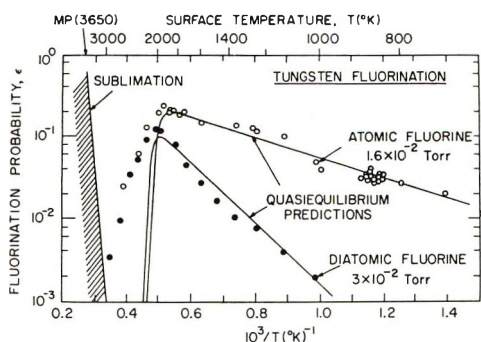


Figure 1. Comparison of predictions of the quasi-equilibrium model with experimental data of Rosner and Allendorf,<sup>1</sup> where the fluorination probability  $\epsilon$  is defined as the ratio of the rate of removal of W atoms from the specimen to the rate at which fluorine atoms or molecule impinge upon the specimen.

our addition of the curves representing the quasi-equilibrium predictions. For simplicity, we have approximated their data for  $T < 1800^\circ\text{K}$  by straight lines, thereby causing the empirically determined equilibration probabilities<sup>2,3</sup> for F and F<sub>2</sub> to be simple exponential functions of temperature.<sup>4</sup> Although the procedure by which the equilibration probabilities are determined<sup>2,3</sup> is responsible for the close agreement of the QE calculations with the experimental data in the region  $T < 1800^\circ\text{K}$ , the maxima appearing near 2000°K result primarily from the fact that the thermodynamic aspect of the quasi-equilibrium model causes the dominant reaction product to change from WF<sub>6</sub> to F as  $T$  increases. (Based on available thermochemical data, WF is negligible under the present conditions.) It seems to us that such predictions provide a satisfactory semiquantitative explanation of the experimental data, but we are disappointed by the increasing discrepancy at the highest temperatures.

*Acknowledgment.* This work was supported in part by the Joint Services Electronics Program [Contract No. DA28-043-AMC-D2536 (E)], by ARPA [Contract No. DAHC15-67-0222], and by NASA [Grant No. NGR-22-009-091].

- (1) D. E. Rosner and H. D. Allendorf, *J. Phys. Chem.*, **75**, 308 (1971).
- (2) J. C. Batty and R. E. Stickney, *J. Chem. Phys.*, **51**, 4475 (1969).
- (3) J. C. Batty and R. E. Stickney, *Oxid. Metals.*, **3**, 331 (1971).
- (4) Although this simplifying assumption does not have a substantial effect on the general (qualitative) nature of the predictions, it does neglect the fact that Rosner and Allendorf's data exhibit definite structure,<sup>1</sup> such as the "bump" in the curve for atomic fluorine at  $T \approx 850^\circ\text{K}$ . We shall not attempt to consider the possible explanations of the structure.

MECHANICAL ENGINEERING DEPARTMENT PHILIP C. ABBOTT  
 MASSACHUSETTS INSTITUTE OF TECHNOLOGY ROBERT E. STICKNEY\*  
 CAMBRIDGE, MASSACHUSETTS 02139

RECEIVED AUGUST 9, 1971

### Reply to "Quasi-Equilibrium Analysis of the Reaction of Atomic and Molecular Fluorine with Tungsten"

Publication costs assisted by the U. S. Army Research Office (Durham N. C.)

Sir: The quasi-equilibrium (QE) model underprediction of rates at and above 2000°K shown in Abbott

and Stickney's Figure 1<sup>1</sup> was in fact one *basis* for our earlier conclusion.<sup>2</sup> There is no question that the quasi-equilibrium model, with WF<sub>6</sub> and F assumed as the dominant products, predicts a decrease in reaction probability above some intermediate temperature—in qualitative agreement with our experimental data.<sup>2</sup> However, in our opinion, too many additional factors are involved in the tungsten fluorination reaction to be content with the qualitative agreement pointed out by Abbott and Stickney. Thus,<sup>2</sup> (i) the complex temperature dependence of the W removal rate (more than one local maximum), (ii) the inadequacy of thermodynamic data for the lower fluorides (WF<sub>n</sub>(g), *n* < 6), and (iii) the magnitude of the observed peak W atom removal probability<sup>2</sup> ( $\epsilon_{\max} > 1/6$ ; see especially the Mo/F data of ref 2), when combined with the QE underprediction of rates (in the only portions of Figure 1 of ref 1 which are *bona fide* predictions) seem to us to preclude WF<sub>6</sub>(g) as the only significant W-containing product, especially above 2000°K. Moreover, it is significant that the QE underpredictions of rate above 2000°K (well over three decades at 2500°K) far exceed discrepancies that could reasonably be attributed to experimental uncertainties in (i) reactant arrival rate, (ii) WF<sub>6</sub>(g) thermochemical data, and/or (iii) oxygen impurity level.

Without more complete thermodynamic data for the gaseous tungsten fluorides and/or product distribution measurements for this and similar reactions it is difficult (i) to decide on the accuracy of QE in the W-F<sub>2</sub> reaction and (ii) to answer the more subtle question of whether the assumptions *underlying* QE models<sup>3,4</sup> break down for atom-metal reactions in which product formation by Rideal-Eley elementary steps may play an important role.<sup>5</sup> Indeed, the use of atomic reactants to study the gasification kinetics of refractory solids<sup>6,7</sup> could shed light on this interesting question.<sup>2</sup>

## Optical Absorption of Solvated Electrons in Alcohols and Their Mixtures with Alkanes

*Publication costs assisted by the U. S. Atomic Energy Commission<sup>1</sup>*

*Sir:* As noted by others,<sup>2-9</sup> the alcohols and their mixtures, especially with alkanes, are particularly suitable media for study of the factors that influence the formation, structure, and decay of solvated electrons. We have initiated a broad and thorough study of the time dependence of solvated electron absorption spectra in such media. The initial results of that study are of special interest and significance in relation to certain previously published experimental work<sup>2,4-6</sup> and models<sup>10-13</sup> for the solvated electron. Absorption spectra have been determined for the solvated electron in 22 alcohols (for 15 of which the e<sub>s</sub><sup>-</sup> spectrum has not been reported) and in binary mixtures of a number of alcohols and cyclohexane. Some salient aspects of the results are reported in this Communication.

The best available grade of each alcohol was purified by distillation with a Nester-Faust spinning-band column. Water content of an alcohol never exceeded 0.2% and generally was less than 0.1%. Fisher Certified cyclohexane was used without further purification. Solutions were deaerated by nitrogen bubbling and irradiated in 1-cm quartz cells at ~30° with 5- or 10-nsec pulses of ~8-MeV electrons (estimated dose per pulse of ~10<sup>18</sup> eV ml<sup>-1</sup>) from the Notre Dame Arco Model LP-7 linear accelerator. The light source for measurement of the optical absorption was a 450-W xenon lamp (Ushio UXL 451-0) that was pulsed to 50 times the steady-state output for a 5-msec period within which the absorption was recorded. Trans-

(1) The Radiation Laboratory of the University of Notre Dame is operated under contract with the U. S. Atomic Energy Commission. This is AEC Document No. COO-38-851.

(2) M. C. Sauer, Jr., S. Arai, and L. M. Dorfman, *J. Chem. Phys.*, **42**, 708 (1965); L. M. Dorfman, *Advan. Chem. Ser.*, No. 50, 36 (1965).

(3) S. Arai and M. C. Sauer, Jr., *J. Chem. Phys.*, **44**, 2297 (1966).

(4) T. J. Kemp, G. A. Salmon, and P. Wardman in "Pulse Radiolysis," M. Ebert, J. P. Keene, A. J. Swallow, and J. H. Baxendale, Ed., Academic Press, London, 1965, pp 247-257.

(5) B. J. Brown, N. T. Barker, and D. F. Sangster, *J. Phys. Chem.*, **75**, 3639 (1971).

(6) L. B. Magnusson, J. T. Richards, and J. K. Thomas, *Int. J. Radiat. Phys. Chem.*, **3**, 295 (1971).

(7) J. H. Baxendale and P. Wardman, *Nature (London)*, **230**, 449 (1971).

(8) J. T. Richards and J. K. Thomas, *J. Chem. Phys.*, **53**, 218 (1970).

(9) H. Hase, M. Noda, T. Higashimura, and K. Fueki, *ibid.*, **55**, 5411 (1971).

(10) J. Jortner, *ibid.*, **30**, 839 (1959); J. Jortner, *Radiat. Res. Suppl.*, **4**, 24 (1964); J. Jortner and S. A. Rice, *Advan. Chem. Ser.*, No. 50, 7 (1965).

(11) M. Natori, *J. Phys. Soc. Jap.*, **24**, 913 (1968); M. Natori and T. Watanabe, *ibid.*, **21**, 1573 (1966); S. Noda, K. Fueki, and Z. Kuri, *Bull. Chem. Soc. Jap.*, **42**, 16 (1969).

(12) K. Fueki, D.-F. Feng, L. Kevan, and R. E. Christoffersen, *J. Phys. Chem.*, **75**, 2297 (1971); K. Fueki, D.-F. Feng, and L. Kevan, *Chem. Phys. Lett.*, **10**, 504 (1971).

(13) D. A. Copeland, N. R. Kestner, and J. Jortner, *J. Chem. Phys.*, **53**, 1189 (1970).

- (1) P. C. Abbott and R. E. Stickney, *J. Phys. Chem.*, **75**, 2930 (1971).
- (2) D. E. Rosner and H. D. Allendorf, *ibid.*, **75**, 308 (1971).
- (3) J. C. Batty and R. E. Stickney, *J. Chem. Phys.*, **51**, 4475 (1969); see also J. E. Franklin and R. E. Stickney, *High Temp. Sci.*, **3**, 401 (1971).
- (4) J. C. Batty and R. E. Stickney, *Oxid. Metals*, **3**, 331 (1971).
- (5) D. E. Rosner and H. D. Allendorf, *J. Electrochem. Soc.*, **114**, 305 (1967).
- (6) D. E. Rosner and H. D. Allendorf, *Proc. Int. Symp. High Temp. Techn.*, 1969, 707 (1969).
- (7) D. E. Rosner and H. D. Allendorf in "Heterogeneous Kinetics at Elevated Temperatures," Plenum Press, New York, N. Y., 1970, pp 231-251.

DEPARTMENT OF ENGINEERING AND  
APPLIED SCIENCE  
YALE UNIVERSITY  
NEW HAVEN, CONNECTICUT 06520

DANIEL E. ROSNER\*  
PAUL C. NORDINE

RECEIVED SEPTEMBER 13, 1971

mitted light was focused onto the slits of a Bausch and Lomb monochromator with the exit slit widths at 0.5–1 mm. Corning filters were placed between light source and cell to remove wavelengths less than 300 nm and before the monochromator slits to eliminate second-order contributions. Light intensity in the visible and infrared was measured with a 50-ohm impedance-matched system comprising either a Hewlett-Packard HP 4207(400–1050 nm) or a special Philco Ford L 4521(800–1500 nm) photodiode coupled to a Lecroy 133 nanosecond amplifier and Tektronix 7704-(150 MHz) or 7904(500 MHz) oscilloscope. The absorption signal displayed on the oscilloscope was recorded on Polaroid 410 high-speed film. Initial light intensity was recorded on a Tektronix 564 storage oscilloscope a few microseconds before the Linac pulse. Response time of the system was  $\sim 2$  nsec with the HP 4207 photodiode and  $\sim 15$  nsec with the L 4521 photodiode.

Solvated electron spectra were determined to  $\pm 5$  nm at wavelengths between 400 and 1500 nm (or the onset of solvent absorption). Each spectrum was a broad band, asymmetric with respect to absorption energy, and without discernible fine structure. In each case, the spectrum was present immediately within a 5-nsec pulse and was unchanged in position and shape at the longest times for which spectra were recorded (100 nsec for neat alcohols and  $\sim 20$  nsec for mixtures). The wavelength,  $\lambda_{\max}$ , and transition energy,  $E_{\max}$ , at the  $e_s^-$  absorption maximum are given in Table I for each of the neat alcohols studied along with the static dielectric constant,  $D_s$ , and refractive index,  $n$ . Values of  $\lambda_{\max}$  for methanol, ethanol, the propanols, 1-butanol, and ethylene glycol agree well with published values;<sup>2,3</sup> spectra have not been reported for  $e_s^-$  in the other alcohols. For 1-hexadecanol (a solid at 30°) a spectrum of  $e_s^-$  with  $\lambda_{\max} = 800$  nm ( $E_{\max} = 1.54$  eV) was obtained for a 0.45 *M* solution in cyclohexane; however, the lower  $E_{\max}$  relative to those of other *normal* alcohols (*cf.* Table I) may not be characteristic of the neat alcohol. Thus, for 0.1 *M* (1.1 mol %) methanol, ethanol, 1-butanol, or 1-pentanol in cyclohexane, we find that  $E_{\max}$  is lower than that for the neat alcohol by 0.2 to 0.3 eV. Such an observation is consistent with results for solutions of methanol in cyclohexane<sup>4</sup> and in 3-methylhexane<sup>5</sup> and is not necessarily inconsistent with results for solutions of ethanol in *n*-hexane.<sup>5</sup>

In polaron or dielectric continuum models<sup>10</sup> of the solvated electron, the energy levels are determined by long-range interactions of the electron with the field produced by polarization of the medium by the electron itself, and the lowest observable transition energy is related to the quantity  $(1/n^2 - 1/D_s)$ , proportional to  $\beta$  in Table I. Clearly, there is no discernible relationship between values of  $E_{\max}$  and  $\beta$  in the last two columns of Table I. Moreover, as shown in Figure 1, there is

**Table I:** Wavelength,  $\lambda_{\max}$ , and Transition Energy,  $E_{\max}$ , at the Absorption Maximum of the Solvated Electron in Alcohols

Alcohol	$\lambda_{\max}^a$ , nm	$n$	$D_s$	$E_{\max}$ , eV	$\beta^b$
CH <sub>3</sub> OH	640	1.33	32.6	1.93	1.93
C <sub>2</sub> H <sub>5</sub> OH	725	1.36	24.3	1.70	1.80
<i>n</i> -C <sub>3</sub> H <sub>7</sub> OH	740	1.39	20.1	1.67	1.69
2-C <sub>3</sub> H <sub>7</sub> OH	830	1.38	18.3	1.49	1.70
<i>n</i> -C <sub>4</sub> H <sub>9</sub> OH	680	1.40	17.1	1.82	1.63
<i>i</i> -C <sub>4</sub> H <sub>9</sub> OH	770	1.40	17.9	1.60	1.64
<i>t</i> -C <sub>4</sub> H <sub>9</sub> OH	1250	1.39	10.9	0.99	1.53
<i>n</i> -C <sub>5</sub> H <sub>11</sub> OH	660	1.41	13.9	1.87	1.56
<i>i</i> -C <sub>5</sub> H <sub>11</sub> OH	690	1.41	14.7	1.79	1.57
<i>t</i> -C <sub>5</sub> H <sub>11</sub> OH	1250	1.41	5.8	0.99	1.19
<i>c</i> -C <sub>5</sub> H <sub>9</sub> OH	820	1.45	15 <sup>c</sup>	1.51	1.47 <sup>c</sup>
<i>n</i> -C <sub>6</sub> H <sub>13</sub> OH	680	1.42	13.3	1.82	1.52
<i>c</i> -C <sub>6</sub> H <sub>11</sub> OH	750	1.47	15.0	1.65	1.43
4-C <sub>7</sub> H <sub>15</sub> OH	950	1.42	5.9	1.30	1.18
<i>n</i> -C <sub>8</sub> H <sub>17</sub> OH	670	1.43	10.3	1.85	1.42
2-C <sub>8</sub> H <sub>17</sub> OH	860	1.43	7.8	1.44	1.30
<i>n</i> -C <sub>9</sub> H <sub>19</sub> OH	670	1.43	9.1	1.85	1.37
<i>n</i> -C <sub>10</sub> H <sub>21</sub> OH	650	1.44	7.8	1.90	1.28
<i>n</i> -C <sub>11</sub> H <sub>23</sub> OH	685	1.44	5.9	1.80	1.13
(CH <sub>2</sub> OH) <sub>2</sub>	580	1.43	37.7	2.13	1.67

<sup>a</sup>  $\pm 10$  nm below  $\sim 900$  nm and  $\pm 20$  nm above. <sup>b</sup>  $\beta \equiv (1/n^2 - 1/D_s)$  normalized to give 1.93 for methanol. <sup>c</sup> Upper limit.

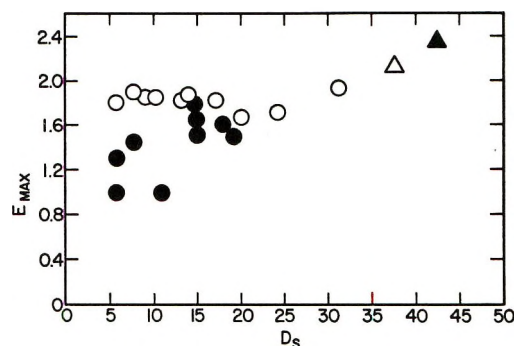


Figure 1. Plot of transition energy,  $E_{\max}$ , at the absorption maximum of the solvated electron in neat alcohols vs. static dielectric constant,  $D_s$ : O, *normal* alcohols; ●, branched alcohols; Δ, ethylene glycol; ▲, glycerol.<sup>3</sup>

no correlation between  $E_{\max}$  and  $D_s$  as was suggested by results for only methanol, ethanol, the propanols, and ethylene glycol.<sup>2</sup> Absence of any kind of correlation between  $E_{\max}$  and  $D_s$  is illustrated strikingly by comparison of the data for the C<sub>9</sub>, C<sub>10</sub>, and C<sub>11</sub> *normal* alcohols in Table I with the following data for tetrahydrofuran:  $\lambda_{\max} = 2100$  nm,<sup>14</sup>  $n = 1.40$ ,  $D_s = 7.4$ ,  $E_{\max} = 0.59$  eV, and  $\beta = 1.36$ . Such comparisons indicate that a long-range interaction determined by  $D_s$  has a negligible effect on  $E_{\max}$  and, therefore, that a short-range interaction largely determines the binding and transition energies of  $e_s^-$  in the alcohols.<sup>15</sup>

(14) L. M. Dorfman, F. Y. Jou, and R. Wageman, *Ber. Bunsenges. Phys. Chem.*, **75**, 681 (1971).

The results in Table I suggest two more specific conclusions: (1) the binding and transition energies of  $e_s^-$  in the alcohols are determined by interaction of the electron with an optimum configuration of OH dipoles in a small solvation domain, perhaps a single shell; (2) the optimum configuration for  $e_s^-$  is affected by molecular structure of the alcohol. Comparison of  $E_{max}$  for the *normal* alcohols (*cf.* Table I or Figure 1) shows that the optimum configuration is little affected by the number of C atoms (particularly for C<sub>4</sub> through C<sub>11</sub>); thus, the linear alkyl chains of OH groups bound by the electron appear to extend radially into the solution with negligible steric hindrance. However, an effect of molecular structure on the optimum configuration is clearly evident in the lower values of  $E_{max}$  for the branched alcohols, for which steric hindrance apparently decreases the interaction between the OH groups and the electron. Our most recent experiments give a  $\lambda_{max}$  of at least 1500 nm for 3-methyl-3-pentanol and 3-ethyl-3-pentanol. A decrease in steric hindrance with increase in distance of the branch point from the OH group, as might be expected, is indicated by the values of  $E_{max}$  for the butanol and pentanol isomers. Of particular interest are the large values of  $E_{max}$  for ethylene glycol and glycerol<sup>3</sup> (*cf.* Figure 1); a chelate-like structure of  $e_s^-$  with enhanced binding energy is suggested.

Results for alcohol-alkane mixtures are consistent with interpretations presented for the neat alcohols. Present results and those of Brown, *et al.*,<sup>5</sup> and Magnusson, *et al.*,<sup>6</sup> indicate that an alcohol can be diluted with an alkane to a concentration at which  $D_s$  is essentially indistinguishable from that of the neat alkane and yet exhibit relatively little or no shift of  $\lambda_{max}$  from that of the neat alcohol toward that of the neat alkane (for which  $\lambda_{nmax} > 2000$  nm<sup>16</sup>). Clearly, such results are not compatible with dielectric continuum models but are compatible with the suggested predominance of the role of a solvation domain. The transition energy is determined by composition of the solvation domain. The equilibrium composition of the solvation domain is determined by (1) composition of the binary mixture, (2) relative strength of the attractive interactions of  $e^-$  with the mixture components (reflected by  $E_{max}$  of the neat components), and (3) strength of the attractive interactions between the mixture components. For alcohol-alkane mixtures in which there is weak interaction between the components and a large difference in the strength of their interactions with  $e^-$ , the solvation domain remains essentially saturated with alcohol down to very low concentrations. However, for binary mixtures in which the interaction between components is strong or the difference in strength of their interactions with  $e^-$  is small or both, a different dependence of the solvation domain composition and, therefore, of  $E_{max}$  on solution composition is to be expected.<sup>14</sup>

In the mixtures studied, as in the neat alcohols, the

$e_s^-$  spectra are present within the 5-nsec pulse and do not change over at least a 20-nsec period. Clusters of alcohol molecules exist in alkane solutions even at 0.1 M alcohol<sup>17</sup> and provide a distribution of preexisting sites of diverse compositions for trapping (localization) of the thermalized electrons. Evidently, relaxation of such trapped electrons to the equilibrium composition and configuration of  $e_s^-$  is complete within 5 nsec in the 0.1 M solutions of alcohol in cyclohexane. Such an observation is in accord with recent calculations by Mozumder<sup>18</sup> on the time dependence of electron solvation as a function of the concentration of single dipole molecules randomly dispersed in a nonpolar medium. For elucidation of the solvation mechanism in alcohol-alkane mixtures, the studies are being extended to lower alcohol concentrations, alkanes of greater viscosity, lower temperatures, and shorter times (for which purpose we have developed a new infrared picosecond pulse-radiolysis system utilizing an injection laser diode).

(15) I. A. Taub and K. Eiben, *J. Chem. Phys.*, **49**, 2499 (1968), reached such a conclusion for  $e_{aq}^-$  from comparison of the spectrum with that of trapped electrons in ice at low temperatures; some models for  $e_s^-$  are based on<sup>11</sup> or include<sup>12,13</sup> short-range interactions,

(16) H. A. Gillis, N. V. Klassen, G. G. Teather, and K. H. Lokan, *Chem. Phys. Lett.*, **10**, 481 (1971).

(17) J. Crossley, *J. Phys. Chem.*, **75**, 1790 (1971); H. C. Van Ness, J. Van Winkle, H. H. Richtol, and H. B. Hollinger, *ibid.*, **71**, 1483 (1967); A. N. Fletcher and C. A. Heller, *ibid.*, **71**, 3742 (1967).

(18) A. Mozumder, *ibid.*, in press.

DEPARTMENT OF CHEMISTRY AND ROBERT R. HENTZ\*  
THE RADIATION LABORATORY GERALDINE KENNEY-WALLACE  
UNIVERSITY OF NOTRE DAME  
NOTRE DAME, INDIANA 46556

RECEIVED MAY 26, 1972

### Calculation of $\Delta H_{d(g)}^\circ - \Delta H_{d(l)}^\circ$ for Dissociating Dimers via the "Dissociation-Vaporization"

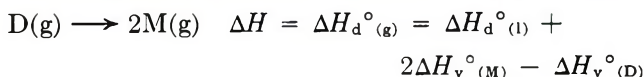
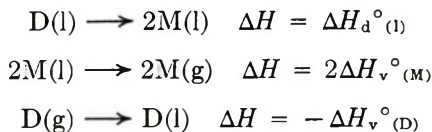
#### Rule. The $\Delta H_{d(l)}^\circ$ of Trimethylaluminum

*Publication costs assisted by the Ethyl Corporation*

*Sir:* For dissociating dimers such as the aluminum alkyls, both the heat of dissociation in the liquid phase ( $\Delta H_{d(l)}^\circ$ ) and that in the gaseous phase ( $\Delta H_{d(g)}^\circ$ ) are of considerable interest. Since it is often the case that one of these quantities is known, but not the other, a method of calculating one value from the other would be very useful. For example, the  $\Delta H_{d(l)}^\circ$  for trimethylaluminum (TMA), often needed for the interpretation of kinetic data, has not been determined experimentally. It would be very helpful if  $\Delta H_{d(l)}^\circ$  could be derived from the experimental value for  $\Delta H_{d(g)}^\circ$  (20.40 kcal/mol of dimer<sup>1</sup>).

(1) C. H. Henrickson and D. P. Eymann, *Inorg. Chem.*, **6**, 1461 (1967).

We wish to call attention to a general method of evaluating the difference  $\delta_H \equiv \Delta H_{d^\circ(g)} - \Delta H_{d^\circ(l)}$  for dissociating dimers. The relationship between  $\Delta H_{d^\circ(g)}$  and  $\Delta H_{d^\circ(l)}$  is readily obtained by summing simple equations. At any given temperature ( $D$  = dimer,  $M$  = monomer)



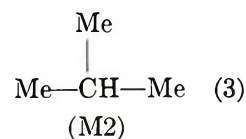
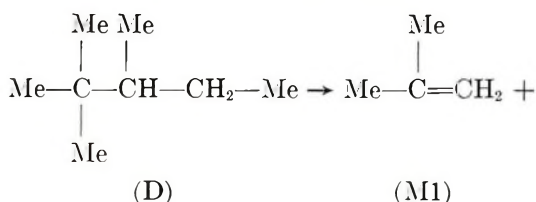
$$\delta_H(25^\circ) \equiv \Delta H_{d^\circ(g,25^\circ)} - \Delta H_{d^\circ(l,25^\circ)} = 2\Delta H_{v^\circ(M,25^\circ)} - \Delta H_{v^\circ(D,25^\circ)} \quad (1)$$

Since  $\Delta H_{d^\circ(g)}$  and  $\Delta H_{d^\circ(l)}$  are customarily taken as constants (experimental data are not usually accurate enough to establish their temperature variation), these values will be assumed to apply at 25°. Equation 1 may then be written as

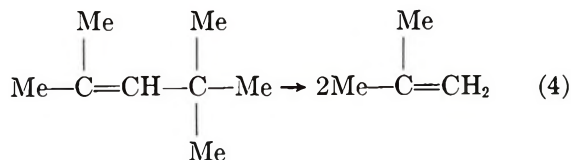
$$\delta_H \equiv \Delta H_{d^\circ(g)} - \Delta H_{d^\circ(l)} = 2\Delta H_{v^\circ(M,25^\circ)} - \Delta H_{v^\circ(D,25^\circ)} \quad (2)$$

It is convenient to refer to eq 2 as the "Dissociation-Vaporization Rule." (It is noted that similar rules can be written for other extensive properties such as entropy and free energy.)

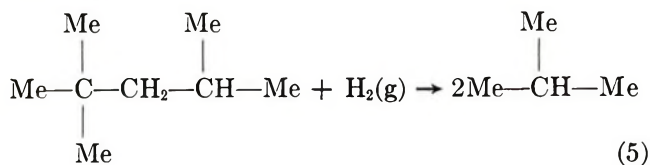
Determination of  $\delta_H$  for a particular monomer-dimer system consists of the evaluation of the "vaporization difference" for that system. It might be expected that the vaporization difference (and therefore the value of  $\delta_H$ ) would have about the same value for different monomer-dimer systems. It will be of interest to test this expectation and to determine the range of  $\delta_H$  values for a particular class of compounds, namely, the aluminum alkyls. Since heats of vaporization of pure monomers and pure dimers are not available, we must turn to analogous compounds for which the necessary data are available. The branched aliphatic hydrocarbons, both saturated and olefinic, are well suited to this purpose. Like pure aluminum alkyl monomers and dimers, they are "normal" liquids which obey Trouton's rule. Individual hydrocarbons can be selected which bear a close structural resemblance to particular monomers and dimers. For example, we can write the following equations simulating the dissociation of TMA dimer into monomer<sup>2</sup>



$$\delta_H = \Delta H_{v^\circ(M1,25^\circ)} + \Delta H_{v^\circ(M2,25^\circ)} - \Delta H_{v^\circ(D,25^\circ)} = 0.93 \text{ kcal}$$



$$\delta_H = 1.14 \text{ kcal}$$



$$\delta_H = 1.04 \text{ kcal (H}_2(\text{g}) \text{ disregarded in the calculation).}$$

The close agreement of the three values for  $\delta_H$  is noted. To obtain comparable values of  $\delta_H$  for a series of (simulated) aluminum alkyls, it is convenient to write equations similar to eq 5 and calculate the necessary values of  $\Delta H_{v^\circ(25^\circ)}$  from Morawetz's<sup>3</sup> correlation of heats of vaporization of isomeric alkanes with molecular structure. The following values of  $\delta_H$  in kcal/mol of dimer were derived in this manner: 0.99 for (simulated)  $\text{Me}_3\text{Al}$ , 1.06 for  $\text{Me}_2\text{AlEt}$ , 1.13 for  $\text{MeAlEt}_2$ , 1.13 for  $\text{Et}_3\text{Al}$ , 1.20 for  $\text{Et}_2\text{AlPr}$ , and 1.26 for  $\text{EtAlPr}_2$ . The value of  $\delta_H$  for the simulated aluminum alkyls increases quite slowly with increasing molecular size and it would be expected that  $\delta_H$  for the actual aluminum alkyls would do the same.

The hydrocarbons simulating TMA dimer (or monomer) in eq 3, 4, and 5 boil about 15–30° lower than pure TMA dimer (or monomer). As just shown, however, the value of  $\delta_H$  is affected only slightly by a moderate change in boiling point. It is concluded that  $\delta_H$  for TMA is about 1.04 kcal/mol of dimer (average for eq 3, 4, and 5). Using Henrickson and Eyman's<sup>1</sup> value of 20.40 kcal for  $\Delta H_{d^\circ(g)}$ , we obtain  $\Delta H_{d^\circ(l)}(\text{TMA}) = \Delta H_{d^\circ(g)} - \delta_H = 20.40 - 1.04 = 19.4 \text{ kcal/mol of dimer.}$

In an earlier paper,<sup>4</sup> based on heat of dilution experiments, we reported the  $\Delta H_{d^\circ(l)}$  of triethylaluminum (TEA) as  $16.93 \pm 0.23 \text{ kcal/mol of dimer.}$  We have determined from heat of mixing experiments on TMA-TEA (to be described in a forthcoming paper) that  $\Delta H_{d^\circ(l)}(\text{TMA}) - \Delta H_{d^\circ(l)}(\text{TEA}) = 2.47 \pm 0.05$

(2) The thermochemical data were taken from F. D. Rossini, *et al.*, "Selected Values of Physical and Thermodynamic Properties of Hydrocarbons and Related Compounds," Carnegie Press, Pittsburgh, Pa., 1953, and Supplements.

(3) E. Morawetz, *J. Chem. Thermodyn.*, **4**, 145 (1972).

(4) M. B. Smith, *J. Phys. Chem.*, **71**, 364 (1967).

kcal/mol of dimer at 25°. This leads to the experimental value  $16.93 + 2.47 = 19.40 \pm 0.30$  kcal/mol of dimer for  $\Delta H_d^\circ(1)$  of TMA, in excellent agreement with the value derived by hydrocarbon simulation.

It is concluded that (1) the proposed general method of calculating  $\delta_H \equiv \Delta H_d^\circ(g) - \Delta H_d^\circ(1)$  for dissociating dimers is supported by experimental results in the case of the aluminum alkyls; (2) the method is readily extensible to other dissociating dimers (such as carboxylic acids) and to other properties (such as entropy and free energy); (3) the value of  $\delta_H$  is about 1.04 kcal/mol of dimer for TMA and increases quite slowly with increasing molecular size; (4) the value of  $\Delta H_d^\circ(1)$  for TMA is established as  $19.40 \pm 0.30$  kcal/mol of dimer.

*Acknowledgments.* The helpful suggestions of Dr. K. E. Wiegand are gratefully acknowledged.

CHEMICAL RESEARCH AND DEVELOPMENT      MARTIN B. SMITH  
ETHYL CORPORATION  
BATON ROUGE, LOUISIANA 70821

RECEIVED MAY 30, 1972

## Resolution of Components of the Optical Rotation Tensor of Collagen

*Publication costs assisted by the National Institutes of Health and the National Science Foundation*

*Sir:* The optical activity of collagen in dilute solution has been studied (*e.g.*, ref 1 and 2) and the results have been reviewed comprehensively.<sup>3,4</sup> By contrast, the optical activity in the solid state has not received much attention although the early measurements of Smith,<sup>5</sup> Robinson and Bott,<sup>6</sup> Robinson,<sup>7</sup> Cohen,<sup>1</sup> and Elliott<sup>8</sup> on solid films of denatured collagen (gelatin) are noteworthy exceptions to such paucity of interest.

In the solid state, collagen appears to possess much stronger optical activity than in solution. At the reference wavelength 365 m $\mu$ , for example, the well-known dilute solution value of the specific rotation is  $-1300$ ,<sup>9</sup> whereas the specific rotation of a solid film cast from a dilute solution of rat tail collagen at room temperature and containing *ca.* 85 wt% collagen is as high as  $-3200$ .<sup>10,11</sup> Early work<sup>1,5,6</sup> with films of gelatin cast at room temperature or below (cold-cast gelatin) has shown that the specific rotation of this partly denatured form of collagen is also considerably higher in the solid state than in solution. No convincing explanation has been previously given for this phenomenon.

The question immediately arises whether the triple-helical structure of the collagen molecule undergoes a significant change in its dimensions in going from a relatively unperturbed existence in dilute solution to the highly crowded solid state. Furthermore, since the

weight ratio of protein to aqueous solvent changes from about  $10^{-3}$  to about 6 as collagen goes from dilute solution to the solid state (*ca.* 15 wt% water), the question of the possible effect of water content on the conformation of the helix also poses itself.

To resolve these questions, we consider the optical activity of a crystal as a second-rank tensor<sup>12</sup>

$$\alpha = \alpha_{ij}l_i l_j \quad (i, j = 1, 2, 3) \quad (1)$$

where  $\alpha_{ij}$  are the components of the tensor and  $l_i, l_j$  are the direction cosines of the light beam with respect to the molecular axes 1, 2, and 3. Due to the cylindrical symmetry of the collagen helix, all nondiagonal components of the optical activity tensor of collagen are zero and, furthermore,  $\alpha_{11} = \alpha_{22}$ . In this notation,  $\alpha_{11} = \alpha_{22}$  is the optical activity measured with the light beam perpendicular to the helical axis, while  $\alpha_{33}$  is the optical activity measured parallel to that axis. In dilute solution, where the helical macromolecules interacting with the light beam are randomly oriented in the solvent, it can be easily shown that

$$\alpha_{\text{solution}} = \frac{2\alpha_{11} + \alpha_{33}}{3} \quad (2)$$

A distinction between the optical activity in dilute solution and in the solid state can be drawn by measuring the individual components  $\alpha_{ii}$  ( $i = 1, 2, 3$ ) in solid specimens and then comparing their arithmetic average directly with the optical activity in dilute solution which, according to eq 2, is the arithmetic average of the tensorial components in that state also. We report here the results of such a comparison. Since there is a significant difference in refractive index between a dilute solution specimen and a solid specimen, the Lorentz correction factor<sup>13</sup> has been applied to all values of specific rotation reported below; values of specific rotation  $[\alpha]$  reduced in this manner are distinguished by the subscript r (*e.g.*,  $[\alpha_{11}]_r$ ). Even though the specific rotation was determined over a

- (1) C. Cohen, *J. Biophys. Biochem. Cytol.*, **1**, 203 (1955).
- (2) E. R. Blout, J. P. Carver, and J. Gross, *J. Amer. Chem. Soc.*, **85**, 644 (1963).
- (3) P. H. von Hippel, "Treatise on Collagen," Vol. 1, G. N. Ramachandran, Ed., Academic Press, London, 1967, Chapter 6.
- (4) J. P. Carver and E. R. Blout, ref 3, Chapter 9.
- (5) C. R. Smith, *J. Amer. Chem. Soc.*, **41**, 135 (1919).
- (6) C. Robinson and M. J. Bott, *Nature (London)*, **168**, 325 (1951).
- (7) C. Robinson, "Nature and Structure of Collagen," J. T. Randall, Ed., Butterworths, London, 1953, p 96.
- (8) A. Elliott, "Recent Advances in Gelatin and Glue Research," G. Stainsby, Ed., Pergamon Press, Elmsford, N. Y., 1958, p 267.
- (9) P. F. Davison and M. P. Drake, *Biochemistry*, **5**, 313 (1966).
- (10) I. V. Yannas and C. Huang, *Macromolecules*, **5**, 99 (1972).
- (11) I. V. Yannas, *Rev. Macromol. Chem.*, **C7(1)**, 49 (1972).
- (12) J. F. Nye, "Physical Properties of Crystals," Oxford University Press, Oxford, 1957.
- (13) P. Urnes and P. Doty, *Advan. Protein Chem.*, **16**, 401 (1961).

wide range of wavelengths, all values reported here were obtained at the reference wavelength 365 m $\mu$ .

Measurements reported here were obtained with solid films or with tendon fibers containing ca. 85 wt % collagen; at this concentration level, specimens are essentially at equilibrium with the usual ambient humidities. The water content of the solid specimens was determined by a modification of the Fischer titration giving results that were identical within experimental error with the results of a high-temperature vacuum dehydration procedure, previously described,<sup>14</sup> which leaves the amino acid composition of collagen unchanged.<sup>11</sup>

The component  $\alpha_{11}$  was determined as follows. Collagen was extracted from rat tail tendon with 0.05 M acetic acid, using the method of Piez, Lewis, Martin, and Gross<sup>15</sup> and the nativity of collagen in solution prepared in this manner was verified by measuring the specific rotation and the intrinsic viscosity and comparing the observed results with published values for solutions of native collagen.<sup>1,9,16,17</sup> Most of the aqueous solvent was then removed by slow evaporation under vacuum at room temperature and a transparent film of collagen 5–10  $\mu$  thick and incorporating about 15 wt % water was thereby prepared. Careful casting under such conditions did not seem to affect the nativity of collagen as shown by redissolving control films and measuring the specific rotation and intrinsic viscosity once more. Close control of the casting process was necessary before films free from birefringence (a property which greatly complicates measurement of optical activity with solid specimens<sup>11</sup>) could be reproducibly prepared; the absence of birefringence was demonstrated by observing that the optical activity was independent of rotation of the film about the axis of the light beam. Wide-angle X-ray diffraction photographs obtained with the beam normal as well as parallel to the plane of collagen films so prepared showed Debye–Scherrer rings, or arc reflections, respectively, which corresponded to spacings that have been attributed to the triple helical structure of native collagen.<sup>18–20</sup> Analysis of the X-ray diagrams led to the conclusion that the axes of the helical macromolecules in these films were lying almost entirely in the plane of the film, but were randomly oriented otherwise. Nevertheless, the orientation was not perfectly planar: the helical axis was, on the average, inclined at an angle of about 12° to the plane of the film and this deviation was taken into account and corrected for in the determination of  $[\alpha_{11}]_r$ . The film was then placed in a Cary 60 CD spectropolarimeter and the optical rotation was determined with the light beam normal to the plane of the film. For planar orientation of the molecules in the film, the average values of the direction cosines are  $\bar{l}_1^2 = \bar{l}_2^2 = 1/2$  and  $\bar{l}_3^2 = 0$ , so that the optical activity measured with the beam normal to the film surface is

$$\alpha_{film} = \frac{\alpha_{11} + \alpha_{22}}{2} = \alpha_{11} = \alpha_{22} \quad (3)$$

In this manner, the specific rotation normal to the helical axis,  $[\alpha_{11}]_r$ , was found equal to  $-2360 \pm 140$ .

The component  $\alpha_{33}$  was determined by two independent methods. First, a direct measurement was made, using a rat-tail tendon fiber which was carefully mounted inside a 0.75 mm-diameter hole drilled in a thin stainless steel plate; the fiber was subsequently sectioned on either side of the hole to provide a tendon fiber slice of 0.132 mm thickness through which the polarized light beam was transmitted. A correction was made for the slight misalignment of constituent filaments (average diameter about 10  $\mu^{21}$ ) along the beam direction and the true specimen cross section was determined directly by light microscopic examination. The value of  $[\alpha_{33}]_r$  measured in this manner was  $+1110 \pm 140$ .

An indirect determination of the component  $\alpha_{33}$  was made by measuring the optical activity of a collagen film, cast on a fused quartz disk, at several levels of the angle between the beam direction and the normal to the plane of the film (tilt angle) and extrapolating the data to a tilt angle of 90°; at this point, the optical activity can easily be shown to be equal to  $(1/2)(\alpha_{11} + \alpha_{33})$ . The data observed at the various tilt angles were found to vary in accord with an analytical expression relating optical activity with tilt angle  $\theta$  which we derived purely on trigonometric grounds

$$\alpha_{\theta} = \alpha_{11} + \frac{(\alpha_{33} - \alpha_{11})}{2} \sin^2 \theta \quad (4)$$

Nevertheless, several corrections were applied to the data, most important of which were a correction for the change in angle to the plane of polarized light as it was refracted by the specimen and supporting disk and a correction for the increase in path length which accompanies tilting. The value of  $[\alpha_{33}]_r$  determined by this method was found to be  $+1310 \pm 190$ .

It is now possible to compute the arithmetic average of the components  $\alpha_{ii}$  obtained with solid specimens and compare this value with the arithmetic average of components obtained by measurements in dilute solution. Using  $-2360 \pm 140$  for the value of  $[\alpha_{11}]_r$  in

(14) I. V. Yannas and A. V. Tobolsky, *Nature (London)*, **215**, 509 (1967).

(15) K. A. Piez, M. S. Lewis, G. R. Martin, and J. Gross, *Biochim. Biophys. Acta*, **53**, 596 (1961).

(16) H. Boedtker and P. Doty, *J. Amer. Chem. Soc.*, **78**, 4267 (1956).

(17) H. Noda, *Biochim. Biophys. Acta*, **17**, 92 (1955).

(18) P. M. Cowan, A. C. T. North, and J. T. Randall, *Symp. Soc. Exp. Biol.*, **9**, 115 (1955).

(19) G. N. Ramachandran and G. Kartha, *Nature (London)*, **174**, 269 (1954); **176**, 593 (1955).

(20) A. Rich and F. H. C. Crick, *ibid.*, **176**, 915 (1955); *J. Mol. Biol.*, **3**, 483 (1961).

(21) I. V. Yannas and C. Huang, *J. Polymer Sci., Part A-2*, **10**, 577 (1972).

the solid state and  $+1210 \pm 170$  for  $[\alpha_{33}]_r$  (the average of the two values determined independently), we find that the arithmetic average of the three tensorial components in the solid state is  $-1170 \pm 220$ . This value can be compared with the dilute solution value of  $-1035 \pm 40$ . (Without the Lorentz correction the solution value becomes the often cited  $-1300$ .<sup>9</sup>) It is clear that the optical activity of collagen in the solid state is almost indistinguishable from the activity in dilute solution.

We conclude that the collagen helix does not undergo any appreciable change as it goes from the dilute solution to the solid state (ca. 85 wt% protein). It appears instead that the large apparent difference between the optical activity of collagen in dilute solution and in the form of a solid film can be largely explained in terms of the transition from a random molecular orientation (in solution) to a planar orientation (in the film). Nevertheless, a small but significant difference, undetected in this work, may exist between the helical structure of collagen in these two states.

It is worth recalling that several authors,<sup>22-26</sup> working with synthetic polypeptides, have reported substantial differences between the specific rotation in dilute solution and in solid films cast from solution. We suggest that resolution of the components of the optical rotation tensor of these polypeptides by use of the methodology described here can determine the extent to which the observed discrepancies reflect differences in the folded structure rather than differences in orientation of the macromolecules in these two states.

Previously, estimates of the magnitude of the tensorial components of the optical activity of macromolecules have been obtained by electrical orientation in dilute solution (e.g., Tinoco<sup>26</sup>). The procedure described in this report obviates the use of an electric field.

*Acknowledgment.* We wish to thank Dr. W. Kauzmann for a useful communication and Drs. P. F. Davison, J. N. Vournakis, and D. F. Waugh for helpful discussions. A valuable discussion with Mr. G. Trapani is acknowledged with pleasure. This work was supported partly from the National Institutes of Health (Grant No. AM 11919) and partly from the National Science Foundation (Grant No. GK-19408). This work is based in part on a thesis submitted by N-H. Sung in partial fulfillment of the requirements for the Sc.D. degree in Materials Science and Engineering,

Department of Mechanical Engineering, Massachusetts Institute of Technology, Cambridge, Mass., June 1972.

FIBERS AND POLYMERS LABORATORIES  
DEPARTMENT OF MECHANICAL ENGINEERING  
MASSACHUSETTS INSTITUTE OF TECHNOLOGY  
CAMBRIDGE, MASSACHUSETTS 02139

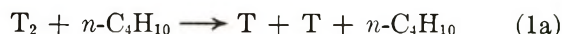
I. V. YANNAS\*  
N-H. SUNG  
C. HUANG

RECEIVED JUNE 5, 1972

## Hydrogen Displacement in *n*-Butane by Fast T<sub>2</sub> Collisions

*Sir:* Beatty and Wexler (BW) have recently reported a molecular beam experiment which is aimed at determining the energy dependence of the reaction cross sections for the hydrogen displacement reactions of T<sub>2</sub> and T<sub>2</sub><sup>+</sup> with *n*-butane.<sup>1</sup> Their experiment seems to be the first of its kind, where neutral tritium molecules with low internal excitation are reacted with a simple hydrocarbon. It complements previous work that has dealt with the reactions of tritium atoms.<sup>2-4</sup> This comment is concerned with BW's inversion of their T<sub>2</sub> data to obtain reaction cross sections, using Porter's kinetic theory.<sup>5</sup> They report cross sections roughly two orders of magnitude smaller than the ones we have determined for the parallel reactions of tritium atoms,<sup>2-4</sup> a result which we wish to examine critically.

BW suggest that their results for the reaction of T<sub>2</sub> with *n*-butane (Figure 5 of ref 1) can be interpreted either in terms of a "single pass" gas-phase reaction, or in terms of a multiple collision process. The latter interpretation seems most feasible. It is true, as BW point out, that their yield curve (Figure 5) is similar to those derived by Karplus, Porter, and Sharma<sup>6</sup> for the collisional dissociation of H<sub>2</sub> and D<sub>2</sub> by fast tritium atoms, although BW's cross sections are, respectively, 5 and 10 times larger. However, a two-step process would be required for the formation of tritiated butane by this mechanism (see Table I of ref 1).



At the reported target density of  $\bar{N} = 8.9 \times 10^{11}$  molecules/cm<sup>2</sup>, and assuming a gas kinetic cross section of 50 Å<sup>2</sup>, the probability that a beam molecule will suffer a collision on passage through the reaction

(22) A. R. Downie, A. Elliott, W. E. Hanby, and B. R. Malcolm, *Proc. Roy. Soc., Ser. A*, **242**, 325 (1957).

(23) A. Elliott, W. E. Hanby, and B. R. Malcolm, *Disc. Faraday Soc.*, **25**, 167 (1958).

(24) G. D. Fasman, *Biopolymers*, **4**, 509 (1966).

(25) G. D. Fasman, H. Hoving, and S. N. Timasheff, *Biochemistry*, **9**, 3316 (1970).

(26) I. Tinoco, Jr., *J. Amer. Chem. Soc.*, **79**, 4248 (1957); **81**, 1540 (1959).

(1) J. W. Beatty and S. Wexler, *J. Phys. Chem.*, **75**, 2417 (1971).

(2) M. Menzinger and R. Wolfgang, *J. Amer. Chem. Soc.*, **89**, 5992 (1967).

(3) M. Menzinger and R. Wolfgang, *J. Chem. Phys.*, **50**, 2991 (1969).

(4) R. L. LeRoy, A. Yench, M. Menzinger, and R. Wolfgang, to be submitted for publication.

(5) R. N. Porter, *J. Chem. Phys.*, **45**, 2284 (1966).

(6) M. Karplus, R. N. Porter, and R. D. Sharma, *ibid.*, **45**, 3871 (1966).

zone is about 0.4%. Thus the probability that the double collision sequence of reaction 1 will occur on a single pass is much less than  $10^{-3}\%$ . BW's high-energy yields are about 0.18%, as calculated from their eq 3, so their results are inconsistent with reaction 1.

This inconsistency is further demonstrated by noting the atomic tritium formed in reaction 1a at high beam energies will have a high translational energy with respect to target butane molecules. Reaction 1b is known<sup>2-4,7</sup> to have a negligible cross section above 15-20 eV.

It is conceivable that the atomic tritium products of reaction 1a could react with butane adsorbed on the walls of the reaction chamber. However, the yield of such a multiple collision reaction is less than 20%,<sup>4,7</sup> so the experimental results would imply a cross section  $>50 \text{ \AA}^2$  for reaction 1a. This is unrealistically high.

BW's "apparent reaction cross-section" (Figure 5 of ref 1) levels out to the high value of  $20 \text{ \AA}^2$  at about 30 eV and then shows no tendency to decline with increasing beam energy, even at 100 eV. This behavior is characteristic of multiple collisions,<sup>2-4</sup> and BW rationalize it in terms of the following kinetic model.

The gas target being optically thin, the beam has, during its first transit through the collision region, only a small chance of colliding with butane (about 0.4%, as shown above), and a much smaller chance of reacting. The unreacted  $T_2$  molecules then strike the rear wall of the apparatus and are reflected with a reduced kinetic energy. This sequence of passage through the collision zone and moderating reflections continues until either a gas-phase reaction takes place or the projectile has dropped below the reactive energy range.

Assuming this model, Beatty and Wexler proceeded to analyze their data by means of the kinetic theory. However, Porter's integral equation (eq 11 of ref 1) simply does not apply to their model. It is only valid if all  $T_2$  molecules suffer their first as well as all subsequent collisions with butane. The reaction model, however, permits at most 0.4% of all collisions to occur with butane in the gas phase. Thus the generalization of Porter's equation to multicomponent systems<sup>5</sup> must be used. In BW's notation this is

$$Y_i(E) = F(E)p_i(E) + F(E) \left[ 1 - \sum_{j=1}^k p_j(E) \right] \times \int_0^\infty \pi_B(E,E') Y_i(E') dE' + [1 - F(E)] \times \int_0^\infty \pi_W(E,E') Y_i(E') dE' \quad (2)$$

for a two-component system, where one component, the wall, is nonreactive.  $F(E)$  is the fraction of  $T_2$  molecules having energy  $E$  which will suffer collision

with a butane molecule, instead of the wall, and  $\pi_B(E,E')$  and  $\pi_W(E,E')$  are the energy loss functions for collisions with butane molecules and the walls, respectively.

Since, as shown above,  $F(E)$  has a maximum value of 0.004, the final term of eq 2 far outweighs the term which precedes it.<sup>8</sup> Thus, incorporating BW's assumption that  $\pi_W(E,E')$  can be approximated by the hard-sphere energy loss expression

$$\pi_W(E,E') = (1 - \beta_W)E \quad \beta_W E < E' < E, \quad (3) \\ = 0 \quad E < E' < \beta_W E$$

eq 2 becomes

$$p_i(E) \simeq \frac{1}{F(E)} \left( Y_i(E) - \frac{1}{(1 - \beta_W)E} \int_{\beta_W E}^E Y_i(E') dE' \right) \quad (4)$$

The denominator on the right-hand side of BW's eq 16 is approximately equal to unity. This is evident, either from direct evaluation or from their statement that computed cross sections are insensitive to the value of  $A_i$ .<sup>9</sup> Thus, from comparison of eq 4 with BW's eq 16, it is clear that the latter expression underestimates the cross section by a factor of approximately 250.

Apart from the inapplicability of the kinetic theory, it is very likely that the yields observed by Beatty and Wexler reflect a more complicated sequence of events than that considered in the simple kinetic model (see above): apart from the moderating reflections from the metal walls, we feel that wall reaction with butane is a process of considerable importance. This would have to be considered in an appropriate kinetic scheme.

In summary, it appears that in this experiment the conditions for the applicability of the kinetic theory are not met, and that the magnitude as well as the functional form of the calculated excitation functions are to be questioned.

(7) M. Menzinger and R. Wolfgang, *J. Phys. Chem.*, **72**, 1789 (1968).

(8) If the energy loss functions can be represented by eq 3, this statement remains true for any choice of  $\beta_B$  and  $\beta_W$ . This includes the extreme case of elastic collisions from a clean wall ( $\beta_W = 1$ ), for any realistic excitation function.

(9) Note that BW's choice of  $A_i = 0.1-1.0$  corresponds to the unphysical situation that the total reaction probability  $\sum_i p_i$  is less than the partial probability  $p_i$ .

DEPARTMENT OF CHEMISTRY  
UNIVERSITY OF TORONTO  
TORONTO 181, ONTARIO, CANADA

MICHAEL MENZINGER\*  
RODNEY L. LEROY  
ANDREW J. YENCHA

RECEIVED SEPTEMBER 24, 1971

## Comments on "Hydrogen Displacement in *n*-Butane by Fast T<sub>2</sub> Collisions"

Publication costs assisted by Argonne National Laboratory

Sir: The preceding communication by Menzinger, *et al.*,<sup>1a</sup> is actually a criticism of our paper.<sup>1b</sup> There are several points of contention and disagreement with their remarks that we wish to bring out.

First, they state that our experiment "complements previous work<sup>2</sup> that has dealt with reactions of tritium atoms." It is very doubtful that the observed tritiated products found from impingement of fast T<sub>2</sub><sup>+</sup> or T<sup>+</sup> on an organic compound condensed on a cold surface are formed exclusively by reactions of fast tritium atoms. Ion-molecule reactions (*e.g.*, dissociative triton transfer is a probable reaction), the effects of surface charges, pyrolysis (with free-radical formation) of the organic compound on a nearby hot filament, and reflection of the fast ions from the surface would all influence and contribute to the observed product yields. Interpretation of data from such an experiment would be very difficult and complicated indeed. Therefore, it is not appropriate for Menzinger, *et al.*, to set up their indirectly measured cross sections for hydrogen displacement as standards by which ours are to be compared, and their statement "... we have determined for the parallel reactions of tritium atoms" is unwarranted.

They write that we have stated in our paper that our results can be interpreted in terms of a "single-pass" gas-phase reaction. Their statement is simply not true, since nowhere in our paper did we talk of a simple "single-pass" experiment. What we write (p 2424) is that since our determined cross section *vs.* kinetic energy curve has a shape similar to the theoretical curve of Karplus, Porter, and Sharma<sup>3</sup> for dissociative collisions, we were led "... to the conclusion that at high kinetic energies the fast tritium species and the butane may undergo collisional dissociation." Indeed, it was the similarity of our experimental curve and their theoretical curve that prompted us to treat our data in terms of single collision processes and thereby arrived at cross sections near gas kinetic at higher energies. It is true that a two-step process would then be required to form the tritiated butane, *i.e.*, the dissociative step of T<sub>2</sub> into tritium atoms followed by a hydrogen displacement step, but we did not say that both steps occurred in the same pass of the fast T<sub>2</sub> through the butane sheath. Menzinger has chosen a two-step mechanism to suit his purposes, but one could suggest another mode which would involve first the *rate-determining* step of collisional dissociation of T<sub>2</sub> into T atoms, followed by eventual reaction of the tritium atoms with *n*-butane in the sheath in subsequent passes. Since the well-collimated T<sub>2</sub> molecular beams at high energies probably pass directly out of the collision

chamber through the aperture leading to the energy-measuring chamber (the corresponding T<sub>2</sub><sup>+</sup> ion beams were focused to do so), this mechanism appears reasonable. Under these conditions the treatment of our data would be valid. One further point in this matter: they keep referring to their work as correct and definitive, *cf.* the statements "Reaction (1b) is known to have a negligible cross section above 15–20 eV" and "However, the yield of such a multiple collision reaction is less than 20%." In view of the difficulties and uncertainties in their experiment cited above their contentions are subject to considerable doubt.

We agree with Menzinger, *et al.*, that the shape of our yield curve is also characteristic of a multiple collision experiment, and since we could not rule out either interpretation, especially at low kinetic energies where the ion beam tends to spread, we consequently treated our data in terms of Porter's theory. Menzinger claims that Porter's generalization to a multicomponent system (here a duocomponent system in which one component, the sheath, is reactive and the other, the wall, is unreactive) must be used rather than his integral equation for a homogeneous single-component gas. This may or may not be true depending on what processes are actually taking place in the collision chamber. They have selected an extreme model in which all hydrogen displacement reactions by fast tritium occur in the sheath and the walls serve only to energy degrade the fast species. This selection, it is true, would then lead to their eq 2–4 and an underestimation of the cross sections by two orders of magnitude. But (as the reviewer has pointed out) an alternative model may be conceived of in which the effects of wall collisions may be ignored to a fair approximation because they may largely pump up the internal energy of the T<sub>2</sub> at relatively little expense of translational energy. If wall collisions can be ignored then use of Porter's one-component integral equation is justified.

However, in the interim since appearance of our publication we have considered an alternative model that would explain our yield curve and make use of Porter's one-component integral equation to arrive at an excitation function for hydrogen displacement in *n*-butane. Although at the time of the experiment we thought we could correct for reactions with butane adsorbed on the chamber walls by subtracting the product yields when alternating the T<sub>2</sub> and *n*-butane beams from the yields when both beams enter the collision chamber simultaneously, it is possible that these experiments do not provide a proper correction. If we

(1) (a) M. Menzinger, R. L. LeRoy, and A. J. Yench, *J. Phys. Chem.*, **76**, 2937 (1972); (b) J. W. Beatty and S. Wexler, *ibid.*, **75**, 2417 (1971).

(2) M. Menzinger and R. Wolfgang, *J. Chem. Phys.*, **50**, 2991 (1969).

(3) M. Karplus, R. N. Porter, and R. D. Sharma, *ibid.*, **45**, 3871 (1966).

assume that butane is adsorbed as a steady-state monolayer on the walls constantly being replenished by stray butane molecules from the sheath, and that the adsorption lifetime of a particular molecule at room temperature is short<sup>4</sup> relative to the duration of an experiment (10 min), virtually all the butane molecules would reach the collection trap. The reactions of fast  $T_2$  molecules could then be with either adsorbed butane or butane in the gas phase, either on first collision at the acceleration energy or after moderating collisions, and the tritiated product would be collected and measured. The conditions of our experiment would then be equivalent to a "thick target" experiment, and Porter's theory would apply exactly to our case. Consequently, the magnitude and form of the derived excitation function (Figure 7 of our paper)

would be valid within the limitations of Porter's theory and our reasonable assumptions.

We wish to thank Menzinger for bringing to our attention (their footnote 9) an apparent peculiar choice of range of  $A_i$ . Unfortunately, a typing error occurred, and p 2425 of our text should read "It was found that the curves obtained for a given energy loss parameter  $\beta$  were the same for all values of  $A_i$  from 10 to 1.0."

(4) The dwell time for physically adsorbed species is less than  $10^{-6}$  sec. See A. W. Adamson, "Physical Chemistry of Surfaces," 2nd ed, Interscience, New York, N. Y., 1967, p 569.

CHEMISTRY DIVISION  
ARGONNE NATIONAL LABORATORY  
ARGONNE, ILLINOIS 60439

S. WEXLER

RECEIVED NOVEMBER 15, 1971

# Reprints from Chemical & Engineering News

On orders of \$10 or less please remit check or money order

Keeping broadly informed challenges every person today. If you missed these features from recent issues of C&EN, you can still get copies by filling in the coupon below.

## Population

A 2-part feature  
David M. Kiefer, C&EN  
Oct. 7 & 14, 1968 **75¢**

Mr. Kiefer finds that population is growing unchecked in much of the world, and that U.S. population will expand 50% in the next 30 years or so. Social as well as technological innovation is needed to thwart this advance. **10148**

## Computers in Chemical Education

Dr. Frederick D. Tabbutt  
Reed College  
Portland, Oregon  
January 19, 1970 **50¢**

A number of experiments with computers in education have been undertaken in the past few years. Some of the approaches to computer-assisted education now show promise as useful adjuncts as surrogate teachers. **11970**

## Arthritis

A 3-part feature  
Howard J. Sanders, C&EN  
July 22, 29, & Aug. 12, 1968 **75¢**

Causes of arthritis are still a mystery, although more and more evidence points to infection as a possible trigger. Mr. Sanders discusses and examines the possible causes and the past, present, and future of treatment. **07228**

## Industrial Research Careers

Howard Reiss  
University of California  
Los Angeles  
June 29, 1970 **50¢**

A major concern of those beginning careers in science is, of course, where to carry out their careers—in a university, private industry, a foundation or wherever. An industrial research career can be a rewarding one, both professionally and financially. **62970**

## Public Policy and the Environment

February 9, 1970 **50¢**  
Speaking at the 158th ACS National Meeting, Lee DuBridge, Herbert Doan, and Barry Commoner urged cooperation among government, industry, and university in tackling environmental improvement. **02970**

## Pollution Control Instrumentation

Michael Heylin, C&EN  
February 15, 1971 **50¢**

Efforts to control air and water resources intelligently depends on the ability to detect and to monitor pollutants. The challenge to produce better instrumentation for this purpose is now receiving intense attention from industry and government researchers. **21571**

## Allergy

Howard J. Sanders, C&EN  
May 11, 1970 **50¢**

Although hay fever, bronchial asthma, and other allergies will not be conquered, they will be better understood and better treated. The expanding study of these diseases in fundamental scientific terms, using the latest research techniques, allergic disorders will yield more and more of their secrets that only a few years ago seemed almost unfathomable. **51170**

## Food Additives

Howard J. Sanders, C&EN  
October 10, 1966 **75¢**

Makers of food additives are keeping their eyes on the spectacular growth of new foods and the shifting moods of regulation-minded Washington. An array of chemicals enhances the wholesomeness, attractiveness, convenience, and nutritional value of American foods. **10176**

## Technology Assessment

David M. Kiefer, C&EN  
October 5, 1970 **50¢**

Technology assessment is an attempt—still halting and uncertain—to establish an early-warning system to control, direct, and, if necessary, restrain technological development so as to maximize the public good while minimizing the public risks. **10570**

## Chemistry and the Atmosphere

Howard J. Sanders, C&EN  
March 28, 1966 **75¢**

The earth's atmosphere is a vast, churning mixture of gases and trace quantities of liquids and solids. Held to the earth by the pull of gravity, it is the transparent envelope without which life on earth would cease to exist. **32866**

## Career Opportunities The New Priorities

March 8, 1971 **50¢**

C&EN's annual career guide for chemists and chemical engineers. In the search for new priorities, new opportunities are emerging. Here C&EN looks at three such areas—food, shelter, and health. **03871**

## Chaos in Science Teaching

Dr. Conrad E. Ronneberg  
Professor Emeritus, Denison University  
June 1, 1970 **50¢**

To many people familiar with the situation in teaching introductory science courses, both in high school and college, the situation is utter chaos. To place attempts to improve science teaching in proper perspective requires a brief review of the progress of science teaching since World II. **06170**

## Artificial Organs

A 2-part feature  
Howard J. Sanders, C&EN  
April 5 and 12, 1971 **75¢**

The implanting of a total artificial heart in a human has been the most dramatic single advance to date in the field of artificial organs. In recent years, however, many other artificial organs have also been developed, and scientists foresee a vast increase in the number of body parts that, in the years ahead, will be replaceable by mechanical devices. **04571**

## Scientific Societies and Public Affairs

K. M. Reese, C&EN  
May 3, 1971 **50¢**

Scientific and engineering societies for many years have fostered research, published papers, and sponsored meetings without great regard for the world beyond their particular disciplines. Only in the past decade or so have the learned societies edged into the realm of public affairs. **05371**

1 to 49 copies—single copy price 50 to 299 copies—20% discount

Prices for larger quantities available on request

10148  11970  07228

62970  02970  51170

21571  10176  10570  32866

03871  06170  04571  05371

TO: REPRINT DEPARTMENT

ACS Publications  
1155 Sixteenth St., N.W.  
Washington, D.C. 20036

FROM:

Name \_\_\_\_\_

Street \_\_\_\_\_

City \_\_\_\_\_

State \_\_\_\_\_ Zip Code \_\_\_\_\_

Amount enclosed \$ \_\_\_\_\_

From The American Chemical Society

# Famous Scientists

**Tape cassettes** from the unique ACS radio program **Men & Molecules**

## NOBEL PRIZE WINNERS

- Dr. Linus Pauling**  
The Committed Scientist  
**Dr. Jacob Bronowski**  
Science and Man
- Dr. Glenn Seaborg** The Atomic World of Glenn Seaborg  
**Dr. George Wald** Vision, Night Blindness, & Professor Wald
- Dr. Melvin Calvin** The Search for Significance—Parts I & II

## BIO-MEDICAL

- Engineering Enzymes**  
Dr. Victor Edwards  
**On Drugs, Plasticizers, & Mass Spec**  
Dr. G. W. A. Milne
- Body Metal** Dr. Thomas Clarkson  
**Judging Technology** Dr. E. G. Mesthene
- Prospects for the Living Filter**  
Dr. Richard Parizek  
**Coral Designs** Dr. Eugene White
- Bones, Teeth, & Ceramics**  
Thomas Driskell  
**PCBs: The Accidental Pollutants**  
Dr. Henry Enos
- Birth Control: Problems & Prospects**  
Dr. Carl Djerassi  
**Hormones, Terpenes, & the German Air Force** Dr. A. J. Birch
- Prospects for Implants**  
Dr. Donald Lyman  
**New Dimensions for Polymers**  
Dr. Alan Michaels
- Fabricating Life** An Essay Report  
**New Ways to Better Food**  
Dr. R. W. F. Hardy
- Chemistry of the Mind: Schizophrenia**  
Dr. Larry Stein  
**Chemistry of the Mind: Depression**  
Dr. Joel Elkes
- The Molecules of Memory**  
Dr. W. L. Byrne & Dr. A. M. Golub  
**The Matter with Memory**  
Dr. J. McGaugh
- Dissonant Harmony**  
Dr. Denham Harman  
**Why We Grow Old** Dr. Howard Curtis

- New Materials for Spare Parts**  
Dr. V. Gott & Dr. A. Rubin  
**Against Individuality**  
Dr. R. Reisfeld & Dr. B. Kahan
- A Richness of Lipids**  
Dr. Roscoe O. Brady  
**Life: Origins to Quality**  
Dr. Stanley Miller
- The Nitrogen Fixer**  
Dr. Eugene van Tamelen  
**Prostaglandins: A Potent Future**  
Dr. E. J. Corey & Dr. S. Bergstrom
- A Glass Revolution** Dr. S. D. Stookey  
**A View of Genes** Dr. Norman Davidson
- Chemical Evolution**  
Dr. Russell Doolittle  
**An Evolving Engine** Dr. R. E. Dickerson

## CANCER RESEARCH

- Cancer Research I—Perspective & Progress** Dr. Frank Rauscher  
**Cancer Research II—Viruses**  
Dr. R. Gallo & Dr. G. Todaro
- Cancer Research III—Chemotherapy**  
Dr. C. Gordon Zubrod  
**Cancer Research IV—Immunology**  
Dr. Paul Levine
- Cancer Research V—Environmental Agents** Dr. Umberto Saffiotti  
**Cancer Research VI—NCI Roundtable**

## ENERGY

- Energy: A Critique**  
Dr. Dean Abrahamson  
**Puzzles of Air Pollution** Arthur Levy
- Fusion: Prospects & Pitfalls—I**  
Dr. H. Furth & Dr. H. Forsen  
**Fusion: Prospects & Pitfalls—II**  
Dr. H. Furth & Dr. H. Forsen
- Antidote to the Energy Crisis**  
George Long  
**Chemicals in the Environment**  
Dr. Samuel Epstein
- Fusion and Fission: An Appraisal**  
Dr. James L. Tuck  
**The Prospects for Energy**  
Dr. M. King Hubert

## ENVIRONMENT

- The Struggle for Clean Water—I**  
**The Struggle for Clean Water—II**
- The Oil Mystery** Harold Bernard  
**The Language of Odors**  
Dr. Stanley Freeman
- The Muskogean County Experiment**  
Dr. W. Bauer & Dr. J. Sheaffer  
**The Sophisticated Dowser**  
Dr. Richard Parizek
- The Lonely Atom** Dr. Philip Skell  
**How Green the Revolution**  
Lester Brown
- Mercury: Another Look, Part I**  
Dr. John Wood  
**Mercury: Another Look, Part II**  
Dr. John Wood & D. G. Langley
- The Troubles with Water**  
Dr. Daniel Okun  
**Pure Oxygen for Polluted Water**  
Dr. Jack McWhirter
- Bubble Machines & Pollution Finders**  
Dr. K. Patel & Dr. L. Kreuzer  
**The Steam Engine: A Modern Approach** Dr. W. Doerner & Dr. M. Bechtold
- Insects: The Elements of Change—Parts I & II** Dr. Carroll M. Williams
- New Weapons Against Insects**  
Dr. G. Staal & Dr. J. Siddall  
**Moths, Drugs, & Pheromones**  
Dr. Wendell Roelofs
- The Lead Issue**  
H. Mayrhoth & M. H. Hyman  
**Smog: An Environmental Dilemma**  
Dr. James Pitts
- The Fusion Torch**  
Dr. B. Eastlund & Dr. W. Gough  
**The Impermanent Plastic**  
Dr. James Guillet

## SCIENCE

- Science, Scientists, & the Public Interest—I**  
**Science, Scientists, & the Public Interest—II**

- Nitrosamines: A Reappraisal**  
Dr. Phillip Issenberg  
**The Emperor of Ice Cream**  
Dr. Wendell Arbuckle
- Ethics and Genetics**  
Dr. Robert F. Murray  
**The American Diet: A Critique**  
Dr. Arnold Schaefer
- Probing Creation** Dr. Myron A. Coler  
**New Directions in U.S. Science**  
Dr. William McElroy
- Aspirins, Enzymes, & Fragrant Redheads** An Essay Report  
**Vitamin D: A New Dimension**  
Dr. Hector DeLuca
- Pica** Dr. J. Julian Chisolm, Jr.  
**Technology in the Nursery**  
Dr. William J. Dorson
- Engineering Microbes**  
Dr. Elmer Gaden  
**Liquid Crystals: A Bright Promise**  
Dr. George Heilmeyer
- Hot Brines in the Red Sea**  
Dr. David Ross  
**Complete Corn** Dr. Edwin T. Mertz
- Lively Xenon** Dr. Neil Bartlett  
**The Repressor Hunt**  
Dr. Mark Ptashne
- The New Prospectors**  
Dr. William Prinz  
**A Sober Look at Alcoholism**  
Dr. Jack Mendelsohn
- Probing the Active Site**  
Dr. David Pressman  
**The Puzzle of Diversity**  
Dr. Oliver Smithies
- Help for the Have Nots**  
Dr. Harrison Brown  
**The Closing Circle** Dr. Preston Cloud

## OUTER SPACE

- Molecules in Space**  
Dr. D. Buhl & Dr. L. Snyder  
**Chemistry Among the Stars**  
Dr. Bertram Donn
- Molecules Meeting Molecules**  
Dr. John Richards  
**The Neutrinos of the Sun**  
Dr. Raymond Davis

	ACS Members	Nonmembers
Single Cassette	\$4.49	\$5.49
Any Six Cassettes	\$3.95/cassette	\$4.95/cassette

Any 18 or more cassettes to one Address \$3.75/cassette

Large Volume Orders Negotiable

For orders outside U.S.A. add 75 cents handling charge

5% Discount if payment accompanies order

Order From: American Chemical Society, 1155 16th Street,  
N.W., Washington, D.C. 20036, ATTN: A. Poulos